Academic Press is an imprint of Elsevier
32 Jamestown Road, London NW1 7BY, UK
Radarweg 29, PO Box 211, 1000 AE Amsterdam, The Netherlands
225 Wyman Street, Waltham, MA 02451, USA
525 B Street, Suite 1900, San Diego, CA 92101-4495, USA

First edition 2011

Library of Congress Cataloging-in-Publication Data
A catalog record for this book is available from the Library of Congress

British Library Cataloguing in Publication Data
A catalogue record for this book is available from the British Library

ISBN: 978-0-12-385904-4
ISSN: 0898-8838

Printed and bound in USA

11 12 13 14 10 9 8 7 6 5 4 3 2 1

LIST OF CONTRIBUTORS

Luis G. Arnaut
Chemistry Department, University of Coimbra, Coimbra, Portugal

Vincenzo Balzani
Dipartimento di Chimica "G. Ciamician", Università di Bologna, via Selmi 2, Bologna, Italy

Giacomo Bergamini
Dipartimento di Chimica "G. Ciamician", Università di Bologna, via Selmi 2, Bologna, Italy

Morgan L. Cable
Planetary Science Section, Jet Propulsion Laboratory, and Beckman Institute, California Institute of Technology, Pasadena, California, USA

Paola Ceroni
Dipartimento di Chimica "G. Ciamician", Università di Bologna, via Selmi 2, Bologna, Italy

Luisa De Cola
Physikalisches Institut, Westfälische Wilhems Universität Münster, Mendesltrasse 7, and Center for Nanotechnology, CeNTech, Heisenbergstrasse 11, Münster, Germany

Harry B. Gray
Beckman Institute, California Institute of Technology, Pasadena, California, USA

Hiroki Inumaru
Department of Chemistry, Tokyo Institute of Technology, Tokyo, Japan

Osamu Ishitani
Core Research for Evolutional Science and Technology (CREST), Japan Science and Technology Agency (JST), Kawaguchi, Saitama, Department of Chemistry, Tokyo Institute of Technology, Tokyo, and Research Seeds Program, Japan Science and Technology Agency (JST), Kawaguchi, Saitama, Japan

James P. Kirby
Planetary Science Section, Jet Propulsion Laboratory, Pasadena, California, USA

Horst Kisch
Department of Chemistry and Pharmacy, Institute of Inorganic Chemistry, Friedrich-Alexander-Universität Erlangen-Nürnbegrg, Egerlandstraße 1, Erlangen, Germany

Günther Knör
Institute of Inorganic Chemistry, Johannes Kepler University (JKU), Linz, Austria

Kazuhide Koike
Core Research for Evolutional Science and Technology (CREST), Japan Science and Technology Agency (JST), Kawaguchi, Saitama, and National Institute of Advanced Industrial Science and Technology, Tsukuba, Ibaraki, Japan

Horst Kunkely
Institut für Anorganische Chemie, Universität Regensburg, 93040 Regensburg, Germany

Dana J. Levine
Beckman Institute, California Institute of Technology, Pasadena, California, USA

Matteo Mauro
Physikalisches Institut, Westfälische Wilhems Universität Münster, Mendesltrasse 7, and Center for Nanotechnology, CeNTech, Heisenbergstrasse 11, Münster, Germany

Uwe Monkowius
Institute of Inorganic Chemistry, Johannes Kepler University (JKU), Linz, Austria

Tatsuki Morimoto
Department of Chemistry, Tokyo Institute of Technology, Tokyo, Japan

B. Ohtani
Catalysis Research Center, Hokkaido University, Sapporo, Japan

Adrian Ponce
Planetary Science Section, Jet Propulsion Laboratory, Pasadena, California, USA

Zofia Stasicka
Faculty of Chemistry, Jagiellonian University, Ingardena 3, Kraków, Poland

Cristian A. Strassert
Physikalisches Institut, Westfälische Wilhems Universität Münster, Mendesltrasse 7, and Center for Nanotechnology, CeNTech, Heisenbergstrasse 11, Münster, Germany

Hiroyuki Takeda
Toyota Central R&D Laboratories, Inc., Nagakute, Aichi, and Core Research for Evolutional Science and Technology (CREST), Japan Science and Technology Agency (JST), Kawaguchi, Saitama, Japan

Arnd Vogler
Institut für Anorganische Chemie, Universität Regensburg, 93040 Regensburg, Germany

PREFACE

Volume 63 of *Advances in Inorganic Chemistry* is a thematic issue devoted to inorganic photochemistry, coedited by Grażyna Stochel from the Jagiellonian University in Kraków, Poland. Photochemistry has always played an important role in inorganic/bioinorganic chemistry, and with the development of sophisticated instrumentation, the underlying physical and chemical processes have been clarified to a significant degree in recent years. Inorganic photochemistry presently finds application in diverse areas such as sensor technology, molecular assemblies, catalysis, medical therapy, biomimetics, activation of small molecules, semiconductors, solid materials, and environmental processes. This volume includes 10 contributions highlighting the role of photochemistry in a broad spectrum of inorganic chemistry. We hope it will prove interesting and inspiring to researchers in this field.

The first chapter by Harry B. Gray and collaborators presents a detailed account on luminescent lanthanide sensors. This is followed by a chapter on the photo-physics of soft and hard molecular assemblies based in luminescent complexes written by Luisa de Cola and collaborators. The photochemistry and photo-physics of metal complexes with dendritic ligands are covered in the following chapter by Vincenzo Balzani and collaborators. In the fourth chapter, Osamu Ishitani and collaborators present an account on the photochemistry and photo-catalysis of rhenium(I) diimine complexes. In the subsequent chapter, Luis G. Arnaut reports on the design of porphyrin-based photosensitizers for photodynamic therapy. Photosensitization and photo-catalysis in bioinorganic, bio-organometallic, and biomimetic systems are covered by Günther Knör and collaborator in the sixth chapter. A short review on recent developments in transition metal complexes as solar photo-catalysts in the environment is presented in the seventh chapter by Zofia Stasicka. This is followed by a contribution from Arnd Vogler and collaborator on the photochemical activation and splitting of water, CO_2, and N_2 induced by charge transfer excitation of redox-active metal complexes. In the ninth chapter, Horst Kisch reports on visible light photo-catalysis by metal halide complexes containing titania as a semiconductor

ligand, and in the final chapter, Bunsho Ohtani presents a contribution on photo-catalysis by inorganic solid materials, in which he revisits the definition, concepts, and experimental procedures.

We appreciate the constructive interaction we had with the authors of these chapters and thank them for their willingness to find time to contribute to this thematic issue. We trust that the readers in the inorganic/bioinorganic chemistry communities will find this volume informative and useful.

Rudi van Eldik
University of Erlangen-Nürnberg
Germany

Grażyna Stochel
Jagiellonian University
Poland
May 2011

LUMINESCENT LANTHANIDE SENSORS

MORGAN L. CABLE[a,b], DANA J. LEVINE[b,1], JAMES P. KIRBY[a], HARRY B. GRAY[b] and ADRIAN PONCE[a]

[a]Planetary Science Section, Jet Propulsion Laboratory, Pasadena, California, USA
[b]Beckman Institute, California Institute of Technology, Pasadena, California, USA

ABSTRACT

Luminescent lanthanide optical sensors have been developed that utilize ancillary ligands to enhance detection of a target analyte. In these systems, the lanthanide (ligand) binary complex serves as the receptor, which upon analyte binding forms a ternary complex resulting in detectable change in lanthanide luminescence (Fig. 1). The ancillary ligand improves many properties of analyte detection by protecting the lanthanide and strengthening analyte binding affinity. Encapsulation shields

[1]Current address: Department of Chemistry, University of California, Berkeley, California, USA

INORGANIC PHOTOCHEMISTRY
VOLUME 63 ISSN 0898-8838 / DOI: 10.1016/B978-0-12-385904-4.00010-X

the lanthanide ion from solvent-quenching effects and interfering ions, improving assay sensitivity and selectivity. The ligand-induced enhancement in binding affinity appears to be the result of an increase in positive charge at the analyte binding site due to the electronegative ancillary ligand bound on the opposite hemisphere of the lanthanide. We have elucidated the effects of ancillary ligands for various lanthanide/analyte systems and shown how such effects can greatly improve sensor performance for medical, planetary science, and biodefense applications.

Keywords: Lanthanide; Sensor; Sensitized luminescence; Dipicolinate; Macrocycle; Ternary complex; Bacterial spore; Ancillary ligand; Gadolinium break; Catecholamine; Salicylic acid; Salicylurate.

I. Introduction

A. Lanthanides

The lanthanides, or lanthanoids, are elements with lives of their own—enigmatic, difficult to separate and purify— and most often pictured as a row orphaned from the rest of the periodic table along with their more radioactive siblings, the actinides. Also known as "rare earth elements" due to the etymology of the term "lanthanide" (derived from the Greek *lanthanein*, meaning "to lie hidden"), they include the 15 elements of the top row in the "f-block" and have electronic configurations [Xe] $4f^n5s^25p^6$, where n varies from 0 to 14. Interestingly, lanthanides are neither rare nor "earths," an old term used to describe certain metal oxides such as lime and magnesia (*1*). Even the rarest lanthanides—thullium and lutetium—are two orders of magnitude more abundant than gold (*2*).

Lanthanides have found uses as catalysts, ceramics, and permanent magnets, as well as in optics and electronics (*3,4*). Solid phosphors containing europium, cerium, and terbium are found in many common fluorescent lighting and color displays. Various lanthanide ions are used in lasers, with neodymium as the most famous in yttrium aluminum garnet (Nd-YAG). The green, blue, and red luminescent bands in Euro banknotes are from europium complexes (*5*). Certain lanthanides are used as tracers in wine chemistry to discriminate wines according to geographical region (*6*). The ratio of europium, which is almost entirely formed in stars, to other rare earth elements in meteorites has helped

us decipher much of the history of processes in our solar system, including the early development of the feldspar-rich lunar crust (*7*).

In aqueous solution, lanthanides are most stable in the tripositive oxidation state, making them difficult to separate and purify. The preference for this oxidation state is due in part to the energy of the 4f electrons being below those of the 5d and 6s electrons (except in the cases of La and Ce). When forming ions, electrons from the 6s and 5d orbitals are lost first so that all Ln^{3+} ions have [Xe] $4f^n$ electronic configurations. Under reducing conditions, certain lanthanides (europium, samarium, and ytterbium) can be stable as dipositive ions, and cerium can adopt a $+4$ oxidation state (*5*).

Lanthanide ions are hard Lewis acids: the 4f orbitals are well shielded by the 5s and 6p orbitals and do not participate directly in bonding, π-bonding is disfavored, and there are no complexes with Ln—O or Ln—N multiple bonds. Coordination to Ln^{3+} is ionic in character, leading to a strong preference for negatively charged or neutral donor groups with large ground state dipole moments (Fig. 1). Combinations of amines and carboxylic acid groups are therefore often used for lanthanide complexation (*8,9*). Coordination geometries in lanthanides are determined by ligand steric factors as opposed to orbital overlap or crystal field effects (*10,11*). In aqueous solution, donor groups containing neutral oxygen or nitrogen atoms generally bind when present in multidentate ligands, such as podands, crown ethers, and cryptates (*12–15*). Relatively few complexes of monodentate nitrogen donors are known, suggesting an oxophilic tendency of lanthanide binding. This preference for oxygen donors also makes lanthanides quite lithophilic and explains their occurrence in silicates as opposed to metallic or sulfidic minerals (*16*).

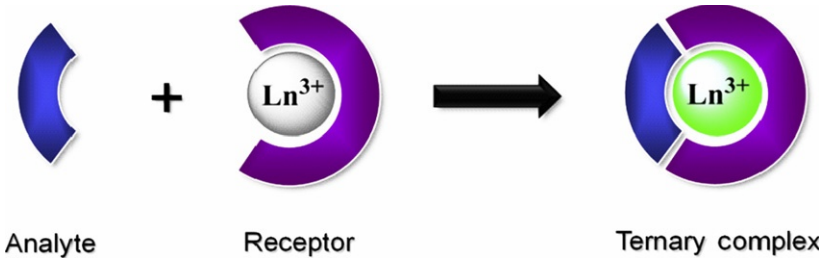

FIG. 1. Binding of an analyte to a lanthanide-based receptor produces a luminescent ternary complex. The ancillary (receptor or helper) ligand is shown in dark gray.

The coordination number of $[Ln(H_2O)_n]^{3+}$ is normally 9 for the early lanthanides (La–Eu) and 8 for those later in the series (Dy–Lu), with the intermediate metals (Sm–Dy) exhibiting a mixture of species. However, the coordination number can be dictated by the steric bulk of the coordinating ligands, and species with coordination numbers as low as 2 and as high as 12 are known (*5,17*).

With the 4f electrons well shielded from the environment, the spectroscopic and magnetic properties of the lanthanides (e.g., electronic spectra and crystal field splittings) are largely independent of environmental factors (solvent, coordinated ligands). The number of electronic configurations is a function of the number of unpaired electrons where $0 \leq x \leq 14$, with the lowest energy term for each ion consistent with the predictions of Hund's first and second rules (*18,19*). Owing in part to spin–orbit coupling, the lanthanides exhibit a rich energy level pattern, with the lowest electronic excited states significantly above the ground state (*20*). As f–f transitions are electric dipole forbidden (but magnetic dipole allowed), lanthanide ion absorptions are very weak ($\epsilon \sim 0.1\ \text{mol}^{-1}\ \text{dm}^3\ \text{cm}^{-1}$) (*5,21–23*). Electronic transitions must involve promotion of an electron without a change in its spin ($\Delta S = 0$) and with a variation of either total angular momentum or total angular quantum number of one unit at most ($\Delta L = \pm 1.0$; $\Delta J = \pm 1.0$). Though absorption of radiation can in theory promote the lanthanide ion to any energetically accessible state, emission normally occurs only from the lowest lying energy level of the first excited term due to rapid internal conversion (IC) (*19*). In cases of low symmetry or vibronic coupling, the f–f transitions can gain intensity through f- and d-state mixing with higher electronic states of opposite parity. Broad $4f^n \rightarrow 4f^{n-1}\ 5d^1$ transitions also can be seen in the infrared region for some lanthanides.

The electronic configurations of Ln^{3+} ions are split by electronic repulsion, with term separations on the order of $10^4\ \text{cm}^{-1}$ (Fig. 2) (*24*). These terms are split further by spin–orbit coupling into J states, with energy differences in the $10^3\ \text{cm}^{-1}$ range (*25*). These spectroscopic levels can be split once again into what are termed Stark sublevels due to ligand-field effects from the coordination sphere around the lanthanide; Stark sublevel splitting is on the order of $10^2\ \text{cm}^{-1}$ (*26*). The emission peak positions in Ln^{3+} complexes do not vary substantially, because the f-electrons are shielded, but an emission profile (defined as the relative intensity and degree of splitting of an emission band) can vary greatly (*21,27*). The number of Stark sublevels depends on the site symmetry of the lanthanide ion, and these can be thermally populated at room temperature, yielding more complex emission spectra.

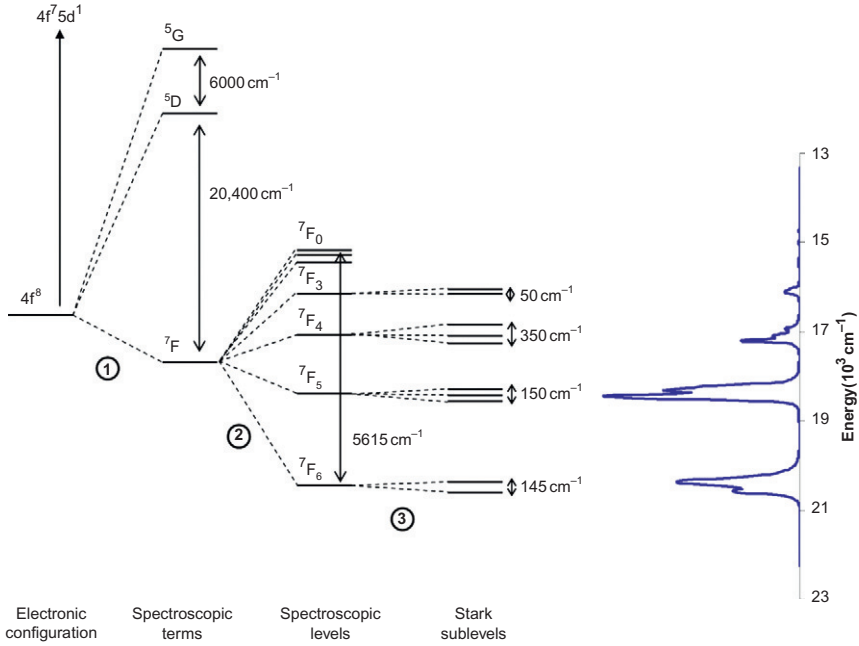

FIG. 2. Splitting of a lanthanide electronic configuration, with Tb^{3+} ($4f^8$) as an example: (1) interelectronic repulsion, (2) spin–orbit coupling, and (3) ligand-field effects. The emission spectrum of $Tb(DPA)_3$ at right is an experimental example of these splittings.

Filling of the inner 4f electron shell across the lanthanide series results in decreases of ionic radii by as much as 15% from lanthanum to lutetium, referred to as the lanthanide contraction (*28*). While atomic radius contraction is not unique across a series (i.e., the actinides and the first two rows of the d-block), the fact that all lanthanides primarily adopt the tripositive oxidation state means that this particular row of elements exhibits a traceable change in properties in a way that is not observed elsewhere in the periodic table. Lanthanides behave similarly in reactions as long as the number of 4f electrons is conserved (*29*). Thus, lanthanide substitution can be used as a tool to tune the ionic radius in a lanthanide complex to better elucidate physical properties.

B. LANTHANIDE SENSITIZATION

The first demonstration of sensitized lanthanide luminescence was due to the efforts of Bhaumik and El-Sayed, who found that if the lowest triplet level of europium tris-hexafluoroacetylacetonate,

$Eu(HFA)_3$, was excited by triplet-to-triplet intermolecular energy transfer (EnT) from another donor (benzophenone), the energy could be transferred to the lanthanide cation (*30,31*). This indirect sensitization bypasses the selection rules that normally limit f–f excitation in lanthanides and can result in luminescence enhancement by three orders of magnitude or more (*24,32,33*).

In sensitized lanthanide luminescence, the chromophore is normally an aromatic or unsaturated organic molecule that is either anionic or is strongly dipolar, thereby promoting binding to the Ln^{3+} ion. To act as an efficient energy harvester or "antenna," (*34*) the chromophore must absorb radiation effectively and transfer most of this energy nonradiatively to the lanthanide ion. This process, known as the absorption-energy transfer-emission (AETE) mechanism, occurs in several steps. First, the light-harvesting ligand is excited from the ground state S_0 to singlet excited states (Fig. 3). Some chromophores have several accessible singlet excited states; nonradiative relaxation from these higher singlet excited states (S_2, S_3, etc.) to the lowest singlet excited state (S_1) via IC can occur readily. Second, a triplet excited state (T_1) is formed through intersystem crossing (ISC), a process that is more efficient near heavy atoms such as lanthanides (*35*). Third, intramolecular EnT from the ligand triplet excited state to the lanthanide excited state occurs, resulting in a populated emissive level. The efficiency of this step, the intramolecular EnT from chromophore to Ln^{3+}, is the most important factor influencing the luminescence properties of lanthanide complexes (*36*). The final step is the luminescence observed as the excited state in the lanthanide decays radiatively to the ground state (*37,38*).

However, there are other pathways, both radiative and nonradiative, that can reduce the efficiency of sensitized lanthanide luminescence. Chromophores can lose energy from the singlet excited state by two mechanisms: (1) fluorescence, where the chromophore radiatively decays from the singlet excited state to the ground state, or (2) nonradiative quenching by photoinduced electron transfer or other means (*12*). The triplet excited state of the chromophore also can decay radiatively (phosphorescence), or nonradiatively by oxygen quenching, though oxygen has been found to have little or no quenching effect on visible-emitting lanthanide complexes (*39,40*). These mechanisms can be mitigated or minimized by judicial choice of chromophore.

The AETE mechanism relies on appropriate alignment of the ligand donating triplet energy level and the lanthanide accepting excited level for efficient EnT. The intramolecular EnT efficiency

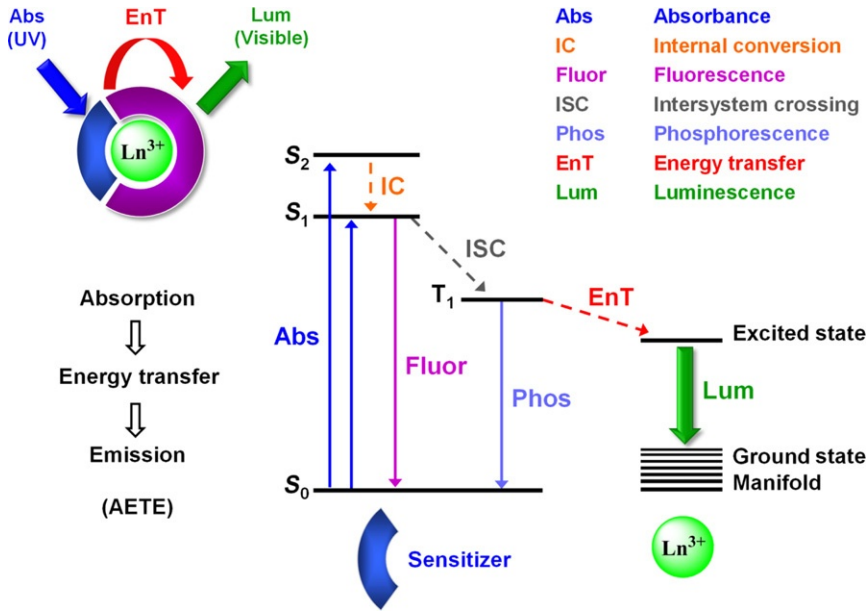

FIG. 3. Jablonski diagram of the absorption-energy transfer-emission (AETE) mechanism from an aromatic sensitizer to Tb^{3+}. Radiative transitions are shown with solid arrows; nonradiative transfers are depicted with dashed arrows. UV radiation is absorbed by the conjugated π-electron system of the aromatic ligand leading to a singlet excited state; this energy transfers to the ligand triplet excited state via intersystem crossing (ISC) and then to the emissive level ($^5D_4$) of the Tb^{3+} ion. Luminescence is observed through radiative decay from the excited state to the seven energy levels of the Tb^{3+} heptet ground state (^7F_J). Note that fluorescence and phosphorescence are not always observed for aromatic donor ligands.

depends mainly on two processes: Dexter resonant exchange and thermal deactivation *(41)*. The donor and acceptor levels must be close enough to allow for efficient EnT, but if they are too close, the energy is lost due to thermal deactivation. The optimal energy gap between chromophore triplet state and lanthanide excited state is approximately $4000 \pm 500\ cm^{-1}$, meaning that the pairing of lanthanide and chromophore is of the utmost importance for achieving efficient EnT (Fig. 4) *(36,42)*.

Lanthanide complexes reveal interesting spectroscopic features not found in other luminescent species. Emission spectra exhibit very narrow bands because both excited and ground states have the same f^n configuration *(12,24)*. These f–f transitions also are largely independent of the chemical environment of the lanthanide

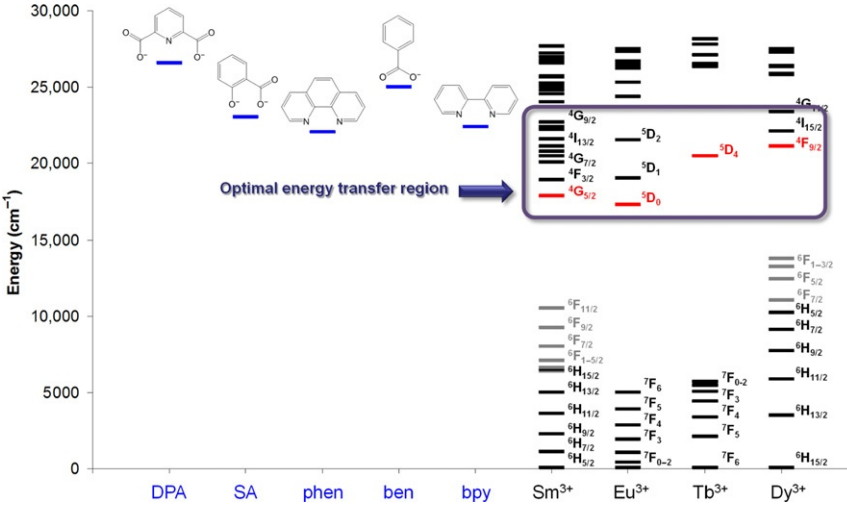

FIG. 4. Energy level diagram depicting the triplet excited states of various aromatic ligands (left) along with the excited and ground states of the four luminescent lanthanides (right). Ground states that do not contribute to luminescence are shown in gray. The area highlighted in the box illustrates the region where the energy gap between ligand triplet state and lanthanide excited state is optimal for efficient energy transfer (4000 ± 500 cm^{-1} less than the ligand triplet state). Aromatic ligands: dipicolinic acid (DPA); salicylic acid (SA); 1,10-phenanthroline (phen); benzoate (ben); 2,2′-bipyridine (bpy).

ion, though peak splittings and relative intensities can vary significantly in some cases. Due to the various EnT steps that occur in lanthanide luminescence (IC, ISC, etc.), there is usually a very large difference between the absorption and emission maxima in these complexes (the Stokes shift) (*39,43*). A larger Stokes shift reduces overlap between absorbance and emission bands which minimizes energy lost to reabsorption. Further, as the major transitions in these complexes are electric dipole forbidden, the excited state lifetimes tend to be very long, often micro- to milliseconds (*21,44*). Though the property of long luminescence lifetime is not necessarily unique, the fact that it occurs under ambient conditions is unusual. Most organic species that exhibit phosphorescence only do so at low temperatures and/or in the absence of oxygen (*19*).

Owing to these unique properties, lanthanides have several advantages over traditional organic fluorophores, quantum dots, or other fluorescent species commonly used as sensors. These

advantages include better spectral resolution due to large Stokes shifts and narrow emission lines and increased temporal resolution due to long lifetimes. The latter property allows for the use of time-gated techniques and bandpass filters to reduce interference from native or autofluorescence in the sample, which occurs on the nanosecond timescale (*21,43*). Lanthanides also are more resistant to photobleaching than organic dyes, as they are effective quenchers of triplet states (*45*). These qualities make lanthanides particularly attractive for optical detection applications, although ways must be found to improve sensitivity, stability, and selectivity. In our work, we have constructed stable and selective luminescence lanthanide sensors containing receptor ancillary ligands designed to detect target analytes of interest.

C. Lanthanide Receptors

A number of factors must be considered when designing lanthanide-based receptors. The choice of lanthanide is paramount. Ionic radius varies across the lanthanide series, and the size of this cation can influence the relative binding affinity of the target analyte. The lanthanide excited state must also align correctly with the triplet excited state of the target analyte; if the energy difference is too great, the EnT efficiency will be low, but if it is too small, quenching effects such as back transfer will dominate. The emission properties of the lanthanide, such as luminescence lifetime and quantum yield, must also be considered to produce an adequate signal. Of all the lanthanides, Eu^{3+}, Tb^{3+}, and Gd^{3+} are the best ions in terms of efficient excited state population, with energy gaps of 12,300 cm^{-1} ($^5D_0 \rightarrow {}^7F_6$), 14,800 cm^{-1} ($^5D_4 \rightarrow {}^7F_0$), and 32,200 cm^{-1} ($^6P_{7/2} \rightarrow {}^8S_{7/2}$), respectively (*12*). While europium and terbium both emit in the visible region, gadolinium emits in the ultraviolet, disfavoring its use in luminescence-based sensing applications due to significant absorption and emission interference at these high-energy wavelengths. (The exactly half-filled f-shell of Gd^{3+} makes this lanthanide better suited to magnetic resonance-based sensing technologies, a rich and broad field beyond the scope of this review.) Dy^{3+} and Sm^{3+} also emit in the visible region, though their emission intensities are muted due to multiple nonradiative decay pathways from several energy-accepting excited states (*39,46*). We therefore focus on terbium and europium as the primary lanthanides used in sensitized luminescence assays, with dysprosium and samarium employed where necessary to elucidate trends based on variations in ionic radii.

Almost as important as the choice of lanthanide is the choice of ancillary ligand, which transforms the lanthanide into a receptor. This helper ligand must bind to the lanthanide with high affinity to prevent solvent coordination, which can severely quench luminescence via nonradiative decay pathways. However, the ligand must not interfere with binding of the target analyte, or the lanthanide loses all functionality as a sensor. Thus, the denticity and stability of the receptor ligand, as well as the size and geometry of the binding pocket it generates, are key factors. Further, as most coordination to lanthanides is based on electrostatic interactions, the charge of the ancillary ligand—and ultimately the entire receptor complex—should influence the binding affinity of the analyte. We will show that there are exceptions to this "rule," as other factors can affect analyte binding in very significant ways.

The goal of our program is to build receptors with lanthanide ions containing ancillary ligands that confer stability, solubility, and high analyte specificity for target molecules. Binding of an aromatic analyte to such a binary complex should trigger intense luminescence upon UV excitation due to an AETE mechanism, producing a signal that is orders of magnitude greater in intensity than emission of the lanthanide alone. We have investigated various binary complexes containing a luminescent lanthanide (Sm^{3+}, Eu^{3+}, Tb^{3+}, and Dy^{3+}) and a helper ligand to optimize detection of a particular analyte of interest. These investigations, which involved analysis of structure, photophysics, stability, and resistance to interferents, turned up some interesting results that forced us to question several basic assumptions regarding lanthanide–ligand interactions.

The common properties attributed to helper ligands in improving lanthanide-based detection techniques include enhanced stability, sensitivity, and selectivity. We will start with the effects of ancillary ligands on lanthanide photophysics and then explore the impacts of these ligands on sensor properties (Section II). Other factors influencing stability, such as sterics and oxophilicity, will be summarized in Section III. A brief discussion of future applications will follow (Section IV).

II. Effects of Ancillary Ligands

A. Photophysics

Ancillary ligands were first applied in lanthanide chemistry due to their ability to encapsulate the metal ion and protect it from solvent *(47,48)*. The greatest vulnerability of sensitized

lanthanide luminescence lies in nonradiative deactivation or relaxation due to solvent interactions, which can reduce emission intensity significantly through energy dissipation by vibronic modes (*24,49*). Typically, this occurs by harmonic oscillators in the lanthanide coordination sphere, though outer-sphere quenching has also been observed (*39*). The most common and efficient quencher of lanthanide luminescence is the O—H oscillator (*50*). To reduce or eliminate this pathway for nonradiative decay, the lanthanide ion must be effectively shielded from the solvent. This can be accomplished using various chelating ligands containing hard donors that bind to the lanthanide ion with high affinity and contain a cavity to encapsulate the ion and prevent solvent coordination. The first "insulating sheath" for lanthanide ions was developed by Halverson in 1964 using fluorinated 1-diketonates (*48*). Since then many ligands have been identified for this purpose, including cyclodextrins, cryptands, podands, calixarenes, porphyrins, crown ethers, and aza-crown macrocyclic and bicylic ligands (*12,13,51–55*).

A well-studied example of improved photophysics due to a helper ligand can be seen in the detection of dipicolinate, an indicator of bacterial spores. Bacterial spores, also known as endospores, are dormant microbial structures that exhibit remarkable resistance to chemical and physical environmental stresses and are considered to be one of the most robust forms of life on Earth (*56*). Discovered in 1876, endospores are formed inside the vegetative cells of certain species of *Bacillus*, *Clostridium*, and *Sporosarcina* (hence the "endo" prefix) in a process called sporulation (*57–60*). Sporulation is often triggered when the cells are exposed to adverse environmental conditions, such as desiccation or starvation. Endospores can remain dormant with no detectable metabolism for potentially millions of years (*61–64*). When conditions become favorable again, as indicated by the presence of water, nutrients, or specific germinants, endospores undergo germination and outgrowth to become vegetative cells, completing the cycle (*65,66*).

In the dormant spore state, endospores are resistant to a wide variety of chemical and physical stresses such as UV and gamma radiation, desiccation, temperature and pressure extremes, and attack by toxic agents (*67–70*). As they are resilient to most sterilization procedures, bacterial spores are used in several industries as biological indicators (*71,72*). Certain species can even survive the vacuum, extreme temperatures, and radiation of space (*73,74*), making them the focus of research concerning planetary protection, panspermia (transfer of life from one

planetary body to another via meteoritic impacts), and life in extreme environments (*75,76*). In addition, detection of bacterial spores became a national priority after the anthrax attacks of 2001, as *Bacillus anthracis* spore powders are the vectors of the anthrax bioweapon (*77–80*). Certain species of anaerobic endospores, such as *Clostridium botulinum* and *Clostridium perfringens*, are pathogenic and the causative agents of food poisoning and other serious diseases (*81*).

Owing to its applications in homeland security, sterilization validation, and astrobiology, bacterial spore detection has become a hot field. However, direct detection of bacterial spores can be challenging for the same reasons that make endospores difficult to irradicate. The tough spore coat is impermeable to staining techniques, so most microscopy and flow cytometry methods are not useful. Endospores are also highly resistant to lysis, meaning that common DNA extraction protocols are difficult to perform. The lack of measurable metabolism renders microcalorimetry and cellular respiration techniques ineffective.

Bacterial spores contain a unique chemical marker—dipicolinic acid, or DPA. DPA is present in nearly all bacterial spores and comprises about 10–15% of a spore's dry weight, or approximately 10^8 molecules per spore (*82–84*). Detection of this chemical marker can therefore serve as a positive signal for the presence of bacterial spores, and the amount of DPA detected can be used to estimate the approximate endospore concentration (*81,85*).

The application of lanthanides to bacterial spore detection was proposed in 1997 with a method using terbium to detect dipicolinate with fluorescence spectrophotometry (*86*). Addition of terbium chloride to a suspension of lysed endospores causes the formation of $[Tb(DPA)_n]^{3-2n}$ complexes, where n varies from 1 to 3, as the Tb^{3+} displaces the Ca^{2+} of calcium dipicolinate (CaDPA). Dipicolinate is an effective absorber of ultraviolet radiation due to the delocalized π-electrons of the aromatic pyridine (Pyr) ring, and the triplet excited state of the DPA anion ($26{,}600\ cm^{-1}$) is also in the appropriate regime to effectively sensitize the Tb^{3+} cation via EnT to the $^5D_4$ emitting level of the terbium ($20{,}500\ cm^{-1}$) through an AETE mechanism (*87–89*). The end result is intense luminescence under UV excitation that is more than three orders of magnitude greater than that of the terbium ion alone (Fig. 5) (*81,90,91*).

Although the method is rapid and straightforward, the use of free terbium as a sensing tool has several weaknesses, such as the potential for false positives or false negatives through complexation of anionic interferents to the exposed tripositive cation.

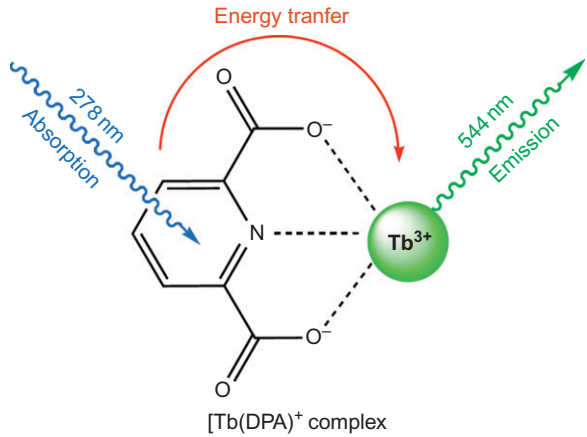

FIG. 5. The method of bacterial spore detection using terbium. Dipicolinic acid (DPA) is released from endospores via lysis or germination and binds to Tb^{3+} with high affinity. The resulting $[Tb(DPA)]^{+}$ complex exhibits intense luminescence in the visible region (544 nm) under UV excitation (278 nm) that is much greater than Tb^{3+} alone.

Another concern is that, for a 9-coordinate lanthanide ion in aqueous solution bound to a single tridentate DPA ligand, the six coordinated water molecules will strongly quench the luminescence (*92*). To eliminate the potential for solvent quenching and improve the sensitivity of the assay, we explored the use of a hexadentate ancillary ligand to encapsulate the Tb^{3+} ion and exclude solvent from the coordination sphere without impeding dipicolinate chelation.

We selected the macrocyclic ligand 1,4,7,10-tetraazacyclododecane-1,7-bisacetate (DO2A) as our helper ligand, as this chelator meets our initial criteria for designing a terbium-containing dipicolinate receptor site. Macrocyclic ligands often have semirigid backbone ring structures. These ligands vary in terms of ring diameter and the extent of substituent functionalization on the ring scaffold. Most macrocycles have a hydrophilic cavity in which an ionic substrate such as a metalion can nest and be shielded from the environment by its lipophilic envelope (*3,93*). Ligands such as the octadentate DOTA (1,4,7,10-tetrakiscarboxymethyl-1,4,7,10-tetraazacyclododecane) have found a convenient niche in the field of bioimaging as magnetic resonance contrast agents due to their tendency to bind gadolinium with high affinity (*94,95*). In fact, most macrocyclic ligands seem to exhibit an unprecedented selectivity for lanthanide ions, and the dissociation of these lanthanide–macrocycle complexes appears to be independent of

foreign metal ion concentration (*96*). Most Ln^{3+}–macrocycles are highly water soluble, thermodynamically stable, kinetically inert at physiological pH, cell permeable, and nontoxic, making them ideal for use as *in vivo* bioprobes. The facile derivatization of ligands bound to lanthanides also makes them easily tailored to bind specific biomolecules such as antigens and proteins.

As described previously, nonradiative decay due to solvent interactions can severely reduce lanthanide luminescence through energy dissipation by vibronic modes, with the O—H oscillator being the most common and efficient quencher. However, if these O—H oscillators are replaced with lower-frequency O—D oscillators, the efficiency of vibronic deactivation decreases substantially. Therefore, the rate constants for luminescence lifetimes (τ_{H_2O}) of lanthanide excited states in water or alcoholic solvents are often much shorter than those in analogous deuterated solvents (τ_{D_2O}). This property can be utilized to determine the degree of solvation for luminescent lanthanides.

The hydration number, or the number of bound water molecules in the lanthanide coordination sphere, can be calculated using a method introduced by Horrocks and Sudnick for terbium and europium complexes (*50*). The relationship between Tb or Eu excited state lifetimes (τ), which are experimentally determined in H_2O and D_2O, and the hydration number (q) is given in Eq. (1)

$$q = A_{Ln}\left(\frac{1}{\tau_{H_2O}} - \frac{1}{\tau_{D_2O}}\right) \tag{1}$$

All lifetimes are in milliseconds, and the A_{Ln} constant is a proportionality factor specific to a given lanthanide that takes into account the energy gap between the ground and excited state manifolds. This equation was later modified by Parker to include quenching effects from coordinated N—H oscillators (Eq. 2), where x is the number of N—H oscillators) and outer-sphere water molecules (*97*).

$$\begin{aligned} q^{Eu} &= A_{Eu}\left[\left(\frac{1}{\tau_{H_2O}} - \frac{1}{\tau_{D_2O}}\right) - 0.25 - 0.075x\right] \\ q^{Tb} &= A_{Tb}\left[\left(\frac{1}{\tau_{H_2O}} - \frac{1}{\tau_{D_2O}}\right) - 0.06\right] \end{aligned} \tag{2}$$

The effect of the DO2A ligand, which contains two N—H oscillators, results in a proportionality factor of 4.6 ± 0.5 ms when coordinated to Tb^{3+}, assuming slow exchange with D_2O (*98*).

TABLE I

LUMINESCENCE LIFETIME MEASUREMENTS ON VARIOUS TERBIUM COMPLEXES (*100*).

Complex	τ_{H_2O} (ms)	τ_{D_2O} (ms)	q
$[Tb(H_2O)_9]^{3+}$	0.4	3.4	8.8 ± 1.1
$[Tb(DPA)(H_2O)_6]^{+}$	0.6	3.5	5.6 ± 0.7
$[Tb(DO2A)(H_2O)_3]^{+}$	1.1	2.6	2.4 ± 0.3
$[Tb(DO2A)(DPA)]^{-}$	1.9	2.2	0.3 ± 0.0

Luminescence lifetime measurements were performed, and the decay curves fit to a monoexponential model to obtain the lifetime of each terbium complex in H_2O and D_2O. The calculated hydration numbers verify that $[Tb(DO2A)(DPA)]^{-}$ excludes all water from the lanthanide coordination sphere, eliminating solvent-quenching effects (Table I) (*99*). Further, encapsulation of the lanthanide also causes a marked improvement in emission lifetime, from 600 μs to nearly 2 ms. This allows for application of time-gated detection techniques, reducing short-lived background fluorescence considerably in environmental samples and demonstrating a significant advantage in achievable limits of detection.

Another example of improved sensitivity due to modulation of lanthanide photophysics by ancillary ligands can be found in the europium and terbium chelates used in time-resolved fluorescence resonance energy transfer (TR-FRET) immunoassays (*100,101*). Due to their line-type emissions and long decay times, the lanthanide chelate is used as a donor, with some visible-absorbing dye such as Alexa® 647 or a rhodamine derivative as the acceptor. Without the helper ligand, the lanthanides would be unprotected from solvent and have much shorter decay times, making them unsuitable for such an assay.

Ancillary ligands improve the photophysical properties of luminescent lanthanide-based assays by encapsulating the cation and protecting it from solvent-quenching effects. In addition to improving signal intensity, the helper ligand also improves the lifetime of the emitting lanthanide. But enhancement of lanthanide photophysics is only one of several improvements observed with use of such receptor ligands.

B. STABILITY

Ancillary ligands have been used in lanthanide-based sensors to improve signal intensity by making the lanthanide more

resistant to solvent-quenching effects. It had not been anticipated that the ancillary ligand also could have a more direct effect—increasing the attraction between lanthanide and analyte.

While investigating the effects of ancillary ligands on the binding of dipicolinate, we developed a binding affinity by competition (BAC) assay to quantify the binding constant of analyte to lanthanide complex (Eq. 3) (*102*).

$$\mathrm{Ln(DO2A)^+ + DPA^{2-} \overset{K'_a}{\rightleftharpoons} Ln(DO2A)(DPA)^-}$$
$$K'_a = \frac{[\mathrm{Ln(DO2A)(DPA)^-}]_{eq}}{[\mathrm{Ln(DO2A)^+}]_{eq}[\mathrm{DPA^{2-}}]_{eq}} \tag{3}$$

This value (K'_a) cannot be measured directly, so we performed a competition experiment to obtain a competition equilibrium constant (K_c), as shown in Eq. (4).

$$\mathrm{Ln(DO2A)(DPA)^- + Ln^{3+} \overset{K_c}{\rightleftharpoons} Ln(DO2A)^+ + Ln(DPA)^+}$$
$$K_c = \frac{[\mathrm{Ln(DO2A)^+}]_{eq}[\mathrm{Ln(DPA)^+}]_{eq}}{[\mathrm{Ln(DO2A)(DPA)^-}]_{eq}[\mathrm{Ln^{3+}}]_{eq}} \tag{4}$$

This competition equilibrium constant is inversely proportional to the association constant K'_a (Eq. 5):

$$K_c = \frac{K_a}{K'_a} \tag{5}$$

where K_a is the association constant of the lanthanide aquo ion with dipicolinate. Using this technique, we were able to compare the dipicolinate binding affinity for the lanthanide alone with that of the lanthanide complex under virtually identical conditions. This assay revealed an enhancement in dipicolinate binding affinity by about an order of magnitude for $[Ln(DO2A)]^+$ as compared to the Ln^{3+} aquo ion (Fig. 6) (*92*). Interestingly, this increase in binding affinity is contrary to predictions based purely on electrostatics. The dianionic DPA^{2-} analyte should be more strongly attracted to tripositive Ln^{3+} than the less-electropositive $[Ln(DO2A)]^+$ complex. The DO2A helper ligand affords an enhancement in DPA affinity that more than counteracts the reduction in positive charge, as dipicolinate binding increases 10-fold.

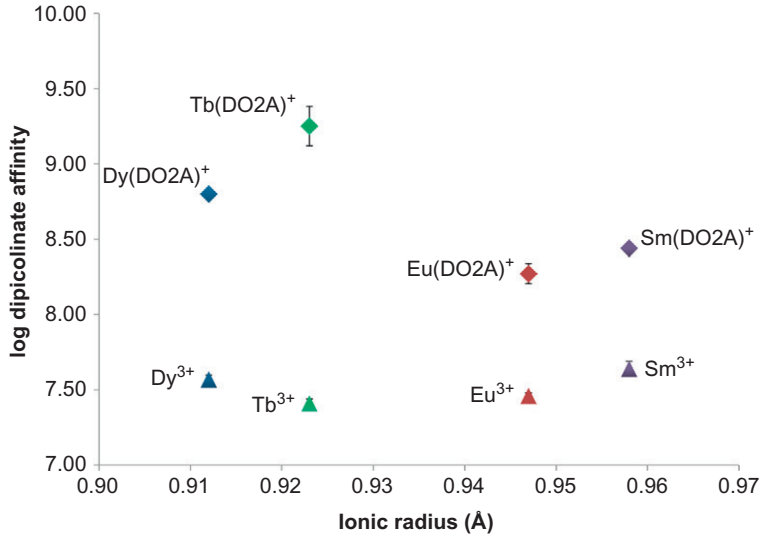

FIG. 6. Plot of association constants for Ln^{3+} and $[Ln(DO2A)]^{+}$ to DPA^{2-} against lanthanide ionic radius, 0.2 M NaOAc, pH 7.5. The addition of DO2A enhances dipicolinate binding affinity by an order of magnitude for most lanthanides investigated and by nearly two orders of magnitude for terbium (light gray).

Evidence for this "enhanced receptor effect" can be found for various other lanthanide/ligand/analyte systems by comparing reported binding affinities with and without a helper ligand under similar conditions (Table II) (*103–107*). In each case, employing an ancillary ligand improves binding affinity of the oxyanion analyte (picolinate, acetate, and lactate) by roughly an order of magnitude, regardless of the type (cyclic or linear), denticity, or charge of the helper ligand. We attribute this enhancement to a shift in electron density of the lanthanide upon receptor ligand chelation, generating a binding site with greater positive character due to the electron-withdrawing oxygen and nitrogen moieties of the helper ligand. Though the net charge of the complex may have decreased, the *local* charge in the binding site may be even greater than the Ln^{3+} aquo case, where the nine solvent molecules are evenly distributed about the lanthanide coordination sphere and the electron density is uniform.

Such a proposal is further supported by another interesting trend in the dipicolinate system: the degree of ligand enhancement is lanthanide dependent. We found a discrepancy in

TABLE II

ENHANCED RECEPTOR EFFECT IN VARIOUS LANTHANIDE/ANALYTE SYSTEMS.

Ligand	Analyte	Δ log K	References
$DO2A^{2-}$	Dipicolinate	0.8–1.8	(*92*)
$EDTA^{2-}$	Picolinate	0.2–1.5[a]	(*103,104*)
L_1	Lactate	0.8–1.5[b]	(*105,106*)
L_2	Acetate	0.1–1.4[c]	(*106,107*)

L_1 = (*SSS*)-1,4,7-tris[1-(1-phenyl)ethylcarbamoylmethyl]-1,4,7,10-tetraazacyclododecane, L_2 = (*SSS*)-1,4,7-tris[1-(1-phenyl)ethylcarbamoylmethyl]-10-methyl-1,4,7,10-tetraazacyclododecane.

Change in the analyte binding affinity (Δ log K = log K'_a − log K_a) due to the ligand in comparison to the lanthanide alone.

[a] log K_a: 0.1 M KNO_3, 25 °C; log K'_a: 0.5 M $NaClO_4$, 25 °C.

[b] log K_a: 0.1 M $NaClO_4$, 20 °C; log K'_a: 0.1 M collidine/HCl, 21.8 °C, pH 7.4.

[c] log K_a: 0.1 M $NaClO_4$, 20 °C; log K'_a: 0.1 M collidine/HCl, 21.8 °C, pH 7.4.

binding affinity that does not track with lanthanide ionic radius, with the greatest difference between terbium and europium. This phenomenon, known as the "gadolinium break," has been reported in various studies of stability constants across the lanthanide series, such as those with acetate and anthranilate (*108*) as well as in investigations of hydration enthalpy and enzyme inhibition properties (*109,110*).

The interesting aspect of the gadolinium break observed in our dipicolinate binding experiments is that it appears to be *induced by binding of the ancillary ligand*. The dipicolinate affinity for the Ln^{3+} aquo ions exhibits little variation, but analogous $[Ln(DO2A)]^+$ complexes show an obvious divide between those to the left of gadolinium (Sm, Eu) and those to the right (Tb, Dy). Another study concerning lanthanide–macrocycle binary complexes also noted a similar trend, in this case using chiral heptadentate 1,4,7,10-tetraazacyclododecane-1,4,7-trisacetate (DO3A) derivatives. The authors noted an increase in the binding affinity of the terbium complex for certain oxyanions (acetate, bicarbonate, and phosphate) in comparison to the analogous europium complex by about the same margin as observed for dipicolinate (Table III). As with our system, lifetime measurements of these complexes indicated no differences in hydration state that might explain the discrepancy, such as a decrease from nine coordinated waters about the larger Eu^{3+} ion to eight around Tb^{3+}. The authors instead attribute the affinity trend to a divergence of pK_a for the two complexes. If the pK_a of the europium complex were lower than that of the terbium complex, the presence of a population of hydroxylated

TABLE III

BINDING AFFINITIES FOR VARIOUS TB AND EU COMPLEXES FOR OXYANIONS, PH 7.4–7.5, 295–298 K, SHOWING THE DIFFERENCE BETWEEN THE TB AND EU SPECIES, Δ(LN).

Ligand	Analyte	log K*		Δ(Ln)
		Tb	Eu	
DO2A	DPA	9.25	8.39	0.86
L_1	HCO_3^-	3.8	2.6	1.2
	$CH_3CO_2^-$	2.3	<1.0	>1.3
	HPO_4^{2-}	≥ 4.7	4.15	≥ 0.55
L_2	HCO_3^-	≥ 4.7	3.75	≥ 0.95
	$CH_3CO_2^-$	3.5	2.4	1.1
	HPO_4^{2-}	>4.7	>4.7	Unknown

L_1 = (*SSS*)-1,4,7-tris[1-(1-phenyl)ethylcarbamoylmethyl]-1,4,7,10-tetraazacyclododecane, L_2 = (*SSS*)-1,4,7-tris[1-(1-phenyl)ethylcarbamoylmethyl]-10-methyl-1,4,7,10-tetraazacyclododecane.
*DPA values from Ref. (*92*), all others from Ref. (*106*) with errors ± 0.2.

species in the former case would reduce the overall binding affinity due to a decrease in electrostatic attraction to the dipositive complex. Differences in pK_a values for Eu and Gd macrocyclic complexes with DOTA derivatives have been noted in the literature, though it is not clear if this trend includes Tb, or if these macrocyclic ligands can be compared directly. We have found no evidence for such a hydroxylated species in our pH dependence studies, as there is no change in stability of [Eu(DO2A)(DPA)]$^-$ compared to [Tb(DO2A)(DPA)]$^-$ at lower pH. With this model ruled out, we return to the previous discussion of perturbations of Ln^{3+} electron density as a possible way to explain both the gadolinium break and the improved binding affinity.

The ability of a chelating ligand to perturb the electron density of an Ln^{3+} cation is dependent on (1) the number and arrangement of electron-withdrawing groups in the ligand and (2) the susceptibility of the lanthanide to polarization. The former property can be tuned by judicial choice of ligand; the latter is defined by how easily the electron density of the lanthanide can be externally influenced, one measure of which is ionization energy. A lanthanide with a low $Ln^{3+} \rightarrow Ln^{4+}$ ionization energy requires less energy to remove an electron and is arguably more susceptible to perturbation by chelating species than a lanthanide with high ionization energy. As shown in Fig. 7, the observed trend in dipicolinate binding affinity is mirrored quite closely by the lanthanide ionization energy. The Tb^{3+} ion has the lowest ionization energy of all the lanthanides investigated, due primarily to

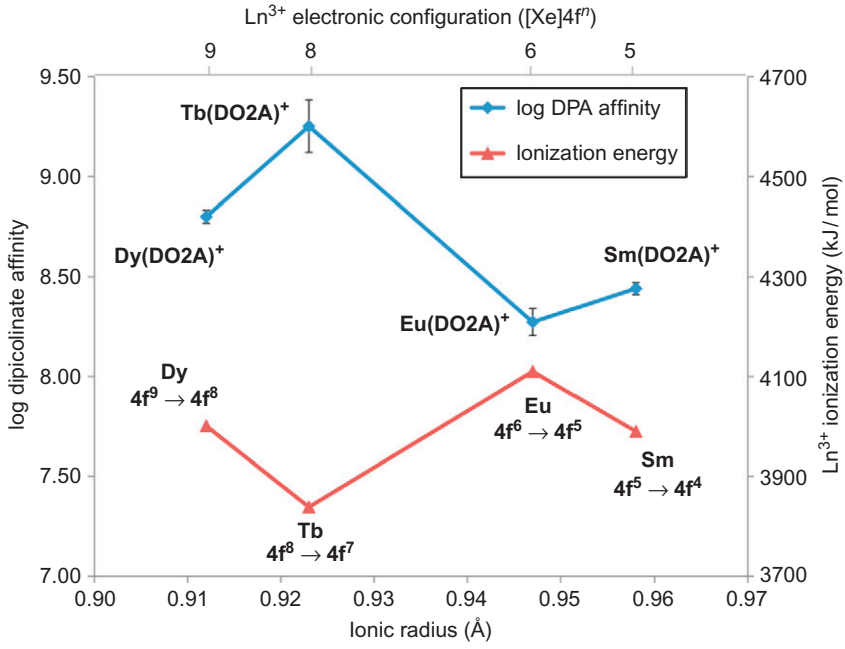

FIG. 7 Relationship between $[Ln(DO2A)]^+$ dipicolinate binding affinity and $Ln^{3+} \rightarrow Ln^{4+}$ ionization energy with lanthanide ionic radius. The $[Tb(DO2A)]^+$ complex has the greatest affinity for DPA^{2-} because the low ionization energy of the Tb^{3+} ion makes it the most susceptible to perturbation by the DO2A ligand, shifting the electron density of the lanthanide and thereby generating the most positive binding site for the DPA^{2-} analyte. Ionization energies from Ref. (*5*).

the fact that the Tb^{4+} ion has an electronic configuration with an *exactly half-filled 4f-shell* (*5*). As a result, this lanthanide is particularly vulnerable to perturbation by an electronegative chelating ligand because the Tb^{3+} ion has the lowest energy barrier to losing an electron. Thus, the observed phenomenon of the ligand-induced gadolinium break is simply *a manifestation of the half-shell effect*, where the lanthanides with the lowest ionization energies are the most significantly affected by electron density perturbations from a chelating ancillary ligand.

We have discovered that ancillary ligands improve analyte binding affinity over the lanthanide alone. This enhanced receptor effect occurs in a variety of systems and appears to be ubiquitous, that is, independent of analyte or ancillary ligand denticity or charge, analyte aromaticity, or the lanthanide employed. In every case, an improvement in the binding affinity of the analyte occurs on the order of 10-fold. We also have found that the degree of

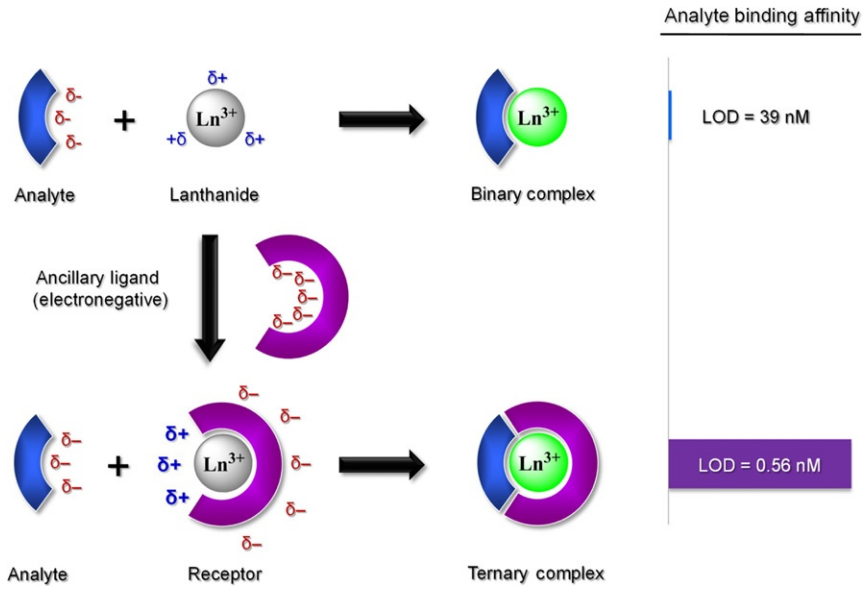

FIG. 8 Enhanced receptor effect on analyte binding affinity. Upon chelation, the electronegative ancillary ligand causes a polarization of the Ln^{3+} ion, inducing an increased positive charge at the binding site. This anisotropy results in an increased binding affinity for the anionic analyte. Limit of detection (LOD) values shown are for the Tb/DO2A/dipicolinate system.

ligand-induced enhancement is lanthanide dependent and is governed by the gadolinium break. We believe this property is due to an induced anisotropy in the electron density of the lanthanide (Fig. 8). Our evidence is that the improvement in binding affinity is directly related to the ionization energy of the lanthanide in question. The greatest effect is seen with terbium, as this lanthanide has the lowest ionization energy because it has exactly one more electron than a half-filled f-shell. Previous explanations for this trend include theories based on a change in basicity of the complex with the helper ligand bound, which our experiments do not support. We conclude that ligand-induced anisotropy of lanthanide ion electron density is a plausible explanation for the observed binding affinity variations.

C. SENSITIVITY

By enhancing the binding affinity between analyte and receptor complex, the ancillary ligand confers additional stability to

the resulting ternary complex. The stronger interaction between analyte and receptor improves the limit of detection (LOD) of the analyte and permits use of the sensor over a much wider pH and concentration range, making the detection technique more sensitive and robust.

In terms of pH, an example of enhancement due to helper ligands can be seen in our initial work on detection of catecholamines (CAs). These "fight-or-flight" hormones, which are part of the sympathetic nervous system, are released by the adrenal glands in response to stress (*111*). CAs produced from the amino acids phenylalanine and tyrosine contain the 1,2-dihydroxybenzene (catechol, Cat) group and either a primary or secondary amine group. CAs are water soluble and circulate in the bloodstream with a half-life of approximately 3 min (*112*). Overstimulation and/or damage of brainstem nuclei can lead to CA toxicity. CA toxicity can also be caused by pheochromocytoma, neuroendocrine tumors in the adrenal medulla, and carcinoid syndrome (carcinoid tumors in the gastrointestinal tract and/or lungs), as well as by a deficiency in monoamine oxidase A, which is normally responsible for the degradation of CAs. High levels of CAs have been associated with various functional and degenerative cardiovascular disorders, such as angina pectoris, arterial hypertension, and atherogenesis (*113*). Decreased dopamine (DA) levels have been linked to Parkinson's disease and attention deficit hyperactivity disorder (ADHD), while elevated levels can cause mood swings, psychosis, and other neurotic disorders (*114–116*). Increased levels of epinephrine (Epi) (when properly administered) can help the body reduce negative allergenic responses and regenerate lost liver cell functions (*117,118*). For all these reasons, rapid detection of CAs in blood and urine can provide vital information that might aid in more efficient diagnosis as well as more effective treatment of various disease states.

Current methods of detection for CAs in biological fluids (urine, plasma, and serum) involve chromatographic separation coupled to either electrochemical (*119,120*) or optical (*121*) techniques. However, most optical methods rely purely on the native fluorescence of CAs ($\lambda_{ex} \sim 280$ nm, $\lambda_{em} \sim 310$ nm) (*122*), which have small Stokes shifts and suffer from signal losses due to reabsorption; others involve pre- or postcolumn derivatization with various fluorophores, such as naphthalene-2,3-dicarboxaldehyde (*123*), 1,2-diphenylethylenediamine (*124,125*), or fluorescamine (*126*). These methods all require significant time for separation using expensive instrumentation and thus are not feasible for rapid CA detection.

We have investigated the potential of lanthanide complexes for the detection of CAs, specifically DA, Epi, and norepinephrine

(NE). The triplet energy levels of CAs (23,800–24,000 cm^{-1}) (*122*) lie in the appropriate range for efficient EnT to the $^5D_4$ energy level of Tb^{3+} (20,500 cm^{-1}) (*89*). CAs coordinate to Cu^{2+}, Co^{2+}, Ni^{2+}, Mn^{2+}, and Zn^{2+} via the two phenolic hydroxyl groups (*127,128*). CAs have also been reported to complex Al^{3+} with submicromolar affinity, though citrate and adenosine triphosphate (ATP) can interfere (*129*). When bound to Y^{3+}, Ca^{2+}, or La^{3+}, a CA still coordinates through the two phenolic groups at neutral pH, but one of the two groups remains protonated (*130–132*). Therefore, to bind to lanthanides in a bidentate fashion with high affinity to allow for efficient EnT, both of these phenol groups must be deprotonated (*133–135*), which requires strongly basic conditions (Table IV) where lanthanides rapidly precipitate as hydroxide salts.

Ancillary ligands such as ethylenediaminetetraacetic acid (EDTA), which bind to lanthanides with high affinities, are able to arrest lanthanide precipitation by preventing hydroxide from coordinating, and previous work using $[Tb(EDTA)]^-$ following capillary electrophoresis has demonstrated that detection limits on the order of 0.1 μM for CAs (DA, NE, Epi, and others) can be achieved (*136*). However, no CA complexes with Ln^{3+}–macrocycles have been reported in the literature, despite the fact that these macrocyclic platforms bind lanthanides with even greater affinities than their linear analogues (Table V) (*96,137,138*). We sought to compare acyclic (linear) to cyclic ancillary ligands and determine the optimal lanthanide–ligand combination to attain better limits of detection for these biologically relevant analytes.

Four ancillary ligands were investigated: three cyclic (DO2A, DO3A, and DOTA) and one acyclic (EDTA), with denticities ranging from hexa- to octadentate (Fig. 9). Assuming chelation via the two hydroxyl moieties, CAs should bind in a bidentate fashion, leaving seven coordination sites remaining on the lanthanide for the helper ligand. We therefore assume that $[Tb(DOTA)]^-$

TABLE IV

PROTONATION CONSTANTS FOR CATECHOL AND VARIOUS CATECHOLAMINES.

Analyte	pK_{a1}	pK_{a2}	pK_{a3}	References
Cat	9.48	12.08	–	(*133*)
Epi	8.64	9.84	13.1	(*134*)
NE	8.58	9.53	12.9	(*134*)
DA	8.89	10.41	13.1	(*135*)

Cat, catechol; Epi, epinephrine; NE, norepinephrine; DA, dopamine.

TABLE V

STABILITY CONSTANTS FOR Tb^{3+} AND Gd^{3+} WITH VARIOUS LINEAR AND MACROCYCLIC LIGANDS.

Type	Ligand	Coord. no.	log K_{Tb}	log K_{Gd}	References
Linear	EDTA	6	17.92	17.35	(*137*)
	DTPA	8	22.71	22.46	(*137*)
Cyclic	DO2A	6	–	19.42	(*138*)
	DO3A	7	–	21.0	(*96*)
	DOTA	8	24.8	24.6	(*96,138*)

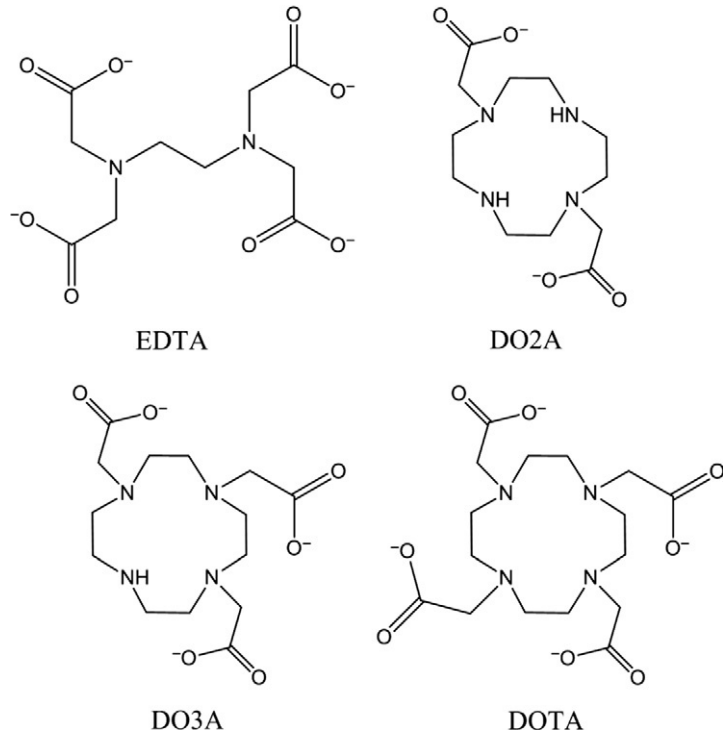

FIG. 9 Linear (EDTA) and cyclic (DO2A, DO3A, and DOTA) ligands utilized for determining binding stoichiometries. EDTA and DO2A are hexadentate, DO3A is heptadentate, and DOTA is octadentate.

should exclude the CA analyte and act as a negative control, while the other three should form Tb(ligand)(CA) ternary complexes, depending on the steric constraints imposed by the receptor ligand on the size and shape of the binding pocket.

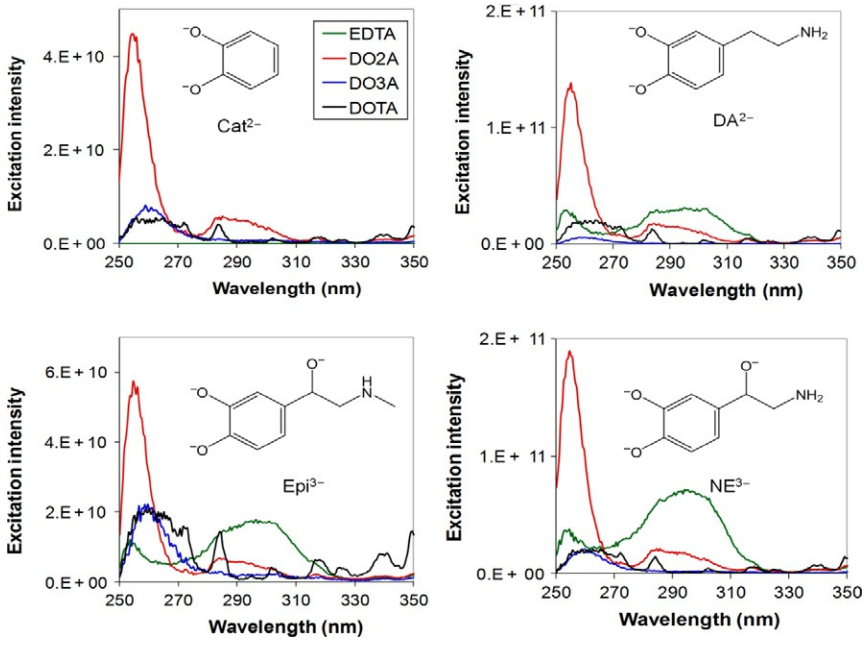

FIG. 10 Excitation spectra ($\lambda_{em} = 544$ nm) of various Tb(ligand)(CA) complexes in 50 mM CAPS buffer, pH 13.5. 10 μM CA, 1.0 mM Tb (ligand) complex. Clockwise from upper left: catechol (Cat), dopamine (DA), norepinephrine (NE), and epinephrine (Epi).

We explored three common CAs—DA, Epi, and NE—along with Cat as a control species. Excitation spectra of the Tb(ligand) (CA) complexes exhibit one band near 255 nm and another centered around 290–295 nm (Fig. 10). The former is assigned as the singlet $\pi \rightarrow \pi^*$ transition L_a (in the notation of Platt (*139*)) of the Cat dianion (256 nm) (*140*), while the latter is consistent with the L_b transition of the Cat dianion, which is blue shifted from 308 to 290 nm when bound to a metal ion (*141*). As expected, the Tb^{3+} complex with DOTA disfavored coordination by the analyte (all four CAs were investigated), as evidenced by the absence of a band at 290 nm and negligible emission intensity. Interestingly, the Tb^{3+} complex with heptadentate DO3A, which should have sufficient space in its inner sphere for a bidentate chelate such as a CA, behaved similarly to $[Tb(DOTA)]^-$. Notably, the two hexadentate ligands, DO2A and EDTA, formed luminescent Tb^{3+} ternary complexes with all three CAs and Cat. The emission spectral profiles for the Tb(DO2A)(CA) complexes are all very similar,

as are the splittings in all four Tb(EDTA)(CA) emission spectra. As Stark splittings of the emission bands report on the composition and geometry of the lanthanide coordination sphere, the data suggest that these CAs all bind to Tb^{3+} in the same fashion for a given Tb(ligand) binary complex. The excitation spectra indicate that the Cat moiety of each analyte is dianionic, and therefore bidentate coordination via deprotonated hydroxyl moieties is very likely. In all cases, the intensity was greater for DO2A complexes than those containing EDTA. We therefore conclude that, although both ancillary ligands are capable of forming ternary complexes with CAs, $[Tb(DO2A)]^+$ is the more effective sensor.

The stability provided by the receptor ligand is integral to the success of this assay. CAs can only bind strongly to cations when fully deprotonated, which means working at high pH, and lanthanides only remain soluble at high pH with the aid of a helper ligand. The use of the ancillary ligand allows these two components—the analyte and the lanthanide—to exist under the same conditions, making this otherwise unwieldy assay sensitive, rapid, and straightforward.

Similar effects are seen with the inclusion of the DO2A helper ligand in the previously described dipicolinate system. A pH dependence study conducted over a range from 6.1 to 10.4 indicates that with the DO2A ligand bound, the lanthanide does not precipitate and the $[Ln(DO2A)(DPA)]^-$ complex is stable over the entire pH range for all lanthanides studied (*92*). In contrast, the $Ln(DPA)^+$ complexes form $Ln(DPA)_3{}^{3-}$ at high pH, indicating precipitation of some of the lanthanide as $Ln(OH)_3$. This further validates the stabilizing effect of the DO2A ancillary ligand, allowing the bacterial spore detection assay to be performed over a much wider range of conditions.

These pH dependence studies have also demonstrated an important point in terms of using lanthanide ions and complexes as sensors. In every dipicolinate system, the luminescence intensity of the $Ln(DPA)^+$ complex varied significantly with pH, due largely to the precipitation of $Ln(OH)_3$ and the resulting formation of more strongly luminescent $Ln(DPA)_n$ species, where $n = 2$ or 3. There was no longer a direct correlation between luminescence intensity and dipicolinate concentration, and the number of bacterial spores could not be quantified. Such intensity variations are undoubtedly a problem with other analyte systems as well, as any bi- or tridentate analyte can form multimeric Ln^{3+} complexes. With the receptor ligand, fortunately, the change in luminescence intensity with pH is no more than 5% for dipicolinate, and therefore the bacterial spore concentration can be determined directly from emission intensity.

Ancillary ligands can dramatically improve detection strategies based on sensitized Ln^{3+} luminescence by stabilizing the lanthanide to pH variations. Such enhancements in stability and reproducibility allow the use of lanthanide sensors *in situ* and also potentially *in vivo*, where free lanthanide ions might precipitate and/or have toxic effects.

D. Selectivity

Ancillary ligands also impart selectivity to lanthanide-based detection strategies, improving resistance to common environmental interferents. For lanthanides, which rely on ionic interactions for analyte binding, the greatest threat is from charged species. Anions, particularly those containing oxygen donors or otherwise have the ability to complex metal ions, could compete with the target analyte for the lanthanide and produce a false negative result. If these anionic interferents are aromatic and capable of transferring energy to the lanthanide, we might also encounter false positives. By encapsulating the lanthanide and limiting the surface area exposed to solvent, the receptor ligand can reduce these undesired interactions and improve analyte detection limits.

A good example of a lanthanide-based detection system made more robust by the inclusion of an ancillary ligand is that of the aspirin metabolite salicylurate (SU). Acetylsalicylic acid (ASA), commonly known as aspirin, is used widely as an anti-inflammatory agent, an analgesic to relieve minor aches and pains, and an antipyretic to reduce fever (*142*). Aspirin is also the primary medication used to treat chronic rheumatic fever, rheumatoid arthritis, and osteoarthritis (*143*). Further, recent studies have shown the antithrombotic benefits of an aspirin regimen in stroke prevention (*144,145*). In the body, ASA is hydrolyzed to salicylic acid (SA) by carboxylesterases in the gut walls and liver, with an elimination half-life of 15–20 min (*146*). SA is then converted primarily to salicyluric acid (SU) and other metabolites, which are excreted in urine (*147,148*). The elimination rate constant for SU is much greater than SA (*149*), and endogenous SU formation only occurs in a limited manner (*150,151*). We can therefore use SU detected in urine as an indicator of SA *in vivo*, and thus we have a noninvasive means of monitoring aspirin dosage and residence in the body. In addition, unusually high or low concentrations of SU in urine have been correlated to a variety of diseases and conditions, such as appendicitis, anemia, abdominal trauma, liver diseases, uremia, and

Down's syndrome (*152*). Hence, detection of SU in urine is a very good way to monitor aspirin dosage as well as provide evidence that could assist in the diagnosis of certain medical conditions.

SU has been shown to bind metal cations such as Cu^{2+} (*153*), Co^{3+} (*154*), VO^{2+} (*155*), and $(CH_3)_2Sn^{2+}$ (*156*). In such complexes, SU is either bidentate or tridentate, coordinating through ligand carbonyl, carboxyl, and phenolate oxygens. As hard ions, lanthanides form strong chelates with oxygen-containing ligands. We therefore explored various lanthanide binary complexes in an effort to detect SU in urine using sensitized lanthanide luminescence. The most promising lanthanide–ligand complex from our screens was $[Tb(DO2A)]^+$. Fluorescence from excited state intramolecular proton transfer (ESIPT) was observed for the $[Tb(DO2A)(SU)]^-$ ternary complex; it is likely that the SU ligand chelates in a bidentate fashion via the carbonyl and carboxyl groups and that the hydroxyl moiety is still protonated (Fig. 11). Using $[Tb(DO2A)]^+$, we were able to detect SU in urine samples from healthy volunteers with a detection limit of 1.8 mg L^{-1} (*157*). For a first iteration receptor site, this result already is competitive with current SU detection techniques based on HPLC and capillary electrophoresis. And, importantly, the analysis can be done in a fraction of the time required in most other methods.

We have seen similar improvements in the dipicolinate system in terms of increased resistance to common cationic and anionic interferents. The inclusion of DO2A improved Tb-DPA binding in the presence of a wide array of interfering ions, most up to concentrations five orders of magnitude greater than that of DPA (*92*). This indicates that $[Tb(DO2A)]^+$ is able to bind

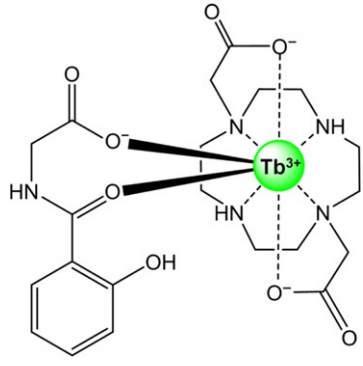

FIG. 11 Likely chelation mode of salicylurate (SU) to $[Tb(DO2A)]^+$.

dipicolinate selectively, even in the presence of similar oxygen-donor ligands such as acetate, carbonate, and citrate. Phosphate, in particular, has been shown to severely inhibit DPA binding and/or decrease luminescence intensity; we have found that not only does DO2A improve resistance to phosphate by several orders of magnitude, but also it is far more effective than aluminum chloride, the current recommended technique for phosphate mitigation (*158,159*).

Other examples of ancillary ligands used to enhance analyte selectivity include amide-modified DO3A (1,4,7,10-tetraazacyclododecane-1,4,7-trisacetate) complexed to Tb^{3+}, which selectively binds the bidentate analytes *p*-dimethylaminobenzoic acid (DMABA) and SA (*160–162*). The binary complex of Tb^{3+} with EDTA can effectively detect SA, 4-aminosalicylic acid and 5-fluorosalicylic acid (*163*). [Tb(EDTA)] also has been used to detect catalysis of hydroxybenzoic acid (HBA) by hemin via formation of a ternary complex with the HBA oxidation product (*164*). Diaza-crown ethers have been utilized with Tb^{3+} and Eu^{3+} to detect phthalate, benzoate, dibenzoylmethide, and picolinate (*165*). The future of these types of sensors lies in the development of lanthanide receptor complexes with greater analyte affinities, perhaps via stronger host–guest interactions such as π-stacking or modification of receptor site topology to generate a "lock and key" hydrophobic pocket.

Ancillary ligands improve the selectivity of lanthanide-based detection techniques by shielding the luminescent reporter from solvent and interferents, thereby reducing the potential for false positives or negatives. By improving selectivity in detection technologies, these receptor ligands make such technologies more robust and broaden the applications for which such schemes may be used.

We have examined the attributes that helper ligands impart to lanthanide-based detection by encapsulating the lanthanide ion and shifting Ln^{3+} ion polarization. Protecting the lanthanide from the quenching effects of solvent molecules as well as detrimental chelation of environmental interferents improves both sensitivity and selectivity. Generation of a more electropositive region on the lanthanide surface by an electronegative ancillary ligand can enhance analyte binding affinity by an order of magnitude or more. We next turn to recent findings concerning steric considerations and oxophilicity that can further optimize detection strategies based on sensitized lanthanide luminescence.

III. Additional Factors That Govern Complex Stability

A. Steric Effects

Initially, ancillary ligands were envisioned as a way to impart steric selectivity for a particular analyte of interest. By leaving only two adjacent coordination sites available on the lanthanide, for instance, it could be assumed that only bidentate ligands would bind to the metal center and that tri- or tetradentate ligands would be excluded from the lanthanide coordination sphere. This design could be further extended by modification of the ancillary ligand to generate a highly specific receptor site, with hydrophobic or hydrophilic regions that would be complementary only to the target analyte.

Our initial work with the dipicolinate system supports this hypothesis. We found that a helper ligand leaving three linear adjacent coordination sites on the terbium ion allowed for optimal dipicolinate binding, while a ligand leaving three coordination sites in a triangular motif resulted in poor binding (Fig. 12). This is consistent with dipicolinate chelation involving oxygen donors from the two carboxyl units and the Pyr nitrogen in a linear arrangement.

However, our work on various other systems has led us to reassess our receptor designs. We have found that, in some cases, a bidentate analyte will chelate more strongly to a lanthanide with a hexadentate helper ligand (i.e., leaving three remaining coordination sites as opposed to two). Cat, the three CAs, and SU, all bidentate analytes, bind more strongly to terbium complexes involving a hexadentate ancillary ligand (DO2A and EDTA) as opposed to a heptadentate one (DO3A). We also have discovered that a cyclic helper ligand is preferred in some cases, while a linear (acyclic) ligand produces better results in others. A ligand screen involving SA clearly indicated a greater binding affinity for EDTA than cyclic DO2A (Fig. 13), and Job's method of continuous variations (*166*) confirms a one-to-one binding stoichiometry of SA^{2-} to $Tb(EDTA)^{3-}$ (Fig. 14). Further study, including molecular modeling, may be necessary to elucidate the mechanism that gives rise to such chelation preferences.

We conclude that the simple explanation based only on steric interactions in the lanthanide coordination sphere is not sufficient, and that there are more complex forces at work. We therefore recommend that ligand screens be performed to determine the optimal ancillary ligand for a given target analyte when designing lanthanide-based sensors.

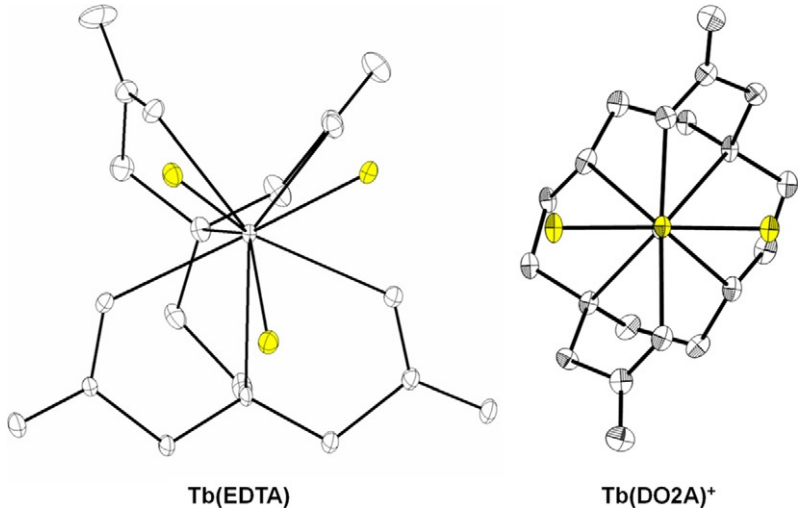

FIG. 12 Crystal structures of Tb(EDTA)·NaOH·2H_2O and TBA·Tb(DO2A)(DPA), showing trigonal and linear coordination sites, respectively, available for dipicolinate binding (dark gray). Thermal ellipsoids are at 50% probability; hydrogens and extraneous atoms omitted for clarity. Tb(EDTA)·NaOH·2H_2O crystallized from deionized water (18.2 MΩ-cm resistivity) at 4 °C.

B. OXOPHILICITY

Most work on lanthanide chelation indicates a strong preference for negatively charged or neutral donor groups with large dipole moments (*5*). In particular, a significant oxophilic tendency has been confirmed by the finding that rarely few lanthanide complexes with monodentate nitrogen donors exist. However, evidence from complexes with aza-crown ligands suggests that neutral nitrogen donors may be slightly preferred over neutral oxygen donors (*167*).

Our work with dipicolinate derivatives also indicates that nitrogen donors can be preferred over oxygen donors in certain cases. To better understand the binding behavior of dipicolinate, we explored the coordination geometries of various DPA analogues with Tb^{3+}. Three structural isomers were examined: pyridine-2,4-dicarboxylic acid (2,4-DPA), pyridine-3,5-dicarboxylic acid (3,5-DPA), and dipicolinate itself (pyridine-2,6-dicarboxylic acid, DPA). Picolinic acid (Pic) and Pyr, which have one and both carboxyl arms eliminated, respectively, were also included. As DPA usually coordinates in a tridentate fashion with the two

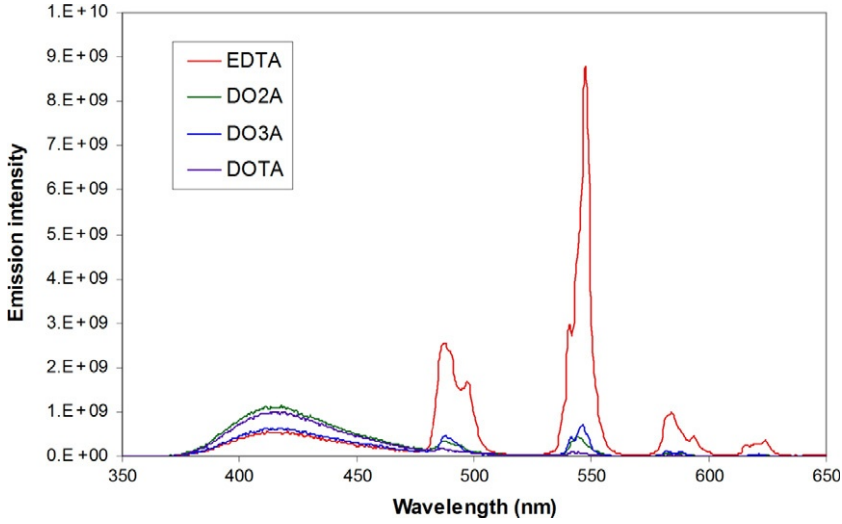

FIG. 13 Emission spectra ($\lambda_{ex} = 326$ nm) of various Tb(ligand)(SA) complexes in 50 mM CAPS buffer, pH 12.5 (DO2A complex in CHES buffer, same concentration, and pH). 10 μM SA, 1.0 mM Tb(ligand) complex. [Tb(EDTA)(SA)] (gray) has the greatest emission intensity.

carboxylates and the Pyr nitrogen as donors, shifting one or both of the carboxyl moieties around the ring will allow multiple bidentate binding modes (Fig. 15).

As expected, emission intensities of the Tb^{3+} chelates in solution follow the order Pyr ≪ Pic < DPA. The finding that monodentate Pyr was the poorest performing ligand and tridentate dipicolinate was best demonstrated that as denticity increases the chromophore can bind with greater affinity to the lanthanide, which in turn leads to more efficient EnT via an AETE mechanism. A blue shift in the Tb^{3+}–picolinate excitation spectrum (approximately 5 nm compared to the analogous dipicolinate complex) also suggests that more energy is required for sensitization as the electron density of the ligand is shifted back onto the Pyr ring. A similar blue shift was also observed with dipicolinate fluorinated in the 4-position, which similarly shifts electron density away from the chelating side of the ligand.

Results from picolinate and the DPA isomers are of interest: using ancillary ligands to limit the available binding sites on the Tb^{3+} ion, we were able to deduce the likely binding motif of each isomer based on the intensity and degree of splitting in the emission spectrum (Fig. 16). Binding of picolinate, 2,4-DPA, and 3,5-DPA to $[Tb(DO2A)]^+$ all produced spectra with comparable

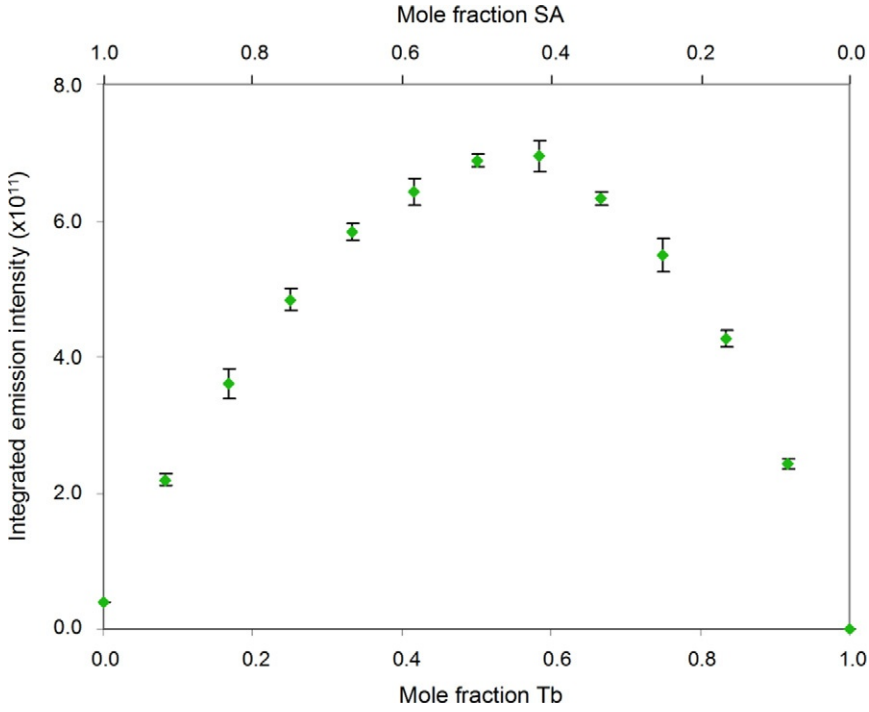

FIG. 14 Method of continuous variations to determine the binding stoichiometry of SA^{2-} to $[Tb(EDTA)]^{-}$. Tb^{3+} and SA^{2-} concentrations varied inversely from 0 to 120 μM in 10 μM increments with 1.00 mM EDTA in 50.0 mM CAPS buffer, pH 13.5 ($\lambda_{ex} = 314$ nm). Emission intensity integrated from 530 to 560 nm. Equilibration time of 24 h.

features, suggesting the Tb^{3+} coordination environment is similar and therefore that all three ligands chelate in the same manner. As picolinate has only one carboxylate moiety, this indicates a bidentate binding mode involving the Pyr nitrogen and a single carboxylate oxygen. The decrease in intensity for 3,5-dipicolinate also supports this motif, as the two donors (Pyr N and carboxylate O) are spaced further apart, weakening chelation for this isomer. Restriction of the number of binding sites to two using the heptadentate DO3A ligand results in little change for picolinate, meaning this analyte remains in the same configuration—bound to Tb^{3+} with one nitrogen and one oxygen. For the dipicolinate isomers, however, things have changed. All three exhibit analogous emission spectra with less splitting for the [Tb(DO3A)] complex, signifying a change in the composition and/or geometry of the lanthanide coordination sphere and consequently a different binding mode. Chelation to the lanthanide via an η^2-carboxylate

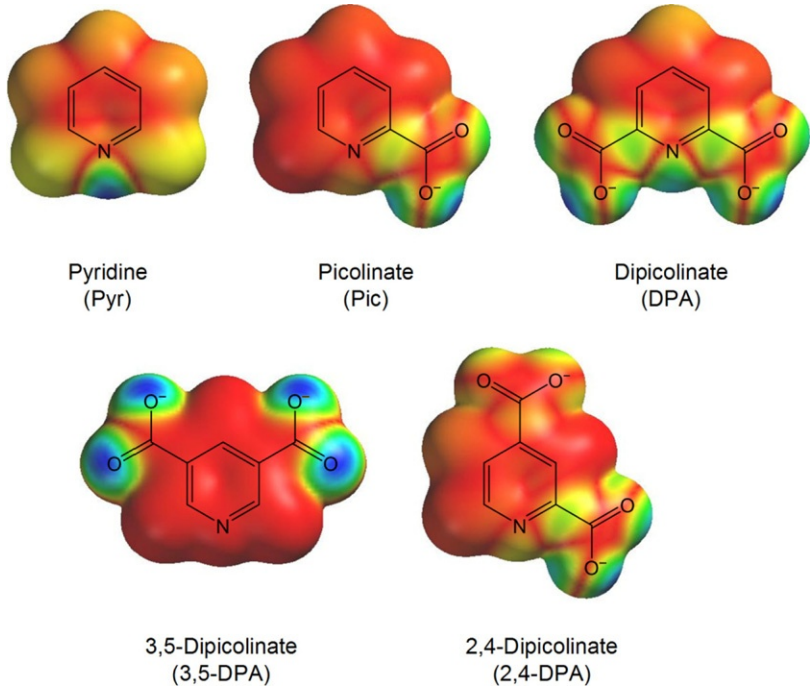

FIG. 15 Structures of pyridine, picolinate, and three structural isomers of dipicolinate, overlaid with an electron density map of the highest occupied molecular orbital (HOMO) for each ligand. These chromophores were explored to better understand the binding properties of DPA. Electron density maps generated using Titan®; higher electron density is in black, lower in white.

would reduce unfavorable steric interactions by moving the second carboxylate group of these species away from the ancillary ligand. For this series of spectra, the intensity decreases in the order 2,6-DPA > 2,4-DPA > 3,5-DPA, which follows with a decrease in electron density at the chelating carboxylate as the functional groups are redistributed evenly about the Pyr ring.

All attempts at crystallization of these species were unsuccessful; the only reported Ln^{3+} crystal structures with these dipicolinate derivatives are of polymeric species obtained under hydrothermal conditions (*168*), which cannot be directly related to our solution results. Although more thorough analyses will be required for the construction of accurate binding models, we have established that the Pyr nitrogen in dipicolinate and related chelators can play an important part in dictating both lanthanide

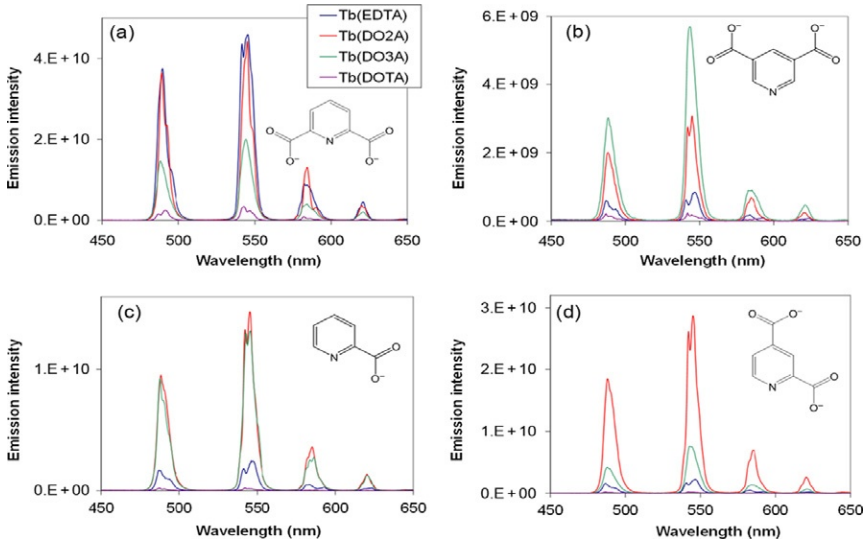

FIG. 16 Emission spectra ($\lambda_{ex} = 278$ nm) of various terbium complexes, 10.0 μM in 50 mM MOPS buffer, pH 7.5. (a) DPA; (b) 3,5-DPA; (c) Pic; and (d) 2,4-DPA.

binding motif and sensitization. Carboxylate oxygens are strong donors but appear to be made even stronger with the help of a proximal nitrogen donor. It follows that analytes with additional nitrogen donors can in principle be detected using lanthanide optical sensors, and work in this area should be undertaken.

IV. Looking to the Future

The future of lanthanide-based sensing technologies is limitless, owing in part to dramatic recent advancements in receptor design. Improvements in the sensitivity, stability, and selectivity of lanthanide receptors will encourage use of such sensors over a wider range of conditions, including both *in situ* and *in vivo* situations. Enhancements in binding affinities will result in better limits of detection, thereby increasing the number and variety of analytes that can be monitored by such systems.

We anticipate further development of lanthanide binary complexes as receptors for aromatic ions, with the ultimate goal of generating highly specific devices capable of sensitive detection in matrices such as environmental samples or biological fluids. The possibility of using several lanthanide sensors

simultaneously then becomes possible. For instance, as SA is broken down into SU in the liver, the ratio of SA to SU could be used as an indicator of liver health and function. A dual assay could be envisioned using $[Tb(DO2A)]^+$ at pH 8.4 to detect SU and $[Tb(EDTA)]^-$ at pH 13.5 to detect SA in aliquots taken from the same plasma or urine sample. Such an assay would be rapid, cost effective, and minimally invasive, providing valuable information with little discomfort to the patient.

We plan to take advantage of ligand-induced enhancement of dipicolinate binding affinity to improve current bacterial spore detection technologies in two ways. The first involves appending terbium(macrocycle) complexes to solid polymer substrates to improve microscopy-based endospore assays. In a second method, we will bind lanthanide complexes to silica to concentrate dipicolinate from very dilute samples on columns.

Covalently attaching $[Tb(DO2A)]^+$ to polydimethylsiloxane (PDMS) could significantly improve the microscopic endospore viability assay (μEVA) that we developed to image bacterial spores. In this assay, endospores are inoculated onto wells of agarose doped with $TbCl_3$ and induced to germinate via the addition of either L- or D-alanine for aerobic or anaerobic spores, respectively (*169,170*). As the bacterial spores germinate and return to a normal vegetative cycle, their DPA is released and binds to the Tb^{3+} ions in the agarose. The resulting "halos" of $Tb(DPA)_n$ complexes ($n = 1$–3) around each endospore are visible using time-gated fluorescence microscopy (*72*). In the current protocol, certain endospores are more easily observed than others, as μEVA only images those capable of germination, and the rate of germination varies significantly among spore species. *Bacillus* spores germinate relatively quickly, on the order of minutes; *Clostridium* spores, however, exhibit germination profiles on the order of hours to days (Fig. 17) (*171*). For slow-germinating species, the rate of DPA diffusion begins to outcompete the rate of germination, and little or no signal results. PDMS is used as a "coverslip" in μEVA to slow agarose drying, limit DPA diffusion, and improve image quality. However, we have just begun to explore the potential of PDMS to serve as a platform upon which dipicolinate-specific sensors can be covalently bound. By appending the lanthanide(macrocycle) complex to the PDMS, we may be able to lengthen the residence time of the DPA proximal to the endospore that released it, expanding our imaging window.

Another problem encountered with μEVA involves microscopy. The agarose surface on which the spores sit is often uneven due to multiple variables in its preparation, meaning that not all

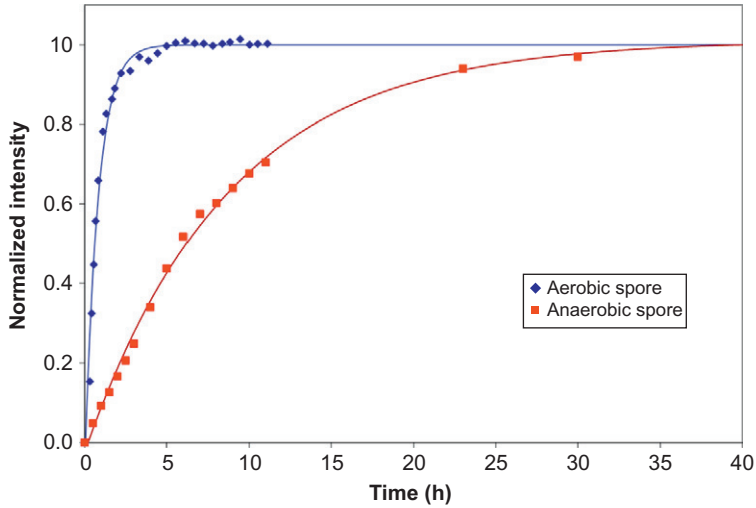

FIG. 17. Germination curves of typical aerobic (*Bacillus atrophaeus*) and anaerobic (*Clostridium sporogenes*) spores. (Data provided by W.-W. Yang.)

spores are present on the same focal plane, rendering an accurate enumeration in any single microscopic view impossible. But, if the dipicolinate released from the germinating spores is effectively bound to a terbium(macrocycle) complex that is itself covalently attached to the PDMS coverslip, the PDMS is the only surface necessary to image. The PDMS could be readily removed from the agarose following germination, placed on a flat surface and imaged separately, eliminating the problem of multiple focal planes.

The second method involves sample concentration to enhance the current LOD of bacterial spores by taking advantage of the pH dependence of dipicolinate binding. Chelation of DPA to $[Tb(DO2A)]^+$ is most effective in the pH range 6–10. Above pH 10, the hydroxide concentration is high enough to compete with the macrocycle and some lanthanide is lost due to precipitation as $Ln(OH)_3$. Below pH 5.5, the macrocycle becomes protonated and $[Tb(DPA)]^+$ dominates (Table VI). The idea of using pH sensitivity of lanthanide complexes is not new; for instance, a pH sensor was developed based on the pH dependence of a europium ternary complex containing a β-diketonate as the chromophore. When the pH shifted out of physiological range, the chromophore dissociated and sensitization was lost (*12*). However, using this property not as an indicator but as a concentration tool has yet to be tested.

TABLE VI

PROTONATION CONSTANTS OF RELEVANT LIGANDS.

Ligand	pK_{a1}	pK_{a2}	pK_{a3}	pK_{a4}	References
DPA	–1.05	2.22	5.22	–	(*159*)
DO2A	2.55	3.85	9.55	10.94	(*96*)

If the terbium(macrocycle) complex was covalently bound to the stationary phase of a column, such as silica or alumina, a dilute DPA solution could be readily concentrated. When applied to environmental samples, this protocol would involve sample collection, DPA release via physical (heating, pressure) or chemical (germinant or lysozyme) means, and filtration to remove any cell debris or other material. The dilute dipicolinate solution, buffered to pH 7–10, could then be passed through the column containing $[Tb(DO2A)]^+$ bound to the solid substrate. The high binding affinity of the terbium(macrocycle) for DPA at this pH would cause the dipicolinate to be retained on the column. After saturation, the addition of a small aliquot of acidic solution (pH $\sim$ 2) would protonate the macrocyclic ligand and release $[Tb(DPA)]^+$, which could then be quantified using fluorescence spectroscopy and correlated to the original filtrate volume to yield a value of spores per milliliter of solution. The column could then be treated with a $TbCl_3$ solution at neutral pH to reform the terbium(macrocycle) in the solid phase for reuse. Current limits of detection of bacterial spores in environmental samples for spectroscopic techniques are in the 10^3–10^4 spores mL^{-1} range (*81,99,158*). The proposed technology could improve the current LOD by several orders of magnitude.

We are currently working to modify the DO2A ligand to append to solid substrates. Recent results indicate a negligible change in binding affinity when one of the acetate moieties is exchanged for an amide group with similar resilience to pH variations (*172*).

V. Conclusions

We have summarized the common attributes of ancillary ligands in improving detection techniques based on sensitized lanthanide luminescence and also introduced a new model for enhanced binding affinity. We suggest that binding affinities can be increased by an order of magnitude or more by ligand-induced anisotropy in

lanthanide ion electron density. Upon chelation of an electronegative helper ligand, the electron density of the lanthanide is shifted away from open coordination sites. The resulting redistribution of charge produces a more electropositive region on the Ln^{3+} surface with greater affinity for an anionic analyte.

We have demonstrated that helper ligands can greatly enhance the binding affinity of an oxyanion with a lanthanide cation, thereby establishing this property as a powerful element in receptor design. What is more, the ligand-induced gadolinium break makes it very attractive to use terbium as the lanthanide of choice in sensors, as the readily polarized electron density of Tb^{3+} will produce the greatest increases in binding affinities if coupled to the right helper ligands.

From their extraction and separation to even the most basic density functional theory (DFT) calculations, life is always more complex when lanthanides are involved and receptor design is no exception. Steric considerations alone do not dictate an *a priori* choice of helper ligand for receptors based on sensitized lanthanide luminescence. To a first approximation, parameters such as ligand denticity and coordination geometry can provide a good basis for designing a functional receptor complex, but in practice, it is difficult to predict how these complexes will interact with their target analytes. We have found that small changes in helper ligand denticity and binding motif can lead to surprising behavior in analyte affinity, which has led us to view these phenomena in a different light.

Abbreviations

acac	acetylacetonate
ADHD	attention deficit hyperactivity disorder
AETE	absorption-energy transfer-emission
ATP	adenosine triphosphate
BAC	binding affinity by competition
CA	catecholamine
Cat	catechol, or 1,2-dihydroxybenzene, or *o*-benzenediol
DA	dopamine
DFT	density functional theory
DMABA	*p*-dimethylaminobenzoic acid
DO2A	1,4,7,10-tetraazacyclododecane-1,7-bisacetate
DO3A	1,4,7,10-tetraazacyclododecane-1,4,7-trisacetate
DOTA	1,4,7,10-tetrakiscarboxymethyl-1,4,7,10-tetraazacyclododecane
DPA	dipicolinic acid, or pyridine-2,6-dicarboxylic acid
2,4-DPA	pyridine-2,4-dicarboxylic acid
3,5-DPA	pyridine-3,5-dicarboxylic acid
EDTA	ethylenediaminetetraacetic acid
EnT	energy transfer

Epi	epinephrine (adrenaline)
ESIPT	excited state intramolecular proton transfer
μEVA	microscopic endospore viability assay
FRET	Förster resonance energy transfer
HBA	hydroxybenzoic acid
HFA	hexafluoroacetylacetonate
IC	internal conversion
ISC	intersystem crossing
Nd:YAG	neodymium-doped yttrium aluminum garnet
NE	norepinephrine (noradrenaline)
PDMS	polydimethylsiloxane
Pic	picolinic acid (pyridine-2-carboxylic acid)
Pyr	pyridine
SA	salicylic acid
SU	salicyluric acid, or 2-hydroxyhippuric acid, or orthohydroxyhippuric acid

Acknowledgments

We thank Larry Henling and Mike Day for crystallographic analyses, Wanwan Yang for providing data for Fig. 17, and Tony Vlcek and Aaron Noell for helpful discussions. The research described in this chapter was carried out at the Jet Propulsion Laboratory, California Institute of Technology, under contract with the National Aeronautic and Space Administration and was sponsored by NASA's Astrobiology and Planetary Protection Programs (A. P. and J. P. K.), the Department of Homeland Security's Chemical and Biological Research & Development Program (A. P.), the NASA Graduate Student Research Program (M. L. C.), and the AmGen Scholars Program (D. J. L.). Work at the Beckman Institute at Caltech was supported by the NIH (DK019038) and the Arnold and Mabel Beckman Foundation (H. B. G.).

References

1. Holden, N. E. *IUPAC General Assembly*. US Department of Energy: Brisbane, Australia, **2001**.
2. Haxel, G. B.; Hedrick, J. B.; Orris, G. J. *Rare Earth Elements—Critical Resources for High Technology*. US Geological Survey: Reston, VA, **2002** pp. 1–4.
3. Arnaudneu, F. *Chem. Soc. Rev.* **1994,** *23*, 235.
4. Bünzli, J. -C. G. *J. Alloys Compd.* **2006,** *408–412*, 934.
5. Cotton, S. In: "Lanthanide and Actinide Chemistry"; Eds. Woolins, D., Crabtree, R., Atwood, D.; Meyer, G.; John Wiley & Sons Ltd.: West Sussex, England, **2006** p. 263.

6. Galgano, F.; Favati, F.; Caruso, M.; Scarpa, T.; Palma, A. *LWT Food Sci. Technol.* **2008,** *41*, 1808.
7. Taylor, S. R.; McLennan, S. M. In: "*Metal Ions in Biological Systems: The Lanthanides and Their Interrelations with Biosystems*"; Eds. Sigel, A.; Sigel, H.; Marcel Dekker, Inc.: New York, **2003** pp. 1–38.
8. Faulkner, S.; Matthews, J. L. In: "*Applications of Coordination Chemistry: Comprehensive Coordination Chemistry II*"; Ed. Ward, M. D.; (2nd edn.). Vol. 9; Elsevier: Amsterdam, **2003**.
9. Petoud, S.; Cohen, S. M.; Bünzli, J. -C. G.; Raymond, K. N. *J. Am. Chem. Soc.* **2003,** *125*, 13324.
10. Gritmon, T. F.; Goedken, M. P.; Choppin, G. R. *J. Inorg. Nucl. Chem.* **1977,** *39*, 2021.
11. Gritmon, T. F.; Goedken, M. P.; Choppin, G. R. *J. Inorg. Nucl. Chem.* **1977,** *39*, 2025.
12. Leonard, J. P.; Nolan, C. B.; Stomeo, F.; Gunnlaugsson, T. *Top. Curr. Chem.* **2007,** *281*, 1.
13. Suarez, S., et al. *New J. Chem.* **2005,** *29*, 1323.
14. Horrocks, W. D.Jr., *Science* **1979,** *206*, 1194.
15. Bünzli, J. C. G.; Wessner, D. *Helv. Chim. Acta* **1981,** *64*, 582.
16. Bulman, R. A. In: "*Metal Ions in Biological Systems: The Lanthanides and Their Interrelations with Biosystems*"; Eds. Sigel, A.; Sigel, H.; Vol. 40; Marcel Dekker, Inc.: New York, **2003** pp. 39–67.
17. Cotton, F. A.; Wilkinson, G. *Advanced Inorganic Chemistry.* John Wiley and Sons: New York, **1988**.
18. van der Ende, B.; Aarts, L.; Meijerink, A. *Phys. Chem. Chem. Phys.* **2009,** *11*, 11081.
19. Parker, D.; Williams, J. A. G. In: "*Metal Ions in Biological Systems: The Lanthanides and Their Interrelations with Biosystems*"; Eds. Sigel, A.; Sigel, H.; Vol. 40; Marcel Dekker, Inc.: New York, **2003** pp. 233–280.
20. Dieke, G. H.; Crosswhite, H. M. *Appl. Opt.* **1963,** *2*, 675.
21. Bünzli, J. -C. G.; Chopin, G. R. *Lanthanide Probes in Life, Chemical and Earth Sciences: Theory and Practice.* Elsevier: New York, **1989**.
22. Parker, D.; Dickins, R. S.; Puschmann, H.; Crossland, C.; Howard, J. A. K. *Chem. Rev.* **2002,** *102*, 1977.
23. Parker, D.; Williams, J. A. G. *J. Chem. Soc., Dalton Trans.* **1996,** *18*, 3613.
24. Sabbatini, N.; Guardigli, M.; Lehn, J. M. *Coord. Chem. Rev.* **1993,** *123*, 201.
25. Carnall, W. T. In: "*Handbook on the Physics and Chemistry of Rare Earths*"; Eds. Gschneider, K. A.; Eyring, L.; Vol. 25; North Holland Publishing Co.: Amsterdam, **1998** p. 508.
26. Walsh, B. M. In: "*Advances in Spectroscopy for Lasers and Sensing*"; Eds. Di Bartolo, B.; Forte, O.; Springer: The Netherlands, **2006** pp. 403–433.
27. Richardson, F. S. *Chem. Rev.* **1982,** *82*, 541.
28. Bünzli, J. C. G. In: "*Metal Ions in Biological Systems*"; Eds. Sigel, A.; Sigel, H.; Vol. 42; Marcel Dekker: Zurich, **2004** p. 39.
29. Johnson, D. A. *J. Chem. Educ.* **1980,** *57*, 475.
30. Bhaumik, M. L.; El-Sayed, M. A. *J. Phys. Chem.* **1965,** *69*, 275.
31. El-Sayed, M. A.; Bhaumik, M. L. *J. Chem. Phys.* **1963,** *39*, 2391.
32. Sammes, P. G.; Yahioglu, G. *Nat. Prod. Rep.* **1996,** *13*, 1.
33. Stryer, L.; Thomas, D. D.; Meares, C. F. *Annu. Rev. Biophys. Bioeng.* **1982,** *11*, 203.
34. Lehn, J. M. *Angew. Chem. Int. Ed.* **1990,** *29*, 1304.

35. de Silva, A. P.; Gunaratne, H. Q. N.; Rice, T. E. *Angew. Chem. Int. Ed.* **1996,** *35*, 2116.
36. Sato, S.; Wada, M. *Bull. Chem. Soc. Jpn.* **1970,** *43*, 1955.
37. Leonard, J. P.; Gunnlaugsson, T. *J. Fluoresc.* **2005,** *15*, 585.
38. Parker, D. *Coord. Chem. Rev.* **2000,** *205*, 109.
39. Hemmila, I.; Laitala, V. *J. Fluoresc.* **2005,** *15*, 529.
40. Prendergast, F. G.; Lu, J.; Callahan, P. J. *J. Biol. Chem.* **1983,** *258*, 4075.
41. Wu, S. L.; Wu, Y. L.; Yang, Y. S. *J. Alloys Compd.* **1992,** *180*, 399.
42. Wang, Q.; Yan, B. *J. Mater. Chem.* **2004,** *14*, 2450.
43. Lakowicz, J. R. *Principles of Fluorescence Spectroscopy* (3rd edn.). Springer Science+Business Media: LLC, Singapore, **2006** p. 954.
44. Lemmetyinen, H., et al. *J. Lumin.* **2000,** *15*, 341.
45. Gassner, A. -L.; Duhot, C.; Bunzli, J. C. G.; Chauvin, A. S. *Inorg. Chem.* **2008,** *47*, 7802.
46. Carnall, W. T.; Fields, P. R.; Rajnak, K. *J. Chem. Phys.* **1968,** *49*, 4424.
47. Brittain, H. G. *J. Lumin.* **1978,** *17*, 411.
48. Halverson, F.; Brinen, J. S.; Leto, J. R. *J. Chem. Phys.* **1964,** *41*, 157.
49. Carnall, W. T. In: "*Handbook on the Physics and Chemistry of Rare Earths*"; Eds. Gschneider, K. A.; Eyring, L.; Vol. 3; North Holland Publishing Co.: Amsterdam, **1979** p. 171.
50. Horrocks, W. D.; Jr., Sudnick, D. R. *J. Am. Chem. Soc.* **1979,** *101*, 334.
51. Tsukube, H.; Shinoda, S. *Chem. Rev.* **2002,** *102*, 2389.
52. Tsukube, H.; Shinoda, S.; Tamiaki, H. *Coord. Chem. Rev.* **2002,** *226*, 227.
53. Rudzinski, C. M.; Hartmann, W. K.; Nocera, D. G. *Coord. Chem. Rev.* **1998,** *171*, 115.
54. Armaroli, N., et al. *Inorg. Chem.* **1999,** *38*, 5769.
55. Horrocks, W. D.; Jr., Wong, C. -P. *J. Am. Chem. Soc.* **1976,** *98*, 7157.
56. Roberts, T. A.; Hitchins, A. D. In: "*The Bacterial Spore*"; Eds. Gould, G. W.; Hurst, A.; Vol. 1; Academic Press: London, **1969** pp. 611–670.
57. Cohn, F. *Beitr. Biol. Pflanz.* **1876,** *2*, 249.
58. Koch, R. *Beitr. Biol. Pflanz.* **1876,** *2*, 277.
59. Koch, R. *Beitr. Biol. Pflanz.* **1877,** *2*, 399.
60. Tyndall, J. *Philos. Trans. R. Soc.* **1877,** *167*, 149.
61. Church, B. D.; Halvorson, H. *Nature* **1959,** *183*, 124.
62. Berg, P. E.; Greez, N. *J. Bacteriol.* **1970,** *103*, 517.
63. Cano, R. J.; Borucki, M. K. *Science* **1995,** *268*, 1060.
64. Vreeland, R. H.; Rosenzweig, W. D.; Powers, D. W. *Nature* **2000,** *407*, 897.
65. Johnstone, K. *J. Appl. Bacteriol.* **1994,** *76*, 17.
66. Setlow, P. *Curr. Opin. Microbiol.* **2003,** *6*, 550.
67. Byrne, A. F.; Burton, T. H.; Koch, R. B. *J. Bacteriol.* **1960,** *80*, 139.
68. Aronson, A. I.; Fitz-James, P. *Bacteriol. Rev.* **1976,** *40*, 360.
69. Bisset, K. A. *Nature* **1950,** *166*, 431.
70. Driks, A. *Proc. Natl. Acad. Sci. USA* **2003,** *100*, 3007.
71. Albert, H.; Davies, D. J. G.; Woodson, L. P.; Soper, C. J. *J. Appl. Microbiol.* **1998,** *85*, 865.
72. Yung, P. T.; Ponce, A. *Appl. Environ. Microbiol.* **2008,** *74*, 7669.
73. Nicholson, W. L.; Munakata, N.; Horneck, G.; Melosh, H. J.; Setlow, P. *Microbiol. Mol. Biol. Rev.* **2000,** *64*, 548.
74. Horneck, G.; Bucker, H.; Reitz, G. *Adv. Space Res.* **1994,** *14*, 41.
75. Nicholson, W. L. *Orig. Life Evol. Biosph.* **2003,** *33*, 621.
76. Shafaat, H. S.; Ponce, A. *Appl. Environ. Microbiol.* **2006,** *72*, 6808.

77. Jernigan, J. A., et al. *Emerg. Infect. Dis.* **2001,** *7*, 933.
78. Sanderson, W. T., et al. *J. Appl. Microbiol.* **2004,** *96*, 1048.
79. Yung, P. T.; Lester, E. D.; Bearman, G.; Ponce, A. *Biotechnol. Bioeng.* **2007,** *84*, 864.
80. Sharp, R. J.; Roberts, A. G. *J. Chem. Technol. Biotechnol.* **2006,** *81*, 1612.
81. Hindle, A. A.; Hall, E. A. H. *Analyst* **1999,** *124*, 1599.
82. Gerhardt, P.; Marquis, R. E. In: "*Regulation of Prokaryotic Development*"; Eds. Smith, I., Slepecky, R. A.; Setlow, P.; American Society for Microbiology: Washington, DC, **1989** pp. 43–63.
83. Murrell, W. G. In: "*The Bacterial Spore*"; Eds. Gould, G. W.; Hurst, A.; Academic Press: New York, **1969** pp. 215–273.
84. Gould, G. W.; Hurst, A. *The Bacterial Spore*. Academic Press: London, **1969**.
85. Slepecky, R.; Foster, J. W. *J. Bacteriol.* **1959,** *78*, 117.
86. Rosen, D. L.; Sharpless, C.; McGown, L. B. *Rev. Anal. Chem* **1999,** *18*, 1.
87. Arnaud, N.; Vaquer, E.; Georges, J. *Analyst* **1998,** *123*, 261.
88. Latva, M., et al. *J. Lumin.* **1997,** *75*, 149.
89. Carnall, W. T.; Fields, P. R.; Rajnak, K. *J. Chem. Phys.* **1968,** *49*, 4447.
90. Horrocks, W. D.; Jr., Sudnick, D. R. *Acc. Chem. Res.* **1981,** *14*, 384.
91. Horrocks, W. D.; Jr., Albin, M. *Prog. Inorg. Chem.* **1984,** *31*, 1.
92. Cable, M. L., et al. *J. Am. Chem. Soc.* **2009,** *131*, 9562.
93. Lehn, J. M. *Struct. Bond.* **1973,** *16*, 1.
94. Eds. Merbach, A. E., Toth, E.; Wiley: West Sussex, England, **2001**.
95. Aime, S., et al. *Inorg. Chem.* **1997,** *36*, 2059.
96. Chang, C. A.; Chen, Y. -H.; Chen, H. -Y.; Shieh, F. -K. *J. Chem. Soc., Dalton Trans.* **1998,** *19*, 3243.
97. Beeby, A., et al. *J. Chem. Soc., Perkin Trans.* **1999,** *2*, 493.
98. Parker, D.; Williams, J. A. G. *J. Chem. Soc., Perkin Trans.* **1995,** *2*, 1305.
99. Cable, M. L.; Kirby, J. P.; Sorasaenee, K.; Gray, H. B.; Ponce, A. *J. Am. Chem. Soc.* **2007,** *129*, 1474.
100. Mathis, G. *Clin. Chem.* **1993,** *39*, 1953.
101. Li, M.; Selvin, P. R. *Bioconjug. Chem.* **1997,** *8*, 127.
102. Kirby, J. P.; Cable, M. L.; Levine, D. J.; Gray, H. B.; Ponce, A. *Anal. Chem.* **2008,** *80*, 5750.
103. Powell, J. E.; Ingemanson, J. W. *Inorg. Chem.* **1968,** *7*, 2459.
104. Elkström, C. -G.; Nilsson, L.; Duncan, I. A.; Grenthe, I. *Inorg. Chim. Acta* **1980,** *40*, 91.
105. Moeller, T., et al. *Chem. Rev.* **1965,** *65*, 1.
106. Bruce, J. I., et al. *J. Am. Chem. Soc.* **2000,** *122*, 9674.
107. Kolat, R. S.; Powell, J. E. *Inorg. Chem.* **1962,** *1*, 293.
108. Silber, H. B.; Paquette, S. J. In: "*Metal Ions in Biological Systems: The Lanthanides and Their Interrelations with Biosystems*"; Eds. Sigel, A.; Sigel, H.; Vol. 40; Marcel Dekker, Inc.: New York, **2003** pp. 69–104.
109. Yang, Z., et al. *Biochem. Biophys. Res. Commun.* **2000,** *274*, 440.
110. Kimura, T.; Kato, Y. *J. Alloys Compd.* **1998,** *278*, 92.
111. Hockenbury, D. H.; Hockenbury, S. E. In "*Psychology*"; (4th edn.). Worth Publishers: New York, **2006**.
112. Whitby, L.; Axelrod, J.; Weil-Malherbe, H. *J. Pharmacol. Exp. Ther.* **1961,** *132*, 191.
113. Raab, W. *Am. J. Cardiol.* **1960,** *5*, 571.
114. Madras, B. K.; Miller, G. M.; Fischman, A. J. *Behav. Brain Res.* **2002,** *130*, 57.
115. Greer, M.; Williams, C. M. *Neurology* **1963,** *13*, 73.

116. Barbeau, A. *Can. Med. Assoc. J.* **1962,** *87*, 802.
117. Middleton, E.; Finke, S. R. *J. Allergy* **1968,** *42*, 288.
118. Lockey, S. D.; Glennon, J. A.; Reed, C. E. *J. Allergy* **1967,** *40*, 349.
119. Riggin, R. M.; Kissinger, P. T. *Anal. Chem.* **1977,** *49*, 2109.
120. Hallman, H.; Farnebo, L. -O.; Hamberger, B.; Jonsson, G. *Life Sci.* **1978,** *23*, 1049.
121. van der Hoorn, F. A. J.; Boomsma, F.; Man In't Veld, A. J.; Schalekamp, M A D H *J. Chromatogr. B Biomed. Sci. Appl.* **1989,** *487*, 17.
122. Yamaguchi, M.; Yutani, Y.; Kohashi, K.; Ohkura, Y. *Anal. Chim. Acta* **1979,** *108*, 297.
123. Robert, F.; Bert, L.; Denoroy, L.; Renaud, B. *Anal. Chem.* **1995,** *67*, 1838.
124. Nohta, H.; Mitsui, A.; Umegae, Y.; Ohkura, Y. *Biomed. Chromatogr.* **1986,** *2*, 9.
125. Nohta, H.; Mitsui, A.; Ohkura, Y. *Anal. Chim. Acta* **1984,** *165*, 171.
126. Imai, K.; Tsukamoto, M.; Tamura, Z. *J. Chromatogr. A* **1977,** *137*, 357.
127. Jameson, R. F.; Neillie, W. F. S. *J. Inorg. Nucl. Chem.* **1966,** *28*, 2667.
128. Jameson, R. F.; Neillie, W. F. S. *J. Inorg. Nucl. Chem.* **1965,** *27*, 2623.
129. Kiss, T.; Sóvágó, I.; Martin, R. B. *J. Am. Chem. Soc.* **1989,** *111*, 3611.
130. Aydin, R. *J. Chem. Eng. Data* **2007,** *52*, 2400.
131. Chakrawarti, P. B.; Vijayvargiya, B. L.; Sharma, H. N. *J. Indian Chem. Soc.* **1983,** *60*, 89.
132. Wu, Z. J.; Gao, F.; Wang, J. P.; Niu, C. J.; Niu, V. J. *J. Coord. Chem.* **2005,** *58*, 473.
133. Borraccino, R., et al. *Water Res.* **2001,** *35*, 3729.
134. Gergely, A.; Kiss, T.; Deák, G.; Sóvágó, I. *Inorg. Chim. Acta* **1981,** *56*, 35.
135. Kiss, T.; Gergely, A. *Inorg. Chim. Acta* **1979,** *36*, 31.
136. Zhu, R. H.; Kok, W. T. *Anal. Chem.* **1997,** *69*, 4010.
137. Martell, A. E.; Smith, R. M. *Critical Stability Constants* **,** (Vol. 1). Plenum Press: New York, **1974**.
138. Kim, W. D.; Hrncir, D. C.; Kiefer, G. E.; Sherry, A. D. *Inorg. Chem.* **1995,** *34*, 2225.
139. Platt, J. R. *J. Chem. Phys.* **1949,** *17*, 484.
140. Vaillancourt, F. H., et al. *J. Am. Chem. Soc.* **2002,** *124*, 2485.
141. Horsman, G. P., et al. *J. Am. Chem. Soc.* **2005,** *127*, 16882.
142. Ed. D. o. H. a. H. Services, "*Federal Register*". U. S. Department of Health and Human Services, Food and Drug Administration: Rockville, MD, **1998**, pp. 56802–56819, Vol. 63.
143. Bayer, A. *Clinicians' Guide to Aspirin.* Chapman & Hall Medical: London, **1998**.
144. Taylor, D. W., et al. *Lancet* **1999,** *353*, 2179.
145. Group, T C C S *N. Engl. J. Med.* **1978,** *299*, 53.
146. Williams, F. M. *Clin. Pharmacokinet.* **1985,** *10*, 392.
147. Liu, J. -H.; Smith, P. C. *J. Chromatogr. B* **1996,** *675*, 61.
148. Miners, J. O. *Clin. Pharmacokinet.* **1989,** *17*, 327.
149. Levy, G.; Amsel, L. P.; Elliott, H. C. *J. Pharm. Sci.* **1969,** *58*, 827.
150. Levy, G. *J. Pharm. Sci.* **1965,** *54*, 959.
151. Paterson, J. R., et al. *J. Agric. Food Chem.* **2008,** *56*, 11648.
152. Eds. Bar-Or, D., U. S. P. a. T. Office, "*Detection of appendicitis by measurement of orthohydroxyhippuric acid*". Appenditech, Inc.: USA, **1995**, pp. 1–16.
153. Bavoso, A.; Menabue, L.; Saladini, M.; Sola, M. *Inorganica Chim. Acta* **1996,** *244*, 207.

154. Ferrer, E. G.; Gonzalez Baro, A. C.; Castellano, E. E.; Piro, O. E.; Williams, P. A. M. *J. Inorg. Biochem.* **2004,** *98*, 413.
155. Kiss, T.; Jakusch, T.; Kilyen, M.; Kiss, E.; Lakatos, A. *Polyhedron* **2000,** *19*, 2389.
156. Jancso, A., et al. *J. Inorg. Biochem.* **2001,** *83*, 187.
157. Esplin, T. L.; Cable, M. L.; Gray, H. B.; Ponce, A. *Inorg. Chem.* **2010,** *49*, 4643.
158. Pellegrino, P. M.; Fell, N. F.; Rosen, D. L.; Gillespie, J. B. *Anal. Chem.* **1998,** *70*, 1755.
159. Jones, G.; Vullev, V. I. *J. Phys. Chem. A* **2002,** *106*, 8213.
160. Gunnlaugsson, T.; Harte, A. J.; Leonard, J. P.; Nieuwenhuyzen, M. *Supramol. Chem.* **2003,** *15*, 505.
161. Gunnlaugsson, T.; Leonard, J. P.; Mulready, S.; Nieuwenhuyzen, M. *Tetrahedron* **2004,** *60*, 105.
162. Gunnlaugsson, T.; Harte, A. J.; Leonard, J. P.; Nieuwenhuyzen, M. *Chem. Commun.* **2002,** *18*, 2134.
163. Arnaud, N.; Georges, J. *Analyst* **1999,** *124*, 1075.
164. Zheng, X. -Y.; Lu, J. -Z.; Zhu, Q. -Z.; Xu, J. -G.; Li, Q. -G. *Analyst* **1997,** *122*, 455.
165. Magennis, S. W., et al. *Polyhedron* **2003,** *22*, 745.
166. Job, P. *C. R. Acad. Sci.* **1925,** *180*, 928.
167. Shestakova, A. K.; Chertkov, V. A.; Schneider, H. -J.; Lysenko, K. A. *Org. Lett.* **2001,** *3*, 325.
168. Min, D.; Lee, S. W. *Inorg. Chem. Commun.* **2002,** *5*, 978.
169. Yang, W. -W.; Ponce, A. *Int. J. Food Microbiol.* **2009,** *133*, 213.
170. Yung, P. T.; Kempf, M. J.; Ponce, A. *IEEE Aerospace Conference*, IEEE: Big Sky, Montana, **2006**.
171. Yang, W. -W. *Fast Viability Assessment of Clostridium spores - Survival in Extreme Environments.* California Institute of Technology: Pasadena, CA, **2009**.
172. Cable, M. L. *Life in Extreme Environments: Lanthanide-Based Detection of Bacterial Spores and Other Sensor Design Pursuits.* California Institute of Technology: Pasadena, CA, **2010**.

PHOTOPHYSICS OF SOFT AND HARD MOLECULAR ASSEMBLIES BASED ON LUMINESCENT COMPLEXES

CRISTIAN A. STRASSERT[a,b], MATTEO MAURO[a,b] and LUISA DE COLA[a,b]

[a]Physikalisches Institut, Westfälische Wilhems Universität Münster, Mendelstrasse 7, Münster, Germany
[b]Center for Nanotechnology, CeNTech, Heisenbergstrasse 11, Münster, Germany

ABSTRACT

In this chapter, we discuss several approaches that have led from molecular entities to supramolecular soft and hard molecular architectures. Systems based on metal complexes with d^6 and d^8 electronic configuration forming assemblies such as micelles, vesicles, and gels, as well as crystalline structures, will be illustrated. The focus is on the role played by the metal complexes chemical structures as well as the choice of the intermolecular interactions in the ground and/or excited electronic states within the arrays. The selected examples, based on noncovalently linked luminescent systems, aim to the development of multifunctional assemblies, in which the self-organization generates new

INORGANIC PHOTOCHEMISTRY
VOLUME 63 ISSN 0898-8838 / DOI: 10.1016/B978-0-12-385904-4.00009-3

functions, for potential applications in optically addressable materials. The question is how much we can rationalize the behavior and predict the structures and their properties on the basis of the design.

Keywords: Self-assembly; Luminescence; Metal complexes; Soft Assemblies; Self-organization.

I. Introduction

Photochemical processes in complex-ordered materials are responsible for life as we know it on our planet's surface. Understanding how light can be absorbed, produced, or transformed in chemical species in assembled components is a major goal involving numerous scientists from different disciplines.

Self-assembly is a nature-inspired process, in which small molecules spontaneously arrange in an ordered fashion, leading to functional structures displaying characteristics which are not present at the level of individual molecules. The information contained within the structure of the small entities is translated into complex functions through the cooperative interactions between these building blocks. To obtain the desired output, the components must be chosen with great care and organized in space, energy, and time. Self-assembly can facilitate the construction of complex systems without employing covalent linkages between subunits, which otherwise would require demanding synthetic procedures and difficult purification steps. Further, a variety of different architectures can be set up with few building blocks that can be repeatedly combined in different ways, just as observed in natural photosystems. The organization in large structures in which intermolecular and noncovalent bonds between two or more chemical entities have been formed is part of supramolecular chemistry defined as *chemistry beyond the molecules* (*1,2*).

Several artificial systems in which intermolecular and noncovalent bonds between two or more chemical entities have been formed have been reported. The driving forces which hold together these entities are mainly dealing with electrostatic interactions, metal coordination, hydrogen bond, π–π stacking as well as hydrophobic, van der Waals, and dispersion interactions. Therefore, such concept has paved the way for designing and building systems with specific and novel features, whose properties could be far beyond the simple sum of

functionalities of the single subentities (*3,4*). Nowadays, one of the most striking goals is to provide building blocks that can be rationally mixed and matched to have functional supramolecular architecture and materials with properties which can be modified upon an external stimulus. Adaptive materials (*5*), self-healing systems (*6*), and dynamic species (*7*), able to reorganize their structure as a response to an input, are the next generation of organized molecular systems which started to appear in the literature.

By mimicking biological systems, it is possible nowadays to create species able to act as (supra)molecular sensors, as well as to develop catalysts which undergo allosteric control (*8*), or produce by light molecular movements (*9*). Moreover, biological systems make strong use of the concept of *multivalency*, which is based on recognition as well as on relatively weak and noncovalent interactions, as hydrophobicity and hydrophilicity (*10,11*), host–guest chemistry (*12,13*), and H-bonding (*14,15*). Thus, taking inspiration from nature offers the possibility to deliberately design cooperative synthetic systems, blossoming novel, and fascinating scientific scenarios in both fundamental and applied research. A more ambitious goal is not to mimic nature but to provide simpler artificial systems which can replace natural ones.

In many cases, in nature, the assemblies are constituted of organic chromophores. Much less common is to encounter assemblies of organometallic species or hybrid organic–inorganic arrays. Organometallic complexes display a variety of outstanding characteristics, among which are photophysical, catalytic, redox, and magnetic properties. Combination of different metal complexes, possessing complementary properties, for example, emission colors, absorption, ability to accept and donate energy and charge, can lead to white-light emission, light-harvesting systems, photoinduced energy and charge-transfer (CT) processes, and photocatalysis.

Herein, we will discuss several approaches that have led from molecular entities to supramolecular soft and hard systems. In particular, we will show how the molecular structure can be modified to induce the controlled self-assembly of transition metal complexes into sophisticated photoactive arrays with unusual properties derived from the structure of the metal complexes and their intermolecular interactions in the ground and/or excited electronic states within the assemblies. We will start with a survey of the photophysical properties of selected transition metal complexes, followed by an overview of the aggregation mechanism they can undergo to. We will focus our attention on soft assemblies

such as micelles, vesicles, and gels, and finish with crystalline materials. Along our journey, we will elaborate on design features, photophysical properties, structure–activity correlation, and potential applications. The selected examples are based on noncovalently linked luminescent systems in which the self-assembly process generates new functions.

II. Basic Photophysics of Selected Transition Metal Complexes

Many excellent reviews and books have been written concerning the photophysics of organometallic species *(16–22)*, a detailed discussion exceeds the scope of this work. We wish to give to the reader only the photophysical basis of selected d^6 and d^8 complexes to follow better the discussion in the next sections. In brief, in a metal complex, its molecular constitution can be described as a metallic center surrounded by an organic coordination sphere. The electronic interplay between these units defines the character of the electronic excited states, which are the ones to undergo subsequent photophysical or photochemical processes.

Ground and excited-state electronic wave functions facilitate the presentation of electron density relocations that can be visualized and interpreted as transitions involving localized molecular orbitals (MOs). However, the limitation of this model should be kept in mind. This is particularly true for the nature of the transitions, which actually occur between electronic states that cannot even be regarded as purely zero-order in nature. Due to electron correlation, interconfigurational mixing is indeed introduced for a more accurate description, namely as configuration interaction of zero-order wave functions. Electronic states are then approximated as combinations of zero-order wave functions, yielding representations of mixed nature *(23,24)*.

For complexes, the combination of metal-centered (MC) d and ligand-centered (LC) orbitals leads to MOs which are denominated according to the predominant atomic orbital contributions. Therefore, transitions between zero-order electronic configurations can be classified as LC, MC, or CT electron density displacements. If contrasted with the ground state, the first two mainly involve changes within the organic portions (LC) or the inorganic part (MC) of the molecule. The latter one (CT) involves a vectorial redistribution within or between the organic ligands (intra- or interligand charge transfer, respectively, ILCT), or more frequently, between the organic part and the metal center. According to the directionality of the electron

density shift, they can be considered either as metal-to-ligand charge-transfer (MLCT) or ligand-to-metal charge-transfer (LMCT) states. Within the orbital approximation, rough electronic wave functions are constructed as linear combinations of basis functions centered on the atomic components, which result in MOs. At this point, the electron spin has not been considered so far. Within the orbital approximation, the excited electronic states involve half-filled orbitals occupied by unpaired electrons. In most cases, purely singlet or triplet wave functions can be constructed as zero-order approximations, which might be fair enough for organic chromophores constituted preponderantly by light atoms. However, relativistic effects due to acceleration of electrons in the immediacy of the elevated nuclear charges of heavy atoms originate a perturbation that, once again, leads to mixing of zero-order wave functions. Representation of electronic states as purely singlet or triplet in nature breaks down and gives way to mixing, by spin–orbit coupling, of electronic wave functions with defined spin. The spin–orbit coupling constant, which determines the magnitude of the perturbation, roughly scales as Z^4, where Z refers to the nuclear charge. The perturbation is the strongest for Au, Re, Os, and Pt.

The properties of photoactive transition metal complexes, such as those described herein, are fundamentally marked by spin–orbit coupling. In metal complexes usually fast intersystem crossing from the optical excited state, mainly of singlet character, to an isoenergetic state, which is predominantly triplet in nature is observed. This radiationless process is followed by fast relaxation into the lowest excited state with preponderant triplet character. From there, emission of light, radiationless deactivation, electron or energy transfer, and chemical reactions can occur. Radiationless deactivation pathways, especially for ruthenium complexes, are often privileged by thermally accessible MC states, which provide a crossing point with the potential energy surface of the ground electronic state, due to their distorted nuclear configuration favored by placement of electrons in unoccupied, antibonding d-orbitals. MC states can be pushed up in energy by the introduction of strong sigma-donating ligands that locate a negative charge density on unoccupied d-orbitals of the metallic center, as well as by the binding of effective π-accepting units that stabilize the occupied d-orbitals of the central atom. Further, the energy level of the lowest electronic excited states can be tuned by a judicious choice of the ligands' "chemical structure" which can critically stabilize or destabilize them with respect to the ground electronic state.

Usually, absorption and emission of light between states of different multiplicity are spin-forbidden. However, due to the mixed multiplicity character of the electronic excited states of transition metal complexes, such processes become, at least, partially allowed, enabling the fabrication of luminescent species with long-lived electronic excited states, due to their predominant triplet character. This opens the possibility for electrical excitation with potentially 100% efficient exciton harvesting: recombinations of holes and electrons lead to electronic excited, singlet and triplet, states which, ultimately, lead to the lowest excited triplet level. Another interesting feature of triplet emitters is their marked Stokes-shift, which is determined by the singlet–triplet splitting of the lowest electronic excited singlet and triplet states, as well as by the energy of structural reorganization upon intersystem crossing and subsequent vibrational relaxation. Moreover, the emitting triplet state can be of a different origin than the optically excited singlet state, thus leading to even more pronounced shifts. The major triplet character of the long-lived, lowest electronic excited states also renders them prone to quenching by molecular oxygen, which can be used for sensing or photosensitizing purposes.

The geometry of complexes of groups 7–9 of the transition metals, in particular, Re(I), Ru(II), Os(II), and Ir(III), is determined by the d^6 electronic configuration that leads to octahedral coordination geometries. The d-orbitals of the central atom can be roughly viewed as split into two sets of triply and doubly degenerate nature, named as t_{2g} and e_g, respectively, where the latter ones are higher in energy, and the splitting is determined by the ligand field (*vide supra*). The metallic center is therefore shielded from the environment, and intermolecular interactions mainly perturb the organic ligands and, consequently, the ground and excited electronic states whose energy content they determine.

For the octahedral Ru(II) complexes, and the other d^6 metal ions, the σ_L and π_L orbitals are completely filled as well as the HOMO $(\pi_M(t_{2g}))^6$ is fully occupied and the ground state configuration is closed shell. The ground state is therefore a singlet, while the excited states are either singlet or triplet. The polypyridine complexes, accounted as paradigmatic examples of MLCT states, involve 4d-orbitals from which electron density is displaced to the organic ligand. In complexes in which the coordinated ligands do not possess accessible π_L^* orbitals, the lowest excited state is a MC. This leads to fast radiationless deactivation to the ground state and/or ligand dissociation reactions. Strong σ-donors and π-acceptors lead to a larger d-orbital splitting and, consequently, destabilize MC states, making thermal activation less accessible.

If compared with their Ru(II) analogues, Os(II) complexes display smaller gaps between the ground and the excited electronic states, as the relevant 5d-orbitals lie higher in energy, thus lowering the energy of the MLCT state. This leads to red-shifted emissions and shortened excited-state lifetimes, due to a faster nonradiative deactivation, which can be rationalized in terms of the energy gap law *(25–28)*. If compared with Ru(II), nonradiative MC states of Os(II) complexes are relatively less thermally accessible due to the lower energy content of the MLCT states. Further, the splitting induced by a given ligand field is more pronounced for the diffuse 5d-orbitals of Os(II) than for the 4d-orbitals of Ru(II), which further increases the gap between the emissive MLCT and the nonradiative MC states.

In the case of Rhenium, Re(I) complexes require the introduction of even stronger π-accepting ligands (typically CO or CN) to stabilize their high lying 5d-orbitals. This is necessary to push up in energy the MLCT states, which otherwise possess a very low-energy content leading to extremely low-emission efficiencies according to the energy gap law. Further, strong field ligands induce a larger splitting of d-orbitals, thus making nonradiative MC states less accessible and favoring radiative processes.

Luminescent Ir(III) complexes are often comprising cyclometalating ligands, and even though they possess the same electronic configuration of the Ru(II) and Os(II), the nature of their excited state is less defined. In fact for many complexes, the lowest emitting excited state is a mixed MLCT and LC, which is reflected in longer excited-state lifetimes and often structured emission. This mixed nature is well shown by the different interplay between the k_r and k_{nr}. For pure ^{3}MLCT, a larger k_r is usually observed than for a pure ^{3}LC states. A remarkable behavior is observed for the excited-state lifetime, as even for larger contribution of the ^{3}LC states, a short lifetime (few microseconds) is recorded which is related to the heavy atom effect which induce a strong triplet-singlet mixing. Another interesting feature of the Ir complexes is their much higher sensitivity toward modifications of the frequently used cyclometalating ligands. Such properties allow a very fine-tuning of the excited-state energies, and the emission maxima can vary from UV to near IR.

In the case of Pt(II), however, the d^8 configuration leads to square-planar coordination geometries. A particular feature of these species is the doubly occupied d_z^2 orbitals, which are normal to the coordination plane. This geometry facilitates the stacking of molecular units into dimers, oligomers, or columnar arrays in which the protruding d_z^2 orbitals can interact, leading

to excited electronic states that involve more than one molecular entity. For the monomeric species, either LC or MLCT excited states (i.e., $\pi\pi^*$ or $d\pi^*$ electronic configurations, respectively) determine the observed photophysical and photochemical properties. However, in the stacked planar complexes, metal–metal-to-ligand charge-transfer (MMLCT) states (i.e., $d\sigma^*\pi^*$ electronic configurations) are populated and can be described as electron density displaced from the interacting metal d_z^2 orbitals to the stacking ligands, which is usually associated to a red-shifted absorption and emission. Further, $d\sigma^*\pi\sigma^*$ electronic configurations can also become relevant when investigating aggregated species. Modulating the intermolecular distance allows, for instance, to tune the absorption and emission wavelengths of the assemblies, as the d–d electronic interaction is a function of distance. Further, the planar nature of Pt(II) complexes also favors excimer formation, which can also display red-shifted emission as compared with the emission of monomeric species. Pd(II) shares structural and chemical features with Pt(II) within the group 10 of the periodic table, even though its photophysical properties are less appealing. Nonetheless, Pd complexes are very well known for their catalytic properties, which might be exploited in photoactive supramolecular architectures.

In the next section, we will divide the d^6 and d^8 metal complexes and describe the possible modulation of their properties upon aggregation.

III. Molecular Systems Based on Aggregates of d^6 Metal Complexes

A. Photoresponsive Assemblies Based on Noncovalent Interactions

Synthetic chemists have applied the concepts of multivalency and cooperativity to supramolecular chemistry to create, for instance, biomimetic receptors able to recognize small molecules (*29,30*), polysaccharides (*31*), and DNA (*32*). Most of these systems are based on calixa[*n*]arenes (*33–35*), cucurbituril (CB) (*36,37*), and cyclodextrine (CD) (*38–40*) (see Fig. 1), and they represent ideal guests for assembling photoactive species.

It has also been shown that organic chromophores can be used to reversibly assemble and disassemble large structures. For example, Zhang and coworkers (*41*) reported the light controlled assembly of a system based on α-CD and diazobenzene-containing surfactant. As depicted in Fig. 2, the

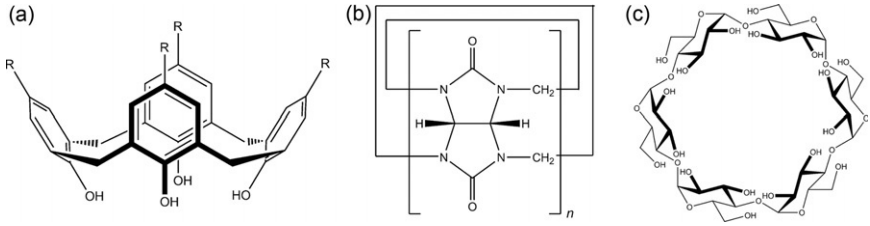

FIG. 1. Schematic representation of some host systems used for host–guest assemblies: from left: calixarene, cucurbituril, and β-cyclodextrine.

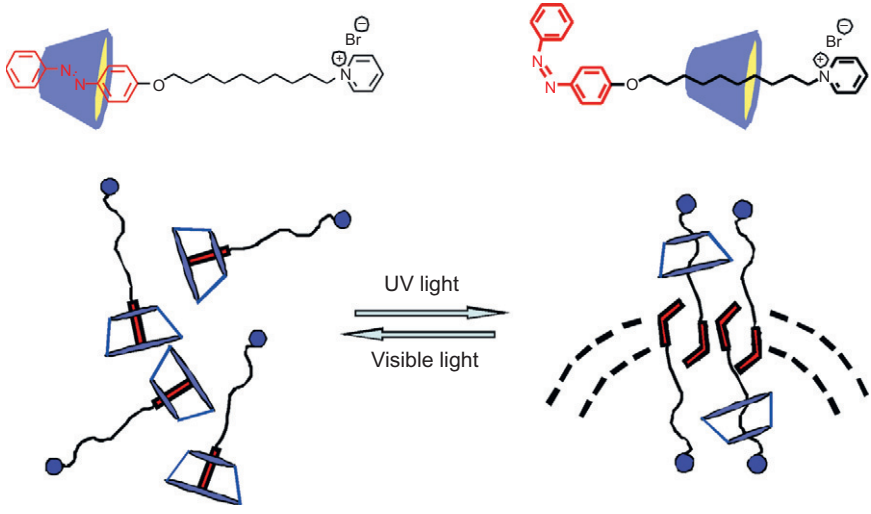

FIG. 2. Schematic light-induced assembly and disassembly process. Reproduced with the permission of Wiley-VCH (*41*).

trans-isomer of 1-[10-(4-phenyl-azophenixy)decyl]pyridinium bromide (namely, *AzoC10*) can be well recognized by α-CD, due to favorable hydrophobic and van der Waals interactions. Upon UV irradiation at 365 nm, the *trans*-diazobenzene moiety undergoes the well-known photoisomerization process to the *cis* form with subsequent disassembling. This is due to the increased steric demand because of the change in conformation of the azobenzene moiety, within the hydrophobic cavity of the α-CD.

Using the same hydrophobic supramolecular interactions, it is possible to create assemblies based on luminescent metal complexes which, if judiciously chosen, can lead to new properties not present in the simple components such as vectorial photoinduced processes.

β-Cyclodextrines, appended to a ruthenium complex, have been employed as hosts for iridium and osmium complexes bearing adamantyl or biphenyl moieties, which form strong host–guest complexes with β-cyclodextrines (see Fig. 3). In such systems, photoinduced energy transfer can occur from the periphery, upon complexation of the iridium units, toward the central ruthenium acceptor, or switched in the other direction, from the ruthenium to the periphery when the osmium moieties are assembled (see Fig. 3) (*42*). The lowest excited state is in fact localized on the osmium center, while the highest luminescent excited state belongs to the iridium complex (see Fig. 3 right).

The system can be made even more complex to achieve vectorial energy transfer in distinct steps, making the central unit asymmetric by substituting the coordinating ligands of the ruthenium with two different CDs. To introduce directionality in the photoinduced process, both α- and β-CDs have been linked onto a ruthenium core, which can act as a junction by the selective binding of tailor-made photoactive guests. In these cases, anthracene and osmium derivatives were employed as final energy donor and acceptor, respectively. After self-assembling of the three different photoactive components (see Fig. 4), and upon excitation of one of the peripheral anthracene moiety, a vectorial unidirectional photoinduced energy transfer process takes place (Fig. 4) (43).

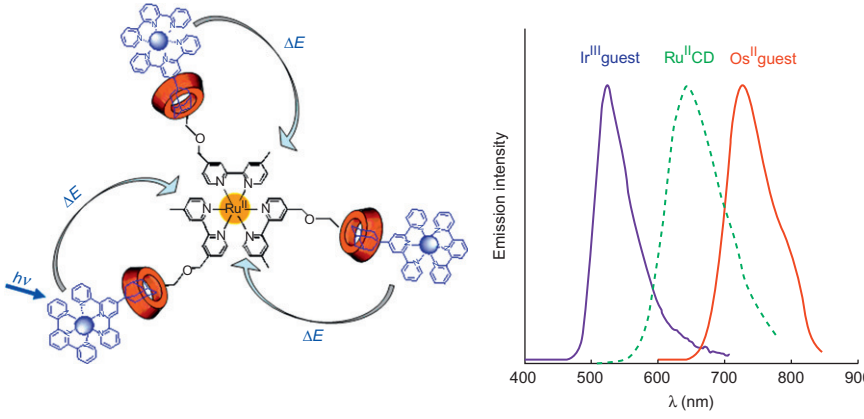

FIG. 3. Schematic representation of the assembled Ru—CD—Ir system in which it is possible, upon light excitation, to funnel the electronic excitation to the ruthenium core. To switch the direction of the energy transfer process, Ir complexes must be replaced with the osmium analogues. Right: emission spectra for the three complexes.

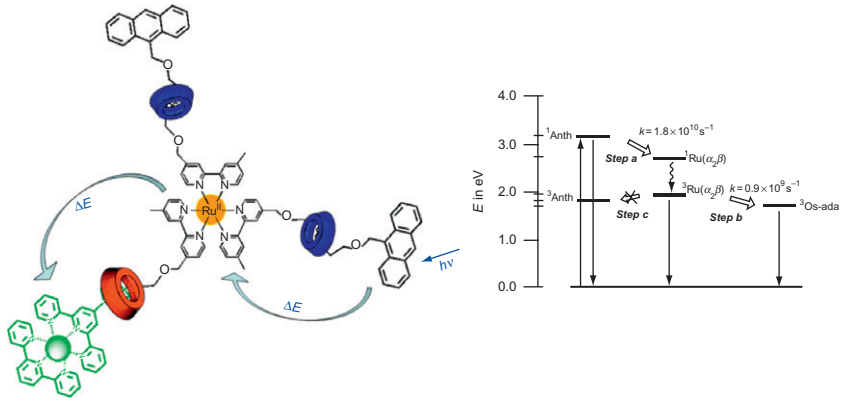

FIG. 4. Schematic formula of the multicomponent system and its energy levels. Due to the energy cascade process, the electronic energy can be transferred from the excited anthracene to the osmium acceptor (green) via the ruthenium moiety (*43*).

An interesting self-assembled light-harvesting antenna system based on a ruthenium complex and a Nd(III) emitter has been reported by Balzani *et al*. (*44*). The three-component assembly containing a dendrimeric 1,4,8,11-tetraazacyclotetadecane (cyclam) core with appended 12 dimethoxybenzene and 16 naphthyl units able to harvest light in the UV region, (**D**), [Ru(bpy)$_2$(CN)$_2$] able to absorb light in the visible but also to coordinate other metal ions, and Nd^{3+} cations able to emit in the infrared region if suitably sensitized. The components were added in equimolar amounts, to form the assembly {**D**·Nd^{3+}·[Ru(bpy)$_2$(CN)$_2$]} (*44*). The cyclam core is able to coordinate the Nd ions, but the dendrimer **D** is not able to directly sensitize the lanthanide ion located in its core. However, the organic chromophores are able to efficiently transfer electronic energy to the [Ru(bpy)$_2$(CN)$_2$] complex, which is coordinated through the cyano groups to the Nd. The excited Ru complex can then emit or sensitize the line-like emission of the Nd^{III} ion, as observed by recording the IR emission spectrum.

Besides hydrophobic and coordinative interactions, hydrogen bonds and electrostatic interactions have been used to assemble luminescent metal complexes. In this context, Barigelletti and coworkers (*45–47*) reported on the luminescent properties of Ru(II) and Os(II) complexes containing bipyridines peripherally functionalized with nucleotide bases, cytosine, and guanine,

namely, **Ru-C** and **Os-G**, respectively. In polar nonprotic solvent, that is, CH_2Cl_2, these compounds are able to associate in pairs through mutually complementary triple hydrogen bonds (C—G nucleotide bases) yielding the couple Ru-C···Os-G. Upon light excitation, a photoinduced energy transfer process from the excited ruthenium moiety to the osmium unit is observed.

We have shown that hydrogen bonds can be successfully employed to decorate the periphery of dendrimers with emitting Re(I) complexes (*48*). The dendrimers were used as multivalent hosts for the barbiturate guests Barbital and for the [Re(Br)$(CO)_3$(barbi-bpy)] (barbi-bpy = 5-[4-(4′-methyl)-2,2′-bipyridyl] methyl-2,4,6-(1*H*,3*H*,5*H*)-pyrimidinetrione) (see Fig. 5). The stable adducts formed between the dendritic architectures (the hosts) and the barbiturate guests were investigated, and energy transfer has been shown from the excited dendrimer to the Re complexes.

Further, electron transfer could be investigated in a system based on the same interaction, in which the electron acceptor, methyl viologen, was bound to the Re(I) complex, acting as an excited-state electron donor (*49*).

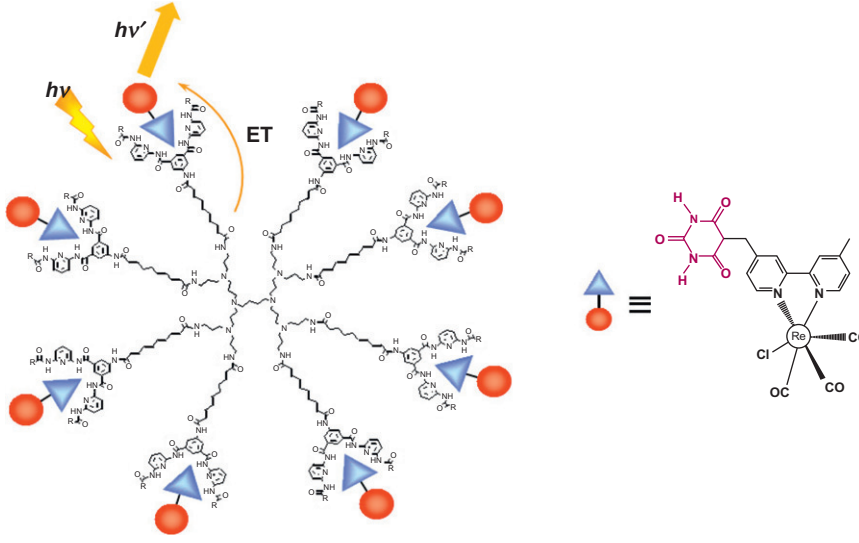

FIG. 5. Schematic formula of the dendrimer and of the Re(I) guest which can complex via hydrogen bonds, at its periphery. Upon irradiation at $\lambda = 330$ nm, where the dendritic structure is almost selectively excited due to the different absorption profile with respect to the rhenium complex, an efficient energy transfer can occur from the dendrimer to the organometallic moiety.

B. Micelles and Vesicles

An interesting approach to have multiple components non-covalent assembled, based on identical or different metal complexes, keeping a well-defined structure, is to organize them in micelles and vesicles. Such self-assembly, in certain solvents, must be promoted by an amphiphilic nature of the metal complex which can be achieved by tailoring the ligands coordinated to the metal ion. A fine-tuning of the ligands could also allow obtaining the correct geometrical shape to be able to discriminate between micelles or double layer structures such as vesicles or eventually linear arrangements such as fibers.

In a general design, the metal complex represents the head group of the surfactant and often constitutes the polar part, as most of the metallosurfactants investigated contain charged complexes. The tails are then the hydrophobic units and can be appended to the coordinated ligands to have a straight geometrical shape or defining a conical form in the case of divergent or double chains. The geometry of the assembly will therefore depend on the relative size ratio chain/metal complex, the length of the chain and its shape, the number and position on the bipyridine ligands, as well as the nature of the counter-ion (*50–52*). However, the rationalization of the assembly is not that straightforward. In fact, secondary intermolecular interactions ($\pi-\pi$, electrostatic, hydrogen bonds, etc.) as well as solvent and temperature could play a major role resulting in assemblies of unpredictable shape and size. Also, so far there are no predictions or experimental evidences on how to interchange from one structure to another one in a reversible or desired way. In simple metallosurfactants, it has been demonstrated by several groups that they all display the typical surfactant-like behaviors, such as adsorbing at interfaces, being it polar/apolar (e.g., micelles, vesicles and liposomes), solid/liquid (e.g., monolayers), or liquid/gas (e.g., Langmuir–Blodgett films). Embedding the typical self-assembling properties of surfactants and the inherent chemical and physical properties of transition metal complexes could provide a clever and straightforward way for incorporating specific functionalities to an interface, such as magnetism, color, or pH sensitivity, and even more importantly, redox, photophysical, and catalytic properties.

Even though metallosurfactants are scarce compared to their nonmetallic organic counterparts, there is an increasing interest due of their multiple applications in fields such as probes in emulsion (*53*), formation of monolayers (*52,54–56*), thin film

optoelectronics (*57,58*), magnetic materials (*59,60*), liquid crystals (*61–63*), templates of mesoporous materials (*64,65*), biologically active compounds (*66*), magnetic resonance imaging (*56,67*), drug delivery (*68,69*), and homogeneous catalysis (*70–74*).

However, much effort has been devoted for shedding light onto the fundamental understanding of the interior structure and dynamics of soft self-assembling materials, as micelles, vesicles, and microemulsion (*53,75*).

Several papers reported on the spatial determination of photoactive molecule in organized assemblies (*76–79*), and Pallavicini and coworkers reviewed on the use of luminescence as probe in self-assembly of multicomponent fluorescent sensors (*80*). Also, luminescence quenching studies on $[Ru(bpy)_3]^{2+}$ in sodium dodecyl sulfate (SDS) micelles and hemimicelles by using a variety of quenchers were reported by Turro and coworkers (*81*) and then reviewed by De Schryver and coworkers (*82*).

Initial studies focused on the lyotropic phase behavior of $[Ru(bpy)_3]^{2+}$ and $[Ru(tpy)_2]^{2+}$ systems (*83,84*), but the first example of micellization was actually observed in solutions of nonlabile metallosurfactants containing a $[Co(polyamine)]^{3+}$ center (*85*).

In this area, Bruce and coworkers extensively reported on amphiphilic metal-containing compounds able to display mesomorphic properties (metallomesogens) (*86,87*). Most of these systems are designed for catalytic purposes (*88*), to act as templating agents for mesoporous materials (*89*), and for optoelectronic application (see d^8-based systems). Moreover, Bruce devoted intensive work to the fundamental understanding of the structure–properties relationship and, in particular, on the role played by the molecular parameters of metal-containing mesogenic molecules, as geometry and volume of the ligands, nature and size of the metal center, on determining aggregation properties and arrangement features of the systems as well as liquid crystalline behavior (*90–93*).

Verani and coworkers widely investigated stimuli-responsive soft materials with interesting optical and redox behaviors. Such materials are able to self-assembly in functional ordered structures, as Langmuir–Blodgett films and liquid crystals, and possess potential applications in molecular electronics and magnetic films as well. These compounds are mainly based on Co(II) (*94*), Co(III) (*95*), Cu(II) (*96*), Fe(II)/Fe(III) (*97*), and Ni (II) and Zn(II) (*98*). A recent overview dedicated to colloidal systems, and their application in different fields has recently appeared in the literature (*99*).

Among all the different coordinating ligands employed, dialkylphenantroline and bipyridines have been successfully used in the

synthesis of ruthenium (*52,100,101*), rhenium- (*102*), and iron-based amphiphiles (*103*). Further, Bruce *et al*. have correlated the shape and chemical nature of the ligand coordinated to the ruthenium ion with the resulting structure of the aggregates. Ruthenium metallosurfactants as the polar head group, which contains a single alkylated bipyridine as hydrophobic part, namely, $[Ru(bpy)_2(R_2\text{-bpy})]^{2+}$, have been also investigated (*50,51,100,104*). Even though these aggregates are potentially luminescent, particularly, ruthenium(II) complexes incorporating bipyridyl units stand out for their robustness, reactivity, as well as rich electro- and photochemical properties (*105,106*), no information on the variation of the photophysical properties were reported for most of the systems.

Going from small molecules to macromolecules-based systems and taking advantage from the well-known tendency of amphiphilic block copolymers to aggregate in micelles in aqueous media, Gohy and coworkers showed the possibility to aggregate metallosupramolecular amphiphilic block copolymers consisting of a core formed by hydrophobic and insoluble poly(styrene) (PS) or poly(ethylene-*co*-butylene) (PEB) blocks, surrounded by a hydrophilic poly(ethylene oxide) (PEO). These two blocks are held together by bis-2,2′:6′,2″-terpyridine-ruthenium moieties, namely, [Ru(R′-tpy)(R″-tpy)], which are thought located at the corona core-corona interface (*107–110*). The metallosupramolecular block copolymer micelles have been recently reviewed by Gohy; thus no more room will be dedicated to this topic hereafter (*111*).

However, Sleiman and coworkers investigated the synthesis of homopolymers block copolymers containing dense arrangement of ruthenium bipyridyl complexes by using ring-opening metathesis polymerization (ROMP). In this case, the hydrophobic polymeric tails face the solvent and act as protecting shield for the polar head, while the core of these aggregates is expected to be formed by the ruthenium moieties. Thus, the block copolymers organized in such a way that the ruthenium moieties displayed a lack of interchromophore interactions with consequent preservation of the redox and photophysical properties (*112,113*).

As already mentioned, to rationalize the shape and size of the aggregate is difficult and also the number of studies on the relationship between structure and the physicochemical properties of these luminescent metalloaggregates remain limited so far (*50,104,114,115*), and mostly dealing with spherical micelles, even though few vesicular systems have been also reported (*116*). In addition, these aggregates have been studied mainly in aqueous solutions, while there are only few known metallosurfactants which aggregate in organic solvents (*116,117*).

Despite most of the investigations on the ruthenium complexes containing micelles deal with the quenching phenomena, there are few papers in which the micelles have been used to enhance the ruthenium emission (*116*). A protection from the environment and a reduction of the quenching by the dioxygen can be achieved by shielding the metal complexes using dendritic structures (*118*) and core/shell nanoparticles (*119,120*). Sauvage and coworkers showed a different effect on investigating the luminescence properties of $Ru(bpy)_2(ppz)$, namely, **Ruppz**, where ppz = dipyrido[3,2-a:2′,3′-c]phenazine, in micellar SDS solution. The complex **Ruppz** did not show any luminescence in water, although it was a modest emitter in organic solvents as ethanol. However, going from pure aqueous solution to a condition in which the concentration of SDS is above its critical micellar concentration (CMC), a dramatic enhancement of the emission intensity was detected, the ratio being larger than a factor of 3 (*121*). The quenching in such a case is not due to the dioxygen but to the protonation of the pyrazine group in water which turns off the emission.

Most of the micellar systems described so far are realized in water. We recently reported on the aggregation features and spectroscopic properties of inverted ruthenium bipyridyl aggregates in low-polarity organic solvents (*116*). Such systems could help to further shed light on the role played by closely organized metal centers. The design of molecules able to self-organize in low-polarity solvents requires shrewd care, thus particular considerations have to be taken into account. Indeed, a surfactant that could be able to aggregate into inverted micelles has to match two different key aspects: a small head group and voluminous hydrophobic substituents. As a result, a molecule with a truncated cone architecture, where the head group represents the narrow extreme of the cone, might be considered.

As far as a $[Ru(bpy)_3]^{2+}$ moiety is concerned, the polar head possesses a rather big volume of about 100 $Å^2$, which requires the hydrophobic tail to be voluminous enough to compensate such a big head group. To reach this goal, we proposed metallosurfactants containing from one to two and either linear or branched alkyl chain substituted bipyridine, of general formula $[Ru(bpy)_{3-n}(bpyR_x)_n]Cl_2$ with $n = 1$ or 2 and where $bpyR_x$ stands for a 4,4′-dialkyl-2,2′-bipyridine ligand with x alkyl chains (Fig. 6).

Due to the amphiphilic nature of the complex, inverted aggregation in apolar organic solvents was realized, leading to the formation or either inverted micelles or inverted vesicles.

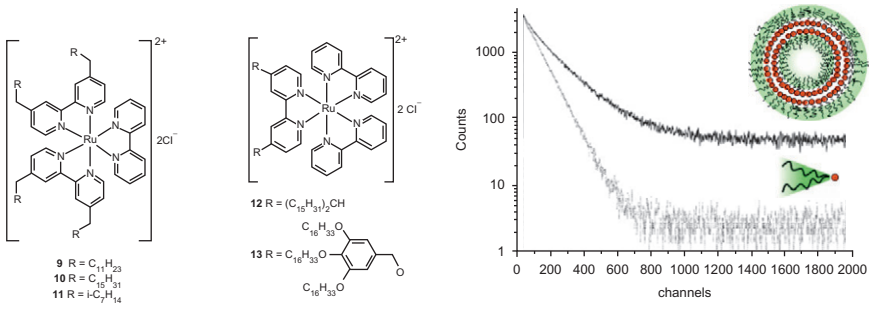

FIG. 6. Chemical structure of the investigated metallosurfactants with two (left) and one (middle) disubstituted bipyridines. Right: room temperature time-resolved emission decays of complex **12** in *n*-hexane (solid line, —) and upon addition of one drop of ethanol (dotted line, ---). Emission was monitored at 644 and 623 nm, respectively.

To compare the properties of the metallosurfactants upon aggregation, the photophysical characteristics of the complexes **9**–**13** were investigated in air-equilibrated *n*-hexane and ethanol conditions. Both absorption and emission spectra of all the complexes are closely related to the ones of $[Ru(bpy)_3]^{2+}$.

However, contrary to the reference complex, a pronounced and unexpected bathochromic shift was detected in the ^{1}MLCT absorption band in *n*-hexane when compared to ethanol. A similar and more evident behavior was observed for the emission spectra indicating that in hexane, the ruthenium moieties experience a more polar environment.

These results suggest the formation of aggregates in the lower polarity solvent, being most likely reversed micelles or reversed vesicles. The cationic heads of the ruthenium complexes being in the core of the aggregates are organized close to each other feeling a higher polarity environment despite the low polarity of the solvent.

The time-resolved analysis of the excited state responsible for such photoluminescence gave further evidence of the formation of aggregates in *n*-hexane, in particular, when compared to ethanol. Figure 6 shows the decays of the complex **12** in air-equilibrated solutions, as monomeric species and in the aggregate form. The long component was assigned to the monomeric nonaggregated ruthenium amphiphilic molecules, while the short component would arise from the aggregated and closely-packed molecules. The quenching effect is due to the triplet–triplet annihilation, which strongly reduces the luminescence excited-state population of the complexes. To support such explanation,

a drop of ethanol into the *n*-hexane was added to disassemble the aggregates. The biexponential decays turned in a monoexponential lifetime (Fig. 6).

The nature and the structure of such aggregates were also investigated by means of dynamic light scattering and atomic force microscopy.

We discussed how the numbers, size, and nature of the akyl chain(s) can influence the formation of inverted vesicles or micelles which could open new perspective toward the synthesis of nanomaterials and, in particular, of photocatalysts. Multichromophoric aggregates can also have an important role as light-harvesting units or for the constitution of multicolor emitting materials.

To exploit this last appealing possibility, we have investigated energy transfer processes in self-assembled aggregates and, in particular, in vesicles constituted of two different (in energy) luminescent metallosurfactants (*122*). Both complexes are charged and contain long chains dialkyl-bipyridine, as the hydrophobic part of the structure. For the electronic energy, acceptor and donor metallosurfactants bis(2,2′-bipyridine)(4,4′-diheptadecyl-2,2′-bipyridine)ruthenium(II) dichloride (1) and bis [(4,6-difluorophenyl)pyridine](4,4'-diheptadecyl-2,2'-bipyridine) iridium(III) chloride (**2**) were chosen, respectively (Fig. 7).

The photophysical properties of these metallosurfactants, namely **1** and **2**, were investigated in air-equilibrated aqueous solution at room temperature, and the results compared with the nonsurfactant analogues, namely, $[Ru(bpy)_3]Cl_2$ and $[Ir(dfppy)_2(bpy)]Cl$ (where bpy = 2,2′-bipyridine and dfppy is 2,4-difluorophenylpyridine). Also, the steady-state and time-resolved emission properties of **1** and **2** were investigated in the presence of a conventional cationic surfactant, as cetyltrimethylammonium bromide (CTAB).

Below the CMC, both the compounds **1** and **2** showed photophysical properties resembling their parental species with a differentiated emission in the red region ($\lambda_{max} = 635$ nm) for the ruthenium complex and a green emission ($\lambda_{max} = 544$ nm) for the iridium compound. Both emissions display monoexponential decays.

However, above the CMC, biexponential lifetime profiles and enhanced emission quantum yields are observed for both complexes. Comparison with the excited lifetime of the parental complexes showed that the longer component can be assigned to the aggregated species. Such findings could be explained in terms of smaller nonradiative rate constant, as consequence of

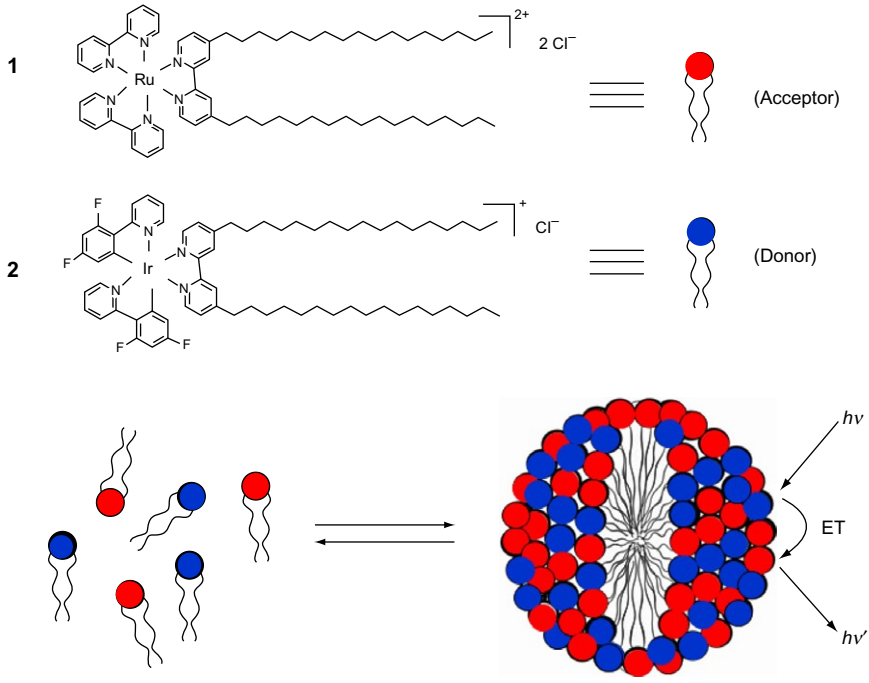

FIG. 7. Schematic formulas of the metallosurfactants and their self-assembly in mixed aggregates.

the reduction of the vibrational modes available to the head groups within the confined environment of the aggregate.

Upon combination of complexes **1** and **2** in an equimolar 0.025 mM aqueous solution, the absorption spectrum displayed features of both complexes. On the contrary, the emission spectrum of such mixture showed a maximum centered at 645 nm, which resembled only one of the complex **1**, while the emission of complex **2** was not detected. The time-resolved emission analysis confirmed that the decay was only related to complex **1** above the CMC. These findings strongly indicate a full and efficient energy transfer process involving the iridium-based metallosurfactant **2**, being quenched by the ruthenium-based amphiphilic complex **1** in a system that can be depicted as a mixed aggregate.

No bimolecular quenching process could be detected at the employed concentrations for the reference complexes.

To gain deeper insight into the energy transfer process as well as to explore the possibility to tune such a process, a "diluting" surfactant as CTAB which possesses a higher CMC

(CMC = 9 mM) was used. The nonluminescent cationic surfactant seemed to play a noninnocent role. Indeed for concentration of CTAB above the CMC, both **1** and **2** displayed an increase of their emission intensity as well as an elongation of their excited-state lifetimes, suggesting an incorporation of the metallosurfactant in the CTAB-based micelles. In Fig. 8 are depicted the emission spectra of equimolar mixtures of the metallosurfactants **1** and **2**, upon variation of the concentration of CTAB. These experiments clearly showed the dependence of the intramicellar energy transfer process occurring between the two amphiphilies due to the micellization equilibrium of CTAB.

Thus, such findings demonstrated the possibility to obtain luminescent soft structure made by self-assembling donor/acceptor metallosurfactants based on ruthenium and iridium complexes, in which the energy transfer process can be easily tuned by addition of a nonluminescent surfactant. As a result, two emission colors can be obtained and one could even imagine to have more than two emitters or to combine other properties within the same aggregate. These aggregates could therefore be employed as novel electroluminescent materials, as the size of the spherical aggregates is compatible with ink-jet printing and the emitters can be tuned in color and efficiency in a desired way.

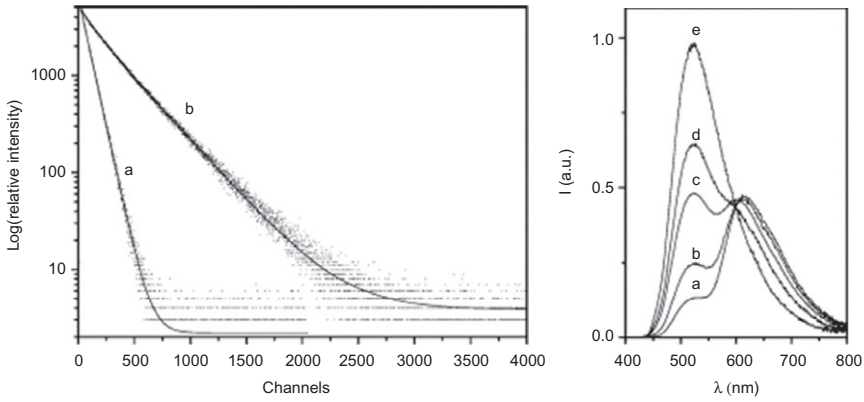

FIG. 8. Left: Time-resolved intensity decays and fits for **1** at (a) 0.01 mM and (b) 0.10 mM in aqueous solutions at room temperature ($\lambda_{exc} = 431$ nm); right: emission spectra of a 1:1 mixture of the complexes **1** and **2**, at different amounts of CTAB. [CTAB] (mM): (a) 0.0, (b) 1.0, (c) 1.5, (d) 2.0, and (e) 3.0 ($\lambda_{exc} = 350$ nm). Reproduced with the permission of the American Chemical Society (*122*).

C. Double Complex Salts

Iridium(III) complexes have been widely explored in the past few decades because of their outstanding photophysical properties and superior photo- and chemical stability (*123–129*). Much effort has been devoted to both neutral and cationic luminescent iridium complexes in which fine-tuning of the energy of their long-lived excited state can be achieved by proper choice of the coordinated ligands (*130–136*).

Work focusing on these compounds was principally prompted by fundamental studies of excited-state electron and energy transfer processes (*137–139*) as well as their potential use as biological sensors (*140*), organic light-emitting diodes (OLEDs) (*141–145*), and light-emitting electrochemical cells (LEECs) (*146–150*).

Besides soft structures containing luminescent metal complexes, strong effort has been devoted to the development of luminescent porous organometallic frameworks as recently reviewed by Allendorf and coworkers (*151*). Also, Kitagawa and coworkers reviewed on the synthetic strategies and properties of functional from 1D to 3D coordination networks (*152–154*). In these materials, the metal atoms play a fundamental role in the structure formation as well as in the spectroscopic properties of the crystalline materials. Several of these structures involve strong covalent interactions as coordination bonds to a mono- or multinuclear metal center, which make them more "robust", as in metal organic frameworks (*155,156*), but also examples consisting of weaker and noncovalent interactions are known (*157*). The latter are usually formed from purely organic compounds linked by hydrogen bonds, and the individual building blocks are commonly referred to as tectons.

Besides these materials, porous organic–inorganic hybrid materials made by organosilica were firstly reported by Inagaki and coworkers (*158*), and since then several examples are known, as reviewed by Fröba and coworkers (*159*) which is, however, a topic outside the aim of this review.

As already mentioned, the supramolecular assemblies can lead to new properties and photoinduced processes which have been studied in great details in solution (see previous section). On the contrary, only few cases of intermolecular photoinduced processes, and in particular, energy transfer, involving transition metal complexes in pure crystalline phases have been reported and will be now discussed. Here, relative orientation and distance between interacting species can be more precisely determined by means of single-crystal X-ray diffractometric analysis.

Taking advantage of weak and noncovalent interactions based on dispersion forces as metallophilic and electrophilic attractions, several efforts were also devoted to assemble extended arrays of metal complexes, for instance, by using double salts of general formula $[M]^+[M]^-$ (*160*). A chain of ligated metal ions with alternating charges require a judicious choice of building blocks with particular steric and electronic needs, as the planarity of the metal complexes involved and the possibility of π-stacking as complementary stabilization force. This theme has been recently reviewed by Doerrer; thus no more room will be devoted to it hereafter (*161*).

Cases of study of double salts in which no metallophilic interaction is involved are also known. In this respect, Schlofer and coworkers first reported an energy transfer studies in Cr(III)-based complexes of formula $[Cr(urea)_6][Cr(CN)_6] \times 3H_2O$. Afterward, Kobayashi (*162,163*), Hauser (*164–166*), and Kaizu (*167–169*), reported on quenching studies in Ru(II)/Cr(III) and Os(II)/Cr(III) mixed double complex salts.

To gain a deeper insight into photoinduced processes in crystalline systems, we recently reported on double complex salts containing more appealing and more luminescent complexes based on iridium phenylpyridil moieties (*170*). These compounds have general formula $[Ir^-][Ir^+]$ and are formed by two highly emitting iridium complexes, which possess different emission colors and complementary charges. Thus, we have combined the cationic orange-emitting compounds $[Ir(dfppy)_2(bpy)]Cl$ (**1a**) and $[Ir(ppy)_2(bpy)]Cl$ (**2a**; dfppy = 4,6-difluorophenylpyridil, ppy = 2-phenylpyridil, and bpy = 2,2′-bipyridil), previously reported by our group, (*140*) with the anionic blue-green-emitting complexes $(n\text{-}Bu_4N^+)[Ir(ppy)_2(CN)_2]$ (**1b**) and $K[Ir(dfppy)_2(CN)_2]$ (**2b**), reported by Grätzel and coworkers (*171*) (see Fig. 9). The double salts are obtained because the small counter-ions yield to easily removable water-soluble salts once the metal complexes are combined. Of course, to have easily detectable and thermodynamically favored processes, the excited-state energies of the two

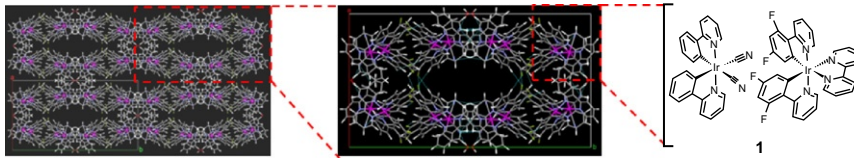

FIG. 9. X-ray crystal structure of a single crystal and its unit cell packing for complex **1**.

complexes must be different. This is the reason for choosing the luminescent ionic complexes possessing complementary colors and high-emission quantum yields.

We were able to precipitate the double salts (**1**) as crystalline materials suitable for single-crystal X-ray analysis, and the structure of one of them shows that they form fascinating 3D porous networks (Fig. 9). As can be easily seen, the pores are formed because of several noncovalent interactions which held together the entire crystalline structure. We noticed that to be able to crystallize the material, a number of characteristics must be incorporated into the building blocks. First, the complexes must have equal and opposite net charges (± 1), the same geometry (in this case, octahedral, C_2 symmetry) to simplify crystal packing, and they must possess as substituents of the coordinated ligands groups able to induce weak interactions as, for example, fluorine to promote halogen–hydrogen or halogen–halogen interactions.

The resulting 3D crystalline supramolecular network devotes about 20% of its volume to host CH_2Cl_2 molecules. The large and isolated channels run along the crystallographic c axis and display an irregular shape with a minimum cross-section of 3.5×11.5 Å^2, which is able to accommodate a sphere whose diameter is 5.1 Å. Interestingly, upon removal of the solvent from the channels, the crystallinity of the compound decreases, but the porosity is maintained. The process of filling and emptying the pores is perfectly reversible, and we demonstrated that the porous network possesses cavities able to host solvent molecules, or electroactive molecules. In the absence of a guest, we observed not only that the emission of the blue-green emitter is completely quenched by energy transfer but also that the emission of the single crystal is bathochromically shifted with respect to the ones which are supposed to be the smaller band gap species, namely, the cations. As revealed by a closer analysis of the packing of single crystal of **1**, a strong π–π interaction ($d = 3.4$ Å) is present between the complementary iridium components. Most likely, this interaction leads to a kind of exciplex formation and emission from a corresponding lower-energy excited state.

Insertion of toluene molecules inside the pores, which most likely increases the distance between the complexes due to the breathing of the crystal, was monitored by confocal microscopy, and a blue shift of the emission accompanied by the visualization of the energy transfer process was detected.

Even more interesting was the possibility to almost selectively quench the cationic iridium complexes by efficient photoinduced electron transfer and to modulate the color of emission of the

crystal. To reach this goal, anthraquinone molecules, good electron acceptors, were inserted by gas-phase inclusion. The photoinduced electron transfer process results in an exoergonic reaction ($\Delta G = -0.51$ eV) for the cationic component, thus leading to the oxidized **2a** and the reduced anthraquinone. As a consequence of the strong quenching of the emission of the red component, the emission spectrum of the crystal displayed an ipsochromic shift, with a shortening of the excited-state lifetime of the red-emitting component (see Fig. 10).

These findings demonstrated for the first time that luminescent complexes made of complementary colors and charges can be used for the creation of a new class of noncovalently linked porous materials and that their properties depend strongly on the intermolecular interactions and on the guests entrapped in their network. Further, due to the different oxidation states of the metals employed, multiredox reactions could be envisaged just upon light excitation. Color modulation has been demonstrated and the active framework could be designed to lead to on/off signal upon recognition of different guests, therefore acting as sensor materials.

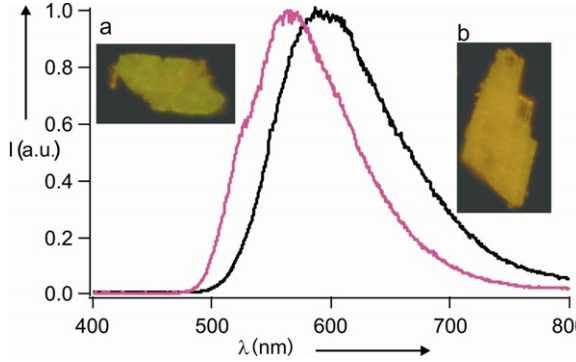

FIG. 10. Confocal microscope emission spectra of a single crystal of complex **1** before (black spectrum) and after (red spectrum) insertion of anthraquinone molecules inside the pores. As can be seen by eyes the emission of the crystal change from orange to green. Reproduced with the permission of Wiley-VCH (*170*).

D. Aggregation-Induced Emission Enhancement in Crystals

It is well known that aggregation of light-emitting compounds, both organic and organometallic, is usually associated with a strong quenching of emission efficiency. This effect was first recognized by Förster and coworker studying the fluorescence of pyrene (*172*). They observed a decrease of the emission intensity upon increasing the concentration of pyrene in fluid solution conditions. Nowadays, it is well established that this phenomenon is almost ubiquitous and involves many aromatic compounds as well as transition metal complexes. Most of the technological applications in which light-emitting molecules are used as emitters in OLED, biological probes and sensors, require a rather high local concentration of such molecules and often the molecules are investigated in solid state. Usually, in these conditions, a strong aggregation-caused quenching effect takes place, which in turn represents a strong limitation in the real world for using these classes of compounds. Finding a way to mitigate this detrimental effect, or even take advantage of aggregation for inducing enhancement of emission, would change the scenario and even create a new class of emitters. In this respect, Tang and coworkers first reported in 2001 on an example of aggregation-induced emission (AIE) (*173,174*). Recently, they reported some possible mechanisms for this phenomena and possible applications of compounds showing AIE effect (*175–178*).

Most of the reported compounds which show this effect are organic molecules (*179–184*), where restriction of intramolecular rotation is generally accounted for being the main cause for AIE (*175,185*). The enhancement is therefore mostly related to the reduction of the nonradiative rate constant rising from the vibrational and rotational mode of the appended groups to the chromophores, which in the aggregates are strongly prevented.

However, few organometallic species based on Cu(I) (*186*), Zn (II) (*187*), Al(III) (*188*), Pt(II) (*189–193*), and Ir(III) (*194–196*) also display color shift, switch on, or enhancement of their emission efficiency upon aggregation. In these cases, several different reasons were considered being involved in the AIE effect, namely metallophilic interaction as in the cases of square-planar Pt(II) complexes, giving rise to new excited state (MMLCT) with larger transition dipole moments associated to increasing radiative rate constants, or π–π stacking of the coordinated ligand. Less common are Ir-based complexes, as the octahedral geometry around the metal center rules out any possible Ir···Ir interaction, thus the formation of intermolecular metal-to-ligand–ligand charge

transfer, restriction of intramolecular relaxation, and establishment of π–π interactions between the cyclometalated ligands in the solid state were arguments to explain the enhancement of the emission (*195–197*).

It is worth to note that crystalline compounds sometimes proved to be more efficient emitters than their amorphous counterparts, showing the influence of molecular packing on the solid-state emission (*177,198*), thus providing optimal conditions to investigate their photophysical properties and the influence of aggregation. The availability of different crystalline phases (polymorphs) of a luminescent molecule is the best example for studying the relationship between crystal packing and optical properties (*188,199–205*). In this respect, we recently reported on two stable concomitant solid-state polymorphs (yellow and orange) of the dinuclear complex $[Re_2(\mu\text{-}Cl)_2(CO)_6(\mu\text{-}4,5\text{-}(Me_3Si)_2pyridazine)]$ (Fig. 11), both showing photoluminescence quantum yields (PLQYs, 0.52 and 0.56), almost one order of magnitude higher than those in solution (*206*).

The compound belongs to the recently reported class of dinuclear, luminescent Re(I) complexes of general formula $[Re_2(\mu\text{-}Cl)_2(CO)_6(\mu\text{-}1,2\text{-diazine})]$ (*207,208*), which display intense, broad, and featureless emission in fluid solution from excited state that can be consistently ascribed to a ^{3}MLCT.

During the crystallization process, the concomitant formation of two crystalline phases of the compound was observed. The concurrent existence of polymorphs provides a unique chance for investigating the factors governing molecular packing. The emission spectra of the two crystalline phases for each single crystal are shown in Fig. 11. As can be seen even by naked eye, the emission has different energies and such a strong shift is most likely due to different local packing of the independent molecules in the

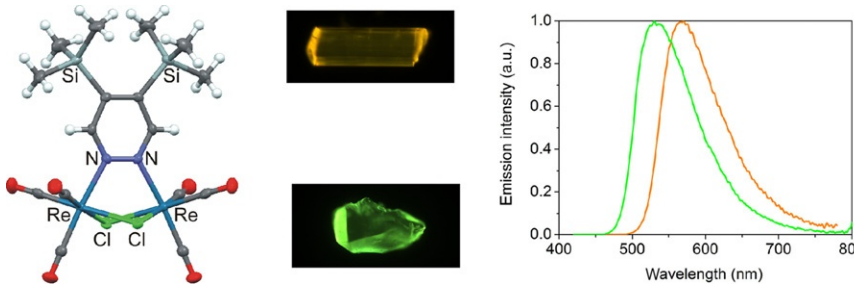

FIG. 11. Left: chemical formula of the crystalline Re(I) complex; middle: images of the two polymorphs under the UV light; right: emission spectra of the two crystalline phases upon excitation at 400 nm.

two polymorphs and, in particular, to the different local organization of molecular dipoles.

Interestingly, both of the crystalline phases exhibit intense photoluminescence (PLQY > 0.50), with excited-state lifetimes in the microsecond regime, suggesting that the emitting excited state has an ^{3}MLCT nature. Most likely, the restricted rotation of the Me_3Si groups in the crystals is responsible for the enhancement of the emission with respect to the solution. This statement is supported by the fact that similar dinuclear complexes lacking the Me_3Si group possess such higher emission quantum yields. This is the first time that intramolecular motions of nonconjugated rotors quench the emission of a luminescent compound in solution.

These findings highlight how packing can strongly perturb the photophysical properties of the molecules even in the absence of particularly short interactions.

IV. Molecular Systems Based on Aggregates of d^8 Metal Complexes

The square-planar coordination geometry of d^8 complexes opens many possibilities for the design of supramolecular architectures. Their tendency toward aggregation and stacking is a crucial feature to trigger self-assembling processes. The preferential stacking geometry imposes a structural constraint that frequently leads to filaments, rods, or needles. Depending on the balance between stacking tendency and solvent affinity, soft or crystalline materials can be obtained. In this sense, the selection of peripheral substituents facilitates a rational design strategy for the manipulation of molecular entities. For instance, balancing the aggregating nature of the square-planar coordination complex with solubilizing moieties of variable aspect ratios and polarities can lead, alternatively, to liquid crystalline structures (*209–211*), flexible fibers (*212–216*), and gelating filaments (*217–221*). The substitution symmetry is a further parameter to be considered for the controlled assembly, while the intrinsic properties of the monomeric constituents can be tuned by judicious choice of ligands.

As previously mentioned, the interaction between protruding, doubly occupied dz^2 orbitals critically affects the photophysical properties upon aggregate formation. Absorption and emission of light, excited-state lifetimes, and redox properties are dramatically affected. A particularly interesting feature is represented by the possibility of tuning the distance between the monomeric units and, consequently, the degree of electronic coupling

between the interacting metal orbitals. The introduction of bridging or spacing ligands can tune the color of dimeric Pt(II) complexes: bringing them closer causes a red-shifted absorption and emission, while widely spaced units resemble the monomeric species. It has been shown that they can form aggregates or even excimers, causing shifts in the emitted wavelengths and affecting the photoluminescence quantum yields (*222,223*). These tunable properties and the fact that platinum complexes emit from a triplet state have been exploited in several optoelectronic applications (*224–232*). Even though these aggregates can be exploited for the construction of white organic light-emitting diodes (*233–236*), it also constitutes a disadvantage for technological applications where color purity is desirable. Therefore, controlling the aggregation and being able to predict and design appropriate compounds with the desired properties are an important step to fully exploit their potential for technological purpose. We will highlight the most important achievement in this area and try to correlate the chemical structures with the observed photophysical behavior. We will discuss not only 1D, 2D and 3D architectures but also crystalline systems. An interesting feature of the crystals is represented by vapochromism: exposure to different solvents, which occupy cavities within the framework, causes the unit cell to "breathe," thus shifting the distance between the metal centers. This variable interaction can be employed for sensing purposes, due to the switchable emission of the frameworks (*237–244*).

A. 1D Arrays

Terpyridine, N^N^N ligands (*245–249*) and their N^C^N and N^N^C analogues (*250–257*) have been successfully coordinated to Pt(II), leading to neutral, mono- or doubly charged species, which in some cases display bright luminescence, both in degassed fluid solutions and frozen matrices. In particular, it has been shown by Che *et al*. that they can form supramolecular structures, such as nanowires, nanosheets, and polymeric mesophases, with interesting optical properties (*214–216,258*).

As an example, cationic cyclometalated/terpyridyl platinum(II) complexes bearing arylisocyanide/arylacetylide ligands possessing highly emissive triplet MLCT or MMLCT excited states in solution and in the solid state (*214*) have been investigated. The molecular aggregation through Pt···Pt or ligand–ligand interactions is significant for these two classes of planar platinum(II) complexes, and as they are robust toward moisture, air, and light irradiation

and exhibit high-emission quantum yields, their use in electrically driven devices has been exploited. The researchers demonstrated that crystalline, waveguiding, semiconducting, and electroluminescent nanowires can be self-assembled through extended intermolecular interactions, and ambipolar organic, light-emitting field effect transistor devices emitting in the red or NIR region have been fabricated by solution processing (Fig. 12).

Che *et al.* (*215*) extended the assembly into aqueous environments, describing the preparation of supramolecular polyelectrolytes by self-organization of cationic organoplatinum (II) complexes in water through extended Pt···Pt and hydrophobic interactions (Fig. 13). Aligned films and discrete uniaxial microfibers with cofacial molecular orientations were readily produced with these phosphorescent viscoelastic mesophases.

Even more interesting are the crystalline, wheel-shaped superstructures described by Che *et al.* (*216*), which grow through a wire-to-wheel metamorphism process involving a ligand-substitution reaction (Fig. 14). Organometallic molecules and noncovalent intermolecular metal–metal and ligand–ligand interactions were employed to construct submicrometer-sized nonlinear superstructures. Due to the optoelectronic properties of organoplatinum(II) complexes, novel mesoscopic applications based on the superstructures could be envisaged. The interplay between closed-shell Pt···Pt interactions and electrostatic/Coulombic interactions leads to the formation of organoplatinum(II) superstructures with diverse morphologies. The preliminary studies carried out have shown that the reported metamorphism

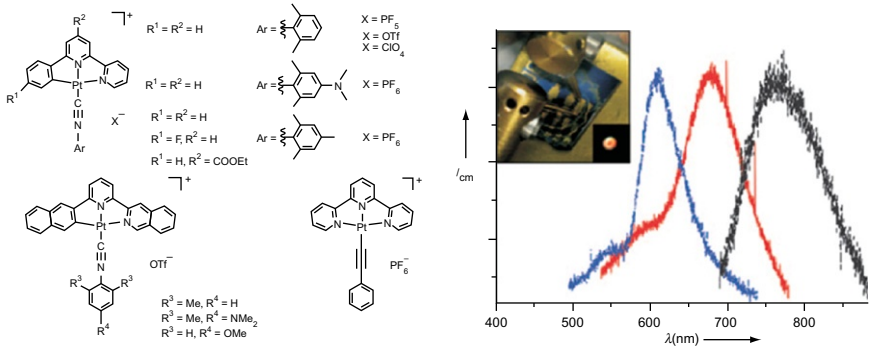

FIG. 12. Molecular structure of Pt(II) complexes and their emission in organic light-emitting field effect transistors. Reproduced with the permission of Wiley-VCH, Ref. (*214*).

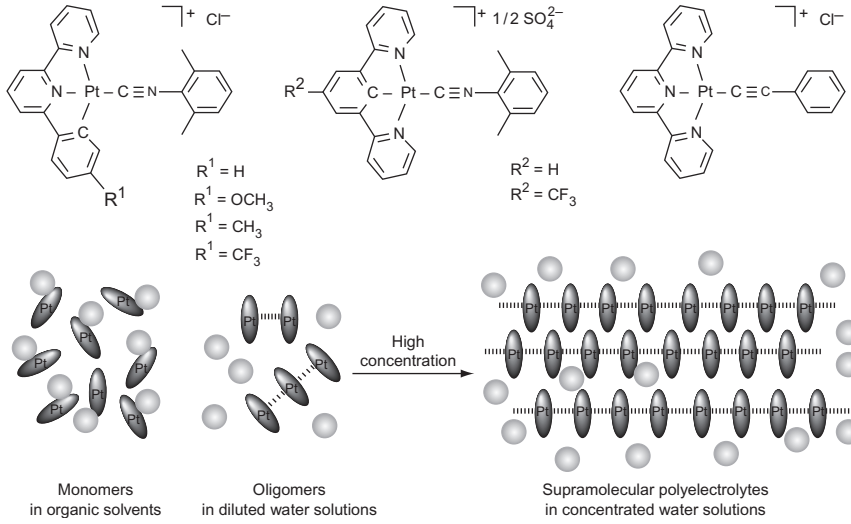

FIG. 13. Self-assembly of ionic Pt(II) complexes in aqueous environments. Reproduced with the permission of Wiley-VCH (*215*).

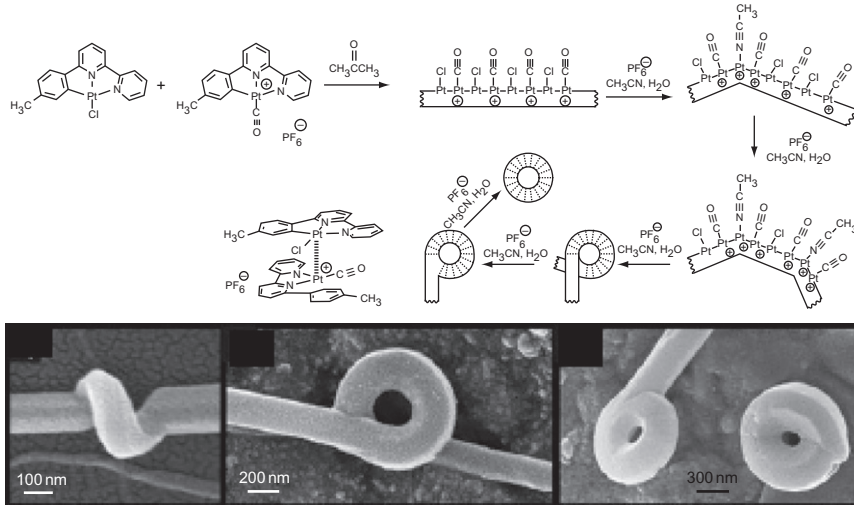

FIG. 14. Assembly of neutral and cationic Pt(II) complexes into linear filaments undergoing a wire-to-wheel metamorphism. SEM micrographs are shown on the bottom. Reproduced with the permission of Wiley-VCH (*216*).

process can tolerate chemical modification on the cyclometalated ligand, which further expands the capabilities of such assemblies.

This work could therefore trigger some interesting developments in the use of labile ligands which could induce conformational changes in nano/microstructures resulting in modulation of mechanical properties.

Employing a rather different structural motif, Aida and coworkers (*212*) successfully developed different types of nanotubes with walls of pyridine–platinum(II) coordination layers by using pyridyl-appended hexabenzocoronene. The self-assembling process was triggered by vapor diffusion or heat–cool cycles. When the nanotubes were suspended in CH_2Cl_2 solutions, all of them disassembled into the corresponding monomers. In contrast, the nanotube obtained by the coassembly with cross-linking *trans*-[$Pt(PhCN)_2Cl_2$] under heat–cool conditions was tolerant against dissociation. However, in the coassembly with *trans*-[$Pt(PhCN)_2Cl_2$], the metal coordination could take place both at an inter and intramolecular level (Fig. 15). Interestingly, structure of the nanotubes affects the electrochemical properties that depend on the degree of shielding of the metallic centers.

B. 2D Arrays

Che and coworkers (*258*) accomplished a further dimensionality in free-standing and crystalline nanosheets self-assembled from neutral pincer-type cyclometalated platinum(II) aryl acetylides. The complexes in solid state display various colors, depending on the substituent on the aryl acetylide ligand (Fig. 16). When electron-withdrawing groups, electron-donating groups, or neutral groups are introduced, the solid is bright yellow, deep red, or dark green in color, respectively. They showed that these organoplatinum(II) complexes can self-assemble into nearly bidimensional nanostructures displaying near infrared phosphorescence and light-modulated conductivity. The molecular organization in the nanosheets is due to orthogonal Pt$\cdots$Pt and C—H$\cdots\pi$(C—C) interactions, highlighting that phosphorescent platinum complexes provide an entry to 2D supramolecular nanomaterials with particular optoelectronic properties derived from metal–metal interactions.

Yam *et al*. (*259*), however, employed platinum(II) 2,6-bis(1-alkylpyrazol-3-yl)pyridyl complexes with various chain lengths of the alkyl groups on the nitrogen atom of the pyrazolyl units to form stable and reproducible Langmuir–Blodgett films at the

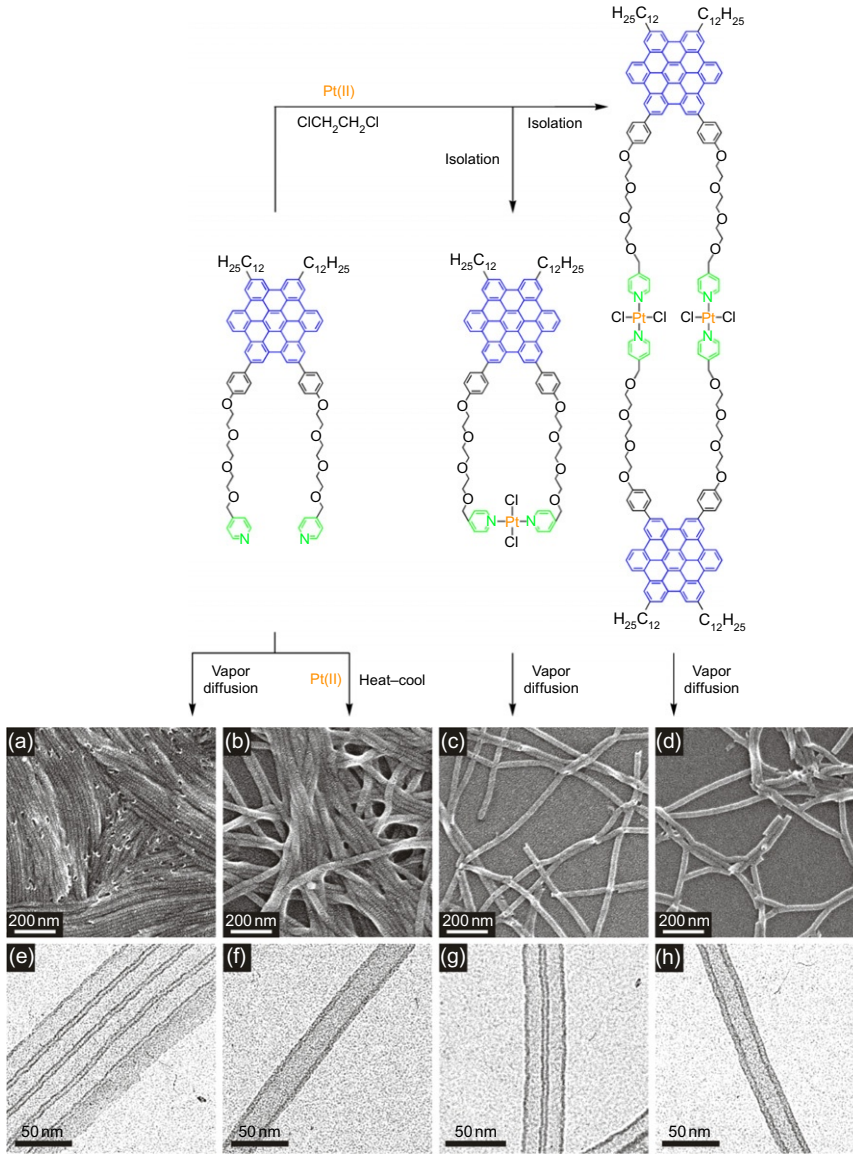

FIG. 15. Molecular structures and supramolecular assemblies obtained under different conditions, as described by Aida *et al*. SEM (a–d) and TEM (e–h) micrographs of the tubes are shown. Reproduced with the permission of Wiley-VCH (*212*).

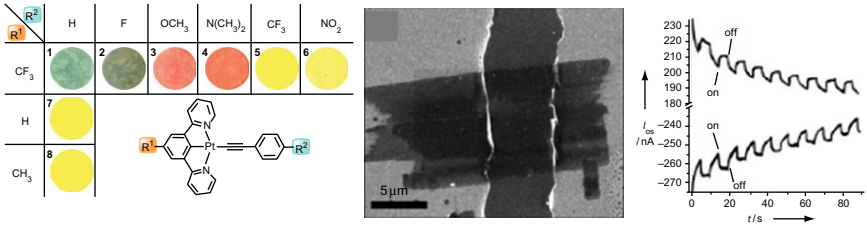

FIG. 16. Structure–color correlation table of Pt(II) complexes (left). The SEM image of a bottom-contact FET device with nanosheets as semiconducting materials is shown (center). Transient conductivity measurement of the FET device (right). The transient channel current was recorded with a light switching on and off every 5 s in a 90-s period. Reproduced with the permission of Wiley-VCH (*258*).

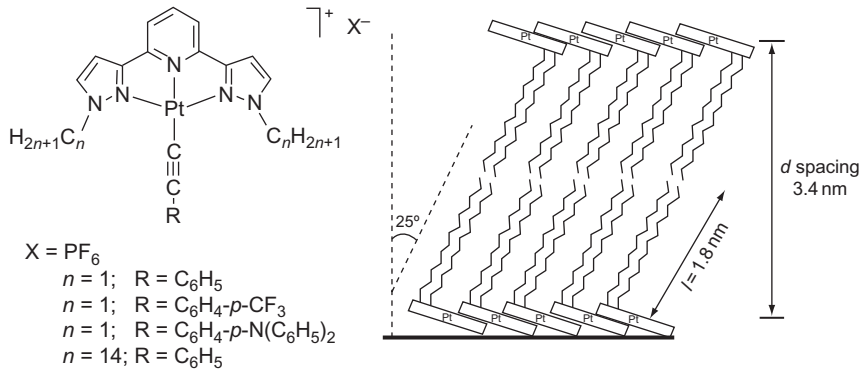

FIG. 17. Selected Pt(II) complexes (left), as described by Yam *et al*. Proposed structure of self-assembled films with $n = 14$, and a chloride replacing the acetylide anion (right). Reproduced with the permission of Wiley-VCH (*259*).

air–water interface (Fig. 17). Surface pressure–area (*p–A*) isotherms, UV/vis spectroscopy, XRD, X-ray photoelectron spectroscopy, FTIR, and polarized IR spectroscopy, as well as luminescence properties in films were successfully investigated. A 47-layer film of the complex with $R = C_6H_5$ $n = 14$ (see Fig. 17) was found to exhibit a low-energy emission band at 693 nm, which is indicative of the presence of Pt···Pt interactions and/or π–π stacking as a result of the close molecular packing in the ordered arrangement, as revealed by the characterization in the *p–A* isotherm and XRD pattern. The origin of these low-energy emission bands was tentatively assigned as MMLCT

and excimeric emissions derived from the stacking of the platinum(II) 2,6-bis(1-tetradecylpyrazol-3-yl)pyridyl moieties in the film.

In a different approach, Bruce and coworkers (*210*) described the preparation of liquid-crystalline derivatives of a N,C,N-Pt (II) luminophore (Fig. 18). Interestingly, they found that emission in the liquid-crystal phase is characteristic of the monomeric complex, while excimer-like emission normally characterizes nonliquid-crystalline analogues. They showed that the emission of pure films is responsive to both method of preparation and tribological stimulation so that it is possible to switch in a controllable manner between monomer- and excimer-like states.

Bruce *et al.* (*211*) also investigated the liquid crystalline and luminescent properties of two rod-like, orthoplatinated complexes bearing a β-diketonate coligand (Fig. 19).

The parent ligands exhibit a rich, smectic polymorphism, but when modified with a fused cyclopentene ring, nematic phases dominate. Reaction of the ligands with tetrachloroplatinate(II) leads to poorly soluble, dimeric complexes that can be cleaved using dimethylsulfoxide; the resulting monomeric complexes are then readily converted to the β-diketonate complexes. All of the complexes are mesomorphic, and the β-diketonate complexes

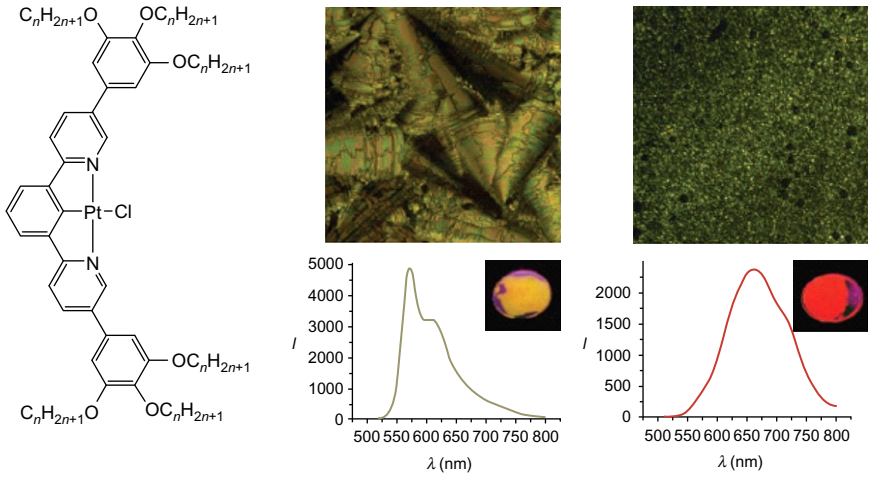

FIG. 18. Selected structure of Pt(II) complexes. For $n = 6$, at room temperature, top: real samples of pure films sandwiched between glass slides; bottom: emission spectra (excitation at 420 nm). Left: fast cooled from the LC phase after the texture is fully developed. Right: fast cooled direct from the isotropic phase. Reproduced with the permission of Wiley-VCH (*210*).

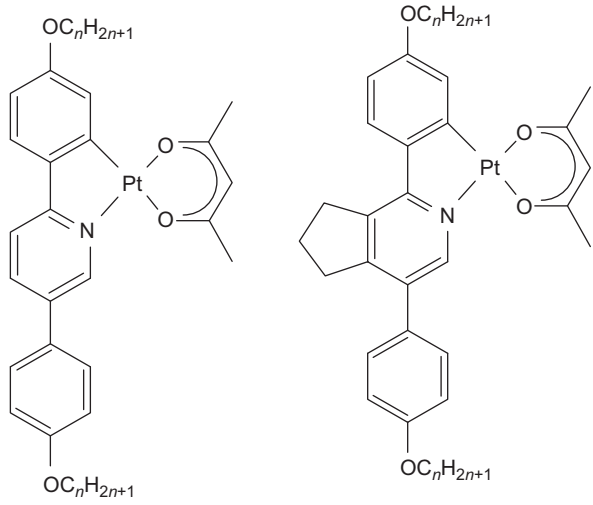

FIG. 19. Orthoplatinated rod-like Pt(II) complexes. Reproduced with the permission of the American Chemical Society (*211*).

have excited-state lifetimes of 27 μs with emission quantum efficiencies exceeding 0.5. Intermolecular organization clearly has a significant effect on emission characteristics. Thus, the combination of emitter and liquid crystalline properties offers control over the nature of the emission via the molecular organization. The high-luminescence efficiency coupled with the potential to align the complexes in the liquid crystal phase promises to yield highly dichroic emission.

C. 3D NETWORKS

Low-molecular weight organo- or hydrogelators have been widely investigated (*260–265*); the operating mechanism of gelation has been identified as a supramolecular effect, where the constituting fibers, usually of microscale lengths and nanoscale diameters, are formed in solution predominantly by unidirectional self-assembly of gelator molecules (*266–269*). The entanglement of many filaments gives a network that entraps the solvent molecules within the compartments. In most cases, the intermolecular interactions are electrostatic, hydrogen bonds and $\pi-\pi$ stacking and are induced by heating and cooling of the solution and most recently by ultrasounds (*270*). We also have demonstrated that gel formation in water can be induced by

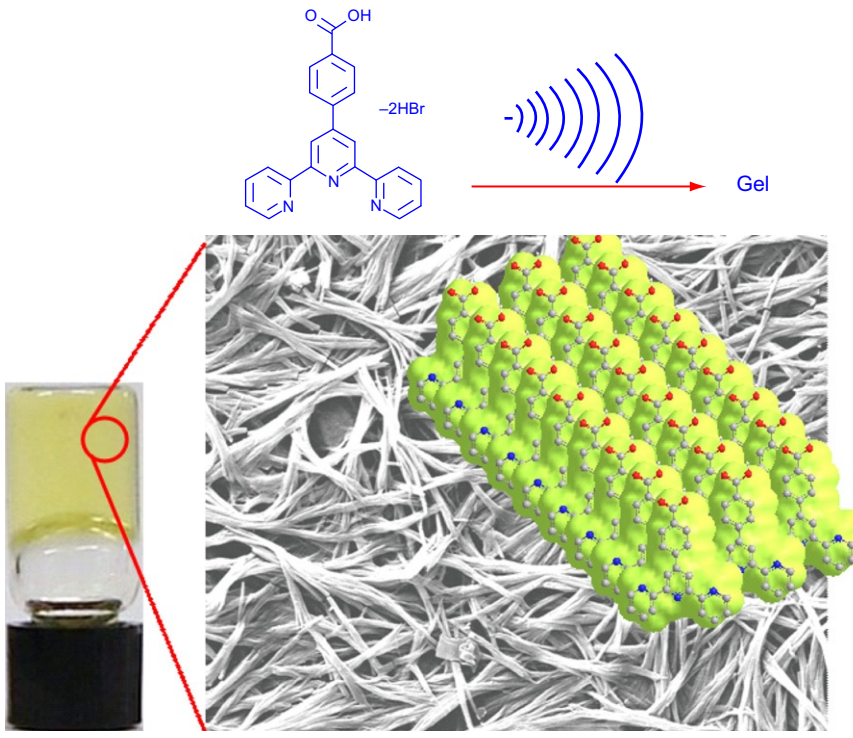

FIG. 20. Stable hydrogel is formed with terpyridine-type systems upon application of ultrasound to the water solution. Left: picture of the gel; right: SEM image of the gel and cartoon representation of possible stacking of the molecules to form 3D networks. The nature of the gels can be modulated by the addition of metal ions. Reproduced with the permission of the Royal Society of Chemistry (*271*).

ultrasounds, which constitutes a reversible process (*271*). Figure 20 shows our findings based on the use of substituted terpyridine ligands which are able to gelate in water even in the presence of metal ions which can coordinate the tridentate ligand. Emission can be observed from the gel depending on the nature of the metal ions.

As supramolecular gels provide fibrous aggregates with long-range order, they are heavily used in biology and medicine as extracellular matrix, drug delivery, and cosmetics, but they could be also of interest in the fields of optoelectronic devices and sensors. In this context, organometallic gelators can display multiple functionalities and properties which combine ligands or organic fragments and metal ions which further can lead to metal–metal interactions influencing their properties (*272*).

Our interest not only in luminescent gels but also in the use of metal complexes to monitor the gelation process started in 2007 (*273*). In these studies, gels were prepared by using alternatively a carboxylate-based aliphatic gelator bearing adamantyl substituents, or an anisole-substituted oxalamide derivative. The cohesion between the small molecules assembling into filaments was given by hydrogen bonds, while the balance between the hydrophobic or hydrophilic backbone bearing adamantane or anisole moieties, respectively, determined the gelating ability either in DMF or water. The gels were doped with an hemicaged Eu(III) complex, which was retained in the cavities containing the entrapped solvent, which was monitored by the excited-state lifetime of the lanthanide complex. The red-emitting unit effectively acted as a sensor of the solvent environment within the gel. However, the self-assembly process yielding the hydrogel was nicely probed with the aid of a Ru(II) complex, which is not luminescent in aqueous environments. The luminescence was turned on upon gelation, due to the fact that the organometallic species intercalated into the hydrophobic pockets of the network, thus allowing a highly sensitive monitoring of the self-assembly.

These findings constitute a basis for the use of luminescent probes, able to change their properties upon solidification of the systems, for the monitoring of bond forming and breaking in soft materials. To make use of the luminescence switching effect upon self-assembly, we developed a Pt(II) complex that by itself is nonluminescent, but is able to stack into luminescent gelating nanofibers (*217*). The neutral, soluble Pt(II) coordination compound bears a dianionic tridentate, terpyridine-like ligand. The coordination of an alkyl-pyridine ancillary moiety to the 2,6-bis-tetrazolyl-pyridine-based complex enhanced the solution processability.

The Pt(II) gelator is nonemissive in diluted solution. However, in frozen CH_2Cl_2 matrix at 77 K and in thin films, it displays a bright unstructured luminescence centered at 570 nm and also shows an intense absorption band around 420 nm, a feature that is not present in solution at room temperature. The photoluminescence quantum yield reaches up to 87%, and the emission spectra do not depend on the excitation wavelength. These results are particularly remarkable considering that Pt(II) complexes usually show rather low-emission intensity and strongly concentration-dependent emission due to aggregate or excimer formation in the solid state and in thin film. The photophysical characteristics unambiguously point toward aggregation processes in the ground state that lead to excited ^{3}MMLCT states, facilitated by the interaction between the axial

dz^2 orbitals of the central Pt(II) atoms. In this case, this phenomenon only becomes evident in frozen matrix and in thin film where aggregate formation is favored. Therefore, the turn on of the bright luminescence upon aggregation can be employed to monitor the assembling process with high sensitivity.

The formation of fibers in solution was clearly revealed by fluorescence microscopy and scanning electron microscopy (see Fig. 21). The fibers self-assemble in larger entangled structures but their emission properties remain unchanged. Diffusion of hexane into the colorless, nonemissive solution of the complex in $CHCl_3$, affords a self-assembled yellow gel that appears highly luminescent under UV irradiation (see Fig. 21, bottom right). A close inspection by SEM revealed a 3D network of fibers responsible for the structure of the emissive soft material, and TEM analysis (see Fig. 21, bottom right) showed the interlocking nature of the nanofibers. The spectroscopic features prove that the gel is an extremely efficient emitter, with up to 90% emission

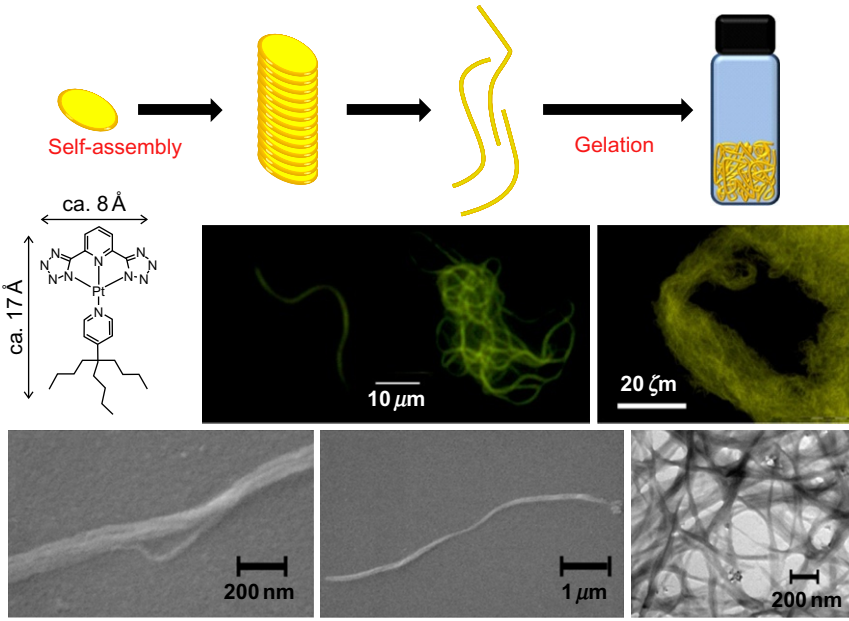

FIG. 21. Top: schematic representation of the subsequent aggregation and gelation processes with the Pt(II) complex. Middle: fluorescence microscopy images of the aggregates, and (right) of the gel. Bottom (left and center): SEM: micrographs of the self-assembled fibers and TEM micrograph (bottom, right) of the self-assembled gel. Reproduced with the permission of Wiley-VCH (*217*).

quantum yield. The soft assembly also displays not only the highest photoluminescence quantum yield and radiative rate constant but also the lowest radiationless deactivation rate, if compared with doped polymethylmetacrylate and neat films. This points to the high degree of order within the filaments, which favors radiative processes and minimizes nonradiative pathways.

Self-assembly of Pt(II) complexes yielding luminescent liquid crystals (*210,211,274*) and AIE (*275–279*) have been already described, but metal complexes forming soft structures with such intense phosphorescence are very rare.

Further, the use of aggregates to build up electroluminescent devices is a new interesting strategy not only to develop novel colors but also to take advantage of the AIE in real applications. Therefore, we have explored the application of the Pt aggregates in solution-processed OLED devices, showing high brightness and good color purity (*217*).

Dötz *et al.* (*218*) developed robust functional organometallic compounds as low-molecular mass gelators, with the aim to introduce the unique properties of organopalladium catalysts into organometallic gelators. They described a palladium pincer bis(carbene) complex constituting an efficient organometallic gelator for a variety of protic and aprotic organic solvents even in concentrations as low as 0.2 wt% (Fig. 22). NMR spectroscopy and X-ray diffraction studies indicated that π stacking of the heteroarene moieties, van der Waals interactions between the alkyl chains, and metal–metal interactions may be responsible for the aggregation. It represents an air-stable organometallic low-molecular mass gelator that is readily accessible from commercial precursors and, moreover, reveals promising catalytic activity in C—C bond formation even in the gel state.

The approach was further extended by the introduction of novel pincer-type, pyridine-bridged bis(benzimidazolylidene)–palladium complexes, which were synthesized reacting readily accessible commercial precursors under microwave assistance (*219*). Despite the simplicity of their structures, the carbene complexes constituted low-molecular mass metallogelators (Fig. 23). They efficiently gelate not only a broad variety of protic and aprotic organic solvents but also different types of ionic liquids (such as imidazolium, pyridinium, pyrazolidinium, piperidinium, and ammonium salts) at concentrations as low as 0.5 mg mL^{-1}. The morphologies of the resulting 3D gel networks composed of long and thin fibers were studied by TEM and light microscopy for a selection of organic and ionic liquids, showing that the achiral gelators assemble into helical fibers. The thermal stability of the gel is enhanced at increasing

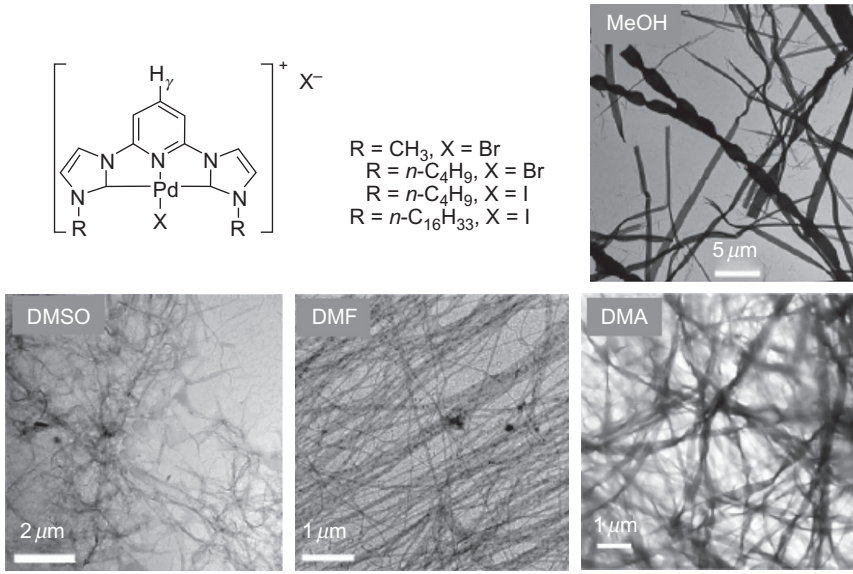

FIG. 22. Structure of gelating Pd(II) complexes described by Dötz *et al*. Selected TEM micrographs of gels obtained from different solvents are shown. Reproduced with the permission of Wiley-VCH (*218*).

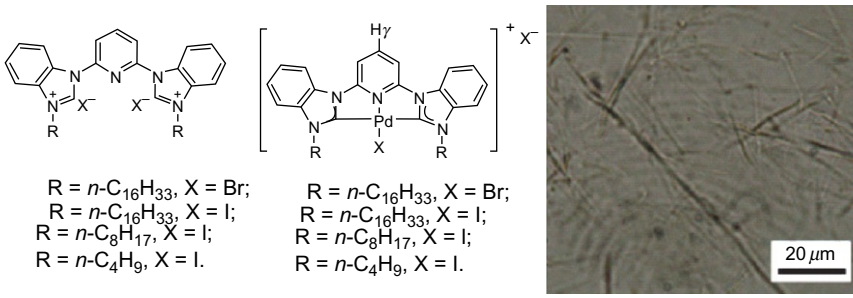

FIG. 23. Structure of gelating Pd(II) CNC pincer ligands and their Pd(II) complexes described by Dötz *et al*. Selected dark-field optical micrograph of a gel obtained with liquid crystals is shown. Reproduced with the permission of Wiley-VCH (*219*).

concentrations of gelator, which was shown by thermoreversible DSC studies. Temperature-dependent NMR and X-ray diffraction experiments, as well as comparisons with analogues substituted with shorter alkyl chains, suggested that the 3D networks

are based on noncovalent interactions, such as π-stacking, van der Waals forces, and hydrogen and metal–metal bonding. Pure ionic liquids and those entrapped within the gels showed comparably high conductivities, which renders pyridine-bridged bis (benzimidazolylidene)–palladium pincer complexes as air-stable metallogelators that efficiently immobilize ionic liquids in low gelator concentrations indicating, apart from catalysis, their potential application in electrochemical devices.

Shinkai *et al*. (*265*), however, employed bidentate ligands to produce planar, stacking complexes of Cu(II), Pd(II), and Pt(II). 8-quinolinol/copper(II)-, palladium(II)-, and platinum(II)-chelate-based organogelators and their nongelling reference compounds were synthesized. The complexes gelated various organic solvents at very low concentrations. Electron microscopy gave visual images of well-developed fibrous structures characteristic of low-molecular weight organogels. UV/vis and FTIR spectroscopy revealed that the outstanding gelation ability arises from the π–π interactions of the chelate moieties and the hydrogen-bond interactions between the amide groups. The nanofibers are evidently different depending on the electronic states of the different central metals. The Pt gel shows unique thermo- and solvatochromism of absorption and emission color in response to a sol–gel transition (Fig. 24). Further, the Pt gel possesses an attractive ability to avoid dioxygen quenching of excited triplet states, which has a positive effect on the phosphorescence

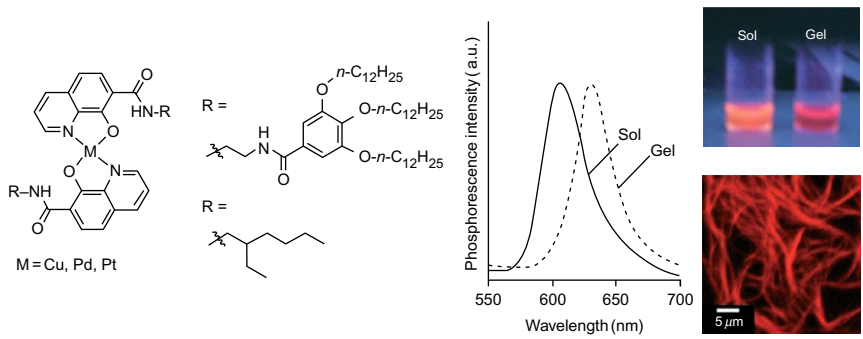

FIG. 24. Quinolinate metal complexes described by Shinkai *et al*. Phosphorescence spectra and photographs of sol and gel phases of a gelating Pt(II) complex are shown, as well as a confocal scanning laser microscopy micrograph of the gel. Reproduced with the permission of Wiley-VCH (*265*).

quantum yield, which is attributed to the isolation of the luminescent chelate from the oxygen dissolved in the liquid phase. These findings consistently indicate that introduction of metal chelates into the gel is one of the most effective strategies toward a variety of photo- and electrochemical nanomaterials.

A last example refers to the complexes described by Yam *et al.* (*220*). They have synthesized a series of alkynylplatinum(II) terpyridyl complexes and investigated their electrochemical, photophysical, and luminescence properties. Some of the complexes were found to exhibit stable thermotropic metallogels in organic solvents and were morphologically characterized by transmission electron microscopy and scanning electron microscopy (Fig. 25). One of them showed drastic color changes from a deep-purple gel to an orange sol during the gel-to-sol phase transition. In the variable temperature UV–vis absorption study of a DMSO gel, the MMLCT absorption shoulder at 580 nm disappears completely above the sol–gel phase-transition temperature (T_{gel}), indicating that Pt···Pt and π–π interactions are involved in the process of metallogelation and are completely destroyed in the sol form at elevated temperature. This is further supported by the observation of the complete switching off of the ^{3}MMLCT emission at 780 nm at T_{gel}. The DMSO metallogels also displayed different colors, with different UV–vis and emission spectral traces depending on the nature of the counter anions, which governs the degree of aggregation and the extent of Pt···Pt and π–π interactions in the gel phases, which results in the formation of different supramolecular architectures. The systematic study of these alkynylplatinum (II) terpyridyl complexes has led to a better understanding of the factors that direct the gel-formation properties. Longer hydrocarbon chains are found to enhance solubility in most common organic solvents hindering the formation of stable metallogels, whereas bulky *tert*-butyl substituents on the terpyridyl ligand forms less stable metallogels, as reflected by its higher critical gelation concentration and lower sol–gel transition temperature than the unsubstituted terpyridyl analogue. Metal–metal and π–π interactions have also been established to play important roles in the stabilization of these metallogels. This demonstrates the subtle interplay of factors influencing the formation and stability of these metallogels and shows that with modifications of the ligands as well as variation of the organic solvents, the electronic absorption, and luminescence properties could readily be tuned.

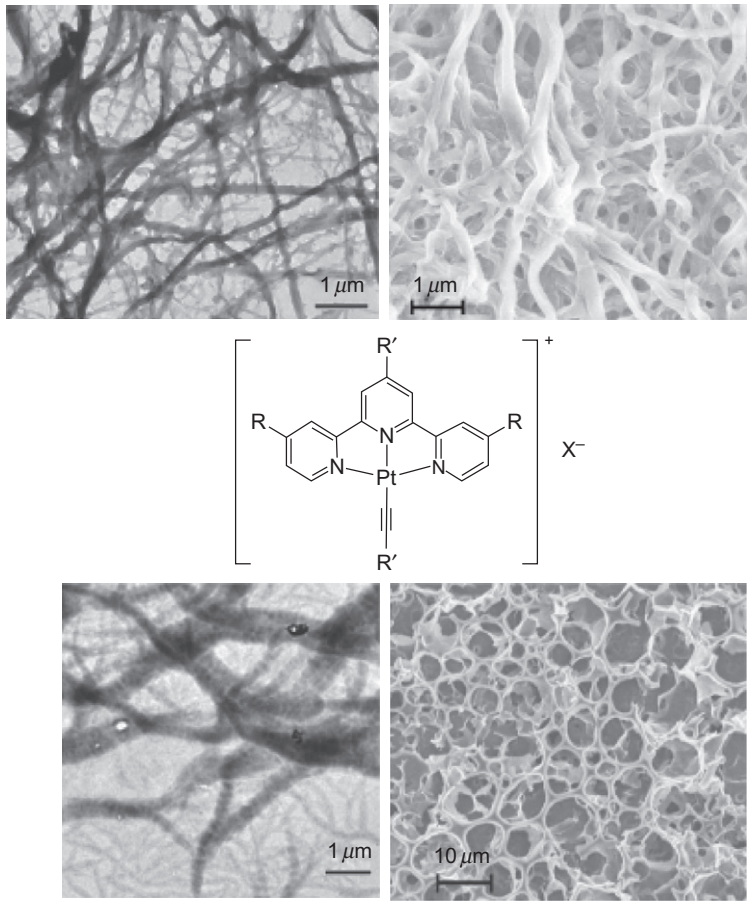

FIG. 25. General structure of gelating terpyridine-based Pt(II) gelators described by Yam *et al*. TEM (left) and SEM (right) images of selected xerogels prepared from a DMSO gel (top), and a benzene gel (bottom). Reproduced with the permission of the American Chemical Society (*220*).

In a further step, Yam and coworkers constructed helical superstructures employing chiral alkynylplatinum(II)–terpyridyl complexes, obtaining metallogels that show helical fibrous nanostructures. The chiral supramolecular structure and the spectroscopic properties depend on the extent of aggregation through Pt···Pt and π–π interactions, which can be influenced by varying the nature of counteranions, as revealed by UV/vis, circular dichroism, and luminescence studies (*221*).

D. Crystalline Assemblies

Eisenberg *et al.* (*240*) reported a Pt(II) terpyridine complex bearing a nicotinamide moiety. The complex is brightly luminescent in the solid state at room temperature exhibiting a remarkable reversible vapochromic behavior and crystallographic change in the presence of several volatile organic solvents (Fig. 26). Upon exposure to methanol vapors, it shifts color from red to orange, and a displacement to higher energy is observed in the emission maximum with an increase in excited-state lifetime and emission intensity. The crystal and molecular structures of the orange and red forms, determined by single-crystal X-ray diffraction on the same single crystal, were equivalent at molecular level and only modestly different in terms of packing. In both

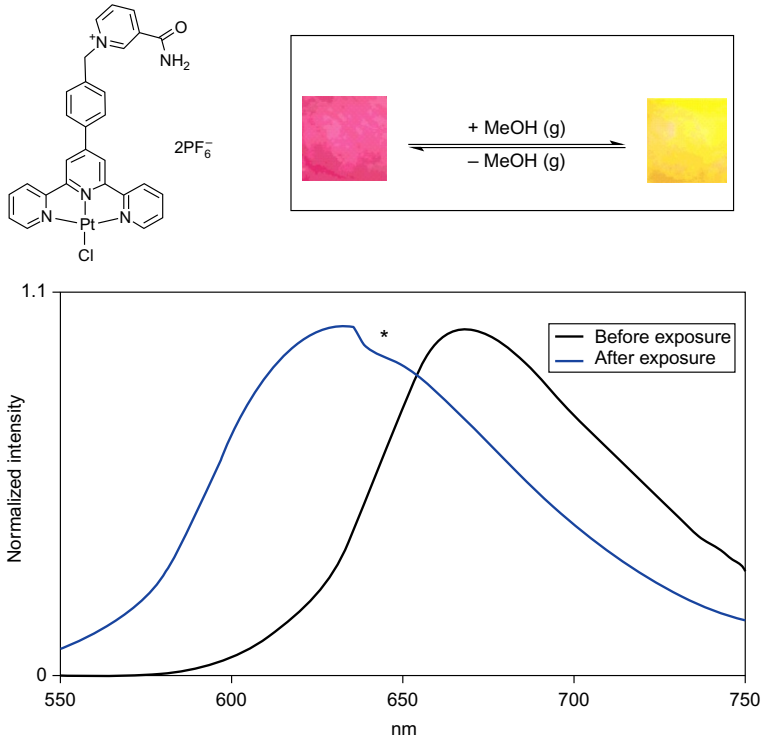

Fig. 26. Pt(II) complex displaying reversible color and luminescence switching after exposure to MeOH vapor, as described by Eisenberg *et al.* Reproduced with the permission of the American Chemical Society (*240*).

forms, the complex possesses a distorted square-planar geometry. Investigation of the orange form's crystal packing revealed the presence of solvent molecules in lattice voids, with Pt···Pt distances averaging 3.75 Å and a zigzag arrangement between nearest neighbor metal centers. However, the red form is devoid of solvent within the crystal lattice and contains complexes stacked with an almost linear arrangement of Pt(II) ions having an average distance of 3.33 Å. These results evidently demonstrate that sorption of methanol vapor induces a change in intermolecular contacts and Pt···Pt interactions in going from red to orange. Disruption of the d^8–d^8 interactions shifts the emitting state from a triplet MMLCT state in the red form to one in which the HOMO corresponds to a more localized metal orbital in the

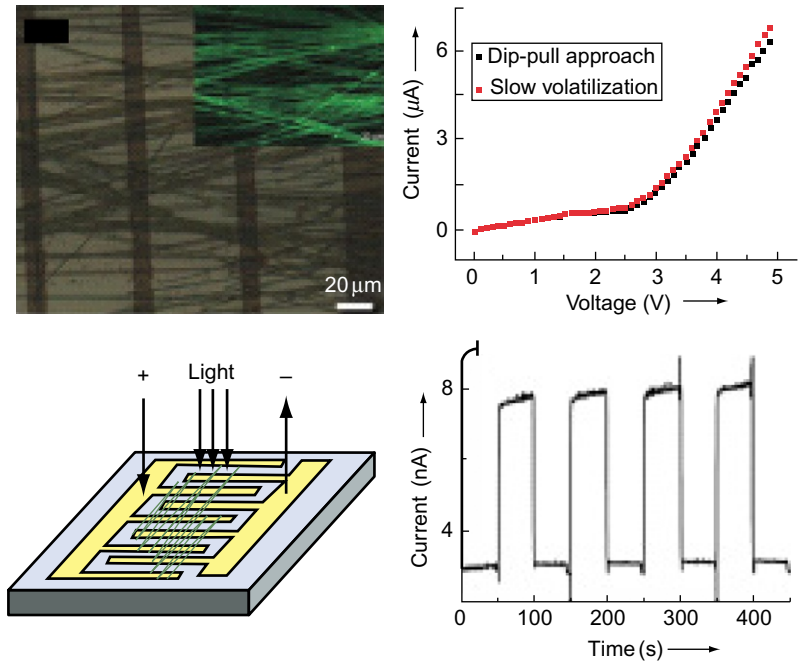

FIG. 27. Top left: image of the device. Inset: luminescence image of microwires. Top right: I–V curves of microwires produced by slow evaporation (red line) and dip-and-pull approach (black line). Bottom left: schematic diagram of the device used for the detection of light. Bottom right: photocurrent of the device (excitation wavelength: 450 nm), which can be switched on/off rapidly by illumination under voltage bias of 0.5 V. Reproduced with the permission of the Royal Society of Chemistry *(244)*.

orange form (triplet MLCT). Further, the complex displays a selective and fully reversible vapochromic response to MeOH, CH_3CN, and pyridine.

Che and coworkers (*244*) went a step further and made use of the vaporesponsive behavior in optoelectronic devices. Semiconducting microwires of $[Pt(CN\text{-}tBu)_2(CN)_2]$ were obtained on substrates by solvent evaporation or dip-and-pull approaches, showing photo- and vapor-responsive conducting characteristics. The characterization of photoresponsive transistors employing the above-mentioned microwires revealed that the microwires constitute ambipolar semiconducting materials (Fig. 27). The photoinduced conducting characteristics suggest that the assembled complex possesses stimuli-responsive features with potential applications in semiconductor devices, such as photodetectors. Interestingly, the exposure to different environments can markedly affect the conductivity.

Changes in the crystal structure can be also triggered by mechanical stimuli, as elegantly shown by Shinozaki *et al.* (*243*). The mechanochemical behavior of Pt(II) complexes bearing cyclometallating tridentate ligands was investigated in terms of solid-state luminescence. The yellow luminescence of the crystalline complex changed to orange when grinded into fine powder (Fig. 28). A broad emission band, which was not detected for the crystal, was observed in the red region of the electromagnetic spectrum for the powder. The phenomenon was very similar to the excimer formation observed in solution. The excimeric state formation is facilitated by the mechanical grinding, and it is described by the quantum chemical mixing of ground and excited

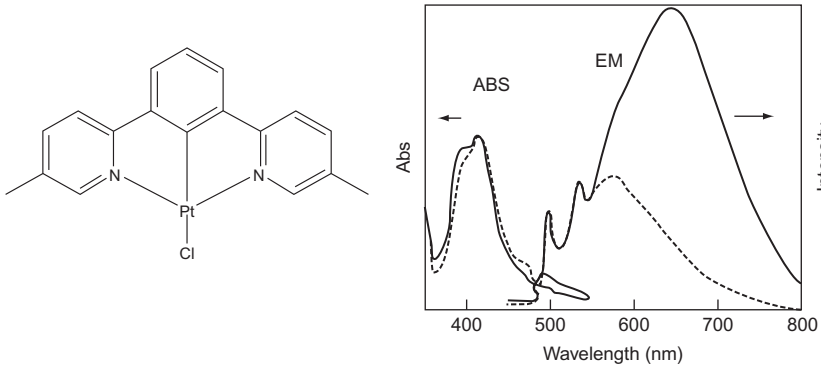

FIG. 28. Mechanoresponsive Pt(II) complex described by Shinozaki *et al.*, which changes color and luminescence upon grinding. Reproduced with the permission of the American Chemical Society (*243*).

electronic states that depend on the distance between the complex molecules. Such crystalline materials could find applications in mechanical sensing.

V. Conclusions and Open Questions

In conclusion, the number of functional aggregates in which new properties are generated by the assembly process is already very large and growing every day. We have shown that it is possible or potentially achievable to modulate optical properties, catalytic activity, conductivity, magnetic and mechanical properties and to have sensing behavior. The role played by the ligands coordinated to the metal ions and the solvents in which the assemblies are formed are key parameters for the interactions within aggregates. In fact, a clever design of the organometallic species can lead to aggregates with emerging properties and novel functions that can be reversibly and dynamically tuned. This behavior resembles the dynamic nature of living systems able to self-organize and adapt in different environments. The question is how much we can rationalize the behavior and predict the soft structures on the basis of the molecular design. Can we foresee that also with metal complexes we are able to interconvert from a soft structure, for example, micelle to another one, for example, fibers or gels by an external input? How far could we go in studying the interactions of such responsive (nano)structures with others, for example, recognition of biomolecules, creation of artificial patterned surfaces, multicatalytic sites using different activatable catalysts? How many different metal complexes acting as energy and electron donor or acceptor species could we organize, for instance, to realize an artificial noncovalent light-harvesting system? Could we have crystalline materials in which we could use the metal complex framework to perform photoinduced multiredox reactions inside the cavities?

Many more questions will arise from the development of this fascinating area combining functional chemical structures and intermolecular interactions. Further, looking at interface problems will be made possible with suitable model systems, and the construction of organic and inorganic hybrid assemblies. We are aware that many scientists all over the world are working on such problems and have answered to some of our questions. And for those who are entering the field, we believe that there are so many exciting systems to create and to study that we will have to write several more book chapters.

References

1. Lehn, J.-M. *Chem. Soc. Rev.* **2007,** *36*, 151.
2. Lehn, J.-M. *Angew. Chem. Int. Ed. Engl.* **1988,** *27*, 89.
3. Balzani, V.; Credi, A.; Venturi, M. *Chem. Eur. J.* **2008,** *14*, 26.
4. Balzani, V.; Bergamini, G.; Ceroni, P. *Coord. Chem. Rev.* **2008,** *252*, 2456.
5. Nishiyabu, R.; Hashimoto, N.; Cho, T.; Watanabe, K.; Yasunaga, T.; Endo, A.; Kaneko, K.; Niidome, T.; Murata, M.; Adachi, C.; Katayama, Y.; Hashizume, M.; Kimizuka, N. *J. Am. Chem. Soc.* **2009,** *131*, 2151.
6. Cordier, P.; Tournilhac, F.; Soulie-Ziakovic, C.; Leibler, L. *Nature* **2008,** *451*, 977.
7. Huc, I.; Lehn, J.-M. *Proc. Natl. Acad. Sci. USA* **1997,** *94*, 2106.
8. Gianneschi, N. C.; Masar, M. S.; III, Mirkin, C. A. *Acc. Chem. Res.* **2005,** *38*, 825.
9. Balzani, V.; Venturi, M.; Credi, A. *Molecular Devices and Machines—A Journey into the Nanoworld.* Wiley-VCH: Weinheim, **2008**.
10. Wang, C.; Zhang, X. *Chem. Soc. Rev.* **2011,** *40*, 94.
11. Mammen, M.; Choi, S. K.; Whitesides, G. M. *Angew. Chem. Int. Ed.* **1998,** *20*, 2755.
12. Pluth, M. D.; Raymond, K. N. *Chem. Soc. Rev.* **2007,** *36*, 161.
13. Lehn, J.-M. *Acc. Chem. Res.* **1978,** *11*, 49.
14. Rehm, T.; Schmuck, C. *Chem. Soc. Rev.* **2010,** *39*, 3597.
15. Sessler, J. L.; Lawrence, C. M.; Jayawickramarajah, J. *Chem. Soc. Rev.* **2007,** *36*, 314.
16. Montalti, M.; Credi, A.; Prodi, L.; Gandolfi, M. T. *Handbook of Photochemistry*. Marcel Dekker Inc.: New York, **2006**.
17. Balzani, V.; Bergamini, G.; Campagna, S.; Puntoriero, F. *Top. Curr. Chem.* **2007,** *280*, 1.
18. Campagna, S.; Puntoriero, F.; Nastasi, F.; Bergamini, G.; Balzani, V. *Top. Curr. Chem.* **2007,** *280*, 117.
19. Kirgan, R. A.; Sullivan, B. P.; Rillema, D. P. *Top. Curr. Chem.* **2007,** *281*, 45.
20. Kumaresan, D.; Shankar, K.; Vaidya, S.; Schmehl, R. H. *Top. Curr. Chem.* **2007,** *281*, 101.
21. Flamigni, L.; Barbieri, A.; Sabatini, C.; Ventura, B.; Barigelletti, F. *Top. Curr. Chem.* **2007,** *281*, 143.
22. Williams, J. A. G. *Top. Curr. Chem.* **2007,** *281*, 205.
23. Szabo, A.; Ostlund, N. S. *Modern Quantum Chemistry: Introduction to Advanced Electronic Structure Theory*. Dover publications, Inc.: Mineola, New York, **1996**.
24. Turro, N. J.; Scaiano, J. C.; Ramamurthy, V. *Modern Molecular Photochemistry of Organic Molecules*. University Science Books: Mill Valley, CA, **2009**.
25. Chen, P.; Meyer, T. J. *Chem. Rev.* **1998,** *98*, 1439.
26. Meyer, T. J.; Caspar, J. V. *J. Phys. Chem.* **1983,** *87*, 952.
27. Kober, E. M.; Caspar, J. V.; Lumpkin, R. S.; Meyer, T. J. *J. Phys. Chem.* **1986,** *90*, 3122.
28. Caspar, J. V.; Kober, E. M.; Sullivan, B. P.; Meyer, T. J. *J. Am. Chem. Soc.* **1982,** *104*, 630.
29. Dalgarno, S. J.; Thallapally, P. K.; Barbour, L. J.; Atwood, J. L. *Chem. Soc. Rev.* **2007,** *36*, 236.
30. Atwood, J. L.; Barbour, L. J.; Jerga, A.; Schottel, B. L. *Science* **2002,** *298*, 1000.

31. Varki, A. *Glycobiology* **1993,** *3*, 97.
32. Sansone, F.; Dudič, M.; Donofrio, G.; Rivetti, C.; Baldini, L.; Casnati, A.; Cellai, S.; Ungaro, R. *J. Am. Chem. Soc.* **2006,** *128*, 14528.
33. Baldini, L. A.; Casnati, A.; Sansone, F.; Ungaro, R. *Chem. Soc. Rev.* **2007,** *2007*(36), 254.
34. Molenveld, P.; Engbersen, J. F. J.; Reinhoudt, D. N. *Chem. Soc. Rev.* **2000,** *29*, 75.
35. Verboom, W.; Vreekamp, R. H.; Rudkeich, D. M.; Reinhoudt, D. N. "*Functionalization and Application of Calixarenes, in Molecular Engineering for Advanced Materials*". Kluver Academic Publisher: Dordrecht, **1995**.
36. Kim, K.; Selvapalam, N.; Ko, Y. H.; Park, K. M.; Kim, D.; Kim, J. *Chem. Soc. Rev.* **2007,** *36*, 267.
37. Jeon, Y. J.; Bharadwaj, P. K.; Choi, S. W.; Lee, J. W.; Kim, K. *Angew. Chem. Int. Ed.* **2002,** *41*, 4474.
38. Wenz, G.; Han, B. H.; Müller, A. *Chem. Rev.* **2006,** *106*, 782.
39. Falvey, P.; Lim, C. W.; Darcy, R.; Revermann, T.; Karst, U.; Giesbers, M.; Marcelis, A. T. M.; Lazar, A.; Coleman, A. W.; Reinhoudt, D. N.; Ravoo, B. J. *Chem. Eur. J.* **2005,** *11*, 1171.
40. Weidner, S.; Pikramenou, Z. *Chem. Commun.* **1998,** 1473.
41. Wang, Y.; Ma, N.; Wang, Z.; Zhang, X. *Angew. Chem. Int. Ed.* **2007,** *46*, 2823.
42. Haider, J. M.; Williams, R. M.; De Cola, L.; Pikramenou, Z. *Angew. Chem. Int. Ed.* **2003,** *42*, 1830.
43. Faiz, J. A.; Williams, R. M.; Pereira Silva, M. J. J.; De Cola, L.; Pikramenou, Z. *J. Am. Chem. Soc.* **2006,** *128*, 4520.
44. Giansante, C.; Ceroni, P.; Balzani, V.; Vögtle, F. *Angew. Chem. Int. Ed.* **2008,** *47*, 5422.
45. Ward, M. D.; Barigelletti, F. *Coord. Chem. Rev.* **2001,** *216–217*, 127.
46. Encinas, S.; Simpson, N. R. M.; Andrews, P.; Ward, M. D.; White, C. M.; Armaroli, N.; Barigelletti, F.; Houlton, A. *New J. Chem.* **2000,** *24*, 987.
47. Armaroli, N.; Barigelletti, F.; Calogero, G.; Flamigni, L.; White, C. M.; Ward, M. D. *Chem. Commun.* **1997,** 2181.
48. Dirksen, A.; Hahn, U.; Schwanke, F.; Nieger, M.; Reek, J. N. H.; Vögtle, F.; De Cola, L. *Chem. Eur. J.* **2004,** *10*, 2036.
49. Dirksen, A.; Kleverlaan, C. J.; Reek, J. N. H.; De Cola, L. *J. Phys. Chem. A* **2005,** *109*, 5248.
50. Bowers, J.; Danks, M. J.; Bruce, D. W.; Heeman, R. K. *Langmuir* **2003,** *19*, 292.
51. Bowers, J.; Danks, M. J.; Bruce, D. W.; Webster, J. R. P. *Langmuir* **2003,** *19*, 299.
52. Domínguez-Gutiérrez, D.; Surtchev, M.; Eiser, E.; Elsevier, C. *Nano Lett.* **2006,** *6*, 145.
53. Turro, N. J.; Yekta, A. *J. Am. Chem. Soc.* **1978,** *100*, 5951.
54. Tran, E.; Cohen, A. E.; Murray, R. W.; Rampi, M. A.; Whitesides, G. M. *J. Am. Chem. Soc.* **2009,** *131*, 2141.
55. Romualdo-Torres, G.; Agricole, B.; Mingotaud, C.; Ravaine, S.; Delhaes, P. *Langmuir* **2003,** *19*, 4688.
56. Li, X.; Zhang, S.; Zhao, P.; Kovacs, Z.; Sherry, A. D. *Inorg. Chem.* **2001,** *40*, 6572.
57. Tuccitto, N.; Ferri, V.; Cavazzini, M.; Quici, S.; Zhavnerko, G.; Licciardello, A.; Rampi, M. A. *Nat. Mater.* **2009,** *8*, 41.
58. Chu, B. W. -K.; Yam, V. W. -W. *Inorg. Chem.* **2001,** *40*, 3324.
59. Cataldo, S.; Pignataro, B.; Ruggirello, A.; Bongiorno, C.; Turco Liveri, V. *Nanotechnology* **2009,** *20*, 225605.

60. Fujigaya, T.; Jiang, D.-L.; Aida, T. *J. Am. Chem. Soc.* **2003,** *125*, 14690.
61. Coco, S.; Cordovilla, C.; Domínguez, C.; Donnio, B.; Espinet, P.; Guillon, D. *Chem. Mater.* **2009,** *21*, 3282.
62. Cardinaels, T.; Ramaekers, J.; Driesem, K.; Nockemann, P.; van Hecke, K.; Van Meervelt, L.; Goderis, B.; Binnemans, K. *Inorg. Chem.* **2009,** *46*, 2490.
63. Shakya, R.; Imbert, C.; Hratchian, H. P.; Lanznaster, M.; Heeg, M. J.; McGarvey, B. R.; Allard, M.; Schlegel, H. B.; Verani, C. N. *Dalton Trans.* **2006,** 2517.
64. Griffiths, P. C.; Fallis, I. A.; Chuenpratoom, T.; Watanesk, R. *Adv. Colloid Interface Sci.* **2006,** *122*, 107.
65. Jervis, H. B.; Raimondi, M. E.; Raja, R.; Maschmeyer, T.; Seddon, J. M.; Bruce, D. W. *Chem. Commun.* **1999,** 2031.
66. Walker, G. W.; Geue, R. J.; Sargeson, A. M.; Behm, C. A. *Dalton Trans.* **2003,** 2992.
67. Storrs, R. W.; Tropper, F. D.; Li, H. Y.; Song, C. K.; Kuniyoshi, J. K.; Sipkins, D. A.; Li, K. C. P.; Bednarski, M. D. *J. Am. Chem. Soc.* **1995,** *117*, 7301.
68. Chou, L. Y. T.; Ming, K.; Chan, W. C. W. *Chem. Soc. Rev.* **2011,** *40*, 233.
69. Kanjappu, J. T.; Kelkar, V. K.; Manohar, C. *Langmuir* **1993,** *9*, 352.
70. Weijnen, J. G. G.; Koudijs, A.; Engbersen, J. F. J. *J. Chem. Soc., Perkin Trans.* **1991,** *2*, 1121.
71. Manabe, K.; Mori, Y.; Wakabayashi, T.; Nagayama, S.; Kobayashi, S. *J. Am. Chem. Soc.* **2000,** *122*, 7202.
72. Kimura, E.; Hashimoto, H.; Koike, T. *J. Am. Chem. Soc.* **1996,** *118*, 10963.
73. Ghirlanda, G.; Scrimin, P.; Kaifer, A. E.; Echegoyen, L. A. *Langmuir* **1996,** *12*, 3695.
74. Kung, H. H.; Kung, M. C. *Top. Catal.* **2005,** *34*, 77.
75. Mishra, B. K.; Valaulikar, B. S.; Kunjappu, J. T.; Manohar, C. *J. Colloid. Interface Sci.* **1989,** *127*, 373.
76. Fuhrhop, J.-H.; Wang, T. *Chem. Rev.* **2004,** *104*, 2901.
77. Meisel, D.; Matheson, M. S.; Rabani, J. *J. Am. Chem. Soc.* **1978,** *100*, 117.
78. Warr, G. G.; Greiser, F. *Chem. Phys. Lett.* **1985,** *116*, 505.
79. Thomas, J. K. *Chem. Rev.* **1980,** *80*, 283.
80. Pallavicini, P.; Diaz-Fernandez, Y. A.; Pasotti, L. *Coord. Chem. Rev.* **2009,** *253*, 2226.
81. Kunjappu, J. T.; Somasundaran, P.; Turro, N. J. *J. Phys. Chem.* **1990,** *94*, 8464.
82. Gehlen, M. H.; De Schryver, F. *Chem. Rev.* **1993,** *93*, 199.
83. Bruce, D. W.; Holbrey, J. D.; Tajbakhsh, A. R.; Tiddy, G. J. T. *J. Mater. Chem.* **1993,** *3*, 905.
84. Hrolbrey, J. D.; Tiddy, G. J. T.; Bruce, D. W. *J. Chem. Soc., Dalton Trans.* **1995,** 1769.
85. Yashiro, M.; Matsumoto, K.; Yoshikawa, S. *Chem. Lett.* **1989,** *18*, 985.
86. Shashikala, I. S.; Bruce, D. W. *Dalton Trans.* **2008,** 1128.
87. Date, R. W.; Fernandez Iglesias, E.; Rowe, K. E.; Elliott, J. M.; Bruce, D. W. *Dalton Trans.* **2003,** 1914.
88. Danks, M. J.; Jervis, H. B.; Nowotny, M.; Zhou, W.; Maschmeyer, T. A.; Bruce, D. W. *Catal. Lett.* **2002,** *82*, 95.
89. Amos, K. E.; Brooks, N. J.; King, N. C.; Xie, S.; Canales-Vázquez, J.; Danks, M. J.; Jervis, H. B.; Zhou, W.; Seddon, J. M.; Bruce, D. W. *J. Mater. Chem.* **2008,** *18*, 528.

90. Fazio, D.; Mongin, C.; Donnio, B.; Galerne, Y.; Guillon, D.; Bruce, D. W. *J. Mater. Chem.* **2001,** *11*, 2852.
91. Bruce, D. W. *Acc. Chem. Res.* **2000,** *33*, 831.
92. Guillevic, M.-A.; Danks, M. J.; Harries, S. K.; Collinson, S. R.; Pidwell, A. D.; Bruce, D. W. *Polyhedron* **2000,** *19*, 249.
93. Liu, X.-H.; Henirich, B.; Manners, I.; Guillon, D.; Bruce, D. W. *J. Mater. Chem.* **2000,** *10*, 637.
94. Shakya, R.; Hindo, S. S.; Wu, L.; Allard, M. M.; Heeg, M. J.; Hratchian, H. P.; McGarvey, B. R.; da Rocha, S. R. P.; Verani, C. N. *Inorg. Chem.* **2007,** *46*, 9808.
95. Canard, G.; Piguet, C. *Inorg. Chem.* **2007,** *46*, 3511.
96. Driscoll, J. A.; Keyes, P. H.; Heeg, M. J.; Heiney, P. A.; Verani, C. N. *Inorg. Chem.* **2008,** *47*, 7225.
97. Lesh, F. D.; Shanmugam, R.; Allard, M. M.; Lanznaster, M.; Heeg, M. J.; Rodgers, M. T.; Shearer, J. M.; Verani, C. N. *Inorg. Chem.* **2010,** *49*, 7226.
98. Lesh, F. D.; Hindo, S. S.; Heeg, M. J.; Allard, M. M.; Jain, P.; Peng, B.; Hryhorczuk, L.; Verani, C. N. *Eur. J. Inorg. Chem.* **2009,** 345.
99. see for instance the dedicated issue *Coord. Chem. Rev.* **2009**, *253*, 2131.
100. Bowers, J.; Amos, K. E.; Bruce, D. W.; Heenan, R. K. *Langmuir* **2005,** *21*, 5696.
101. Domínguez-Gutiérrez, D.; Eiser, E.; Elsevier, C. J. *Eur. J. Inorg. Chem.* **2008,** 1088.
102. Cardinaels, T.; Ramaekers, J.; Nockemann, P.; Driesen, K.; Van Hecke, K.; Van Meervelt, L.; Wang, G.; De Feyter, S.; Fernandez Iglesias, E.; Guillon, D.; Donnio, B.; Binnemans, K.; Bruce, D. W. *Soft Matter* **2008,** *4*, 2172.
103. Garcia, P.; Marques, J.; Pereira, E.; Gameiro, P.; Salema, R.; de Castro, B. *Chem. Commun.* **2001,** 1298.
104. Bowers, J.; Amos, K. E.; Bruce, D. W.; Webster, J. R. P. *Langmuir* **2005,** *21*, 1346.
105. Kalyanasundaram, K. *Photochemistry of Polypyridine and Porhyrin Complexes*. Academic Press: London, **1992**.
106. Balzani, V.; Juris, A. *Coord. Chem. Rev.* **2001,** *211*, 97.
107. Gohy, J.-F.; Lohmeijer, B. G. G.; Schubert, U. S. *Chem. Eur. J.* **2003,** *9*, 3472.
108. Lohmeijer, B. G. G.; Schubert, U. S. *Angew. Chem. Int. Ed.* **2002,** *41*, 3825.
109. Gohy, J.-F.; Lohmeijer, B. G. G.; Varshney, S. K.; Schubert, U. S. *Macromolecules* **2002,** *35*, 7427.
110. Gohy, J.-F.; Lohmeijer, B. G. G.; Schubert, U. S. *Macromolecules* **2002,** *35*, 4560.
111. Gohy, J.-F. *Coord. Chem. Rev.* **2009,** *253*, 2214.
112. Chen, B.; Metera, K.; Sleiman, H. F. *Macromolecules* **2005,** *38*, 1084.
113. Chen, B.; Sleiman, H. F. *Macromolecules* **2004,** *37*, 5866.
114. Griffiths, P. C.; Fallis, I. A.; Willock, D. J.; Paul, A.; Barrie, C. L.; Griffiths, P. M.; Williams, G. M.; King, S. M.; Heenan, R. K.; Görgl, R. *Chem. Eur. J.* **2004,** *10*, 2022.
115. Draeger, C.; Böttcher, C.; Messerschmidt, C.; Schulz, A.; Ruhlmann, L.; Siggel, U.; Hammarström, L.; Berglund-Baudin, H.; Fuhrhop, J. H. J. -H. *Langmuir* **2000,** *16*, 2069.
116. Domínguez-Gutiérrez, D.; De Paoli, G.; Guerrero-Martínez, A.; Ginocchietti, G.; Ebeling, D.; Eiser, E.; De Cola, L.; Elsevier, J. C. *J. Mater. Chem.* **2008,** *18*, 2762.

117. Gameiro, P.; Pereira, E.; Garcia, P.; Breia, S.; Burgess, J.; de Castro, B. *Eur. J. Inorg. Chem.* **2001,** 2755.
118. Vögtle, F.; Plevoets, M.; Nieger, M.; Azzellini, M. C.; Credi, A.; De Cola, L.; De Marchis, V.; Venturi, M.; Balzani, V. J. *J. Am. Chem. Soc.* **1999,** *121*, 6290.
119. Zanarini, S.; Rampazzo, E.; Bonacchi, S.; Juris, R.; Marcaccio, M.; Montalti, M.; Paolucci, F.; Prodi, L. *J. Am. Chem. Soc.* **2009,** *131*, 14208.
120. Zanarini, S.; Rampazzo, E.; Della Ciana, L.; Marcaccio, M.; Marzocchi, E.; Montalti, M.; Paolucci, F.; Prodi, L. *J. Am. Chem. Soc.* **2009,** *131*, 2260.
121. Chambron, J. C.; Sauvage, J.-P. *Chem. Phys. Lett.* **1991,** *182*, 603.
122. Guerrero-Martínez, A.; Vida, Y.; Domínguez-Gutiérrez, D.; Albuquerque, R. Q.; De Cola, L. *Inorg. Chem.* **2008,** *47*, 9131.
123. Baldo, M. A.; O'Brien, D. F.; You, Y.; Shoustikov, A.; Sibley, S.; Thompson, M. E.; Forrest, S. R. *Nature* **1998,** *395*, 151.
124. Orselli, E.; Albuquerque, Q. R.; Fransen, P. M.; Fröhlich, R.; Janssen, H. M.; De Cola, L. *J. Mater. Chem.* **2008,** *18*, 4579.
125. Yang, C.-H.; Cheng, Y. M.; Chi, Y.; Hsu, C. J.; Fang, F. -C.; Wong, K. -T.; Chou, P.-T.; Chang, C. -H.; Tsai, M. -H.; Wu, C. -C. *Angew. Chem. Int. Ed.* **2007,** *46*, 2418.
126. Huang, W. -S.; Lin, J. T.; Chien, C. -H.; Tao, Y. T.; Sun, S. S.; Wen, Y. -S. *Chem. Mater.* **2004,** *16*, 2480.
127. Lamansky, S.; Djurovich, P.; Murphy, D.; Abdel-Razzaq, F.; Lee, H. -E.; Adachi, C.; Burrows, P. E.; Forrest, S. R.; Thompson, M. E. *J. Am. Chem. Soc.* **2001,** *123*, 4304.
128. Nazeeruddin, K.; Humphry-Baker, R.; Berner, D.; Rivier, S.; Zuppiroli, L.; Graetzel, M. *J. Am. Chem. Soc.* **2003,** *125*, 8790.
129. Tamayo, A. B.; Alleyne, B. D.; Djurovich, P. I.; Lamansky, S.; Tsyba, I.; Ho, N. N.; Bau, R.; Thompson, M. E. *J. Am. Chem. Soc.* **2003,** *125*, 7377.
130. Chi, Y.; Chou, P. T. *Chem. Soc. Rev.* **2010,** *39*, 638.
131. You, Y.; Park, S. Y. *Dalton Trans.* **2009,** 1267.
132. Yang, L.; Okuda, F.; Kobayashi, K.; Nozaki, K.; Tanabe, Y.; Ishii, Y.; Haga, M. *Inorg. Chem.* **2008,** *47*, 7154.
133. Lowry, M. S.; Bernhard, S. *Chem. Eur. J.* **2006,** *12*, 7970.
134. You, Y.; Park, S. Y. *J. Am. Chem. Soc.* **2005,** *127*, 12438.
135. Li, J.; Djurovich, P. I.; Alleyne, B. D.; Yousufuddin, M.; Ho, N. N.; Thomas, J. C.; Peters, J. C.; Bau, R.; Thompson, M. E. *Inorg. Chem.* **2005,** *44*, 1713.
136. Coppo, P.; Plummer, E. A.; De Cola, L. *Chem. Commun.* **2004,** 1774.
137. Welter, S.; Lafolet, F.; Cecchetto, E.; Vergeer, F.; De Cola, L. *Chem. Phys. Chem.* **2005,** *6*, 2417.
138. Plummer, E. A.; Hofstraat, J. W.; De Cola, L. *Dalton Trans.* **2003,** 2080.
139. Lafolet, F.; Welter, S.; Popović, Z.; De Cola, L. *J. Mater. Chem.* **2005,** *15*, 2820.
140. Fernández-Moreira, V.; Thorp-Greenwood, F. L.; Coogan, M. P. *Chem. Commun.* **2010,** *46*, 186.
141. Wong, W.-Y.; Ho, C. L. *J. Mater. Chem.* **2009,** *19*, 4457.
142. Di Censo, D.; Fantacci, S.; De Angelis, F.; Klein, C.; Evans, N.; Kalyanasundaram, K.; Bolink, H. J.; Grätzel, M.; Nazeeruddin, Md.K. *Inorg. Chem.* **2008,** *47*, 980.
143. Chou, P.-T.; Chi, Y. *Chem. Eur. J.* **2008,** *13*, 380.

144. Orselli, E.; Kottas, G. S.; Konradsson, A. E.; Coppo, P.; Fröhlich, R.; De Cola, L.; van Dijken, A.; Büchel, M.; Börner, H. *Inorg. Chem.* **2007,** *46*, 11082.
145. Tamayo, A. B.; Garon, S.; Sajoto, T.; Djurovich, P. I.; Tsyba, I. M.; Bau, R.; Thompson, M. E. *Inorg. Chem.* **2005,** *44*, 8723.
146. Yang, C.-H.; Beltran, J.; Lemaur, V.; Cornil, J.; Hartmann, D.; Sarfert, W.; Fröhlich, R.; Bizzarri, C.; De Cola, L. *Inorg. Chem.* **2010,** *49*, 9891.
147. Mydlak, M.; Bizzarri, C.; Harmann, D.; Sarfert, W.; Schmid, G.; De Cola, L. *Adv. Funct. Mater.* **2010,** *20*, 1812.
148. Bolink, H. J.; Coronado, E.; Costa, R. D.; Lardiés, N.; Ortí, E. *Inorg. Chem.* **2008,** *47*, 9149.
149. Bolink, H. J.; Cappelli, L.; Coronado, E.; Grätzel, M.; Ortí, E.; Costa, R. D.; Viruela, P. M.; Nazeeruddin, Md.K. *J. Am. Chem. Soc.* **2006,** *128*, 14786.
150. Slinker, J. D.; Gorodetsky, A. A.; Lowry, M. S.; Wang, J.; Parker, S.; Rohl, R.; Bernhard, S.; Malliaras, G. G. *J. Am. Chem. Soc.* **2004,** *126*, 2763.
151. Allendorf, M. D.; Bauer, C. A.; Bhakta, R. K.; Houk, R. J. T. *Chem. Soc. Rev.* **2009,** *38*, 1330.
152. Uemura, T.; Yanai, N.; Kitagawa, S. *Chem. Soc. Rev.* **2009,** *38*, 1228.
153. Kitagawa, S.; Matsuda, R. *Coord. Chem. Rev.* **2007,** *251*, 2490.
154. Kitagawa, S.; Kitaura, R.; Noro, S. *Angew. Chem. Int. Ed.* **2004,** *43*, 2334.
155. Tranchemontagne, D.; Mendoza-Cortés, J. L.; O'Keeffe, M.; Yaghi, O. M. *Chem. Soc. Rev.* **2009,** *38*, 1257.
156. Li, H.; Eddaoudi, M.; O'Keeffe, M.; Yaghi, O. M. *Nature* **1999,** *402*, 276.
157. Hosseini, M. W. *Acc. Chem. Res.* **2005,** *38*, 313.
158. Inagaki, S.; Guan, S.; Ohsuna, T.; Terasaki, O. *Nature* **2002,** *416*, 304.
159. Hoffmann, F.; Cornelius, M.; Morell, J.; Fröba, M. *Angew. Chem. Int. Ed.* **2006,** *45*, 3216.
160. Phillips, V.; Willard, K. J.; Golen, J. A.; Moore, C. J.; Rheingold, A. L.; Doerrer, L. H. *Inorg. Chem.* **2010,** *49*, 9265, and refs therein.
161. Doerrer, L. H. *Dalton Trans.* **2010,** 3543.
162. Fujita, I.; Kobayashi, H. *J. Chem. Phys.* **1973,** *59*, 2902.
163. Fujita, I.; Kobayashi, H. J. *J. Chem. Phys.* **1970,** *52*, 4904.
164. von Arx, M. E.; Burattini, E.; Hauser, A.; van Pieterson, L.; Pellaux, R.; Decurtins, S. *J. Phys. Chem. A* **2000,** *104*, 883.
165. Langford, V. S.; von Arx, M. E.; Hauser, A. *J. Phys. Chem. A* **1999,** *103*, 7161.
166. von Arx, M. E.; Hauser, A.; Riesen, H.; Pellaux, R.; Decurtins, S. *Phys. Rev. B* **1996,** *54*, 15800.
167. Otsuka, T.; Sekine, A.; Fujigasaki, N.; Ohashi, Y.; Kaizu, Y. *Inorg. Chem.* **2001,** *40*, 3406.
168. Otsuka, T.; Takahashi, N.; Fujigasaki, N.; Sekine, A.; Ohashi, Y.; Kaizu, Y. *Inorg. Chem.* **1999,** *38*, 1340.
169. Otsuka, T.; Kaizu, Y. *Chem. Lett.* **1997,** *26*, 79.
170. Mauro, M.; Schuermann, K. C.; Prétôt, R.; Hafner, A.; Mercandelli, P.; Sironi, A.; De Cola, L. *Angew. Chem. Int. Ed.* **2010,** *49*, 1222.
171. Nazeeruddin, K.; Wegh, R. T.; Zhou, Z.; Klein, C.; Wang, Q.; De Angelis, F.; Fantacci, S.; Grätzel, M. *Inorg. Chem.* **2006,** *45*, 9245.
172. Förster, Th.; Kasper, K. *Z. Phys. Chem.* **1954,** *1*, 275.
173. Luo, J.; Xie, Z.; Lam, J. W. Y.; Cheng, L.; Chen, H.; Qiu, C.; Kwok, H. S.; Zhan, X.; Liu, Y.; Zhu, D.; Tang, B. Z. *Chem. Commun.* **2001,** 1740.

174. Tang, B. Z.; Zhan, X.; Yu, G.; Lee, P. P. S.; Liu, Y.; Zhu, D. *J. Mater. Chem.* **2001,** *11*, 2974.
175. Hong, Y.; Lam, J. W. Y.; Tang, B. Z. *Chem. Commun.* **2009,** 4332.
176. Hong, Y.; Häubler, M.; Lam, J. W. Y.; Li, Z.; Sin, K. K.; Dong, Y.; Tong, H.; Liu, J.; Qin, A.; Renneberg, R.; Tang, B. Z. *Chem. Eur. J.* **2008,** *14*, 6428.
177. Dong, Y.; Lam, J. W. Y.; Qin, A.; Li, Z.; Sun, J.; Sung, H. H.-Y.; Williams, I. A.; Tang, B. Z. *Chem. Commun.* **2007,** 40.
178. An, B.-K.; Kwon, S.-K.; Jung, S.-D.; Park, S.-Y. *J. Am. Chem. Soc.* **2002,** *124*, 14410.
179. Zhao, Z.; Chen, S.; Shen, X.; Mahtab, F.; Yu, Y.; Lu, P.; Lam, J. W. Y.; Kwok, H. S.; Tang, B. Z. *Chem. Commun.* **2010,** *46*, 686.
180. Zhang, G.; Lu, J.; Sabat, M.; Fraser, C. L. *J. Am. Chem. Soc.* **2010,** *132*, 2160.
181. Tong, H.; Hong, Y.; Dong, Y.; Ren, Y.; Häussler, M.; Lam, J. W. Y.; Wong, K. S.; Tang, B. Z. *J. Phys. Chem. B* **2007,** *111*, 2000.
182. Sagara, Y.; Mutai, T.; Yoshikawa, I.; Araki, K. *J. Am. Chem. Soc.* **2008,** *129*, 1520.
183. Kim, S.; Zheng, Q.; He, G. S.; Bharali, D. J.; Pudavar, H. E.; Baev, A.; Prasad, P. N. *Adv. Funct. Mater.* **2006,** *16*, 2317.
184. Lee, S. H.; Jang, B.-B.; Kafafi, Z. H. *J. Am. Chem. Soc.* **2005,** *127*, 9071.
185. Chen, J.; Xu, B.; Ouyang, X.; Tang, B. Z.; Cao, Y. *J. Phys. Chem. A* **2004,** *108*, 7522.
186. Zhang, L.; Li, B.; Su, Z. *Langmuir* **2009,** *25*, 2068.
187. Sapochak, L. S.; Benincasa, F. E.; Schofield, R. S.; Baker, J. L.; Riccio, K. K. C.; Fogarty, D.; Kohlmann, H.; Ferris, K. F.; Burrows, P. E. *J. Am. Chem. Soc.* **2002,** *124*, 6119.
188. Brinkmann, M.; Gadret, G.; Muccini, M.; Taliani, C.; Masciocchi, N.; Sironi, A. *J. Am. Chem. Soc.* **2000,** *122*, 5147.
189. Yam, V. W.-W.; Chan, K. H.-Y.; Wong, K. M.-C.; Zhu, N. *Chem. Eur. J.* **2005,** *11*, 4535.
190. Kato, M.; Shishido, Y.; Ishida, Y.; Kishi, S. *Chem. Lett.* **2008,** *37*, 16.
191. Ma, B.; Djurovich, P. I.; Yousufuddin, M.; Bau, R.; Thompson, M. E. *J. Am. Chem. Soc.* **2005,** *127*, 28.
192. Büchner, R.; Field, J. S.; Haines, R. J.; Cunningham, C. T.; McMillin, D. R. *Inorg. Chem.* **1997,** *36*, 3952.
193. Connick, W. B.; Marsh, R. E.; Schaefer, W. P.; Gray, H. B. *Inorg. Chem.* **1997,** *36*, 913.
194. Shin, C. H.; Huh, J. O.; Lee, M. H.; Do, Y. *Dalton Trans.* **2009,** 6476.
195. Zhao, Q.; Li, L.; Li, F.; Yu, M.; Liu, Z.; Yi, T.; Huang, C. *Chem. Commun.* **2008,** 685.
196. You, Y.; Huh, H. S.; Kim, K. S.; Lee, S. W.; Kim, D.; Park, S. Y. *Chem. Commun.* **2008,** 3998.
197. Huang, K.; Wu, H.; Shi, M.; Li, F.; Yi, T.; Huang, C. *Chem. Commun.* **2009,** 1243.
198. Han, M.; Hara, M. *J. Am. Chem. Soc.* **2005,** *127*, 10951.
199. Talarico, A. M.; Aiello, I.; Bellusci, A.; Crispini, A.; Ghedini, M.; Godbert, N.; Pugliese, T.; Szerb, E. *Dalton Trans.* **2010,** *39*, 1709.
200. Kitagawa, H.; Ozawa, Y.; Toriumi, K. *Chem. Commun.* **2010,** 6302.
201. Fan, Y.; Zhao, Y.; Ye, L.; Li, B.; Yang, G.; Wang, Y. *Cryst. Growth Des.* **2009,** *9*, 1421.
202. Field, J. S.; Ledwaba, L. P.; Munro, O. Q.; McMillin, D. R. *CrystEngComm* **2008,** *10*, 740.

203. Zhang, H.; Zhang, Z.; Ye, K.; Zhang, J.; Wang, Y. *Adv. Mater.* **2006,** *18*, 2369.
204. Davis, R.; Rath, N. P.; Das, S. *Chem Commun.* **2004,** 74.
205. Yam, V. W.-W.; Wong, K. M.-C.; Zhu, N. *J. Am. Chem. Soc.* **2002,** *124*, 6506.
206. Quartapelle Procopio, E.; Mauro, M.; Panigati, M.; Donghi, D.; Mercandelli, P.; Sironi, A.; D'Alfonso, G.; De Cola, L. *J. Am. Chem. Soc.* **2010,** *132*, 14397.
207. Mauro, M.; Quartapelle Procopio, E.; Sun, Y.; Chien, C. H.; Donghi, D.; Panigati, M.; Mercandelli, P.; Mussini, P.; D'Alfonso, G.; De Cola, L. *Adv. Funct. Mater.* **2009,** *19*, 2607.
208. Donghi, D.; D'Alfonso, G.; Mauro, M.; Panigati, M.; Mercandelli, P.; Sironi, A.; Mussini, P.; D'Alfonso, L. *Inorg. Chem.* **2008,** *28*, 4243.
209. Camerel, F.; Ziessel, R.; Donnio, B.; Bourgogne, C.; Guillon, D.; Schmutz, M.; Iacovita, C.; Bucher, J. P. *Angew. Chem. Int. Ed.* **2007,** *46*, 2659.
210. Kozhevnikov, V. N.; Donnio, B.; Bruce, D. W. *Angew. Chem. Int. Ed.* **2008,** *47*, 6286.
211. Santoro, A.; Whitwood, A. C.; Williams, J. A. G.; Kozhevnikov, V. N.; Bruce, D. W. *Chem. Mater.* **2009,** *21*, 3871.
212. Zhang, W.; Jin, W.; Fukushima, T.; Ishii, N.; Aida, T. *Angew. Chem. Int. Ed.* **2009,** *48*, 4747.
213. Sun, Y.; Ye, K.; Zhang, H.; Zhang, J.; Zhao, L.; Li, B.; Yang, G.; Yang, B.; Wang, Y.; Lai, S.-W.; Che, C.-M. *Angew. Chem. Int. Ed.* **2006,** *45*, 5610.
214. Yuen, M.-Y.; Roy, V. A. L.; Lu, W.; Kui, S. C.-F.; Tong, G. S. M.; Chui, S. S.-Y.; Muccini, M.; Ning, J. Q.; Xu, S. J.; Che, C.-M. *Angew. Chem. Int. Ed.* **2008,** *47*, 9895.
215. Lu, W.; Chen, Y.; Roy, V. A. L.; Chui, S. S.-Y.; Che, C.-M. *Angew. Chem. Int. Ed.* **2009,** *48*, 7621.
216. Lu, W.; Chui, S. S.-Y.; Ng, K.-M.; Che, C.-M. *Angew. Chem. Int. Ed.* **2008,** *47*, 4568.
217. Strassert, C. A.; Chien, C.-H.; Galvez-Lopez, M. D.; Korkoulos, D.; Hertel, D.; Meerholz, K.; De Cola, L. *Angew. Chem. Int. Ed.* **2011,** *50*, 946.
218. Peterlik, H.; Weisbarth, R.; Nieger, M.; Dötz, K. H. *Angew. Chem. Int. Ed.* **2007,** *46*, 6368.
219. Bao, X. L.; Assenmacher, W.; Peterlik, H.; Daniels, J.; Dötz, K. H. *Chem. Eur. J.* **2009,** *15*, 1853.
220. Tam, A. Y.-Y.; Wong, K. M.-C.; Zhu, N.; Wang, G.; Yam, V. W.-W. *Langmuir* **2009,** *25*, 8685.
221. Tam, A. Y.-Y.; Wong, K. M.-C.; Yam, V. W.-W. *Chem. Eur. J.* **2010,** *15*, 4775.
222. Develay, S.; Williams, J. A. G. *Dalton Trans.* **2008,** 4562.
223. Ma, B.; Djurovich, P. I.; Thompson, M. E. *Coord. Chem. Rev.* **2005,** *249*, 1501.
224. Chang, S.-Y.; Chen, J.-L.; Chi, Y. *Inorg. Chem.* **2007,** *46*, 11202.
225. Accorsi, G.; Listorti, A.; Yoosaf, K.; Armaroli, N. *Chem. Soc. Rev.* **2009,** *38*, 1690.
226. Rachford, A. A.; Hua, F.; Adams, C. J.; Castellano, F. N. *Dalton Trans.* **2009,** 3950.
227. Scarpaci, A.; Monnereau, C.; Hergue, N.; Blart, E.; Legoupy, S.; Odobel, F.; Gorfo, A.; Perez-Moreno, J.; Clays, K.; Asselberghs, I. *Dalton Trans.* **2009,** 4538.

228. Tong, W. -L.; Chan, M. C. W.; Zhub, N.; Leunga, S. K. *Dalton Trans.* **2009,** 4741.
229. Unger, Y.; Zeller, A.; Taige, M. A.; Strassner, T. *Dalton Trans.* **2009,** 4786.
230. Sun, Y.; Wang, S. *Inorg. Chem.* **2009,** *48*, 3755.
231. Niedermair, F.; Sandholzer, M.; Kremser, G.; Slugovc, C. *Organometallics* **2009,** *28*, 2888.
232. Kozhevnikov, D. N.; Kozhevnikov, V. N.; Ustinova, M. M.; Santoro, A.; Bruce, D. W.; Koenig, B.; Czerwieniec, R.; Fischer, T.; Zabel, M.; Yersin, H. *Inorg. Chem.* **2009,** *48*, 4179.
233. Adamovich, V.; Brooks, J.; Tamayo, A.; Alexander, A. M.; Djurovich, P. I.; D'Andrade, B. W.; Adachi, C.; Forrest, S. R.; Thompson, M. E. *New J. Chem.* **2002,** *26*, 1171.
234. Yang, X.; Wang, V.; Madakuni, S.; Li, J.; Jabbour, G. E. *Adv. Mater.* **2008,** *20*, 2405.
235. Ma, B.; Djurovich, P. I.; Garon, S.; Alleyne, B.; Thompson, M. E. *Adv. Funct. Mater.* **2006,** *16*, 2438.
236. Zhou, G.; Wang, Q.; Ho, C. L.; Wong, W. Y.; Ma, D.; Wang, L. *Chem. Commun.* **2009,** 3574.
237. Extrom, C. L.; Sowa, J. R.; Daws, C. A.; Janzen, D.; Mann, K. R. *Chem. Mater.* **1995,** *7*, 15.
238. Buss, C. E.; Anderson, C. E.; Pomije, M. K.; Lutz, C. M.; Britton, D.; Mann, K. R. *J. Am. Chem. Soc.* **1998,** *120*, 7783.
239. Buss, C. E.; Mann, K. R. *J. Am. Chem. Soc.* **2002,** *124*, 1031.
240. Wadas, T. J.; Wang, Q.-M.; Kim, Y.-J.; Flaschenreim, C.; Blanton, T. N.; Eisenberg, R. *J. Am. Chem. Soc.* **2004,** *126*, 16841.
241. Kato, M. *Bull. Chem. Soc. Jpn.* **2007,** *80*, 287.
242. Grove, L. J.; Oliver, A. G.; Krause, J. A.; Connick, W. B. *Inorg. Chem.* **2008,** *47*, 1408.
243. Abe, T.; Akura, T.; Ikeda, N.; Shinozaki, K. *Dalton Trans.* **2009,** 711.
244. Zhang, Y.; Zhang, H.; Mu, X.; Lai, S. -W.; Xu, B.; Tian, W.; Wang, Y.; Che, C. -M. *Chem. Commun.* **2010,** *46*, 7727.
245. Moussa, J.; Wong, K. M.-C.; Chamoreau, L. -M.; Amouri, H.; Yam, V. W.-W. *Dalton Trans.* **2007,** 3526.
246. Tang, R. P.-L.; Wong, K. M.-C.; Zhu, N.; Yam, V. W.-W. *Dalton Trans.* **2009,** 3911.
247. Jarozs, P.; Lotito, K.; Schneider, J.; Kumaresan, D.; Schmehl, R.; Eisenberg, R. *Inorg. Chem.* **2009,** *48*, 2420.
248. Zhang, H.; Zhang, B.; Li, Y.; Sun, W. *Inorg. Chem.* **2009,** *48*, 3617.
249. Tam, A. Y. Y.; Wong, K. M. C.; Yam, V. W. W. *J. Am. Chem. Soc.* **2009,** *131*, 6253.
250. Develay, S.; Blackburn, O.; Thompson, A. L.; Williams, J. A. G. *Inorg. Chem.* **2008,** *47*, 11129.
251. Williams, J. A. G. *Chem. Soc. Rev.* **2009,** *38*, 1783.
252. Rochester, D. L.; Develay, S.; Zalis, S.; Williams, J. A. G. *Dalton Trans.* **2009,** 1728.
253. Williams, J. A. G.; Beeby, A.; Davies, E. S.; Weinstein, J. A.; Wilson, C. *Inorg. Chem.* **2003,** *42*, 8609.
254. Farley, S. J.; Rochester, D. L.; Thompson, A. L.; Howard, J. A. K.; Williams, J. A. G. *Inorg. Chem.* **2005,** *44*, 9690.
255. Schneider, J.; Du, P.; Wang, X.; Brennessel, W. W.; Eisenberg, R. *Inorg. Chem.* **2009,** *48*, 1498.

256. Shao, P.; Li, Y.; Azenkeng, A.; Hoffmann, M. R.; Sun, W. *Inorg. Chem.* **2009,** *48*, 2407.
257. Schneider, J.; Du, P.; Jarosz, P.; Lazarides, T.; Wang, X.; Brennessel, W. W.; Eisenberg, R. *Inorg. Chem.* **2009,** *48*, 4306.
258. Chen, Y.; Li, K.; Lu, W.; Chui, S. S. -Y.; Ma, C. -W.; Che, C. -M. *Angew. Chem. Int. Ed.* **2009,** *48*, 9909.
259. Zhao, L.; Wong, K. M. -C.; Li, B.; Li, W.; Zhu, N.; Wu, L.; Yam, V. W. -W. *Chem. Eur. J.* **2010,** *16*, 6797.
260. Estroff, L. A.; Hamilton, A. D. *Chem. Rev.* **2004,** *104*, 1201.
261. Terech, P.; Weiss, R. G. *Chem. Rev.* **1997,** *97*, 3133.
262. van Esch, J. H.; Feringa, B. L. *Angew. Chem. Int. Ed.* **2000,** *39*, 2263.
263. Sangeetha, N. M.; Maitra, U. *Chem. Soc. Rev.* **2005,** *34*, 821.
264. Fages, F. *Angew. Chem. Int. Ed.* **2006,** *45*, 1680.
265. Shirakawa, M.; Fujita, N.; Tani, T.; Kaneko, K.; Ojima, M.; Fujii, A.; Ozaki, M.; Shinkai, S. *Chem. Eur. J.* **2007,** *13*, 4155.
266. de Loos, M.; van Esch, J. H.; Kellogg, R. M.; Feringa, B. L. *Angew. Chem. Int. Ed.* **2001,** *40*, 613.
267. Mieden-Gundert, G.; Klein, L.; Fischer, M.; Vögtle, F.; Heuze, K.; Pozzo, J. L.; Vallier, M.; Fages, F. *Angew. Chem. Int. Ed.* **2001,** *40*, 3164.
268. Hanabusa, K.; Yamada, M.; Kimura, M.; Shirai, H. *Angew. Chem. Int. Ed. Engl.* **1996,** *35*, 1949.
269. Rowan, S. J.; Beck, J. B. *Faraday Discuss.* **2005,** *128*, 43.
270. Cravotto, P.; Cintas, G. *Chem. Soc. Rev.* **2009,** *38*, 2684.
271. Sambri, L.; Cucinotta, F.; De Paoli, G.; Stagni, S.; De Cola, L. *New J. Chem.* **2010,** *34*, 2093.
272. Gansäuer, A.; Winkler, I.; Klawonn, T.; Nolte, R. J. M.; Feiters, M. C.; Börner, H. G.; Hentschel, J.; Dötz, K. H. *Organometallics* **2009,** *28*, 1377.
273. De Paoli, G. B.; Dzolic, Z.; Rizzo, F.; De Cola, L.; Vögtle, F.; Müller, W. M.; Richardt, G.; Zinic, M. *Adv. Funct. Mater.* **2007,** *17*, 82.
274. Cîrcu, V.; Horton, P. N.; Hursthouse, M. B.; Bruce, D. W. *Liq. Cryst.* **2007,** *34*, 1463.
275. Sagara, Y.; Kato, T. *Nat. Chem.* **2009,** *1*, 605.
276. An, B.-K.; Lee, D.-S.; Lee, J.-S.; Park, Y.-S.; Song, H.-S.; Park, S. Y. *J. Am. Chem. Soc.* **2004,** *126*, 10232.
277. Yu, G.; Yin, S. W.; Liu, Y. Q.; Chen, J. S.; Xu, X. J.; Sun, X. B.; Ma, D. G.; Zhan, X. W.; Peng, Q.; Shuai, Z. G.; Tang, B. Z.; Zhu, D. B.; Fang, W. H.; Luo, Y. *J. Am. Chem. Soc.* **2005,** *127*, 6335.
278. Tong, X.; Zhao, Y.; An, B.-K.; Park, S. Y. *Adv. Funct. Mater.* **2006,** *16*, 1799.
279. Chen, K.-H.; Yang, J.-S.; Hwang, C.-Y.; Fang, J.-M. *Org. Lett.* **2008,** *10*, 4401.

PHOTOCHEMISTRY AND PHOTOPHYSICS OF METAL COMPLEXES WITH DENDRITIC LIGANDS

VINCENZO BALZANI, GIACOMO BERGAMINI and PAOLA CERONI

Dipartimento di Chimica "G. Ciamician", Università di Bologna, via Selmi 2, Bologna, Italy

ABSTRACT

Combinations of suitably chosen metal ions and dendritic ligands may lead to giant metal complexes that display interesting spectroscopic properties, particularly as far as luminescence is concerned. This chapter illustrates some fundamental aspects of the interaction of light with dendrimers and then reviews results obtained with dendrimers (i) containing one or more metal complexes as branching centers or as a core, (ii) capable of coordinating one or more metal ions in their cavities, (iii) assembled around metal ions without or with other ligands. The study of the luminescent properties reveals that these compounds can be useful for several purposes, including light harvesting, sensing with signal amplification, conversion of the absorbed light into emitted light of quite different wavelengths (e.g., UV light into IR light), and information processing.

INORGANIC PHOTOCHEMISTRY
VOLUME 63 ISSN 0898-8838 / DOI:10.1016/B978-0-12-385904-4.00008-1

Keywords: Luminescence; Energy transfer; Electron transfer; Lanthanide ions; Sensors.

I. Dendrimers: A New Class of Ligands

Dendrimers (*1*) are macromolecules that exhibit a defined structure and not only a high degree of order but also a high degree of complexity. From a topological viewpoint, dendrimers contain three different regions: core, branches, and surface (Fig. 1). A most important feature of dendrimer chemistry is the possibility to insert selected chemical units in predetermined sites of their architecture. Further, because of their three-dimensional structure, dendrimers exhibit internal dynamic cavities where ions or molecules can be hosted.

Dendrimers were initially developed in the field of organic chemistry. More recently, a number of dendrimers based on or containing metal ions have been prepared and investigated. The study of these species has considerably expanded the scope of metal coordination chemistry.

By using dendrimers, it is possible to construct large nanoobjects capable of performing complex functionalities that derive from the integration of the specific properties of the constituent moieties. Nowadays both chemistry and physics of dendritic

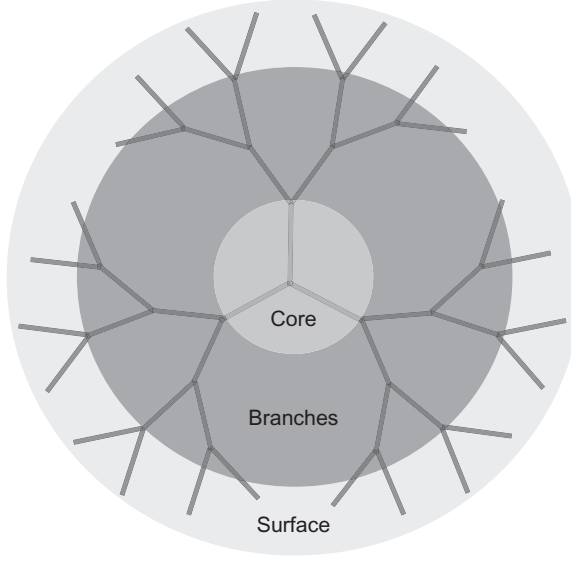

FIG. 1. Schematic representation of a dendrimer, evidencing three different regions: core, branches, and surface.

molecules are rapidly expanding for fundamental research as well as for technological applications (*2*).

Dendrimers are ideal scaffolds to organize many luminescent units in a restricted space according to a predetermined pattern. Because of their proximity, the various functional groups of a dendrimer can easily give rise to energy- and electron-transfer processes with one another, or with molecules or ions hosted in the dendritic cavities or associated to the dendrimer surface (*3*).

Combination of the chemistry of metal ions with the chemistry of dendrimers can lead to a great variety of novel compounds. In this chapter, we will deal with six exemplifying cases (Fig. 2) belonging to three classes of compounds, namely,

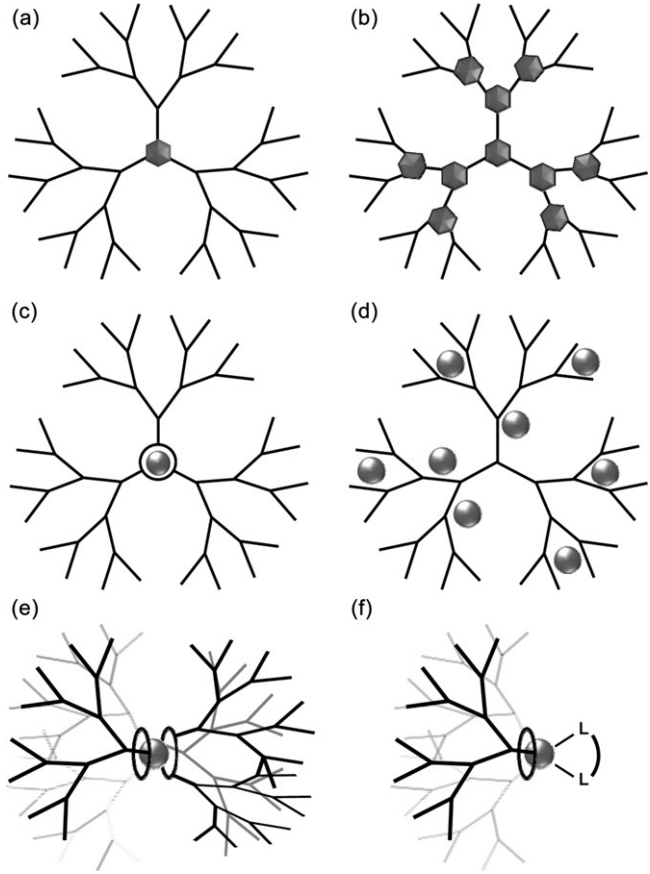

FIG. 2. Schematic representation of the six cases of metal complexes with dendritic ligands: dendrimers containing one (a) or more (b) metal complexes (hexagons) as branching centers; dendrimers capable of coordinating one (c) or multiple (d) metal ions (circles); dendrimers assembled around metal ions without (e) or with (f) other ligands (L–L).

– dendrimers with one or more metal complexes as branching centers (Fig. 2a and b);
– dendrimers capable of coordinating one or more metal ions in their cavities (Fig. 2c and d);
– dendrimers assembled around metal ions without or with other ligands (Fig. 2e and f).

We will focus on the remarkable luminescent properties of selected examples of compounds belonging to the above-mentioned categories.

For the sake of simplicity, electronic transitions in metal complexes are usually classified on the basis of the predominant localization, on the metal or on the ligand(s), of the molecular orbitals involved in the transition (*4*). This assumption leads to the well-known classification of the electronic excited states of metal complexes into three types, namely, metal-centered (MC), ligand-centered (LC), and charge-transfer (CT). The CT excited states can be further classified as ligand-to-metal charge-transfer (LMCT) and metal-to-ligand charge-transfer (MLCT).

II. Intrinsic Photochemical and Photophysical Properties of Organic Dendrimers

Organic dendrimers are constituted by molecular components that can absorb light and, often, undergo luminescence. It is therefore worthwhile recalling some fundamental aspects of the processes that follow light excitation of an organic molecule and then the complications that may arise because of the interactions among nearby molecular components.

Figure 3a shows a schematic energy level diagram for a molecule that could be a chromophoric and luminescent unit of an organic dendrimer. In most cases, the ground state of a molecule is a singlet state (S_0), and the excited states are either singlets (S_1, S_2, etc.) or triplets (T_1, T_2, etc.). In principle, transitions between states having the same spin value are allowed, whereas those between states of different spin are forbidden. Therefore, the electronic absorption bands observed in the UV–visible spectrum of molecules usually correspond to $S_0 \rightarrow S_n$ transitions. When a molecule is excited to upper singlet excited states, it usually undergoes a fast and 100% efficient radiationless deactivation (internal conversion, ic) to the lowest excited singlet, S_1. Such an excited state undergoes deactivation via three competing processes: nonradiative decay to the ground state (internal

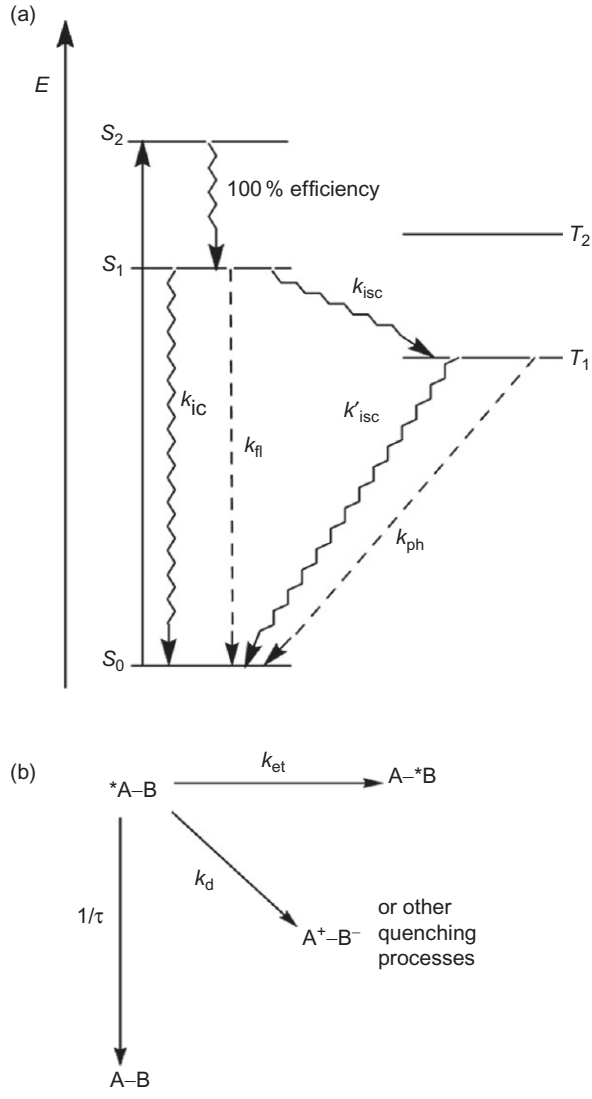

FIG. 3. (a) Schematic energy level diagram for a generic molecule. For more details, see text. (b) Schematic deactivation processes of an excited state in a supramolecular species.

conversion, rate constant k_{ic}); radiative decay to the ground state (fluorescence, k_{fl}); conversion to the lowest triplet state T_1 (intersystem crossing, k_{isc}). In its turn, T_1 can undergo deactivation via nonradiative (intersystem crossing, k'_{isc}) or radiative (phosphorescence, k_{ph}) decay to the ground state S_0.

The kinetic constants of the deactivation processes usually cannot be measured directly. What can be easily measured is the lifetime (τ) of an excited state:

$$\tau(S_1) = \frac{1}{(k_{ic}+k_{fl}+k_{isc})} \tag{1}$$

$$\tau(T_1) = \frac{1}{(k'_{isc}+k_{ph})} \tag{2}$$

The orders of magnitude of $\tau(S_1)$ and $\tau(T_1)$ are approximately 10^{-9}–10^{-7} and 10^{-3}–10^{0} s, respectively.

Other quantities that can be measured are the quantum yields of fluorescence and phosphorescence:

$$\Phi_{fl} = \frac{k_{fl}}{(k_{ic}+k_{fl}+k_{isc})} \tag{3}$$

$$\Phi_{ph} = \left[\frac{k_{ph}}{(k'_{isc}+k_{ph})}\right] \times \left[\frac{k_{isc}}{(k_{ic}+k_{fl}+k_{isc})}\right] \tag{4}$$

Deactivation of an excited state in fluid solution can occur not only by the above-mentioned intrinsic (first order) decay channels but also by interaction with other species (called "quenchers") following second order kinetics. The two most important types of interactions are those leading to energy (Eq. 6) or electron (Eqs. 7 and 8) transfer (*A and *B stand for excited molecules):

$$A + h\nu \rightarrow {}^{*}A \tag{5}$$

$${}^{*}A + B \rightarrow A + {}^{*}B \tag{6}$$

$${}^{*}A + B \rightarrow A^{+} + B^{-} \tag{7}$$

$${}^{*}A + B \rightarrow A^{-} + B^{+} \tag{8}$$

In both cases, the luminescence of the species A is quenched, and in the case of energy transfer, it can be replaced by the luminescence of species B (sensitization process). In dendrimers, energy- and electron-transfer processes can also occur among nearby molecular components incorporated in the dendrimer structure. For example, in a dendrimer containing A and B component units, excitation of A may be followed by energy (Eq. 10) or electron (Eqs. 11 and 12) transfer to B (*5*) (Fig. 3b):

$$A - B + h\nu \rightarrow {}^{*}A - B \tag{9}$$

$${}^{*}A - B \rightarrow A - {}^{*}B \tag{10}$$

$${}^{*}A - B \rightarrow A^{+} - B^{-} \tag{11}$$

$${}^{*}A - B \rightarrow A^{-} - B^{+} \tag{12}$$

These types of processes can also occur between molecular components of a dendrimer and molecules or ions hosted in the dendritic cavities or associated to the dendrimer surface. Particularly interesting is the case in which a dendrimer light absorption by a component A is followed by energy transfer to a luminescent component B (Eqs. 9 and 10). The quantum yield of the sensitized emission of B, Φ_{sens}, is given by the product of the efficiency η_{et} of energy transfer from *A to B and the emission quantum yield of B upon direct excitation of this component, $\Phi_{*\text{B}}$,

$$\Phi_{\text{sens}} = \eta_{\text{et}} \Phi_{*\text{B}} \tag{13}$$

$$\eta_{\text{et}} = \frac{k_{\text{et}}}{(k_{\text{et}} + 1/\tau + k_{\text{d}})} \tag{14}$$

where k_{et} is the first order rate constant for energy transfer from *A to B (Eq. 10), τ is the intrinsic lifetime of the relevant ($\tau(S_1)$ or $\tau(T_1)$, Eqs. 1 and 2) excited state of A involved in the process, and k_{d} is the rate constant of other deactivation processes that compete with energy transfer (e.g., electron transfer, Eqs. 11 and 12).

Energy transfer requires electronic interactions and therefore its rate decreases with increasing distance, r. Depending on the electronic interaction mechanism, the distance dependence may follow a $1/r^6$ (resonance, also called Förster-type, mechanism) or e^{-r} (exchange, also called Dexter-type, mechanism) (*6*). In both cases, energy transfer is favored when the emission spectrum of the donor overlaps the absorption spectrum of the acceptor.

For a more exhaustive discussion on photo-induced energy and electron transfer in supramolecular systems, please refer to Refs. (*5–7*).

Quenching of an excited state by electron transfer needs electronic interaction between the two partners and obeys the same rules as electron transfer between ground state molecules (Marcus equation and related quantum mechanical elaborations (*7*)), taking into account that the excited-state energy can be used, to a first approximation, as an extra free energy contribution for the occurrence of both oxidation and reduction processes.

When an excited state of a molecule undergoes strong electronic interaction with a nearby ground state molecule, new chemical species originate, which are called excimers (from *excited dimers*) or exciplexes (from *excited complexes*), depending on whether the two interacting units have the same or different chemical nature (Fig. 4a). It is important to notice that excimer and exciplex formation is a reversible process and that both excimers and exciplexes sometimes (but not always!) can give luminescence (Fig. 4b). Compared with the "monomer" emission, the emission of an excimer or exciplex is always displaced to lower energy (longer wavelengths) and usually corresponds to a broad and rather weak band.

Excimers are usually obtained when an excited state of an aromatic molecule interacts with the ground state of a molecule of the same type. Exciplexes are obtained when an electron donor (acceptor) excited state interacts with an electron acceptor

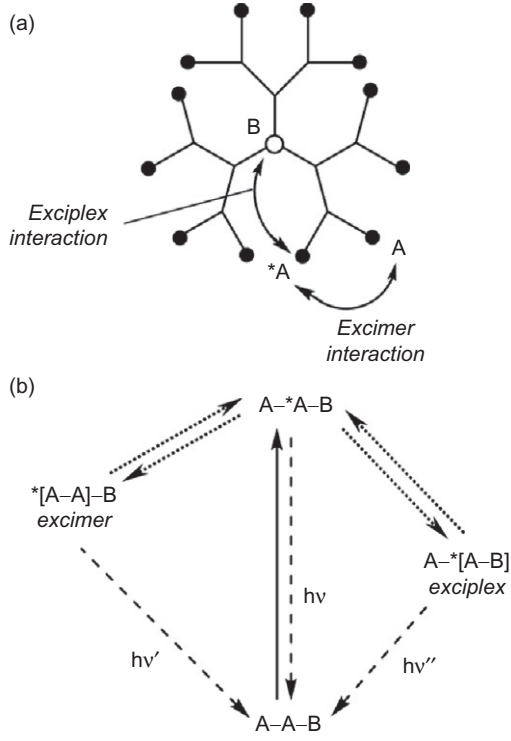

FIG. 4. Schematic (a) representation of excimer and exciplex formation in a dendrimer and (b) energy level diagram showing the three types of emissions that can result.

(donor) ground state molecule; for example, between excited states of aromatic molecules (electron acceptors) and amines (electron donors). In dendrimers containing a variety of components, both exciplex and excimer formation can take place (see e.g., Refs. (*8,9*)). In such a case, as many as three different types of luminescence can be observed, namely, "monomer" emission, exciplex emission, and excimer emission (Fig. 4b).

If there is a nonnegligible electronic interaction between adjacent chromophoric units already in the ground state, the absorption spectrum of the species may substantially differ from the sum of the absorption spectra of the component units. When the units have the same chemical nature, the interaction leads to formation of dimers. When the two units are different, the interaction is usually CT in nature with formation of CT complexes. Excitation of such dimers leads to an excited state that is substantially the same as the corresponding excimers, and excitation of the CT ground state complexes leads to an excited state that is substantially the same as that of the corresponding exciplexes.

III. Dendrimers with One or More Metal Complexes as Branching Centers

In this section, we will describe selected examples in which metal complexes constitute the core (Fig. 2a) or the branching points (Fig. 2b) of the dendritic architecture. Therefore, the dendrimer does not exist by itself as a ligand.

A. A Metal Complex as Core

Dendrimer $\mathbf{1}^{2+}$ (Fig. 5) is a classical example of a dendrimer built around a metal complex core. In this compound, the 2,2′-bipyridine ligands, that constitute the first coordination sphere of the Ru^{2+} ion, carry branches containing 1,3-dimethoxybenzene and 2-naphthyl chromophoric units separated by aliphatic connectors (*10*). Since the interchromophoric interactions are weak, the absorption spectrum of $\mathbf{1}^{2+}$ is substantially equal to the summation of the spectra of $[Ru(bpy)_3]^{2+}$, which is characterized by a broad spin-allowed $Ru \rightarrow bpy$ metal-to-ligand (MLCT) band around 450 nm (*11*), and of the chromophoric groups contained in the branches, which show very intense bands in the near UV region.

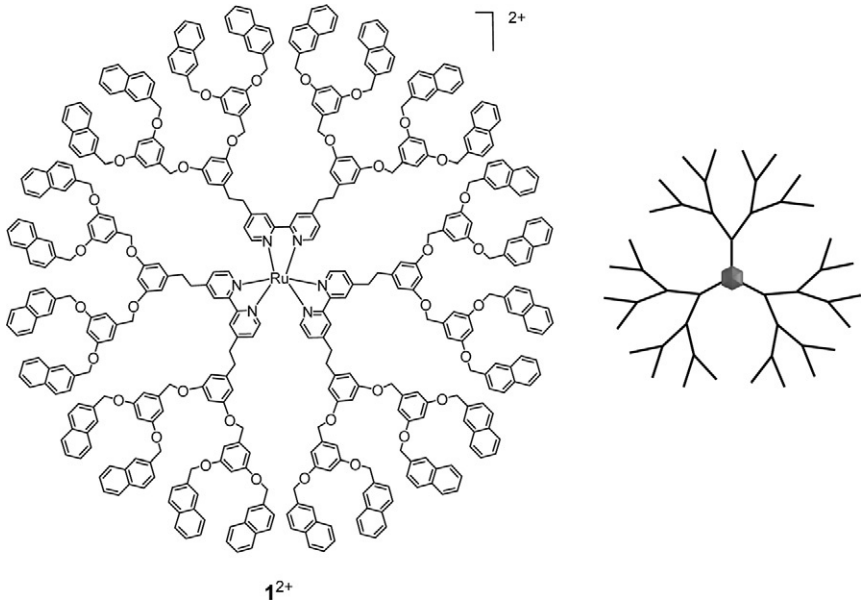

FIG. 5. Formula of a dendrimer with a $[Ru(bpy)_3]^{2+}$ core, and the corresponding scheme (Fig. 2a).

It should be noted that the 1,3-dimethoxybenzene and 2-naphthyl chromophoric units contained in the branches of the dendrimer are not involved in metal coordination. In some way, they belong to a second coordination sphere. If $\mathbf{1}^{2+}$ is considered a large metal complex, the absorption and emission bands of the 1,3-dimethoxybenzene and 2-naphthyl chromophoric units can formally be classified as LC. However, $\mathbf{1}^{2+}$ can be more properly viewed as a supramolecular (multicomponent) species (*12*). In such species, each chromophoric unit displays its own absorption spectrum since there is no appreciable interactions among them in the ground state, but in the excited state even weak interactions can cause intercomponent energy or electron-transfer processes. This kind of reasoning can also be applied to all the other systems discussed in this chapter.

The lowest excited state of dendrimer $\mathbf{1}^{2+}$ is an ^{3}MLCT level of the $[Ru(bpy)_3]^{2+}$ unit; because of the presence of the heavy metal atom, this level is populated with unitary efficiency from the upper lying ^{1}MLCT excited state. All the three types of chromophoric groups present in the dendrimer, namely, $[Ru(bpy)_3]^{2+}$, dimethoxybenzene, and naphthalene, are potentially luminescent species. In dendrimer $\mathbf{1}^{2+}$, however, the UV fluorescence of the dimethoxybenzene- and naphthyl-type units is almost

completely quenched with concomitant sensitization of the orange $[Ru(bpy)_3]^{2+}$ phosphorescence ($\lambda_{max} = 610$ nm). These results show that energy-transfer processes with very high efficiency (ca. 90%) take place from the very short lived (nanosecond time scale) potentially fluorescent excited states of the aromatic units of the wedges to the relatively long lived (microsecond time scale) ^{3}MLCT level of metal-based dendritic core. Dendrimer $\mathbf{1}^{2+}$ is therefore an example of a light-harvesting antenna system, as well as of a species capable of changing the color of the incident light. It should also be noted that in aerated solution, the phosphorescence intensity of the $[Ru(bpy)_3]^{2+}$ dendritic core is more than twice intense as that of the "free" $[Ru(bpy)_3]^{2+}$ parent compound because the dendrimer branches protect the core from dioxygen quenching *(13)*.

A light-harvesting antenna based on the same chromophores has been obtained by a proton-driven self-assembly of the $[Ru(bpy)(CN)_4]^{2-}$complex and a dendrimer containing a 1,4,8,11-tetraazacyclotetradecane (cyclam) core appended with four dendrons identical to that of compound $\mathbf{1}^{2+}$ *(14)*. In the self-assembled structure, the two protons are shared between the cyclam core and the cyanide ligand of the Ru(II) complex. The advantage of the present system is the possibility of tuning the emission wavelength by careful choice of a different metal complex without a time-consuming synthesis of a new dendrimer.

B. Dendrimers with Metal Complexes as Branching Centers

In dendrimers with metal complexes as branching centers (Fig. 2b), a key role is played by polytopic-chelating ligands (the *bridging ligands*), which can coordinate more than a single metal center and control the shape of the polynuclear array and the electronic interaction between metal chromophores, thereby allowing for intercomponent energy or electron-transfer processes.

Among such type of dendrimers, an important family is based on the 2,3-bis(2′-pyridyl) pyrazine (dpp) bridging ligand. Within such a family, the largest species contains 22 metal centers *(15)*. The decanuclear compound **2** shown in Fig. 6 is a second-generation dendrimer of this family *(16)*. For the dendrimers of this series, the modular synthetic strategy allows a high degree of synthetic control in terms of the nature and position of metal centers, bridging ligands, and terminal ligands. Since the excited-state level of each metal center in the dendrimer depends on the nature of the metal, its coordination sphere (which in its

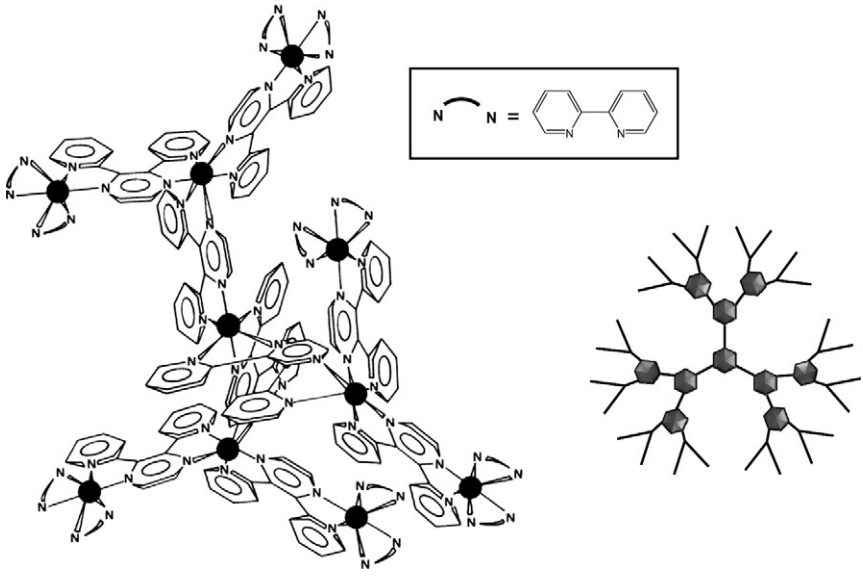

FIG. 6. Formula of a decanuclear Ru^{2+} metal complex with 2,3-bis (2′-pyridyl) pyrazine (dpp) bridging ligands and 2,2′- bipyridine (bpy) peripheral ligands, and the corresponding scheme (Fig. 2b).

turn depends on the metal position, inner or outer, within the dendritic array), and the ligands, each metal-based subunit is characterized by specific excited-state properties, which because of the symmetry of the dendritic structure are usually identical for each metal-based subunit belonging to the same dendritic layer. Therefore, a judicious design allows that the synthetic control translates into control on specific properties, such as the direction of electronic energy flow within the dendritic array (antenna effect) (*17*). For example, in the complex shown in Fig. 6, the lowest excited-state level involves the peripheral subunit(s), and the emission of the species (acetonitrile, room temperature: $\lambda_{max} = 780$ nm; $\tau = 60$ ns; $\Phi_{em} = 3 \times 10^{-3}$) is assigned to a $(bpy)_2Ru \rightarrow \mu$-dpp CT triplet state (*16*). Excitation spectroscopy indicates that quantitative energy transfer takes place from inner subunits to the peripheral ones (*16*). Because of the energy gradient between the dendritic layers, the energy transfer is ultrafast (femtosecond timescale). On the basis of the above discussion, it is not surprising that all the homometallic dendrimers of the same family, independent of the number of Ru subunits (i.e., tetranuclear (*18*), decanuclear (*15*), docosanuclear (*16*), as well as hexanuclear (*19*), heptanuclear (*20*), and tridecanuclear species (*21*), which have particular connections/geometries)

exhibit practically identical photophysical properties, since the lowest energy subunit(s) is in all the cases the identical peripheral $(bpy)_2Ru \rightarrow \mu$-dpp CT state(s).

For heterometallic species, on increasing nuclearity, an unidirectional gradient (center-to-periphery or vice versa) for energy transfer is hardly obtained with only two types of metals (commonly, Ru(II) and Os(II)) and ligands (bpy and 2,3-dpp). In fact, by using a divergent synthetic approach starting from a metal-based core, it becomes unavoidable that metal-based building blocks with high-energy excited states (*high-energy subunits*) are interposed between donor and acceptor subunits of the energy-transfer processes (*17*). For example, while in the tetranuclear $Os[(\mu\text{-dpp})Ru(bpy)_2]_3^{8+}$ ($OsRu_3$) species, in which a central $\{Os(\mu\text{-dpp})_3\}^{2+}$ subunit is surrounded by three $\{Ru(bpy)_2\}^{2+}$ subunits, only the osmium-based core emission is obtained (acetonitrile, room temperature: $\lambda_{max} = 860$ nm; $\tau = 18$ ns; $\Phi_{em} = 1 \times 10^{-3}$) (*22*), indicating quantitative energy transfer from the peripheral Ru-based chromophore to the center Os-based site, for the larger systems peripheral Ru-based emission is not quenched (*17*). This highlights that although downhill or even isoergonic energy transfer between nearby building blocks in the dendrimers based on 2,3-dpp bridging ligand is fast and efficient, direct downhill energy transfer between partners separated by high-energy subunits is much slower and can be highly inefficient. This problem has been overcome (i) by using a third type of metal center, namely, a Pt(II) one, to prepare decanuclear species (second-generation dendrimers) having different metal centers in each "generation" layer (schematically, $OsRu_3Pt_6$ species) (*23*) or, more recently, (ii) in a heptanuclear dendron where the barrier made of high-energy subunits is bypassed via the occurrence of consecutive electron-transfer steps (*24*). Quite interestingly, this latter study also suggests that long-range photo-induced electron-transfer processes do not appear to be dramatically slowed down by interposed high-energy subunits in this class of dendrimers.

IV. Coordination of Metal Ions Inside Dendrimers

Dendrimers containing coordination sites (e.g., amine, amide groups) in their structure can act as ligands of metal ions. We can distinguish dendrimers containing a single coordination site, for example, in the core (Fig. 2c), or multiple coordination sites in the branches (Fig. 2d).

For historical reasons, examples of case 2d, containing multiple amine or amide groups in their branches, will be discussed first. These types of dendrimers give rise to metal complexes of variable stoichiometry and unknown structures since they contain several more or less equivalent ligand units and not well-defined coordination sites.

A. Dendrimers with Multiple Coordination Sites

A.1. Amide coordinating units

Dendrimer **3** (Fig. 7), which is based on a benzene core branched in the 1, 3, and 5 positions, contains 18 amide groups in its branches and 24 chromophoric dansyl units in the periphery. It is well known that, in sufficiently basic solution, amide groups (*25*), including the dansylamide units (*26*) can undergo deprotonation and coordination of transition metal ions. The dansyl units show strong absorption bands in the near UV

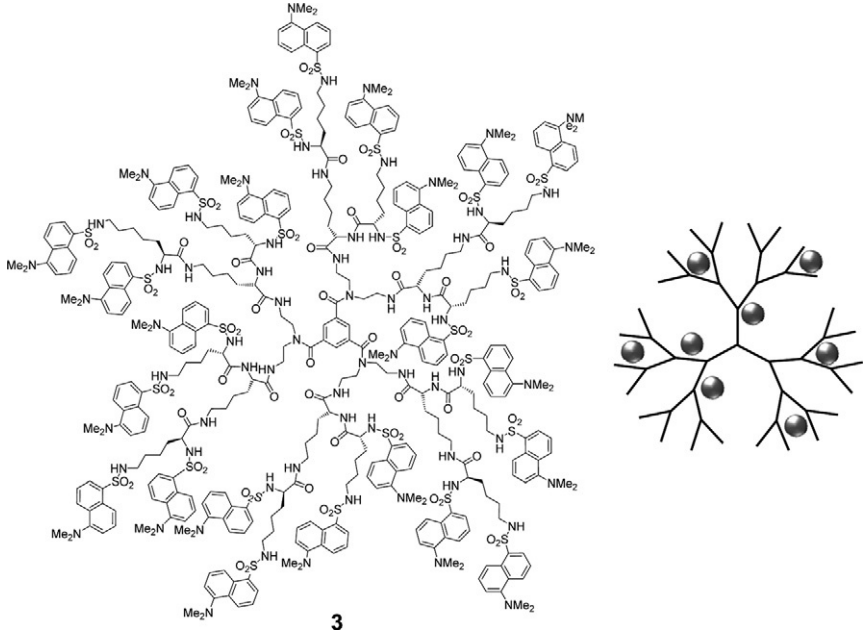

3

Fig. 7. Formula of a dendrimer containing 18 amide groups in its branches and 24 chromophoric dansyl units in the periphery, capable of coordinating metal ions (Co^{2+}, Ni^{2+}, or lanthanide ions), and the corresponding scheme (Fig. 2d).

spectral region and an intense fluorescence band in the visible region. In acetonitrile/dichloromethane (5:1, v/v) solution, the absorption spectrum and the fluorescence properties of the dendrimer are those expected for a species containing 24 noninteracting dansyl units (*27*). Upon addition of Co^{2+} or Ni^{2+} ions to a solution of **3** in the presence of a weak base, the absorption band of the dansyl units did not show any appreciable change, but a strong static quenching of the dansyl fluorescence was observed (*27*). These results indicate that the metal ions are coordinated by the aliphatic amide units and can quench the dansyl fluorescent excited state by energy or electron transfer. Under conditions in which each dendrimer can coordinate no more than a single metal ion (Fig. 2c), about 9 out of 24 dansyl units are quenched.

Investigations have also been performed (*28*) by using lanthanide ions since amide groups are known to be good ligands for such metal ions (*29*). Addition of lanthanide ions to solutions containing dendrimer **3** showed that (*28*) (a) the absorption spectrum of the dendrimer is almost unaffected; (b) the fluorescence of the dansyl units is quenched; (c) the quenching effect is very large for Nd^{3+} and Eu^{3+}, moderate for Er^{3+} and Yb^{3+}, small for Tb^{3+}, and very small for Gd^{3+}; (d) in the case of Nd^{3+}, Er^{3+}, and Yb^{3+}, the quenching of the dansyl fluorescence is accompanied by the sensitized near-infrared emission of the lanthanide ion. Interpretation of the results obtained on the basis of the energy levels (Fig. 8) and redox potentials of the dansyl unit and of the metal ions has led to the following conclusions: (i) at low metal ion concentrations, each dendrimer hosts only one metal ion (Fig. 2e); (ii) the very small quenching effect observed for Gd^{3+} is assigned to charge perturbation of the S_1 dansyl excited state, indicating that the effect on intersystem crossing is small, if any; (iii) when the hosted metal ion is Nd^{3+} or Eu^{3+}, all the 24 dansyl units of the dendrimer are quenched with unitary efficiency; (iv) quenching by Nd^{3+} and Er^{3+} takes place by direct energy transfer from the fluorescent (S_1) excited state of dansyl to a manifold of Nd^{3+} energy levels, followed by sensitized near-infrared emission from the metal ion ($\lambda_{max} = 1064$ nm for Nd^{3+} and $\lambda_{max} = 1525$ for Er^{3+}); (v) quenching by Eu^{3+} does not lead to any sensitized emission since the lowest excited state of the system is a nonemissive electron-transfer excited state; upon protonation of the dansyl units, however, the electron-transfer excited state moves to very high energy, and at 77 K, a sensitized Eu^{3+} emission is observed. Since the sensitization is not accompanied by quenching of the protonated dansyl fluorescence, energy transfer originates from the T_1 excited state of the

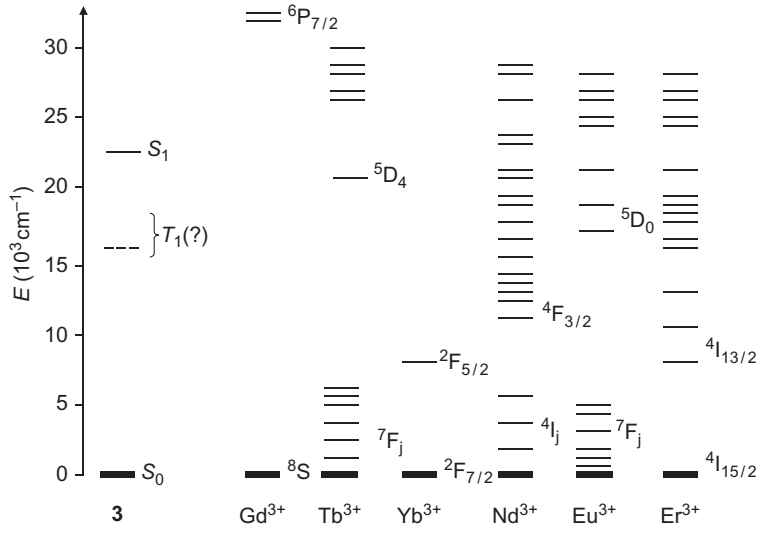

FIG. 8. Energy level diagrams for the dansyl units of dendrimer **3** and the investigated lanthanide ions. The position of the triplet excited state of **3** is uncertain because no phosphorescence can be observed.

protonated dansyl units; (vi) in the case of Yb^{3+}, the sensitization of the near-infrared MC emission occurs via the intermediate formation of a dansyl to Yb^{3+} electron-transfer excited state; at 77 K the electron-transfer excited state moves to higher energy, thus preventing the population of the Yb^{3+} emitting excited state; (vii) the small quenching effect observed for Tb^{3+} is partly caused by a direct energy transfer from the fluorescent (S_1) excited state of dansyl; on protonation of the dansyl units, a strong Tb^{3+} sensitized emission is observed at 77 K, originating from the T_1 excited state of the protonated dansyl units.

An extension of the present work has recently been published (*30*), in which a supramolecular system constituted by five luminescent components, namely, one dendrimer **3**, two Nd^{3+} ions, and two molecular clips, have been assembled in solution with light-harvesting properties.

A.2. Amine coordinating units

Dendrimers of the poly(propylene amine) family can be easily functionalized in the periphery with luminescent units such as dansyl (*31*). The resulting dendrimers *n*D, where the generation number *n* goes from 1 to 5, comprise $2^{(n+1)}$ dansyl functions in the periphery and $2^{(n+1)}-2$ tertiary amine units in the interior.

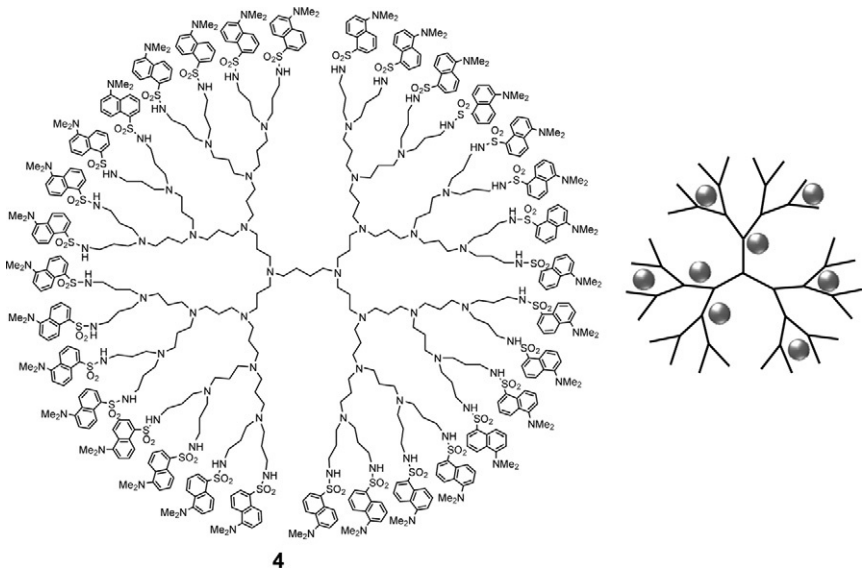

FIG. 9. Formula of a dendrimer constituted by a poly(propylene amine) structure functionalized with 32 dansyl units at the periphery, capable of coordinating Co^{2+} ions, and the corresponding scheme (Fig. 2d).

Compound **4** (Fig. 9) is the fourth generation dendrimer 4D that contains 30 tertiary amine units and 32 dansyl functions. The dansyl units behave independently from one another so that these dendrimers display light absorption and emission properties characteristic of the dansyl chromophoric group. Because of the presence of the aliphatic amine groups in their interior, these dendrimers can be used as ligands for transition metal ions. It should be noted that the dansyl units are not involved in metal coordination, so that, as we have seen in Section IV.A.1, they may be considered as components of a second coordination sphere covalently linked to the amine ligands that constitute the first coordination sphere of the metal ions. Therefore, the absorption and emission bands of dansyl can be classified as LC, but as discussed above, it is convenient to consider the metal complexes of **4** and of the related dendrimers as supramolecular species where the component chromophoric units do not interact in the ground state but excited-state interactions can lead to intercomponent energy and electron-transfer processes.

The titration of these dansyl-functionalized dendrimers with Co^{2+} ions has been carefully investigated (32). For comparison purposes, the behavior of a monodansyl reference compound has also been studied. The results obtained have shown that

(i) the absorption and fluorescence spectra of a monodansyl reference compound are not affected by addition of Co^{2+} ions; (ii) in the case of the dendrimers, the absorption spectra are unaffected, but a strong quenching of the fluorescence of the peripheral dansyl units is observed; (iii) the fluorescence quenching takes place by a static mechanism involving coordination of metal ions in the interior of the dendrimers; (iv) metal ion coordination by the dendrimers is a fully reversible process; (v) a strong amplification of the fluorescence quenching signal is observed with increasing dendrimer generation. The results obtained show that metal coordination involves the amine groups and that the poly(propylene amine) dendrimers functionalized with luminescent dansyl units can be profitably used as supramolecular fluorescent sensors for metal ions. The advantage of a dendrimer for this kind of application is related to the fact that a single analyte can interact with a great number of fluorescent units, which results in signal amplification. For example, when a Co^{2+} ion enters dendrimer **3**,the fluorescence of all the 32 dansyl units is quenched, with a 32 times increase in sensitivity with respect to a normal dansyl sensor. This concept is illustrated in Fig. 10.

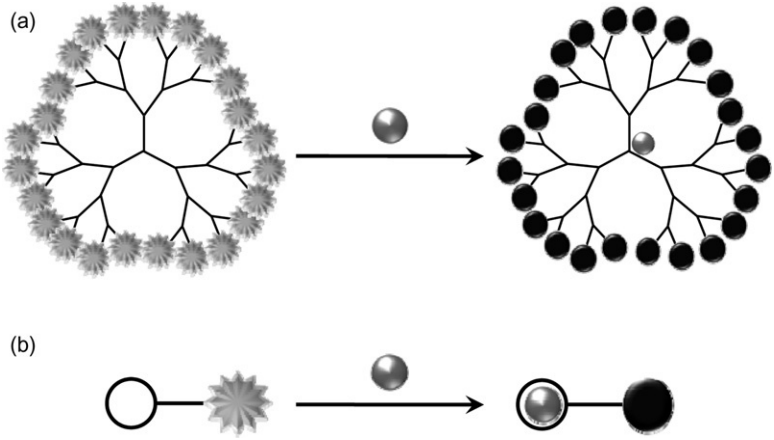

FIG. 10. Schematic representation of (a) a fluorescent sensor with signal amplification and (b) a conventional fluorescent sensor. In the case of a dendrimer, the absorbed photon excites a single fluorophore component, that is quenched by the metal ion, regardless of its position. For more details, see text.

B. Dendrimers with a Single Coordination Site

A much better defined coordination arrangement around a metal ion is obtained when a dendrimer contains a precise coordination site, for example, in the core.

Dendrimer **5** (Fig. 11) consists of a cyclam core appended with 12 dimethoxybenzene and 16 naphthyl units. Cyclam is one of the most extensively investigated ligands in coordination chemistry (*33*). Both cyclam and its 1,4,8,11-tetramethyl derivative in aqueous solution can be protonated and can coordinate metal ions such as Co(II), Ni(II), Cu(II), Zn(II), Cd(II), and Hg(II) with high stability constants (*34*).

In acetonitrile–dichloromethane 1:1 (v/v) solution, the absorption spectrum of dendrimer **5** is dominated by naphthalene absorption bands and the dendrimers exhibit three types of emission bands, assigned to naphthyl-localized excited states ($\lambda_{max} = 337$ nm), naphthyl excimers (λ_{max} ca. 390 nm), and naphthyl-amine exciplexes ($\lambda_{max} = 480$ nm) (*35*).

Extensive investigations have been performed on the interaction of dendrimers of this class with metal ions (*36*). Coordination of Zn^{2+}, a metal ion that is difficult to oxidize and reduce and that exhibits a d^{10} electronic configuration, leads to

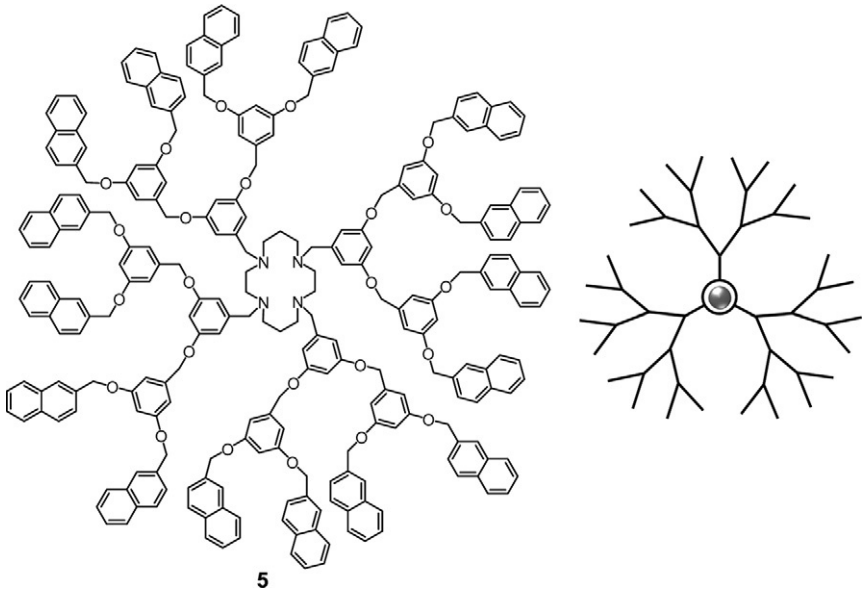

Fig. 11. Formula of a dendrimer consisting of a cyclam core, capable of coordinating a Zn^{2+} ion, and the corresponding scheme (Fig. 2c).

complexes that cannot exhibit MC or CT excited states at low energy. Nevertheless, Zn^{2+} coordination by the dendrimer causes strong changes in the emission spectrum of the dendrimer since engagement of the nitrogen lone pairs in the coordination of the metal ion prevents exciplex formation, with a resulting increase of the naphthyl fluorescence. Such a fluorescent signal is quite suitable for monitoring the formation of the complexes in dendrimer/metal titration experiments.

Complexation of dendrimer **5** with lanthanide ions (Nd^{3+}, Eu^{3+}, Gd^{3+}, Tb^{3+}, Dy^{3+}) [3636b] leads to qualitatively similar results.

V. Coordination of Dendrimers Around Metal Ions

When a dendrimer contains a precise coordination site, as previously reported for case 2c, more than one dendrimer (Fig. 2e) or a dendrimer and other ligands (Fig. 2f) can be assembled around a metal ion.

A. Coordination of Dendrimers Alone

We have seen in Section IV.B that dendrimer **5** is able to form 1:1 complex with Zn^{2+} ions in acetonitrile/dichloromethane solution. The $[Zn(\mathbf{5})]^{2+}$ complex is stable as long as the Zn^{2+} concentration is equal or higher than that of dendrimer **5**, while at low Zn^{2+} concentration, dendrimer **5** gives rise only to complexes with 2:1 dendrimer/metal stoichiometry with a high formation constant ($>10^{13}\,M^{-2}$), as evidenced by both fluorescence and ^1H NMR titrations. The $[Zn(\mathbf{5})_2]^{2+}$ species is an example of case 2e: the dendrimer branches not only do not hinder but also in fact favor coordination of cyclam to Zn^{2+} with respect to coordination of solvent molecules or counter ions. Two limiting structures can be proposed for the 2:1 complexes: (i) an "inward" structure, stabilized by the intermeshing of the branches of the two coordinated dendrimers; (ii) an "outward" structure in which the branches of the two coordinated dendrimers do not interact but impose to the cyclam core a very specific coordination structure. Indeed, an "inward" structure for the 2:1 complex stabilized by branch intermeshing should increase the probability of excimer formation compared with the 1:1 species. In such a case, the intensity of the excimer band (λ_{max} ca. 390 nm) should grow more rapidly at the beginning of the titration, when formation of a 2:1 species is favored. This seems not to be the case for dendrimer **5**. Therefore, in the $[Zn(\mathbf{5})_2]^{2+}$ species, the dendrimer

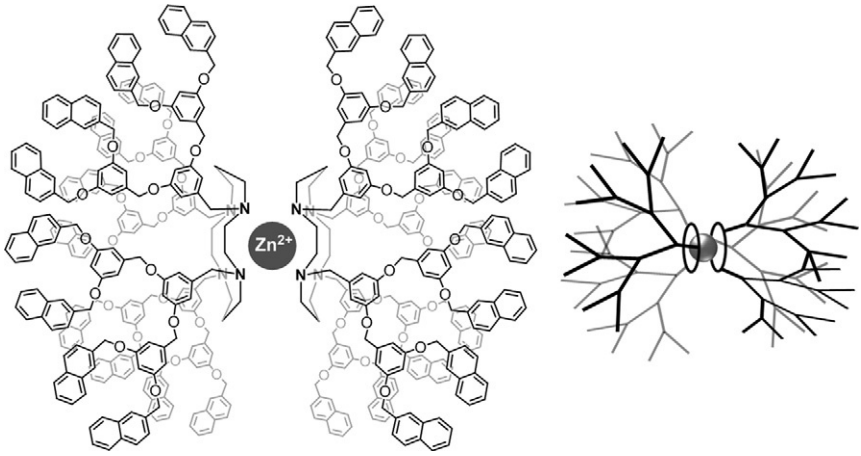

FIG. 12. Schematic representation of a metal complex containing a Zn^{2+} ion coordinated by two cyclam-cored dendrimer **5**, and the corresponding scheme (Fig. 2e).

branches are likely extending outward (Fig. 12). Further, the two cyclam cores, to account for the coordination number (≤ 6) of Zn^{2+}, are likely forced to adopt a structure in which not all of the four N atoms are available for Zn^{2+} coordination, thereby favoring a 2:1 stoichiometry.

In the case of lanthanide ions (Nd^{3+}, Eu^{3+},Gd^{3+}, Tb^{3+}, Dy^{3+}) [3636b], the complex stoichiometry is different: at low metal ion concentration, the formation of 1:3 (metal/dendrimer) complex ($\log \beta_{1:3} = 20.3$) is demonstrated by fluorescence and NMR titration. It is likely that, in the $[M(\mathbf{5})_3]^{3+}$ complex, not all the 12 nitrogens of the three cyclam cores are engaged in metal ion coordination. However, upon metal coordination, the exciplex emission band completely disappears, as it is was previously observed upon acid titration. Clearly, as is also shown by NMR results, the presence of the 3^+ ion is "felt" by all the nitrogens of the three cyclam moieties, thereby raising the energy of the exciplex excited state above that of the naphthyl-based one. For all the lanthanide complexes of **5**, no sensitized emission from the lanthanide ion was observed. Therefore, energy transfer from either the S_1 or the T_1 excited state of the naphthyl units of **5** to the lanthanide ion is inefficient. By contrast, efficient energy transfer from naphthalene-like chromophores to Eu^{3+} has been reported in the case in which naphthalene is linked through an amide or carboxylate bond to the lanthanide (*37*). Apparently, the nature of the first coordination sphere plays an important role concerning energy-transfer efficiency.

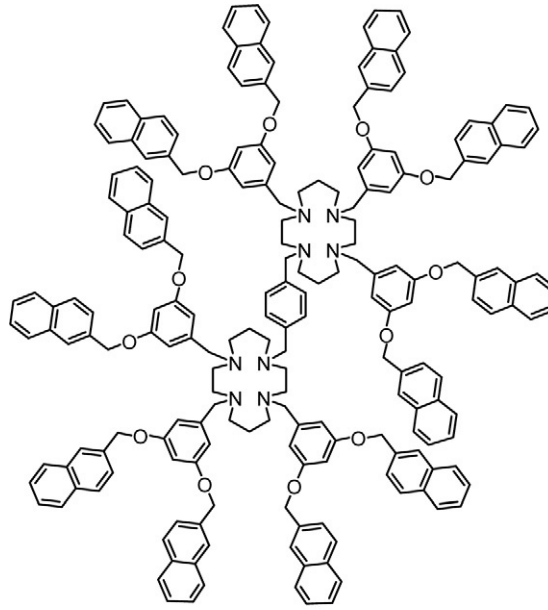

6

FIG. 13. Formula of a dendrimer constituted by a bis-cyclam core.

A step further in cyclam-based dendritic ligands for metal ions is constituted by dendrimer **6** (Fig. 13), containing two covalently linked cyclam units as a core, appended to six branches, each one of them consisting of a dimethoxybenzene and two naphthyl units (*38*). Its photophysical properties are qualitatively similar to that observed for **5**. For example, the emission spectrum evidences the presence of naphthyl-localized excited states ($\lambda_{max} = 337$ nm), naphthyl excimers (λ_{max} ca. 390 nm), and naphthyl-amine exciplexes ($\lambda_{max} = 480$ nm).

Dendrimer **6** ability to coordinate Zn(II) and Cu(II) in acetonitrile/dichloromethane 1:1 (v/v) solution has been carefully investigated (*38*).

Upon titration with $Zn(CF_3SO_3)_2$, no change was observed in the absorption spectrum, whereas strong changes were observed in the emission spectrum. Such changes, qualitatively similar to those caused by protonation, indicate that a 1:1 complex, $[Zn(\mathbf{6})]^{2+}$, is first formed and then replaced by a 2:1 species $[Zn_2(\mathbf{6})]^{4+}$ ($\log \beta_{1:1} = 9.7$ and $\log \beta_{2:1} = 16.1$ for these two species, respectively). In the 1:1 complex $[Zn(\mathbf{6})]^{2+}$, the metal ion is likely sandwiched between the two cyclam units. As previously observed in the case of dendrimer **5**, apparently, the dendrimer

branches favor coordination of cyclam units to metal ions with respect to solvent molecules and counter ions. Further, the experimental observation that, in going from $[Zn(\mathbf{6})]^{2+}$ to $[Zn_2(\mathbf{6})]^{4+}$, the intensity of the excimer band does not change suggests that, in these sandwich-type complexes, the dendrimer branches extend outward and maintain the same structure in both species.

Quite different results were obtained upon titration with $Cu(CF_3SO_3)_2$ both in absorption and emission spectra. The absorption spectrum showed the appearance of a broad tail in the 300–400 nm region, assigned to LMCT transitions (a similar absorption band was observed also in the case of mere cyclam). The absorbance values increase almost linearly up to the addition of 2 eq. of metal ion per dendrimer. Therefore, we can conclude that upon addition of $Cu(CF_3SO_3)_2$ to **6**, both the cyclam units of the dendrimer coordinate a Cu^{2+} ion (log $\beta_{2:1} = 11.9$). At variance with the case of Zn^{2+}, the decrease in the intensity of the exciplex emission, caused by the engagement of the cyclam N atoms by protons or metal ions, is not accompanied by an increase in the intensity of the naphthyl-localized emission. This result can be easily rationalized considering that coordination of Cu^{2+}, while preventing deactivation of the excited naphthyl units via exciplex formation, introduces another deactivation channel related to the presence of the low energy LMCT state. Further, analysis of the emission spectral changes upon addition of Cu^{2+} evidences the formation of a 1:1 complex, $[Cu(\mathbf{6})]^{2+}$, then replaced by a 2:1 species, $[Cu_2(\mathbf{6})]^{4+}$.

The $[M(\mathbf{6})]^{2+}$ complexes (M = Zn, or Cu) are examples of the dendritic complexes schematized in Fig. 2e in which the two dendrimer are covalently linked.

B. Coordination of Dendrimers and Other Ligands

We have seen above that a metal ion can assemble two or even three dendrimers **5**. A step further in the complexity of the system is constituted by assembling around a metal ion a dendrimer together with another ligand (Fig. 2f). An example (*39*) is given by the assembly around a metal ion of dendrimer **5** and a molecular clip $\mathbf{C}^{2-}$(Fig. 14) consisting of two anthracene sidewalls and a benzene bridge carrying two sulfate substituents on the para positions.

Upon addition of $Zn(CF_3SO_3)_2$ to an equimolar solution of dendrimer **5** and clip $\mathbf{C}^{2-}$, changes in the absorption and, particularly, in the emission spectra are registered. Upon excitation at

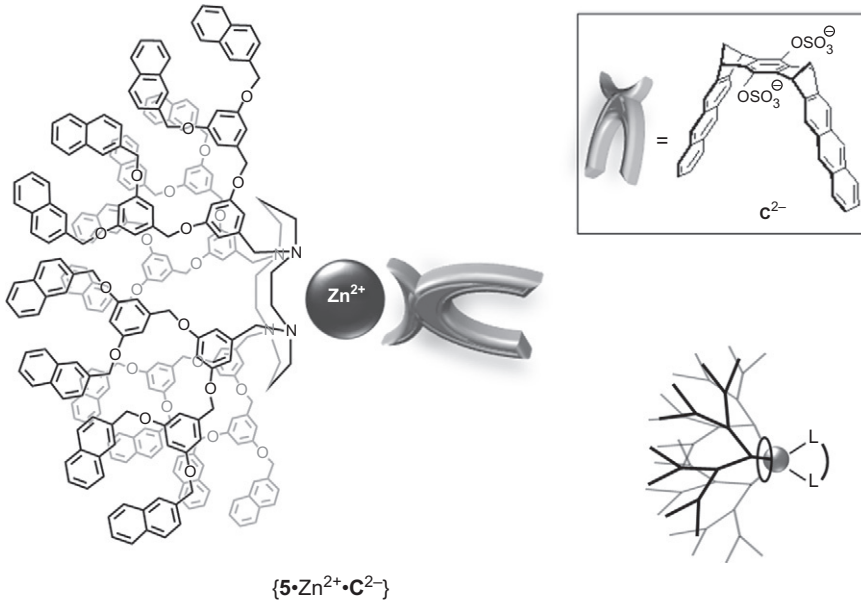

FIG. 14. Schematic representation of a metal complex constituted by dendrimer **5**, a Zn^{2+} ion, and one molecular clip $\mathbf{C}^{2-}$, and the corresponding scheme (Fig. 2f).

288 nm where most of the light is absorbed by the 16 naphthalene chromophores of **5**, a strong increase of the anthracene emission at 400 nm is registered together with changes in intensity of the naphthyl band at 335 nm. A closer look to the titration profiles shows that (i) changes in absorption and emission bands of the clip are significant only after addition of ca. 0.2 eq. of Zn(II); (ii) changes in the naphthyl fluorescence at 335 nm are effective since the beginning with an increase up to ca. 0.6 eq. of Zn(II) and then a minimum at 1.1 Zn(II) eq. These results can be interpreted by formation of a $[Zn(\mathbf{5})_2]^{2+}$ complex at low Zn(II) ion concentration since naphthyl-based emission increases, while clip absorption and emission spectra are not affected. Indeed, as previously discussed, dendrimer **5** forms a very stable complex with 2:1 ligand to metal stoichiometry. Upon further addition of metal ion, the $[Zn(\mathbf{5})_2]^{2+}$ complex is disrupted and Zn(II) is coordinated by both **5** and $\mathbf{C}^{2-}$ forming a [**5**Zn**C**] complex, as demonstrated by the quenching of the naphthyl emission and the sensitization of the anthracene emission. These quenching/sensitization processes has an efficiency higher than 95% and it cannot take place by dynamic mechanisms because of the short lifetime of the fluorescent naphthyl-excited state of

the dendrimer ($\tau < 10$ ns) and the low concentration of the clip acceptor. Upon addition of an excess of Zn(II) (ca. 80 eq.), the fluorescence of both the dendrimer and the clip are those expected for the two separated $[Zn\mathbf{5}]^{2+}$ and [Zn**C**] complexes, demonstrating that the three-component system is destroyed.

Another tool to investigate the formation of the [**5**Zn**C**] complex is represented by fluorescence anisotropy *(40)*. For a simple molecule randomly oriented in fluid solution, the value of anisotropy r is dependent on the angle between the absorption and emission transition moments, an intrinsic property of the fluorophore, and on the rate of the molecule rotation in solution. In principle, the formation of a complex can be followed by a change in fluorescence anisotropy since the complex rotation in solution is expected to be slower compared to that of the ligand because of the bigger dimension. The measured value r_{exp} is given by the following equation:

$$r_{exp} = F_L r_L + F_A r_A$$

where F_L and F_A are the fractional fluorescence intensities, and r_L, r_A are the fluorescence anisotropy of the ligand L and associated species A. For a supramolecular system containing multiple identical fluorophores, other channels of depolarization are represented by local movements of the fluorophore inside the multicomponent structure and by energy migration between identical fluorophores.

In the case of the clip, two anthracene chromophores are linked by a quite rigid bridge, so that depolarization can only be caused by global rotation of the clip and by energy migration: the resulting value of steady-state anisotropy in CH_3CN/CH_2Cl_2 1:1 (v/v) solution at 298 K is very low ($r_{ss} \approx 0.01$). Upon addition of 1 eq. of Zn(II) and formation of the [Zn**C**] complex, the value of r_{ss} does not show a significant variation, demonstrating that the resulting complex is still rotating very fast. However, upon addition of the dendrimer and formation of the [**5**Zn**C**] complex, a significant increase of the anthracene anisotropy is observed ($r_{ss} \approx 0.02$). Upon complexation of **5**, the mass and dimension increase to a significant extent and rotation of the whole resulting complex is sufficiently slow that the measured steady-state anisotropy doubles.

To the best of our knowledge, this is the first time in which the formation of a metal ion complex in solution is followed by fluorescence anisotropy. Indeed, this has been made possible in low-viscosity solvents because of the profound change of mass and dimension between the [ZnC] complex and the [**5**Zn**C**] complex. In the self-assembled structure [**5**Zn**C**], the clip may function as a ditopic

receptor: on one side the sulfate substituents coordinated to Zn(II) and, on the other side, the highly negative electrostatic potential on the inner van-der-Waals surface of the clip cavity offers a further recognition site for electron-deficient guest molecules.

To overcome the lack of sensitization of the lanthanide emissions for the complex of dendrimers **5** (see above), a supramolecular approach has been pursued (*41*). It was known that complexes of Ru^{2+} containing 2,2′-bipyridine (bpy) and cyanide ligands, that is, $[Ru(bpy)_2(CN)_2]$ and $[Ru(bpy)(CN)_4]^{2-}$, are luminescent and can play the role of ligands giving rise to supercomplexes (*42,43*). Titration of an acetonitrile:dichloromethane 1:1 (v/v) solution of $[Ru(bpy)_2(CN)_2]$ with Nd^{3+} causes changes in the absorption spectrum and quenching of the Ru^{2+} complex emission, accompanied by sensitized Nd^{3+} emission, demonstrating the ability of $[Ru(bpy)_2(CN)_2]$ to complex the lanthanide metal ion. Titration of a 1:1 mixture of dendrimer **5** and $[Ru(bpy)_2(CN)_2]$ in acetonitrile:dichloromethane 1:1 (v/v) with Nd $(CF_3SO_3)_3$ brings about changes in the absorption and emission spectra. The lowest energy absorption band is blue-shifted, as observed for the titration of $[Ru(bpy)_2(CN)_2]$ in the absence of dendrimer. Upon excitation at 260 nm, where most of the light is absorbed by dendrimer **1**, the intensity of the naphthyl monomer emission at 337 nm does not show a monotonous increase, as observed in the absence of the $[Ru(bpy)_2(CN)_2]$ complex, reaches a maximum at 0.5 eq., and then decreases up to about 1.0 eq. of Nd^{3+} to rise again for higher metal ion concentration. The emission intensity at 1.0 eq. is lower than that observed in the absence of $[Ru(bpy)_2(CN)_2]$. These results show that a three-component system $\{\mathbf{5}\cdot Nd^{3+}\cdot[Ru(bpy)_2(CN)_2]\}$ (Fig. 15) is formed in which the dendrimer emission is quenched. The three-component system can be disassembled by addition of an excess of each component, or of cyclam. The main photophysical processes of the $\{\mathbf{5}\cdot Nd^{3+}\cdot[Ru(bpy)_2(CN)_2]\}$ adduct are summarized in Fig. 16, which shows the energy levels of the three components. In the two-component dendrimer–Nd^{3+} system, energy transfer from either the lowest singlet (S_1) or triplet (T_1) excited state of the naphthyl units of the dendrimer to the lanthanide ion does not occur. Sensitization of the Nd^{3+} emission upon dendrimer excitation in the three-component system is mediated by the $[Ru(bpy)_2(CN)_2]$ component. Comparison between the emission quantum yield of $[Ru(bpy)_2(CN)_2]$ upon excitation at 260 nm (dendrimer absorption) and 450 nm ($[Ru(bpy)_2(CN)_2]$ absorption) has allowed to estimate that the energy-transfer efficiency from the S_1 excited state of the naphthyl groups to the ^{1}MLCT excited state of $[Ru(bpy)_2(CN)_2]$ is about 60% (Fig. 16). The energy-transfer

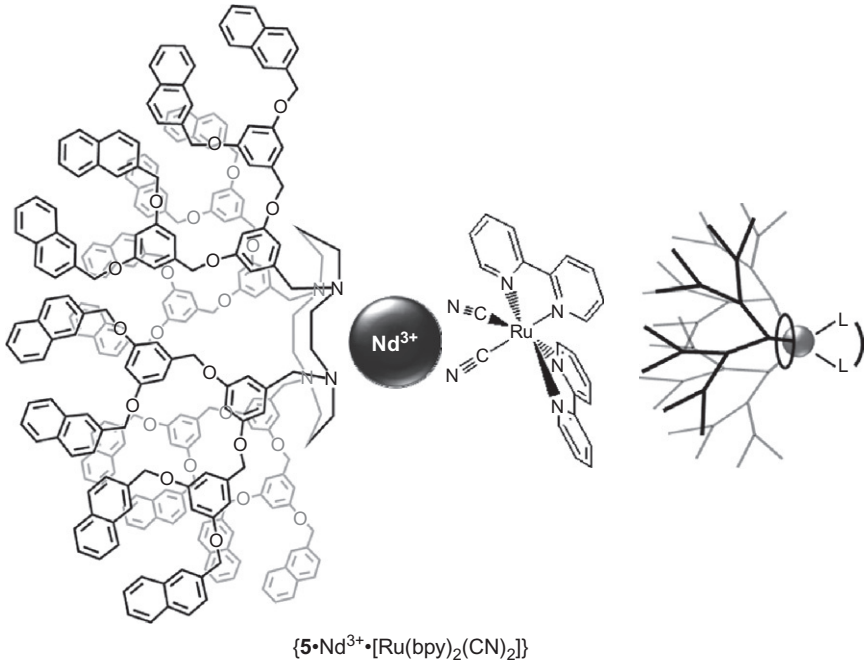

FIG. 15. Schematic representation of a metal complex based on dendrimer **5**, one Nd^{3+} and $[Ru(bpy)_2(CN)_2]$ complex, and the corresponding scheme (Fig. 2f).

efficiency from the ^{3}MLCT excited state of $[Ru(bpy)_2(CN)_2]$ to Nd^{3+} can be assumed to be equal to the efficiency of the quenching of the $[Ru(bpy)_2(CN)_2]$ emission (ca. 90%) because quenching by electron transfer can be ruled out in view of the Nd^{3+} redox properties. No evidence of energy transfer in the adduct from the naphthyl-localized T_1 excited state of the dendrimer to the lowest ^{3}MLCT state of $[Ru(bpy)_2(CN)_2]$ has been found since no change in the T_1 lifetime at 77 K has been observed.

The three components of the self-assembled structure have complementary properties so that new functions emerge from their assembly. Dendrimer **5** has a very high molar absorption coefficient in the UV spectral region because of 12 dimethoxybenzene and 16 naphthyl units, but it is unable to sensitize the emission of an Nd^{3+} ion placed in its cyclam core. The $[Ru(bpy)_2(CN)_2]$ complex can coordinate (by the cyanide ligands) and sensitize the emission of Nd^{3+} ions. Self-assembly of the three species leads to a quite unusual Nd^{3+} complex which exploits a dendrimer and an Ru^{2+} complex as ligands. Such a system behaves as an antenna that can harvest UV to VIS light absorbed by both the

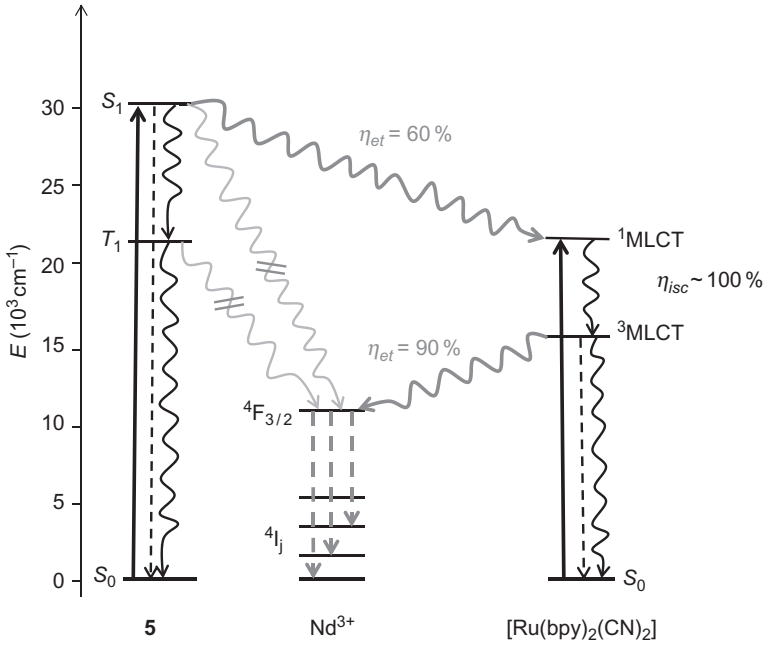

FIG. 16. Energy level diagram showing the excited states involved in the main photophysical processes (absorption: solid lines; radiative deactivation: dashed lines; nonradiative deactivation processes: wavy lines) of the {**5**·Nd^{3+}·$[Ru(bpy)_2(CN)_2]$} three-component system. For the sake of clarity, naphthyl excimer energy level has been omitted.

Ru^{2+} complex and the dendrimer and emit in the NIR region with line-like bands. In principle, the emission wavelength can be tuned by replacing Nd^{3+} with other lanthanide ions possessing low-lying excited states.

VI. Conclusion

The introduction of dendrimers as ligands has greatly expanded the scope of metal coordination chemistry and, in particular, has revitalized the study of luminescent metal complexes. The great potential of dendrimers as light-absorbing ligands and the diversity of their composition, coupled with the variety of metal ions that can be involved and of the dendrimer–metal coordination structures (Fig. 2), has allowed to build systems capable of exhibiting very complex luminescence properties. Such systems are quite suitable to get insight on the mechanisms of energy and electron-transfer processes. Another important feature of this

novel coordination chemistry is the extensive use of fluorescence techniques (including fluorescence anisotropy) to study metal–ligand coordination processes. The role of metal ions can be multifarious: (1) quencher or enhancer of the organic dendrimer luminescence, a phenomenon that can be exploited for sensing purposes; (2) acceptor of the excitation energy of the dendrimer chromophores with generation of intense metal-centered luminescence (antenna effect); (3) controller of the intensity of the various types of ligand-centered luminescence (fluorescence and phosphorescence of molecular component units of the dendrimer, emission from excimer and exciplex species), which might be exploited for information processing.

References

1. (a) Vögtle, F.; Richardt, G.; Werner, N. *"Dendrimer Chemistry"*. Wiley-VCH: Chichester, **2009**. (b) Newkome, G. R.; Vögtle, F. *"Dendrimers and Dendrons"*. Wiley-VCH: Weinheim, **2001**. (c) In: "*Dendrimers and Other Dendritic Polymers*"; Eds. Fréchet, J. M. J.; Tomalia, D. A.; John Wiley & Sons: Chichester, **2001**.
2. (a) Franc, G.; Kakkar, A. K. *Chem. Soc. Rev.* **2010,** *39*, 1536. (b) Wilms, D.; Stiriba, S. E.; Frey, H. *Acc. Chem. Res.* **2010,** *43*, 129. (c) Deloncle, R.; Caminade, A. -M. *J. Photochem. Photobiol. C* **2010,** *11*, 25. (d) Jang, W. -D.; Selim, K. M. K.; Lee, C. -H.; Kang, I. -K. *Prog. Polym. Sci.* **2009,** *34*, 1. (e) Li, W. -S.; Aida, T. *Chem. Rev.* **2009,** *109*, 6047. (f) Astruc, D.; Ornelas, C.; Ruiz, J. *Acc. Chem. Res.* **2008,** *41*, 841. (g) Special Issue on DendrimersIn: Ed. Majoral, J. -P.; *New J. Chem.* **,** *31*. (h) Gingras, M.; Raimundo, J. -M.; Chabre, Y. M. *Angew. Chem. Int. Ed.* **2007,** *46*, 1010.
3. (a) Hwang, S. -H.; Shreiner, C. D.; Moorefield, C. N.; Newkome, G. R. *New J. Chem.* **2007,** *31*, 1192. (b) Ceroni, P.; Bergamini, G.; Marchioni, F.; Balzani, V. *Prog. Polym. Sci.* **2005,** *30*, 453.
4. Balzani, V.; Balzani, V. compiled by In: "*Handbook of Photochemistry*"; Eds. Montalti, M., Credi, A., Prodi, L.; Gandolfi, M. T.; Taylor & Francis Group: Boca Raton, **2006**, ch.1.
5. Balzani, V.; Scandola, F. "*Supramolecular photochemistry*". Horwood: Chichester, **1991**.
6. (a) Klàn, P.; Wirz, J. *"Photochemistry of Organic Compounds. From Concepts to Practice"*. Wiley: Chichester, **2009**, Ch. 2. (b) Turro, N. J.; Ramamurthy, V.; Scaiano, J. C. *"Principles of Molecular Photochemistry. An Introduction"*. University Science Books: Sausalito, **2009**, Ch. 7.
7. Piotrowiak, P. In: "*Electron Transfer in Chemistry*"; Ed. Balzani, V.; Vol. I; Wiley-VCH: Weinheim, **2001**, p. 215.
8. Meskers, S. C. J.; Bender, M.; Hübner, J.; Romanovskii, Y. V.; Oestreich, M.; Schenning, A P H J; Meijer, E. W.; Baessler, H. *J. Phys. Chem. A* **2001,** *105*, 10220.
9. (a) Hofkens, J.; Latterini, L.; De Belder, G.; Gensch, T.; Maus, M.; Vosch, T.; Karni, Y.; Schweitzer, G.; De Schryver, F. C.; Hermann, A.; Müllen, K. *Chem. Phys. Lett.* **1999,** *304*, 1. (b) Karni, Y.; Jordens, S.;

De Belder, G.; Schweitzer, G.; Hofkens, J.; Gensch, T.; Maus, M.; De Schryver, F. C.; Hermann, A.; Müllen, K. *Chem. Phys. Lett.* **1999,** *310*, 73.
10. Pleovets, M.; Vögtle, F.; De Cola, L.; Balzani, V. *New J. Chem.* **1999,** *23*, 63.
11. Balzani, V.; Bergamini, G.; Marchioni, F.; Ceroni, P. *Coord. Chem. Rev.* **2006,** *250*, 1254.
12. (a) Balzani, V.; Credi, A.; Venturi, M. *Chem. Eur. J.* **2002,** *8*, 5524. (b) Balzani, V.; Credi, A.; Venturi, M. *"Molecular Devices and Machines—A Journey in the Nano World"*. Wiley-VCH: Weinheim, **2008**.
13. Vögtle, F.; Plevoets, M.; Nieger, M.; Azzellini, G. C.; Credi, A.; De Cola, L.; De Marchis, V.; Venturi, M.; Balzani, V. J. *Am. Chem. Soc.* **1999,** *121*, 6290.
14. Bergamini, G.; Saudan, C.; Ceroni, P.; Maestri, M.; Balzani, V.; Gorka, M.; Lee, S. -K.; van Heyst, J.; Vögtle, F. J. *Am. Chem. Soc.* **2004,** *126*, 16466.
15. (a) Serroni, S.; Denti, G.; Campagna, S.; Juris, A.; Ciano, M.; Balzani, V. *Angew. Chem. Int. Ed.* **1992,** *31*, 1493. (b) Serroni, S.; Juris, A.; Venturi, M.; Campagna, S.; Resino, I.; Denti, G.; Credi, A.; Balzani, V. *J. Mater. Chem.* **1997,** *7*, 1227.
16. Denti, G.; Campagna, S.; Serroni, S.; Ciano, M.; Balzani, V. *J. Am. Chem. Soc.* **1992,** *114*, 2944.
17. Balzani, V.; Campagna, S.; Denti, G.; Serroni, S.; Juris, A.; Venturi, M. *Acc. Chem. Res.* **1998,** *31*, 26.
18. (a) Campagna, S.; Denti, G.; Sabatino, L.; Serroni, S.; Ciano, M.; Balzani, V. *Inorg. Chem.* **1990,** *29*, 4750. (b) Serroni, S.; Campagna, S.; Denti, G.; Keyes, T. E.; Vos, J. G. *Inorg. Chem.* **1996,** *35*, 4513.
19. (a) Campagna, S.; Denti, G.; Serroni, S.; Ciano, M.; Balzani, V. *Inorg. Chem.* **1991,** *30*, 3728. (b) Denti, G.; Serroni, S.; Campagna, S.; Ricevuto, V.; Juris, A.; Ciano, M.; Balzani, V. *Inorg. Chim. Acta* **1992,** *507*, 198–200.
20. Denti, G.; Campagna, S.; Sabatino, L.; Serroni, S.; Ciano, M.; Balzani, V. *Inorg. Chim. Acta* **1990,** *176*, 175.
21. Campagna, S.; Denti, G.; Serroni, S.; Juris, A.; Ciano, M.; Balzani, V. *Inorg. Chem.* **1991,** *31*, 2982.
22. Campagna, S.; Denti, G.; Sabatino, L.; Serroni, S.; Ciano, M.; Balzani, V. *J. Chem. Soc. Chem. Commun.* **1989,** 1500.
23. Sommovigo, M.; Denti, G.; Serroni, S.; Campagna, S.; Mingazzini, C.; Mariotti, C.; Juris, A. *Inorg. Chem.* **2001,** *40*, 3318.
24. Puntoriero, F.; Serroni, S.; Galletta, M.; Juris, A.; Licciardello, A.; Chiorboli, C.; Campagna, S.; Scandola, F. *Chem. Phys Chem.* **2005,** *6*, 129.
25. (a) Fabbrizzi, L.; Forlini, F.; Perotti, A.; Seghi, B. *Inorg. Chem.* **1984,** *23*, 807. (b) Fabbrizzi, L.; Licchelli, M.; Pallavicini, P.; Perotti, A.; Taglietti, A.; Sacchi, D. *Chem. Eur. J.* **1996,** *2*, 75. (c) Amendola, V.; Fabbrizzi, L.; Mangano, C.; Pallavicini, P.; Perotti, A.; Taglietti, A. *J. Chem. Soc., Dalton Trans.* **2000,** 185.
26. Prodi, L.; Bolletta, F.; Montalti, M.; Zaccheroni, N. *Eur. J. Inorg. Chem.* **1999,** 455.
27. Balzani, V.; Ceroni, P.; Gestermann, S.; Gorka, M.; Kauffmann, C.; Vögtle, F. *J. Chem. Soc., Dalton Trans.* **2000,** 3765.
28. (a) Vögtle, F.; Gorka, M.; Vicinelli, V.; Ceroni, P.; Maestri, M.; Balzani, V. *ChemPhysChem* **2001,** *12*, 769. (b) Vicinelli, V.; Ceroni, P.; Maestri, M.; Balzani, V.; Gorka, M.; Vögtle, F. *J. Am. Chem. Soc.* **2002,** *124*, 6461.
29. Cross, J. P.; Lauz, M.; Badger, P. D.; Petoud, S. *J. Am. Chem. Soc.* **2004,** *126*, 16278.

30. Branchi, B.; Ceroni, P.; Balzani, V.; Klärner, F. -G.; Vögtle, F. *Chem. Eur. J.* **2010,** *16*, 6048.

31. Vögtle, F.; Gestermann, S.; Kauffmann, C.; Ceroni, P.; Vicinelli, V.; De Cola, L.; Balzani, V. *J. Am. Chem. Soc.* **1999,** *121*, 12161.

32. (a) Balzani, V.; Ceroni, P.; Gestermann, S.; Kauffmann, C.; Gorka, M.; Vögtle, F. *Chem. Commun.* **2000,** 853.. (b) Vögtle, F.; Gestermann, S.; Kauffmann, C.; Ceroni, P.; Vicinelli, V.; Balzani, V. *J. Am. Chem. Soc.* **2000,** *122*, 10398.

33. (a) Lukeš, I.; Kotek, J.; Vojtíšek, P.; Hermann, P. *Coord. Chem. Rev.* **2001,** *287*, 216–217. (b) Hay, B. P.; Hancock, R. D. *Coord. Chem. Rev.* **2001,** *212*, 61.

34. (a) Bianchi, A.; Micheloni, M.; Paoletti, P. *Coord. Chem. Rev.* **1991,** *110*, 17. (b) Kimura, E. *Prog. Inorg. Chem.* **1994,** *41*, 443. (c) Meyer, M.; Dahaoui-Gindrey, V.; Lecomte, C.; Guilard, R. *Coord. Chem. Rev.* **1998,** *178*, 1313. (d) Fabbrizzi, L.; Licchelli, M.; Pallavicini, P.; Sacchi, D. *Supramol. Chem.* **2001,** *13*, 569.

35. Saudan, C.; Balzani, V.; Ceroni, P.; Gorka, M.; Maestri, M.; Vicinelli, V.; Vögtle, F. *Tetrahedron* **2003,** *59*, 3845.

36. (a) Saudan, C.; Balzani, V.; Gorka, M.; Lee, S. -K.; Maestri, M.; Vicinelli, V.; Vögtle, F. *J. Am. Chem. Soc.* **2003,** *125*, 4424. (b) Saudan, C.; Balzani, V.; Gorka, M.; Lee, S. -K.; van Heyst, J.; Maestri, M.; Ceroni, P.; Vicinelli, V.; Vögtle, F. *Chem. Eur. J.* **2004,** *10*, 899. (c) Saudan, C.; Ceroni, P.; Vicinelli, V.; Maestri, M.; Balzani, V.; Gorka, M.; Lee, S. -K.; van Heyst, J.; Vögtle, F. *Dalton Trans.* **2004,** 1597.

37. (a) Beeby, A.; Parker, D.; Williams, J. A. G. *J. Chem. Soc. Perkin Trans.* **1996,** *2*, 1565. (b) Tung, C. -H.; Wu, L. -Z. *J. Chem. Soc. Faraday Trans.* **1996,** *92*, 1381. (c) Parker, D.; Williams, J. A. G. *J. Chem. Soc. Perkin Trans.* **1995,** *2*, 1305.

38. Bergamini, G.; Ceroni, P.; Balzani, V.; Cornelissen, L.; van Heyst, J.; Lee, S. -K.; Vögtle, F. *J. Mater. Chem.* **2005,** *15*, 2959.

39. Branchi, B.; Bergamini, G.; Fiandro, L.; Ceroni, P.; Vögtle, F.; Klärner, F. -G. *Chem. Commun.* **2010,** *46*, 3571.

40. Lakowicz, J. R. *"Principles of Fluorescence Spectroscopy"*. Springer: Singapore, **2006**.

41. Giansante, C.; Ceroni, P.; Balzani, V.; Vögtle, F. *Angew. Chem. Int. Ed.* **2008,** *47*, 5422.

42. (a) Ward, M. D. *Coord. Chem. Rev.* **2006,** *250*, 3128. (b) Scandola, F.; Indelli, M. T. *Pure Appl. Chem.* **1988,** *60*, 973. (c) Balzani, V.; Sabbatini, N.; Scandola, F. *Chem. Rev.* **1986,** *86*, 319.

43. (a) For some recent papers, see:Lazarides, T.; Easun, T. L.; Veyne-Marti, C.; Alsindi, W. Z.; George, M. W.; Deppermann, N.; Hunter, C. A.; Adams, H.; Ward, M. D. *J. Am. Chem. Soc.* **2007,** *129*, 4014.
(b) Bernhardt, P. V.; Bozoglian, F.; Font-Bardia, M.; Martinez, M.; Meacham, A. P.; Sienra, B.; Solans, X. *Eur. J. Inorg. Chem.* **2007,** 5270.
(c) Davies, G. M.; Pope, S. J. A.; Adams, H.; Faulkner, S.; Ward, M. D. *Inorg. Chem.* **2005,** *44*, 4656. (d) Kovács, M.; Horváth, A. *J. Photochem. Photobiol. A: Chem.* **2004,** *163*, 13. (e) Loiseau, F.; Marzanni, G.; Quici, S.; Indelli, M. T.; Campagna, S. *Chem. Commun.* **2003,** 286.

PHOTOCHEMISTRY AND PHOTOCATALYSIS OF RHENIUM(I) DIIMINE COMPLEXES

HIROYUKI TAKEDA[a,b], KAZUHIDE KOIKE[b,c], TATSUKI MORIMOTO[d], HIROKI INUMARU[d] and OSAMU ISHITANI[b,d,e]

[a]Toyota Central R&D Laboratories, Inc., Nagakute, Aichi, Japan
[b]Core Research for Evolutional Science and Technology (CREST), Japan Science and Technology Agency (JST), Kawaguchi, Saitama, Japan
[c]National Institute of Advanced Industrial Science and Technology, Tsukuba, Ibaraki, Japan
[d]Department of Chemistry, Tokyo Institute of Technology, Tokyo, Japan
[e]Research Seeds Program, Japan Science and Technology Agency (JST), Kawaguchi, Saitama, Japan

INORGANIC PHOTOCHEMISTRY
VOLUME 63 ISSN 0898-8838 / DOI: 10.1016/B978-0-12-385904-4.00007-X

ABSTRACT

Rhenium(I) diimine carbonyl complexes have been well investigated because of their functionalities, such as the intense emission properties, capabilities as a building block for multinuclear complexes, and photocatalytic activities.

This chapter describes the following three topics of the rhenium complexes including recent reported works: photophysics, photochemical reactions, and photocatalyses.

After Section I, the photophysical processes of the rhenium complexes are briefly summarized: the electronic structures, the photophysical relaxation processes, and the effects of intramolecular weak interaction between ligands on the photophysical properties.

The next section about photochemical reactions includes ligand substitution, homolysis, and reactions of the ligand on the rhenium complexes. This section also includes synthesis of emissive multinuclear rhenium(I) complexes using the photochemical ligand substitution.

The last section describes unique and high photocatalytic activities of the rhenium(I) diimine carbonyl complexes, especially for CO_2 reduction. The photocatalyses of mononuclear rhenium complexes, multicomponent systems, supramolecular systems with a Ru(II) complex as a photosensitizer, and a rhenium complex with periodic mesoporous organosilica as a light-harvesting system.

Keywords: Rhenium complex; Photophysics; Photochemistry; Photocatalyst.

I. Introduction

The photophysics and photochemistry of d^6 transition metal complexes, such as Re(I), Ru(II), Os(II), and Ir(III), with α-diimines as electron acceptor ligands have been widely investigated during past four decades. These complexes have been frequently used as photofunctional molecules because of the following common properties (*1–16*):

1. Quantum yields for the formation of stable triplet metal-to-ligand charge transfer (MLCT) and/or ππ* excited states are very high, usually almost unity.
2. Many of the complexes are emissive even in solution at room temperature, and the lifetimes of the lowest excited state are long, typically several hundred nanoseconds.

3. The ^{3}MLCT excited states of the complexes have strong oxidation and/or reduction power.

For example, rhenium(I) complexes have been used as emitter materials in electroluminescent devices (*17–20*) and biological probes (*11*), as dye for dye-sensitized solar cells (*21*), as chromophores for photochemical electron or energy transfer studies (*14,17,22*), and as a redox photosensitizer (*23*).

In addition, the family of rhenium(I) diimine carbonyl complexes *fac*-$[Re(LL)(CO)_2(X)(Y)]^{n+}$ (LL = α-diimine) has unique properties and application as follows:

(a) They can be used as photocatalysts for multielectron transfer reactions, especially for CO_2 reduction.
(b) They have been used as building blocks of emissive multinuclear complexes because they have at least three different ligands.
(c) Some of them show unique photoreactivities that are strongly dependent on the ligands.
(d) They have been used as target molecules for time-resolved IR measurements because the CO ligands have strong stretching absorption bands that are very sensitive to electron density at the central rhenium atom.

In this chapter, we focus on these unique photochemical properties of rhenium(I) diimine carbonyl complexes (Fig. 1), especially photochemical reactions and photocatalysis.

II. Photophysics of Rhenium(I) Diimine Complexes

A. Electronic Structure of Rhenium(I) Diimine Complexes

Rhenium diimine carbonyl complexes generally have octahedral coordination geometries. Their electronic states are structured by the electronic interactions between the d orbitals of the central rhenium ion and the molecular orbitals of the ligands, such as CO, which has a strong π-accepting character, and α-diimines, which can act as an electron pool (Fig. 2) (*24,25*). The excited states pertaining to the useful photophysical and photochemical properties of these complexes are (a) the ligand-field (LF) excited states of the central rhenium, (b) ππ* excited states localized on the diimine ligand (LC), and (c) the MLCT state from the rhenium to the diimine ligand. The empty d orbital energy of the central rhenium(I) is high due to the large LF splitting resulting from the low-oxidation state of the central

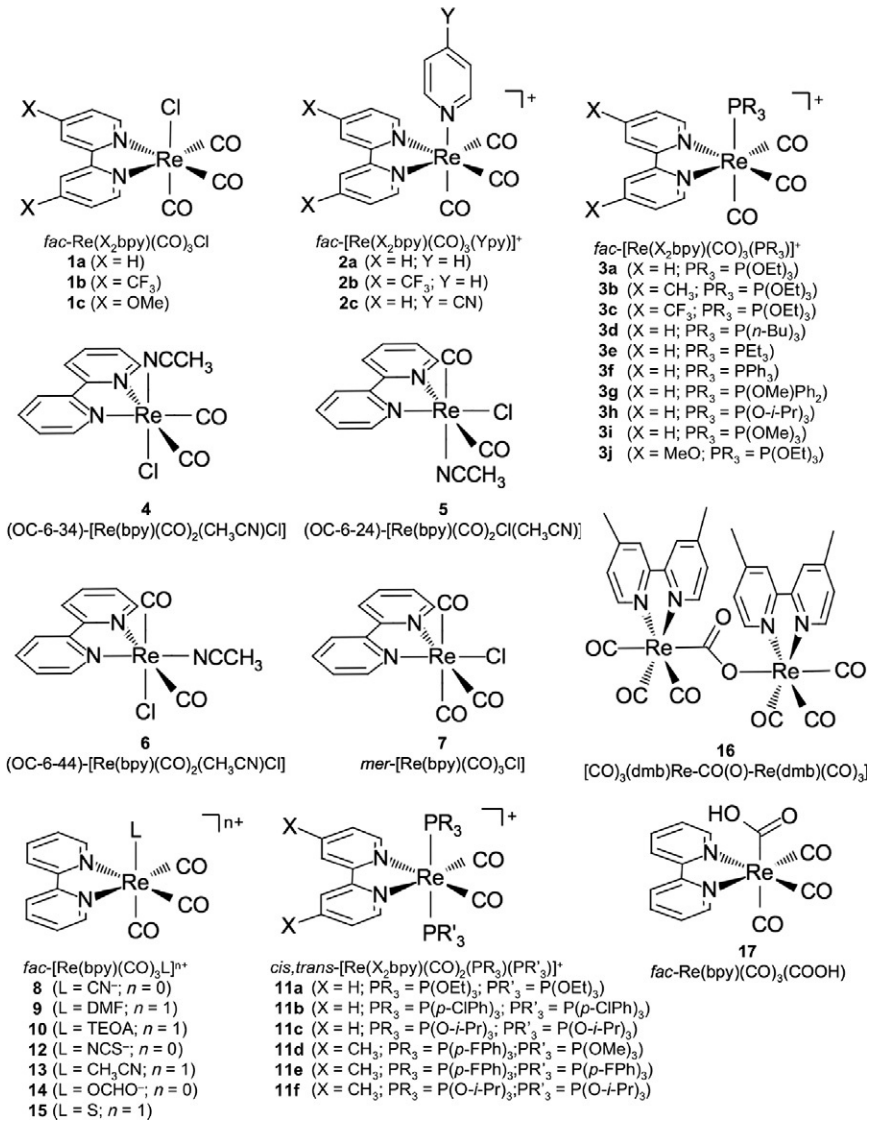

FIG. 1. Structures of rhenium(I) diimine complexes with abbreviations.

metal and the presence of the CO ligands with the strong LF. However, the energies of the empty π* orbitals localized on diimine ligands, typically 2,2′-bipyridine (bpy) and 1,10-phenanthroline, are low because of the relatively large conjugated π system. Therefore, the ligand π* orbital energy is lower

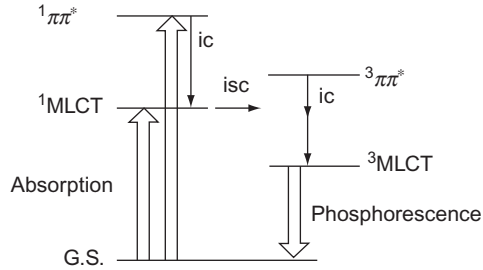

FIG. 2. The schematic energy diagram of the electronic states of the rhenium(I) diimine complexes.

than that of the lowest-energy empty d orbital of Re(I), making the MLCT state the lowest excited state in many cases (Fig. 2).

The electronic transition to the MLCT and ππ* excited states are optically allowed transitions, and they have relatively large transition moments. They do not involve the population of an orbital that is antibonding with regard to the M—L bonds, in contrast to the forbidden transitions to the LF excited states. This is one of the reasons for photostability of Re(I) complexes. However, as discussed in the following sections, photoinduced chemical reactions have been reported in some cases, where transitions to reactive higher-energy states arise from photoexcitation with shorter wavelength irradiation or thermal activation from lowest excited state.

In reality, the electronic states of Re(I) complexes are mixed with each other by configuration interactions, and the "real" electronic states are best viewed as composites of the "virtual" pure electronic states such as MLCT and ππ* excited states, etc. In this chapter, the "real" electronic states will be represented by the "virtual" pure state which has the largest contribution to the excited state properties.

B. PHOTOPHYSICAL RELAXATION PROCESS OF RHENIUM(I) DIIMINE COMPLEXES

As the lowest excited state of many Re(I) diimine complexes is the emissive ^{3}MLCT state, it can be tuned by chemical modification of the diimine ligand and the identity of the monodentate ligands. Figure 3 shows the UV/Vis absorption and emission spectra of a typical rhenium(I) diimine complex, *fac*-Re(bpy)$(CO)_3$Cl (bpy = 2,2′-bipyridine) (**1a**), measured in CH_3CN.

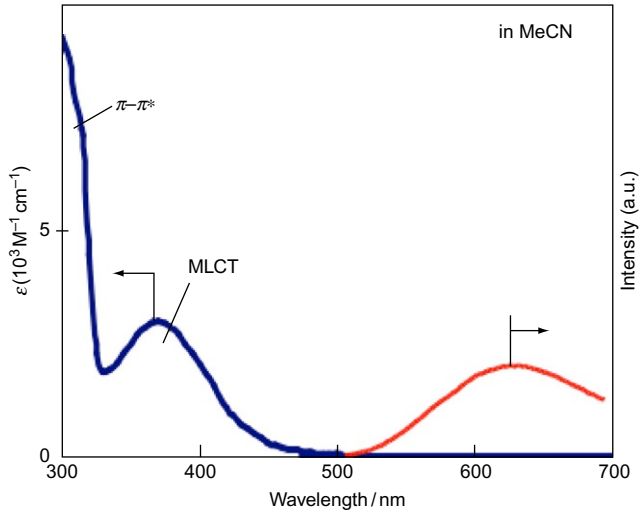

FIG. 3. UV/Vis absorption and emission spectra of *fac*-Re(bpy)$(CO)_3Cl$ (**1a**) complex measured in an CH_3CN solution.

In the UV/Vis absorption spectrum, a broad band at $\lambda_{abs} = 370$ nm and a more intense one at 292 nm are attributed to transitions to the ^{1}MLCT and the $^1\pi\pi^*$ (^{1}LC) excited states, respectively. Such characteristics are common for many rhenium(I) diimine carbonyl complexes (Table I). The emission spectrum comprises a single broad band, which arises from a transition from the lowest ^{3}MLCT excited state to the ground state. The lifetime of the ^{3}MLCT excited state is relatively short (Table I).

In the case of the rhenium(I) bipyridine tricarbonyl complexes with a phosphorous ligand such as **3a** in Table I, both the ^{1}MLCT absorption and the emission bands are blue shifted because of the stronger LF induced by the phosphorous ligand. This causes the lifetime of the ^{3}MLCT excited state to be longer. The photophysical parameters of some typical Re(I) complexes are summarized in Table I (*5,26*).

Concerning the relaxation processes of Ru(II) tris(diimine) complexes whose lowest excited state is the ^{3}MLCT state, a good linear relationship between the logarithm of the nonradiative decay rate (k_d) and the energy gap ($E_{00}(^3\text{MLCT})$), the energy difference from the ground state to the ^{3}MLCT state, is observed. This is termed as the Energy Gap Law (*5,27*). In a series of rhenium(I) bipyridine tricarbonyl complexes, such a linear correlation was also observed (Fig. 4) (*26,27*), where the net

TABLE I

PHOTOPHYSICAL PROPERTIES OF SOME Re(I) BIPYRIDINE COMPLEXES IN AN CH_3CN SOLUTION AT ROOM TEMPERATURE (26).

$[Re(X_2bpy)(CO)_3(L)]^+$			$\lambda_a(^1MLCT)$ (nm)	λ_e (nm)	τ_e (ns)	Φ_e	Φ_r
Abbr.	X	L					
1a	H	Cl^-	370[a]	622[b]	25[b]	0.005[c]	–
2a	H	py	351[d]	545[d]	250[d]	0.059[e]	–
3a	H	$P(OEt)_3$	336	542	1034	0.155	0.0089
3b	CH_3	$P(OEt)_3$	330	533	936	0.175	0.16
3c	CF_3	$P(OEt)_3$	363	622	162	0.031	0.0003

[a]Ref. (27).
[b]Ref. (28).
[c]In CH_2Cl_2, Ref. (5).
[d]Ref. (29).
[e]Ref. (30).

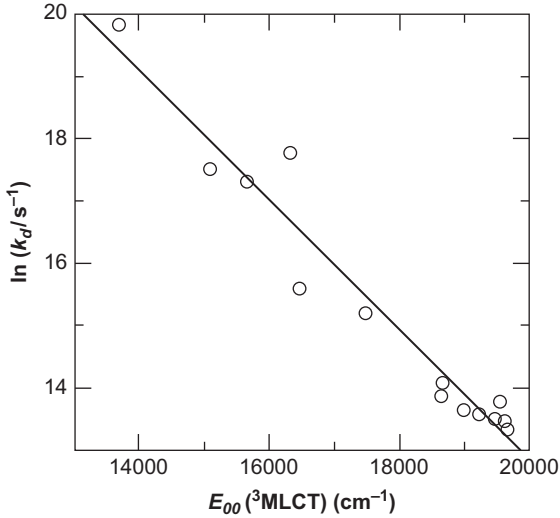

FIG. 4. Plots of ln k_d of various rhenium(I) diimine tricarbonyl complexes versus $E_{00}(^3MLCT)$ at 25 °C in a degassed CH_3CN solution.

nonradiative decay rate was calculated by subtracting the contribution of the photochemical reaction from the inverse of the emission lifetime (τ_e). The slope ($-8.4\ eV^{-1}$) for the rhenium(I) complexes was similar to that of the Ru(II) complexes ($-7.54\ eV^{-1}$).

C. Effect of Weak Interactions Between Ligands on Electronic Structure

Tricarbonyl monophosphine rhenium(I) complexes *fac*-[Re(diimine)$(CO)_3(PR_3)]^+$ can be readily converted into the corresponding biscarbonyl bisphosphine rhenium(I) complexes *cis, trans*-[Re(diimine)$(CO)_2(PR_3)(PR'_3)]^+$ by means of a photochemical ligand substitution reaction (see Section III.D) *(26,31)*. Due to the strong π-acidity of the carbonyl ligand, substitution by a phosphine ligand causes a destabilization of the HOMO level (dπ orbital of the Re center, see Section III) and bathochromic shifts in the absorption and emission spectra. For example, *cis,trans*-[Re(bpy)$(CO)_2${P$(OEt)_3\}_2]^+$ (**11a**) has an MLCT absorption band and an emission maxima in a longer wavelength region compared to *fac*-[Re(bpy)$(CO)_3$P$(OEt)_3]^+$ (**3a**) (Fig. 5). Moreover, the emission quantum yield of the **11a** (1.7%) was much smaller than that of **3a** (8.8%) *(32)*, which obeys the Energy Gap Law (see Section II.B).

However, the nature of the phosphine ligands is another critical factor for controlling the photophysical properties of this family of complexes. In particular, the introduction of triarylphosphine ligand(s) was found to bring about drastic changes in the photophysical and electrochemical properties *(33,34)*. For example, a Re(I) complex with two tris(*p*-chlorophenyl)phosphine ligands (**11b**) exhibited a red-shifted MLCT absorption band but blue-shifted emission compared to the bis(*iso*-propylphosphite) Re(I) complex (**11c**) (Fig. 6). As these two ligands have comparable electron-withdrawing abilities estimated from Tolman's χ values

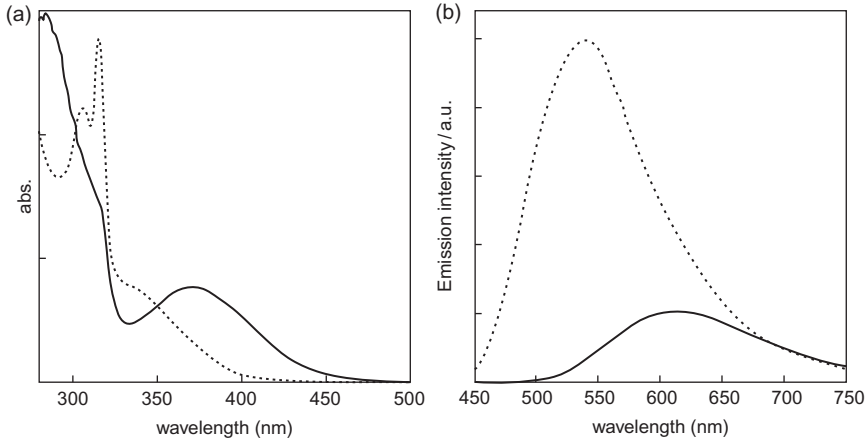

Fig. 5. UV/Vis absorption (a) and emission (b) spectra of *cis,trans*-[Re(bpy)$(CO)_2${P$(OEt)_3\}_2]^+$ (**11a**, solid line) and *fac*-[Re(bpy)$(CO)_3$(P$(OEt)_3)]^+$ (**3a**, dotted line).

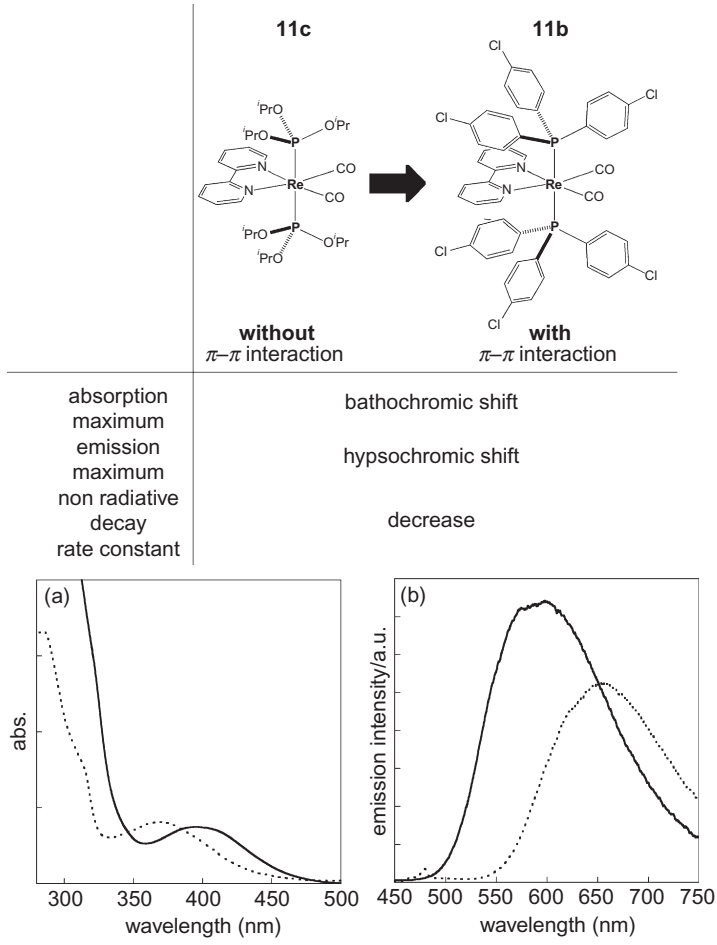

FIG. 6. The effects of the interligand π–π interaction to the fundamental properties of rhenium(I) complexes. The absorption (a) and emission (b) spectra of rhenium(I) complexes with (**11b**, solid line) and without (**11c**, dotted line) π–π interaction.

($\Sigma\chi = 33.6$ and 38.1 for **11b** and **11c**, respectively), this clearly shows that interligand π–π interactions between the aromatic diimine ligand and the aryl groups in the phosphine ligands have a profound influence on the photophysical properties of the complex. Close contacts between the two aromatic moieties in the solid state were observed by X-ray crystallography and in solution by nuclear magnetic resonance (NMR) and infrared spectroscopies. The interligand aromatic interactions decrease the nonradiative decay rate constant from the ^{3}MLCT excited state of the complex, prolong the excitation lifetime, and strengthen the oxidation power of the complex.

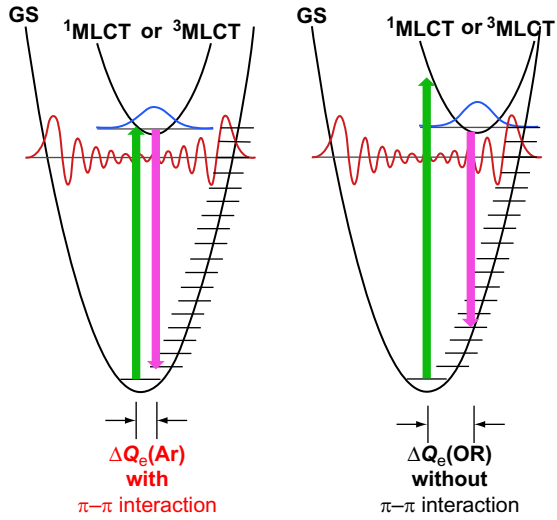

FIG. 7. Energy surfaces of the ground state and the ^{1}MLCT or ^{3}MLCT excited state depending on the absence and presence of the interligand π–π interaction.

The changes to the photophysical properties can be rationalized by the following energy surfaces of the ground and ^{1}MLCT or ^{3}MLCT excited states of Re(I) complexes. It is reasonable to assume that the interligand interaction decreases the lateral displacement ΔQ_e of the MLCT excited state from the ground state by the delocalization of the electron that is transferred onto the diimine ligand in the MLCT excited state through the interaction (Fig. 7). In this case, less energy should be required for excitation process, and the ^{3}MLCT excited state can emit a higher-energy photon. In other words, interligand interactions induce bathochromic and hypsochromic shifts in absorption and emission spectra, respectively. Further, the smaller lateral displacement gives a smaller Franck–Condon factor, that is, a smaller nonradiative decay constant, which results in an increase in the excitation lifetime.

III. Photochemistry of Rhenium(I) Complexes

A. Photochemical CO Elimination Reaction of a Re(I) Hexacarbonyl Complex

$[Re(CO)_6]^+$ belongs to the O_h point group and has a low-spin d^6 electron configuration. This configuration is the same as the neutral hexacarbonyl complexes of the Group 6 elements (Cr, Mo, W), and they show similar photochemical reactivities.

The coordination bonds between the rhenium(I) and the CO ligands consist of two electron-donating mechanisms: σ-donation from the lone-pair electrons of the CO ligand to the rhenium(I), and the π-back donation from the occupied t_{2g} orbital electron of the rhenium(I) to the empty π* orbital of the CO ligands. The photoexcitation process of this complex is attributed to two types of electronic transition, that is, an LF transition (Re $t_{2g} \rightarrow$ Re e_g) in a lower-energy region and an MLCT transition (Re $d\pi \rightarrow$ CO π^*) in a higher region. Although the molar extinction coefficient of the LF absorption band is very small because it is a forbidden transition, it causes a photochemical reaction. The LF transition weakens the Re—CO bond, and one CO ligand is eliminated (Eq. 1) because an electron located on the bonding t_{2g} orbital is excited to an antibonding e_g orbital. The rate constant of CO elimination from the LF excited state is accelerated by a factor of 10^{16} compared to the ground state, and the reaction quantum yield is close to unity. For the presence of the good ligands (L), a photoinduced ligand substitution reaction can proceed to give $Re(CO)_5L$ (Eq. 2).

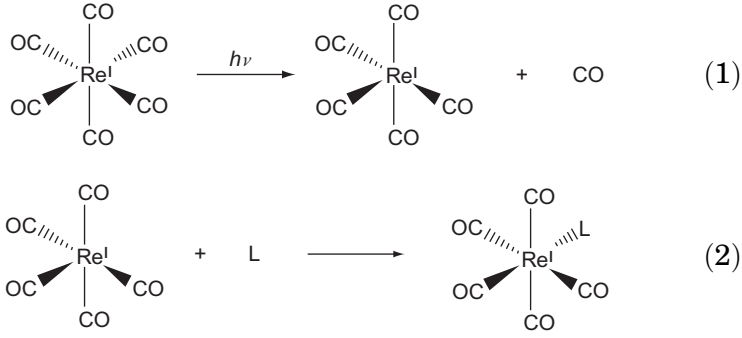

B. Re–Re, Re–M, and Re–C Bond Homolysis Reactions

For Re(I) dimers with a Re—Re bond, photoexcitation induces homolysis of the Re—Re bond. The two rhenium(0) metal centers in $Re_2(CO)_{10}$ each donate one electron from their d_{z^2} orbitals to make a σ M—M bond. Upon photoirradiation, the bonding σ-orbital (σ_b) electron is excited into the antibonding σ-orbital (σ_z^*), which leads to metal–metal bond cleavage. It has been also reported that a CO ligand elimination proceeds competitively with the metal–metal bond homolysis reaction. When a cyclohexane solution of $Re_2(CO)_{10}$ was irradiated by the 355-nm laser light, the ratio of the reaction quantum yields of Re—Re bond

cleavage (Y_1) and CO elimination (Y_2) was evaluated as $Y_1/Y_2 = 0.13$ (*35*).

Irradiation of $L_nMRe(CO)_3(L–L)$ ($L_nM = (CO)_5Mn$, $(CO)_5Re$, Ph_3Sn, Me_3Sn; a diimine ligand (L–L) coordinated on one of the metal centers) complexes also causes Re—M bond homolysis, but the reaction pathway is different. The longest wavelength absorption band of this type of complex was attributed to a ^{3}MLCT(Re $d\pi \rightarrow \pi^*$(L–L)) transition. Stufkens *et al*. reported that the Re—M bond homolysis proceeds via the $\sigma_b \rightarrow \pi^*$(L–L) excited state produced by internal conversion from the ^{3}MLCT excited state (*36*).

It has been also reported that Re—R bond homolysis can be promoted by the photoexcitation of mononuclear rhenium(I) complexes with a Re—alkyl bond, *fac*-[$Re(CO)_3$(α-diimine)R] (R = alkyl ligand). This type of the reaction also proceeds via a $^3\sigma\pi^*$ state, which is produced by the relaxation from the ^{3}MLCT excited state. In the cases of R = ethyl (Et) and benzyl (Bz), the homolysis reaction proceeds efficiently. However, the reaction efficiency is much lower in the case R = methyl (Me) because the transition from ^{3}MLCT to $^3\sigma\pi^*$ requires extra energy (Scheme 1). Using transient absorption spectroscopy, the $^3\sigma\pi^*$ state was directly detected as a reaction intermediate with an absorption band at 500 nm. It was concluded that the potential curve of the $^3\sigma\pi^*$ excited state should have a distinct minimum and that the homolysis reaction will proceed competitively with the nonradiative decay process to the ground state (Scheme 1) (*37*).

C. Photochemistry of Re(I) Diimine Tetracarbonyl Complexes

Rillema *et al*. have presented a comprehensive report on the rhenium diimine tetracarbonyl complexes, [Re(L–L)$(CO)_4$]

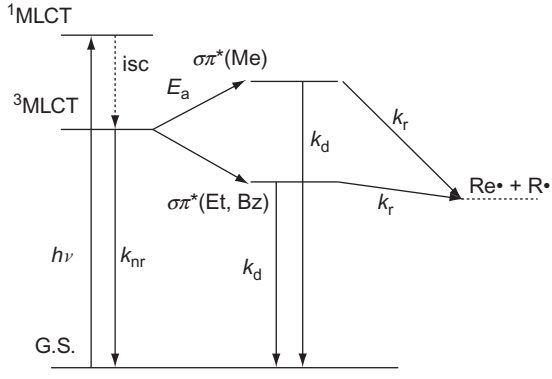

Scheme 1. Energy diagram of [Re(α-diimine) $(CO)_3$R].

(CF_3SO_3) (L–L = 2,2′-bipyrimidine (bpm), 4,4′-dimethyl-2,2′-bipyridine (dmb), 2,2′-bipyridine (bpy), and 1,10-phenanthroline (phen)), including their electronic states, photophysics, and photochemistry (*38*). These complexes have a $d\pi \rightarrow \pi^*$ charge-transfer absorption band in the region of 300–400 nm and $\pi\pi^*$ (diimine) transition bands in the shorter wavelength region of 300 nm. Even at room temperature, these complexes emit phosphorescence from the lowest triplet excited state (Table II). Because the bpm complex shows a nonstructured broad emission band in dichloromethane solution at room temperature, the lowest excited triplet state was identified as the ^{3}MLCT state. However, bpy, dmb, and phen complexes showed a vibrational structured emission spectra, and therefore, the lowest excited state was attributed to the $^3\pi\pi^*$ state localized on the diimine ligands.

Irradiation of these tetracarbonyl complexes caused the elimination of a CO ligand (Eq. 3).

$$[\mathrm{Re(diimine)(CO)_4}]^+ + \mathrm{CF_3SO_3}^- \xrightarrow{h\nu} [\mathrm{Re(diimine)(CO)_3(CF_3SO_3)}] + \mathrm{CO} \quad (3)$$

The reaction quantum yields were varied from 0.03 to 0.9 (Table I).

It was suggested that the photoinduced ligand substitution reactions proceed via the ^{3}LF state as a reactive state, but the relative energy of this state compared to the lowest excited state, that is, ^{3}LC, was not clearly estimated. The ^{3}MLCT state was also proposed as another candidate of the reactive state because the Re—C bond strength should be lower in the ^{3}MLCT state compared to the ground state owing to the removal of an electron from a bonding $d\pi$ orbital.

TABLE II

EMISSION PEAK (λ_E), EMISSION QUANTUM YIELD (Φ_E), EMISSION LIFETIME (τ_E), AND PHOTOREACTION QUANTUM YIELD (Φ_R) OF [RE(DIIMINE)(CO)$_4$](CF$_3$SO$_3$) IN CH_2Cl_2 UNDER CO AT ROOM TEMPERATURE.

L–L	λ_e (nm)	Φ_e	τ_e (μs)	Φ_r
bpm	521	0.037	0.75	0.5
bpy	448, 476, 506	0.031	4.7	0.3
dmb	444, 473, 505	0.033	2.3	0.9
phen	459, 489, 525	0.008	3.8	0.05

D. Photochemical Ligand Substitution Reaction of *fac*-[Re(Diimine)$(CO)_3PR_3]^+$

Recently, the excited states of the rhenium complexes have been investigated by using advanced computational methods, which can handle chemical systems that contain heavy atoms. Although direct observation of the reactive states remains important in order to confirm the photochemical reaction mechanism, it is sometimes very difficult because the concentrations of reactive states are very small when their potential curves are repulsive. Systematic investigations of the effects of various experimental parameters on reaction yields are also useful for getting mechanistic information. For example, energetic characteristics of the reactive states can be elucidated by investigating the dependence of emission and reaction quantum yields on temperature and chemical modification of the ligands.

Most rhenium diimine tricarbonyl complexes were considered to be relatively stable against photosubstitution, with some exceptions described above, until the photochemical ligand substitution reactions of complexes with phosphorous ligands, phosphorous complexes, and *fac*-$[Re(LL)(CO)_3(PR_3)]^+$ were reported.

When the complex **3a** with triethylphosphite as a monodentate ligand was irradiated at 365 nm in MeCN, the UV/Vis absorption spectrum changed with some isosbestic points (Fig. 8). This photochemical reaction gave exclusively *cis*,*trans*-[Re(bpy)$(CO)_2${P

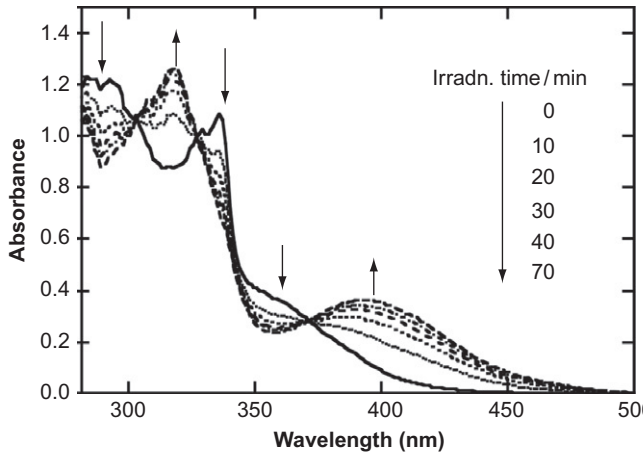

Fig. 8. UV/Vis absorption spectral changes of an CH_3CN solution containing **1a** (0.12 mM) under an Ar atmosphere during 365-nm irradiation (4.24×10^{15} photon s^{-1}). Copyright 2002 American Chemical Society.

$(OEt)_3\}(CH_3CN)]^+$, in which an MeCN ligand occupies a position trans to the $P(OEt)_3$ ligand. This product was obtained quantitatively, and no other isomers were produced (Eq. 4). The same photoinduced ligand substitution reaction was observed for complexes with other phosphorous ligands.

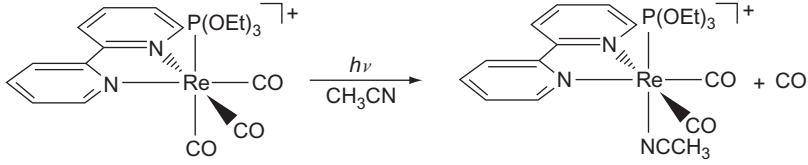

(4)

Generally, there are two reaction mechanisms for photochemical ligand substitution reactions on metal complexes, that is, "dissociative" and "associative" mechanisms. The photochemical reaction of **3a** in CH_2Cl_2 solution was investigated in the presence of molecules with different coordinative abilities (CH_3CN, pyridine, $P(OEt)_3$). In all the cases, the photochemical ligand substitution reactions proceeded quantitatively and the reaction rates did not depend on the identity of the incoming ligand. This clearly shows that photochemical reaction proceeds through the dissociative mechanism.

A $CDCl_3$ solution containing **3a** was irradiated under a ^{13}CO atmosphere. The ^{13}C NMR measurement revealed that only the CO ligand in the trans-position to $P(OEt)_3$ was substituted (Fig. 9). This result indicates that the primary process of the photochemical ligand substitution reaction is the elimination of the CO ligand in the trans-position to $P(OEt)_3$ ligand, and a new ligand should be promptly introduced at the same position. The coordinatively unsaturated species do not undergo any structural rearrangements which cause isomerization of the complex.

The CO stretching vibrational bands of rhenium carbonyl complexes are useful spectroscopic probes for studying their electronic excited states. As these IR absorption bands reside in the frequency region where few absorption bands exist, their absorption cross section are large and the band frequencies are greatly influenced by the amount of electron density on the central rhenium(I). Therefore, transient IR absorption (TR-IR) measurements should be one of the ultimate tools for the study of the photophysics and photochemistry of the rhenium carbonyl complexes.

TR-IR spectra of the complex **3a** were measured in an CH_3CN solution following irradiation with 355-nm laser light (Fig. 10). Immediately after laser pulse, the three absorption peaks (at 1928, 1962, 2047 cm^{-1}) attributed to the three ground-state CO

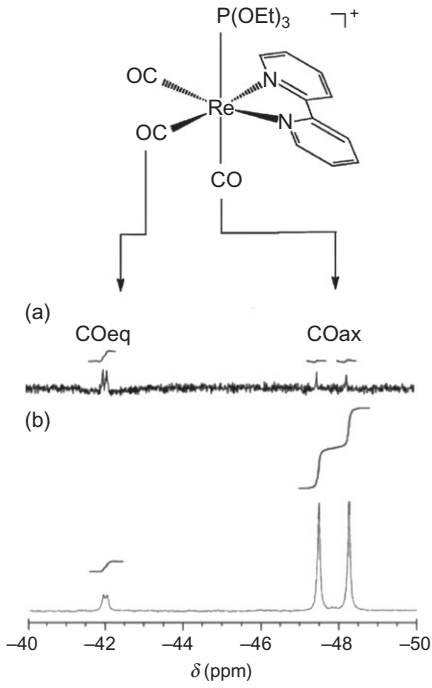

FIG. 9. ^{13}C NMR spectra of **3a** in a degassed $CDCl_3$ solution under ^{13}CO atmosphere: (a) before irradiation, (b) after 60-min irradiation. Copyright 2002 American Chemical Society.

ligands were bleached, and other three absorption peaks (at $\sim$1970, 2017, $\sim$2070 cm^{-1}) attributed to the lowest excited state, ^{3}MLCT, were produced. Although the additional three peaks decayed at the same rate as that observed in the emission decay experiment, the peak intensities of the ground state did not recover to their original magnitudes. On the same timescale, a new couple of IR absorption bands appeared (at 1876, 1951 cm^{-1}), which can be attributed to the ligand substitution reaction product *cis*,*trans*-$[Re(bpy)(CO)_2\{P(OEt)_3\}(CH_3CN)]^+$. The rise of the IR absorption band of the product was proportional to the amount of the ^{3}MLCT state complex formed immediately after laser irradiation. This result suggested that this photochemical ligand substitution reaction proceeds from the ^{3}MLCT state or the ^{3}LF state, which is in thermal equilibrium with the ^{3}MLCT state (Scheme 2).

As these excited states were attributed to the transitions from the central metal dπ orbital to the bipyridine π^* orbital (^{3}MLCT) and to the central metal dσ^* orbital (^{3}LF), respectively, the state

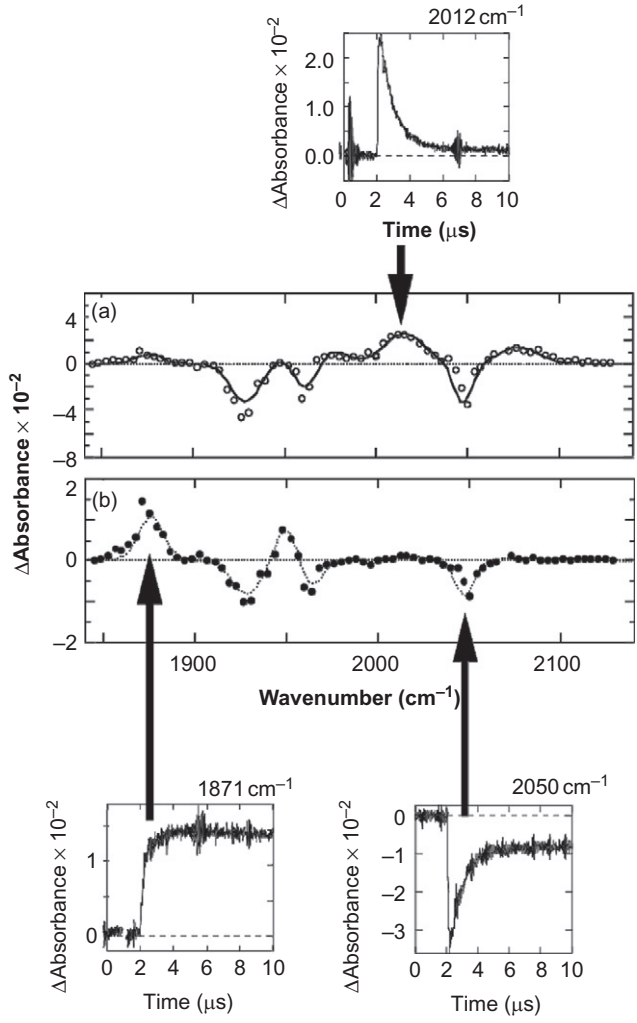

FIG. 10. TR-IR spectra of **3a** in a degassed CH_3CN solution taken at 50 ns (a) and 5 μs (b) after 355-nm laser excitation. The three small figures are the decay traces for typical IR bonds. (Copyright 2002 American Chemical Society.)

energies of these states can be controlled by systematic chemical modification of the bipyridine and axial ligands. In doing so, the energy gap between ^{3}MLCT and ^{3}LF states can be tuned. Such modification effects are summarized as follows:

1. Modification of the bipyridine ligand with introduction of electron-withdrawing (donating) groups at the 4,4′-positions

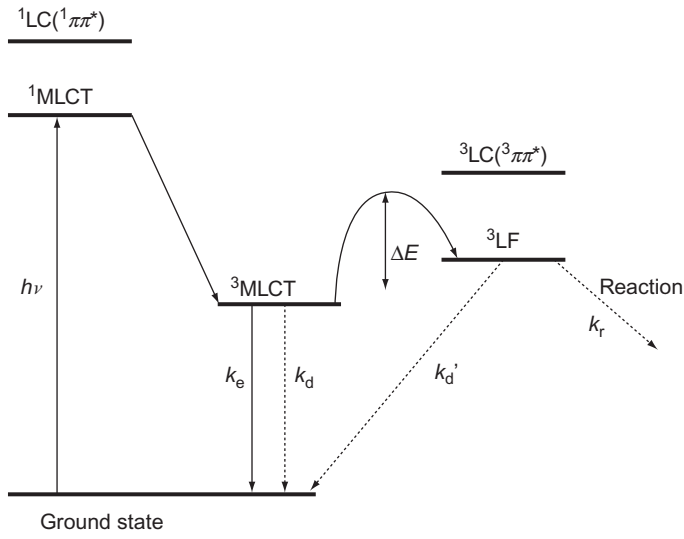

SCHEME 2. Schematic energy diagram of *fac*-[Re(bpy)(CO)$_3${P(OEt)$_3$}]$^+$ (**3a**).

should cause stabilization (destabilization) of the π* orbital of the bipyridine ligand, with only a small effect on the central metal d orbital energy.

2. Introducing a phosphorous ligand with a strong (weak) LF ligand should cause both stabilization (destabilization) of the rhenium dπ orbitals and destabilization (stabilization) of the rhenium dσ* orbitals, it does only a small effect on the bipyridine π* orbital.

The energy of the ^{3}MLCT excited state (E_{00}(^{3}MLCT)) can be evaluated from the emission spectrum. Emission peak wavelength (λ_e), emission quantum yields (Φ_e), emission lifetimes (τ_e), and reaction quantum yields of the photochemical ligand substitution reactions (Φ_r) are summarized in Table III. The modification of the bipyridine ligand caused changes in E_{00}(^{3}MLCT) as large as 2400 cm^{-1}.

The relaxation processes from the ^{3}MLCT state can be evaluated quantitatively by measuring the temperature dependence of the emission yield and lifetime because the ^{3}MLCT state is both the lowest and emissive excited state. Higher temperature caused larger Φ_r. However, Φ_e and τ_e became smaller and shorter at higher temperature, respectively. These experimental results could be well simulated by assuming that the photochemical reactions occur via the thermally accessible higher excited

TABLE III

PHOTOPHYSICAL PROPERTIES OF $[Re(X_2bpy)(CO)_3(PR_3)]^+$ (**3**) IN CH_3CN AT 298 K.

	$[Re(X_2bpy)(CO)_3(PR_3)]^+$		λ_e (nm)	$E_{00}(^3MLCT)^a$ (cm^{-1})	τ_e (ns)	Φ_e	Φ_r
	X	PR_3					
3a	H	$P(OEt)_3$	542	19,470 ± 55	1034	0.155	0.089
3b	CH_3	$P(OEt)_3$	533	19,637 ± 50	936	0.175	0.16
3c	CF_3	$P(OEt)_3$	623	17,272 ± 49	162	0.031	0.0003
3d	H	$P(n\text{-}Bu)_3$	561	18,672 ± 50	621	0.091	0.095
3e	H	PEt_3	561	18,649 ± 51	654	0.153	0.15
3f	H	PPh_3	540	19,000 ± 31	416	0.097	0.55
3g	H	$P(OMe)Ph_2$	542	19,553 ± 46	644	0.127	0.25
3h	H	$P(Oi\text{-}Pr)_3$	543	19,239 ± 52	952	0.247	0.099
3i	H	$P(OMe)_3$	543	19,678 ± 43	1076	0.216	0.118

[a] 0–0 band energy gap between the ^{3}MLCT and the ground states.

state from the ^{3}MLCT state (Scheme 2) and by using Eqs. (5)–(10) as shown in Figs. 11 and 12.

$$k_r = \frac{\Phi_r}{\tau_e} = k_r^0 \exp\left(\frac{-\Delta E}{RT}\right) \tag{5}$$

$$k_e = \frac{\Phi_e}{\tau_e} = k_e^0 \exp\left(\frac{-\Delta E}{RT}\right) \tag{6}$$

$$k'_d = k'^0_d \exp\left(\frac{-\Delta E}{RT}\right) \tag{7}$$

$$\Phi_e = \frac{k_e}{(k_e + k_d + k'_d + k_r)} \tag{8}$$

$$\Phi_r = \frac{k_r}{(k_e + k_d + k'_d + k_r)} \tag{9}$$

$$\tau_e = \frac{1}{(k_e + k_d + k'_d + k_r)} \tag{10}$$

The energy differences between the lowest excited ^{3}MLCT states and the transition states of the photochemical ligand substitution reactions could be estimated from analysis of the temperature effects (Table IV). The evaluated $\Delta G^{\neq}$ values were found to vary with the substituents on the bpy ligand (3650–4820 cm^{-1}).

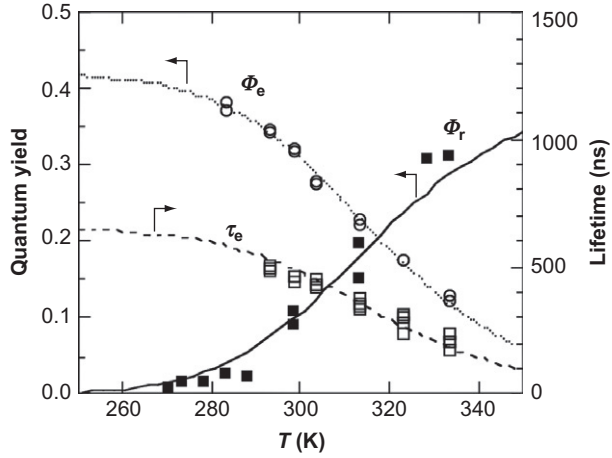

FIG. 11. Temperature dependence of the emission yield (Φ_e), the lifetime (τ_e), and the quantum yield of the photochemical ligand substitution reaction (Φ_r) of **3a** in a degassed CH_3CN solution. Copyright 2002 American Chemical Society.

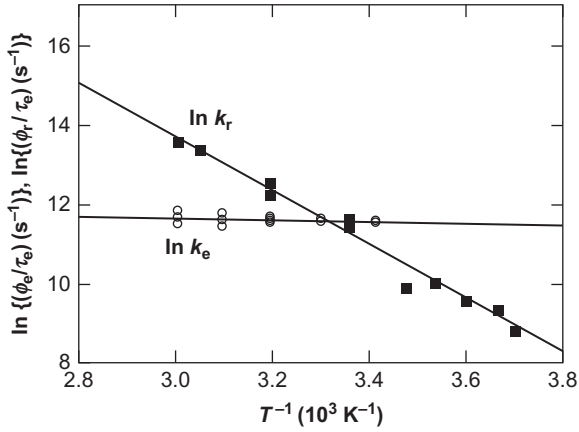

FIG. 12. Arrhenius plots of the radiative decay rate (k_e) and the reaction rate of the photochemical ligand substitution reaction (k_r) of **3a** in a degassed CH_3CN solution. Copyright 2002 American Chemical Society.

Interestingly, this effect was inversely proportional to the energy of the ^{3}MLCT state (E_{00} in Tables III and IV). Therefore, the energy gap between the ground state and the transition state of the photochemical ligand substitution reaction ($E_{00}+\Delta G^{\neq}$) is not affected by the modification of the bipyridine ligand as much

TABLE IV

THERMODYNAMIC DATA FOR THE PHOTOCHEMICAL LIGAND SUBSTITUTION REACTIONS OF $[Re(X_2bpy)(CO)_3(PR_3)]^+$ (**3**) IN CH_3CN.

$[Re(X_2bpy)(CO)_3(PR_3)]^+$						
	X	PR_3	$E_{00}(^3MLCT)$[a] (cm^{-1})	k_d ($10^5\ s^{-1}$)	$\Delta G^{\neq}_{298}$[b] (cm^{-1})	$(E_{00}+\Delta G^{\neq})_{298}$ (cm^{-1})
3a	H	$P(OEt)_3$	$19{,}470 \pm 55$	6.9	3810 ± 590	$23{,}280 \pm 650$
3b	CH_3	$P(OEt)_3$	$19{,}637 \pm 50$	4.1	3650 ± 80	$23{,}290 \pm 130$
3c	CF_3	$P(OEt)_3$	$17{,}272 \pm 49$	60	4820 ± 140	$22{,}090 \pm 190$
3d	H	$P(n\text{-}Bu)_3$	$18{,}672 \pm 50$	11	3480 ± 830	$22{,}150 \pm 880$
3e	H	PEt_3	$18{,}649 \pm 51$	11	3390 ± 610	$22{,}030 \pm 660$
3f	H	PPh_3	$19{,}000 \pm 31$	8.5	3230 ± 1650	$22{,}230 \pm 1680$
3g	H	$P(OMe)Ph_2$	$19{,}553 \pm 46$	9.7	3240 ± 440	$22{,}790 \pm 490$
3h	H	$P(Oi\text{-}Pr)_3$	$19{,}239 \pm 52$	7.9	3610 ± 760	$22{,}840 \pm 810$
3i	H	$P(OMe)_3$	$19{,}678 \pm 43$	6.2	3740 ± 760	$23{,}420 \pm 800$

[a] 0–0 band energy gap between the ^3MLCT and the ground states.
[b] Free activation energy change at 298 K.

as the excitation energy of the ^{3}MLCT state (E_{00}). However, variation of the phosphorous ligand, which should give larger effects on the d–d splitting, had an effect on $E_{00}+\Delta G^{\neq}$ similar to or larger than that on E_{00}. These results clearly indicate that the photochemical ligand substitution reactions proceed via the ^{3}LF excited state thermally produced from the ^{3}MLCT state.

Scheme 3 illustrates the potential energies of the ground state, ^{3}MLCT state, and ^{3}LF state versus the bond distance Re—CO.

In the cases of most rhenium(I) diimine tricarbonyl complexes with a phosphorous ligand, the activation energies ($\Delta G^{\neq}$) are enough small to be overcome even at room temperature ($k_BT=207.1\ cm^{-1}$ at 298 K). The evaluated activation energy of **3a** was $3810\ cm^{-1}$ and the quantum yield of the photochemical ligand substitution reaction was 0.089 using 366-nm light (Tables III and IV). However, the complexes which do not have a phosphorous ligand, such as *fac*-Re{$(MeO)_2$bpy}$(CO)_3$Cl (**1c**) and *fac*-[Re(bpy)$(CO)_3$(py)]$^+$ (**2a**), do not react at all under the same conditions using 366-nm light. Activation energies ($\Delta G^{\neq}$) of these complexes, as evaluated from the temperature dependence of the emission lifetime and the emission quantum yield, are drastically smaller. For instance, the $\Delta G^{\neq}$ of **1c** was estimated as $252\ cm^{-1}$. This is the same order of the magnitude

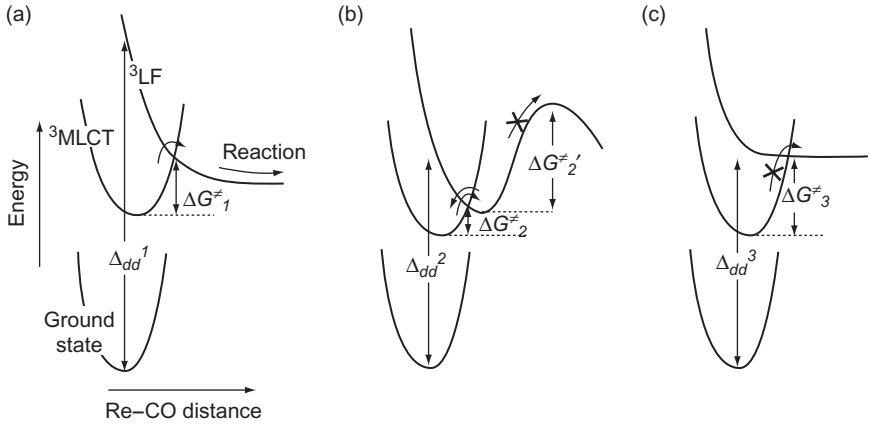

SCHEME 3. Energy versus Re—CO distance for rhenium(I) complexes. Illustrating the three lowest-lying electronic states: (a) *fac*-[Re{$(CF_3)_2$bpy}$(CO)_3${P$(OEt)_3$}]$^+$ (**3c**), (b) *fac*-[Re(bpy)$(CO)_3$(py)]$^+$ (**2a**) and *fac*-Re{$(MeO)_2$bpy}$(CO)_3$Cl (**1c**) for the case of a nonreactive ^{3}LF state, and (c) **2a** and **1c** for the case of a large activation energy from the ^{3}MLCT to ^{3}LF states. Copyright 2002 American Chemical Society.

as the energy caused by dependence of the solvent viscosity on temperature, and therefore, it should not be attributed to $\Delta G^{\neq}$ of the thermal activation from the ^{3}MLCT state to the ^{3}LF state.

The reasons why these complexes are not active in the photochemical ligand substitution reaction can be classified into two cases. One is that although the thermal activation from ^{3}MLCT to ^{3}LF is preferable, the energy surface of ^{3}LF is not repulsive and a large activation energy ($\Delta G_2^{\neq}$) is required to eliminate the CO ligand at room temperature (Scheme 3b). The other case is that the energy gap from ^{3}MLCT to ^{3}LF ($\Delta G_1^{\neq}$) is too large to produce the ^{3}LF state at room temperature (Scheme 3c).

As the pyridine ligand has a relatively weak LF compared to the phosphorous ligands, the d–d splitting of the pyridine complex should be smaller. Therefore, the ^{3}MLCT state energies (E_{00}) of the pyridine complexes are relatively low, for example, 17,490 cm^{-1} for **2a**. The energy was as low as 17,270 cm^{-1} for *fac*-[Re{$(CF_3)_2$bpy}$(CO)_3${$P(OEt)_3$}]$^+$ (**3c**), which has the strong electron-withdrawing CF_3 groups at the 4,4′-positions of the bpy ligand. These serve to stabilize the π* state. The similar situation can be seen in the case of the rhenium(I) complexes with a Cl^- ligand where LF is even smaller than complexes with pyridine as a ligand. For example, the ^{3}MLCT state energy of *fac*-Re{$(MeO)_2$bpy}$(CO)_3$Cl (**1c**), which features two electron-donating substituents on the bpy ligand, was 16,320 cm^{-1}, which is slightly lower energy than that of **3c**. The ^{3}LF excited state energies of both **1c** and **2a** should be smaller than that of **3c** owing to the smaller LFs than the phosphorous ligands. Therefore, the ^{3}MLCT–^{3}LF energy gaps of **1c** and **2a** should be similar or less than that of **3c**. Although **3c** was photoreactive under 366-nm irradiation, **2a** and **1c** were not at all reactive, as mentioned above. This result clearly indicates that the photostabilities of **2a** and **1c** are not caused by a large $\Delta G^{\neq}$ that prevents thermal activation to the reactive ^{3}LF state from the ^{3}MLCT state (Table V).

Based on the above discussion, the following interpretation has been proposed using Scheme 3b. Although the potential curves of the ^{3}LF state and the ^{3}MLCT state cross each other in a relatively low-energy region, it is necessary to overcome another higher-potential barrier for Re—CO bond scission. The Re—CO bond of **3c** should be weakened due to the π-acidity of the phosphorous ligand in the trans-position to the released CO ligand. However, it should be reasonable that the Re—CO bonds of **1c** and **2a** should be stronger than **3c** because the pyridine ligand is a weak π-acid and the Cl^- ligand is a π-base (Scheme 4).

TABLE V

PHOTOPHYSICAL AND THERMODYNAMIC DATA FOR THE PHOTOCHEMICAL LIGAND SUBSTITUTION REACTIONS OF *fac*-$[Re(X_2bpy)(CO)_3(Y)]^+$ IN CH_3CN.

Complex				k_d (10^5 s^{-1})	$E_{00}(^3MLCT)$[a] (cm^{-1})	$\Delta G^{\neq}_{298}$[b] (cm^{-1})
	X	Y	n			
1a	H	Cl^-	0	320	15,660 ± 30	250 ± 21
1b	CF_3	Cl^-	0	4100	13,680 ± 20	252 ± 94
1c	OMe	Cl^-	0	520	16,320 ± 1	252 ± 40
2a	H	py	1	40	17,490 ± 15	−36 ± 15
2b	CF_3	py	1	400	15,090 ± 15	84 ± 8
3c	CF_3	$P(OEt)_3$	1	60	17,270 ± 50	4820 ± 140

[a] 0–0 band energy gaps between the ^{3}MLCT and the ground states.
[b] Free activation energy change at 298 K.

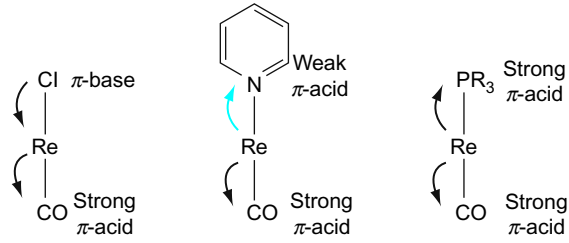

SCHEME 4. Trans-effects of the ligands to the Re—CO bond.

E. MULTINUCLEAR RHENIUM(I) COMPLEXES

Because of the significant features of the rhenium(I) complexes, such as strong photoabsorption, intense emission, and catalytic activities, they have been adopted as building blocks for constructing various multinuclear complexes. For instance, rhenium complexes introduced as pendant molecules on polymer chains have been reported (Fig. 13).

All these polymers, A (*39*), B (*40*), C (*41,42*), D (*43*), showed distinctive absorption and emission due to the MLCT transition of the rhenium(I) diimine complexes. Among these rhenium-containing polymers, polymer C has the most notable emission properties, with an emission quantum yield and a lifetime ($\Phi_e = 0.132$, $\tau_e = 2019$ ns in a deaerated CH_2Cl_2 solution) comparable to those of the corresponding mononuclear complex ($\Phi_e = 0.181$, $\tau_e = 2200$ ns) (*43*).

fac-$[Re(diimine)(CO)_3X]^{m+}$ ($m = 0, 1$) type complexes have been also employed as "L-shaped" building blocks for constructing

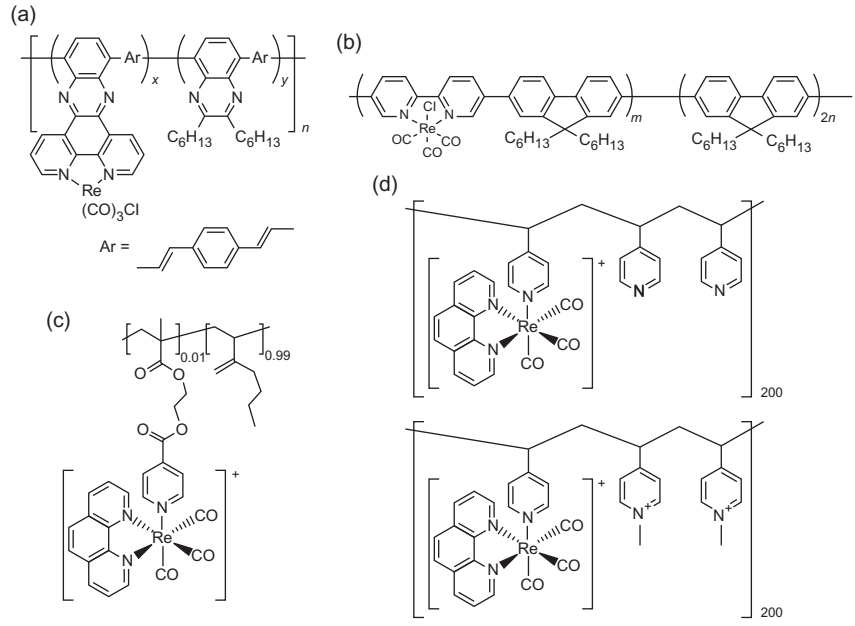

FIG. 13. Polymer molecules containing rhenium(I) tricarbonyl complexes as pendant molecules.

"molecular polygons" because various kinds of molecules could be introduced into these complexes as the diimine ligand and the monodentate ligand X (Fig. 14a *(44)*, b *(45)*, c *(45)*, d *(46)*). Many of these molecular polygons emit in solution even at room temperature.

Recently, a series of linear-shaped rhenium multinuclear complexes were synthesized by applying the photochemical ligand substitution reaction of the rhenium(I) diimine complexes with a phosphorus ligand to the rhenium(I) binuclear complexes bridged with a bidentate phosphorous ligand. First, two CO ligands in the trans-position to the phosphorous ligands were photochemically substituted sequentially with CH_3CN, which can be easily substituted by thermal activation (Scheme 5) *(47)*. This product can be polymerized by the reaction with the appropriate amount of a bidentate ligand such as bidentate phosphorous ligands and 4,4′-bipyridine *(48–50)*. This produces linear-shaped rhenium(I) multinuclear complexes with 2–20 nuclei, which were successfully isolated by size-exclusion chromatography (Fig. 15).

All the linear-shaped multinuclear complexes emit in solution at room temperature. Although UV/Vis light can be absorbed by all the Re(I) units, most of the emission comes from the interior Re(I) biscarbonyl unit(s) because excitation energy absorbed

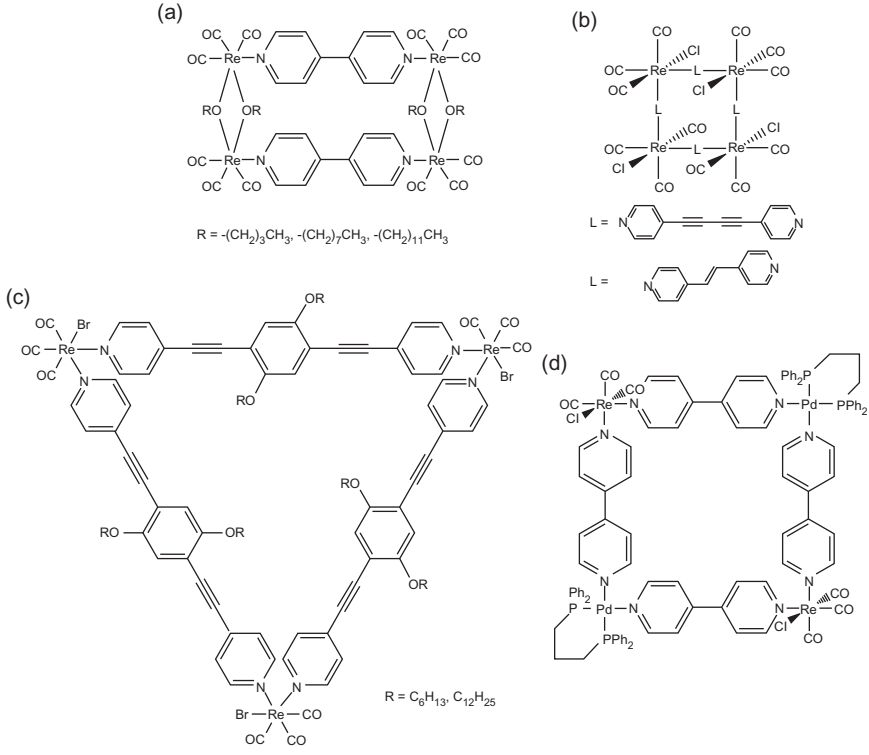

FIG. 14. Rhenium molecular rectangle (a), square (b), triangle (c), and Re/Pd square (d).

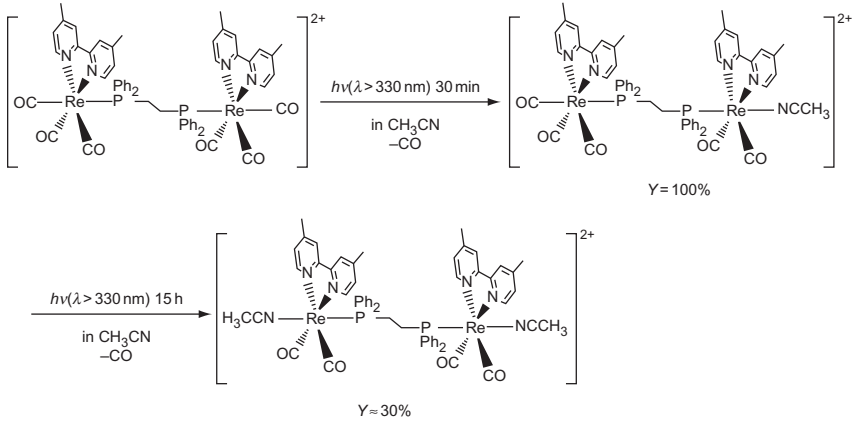

SCHEME 5. Photochemical ligand substitution reactions for introducing replaceable solvent molecules (CH_3CN).

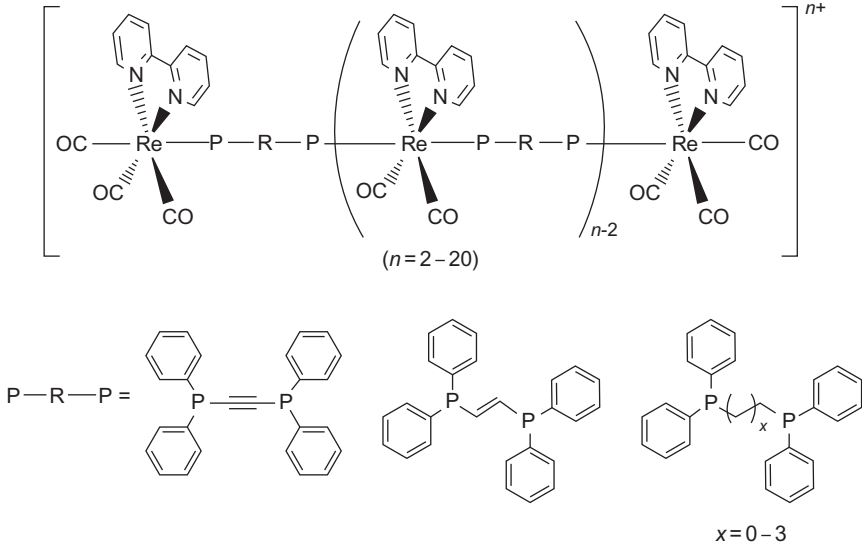

FIG. 15. Linear-shaped Re(I) oligomers and polymers constructed with bidentate phosphine ligands.

by the edge Re(I) tricarbonyl units is rapidly transferred to the interior units (*49*). The photophysical properties of linear-shaped multinuclear complexes bridged by 1,2-bis(diphenylphosphino) ethane (dppe) are summarized in Table VI.

F. PHOTOCHEMICAL REACTIONS OF *fac*-Re(bpy)$(CO)_3$Cl FROM HIGHER EXCITED STATES

As described above, most rhenium(I) diimine tricarbonyl complexes for which the lowest excited state is the ^{3}MLCT state are stable against irradiation with light of wavelength longer than 340 nm. The exception is complexes with phosphorous ligands (Section III.D). Actually, this kind of photochemical ligand substitution reaction of *fac*-Re(diimine)$(CO)_3$Cl and *fac*-[Re(diimine)$(CO)_3$(X-py)]$^+$ (X-py = pyridine derivative) does not proceed by irradiation using $\lambda > 330$ nm light. However, it has been recently reported that photochemical ligand substitution and photochemical isomerization of **1a** occur from higher excited states.

Although **1a** was photostable under 366-nm irradiation, irradiation with higher-energy light than 340 nm does cause

TABLE VI

PHOTOPHYSICAL PROPERTIES OF $[Re(bpy)(CO)_3(dppe)\{Re(bpy)(CO)_2(dppe)\}_{N-2}Re(bpy)(CO)_3]^{N+}$ COMPLEXES[a]

			τ_e[b] (ns)						
			Observed at 480 nm			Observed at 575 nm			
n	λ_{em} (nm)	Φ_e	τ_1	τ_2	τ_3	τ_1	τ_2	τ_3	k_{et}[c] (10^7 s^{-1})
2	523	0.072	865(100)	–	–	865(100)	–	–	–
3	572	0.073	11(91)	–	823(9)	–	–	833(100)	8.98
4	572	0.066	11(73)	128(7)	798(20)	–	128(12)	798(88)	8.98
5	572	0.062	11(83)	112(1)	796(16)	–	112(5)	796(95)	8.98
6	571	0.058	11(57)	129(5)	768(38)	–	129(12)	768(88)	8.98
8	571	0.056	10(86)	110(2)	763(12)	–	110(11)	763(89)	9.88
10	572	0.053	8(81)	168(12)	720(8)	–	168(21)	720(79)	12.38
12	572	0.051	7(82)	118(4)	758(14)	–	118(15)	758(85)	14.17
15	572	0.049	4(96)	162(4)	–	–	162(20)	764(80)	24.88
16	572	0.048	5(87)	64(3)	757(10)	–	64(22)	757(78)	19.88
20	572	0.046	4(92)	132(8)	–	–	132(14)	747(86)	24.88

[a]Measured in a deoxygenated acetonitrile solution at 298 K.
[b]Lifetime. Numbers in parentheses are percentages of preexponential factors of triexponential decay fitting results.
[c]Energy-transfer rates from the edge units to the interior ones (k_{et}).

photochemical reactions. Irradiation of **1a** using 313-nm light in an Ar-saturated acetonitrile solution gave (OC-6-34)-[Re(bpy)$(CO)_2(CH_3CN)Cl$] (**4**), which is a CO ligand substitution product and (OC-6-24)-[Re(bpy)$(CO)_2Cl(CH_3CN)$] (**5**), an isomer of **4** (Eq. 11). Complex **5** was isomerized to (OC-6-44)-[Re(bpy)$(CO)_2(CH_3CN)Cl$] (**6**) even in the dark (*51*). The reaction quantum yield evaluated from the consumption of complex **1a** was 0.01 ± 0.001, which increased using higher-energy light.

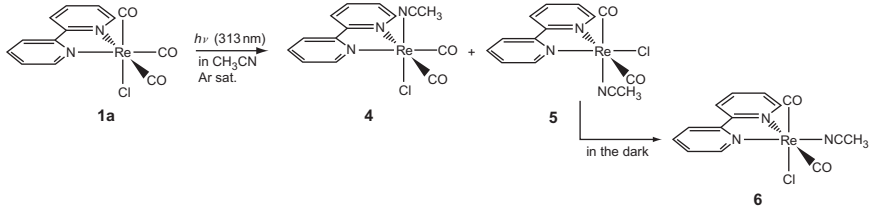

1a 4 5 6

(11)

Photochemical isomerization of **1a** to the *mer*-isomer (**7**) in a CO-saturated THF solution proceeded by 313-nm irradiation instead of the ligand substitution reaction (Eq. 12) (*52*).

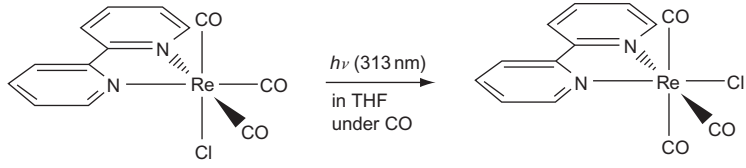

fac-[Re(bpy)$(CO)_3Cl$] *mer*-[Re(bpy)$(CO)_3Cl$]

1a **7**

(12)

The photochemical ligand substitution reaction of **1a** was investigated by ultrafast TR-IR spectroscopy (Fig. 16) (*51*). An acetonitrile solution of **1a** was irradiated by a 266-nm laser pulse ($\sim$150 fs pulse width). A broad IR absorption band which was attributed to the reaction products in higher vibrational excited states was produced within 1 ps after the laser flash. The broad band sharpened and a ν_{00} peak at 1828 cm^{-1} of the reaction product was observed in the 50- to 100-ps duration. This time scale is much shorter than the decay of the lowest ^{3}MLCT excited state (right-hand side of Fig. 16). The TR-IR results indicate that this photochemical reaction proceeds from higher vibrational states or high-energy electronic excited states instead of the lower vibrational excited states of ^{3}MLCT and thermal accessible states from ^{3}MLCT such as the ^{3}LF state.

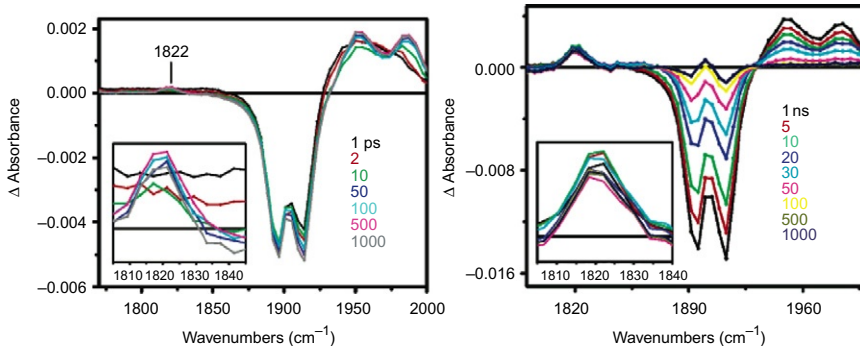

FIG. 16. Picosecond (left) and nanosecond (right) difference TR-IR spectra of **1a** in MeCN measured at selected time delays after excitation (ps pulse: 266 nm, ~150 fs with Ti:Sapphire laser; ns pulse: 267 nm–1 ns with Nd:YAG laser). Experimental points are separated by 4–5 cm^{-1}. Inset: expansion of the low-wavenumber region showing the formation of the photoproduct band. Copyright 2007 American Chemical Society.

G. PHOTOCHEMICAL REACTIONS OF THE LIGAND IN Re(I) COMPLEXES

Three types of photochemical reactions of the ligand in rhenium(I) diimine carbonyl complexes have been reported by several authors.

fac-[Re(bpy)$(CO)_3$(4-cyanopyridine)]$^+$ (**2c**) was irradiated at 355 nm in a CO_2-saturated triethanolamine (TEOA)–DMF (1:5 v/v) solution giving *fac*-[Re(bpy)$(CO)_3$(CN)] (**8**) with a 53% quantum yield (Eq. 13) (*53*). This reaction proceeds via the photochemical reduction of **2c** by TEOA.

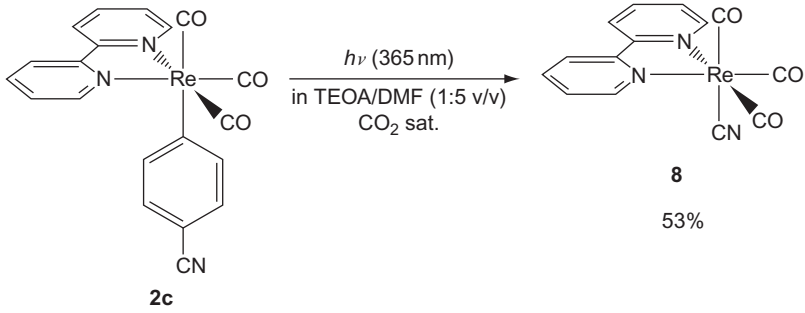

(13)

The second example is the photoinduced alkylation of the bipyridine ligand in *fac*-Re(bpy)$(CO)_3$Br in the presence of triethylamine (TEA) in a DMF solution (Eq. 14) (*54*).

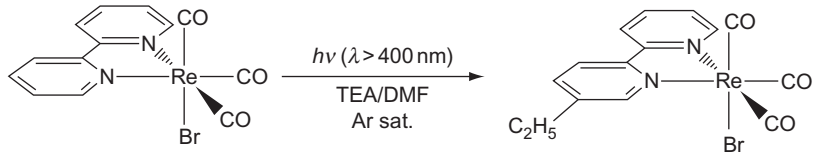

(14)

The formation yield was 10–43% depending on reaction conditions. This reaction is also initiated by photochemical reduction of the Re(I) complex by TEA. Interestingly, the ethyl group was only introduced at the 5-position of the bpy ligand.

The *trans–cis* photoisomerization of the "stilbene-type" ligand in the Re(I) diimine complexes has been reported (*55*).

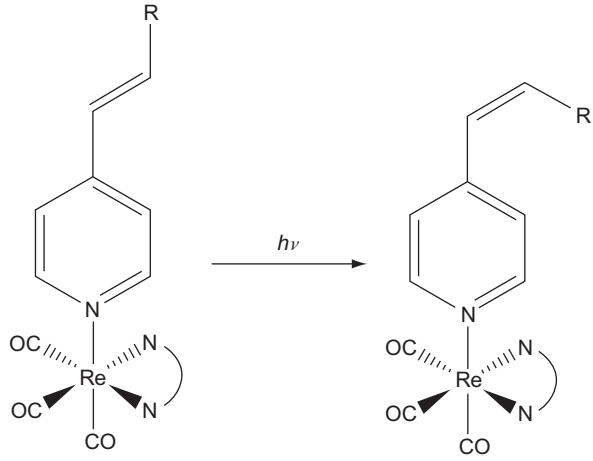

(15)

For instance, *fac*-[Re(phen)(CO)$_3$(*trans*-stpy)]$^+$ (phen = 1, 10-phenanthroline, *trans*-stpy = *trans*-4-styrylpyridine) was irradiated at three different wavelengths (313, 334, and 365 nm) in an acetonitrile solution. Although there is no absorption by free *trans*-stpy at 365 nm, isomerization of the *trans*-stpy ligand to the *cis*-form proceeded with reaction quantum yields of 0.35, 0.36, and 0.31, respectively (*56*). The photochemical isomerization proceeds via intramolecular sensitization, that is, ^{1}MLCT, $^1\pi\pi \rightarrow {}^3$MLCT $\rightarrow {}^3\pi\pi$(*trans*-stpy) $\rightarrow {}^3\pi\pi^*$ of which *trans*-stpy ligand is twisted (*57*).

IV. Rhenium(I) Complexes as Highly Efficient Photocatalyst

As noted above (Section II), rhenium(I) complexes have relatively long excitation lifetimes in solution at room temperature and can be used as redox photosensitizers that drive

single-electron transfer with a strong oxidation power. Further, by choosing appropriate ligands, these complexes can act as electrochemical catalysts that drive the two-electron reduction of CO_2 (*58*). These are the reasons why rhenium(I) complexes can "single-handedly" work as photocatalysts. The high photocatalytic abilities of some rhenium(I) complexes toward CO_2 reduction have received great attention.

As the utilization of CO_2 using solar energy is a promising technique toward resolving both serious problems of global warming and the exhaustion of fossil fuels, development of photocatalysts as a key player for this technique is desired. Although many studies regarding photocatalytic systems simultaneously using $Ru(bpy)_3^{2+}$ (bpy = 2,2′-bipyridine) as a photosensitizer and metal complexes, enzymes, and metal colloids as a catalyst, which can convert photochemical single-electron transfer into multielectron reduction, and also about semiconductor photocatalysts, have been reported, there still exist problems such as low-reaction efficiencies and product selectivities. Rhenium complexes, however, are some of the few photocatalysts that allow both a high reaction efficiency and product selectivity. This section gives an overview about the eminent photocatalyses of rhenium complexes.

A. Mononuclear Rhenium(I) Complexes

Almost 30 years ago, Lehn *et al.* (*59,60*) first reported the photocatalytic reduction of CO_2 by a rhenium(I) complex. They found that *fac*-$Re(bpy)(CO)_3Cl$ (**1a**) could efficiently produce CO from CO_2 using TEOA as a sacrificial reductant. The quantum yield (Φ_{CO}) of this reaction was 0.14, and **1a** was the most efficient photocatalyst for CO_2 reduction at the time. The other outstanding feature of this photocatalytic reaction is its high-product selectivity. That is, the product produced using **1a** is almost exclusively CO, while most other photocatalytic systems yield H_2 and/or formic acid as side products (Table VII).

The identity of the ancillary monodentate ligand greatly influences on the photocatalytic ability of the rhenium complexes. *fac*-$[Re(bpy)(CO)_3\{P(OEt)_3\}]^+$ (**3a**) is a superior photocatalyst ($\Phi_{CO} = 0.38$) to **1a** (*61*). However, the quantum yield of CO production reduces to 0.05 if *fac*-$[Re(bpy)(CO)_3(PPh_3)]^+$ (**3f**) is employed (*62*). *fac*-$[Re(bpy)(CO)_3(py)]^+$ (**2a**), with a pyridine ligand, does not function effectively as a photocatalyst (*29*). The complex *fac*-$Re(bpy)(CO)_3(NCS)$ (**12**), with an anionic ancillary ligand, is a good

TABLE VII

PHOTOCATALYTIC CO_2 REDUCTION USING RHENIUM(I) BIPYRIDINE COMPLEXES.

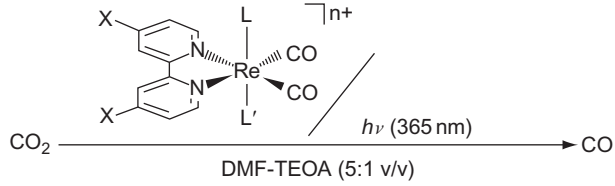

Rhenium complex							
Entry	X	L	L′	n	$E_{1/2}^{red}$ [a] (V)	Φ_{CO} [b]	Ref.
(1) *fac*-[Re(4,4′-X_2-bpy)$(CO)_3$L]$^{n+}$							
1a	H	Cl^-	CO	0	−1.67	0.14	(*60,64*)
3a	H	$P(OEt)_3$	CO	1	−1.43	0.38	(*61,65*)
3j	MeO	$P(OEt)_3$	CO	1	−1.67	0.33	(*64*)
3c	CF_3	$P(OEt)_3$	CO	1	−1.03	0.005	(*65*)
3f	H	PPh_3	CO	1	−1.40	0.05	(*62,65*)
2a	H	py	CO	1		0.03	(*29*)
12	H	NCS^-	CO	0	−1.61	0.30	(*64*)
8	H	CN^-	CO	0	−1.67	0	(*64*)
MS	MeO	$P(OEt)_3$	CO	1	−1.67	0.59	(*64*)
	H	CH_3CN	CO	1	−1.49[c]		
13	H	CH_3CN	CO	1	−1.49[c]	0.04	(*64*)
14	H	$OCHO^-$	CO	0	−1.72[c]	0.05	(*62*)
(2) *cis,trans*-[Re(4,4′-X_2-bpy)$(CO)_2$LL′]$^{n+}$							
11a	H	$P(OEt)_3$	$P(OEt)_3$	1	−1.69	∼0	(*66*)
11d	Me	$P(p\text{-}FPh)_3$	$P(OMe)_3$	1	−1.74	0.09	(*33,67*)
11e	Me	$P(p\text{-}FPh)_3$	$P(p\text{-}FPh)_3$	1	−1.73	0.20	(*33,67*)
11f	Me	$P(Oi\text{-}Pr)_3$	$P(Oi\text{-}Pr)_3$	1	−1.86	0.02	(*33,67*)

[a] Reduction potentials of the complexes versus $Ag/AgNO_3$ measured in CH_3CN.
[b] Quantum yields of CO formation.
[c] Reduction potential converted from Ref. (*71*) with $E_{1/2}^{red}$ versus Fc/Fc^+ + 0.09 V.

photocatalyst, while *fac*-Re(bpy)$(CO)_3(CN)$ (**8**), which also possess an anionic ligand, cannot photocatalyze CO_2 reduction (*63,64*).

The substituents on the bipyridine ligand are also of importance (*65*). The complex **3c**, which has electron-withdrawing CF_3 groups, shows only low CO_2-reducing abilities ($\Phi_{CO} = 0.005$). However, the introduction of electron-donating MeO groups did not influence the photocatalytic ability of the rhenium complex **3j**.

A strong correlation between the first reduction potential and the photocatalytic ability of rhenium complexes has been reported (*65*). For example, complexes with $E_{1/2}^{red} > -1.4$ V versus $Ag/AgNO_3$ show only low photocatalytic ability for CO_2

reduction. Conversely, many of the complexes with $E_{1/2}^{red} < -1.4\,V$ versus $Ag/AgNO_3$ show high photocatalytic ability. Although **3f**, **2a**, and **8** are exceptions, the reasons for this have been clarified. For **3f**, the PPh_3 ligand dissociated relatively quickly from the one-electron reduced (OER) species $[Re(bpy)(CO)_3(PPh_3)]$, which is produced by photochemical electron transfer from the reductant TEOA (Eq. 16). Because the OER species of the solvent complex $[Re(bpy)(CO)_3(S)]$ (**15**, S = DMF, TEOA) has a more negative $E_{1/2}^{red}$ than that of **3f**, electron transfer from $\mathbf{15}^-$ to **3f** proceeds (Eq. 17). Due to Eqs. (16) and (17) occurring repeatedly, **3f** is converted into **15** in a chain reaction. A similar chain reaction occurs with **2a**. The quantum yields of this ligand substitution via light-induced electron transfer are reported as 16.9 for **3f** and 50.3 for **2a** (*29,62*). Due to the short lifetime of its excited state, **15** shows only a low photocatalytic ability.

$$\left[Re(bpy^{\bullet-})(CO)_3(PPh_3)\right] + S \rightarrow \left[Re(bpy^{\bullet-})(CO)_3(S)\right] + PPh_3 \tag{16}$$

$$\begin{aligned} &\left[Re(bpy)(CO)_3(PPh_3)\right]^+ + \left[Re(bpy^{\bullet-})(CO)_3(S)\right] \\ &\rightarrow \left[Re(bpy^{\bullet-})(CO)_3(PPh_3)\right] + \left[Re(bpy)(CO)_3(S)\right]^+ \end{aligned} \tag{17}$$

The reason why **8** does not work as a photocatalyst will be discussed later.

The photocatalytic CO_2 reduction abilities of the biscarbonyl complexes *cis,trans*-$[Re(4,4'\text{-}X_2\text{-}2,2'\text{-bpy})(CO)_2(PR_3)(PR'_3)]^+$ have been also reported. Generally, switching of the strongly electron-attracting CO ligand by other ligands results in a decrease of the excitation energy of the lowest ^{3}MLCT excited state and leads to shortening of the excited state lifetime according to the Energy Gap Law (*5*). Although this is favorable considering the use of the solar energy as such complexes are able to absorb light of longer wavelengths, it also means that light-induced electron transfer, which is the initiating reaction in the photocatalytic reaction, is suppressed due to the lowering of the oxidation power of the excited state. In fact, CO_2 reduction does not proceed with *cis,trans*-$[Re(LL)(CO)_2\{P(OEt)_3\}_2]^+$ (**11a**, LL = bpy, 4,4′-Me_2-2,2′-bpy) even under the same conditions as the photocatalytic reaction of **3a** (*66*). However, biscarbonyl complexes with two triphenylphosphine derivatives show exceptional photocatalytic behavior. Photocatalytic CO_2 reduction proceeded with quantum yield of 0.20 using **11e**, which has electron-withdrawing F atoms at the *p*-positions of the phenyl groups (*33,67*). This is a result of the emergence of π–π interactions between the aryl groups of the

phosphine ligands and the diimine ligand (see Section II.C). This weak interaction between the ligands red-shifts the MLCT absorption band, but blue-shifts the emission from the ^{3}MLCT excited state. The excited state lifetime becomes longer ($\tau = 1.0$ μs), and the oxidation power of the excited state is enhanced. These changes in the complexes' properties are all positive in terms of promoting the photocatalytic reaction.

Aiming at enhancing the efficiency of the photocatalytic reaction using rhenium complexes, CO_2 reduction under various conditions were considered. Under a pressurized CO_2 atmosphere (2.45 MPa), the photocatalytic ability of *fac*-Re(bpy)$(CO)_3$Cl increases as compared to atmospheric pressure and the turnover number (TN_{CO} = the number of CO molecules produced/the number of rhenium complex molecules used) become 5.1 times greater (*68*). At a pressure of 1.36 MPa, *fac*-[Re(bpy)$(CO)_3${P(O*i*-Pr)$_3$}]$^+$ showed a 3.8-fold increase in TN_{CO} (*69*). The explanation given for such increase in the durability of rhenium complexes as photocatalysts is the suppression of the decomposition of the rhenium complexes by side reactions. From the same perspective, photocatalytic CO_2 reduction using rhenium complexes in supercritical or liquid CO_2, which has been given great attention as a clean solvent, has been considered. The complex employed in this study was *fac*-[Re(bpy)$(CO)_3${P$(OC_6H_{13})_3$}] (BArF) (*70*), which has a fluorinated counter anion BArF$^-$ (tetrakis[3,5-bis(trifluoromethyl)phenyl]borate) to increase solubility in liquid CO_2. CO production in liquid CO_2 at 7.0 MPa was confirmed to have a TN_{CO} of 2.2 using this complex.

Further, gas–solid state reactions are possible with solid catalysts that have *fac*-Re(bpy)$(CO)_3$Cl or *fac*-[Re(bpy)$(CO)_3$(py)]$^+$ embedded in the pores of porous materials such as zeolite (NaY) and mesoporous silica (AlMCM-41). CO production using these catalysts with adsorbed water and CO_2 has been confirmed (*72,73*). From the fact that CO_2 reduction proceeds without the addition of a reducing agent, the AlMCM-41 framework has been suspected as serving as the reducing agent.

As noted above, in most cases, in which rhenium(I) complexes are employed as a photocatalyst, CO_2 reduction to CO selectively proceeds, and hydrogen and formic acid are barely formed even under conditions associated with significant quantities of proton donors such as water and TEOA. However, only the following two cases of hydrogen-generating photocatalytic reactions using rhenium complexes have been reported. In ether solvents such as THF, irradiation of *fac*-Re(bpy)$(CO)_3$Br under an Ar atmosphere in the presence of TEA generated hydrogen catalytically ($TN_{H2} = 7$–10) (*74*). Also, it has been reported that rhenium

complexes intercalated between layers of Hectorite function as hydrogen-generating photocatalysts (*75*).

Reactions using rhenium complexes as redox photosensitizers for hydrogen generation have also been reported. The coexistence of Co complexes (*76,77*) or Fe complexes (*78*) as catalyst induced efficient hydrogen generation.

B. Reaction Mechanism

The lowest excited state of the rhenium complexes used in photocatalytic reactions is almost without exception the ^{3}MLCT state. As stated in Section II, the ^{3}MLCT state has a long lifetime and is reduced into an OER species by a suitable reductant (Eq. 18).

$$\left[\mathrm{Re}^{I}(\mathrm{LL})(\mathrm{CO})_3\mathrm{X}\right]^{n+} + \mathrm{D} \xrightarrow{h\nu} \left[\mathrm{Re}^{\mathrm{I}}(\mathrm{LL}^{\bullet-})(\mathrm{CO})_3\mathrm{X}\right]^{(n-1)+} + \mathrm{D}^{\bullet+},$$

$$\mathrm{D} = \mathrm{TEOA},\ \mathrm{TEA} \tag{18}$$

The ^{3}MLCT excited state of the rhenium complexes is a more powerful oxidizing agent than the ground state. While the first reduction wave of **1a** in the ground state is $E_{1/2}{}^{\mathrm{red}} = -1.35\,\mathrm{V}$ vs. SCE (*79*), in the ^{3}MLCT excited state, it becomes $^*E_{1/2}{}^{\mathrm{red}} = +1.15\,\mathrm{V}$, with the oxidation power enhanced by the excitation energy (2.50 eV) (*80*). Therefore, the ^{3}MLCT excited state is reductively quenched by TEOA ($E_0 = +0.80$ V vs. SCE (*28*)) or TEA ($E_{1/2}{}^{\mathrm{ox}} = +1.15$ V vs. SCE (*81*)). For **1a** and **3a**, the rate constants of quenching by TEOA are $k_q = 8.0 \times 10^7$ and $1.1 \times 10^9\ \mathrm{M}^{-1}\,\mathrm{s}^{-1}$, respectively. The initial process of this photocatalytic reaction has been studied in detail by Kutal *et al.* (*82,83*), Kalyanasundaram *et al.* (*28*), and Turner *et al.* (*84*) by laser flash photolysis. The formation of the OER species, *fac*-[$\mathrm{Re}^{\mathrm{I}}(\mathrm{bpy}^-)(\mathrm{CO})_3\mathrm{X}$] (X = Cl, Br), has been clearly demonstrated.

Because the potential of the one-electron reduction of CO_2 is -1.9 V (vs. NHE), neither the ^{3}MLCT excited state nor the OER species of rhenium complexes can reduce CO_2 with a single electron through outer-sphere electron transfer. As shown in Eq. (19), however, the potential for obtaining CO by two-electron reduction of CO_2 shifts positively to -0.53 V (vs. NHE: these potentials of CO_2 reduction are close to the values in CH_3CN vs. SCE (*80*)). Such two-electron reduction of CO_2 has been reported to proceed efficiently using rhenium(I) complexes as electrochemical catalyst (Eqs. 20–22) (*79,85*).

$$CO_2 + 2H^+ + 2e^- \rightarrow CO + H_2O \quad (19)$$

$$\left[Re(bpy)(CO)_3Cl\right] + 2e^- \rightarrow \left[Re(bpy)(CO)_3\right]^- + Cl \quad (20)$$

$$\left[Re(bpy)(CO)_3\right]^- + CO_2 \rightarrow \left[Re(bpy)(CO)_3CO_2\right]^- \quad (21)$$

$$\left[Re(bpy)(CO)_3CO_2\right]^- + CO_2 \xrightarrow{Cl^-} \left[Re(bpy)(CO)_3Cl\right] + CO + CO_3^{2-} \quad (22)$$

In photoreactions, however, in principle, only one-electron transfer occurs with one photon and two electrons cannot be simultaneously inserted into the complex, as can be achieved electrochemically. The OER species of *fac*-[Re(LL)(CO)$_3$(PR$_3$)]$^+$-type complexes are especially stable, and their accumulation can be detected even during photocatalytic CO_2 reduction (*65*). This allows the reaction between this OER species and CO_2 to be studied in detail. For example, the OER species of *fac*-[Re(dmb)(CO)$_3${P(OEt)$_3$}]$^+$ decayed slowly according to a second-order kinetics under an Ar atmosphere, but became faster according to pseudo-first-order kinetics under CO_2 ($k_1 = 5.6 \times 10^{-4}\,M^{-1}\,s^{-1}$ at $[CO_2] = 0.139\,M$) (*65*). This rate constant increased with higher CO_2 concentration. The first reduction potentials ($E_{1/2}^{red}$) of rhenium complexes, which is attributable to the reduction of bpy ligand reduction (bpy/bpy$^-$), the reaction rates of the corresponding OER species and CO_2, and the CO production quantum yields of known photocatalysts are summarized in Table VIII. It is noteworthy that k_1 is relatively large for complexes with $E_{1/2}^{red} < -1.4\,V$, and they function well as photocatalysts for CO_2 reduction. This potential is important as complexes with $E_{1/2}^{red} > -1.4\,V$ have low photocatalytic abilities and react slowly with CO_2.

The three rhenium complexes with anionic ligands, *fac*-[Re(bpy)(CO)$_3$(L)] (**12**: L = NCS$^-$, **8**: CN$^-$, **1a**: Cl$^-$), show similar photophysical and electrochemical characteristics (Table IX).

However, their photocatalytic abilities differ significantly. Specifically, while **12** is a better photocatalyst than **1a**, **8** shows absolutely no photocatalytic behavior. The reason for **8** not to show photocatalytic behavior is that elimination of the CN$^-$ ligand from the OER species does not proceed. As elimination of the Cl$^-$ ligand from the OER species of **1a** (Eq. 23) is relatively fast, only a minute accumulation of the OER species is observed under standard photocatalytic conditions. This elimination reaction was also observed by spectroelectrochemistry (*71,86–88*).

TABLE VIII

PHOTOCATALYTIC CO_2 REDUCTION USING *fac*-[Re(4,4′-X_2bpy)$(CO)_3(PR'_3)]^+$,[a] REACTION OF THE CORRESPONDING OER SPECIES WITH CO_2, AND THEIR REDUCTION POTENTIALS.

[Re(4,4′-X_2,-bpy)$(CO)_3(PR'_3)]^+$					
Entry	X	PR'_3	$E_{1/2}^{red}$ [b] (V)	k_1 [c] (10^{-5} M^{-1} s^{-1})	Φ_{CO} [d]
3d	H	P(*n*-Bu)$_3$	−1.39	10.7	0.013
3e	H	PEt_3	−1.39	3.5	0.024
3h	H	P(O*i*-Pr)$_3$	−1.44	94.2	0.20
3a	H	P(OEt)$_3$	−1.43	56.0	0.16
3i	H	P(OMe)$_3$	−1.41	60.0	0.17
3b	Me	P(OEt)$_3$	−1.55	186	0.18
3c	CF_3	P(OEt)$_3$	−1.03	5.2	0.005

Adapted with permission from Ref. (65). Copyright 1997 American Chemical Society.
[a]A DMF-TEOA (5:1 v/v) solution containing a complex (2.6 mM) was irradiated at 365 nm (light intensity, 1.27×10^{-8} einstein s^{-1}).
[b]Reduction potentials of the complexes versus $Ag/AgNO_3$.
[c]Second-order reaction rate constants of the OER species and CO_2 (0.139 M).
[d]Quantum yield of CO formation.

TABLE IX

PHOTOPHYSICAL AND ELECTROCHEMICAL PROPERTIES OF RHENIUM COMPLEXES.

Complex	λ_{max}^{abs} [a] (nm)	λ_{max}^{em} [b] (nm)	τ [c] (ns)	$E_{1/2}^{red}$ [d] (V)	Φ_{CO} [e]	TN_{CO} [f]
1a	376	637	25[g]	−1.67	0.14	15
12	371	635	30	−1.61	0.30	30
8	356	611	87	−1.67	0	0

Copyright 2008 American Chemical Society.
Adapted with permission from Ref. (64)
[a]Absorption maxima in DMF.
[b]Emission maxima in DMF at room temperature.
[c]Excited state lifetimes in DMF at room temperature under an Ar atmosphere.
[d]Reduction potentials of the complexes versus $Ag/AgNO_3$.
[e]Quantum yields of CO formation (365-nm light irradiation with 7.5×10^{-9} einstein s^{-1}).
[f]Turnover numbers of CO formation.
[g]in MeCN, Ref. (28).

$$\left[\mathrm{Re^{I}(bpy^{\bullet -})(CO)_3Cl}\right]^- \rightarrow \left[\mathrm{Re^{I}(bpy^{\bullet -})(CO)_3}\right] + \mathrm{Cl^-} \leftrightarrow \left[\mathrm{Re^{0}(bpy)(CO)_3}\right] + \mathrm{Cl^-} \quad (23)$$

As the active species formed by elimination of the Cl^- ligand possesses the characteristics of a 17-electron species (Eq. 23),

it reacts with CO_2 to generate the corresponding "CO_2 adduct" (Eq. 24). Two-electron reduction of CO_2 proceeds due to a second one-electron reduction of this CO_2 adduct by another molecule of the OER species (Eq. 25). At this point, **1a** is regenerated by recoordination of Cl^-.

$$\left[\mathrm{Re(bpy)(CO)_3}\right] + \mathrm{CO_2} \rightarrow \text{“}\mathrm{CO_2}\,\text{adduct”} \tag{24}$$

$$\text{“}\mathrm{CO_2}\,\text{adduct”} + \left[\mathrm{Re^{I}(bpy^{\bullet -})(CO)_3Cl}\right]^- \xrightarrow{\mathrm{Cl^-}} \mathrm{CO} + 2\left[\mathrm{Re^{I}(bpy)(CO)_3Cl}\right] \tag{25}$$

The photocatalytic reaction proceeds via a similar mechanism with complex **12** (Scheme 6). However, the elimination reaction of the SCN^- ligand from the OER species of **12** is slower than that of the Cl^- ligand from **1a**. Thus, the photocatalytic reaction proceeds with OER species accumulated to some extent in the solution. Therefore, it is believed that the high photocatalytic activity of **12** arises as a result of the rapid electron transfer from the OER species to the "CO_2 adduct" *(64)*.

If the lifetime of the OER species is relatively long, an inner filter effect is observed, as the OER species is able to absorb over a wide spectrum, ranging from the ultraviolet region to the visible region. Due to the inner filter effect, the ratio of photons absorbed by the initial complex decreases, lowering the apparent quantum yield of CO_2 reduction under high light intensity. Further, photolysis of the OER species proceeds under such conditions, also lowering TN_{CO}, in many cases.

However, the rhenium complexes for which the corresponding OER species rapidly lose the monodentate ligand, such as **1a**, **3f**, and **2a**, have been reported to be converted into *fac*-[Re(bpy)$(CO)_3$(OCHO)] (**14**) during the photocatalytic reaction. Due to its low CO_2 reduction photocatalysis efficiency ($\Phi_{CO} = 0.05$), the photocatalysis diminishes as this complex forms *(29,62)*. It is proposed

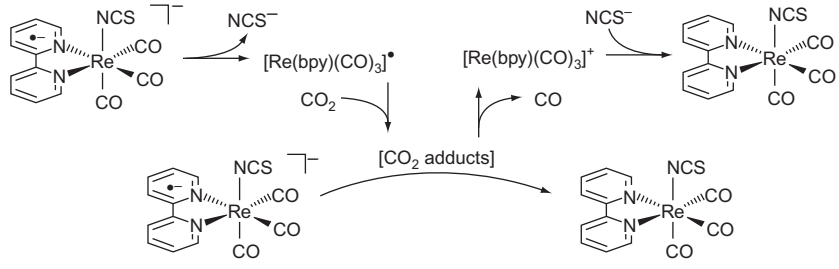

SCHEME 6. Reaction mechanism of the OER species of *fac*-[Re(bpy)$(CO)_3$(NCS)] (**12**) and CO_2.

that a rhenium hydride complex is an intermediate in the pathway to this formate complex (*60*), but this remains speculative.

Although the structure of the "CO_2 adduct," which is an important intermediate in the photocatalysis of the rhenium complexes, has not yet been confirmed, several proposals have been made. As candidates, a CO_2-bridged binuclear complex $(CO)_3(dmb)Re—CO_2—Re(dmb)(CO)_3$ (**16**, dmb = 4,4′-dimethyl-2,2′-bipyridine) and a rhenium carboxylate complex Re(bpy)$(CO)_3$(COOH) (**17**) were synthesized.

Fujita *et al*. (*89–91*) reported that **16** is produced by irradiating the rhenium dimer complex, $(CO)_3(dmb)Re—Re(dmb)(CO)_3$, in THF under a CO_2 atmosphere. This reaction has been reported to proceed by the reaction between CO_2 and the 17-electron species [Re(dmb)$(CO)_3$] generated by light-induced homolysis of the dimer (see Section III.B for homolysis of the Re—Re bond). The photoreaction of $(CO)_3(dmb)Re—CO_2—Re(dmb)(CO)_3$ with CO_2 quantitatively yielded CO and CO_3^{2-}.

17 is synthesized by reacting Re(bpy)$(CO)_4^+$ with OH^-. This reaction is reversible, producing Re(bpy)$(CO)_4^+$ through the elimination of OH^- from Re(bpy)$(CO)_3$(COOH) (Eq. 26). When exposed to light, Re(bpy)$(CO)_4^+$ released one CO ligand (see Section III.C for the photochemical reaction of this complex) and was thereby converted efficiently into *fac*-[Re(bpy)$(CO)_3$S]$^+$ (S = solvent) (*92–94*).

$$\left[\mathrm{Re(bpy)(CO)_4}\right]^+ + \mathrm{OH^-} \rightleftarrows \left[\mathrm{Re(bpy)(CO)_3(COOH)}\right] \qquad (26)$$

The formation of the formate complex **14** as an alternate CO_2 adduct has been noted above. No CO is directly produced from this complex, however, and also due to its low photocatalytic ability, **14** itself is seen as a "dead end" product rather than a reaction intermediate (*60,62*). Recently, Fujita *et al*. (*95*) have proposed a possibility that there is a switch between the two "CO_2 adducts" as the photocatalytic reaction proceeds. That is, a mechanism in which dimer **16** is the main intermediate early in the photocatalytic reaction, but due to the increase in H^+ concentration as the reaction proceeds, the carboxylate complex **17** becomes the intermediate (*95*). However, no report detecting either "CO_2 adduct" in photocatalytic reaction solution has been published, indicating a need for further research.

C. Multicomponent Systems

As stated above, CO_2 reduction proceeds by the OER species of the rhenium complex serving two roles. That is, (1) serving as a single-electron donor and (2) ligand elimination to generate a

17-electron species that reacts directly with CO_2. For the OER species to serve these two roles (1) requires stability while (2) requires instability, demanding contradicting features. Based on this consideration, high photocatalytic attributes have been achieved by employment of a mixture of two rhenium complexes (**MS**), each with optimized functions. *fac*-[Re{4,4′-$(MeO)_2$bpy}$(CO)_3${$P(OEt)_3$}]$^+$ (**3j**) yields the corresponding OER species with high efficiency ($\Phi = 1.6$) under photocatalytic reaction conditions, and this OER species has a strong oxidation power ($E_{1/2}^{red} = -1.67$ V vs. $Ag/AgNO_3$). Although the CO_2 reduction quantum yield using this complex alone is fairly high at 0.33, the addition of a small amount of *fac*-[Re(bpy)$(CO)_3(CN_3CN)$]$^+$ (**13**), which shows nearly no CO_2 reducing ability, led to the most efficient CO_2 photoreduction among known homogeneous photocatalysts ($\Phi_{CO} = 0.59$) (*64*). Complex **3j** functions as a photosensitizer for single-electron transfer in this mixed photocatalyst system. However, *fac*-[Re(bpy)$(CO)_3(CN_3CN)$]$^+$ (**13**) forms 17-electron species efficiently, as elimination of the monodentate ligand occurs rapidly after receiving one electron from the OER species of **3j**. After reacting with CO_2, the CO_2 adduct receives another electron from the OER species of **3j** to produce CO and complete its role as a catalyst (Scheme 7).

One drawback of rhenium tricarbonyl complexes, *fac*-[Re(bpy)$(CO)_3$L]$^{n+}$, is that their absorption of visible light is weak (see

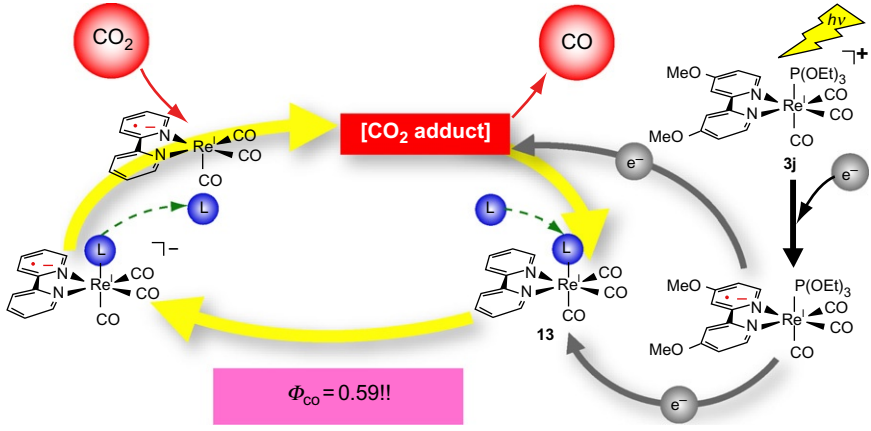

SCHEME 7. Schematic representation of multicomponent system with **3j** as photosensitizer and **13** as catalyst of which acetonitrile ligand can be substituted with L such as DMF and TEOA in the reaction solution. Adapted with permission from Ref. (*64*). Copyright 2008 American Chemical Society.

Fig. 3). However, $[Ru^{II}(dmb)_3]^{2+}$ (dmb = 4,4′-dimethyl-2,2′-bipyridine) strongly absorbs light in the visible region and has a long excited state lifetime of 881 ns and therefore can be employed as a redox photosensitizer. Because the OER species $[Ru^{II}(dmb)_2(dmb^-)]^+$, produced by reductive quenching of its ^{3}MLCT excited state by a reductant such as 1-benzyl-1,4-dihydronicotinamide (BNAH), has a strong reducing power of −1.77 V vs. $Ag/AgNO_3$, it can reduce rhenium complexes such as *fac*-Re(dmb)$(CO)_3$Cl ($E_{1/2} = -1.78$ V vs. $Ag/AgNO_3$), *fac*-[Re(dmb)$(CO)_3${P$(OEt)_3$}]$^+$ ($E_{1/2} = -1.60$ V vs. $Ag/AgNO_3$), and *fac*-[Re(dmb)$(CO)_3$(py)]$^+$ ($E_{1/2} = -1.64$ V vs. $Ag/AgNO_3$) by electron transfer to give the corresponding OER species. In fact, irradiation of a 1:1 mixture of $[Ru(dmb)_3]^{2+}$ and *fac*-Re(dmb)$(CO)_3$Cl using >500-nm light in the presence of BNAH photocatalytically reduced CO_2 to CO ($\Phi_{CO} = 0.062$, $TN_{CO} = 101$) (*96*).

D. Ruthenium(II)–Rhenium(I) Supramolecular Photocatalysts

Aiming to promote electron transfer from the OER species of $[Ru(dmb)_3]^{2+}$ to the rhenium complex, supramolecular complexes connecting these two molecules have been synthesized (Scheme 8). The photocatalytic reaction of **RuC3(OH)ReCl** that has $[Ru(dmb)_3]^{2+}$ and *fac*-Re(dmb)$(CO)_3$Cl connected with a $-CH_2CH(OH)CH_2-$ group between each one of diimine ligands was reported first. The CO_2 reduction photocatalytic ability of this supramolecular complex is higher than the mixture of the corresponding mononuclear complexes, reaching $\Phi_{CO} = 0.12$ and $TN_{CO} = 170$ (*96*).

Photocatalysis using these supramolecular complexes shows a strong dependence on the number of carbon atoms within the bridge and as can be seen from the results of **RuC2Re** ($\Phi_{CO} = 0.13$, $TN_{CO} = 180$), **RuC4Re** ($\Phi_{CO} = 0.11$, $TN_{CO} = 120$), and **RuC6Re** ($\Phi_{CO} = 0.11$, $TN_{CO} = 120$). Bridging by a $-C_2H_4-$ group gave the highest CO_2 reduction photocatalytic ability (*97*). The effect of the monodentate ligand of the rhenium unit is also important. The complex with a $P(OEt)_3$ ligand **RuC3(OH)ReP$(OEt)_3$** showed superior photocatalytic behavior ($\Phi_{CO} = 0.21$, $TN_{CO} = 232$), but on the contrary, **RuC3(OH)Repy** exhibited reduced durability ($TN_{CO} = 97$) (*98*).

Supramolecular photocatalysts connecting several rhenium complexes to a ruthenium complex and connecting several ruthenium complexes to one rhenium complex have also been synthesized. The photocatalytic abilities toward CO_2 reduction of each were **RuRe2** ($TN_{CO} = 190$), **Ru2Re** ($TN_{CO} = 110$) (*99,100*), **RuRe3** ($\Phi_{CO} = 0.093$, $TN_{CO} = 240$) (*96*).

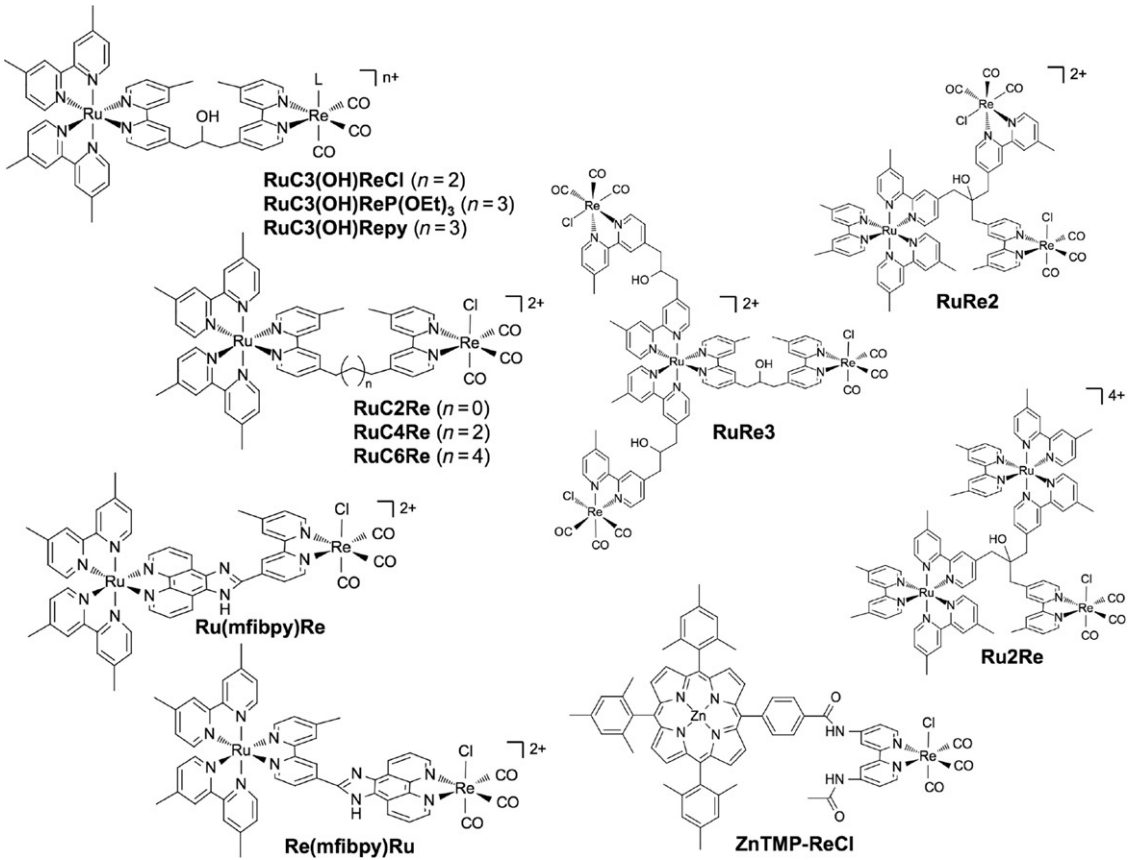

SCHEME 8. Structures and abbreviations of supramolecular photocatalysts.

However, photocatalytic activity was lowered in the cases of **Ru(mfibpy)Re** and **Re(mfibpy)Ru** with conjugated bridges. This is thought to be due to more favorable electron transfer between the Ru and Re units ($TN_{CO} = 14$, 28, respectively) (*96*). A decrease in the reducing power of the rhenium complex due to the use of the conjugate bridging ligand is the cause of the attenuated photocatalysis. As stated in Section IV.A, rhenium complexes cannot photocatalyze CO_2 reduction unless the redox potentials $E_{1/2}{}^{red}$ are more positive than -1.4 V vs. $Ag/AgNO_3$. As $E_{1/2}{}^{red} = -1.10$ V for **Ru(mfibpy)Re** and $E_{1/2}{}^{red} = -1.10$ V for **Re(mfibpy)Ru**, this condition is not satisfied. This is likely to be the reason why these supramolecules demonstrated only low photocatalytic abilities.

Photocatalytic CO_2 reduction of a supramolecule with a Zn porphyrin unit, which is a redox photosensitizer that can absorb even wider ranges of visible light, connected to a rhenium complex (**ZnTMP-ReCl**) was considered (*101,102*). In this system, ultrafast ($1.3 \times 10^{12}\ s^{-1}$) electron transfer from the S_2 excited state of the ZnTMP unit to the rhenium unit was observed. Reduction of CO_2 proceeded with generation of the OER species of the rhenium unit by the reduction of this intramolecular charge-transfer state by TEA.

E. Light-Harvesting System with Periodic Mesoporous Organosilica

The low light density of sunlight may be a problem for solar energy conversion. Photosynthesis alleviates this problem by capturing sunlight with light-antennae unit consisting of chlorophyll stacks and concentrating the energy to reaction centers by excitation energy transfer. Artificial systems that mimic the light-antennae's light-harvesting abilities using chlorophyll analogs (*103*) and porphyrin (*104*) have been an active field of research for the past two decades. However, nearly no applications of these artificial systems to photocatalytic reactions have been made.

Recently, photocatalytic CO_2 reduction using a periodic mesoporous organosilica (PMO, Scheme 9) as the light-harvesting antenna has been reported. PMO has well-ordered pores with a narrow pore size distribution and consists of organosilica frameworks with aromatic rings aligned in a high-density arrangement (*105–108*). The organosilica framework can absorb light efficiently and efficiently transfer energy to guest molecules situated within the pores, thereby efficiently generating the excited state of the guest molecule.

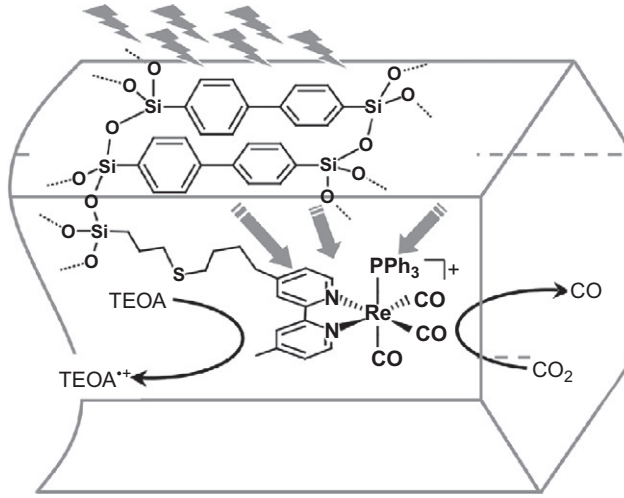

SCHEME 9. Light-harvesting system consisting of periodic mesoporous organosilica with the rhenium complex as the reaction center.

A hybrid material has been synthesized by covalently fixing *fac*-$[Re(dmb)(CO)_3(PPh_3)]^+$ within the 3.5 nm diameter pores of a stable biphenyl-bridged mesoporous organosilica (Bp-PMO). Efficient energy transfer from the biphenylene units to the rhenium complex was observed. Irradiation of dispersed particles of this material in CH_3CN in the presence of TEOA using 280-nm light enables the photocatalytic reduction of CO_2 (*109*). 4.4 times more CO was produced in comparison to the direct irradiation of the rhenium complex with 350-nm light. Rhenium complexes are known to decompose upon direct absorption of 280-nm light through CO elimination (see Section III.F) (*51*). The organosilica framework demonstrates a filtering effect, inhibiting direct excitation of the rhenium complex within the PMO pore, thereby increasing the photocatalyst durability. Further, the chain reaction that induces elimination of the PPh_3 ligand observed in DMF solution (see Section IV.A) was not seen with the PMO hybrids. The cause for this is suspected to be that after the CO_2 reduction, recoordination of PPh_3 to the rhenium center occurs more readily due to the detached PPh_3 being contained within the pore.

ACKNOWLEDGMENTS

We are grateful to Dr. Shane Telfer, Massey University for his assistance in the preparation of this chapter.

References

1. Balzani, V. Ed.: "*Supramolecular Photochemistry*"; D. Reidel: Dordrecht, **1987**.
2. Balzani, V.; Juris, A.; Venturi, M.; Campagna, S.; Serroni, S. *Chem. Rev.* **1996,** *96*, 759–833.
3. Bergman, S. D.; Goldberg, I.; Barbieri, A.; Barigelletti, F.; Kol, M. *Inorg. Chem.* **2004,** *43*, 2355–2367.
4. Butler, J. M.; George, M. W.; Schoonover, J. R.; Dattelbaum, D. M.; Meyer, T. J. *Coord. Chem. Rev.* **2007,** *251*, 492–514.
5. Caspar, J. V.; Meyer, T. J. *J. Phys. Chem.* **1983,** *87*, 952–957.
6. Evans, R. C.; Douglas, P.; Winscom, C. J. *Coord. Chem. Rev.* **2006,** *250*, 2093–2126.
7. George, M. W.; Poliakoff, M.; Turner, J. J. *Analyst* **1994,** *119*, 551–560.
8. Juris, A.; Balzani, V.; Barigelletti, F.; Campagna, S.; Belser, P.; Vonzelewsky, A. *Coord. Chem. Rev.* **1988,** *84*, 85–277.
9. Kalyanasundaram, K. In: "*Photochemistry of Polypyridine and Porphyrin*"; Academic Press Limited: London, **1992,** pp. 311.
10. Kalyanasundaram, K. In: "*Photosensitization and Photocatalysis Using Inorganic and Organometallic Compounds*"; Ed. Kalyanasundaram, K. et al.; Kluwer Academic Publishers: Dordrecht, **1993,** pp. 113–160.
11. Lo, K. K.-W.; Louie, M.-W.; Zhang, K. Y. *Coord. Chem. Rev.* **2010,** *254*, 2603–2622.
12. Sauvage, J. P.; Collin, J. P.; Chambron, J. C.; Guillerez, S.; Coudret, C.; Balzani, V.; Barigelletti, F.; Decola, L.; Flamigni, L. *Chem. Rev.* **1994,** *94*, 993–1019.
13. Schanze, K. S.; MacQueen, D. B.; Perkins, T. A.; Cabana, L. A. *Coord. Chem. Rev.* **1993,** *122*, 63–89.
14. Schanze, K. S.; Walters, K. A. In: "*Organic and Inorganic Photochemistry, vol. 2*"; Ed. Ramamurthy, V.et al.; Marcel Dekker, Inc.: New York, **1998,** pp. 75–127.
15. Slone, R. V.; Benkstein, K. D.; Belanger, S.; Hupp, J. T.; Guzei, I. A.; Rheingold, A. L. *Coord. Chem. Rev.* **1998,** *171*, 221–243.
16. Ziessel, R. F. J. *Chem. Educ.* **1997,** *74*, 673–679.
17. Kumar, A.; Sun, S. S.; Lees, A. J. *Top. Organomet. Chem.* **2010,** *29*, 1–35.
18. Li, F.; Cheng, G.; Zhao, Y.; Feng, J.; Liu, S.; Zhang, M.; Ma, Y.; Shen, J. *Appl. Phys. Lett.* **2003,** *83*, 4716–4718.
19. Ranjan, S.; Lin, S. Y.; Hwang, K. C.; Chi, Y.; Ching, W. L.; Liu, C. S.; Tao, Y. T.; Chien, C. H.; Peng, S. M.; Lee, G. H. *Inorg. Chem.* **2003,** *42*, 1248–1255.
20. Yam, V. W.-w.; Li, B.; Yang, Y.; Chu, B. W.-k.; Wong, K. M.-c.; Cheung, K.-k. *Eur. J. Inorg. Chem.* **2003,** 4035–4042.
21. Hasselmann, G. M.; Meyer, G. J. *Z. Phys. Chem.* **1999,** *212*, 39–44.
22. Chen, P. Y.; Westmoreland, T. D.; Danielson, E.; Schanze, K. S.; Anthon, D.; Neveux, P. E.; Meyer, T. J. *Inorg. Chem.* **1987,** *26*, 1116–1126.
23. Pac, C.; Kaseda, S.; Ishii, K.; Yanagida, S.; Ishitani, O. In: "*Photochemical Processes in Organized Molecular Systems*"; Ed. Honda, K.et al.; Elsevier: Amsterdam, **1991** pp. 177–186.
24. Kirgan, R. A.; Sullivan, B. P.; Rillema, D. P. In: "*Photochemistry and Photophysics of Coordination Compounds II, vol. 281*"; Ed. Balzani, V. et al.; Springer, Verlag: Berlin, Heidelberg, **2007** pp. 45–100.
25. Vos, J. G.; Pryce, M. T. *Coord. Chem. Rev.* **2010,** *254*, 2519–2532.

26. Koike, K.; Okoshi, N.; Hori, H.; Takeuchi, K.; Ishitani, O.; Tsubaki, H.; Clark, I. P.; George, M. W.; Johnson, F. P. A.; Turner, J. J. J. *Am. Chem. Soc.* **2002,** *124*, 11448–11455.
27. Worl, L. A.; Duesing, R.; Chen, P. Y.; Dellaciana, L.; Meyer, T. J. *J. Chem. Soc. Dalton Trans.* **1991,** 849–858.
28. Kalyanasundaram, K. *J. Chem. Soc. Faraday Trans.* **1986,** *82*, 2401–2415.
29. Hori, H.; Ishihara, J.; Koike, K.; Takeuchi, K.; Ibusuki, T.; Ishitani, O. *J. Photochem. Photobiol. A Chem.* **1999,** *120*, 119–124.
30. Sacksteder, L.; Zipp, A. P.; Brown, E. A.; Streich, J.; Demas, J. N.; Degraff, B. A. *Inorg. Chem.* **1990,** *29*, 4335–4340.
31. Koike, K.; Tanabe, J.; Toyama, S.; Tsubaki, H.; Sakamoto, K.; Westwell, J. R.; Johnson, F. P. A.; Hori, H.; Saitoh, H.; Ishitani, O. *Inorg. Chem.* **2000,** *39*, 2777–2783.
32. Hori, H.; Koike, K.; Ishizuka, M.; Takeuchi, K.; Ibusuki, T.; Ishitani, O. *J. Organomet. Chem.* **1997,** *530*, 169–176.
33. Tsubaki, H.; Sekine, A.; Ohashi, Y.; Koike, K.; Takeda, H.; Ishitani, O. *J. Am. Chem. Soc.* **2005,** *127*, 15544–15555.
34. Tsubaki, H.; Tohyama, S.; Koike, K.; Saitoh, H.; Ishitani, O. *Dalton Trans.* **2005,** 385–395.
35. Yasufuku, K.; Noda, H.; Iwai, J.; Ohtani, H.; Hoshino, M.; Kobayashi, T. *Organometallics* **1985,** *4*, 2174–2176.
36. Rossenaar, B. D.; Vandergraaf, T.; Vaneldik, R.; Langford, C. H.; Stufkens, D. J.; Vlček, A. *Inorg. Chem.* **1994,** *33*, 2865–2873.
37. Rossenaar, B. D.; Kleverlaan, C. J.; vandeVen, M. C. E.; Stufkens, D. J.; Vlček, A. *Chem. Eur. J.* **1996,** *2*, 228–237.
38. Shaver, R. J.; Rillema, D. P. *Inorg. Chem.* **1992,** *31*, 4101–4107.
39. Chan, W. K.; Ng, P. K.; Gong, X.; Hou, S. J. *J. Mater. Chem.* **1999,** *9*, 2103–2108.
40. Ming, Z.; Ping, L.; Wang, X. M.; Lin, H.; Hong, X.; Wu, Z.; Bing, Y.; Liu, L. L.; Li, Y.; Min, Y.; Ma, Y. G.; Feng, J. K.; Wang, D. J.; Tamai, N. *J. Phys. Chem. B* **2004,** *108*, 13185–13190.
41. Bignozzi, C. A.; Ferri, V.; Scoponi, M. *Macromol. Chem. Phys.* **2003,** *204*, 1851–1862.
42. Zhang, M.; Lu, P.; Wang, X. M.; Xia, H.; Zhang, W.; Yang, B.; Liu, L. L.; Yang, L.; Yang, M.; Ma, Y. G.; Feng, J. K.; Wang, D. J. *Thin Solid Films* **2005,** *477*, 193–197.
43. Feliz, M. R.; Ferraudi, G. *Inorg. Chem.* **2004,** *43*, 1551–1557.
44. Woessner, S. M.; Helms, J. B.; Shen, Y. B.; Sullivan, B. P. *Inorg. Chem.* **1998,** *37*, 5406–5407.
45. Sun, S. S.; Lees, A. J. *J. Am. Chem. Soc.* **2000,** *122*, 8956–8967.
46. Slone, R. V.; Yoon, D. I.; Calhoun, R. M.; Hupp, J. T. *J. Am. Chem. Soc.* **1995,** *117*, 11813–11814.
47. DelNegro, A. S.; Woessner, S. M.; Sullivan, B. P.; Dattelbaum, D. M.; Schoonover, J. R. *Inorg. Chem.* **2001,** *40*, 5056–5057.
48. Ishitani, O.; Kanai, K.; Yamada, Y.; Sakamoto, K. *Chem. Commun.* **2001,** 1514–1515.
49. Yamamoto, Y.; Sawa, S.; Funada, Y.; Morimoto, T.; Falkenstrom, M.; Miyasaka, H.; Shishido, S.; Ozeki, T.; Koike, K.; Ishitani, O. *J. Am. Chem. Soc.* **2008,** *130*, 14659–14674.
50. Takeda, H.; Yamamoto, Y.; Nishiura, C.; Ishitani, O. *Anal. Sci.* **2006,** *22*, 545–549.

51. Sato, S.; Sekine, A.; Ohashi, Y.; Ishitani, O.; Blanco-Rodriguez, A. M.; Vlcek, A. Jr.; Unno, T.; Koike, K. *Inorg. Chem.* **2007,** *46*, 3531–3540.
52. Sato, S.; Morimoto, T.; Ishitani, O. *Inorg. Chem.* **2007,** *46*, 9051–9053.
53. Hori, H.; Ishihara, J.; Koike, K.; Takeuchi, K.; Ibusuki, T.; Ishitani, O. *Chem. Lett.* **1997,** 1249–1250.
54. Ishitani, O.; Namura, I.; Yanagida, S.; Pac, C. *J. Chem. Soc. Chem. Commun.* **1987,** 1153–1154.
55. Polo, A. S.; Itokazu, M. K.; Frin, K. M.; Patrocinio, A. O. D.; Iha, N. Y. M. *Coord. Chem. Rev.* **2006,** *250*, 1669–1680.
56. Polo, A. S.; Itokazu, M. K.; Iha, N. Y. M. *J. Photochem. Photobiol. A Chem.* **2006,** *181*, 73–78.
57. Dattelbaum, D. M.; Itokazu, M. K.; Iha, N. Y. M.; Meyer, T. J. *J. Phys. Chem. A* **2003,** *107*, 4092–4095.
58. Takeda, H.; Ishitani, O. *Coord. Chem. Rev.* **2010,** *254*, 346–354.
59. Hawecker, J.; Lehn, J.-M.; Ziessel, R. *J. Chem. Soc. Chem. Commun.* **1983,** 536–538.
60. Hawecker, J.; Lehn, J.-M.; Ziessel, R. *Helv. Chim. Acta* **1986,** *69*, 1990–2012.
61. Hori, H.; Johnson, F. P. A.; Koike, K.; Ishitani, O.; Ibusuki, T. *J. Photochem. Photobiol. A Chem.* **1996,** *96*, 171–174.
62. Hori, H.; Johnson, F. P. A.; Koike, K.; Takeuchi, K.; Ibusuki, T.; Ishitani, O. *J. Chem. Soc. Dalton Trans.* **1997,** 1019–1023.
63. Kurz, P.; Probst, B.; Spingler, B.; Alberto, R. *Eur. J. Inorg. Chem.* **2006,** 2966–2974.
64. Takeda, H.; Koike, K.; Inoue, H.; Ishitani, O. *J. Am. Chem. Soc.* **2008,** *130*, 2023–2031.
65. Koike, K.; Hori, H.; Ishizuka, M.; Westwell, J. R.; Takeuchi, K.; Ibusuki, T.; Enjouji, K.; Konno, H.; Sakamoto, K.; Ishitani, O. *Organometallics* **1997,** *16*, 5724–5729.
66. Ishitani, O.; George, M. W.; Ibusuki, T.; Johnson, F. P. A.; Koike, K.; Nozaki, K.; Pac, C.; Turner, J. J.; Westwell, J. R. *Inorg. Chem.* **1994,** *33*, 4712–4717.
67. Tsubaki, H.; Sugawara, A.; Takeda, H.; Gholamkhass, B.; Koike, K.; Ishitani, O. *Res. Chem. Intermed.* **2007,** *33*, 37–48.
68. Hori, H.; Takano, Y.; Koike, K.; Sasaki, Y. *Inorg. Chem. Commun.* **2003,** *6*, 300–303.
69. Hori, H.; Koike, K.; Suzuki, Y.; Ishizuka, M.; Tanaka, J.; Takeuchi, K.; Sasaki, Y. *J. Mol. Catal. A Chem.* **2002,** *179*, 1–9.
70. Hori, H.; Koike, K.; Takeuchi, K.; Sasaki, Y. *Chem. Lett.* **2000,** 522–523.
71. Johnson, F. P. A.; George, M. W.; Hartl, F.; Turner, J. J. *Organometallics* **1996,** *15*, 3374–3387.
72. Sung-Suh, H. M.; Kim, D. S.; Lee, C. W.; Park, S.-E. *Appl. Organomet. Chem.* **2000,** *14*, 826–830.
73. Hwang, J.-S.; Kim, D. S.; Lee, C. W.; Park, S.-E. *Korean J. Chem. Eng.* **2001,** *18*, 919–923.
74. Pac, C.; Ishii, K.; Yanagida, S. *Chem. Lett.* **1989,** 765–768.
75. Tajik, M.; Detellier, C. *J. Chem. Soc. Chem. Commun.* **1987,** 1824–1825.
76. Probst, B.; Kolano, C.; Hamm, P.; Alberto, R. *Inorg. Chem.* **2009,** *48*, 1836–1843.
77. Probst, B.; Rodenberg, A.; Guttentag, M.; Hamm, P.; Alberto, R. *Inorg. Chem.* **2010,** *49*, 6453–6460.
78. Wang, H.-Y.; Wang, W.-G.; Si, G.; Wang, F.; Tung, C.-H.; Wu, L.-Z. *Langmuir* **2010,** *26*, 9766–9771.

79. Sullivan, B. P.; Bolinger, C. M.; Conrad, D.; Vining, W. J.; Meyer, T. J. *J. Chem. Soc. Chem. Commun.* **1985,** 1414–1416.
80. Fujita, E.; Brunschwig, B. S. In: "*Catalysis, Heterogeneous Systems, Gas Phase Systems*"; Ed. Balzani, V.; vol. 4; Wiley-VCH: Weinheim, **2001** pp. 88–126.
81. Loveland, J. W.; Dimeler, G. R. *Anal. Chem.* **1961,** *33*, 1196–1201.
82. Kutal, C.; Corbin, A. J.; Ferraudi, G. *Organometallics* **1987,** *6*, 553–557.
83. Kutal, C.; Weber, M. A.; Ferraudi, G.; Geiger, D. *Organometallics* **1985,** *4*, 2161–2166.
84. George, M. W.; Johnson, F. P. A.; Westwell, J. R.; Hodges, P. M.; Turner, J. J. *J. Chem. Soc. Dalton Trans.* **1993,** 2977–2979.
85. Smieja, J. M.; Kubiak, C. P. *Inorg. Chem.* **2010,** *49*, 9283–9289.
86. Christensen, P.; Hamnett, A.; Muir, A. V. G.; Timney, J. A. *J. Chem. Soc. Dalton Trans.* **1992,** 1455–1463.
87. Stor, G. J.; Hartl, F.; van Outersterp, J. W. M.; Stufkens, D. J. *Organometallics* **1995,** *14*, 1115–1131.
88. Scheiring, T.; Klein, A.; Kaim, W. *J. Chem. Soc. Perkin Trans.* **1997,** *2*, 2569–2571.
89. Shinozaki, K.; Hayashi, Y.; Brunschwig, B. S.; Fujita, E. *Res. Chem. Intermed.* **2007,** *33*, 27–36.
90. Hayashi, Y.; Kita, S.; Brunschwig, B. S.; Fujita, E. *J. Am. Chem. Soc.* **2003,** *125*, 11976–11987.
91. Fujita, E.; Muckerman, J. T. *Inorg. Chem.* **2004,** *43*, 7636–7647.
92. Gibson, D. H.; Yin, X. J. *Am. Chem. Soc.* **1998,** *120*, 11200–11201.
93. Gibson, D. H.; Yin, X. *Chem. Commun.* **1999,** 1411–1412.
94. Gibson, D. H.; Yin, X.; He, H.; Mashuta, M. S. *Organometallics* **2003,** *22*, 337–346.
95. Morris, A. J.; Meyer, G. J.; Fujita, E. *Acc. Chem. Res.* **2009,** *42*, 1983–1994.
96. Gholamkhass, B.; Mametsuka, H.; Koike, K.; Tanabe, T.; Furue, M.; Ishitani, O. *Inorg. Chem.* **2005,** *44*, 2326–2336.
97. Koike, K.; Naito, S.; Sato, S.; Tamaki, Y.; Ishitani, O. *J. Photochem. Photobiol. A Chem.* **2009,** *207*, 109–114.
98. Sato, S.; Koike, K.; Inoue, H.; Ishitani, O. *Photochem. Photobiol. Sci.* **2007,** *6*, 454–461.
99. Bian, Z.-Y.; Sumi, K.; Furue, M.; Sato, S.; Koike, K.; Ishitani, O. *Inorg. Chem.* **2008,** *47*, 10801–10803.
100. Bian, Z.-Y.; Sumi, K.; Furue, M.; Sato, S.; Koike, K.; Ishitani, O. *Dalton Trans.* **2009,** 983–993.
101. Kiyosawa, K.; Shiraishi, N.; Shimada, T.; Masui, D.; Tachibana, H.; Takagi, S.; Ishitani, O.; Tryk, D. A.; Inoue, H. *J. Phys. Chem. C* **2009,** *113*, 11667–11673.
102. Kiyosawa, K.; Shiraishi, N.; Takeda, H.; Masui, D.; Shimada, T.; Tachibana, H.; Ishitani, O.; Inoue, H. in preparation.
103. Tamiaki, H.; Miyatake, T.; Tanikaga, R.; Holzwarth, A. R.; Schaffner, K. *Angew. Chem. Int. Ed. Engl.* **1996,** *35*, 772–774.
104. Peng, X.; Aratani, N.; Takagi, A.; Matsumoto, T.; Kawai, T.; Hwang, I.-W.; Ahn, T. K.; Kim, D.; Osuka, A. *J. Am. Chem. Soc.* **2004,** *126*, 4468–4469.
105. Inagaki, S.; Guan, S.; Ohsuna, T.; Terasaki, O. *Nature* **2002,** *416*, 304–307.
106. Kapoor, M. P.; Yang, Q.; Inagaki, S. *J. Am. Chem. Soc.* **2002,** *124*, 15176–15177.

107. Inagaki, S.; Ohtani, O.; Goto, Y.; Okamoto, K.; Ikai, M.; Yamanaka, K.; Tani, T.; Okada, T. *Angew. Chem. Int. Ed.* **2009,** *48*, 4042–4046.
108. Takeda, H.; Goto, Y.; Maegawa, Y.; Ohsuna, T.; Tani, T.; Matsumoto, K.; Shimada, T.; Inagaki, S. *Chem. Commun.* **2009,** 6032–6034.
109. Takeda, H.; Ohashi, M.; Tani, T.; Ishitani, O.; Inagaki, S. *Inorg. Chem.* **2010,** *49*, 4554–4559.

DESIGN OF PORPHYRIN-BASED PHOTOSENSITIZERS FOR PHOTODYNAMIC THERAPY

LUIS G. ARNAUT[1]

Chemistry Department, University of Coimbra, Coimbra, Portugal

ABSTRACT

Porphyrin and metalloporphyrin derivatives are at the forefront of the photosensitizers currently investigated for the photodynamic therapy (PDT) of cancer. Earlier examples included various porphyrins and chlorins, some of them already approved for clinical work, but lately emphasis has been given to the development of stable bacteriochlorin derivatives. The spectroscopy, photochemistry, and electrochemistry of porphyrins and bacteriochlorins, and some of their representative metal complexes, are reviewed and related to the design of photosensitizers capable of producing reactive oxygen species with high quantum yields. Efficacy *in vitro* is evaluated in terms of a phototherapeutic index, and efficacy *in vitro* is assessed using tumor growth delays. Guidelines are proposed for the design of more efficient PDT photosensitizers.

[1]Also affiliated with Luzitin SA, R. Bayer, 3045-016 Coimbra, Portugal.

INORGANIC PHOTOCHEMISTRY
VOLUME 63 ISSN 0898-8838 / DOI: 10.1016/B978-0-12-385904-4.00006-8

Keywords: Bacteriochlorin; Photodynamic therapy; Reactive oxygen species; Photodecomposition.

I. Introduction

Porphyrins and their derivatives play critical roles in many biological functions. Some of the most remarkable examples are protoporphyrin IX and its iron complex that constitutes the heme prosthetic group, and the magnesium complexes of pheophytin *a* and bacteriopheophytin *a* that are known as chlorophyll *a* and bacteriochlorophyll *a*, respectively. These natural compounds are illustrated in Fig. 1 together with the structure of porphin,

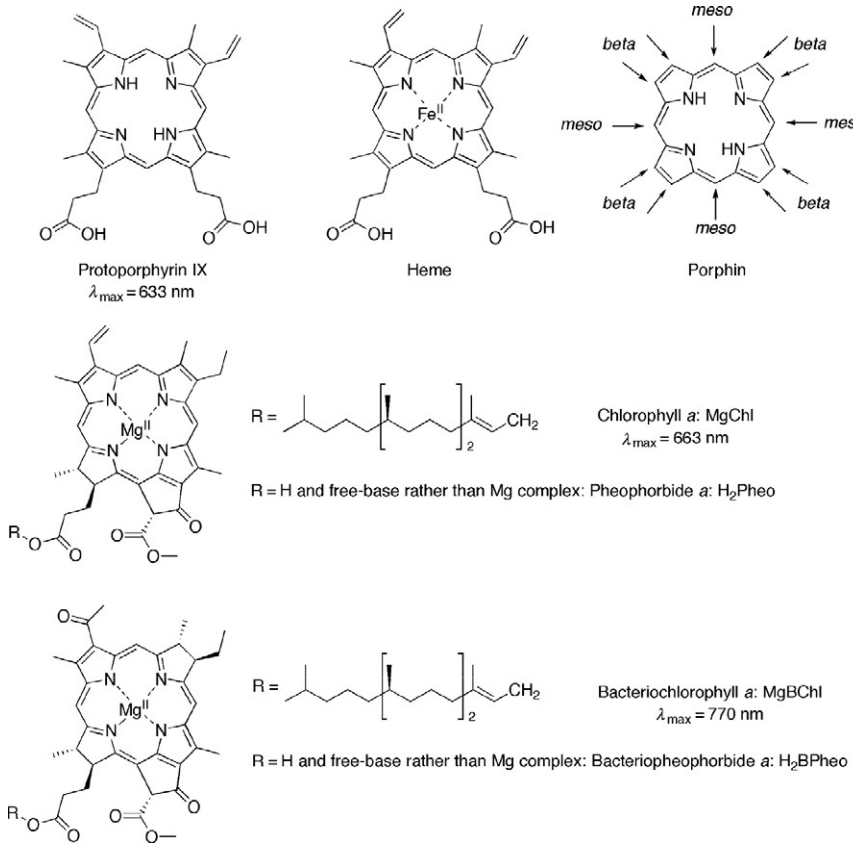

FIG. 1. Structure and absorption maxima of some natural porphyrins and their derivatives. Also shown is the structure of the simplest porphyrin, called porphin, and the names commonly given to substitution positions.

the simplest porphyrin, and the common generic names of the positions of the pyrrole rings. These macrocycles have important absorption bands in the red and near infrared, with the wavelength of the maximum absorption of the lowest energy absorption band (λ_{max}) indicated in the figure.

The photochemistry of porphyrins and their derivatives has been particularly well studied for their relevance in biological processes, as evidenced from the examples above, and also for their use in many other processes such as dye-sensitized solar cells, photocatalysis, molecular electronics, etc. The subject is vast and has been addressed by many excellent books, reviews, and specific journals (*1,2*). More recently, expanded porphyrins, with additional pyrrole rings conjugated to each other through carbon groups (*3*), have contributed to enrich the chemistry of these molecules. A comprehensive view of this subject is beyond the scope of this work. Our work focuses on the photochemistry of the *meso*-tetraphenylporphyrin (TPP) because it is the most easily synthesized porphyrin unit, and on the applications of tetrahydroporphyrins to photodynamic therapy (PDT). This focus is motivated by the need for designed synthetic products obtained from abundant sources at affordable prices in photomedicine, by the increasingly important role of PDT in photomedicine, and by the perception that the versatility and photochemical properties of TPPs have the potential to meet needs of PDT. We emphasize the quest for photostable tetrahydroporphyrins derivatives because of their strong absorptions in the red and infrared as a critical step toward a better use of the phototherapeutic window (720–900 nm, the most penetrating and least harmful radiation to human tissues that can generate reactive oxygen species (ROS)).

Porphyrin derivatives have been extensively tested as photosensitizers for the PDT of cancer for two sets of reasons. First, their strong absorption of light in the phototherapeutic window and efficient photoinduced reactions with molecular oxygen offer a photochemical tool to induce localized cytotoxicity in targeted tissues. Second, porphyrin derivatives have an intrinsic affinity for tumors (*4–6*). Whereas the spectroscopy and photochemistry of porphyrin derivatives are very well understood, the same is not (yet) true for the mechanisms that contribute to their preferential localization and accumulation in tumors. This latter subject is outside the scope of this work, and it will only be briefly mentioned in the context of *in vivo* studies with porphyrin derivatives.

The structure of this work is as follows. First, we offer an overview of simple models that can give a semiquantitative

understanding of electronic states and electronic transitions in porphyrins and metalloporphyrins, and of the lifetimes and yields of their singlet and triplet electronic states. From this spectroscopic and photochemical viewpoint, we address the interaction between electronically excited porphyrins or porphyrins derivatives and molecular oxygen because this interaction can lead to ROS of general interest in photomedicine. Finally, we present some recent results of dyes of this class designed for PDT.

II. Molecular and Electronic Structure

The core of a *porphyrin* is a tetrapyrrole in which the four rings of the pyrrole type are linked together by methine carbon atoms. The most common reduced porphyrins are dihydroporphyrins, and the parent compound of this series is called *chlorin*. Tetrahydroporphyrins in which the saturated carbon atoms are located at nonfused carbon atoms of two diagonally opposite pyrrole rings are called *bacteriochlorins*. An interesting common feature of these species is that they share the same basic chromophore, because the porphyrin macrocycle has 22 π-electrons, but only 18 π-electrons are considered to lie on the main delocalization pathway. Figure 2 illustrates these structures and the numbering scheme recommended by IUPAC. The 2, 3, 7, 8, 12, 13, 17, and 18 positions are commonly referred as "*beta*-positions" and the 5, 10, 15, and 20 positions are referred as "*meso*-positions."

A simple and yet meaningful model to interpret the electronic structure of porphyrins was proposed by Guterman based on the two highest occupied molecular orbitals (HOMOs) and the two lowest unoccupied molecular orbitals (LUMOs) (*7*,*8*). The macrocycles of porphin (H_2P) and 5,10,15,20-tetraphenylporphyrin (H_2TPP) are distorted from the planar (D_{4h}) geometry owing to the presence of the two hydrogens bonded to two opposing central nitrogens and assume a D_{2h} symmetry. The two HOMOs in the D_{4h} point group labeled a_{1u} and a_{2u} correspond to a_u and b_{1u}, respectively, in the D_{2h} point group, and the two LUMOs transform from e_{gx}* and e_{gy}* in D_{4h} to b_{2g} and b_{3g} in D_{2h}. The x molecular axis is defined by the central NH bonds, and the y axis bisects the central nitrogen electron lone pairs, as shown in Fig. 2. In porphyrins, the HOMO a_u and b_{1u} orbitals lie close enough in energy that they be viewed as being essentially degenerate, and the b_{2g} and b_{3g} orbitals are even closer in energy. As a result, the allowed

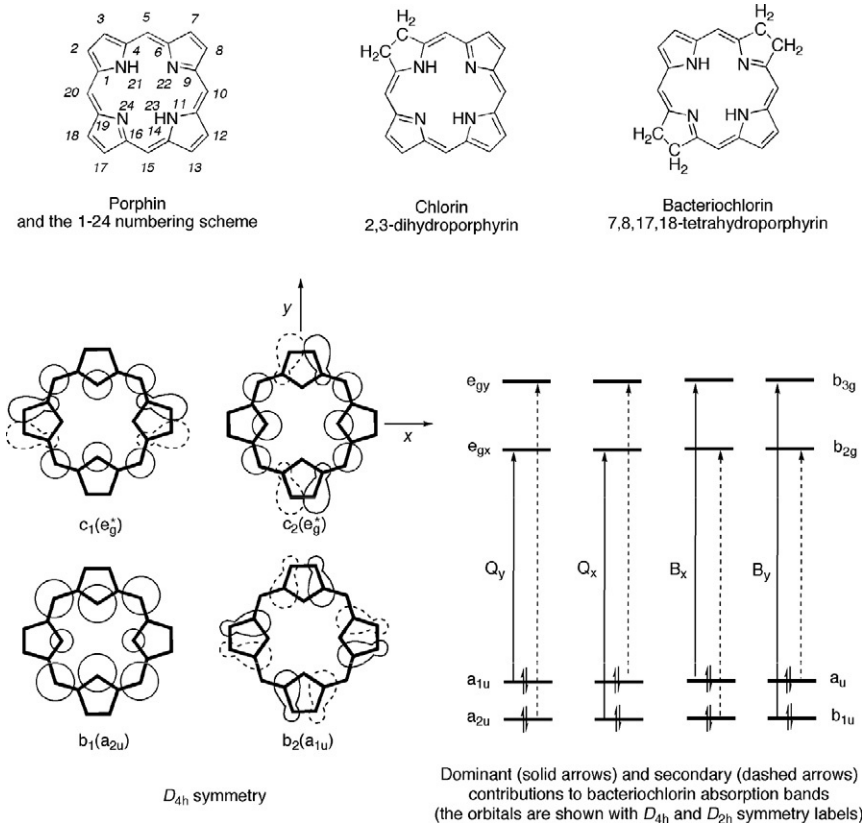

FIG. 2. Fundamental porphyrin systems with numbering scheme, pictorial representation of the HOMOs and LUMOs, and contributions to the absorption bands of bacteriochlorins.

$a_u \rightarrow b_{2g}$ and $b_{1u} \rightarrow b_{3g}$ optical transitions have nearly the same energy as the allowed $b_{1u} \rightarrow b_{2g}$ and $a_u \rightarrow b_{3g}$ transitions, the electronic states undergo configuration interaction and split, giving rise to a pair of low energy and low intensity (Q_x and Q_y) transitions and another of high energy (B_x and B_y) transitions. The pair B_x and B_y is often observed a single intense band called Soret band. Most of the intensity of the transitions is carried by the B bands because they result from the addition of the transition dipoles, whereas the weakness of the Q bands comes from the near cancelation of the transition dipoles. The skeletal distortions in the free-base due to the presence of the NH bonds are responsible for lifting the b_{2g}–b_{3g} orbital degeneracy and for the observed splitting of the Q bands. The lowest energy transition, $b_{1u} \rightarrow b_{2g}$, is polarized along the proton axis and is labeled

Q_x (8). Replacement of the two central hydrogens by a metal ion of appropriate size leads to the D_{4h} geometry and to degeneracy the b_{2g} and b_{3g} orbitals (e_g orbitals in this point group), and only one Q band is observed. The closer the degeneracy of the optical transitions, the weaker the Q band. More sophisticated quantum-mechanical calculations have shown the robustness of the Gouterman model in describing the energy order and character of the porphyrin molecular orbitals (9).

MO calculations for simple porphyrins, chlorins, and bacteriochlorins show that, within the same series, the LUMOs are nearly isoenergetic, that is, they do not change as the number of π electrons is reduced from 22 to 20 and to 18 along the series. However, the increased D_{2h} skeletal distortion destabilizes the HOMOs, and their energies increase systematically (Fig. 3 (10)).

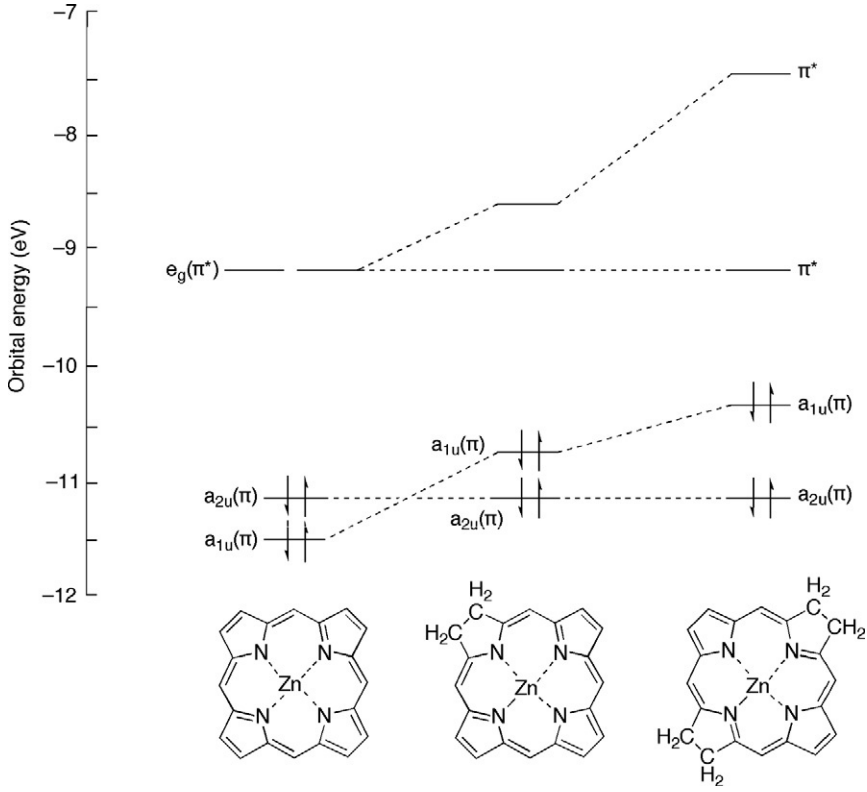

FIG. 3. Calculated energy levels of macrocycle HOMO−1, HOMO, LUMO, and LUMO+1 in porphin, chlorin, and bacteriochlorin complexes with Zn(II). For clarity, the D_{4h} symmetry labels of a_{1u} and a_{2u} were retained for all the macrocycles. Adapted from Ref. (10).

This diminishes the HOMO–LUMO gap from the porphyrin, to the chlorin and to the bacteriochlorin, explaining the bathochromic shift of the Q_y bands. The oxidation and reduction potentials of these species follow the energy changes of the HOMO and LUMO, respectively. Thus, again within a homologous series, the reduction potentials of the porphyrin, chlorin, and bacteriochlorin remain essentially the same, whereas the oxidation potentials become increasingly more facile, with the bacteriochlorin having the lowest oxidation potential and the porphyrin the highest (*10*). These properties are illustrated with some examples in Table I.

Perfluoroalkyl groups are strongly α-electron withdrawing and do not function as π-electron donors. The electron-withdrawing effect of CF_3 groups in the pyrrolic β-positions of *meso*-TPP distorts the macrocycle and forces it to take a fixed 18π-electron pathway, resembling the electronic structure of bacteriochlorin. This is reflected in the HOMO–LUMO gap contraction and in the 0.06 V decrease in the oxidation potential of H_2TPP-β$(CF_3)_4$ with respect to H_2TPP (*12*). However, this decrease is not as accentuated as the 0.20 V decrease observed for H_2TPP-β$(CH_3)_4$ because it is compensated by the strong electron-withdrawing ability of the trifluoromethyl group (*12*). The electron-withdrawing effect is also responsible for making the reduction easier. β-Octahalogenation of TPPs with Cl or Br atoms also produces steric hindrance at the ligand periphery and leads to highly nonplanar porphyrin cores, but β-octafluoro-*meso*-TPPs are nearly planar (*14*). This is corroborated by the hypsochromic shift of the absorption bands of both free-base and zinc complex, and by the remarkable increase of the oxidation potentials of β-fluorinated porphyrins (*13*).

Fluorinating the phenyl groups of TPP in the *meso*-positions also introduces electron-withdrawing substituents that operate exclusively through the inductive effect, as shown in the replacement of phenyl by *o*,*o*′-difluorophenyl rings (TF_2PP), in free-base, Mg, and Zn porphyrins (*20*). Comparison between the oxidation potentials of Mg^{II}TPP and $Mg^{II}(TF_2PP)$ or of Zn^{II}TPP and $Zn^{II}(TF_2PP)$ reveals an increase in 0.26–0.27 eV in the oxidation potential, assigned to a stabilization of both a_{2u} and a_{1u} orbitals. However, the a_{2u} orbital is expected to be preferentially stabilized relative to the a_{1u} orbital because the halogenated phenyl rings are bonded to the *meso*-carbon atoms, where the electronic density of the a_{2u} orbital is higher. The 3d metal orbitals of Mg^{II}TPP and Zn^{II}TPP are of lower energy than the HOMO and do not change the ordering of the active orbitals (*21*), hence the changes in oxidation potentials of fluorinated Mg^{II} and Zn^{II} porphyrins are representative of the corresponding changes in free bases.

TABLE I

REDOX POTENTIALS VERSUS SCE AND OPTICAL CHARACTERISTICS OF PORPHYRIN DERIVATIVES

Compound	Half-wave potential (V)			Q(0,0) absorption band	
	$E_{1/2}^{ox}$[a]	$E_{1/2}^{red}$[a]	$\Delta E^{\pm}$[a]	E_{S1} (eV)	λ_{max} (nm)
H_2TPP [b]	0.95	−1.08	2.03	1.92	647
H_2TPC [b]	0.88	−1.12	2.00	1.91	650
H_2TPB [b]	0.40	−1.10	1.50	1.68	740
H_2TPP-β$(CF_3)_4$[c]	0.89	−0.33	1.42		835
H_2TPP-βF_8[d]	1.26	−0.67	2.13		637
ZnTPP[e]	0.77	−1.35	2.02	2.12	585
ZnTPC[e]	0.60	−1.33	1.93	2.03	610
ZnTPB[e]	0.18	−1.28[f]	1.46	1.64	755
CuTPP[e]	0.99	−1.41	2.40		578
NiTPP[e]	1.10 − 1.00*	−1.28	2.38		
CoTPP[e]	1.19 − 0.52*	−1.29 − 0.92*	2.48		–
FeTPP[e]	1.18 − 0.32*	−1.01*[g]			581
PdTPP[h]	1.02	−1.03	2.02	2.25	553[i]

[a] The redox potentials taken from difference sources were offset by the difference with respect to the redox potentials of H_2TPP or ZnTPP reported in Ref. (*10*), but the differences in redox potentials ($\Delta E^{\pm} = E_{1/2}^{ox} - E_{1/2}^{red}$) were calculated from the original sources whenever possible.

[b] Oxidation potential in CH_2Cl_2 and reduction potential in dimethylformamide or butyronitrile, spectroscopic data in CH_2Cl_2, benzene, or toluene, according to Ref. (*10*); Ref. (*11*) gives the same oxidation potential for H_2TPB and reports $E_{1/2}^{ox} = 0.40$ V versus SCE for MgBChl.

[c] From Ref. (*12*) but offset by the difference of redox potential of H_2TPP.

[d] From Refs. (*13*) and (*14*) but offset by the difference of redox potentials of H_2TPP.

[e] Oxidation potentials in benzonitrile from Ref. (*15*) and reduction potentials in CH_2Cl_2 from Ref. (*16*); an asterisk indicates either the metal oxidation ($2+ \rightarrow 3+$) or the metal reduction ($2+ \rightarrow 1+$).

[f] The macrocycle reduction potential of ZnTPP is −1.52 V in the conditions of Ref. (*16*).

[g] Reduction potentials for the metal reduction ($2+ \rightarrow 1+$) in CH_3ClCH_3Cl from Ref. (*17*).

[h] From Ref. (*18*).

[i] From Ref. (*19*).

The tetrapyrrole ring acts as a tetradentate dianionic ligand and can form complexes with a wide range of transition metal ions. In many cases, additional ligands may occupy the axial positions. Tetrapyrroles closely approach planarity, and D_{4h} symmetry, when coordinated with metals. The e_{gx}* and e_{gy}* orbitals are degenerate and only one Q band is observed in the absorption spectra.

Orbital diagrams of metalloporphyrins may be complicated by the presence of metal orbitals with energies close of the HOMO and LUMO of the prophyrin. Figure 4 shows orbital energy

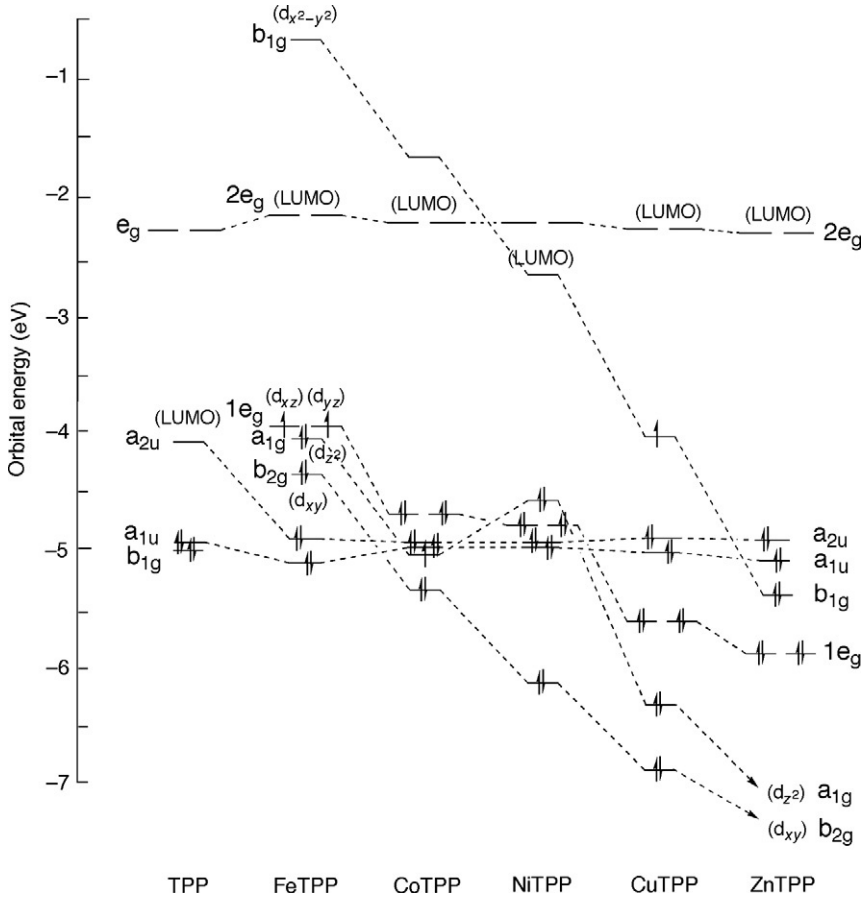

FIG. 4. Calculated energy levels for the frontier molecular orbitals of metal *meso*-tetraphenyl porphyrins and for TPP (with no H atoms in the porphyrin cage). Electron occupancies are indicated for frontier molecular orbitals of the metal. Adapted from Ref. (22) with neglect of various nonactive orbitals.

diagrams for several metal porphyrins (22). The 3d orbitals of ZnTPP are particularly low in energy, and the HOMO is a porphyrin π orbital. The first oxidation of ZnTPP removes an electron from the HOMO a_{2u} and leads to the π-cation radical $[Zn^{II}TPP]^+$, whereas in the first four reduction stages, the successive electrons are added to the LUMO $2e_g(\pi^*)$. The 3d orbitals of CuTPP are also low in energy but the odd electron now occupies the $b_{1g}(d_{x^2-y^2})$ HOMO. Somewhat surprisingly, the first oxidation removes an electron from the porphyrin a_{2u} orbital and not from the HOMO, and the first reduction adds an electron to

the $2e_g(\pi^*)$ and not to the $b_{1g}(d_{x^2-y^2})$, which would give a d^{10} configuration. NiTPP is diamagnetic (closed shell) and now both $a_{1g}(d_{z^2})$ and $1e_g(d_{xz}$ and $d_{yz})$ metal orbitals also raise above the porphyrin a_{2u} and a_{1u} orbitals, with the $a_{1g}(d_{z^2})$ becoming the HOMO and the $b_{1g}(d_{x^2-y^2})$ the LUMO. Experimental oxidation potentials suggested that the first electron is removed from the metal, but calculations show that $[Ni^{III}TPP]^+$ is less stable than the $[Ni^{II}TPP]^+$ radical cation and that the electron must come from the porphyrin a_{2u} or a_{1u} orbitals *(15,22)*. In the reduction of NiTPP, the first three electrons go to the porphyrin $2e_g(\pi^*)$ orbitals because the occupation of this orbital unstabilizes the $b_{1g}(d_{x^2-y^2})$ orbital and inverts their energy order. The $1e_g(d_{xz}$ and $d_{yz})$ orbitals of low-spin CoTPP are situated above the a_{2u} or a_{1u} orbitals of the porphyrin and are the HOMO, whereas the $a_{1g}(d_{z^2})$ orbital is placed below and is singly occupied. The $b_{1g}(d_{x^2-y^2})$ is higher in energy than the $2e_g(\pi^*)$ orbitals, which are the LUMOs of CoTPP. Initial oxidation removes an electron from the porphyrin ring leading to $[Co^{II}TPP^+]$ followed by electron redistribution yielding high-spin $[Co^{III}TPP]^+$ where the $a_{1g}(d_{z^2})$ becomes doubly occupied and $1e_g(d_{xz}$ and $d_{yz})$ orbitals are each singly occupied. Reduction adds an electron to the $a_{1g}(d_{z^2})$ orbital, as expected. All the four occupied 3d-like orbitals $b_{2g}(d_{xy})$, $a_{1g}(d_{z^2})$, and $1e_g(d_{xz}$ and $d_{yz})$ of FeTPP lie above the porphyrin a_{2u} and a_{1u} orbitals, and the unoccupied $b_{1g}(d_{x^2-y^2})$ is much higher in energy. The first oxidation takes place from the central metal (d_{z^2}), and the first and second reductions populate the low-lying half-filled metal d orbitals.

Metalloporphyrins that undergo a metal atom oxidation show a linear dependence of the corresponding oxidation potentials with the third ionization potentials of their metal atoms *(15)*. In general, the reduction potentials become more negative as the electron affinity increases *(23)*. Changes in ligand oxidation or reduction potentials have been correlated with electronegativity and covalent radius changes of the central atom *(24)*. A similar correlation also holds for electronic transition energies *(24)*.

The stability of axial ligands depends on the electron configuration of the metal. Diamagnetic Zn^{II}(TPP) binds to a variety of neutral or charged axial ligands, but the five-coordinate 1:1 complexes are very labile. Paramagnetic Cu^{II}(TPP), like other copper porphyrin complexes, has very little tendency to add axial ligands because of the population of the d_{z^2} orbital. Ni^{II}(TPP) has a low-spin d^8 configuration, and axial ligands are usually repelled by the filled d_{z^2} orbital. The low-spin d^7 configuration of Co^{II}(TPP) supports one or two axial ligands, with an odd electron occupying the d_{z^2} orbital. Co^{III}(TPP) is diamagnetic and

isoelectronic with Fe^{II}(TPP) and can also bind axial ligands. Fe^{II}-porphyrin systems have been much investigated because of the biological relevance of its ability to bind CO and O_2 axially. Weakly binding ligands are high spin, either in five- or in six-coordinate complexes. Increasing the binding constant of the ligands leads to a change from high to low spin as the electrons are displaced from the d_{z^2} orbital (*25*). Unlike Fe^{II}-porphyrin, the four-coordinate species $Fe^{III}(TPP)^-$ is unknown. Five-coordinate species such as Fe^{III}(TPP)Cl are high spin, and its electrochemical reduction to $Fe^{II}(TPP)^-$ occurs at -0.31 V versus saturated calomel electrode (SCE) in CH_3ClCH_3Cl (*17*). Under similar conditions, the reduction potential of pentacoordinated high-spin Mn^{III}(TPP)Cl is -0.29 V (*26*).

Two other metals may play important roles in metalloporphyrins designed for PDT: palladium and indium. The first oxidation and reduction potentials of Pd^{II}TPP are $+1.02$ and -1.00 V versus SCE (*27*), which are consistent with ligand-centered redox processes and with the assignment of the Q band to a porphyrin transition. The singlet state energy of Pd^{II}TPP is somewhat higher than that of H_2TPP. The nature of the axial ligand of $In^{III}(TPP)^+$ influences its redox properties. When that ligand in Cl^-, the first oxidation and reduction potentials are $+1.16$ and -1.09 versus SCE in CH_2Cl_2, and the maximum of the Q band is observed at 597 nm in $CHCl_3$ (*28*). The one-electron oxidation or reduction of In^{III}(TPP)Cl is also π-ring-centered reactions.

Breaking the degeneracy of the HOMOs increases the intensity of the Q band. In bacteriochlorins, this is accompanied by a decrease in the HOMO–LUMO gap, and an intense Q band is observed in the near infrared. Following the labeling of the orbitals shown in Fig. 3, the lowest energy transition in a bacteriochlorin represents mainly the configuration $a_{1u} \rightarrow e_{gx}$ (HOMO $\rightarrow$ LUMO) with a small contribution from $a_{2u} \rightarrow e_{gy}$ (HOMO$-1 \rightarrow$ LUMO$+1$) and is labeled Q_y (Fig. 2). In tetraphenylbacteriochlorins, this very intense band is observed at 740–750 nm. The Q_x band has a smaller intensity and is observed at 519–529 nm. It represents mainly $a_{2u} \rightarrow e_{gx}$ with a smaller amount of $a_{1u} \rightarrow e_{gy}$. The B_y absorption near 350–360 nm and the B_x at 370–380 nm are the split Soret band. The B_y band is made up mainly of the $a_{2u} \rightarrow e_{gy}$ configuration while the B_x band is mainly $a_{1u} \rightarrow e_{gy}$ (*29*).

The intense near infrared absorption exhibited by bacteriochlorophyll *a* is a most interesting property for a sensitizer, but bacteriochlorophyll *a* is known to be extremely sensitive to oxidation. For many years, the lability of the bacteriochlorins available directed the research efforts on new photosensitizers

to chlorins (*30*). Lowering the energy of the HOMOs strongly disfavors oxidative destruction of the macrocycle and should contribute to increase stability with respect to oxidation (*31*). Thus, increasing the oxidation potentials provides extra stability toward oxidative degradation of porphyrin-based photosensitizers. This can be achieved, for example, replacing the phenyl rings by *o*,*o*′-difluorophenyl rings in TPPs. In principle, it should be possible to synthesize stable fluorinated tetraphenylbacteriochlorins with intense absorption in the phototherapeutic window. Bacteriochlorins should also be stabilized by complexation with In^{3+} and, to a smaller extent, by complexation with Pd^{2+}.

Another concern specific to the use of porphyrin-based photosensitizers is the fact that singlet state lifetimes are usually less than 10 ns and photosensitization occurs mostly from the triplet state. This requires the selection of systems that efficiently generate triplet states, which is not the case of paramagnetic metalloporphyrins.

III. Electronic Transitions

A. Absorption and Emission

The absorption spectra of free-base porphyrins shows the expected Soret, Q_y and Q_x bands and two additional bands in the visible (Fig. 5). These extra bands are due to vibrational coupling effects and derive from HOMO (b_{1u} orbital) to the first vibrationally excited state of LUMO (b_{2g} orbital) or to LUMO+1 (b_{3g} orbital) transitions. Thus, in order of increasing energies, the optical transitions of H_2TPP are labeled $Q_x(0,0)$, $Q_x(0,1)$, $Q_y(0,0)$, and $Q_y(0,1)$. Typical free-base porphyrins have moderate fluorescence quantum yields ($\Phi_F = 0.10$ for H_2TPP in deaerated toluene) (*32*) and nanosecond fluorescence lifetimes ($\tau_s = 14.7$ ns for H_2TPP) (*33*). Most of the singlet states evolve to the lowest triplets (triplet quantum yield $\Phi_T = 0.73$ for H_2TPP in deaerated toluene) (*32*), which have long lifetimes in deaerated solutions (milliseconds in sufficiently pure solutions).

In general, β-substituents cause steric interactions and, consequently, structural distortion of the porphyrin core, and this is more accentuated in TPPs than in porphins. Such steric interactions are evident in the red shift of the Q and B bands of β-octabromo and β-octatrifluoromethyl porphyrins (*12,34*). However, β-octafluoro porphyrins remain nearly planar, and the absorption bands are blue shifted (*14*).

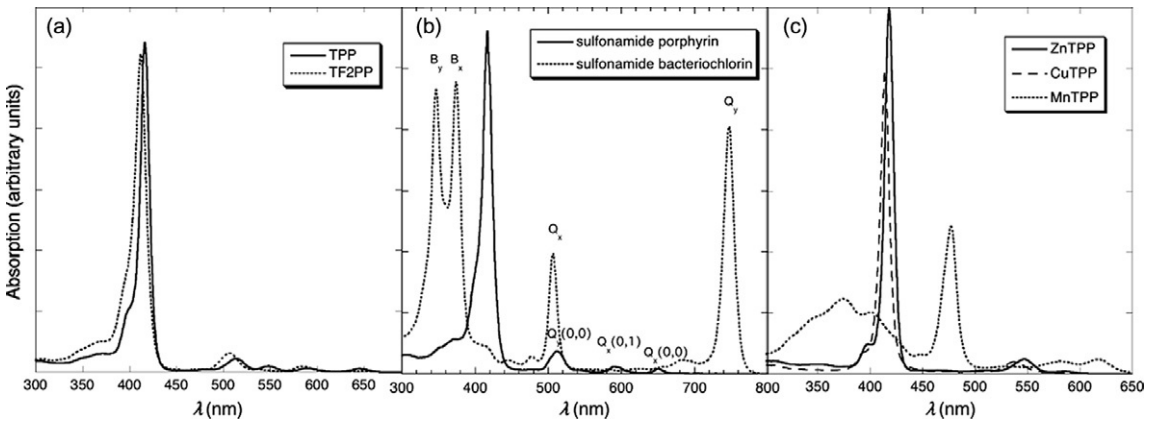

FIG. 5. Absorption spectra of: (a) H_2TPP (full line) and H_2TF_2PP (dashed line); (b) $H_2TCl_2PPethyl$ (full line) and $H_2TFPBmethyl$ (dashed line); and (c) $Zn^{II}TPP$ (regular metalloporphyrin, solid line), $Cu^{II}TPP$ (hypso-type spectrum, dashed line), and $Mn^{III}TPPCl$ in toluene (hyper-type spectrum, dotted line).

The introduction of trifluoromethyl (H_2TCF_3P) or phenyl groups (H_2TPP) in the four *meso*-positions of porphin leads to relatively small and nearly identical blue shifts of the Q and B bands. However, the fluorescence lifetime is reduced by nearly one order of magnitude from H_2TPP to H_2TCF_3P, and the fluorescence quantum yields follow the same trend (*34*). This is consistent with the internal heavy-atom effect to be discussed in the next section.

The presence of strongly electron-withdrawing groups, such as fluorines, in the phenyl rings of H_2TPP or MTPP lower the energy of a_{2u} relative to that of a_{1u}, as the latter has nodes at the methine carbon atoms (*35*). This is confirmed by the blue shifts of the Q bands observed when fluorine atoms are introduced in the phenyl rings of free-base or zinc TPPs (*32*).

The atomic orbitals of metal ions with a closed shell of valence electrons interact only weakly with the π-molecular orbitals of the porphyrin. The absorption and emission spectra of the corresponding metalloporphyrins are largely determined by the porphyrin's π-electrons and are classified as "regular." An example of this class is $Zn^{II}TPP$. Regular metalloporphyrins give *normal* spectra, with the Soret band in the near-UV (390–425 nm) and two Q bands. The longest wavelength band occurs within the range 570–610 nm for complexes with the macrocycle substituted in the β-positions and between 590 and 630 when the macrocycle is substituted in the *meso*-positions (*36*). It should be remembered that the number of Q bands decreases from four to two upon the coordination of the metal ions to free-base porphyrins because of the change from D_{2h} to D_{4h} symmetry. Metalloproteins with closed metal shells, such as Mg^{II}(TPP) and Zn^{II}(TPP), are less fluorescent than the parent free-base porphyrin ($\Phi_F = 0.033$ for ZnTPP in deaerated toluene) (*32*), have shorter fluorescence lifetimes ($\tau_s = 1.9$ ns for ZnTPP) (*33*), and higher intersystems crossing to triplet states ($\Phi_T = 0.86$ for ZnTPP in deaerated toluene) (*32*) promoted by the spin–orbit coupling mechanism described in the next section. In PdTPP, this becomes so pronounced that $\Phi_F = 2 \times 10^{-4}$ and $\Phi_T \approx 1$ (*18*).

"Irregular" metalloporphyrins show mainly three types of spectra, called normal, *hypso*, and *hyper*. The normal spectra are observed when the metal d or f electrons are of such low energy that they do not interact appreciably with the porphyrin π-electrons. Hypso-type spectra resemble the normal spectra, except for a hypsochromic (blue) shift. The origin of this shift is the back-bonding between d_{xy} and d_{yz} orbitals of metals from groups VIII to IB (d^6–d^9 transition metals, such as low-spin Fe^{II}, Co^{II}, Ni^{II}, Pd^{II}, or Cu^{II}) and the porphyrins's empty π* orbitals

thus raising their energy. Hyper-type spectra exhibit additional bands coming either from charge transfer (CT) from the metal p orbitals into the empty porphyrins π^* orbitals (d^1–d^5 transition metals, such as Fe^{III}, Mn^{III}, Cr^{III}) or from the porphyrins π orbitals into vacancies in the transition metal's d orbital (cation with an open shell outer electronic configuration, such as Sn^{II} or Pb^{II}) (*36*). Figure 5 compares the UV–Vis absorption spectra of free-base and metalloporphyrins.

Paramagnetic complexes such as Cu^{II}TPP or Co^{II}TPP have one odd electron that can couple to the spin of the porphyrin triplet yielding a "tripdoublet" and a "tripquartet" state. Similarly, that odd electron can couple its spin with that of the porphyrin first excited singlet state, leading to singmultiplet states. Moreover, the singmultiplet states couple efficiently with the tripmultiplet states resulting in rapid intersystems crossing from the excited singlet state to the triplet manifold. This coupling mechanism deactivates the singlet states rapidly and quenches almost completely the fluorescence of paramagnetic complexes of porphyrins ($\Phi_F < 10^{-4}$). However, this coupling is responsible for the observation of direct absorption from the ground state doublet of Cu^{II}TPP to the "spin-forbidden" tripdoublet, at 670–710 nm (*37*). The phosphorescence from lowest energy (π,π^*) state of Cu^{II}TPP, which is the tripquartet, to the ground state doublet becomes relatively intense and long-lived ($\Phi_P = 6 \times 10^{-2}$ and $\tau_T = 600$ μs) at 77 K in methylcyclohexane (*38*). The luminescence lifetime is reduced to 29 ns at room temperature, and this is ascribed to phosphorescence from the tripdoublet state which is thermally repopulated from the tripquartet state (*39*).

The lowest energy (π,π^*) state of Co^{II}TPP is also the tripquartet, but this and other Co^{II}-porphyrins are not luminescent. This peculiar behavior is due to the presence of a porphyrin $a_{2u}(\pi) \rightarrow$ metal d_{z^2} CT state near the energy of the tripquartet state. In fact, very weak absorption peaks in the 850–905 nm region have been assigned to this CT transition (*40*). The decay of the lowest energy (π,π^*) state of Co^{II}TPP to the CT state occurs with a lifetime of 220 fs in benzene, and the decay of the CT state takes place in 16 ps (*41*).

In addition to the hypsochromic shift of the Soret and Q bands of diamagnetic Ni^{II}TPP, there are various optically invisible lower-energy electronic states in which an electron is promoted from the metal to the porphyrin ring or vice versa and those that correspond to d–d excitation within the metal orbitals. Calculations have shown that there is a multitude of CT states below the first optically allowed state and explain its lack of fluorescence (*42*). The radiationless depopulation of the Q state

occurs in femtoseconds. However, $Pd^{II}TPP$, which is also diamagnetic and d^8, does not show fluorescence but is strongly phosphorescent. This difference was assigned to the tightly bond d orbitals of Pd that push the intermediate states closer in energy to the ground state, disfavoring the radiationless path (*7*).

The electronic structure of $Fe^{II}TPP$ is quite complex, with the four 3d-like orbitals lying close together and above the porphyrin a_{1u} and a_{2u} orbitals. The orbitals generate low-lying triplet states and promote the deactivation of the excited states. Additionally, $Fe^{II}TPP$ has a CT band with a maximum at 714 nm. As a result, no luminescence is observed from $Fe^{II}TPP$. However, $Fe^{II}TPP$ reacts with O_2 to form a dioxygen adduct that eventually leads to $[Fe^{III}TPP]^+$ with axial ligands (*38,43*). High spin $[Fe^{III}TPP]^+$ also exhibits CT absorption bands in the 650–750 nm region, assigned to $a_{1u},a_{2u} \rightarrow e_g$ transitions, whose exact positions depend on the electronegativity of the axial ligand (*44*). Weak luminescence is observed from the tripmultiplet state of $[Fe^{III}TPP]^+$ when it is positioned below the CT state (*38*).

The strongly antibonding $d_{x^2-y^2}$ of $[Mn^{III}TPP]^+$ remains empty, but the other four d orbitals are singly occupied. The $[Mn^{III}TPP]^+$ absorption spectrum provides an impressive example of low-energy CT absorption bands characteristic of hyper-type spectra. The $d\pi$ (d_{xz} an d_{yz}) orbitals of Mn^{III} raise in energy with respect to those of Fe^{III} and approach the energies of the porphyrin e_g* orbitals (*45*). The energetic proximity of orbitals with π symmetry leads to substantial mixing of the orbitals and enhances the intensity of the CT bands. The strong perturbation, the porphyrin π orbitals, leads to the split Soret band with peaks at 370 and 477 nm. The Q band is observed at 596 nm, and the other bands in the visible part of the spectrum are CT bands. Electronic excitation rapidly populates a tripquintet state that repopulates the quintet ground state in less than 30 ps; a competitive decay channel populates a tripseptet state that decays in 80 ps to the ground state presumably via quintet CT state (*46*). The very weak luminescence of $[Mn^{III}TPP]^+$ resembles that of $[Fe^{III}TPP]^+$ (*38*).

Long-lived excited states can be found in free-base porphyrins and closed-shell metalloporphyrins. Open-shell diamagnetic metalloporphyrins may lead to long-lived $^3(\pi,\pi^*)$ states in high yields provided that they lie below the CT states, as in $Pd^{II}TPP$ or $ClIn^{III}TPP$. Thus, the most promising photosensitizers are likely to come from these types of compounds. This does not imply that paramagnetic metalloporphyrins cannot have interesting photochemistry. For example, irradiation of $ClMn^{III}TPP$ at 416 nm was shown to induce the photoreduction of Mn^{III} to Mn^{II} porphyrin with the concomitant loss of the chlorine

atom (*47*). The rapid oxidation of Mn^{II} to Mn^{III} makes this process reversible. Laser photolysis of $ClFe^{III}TPP$ at 355 nm in degassed methanol gave a quantum yield of $Fe^{II}TPP$ formation of 0.02 (*43*). The system reverts to $ClFe^{III}TPP$ in the presence of oxygen. Nevertheless, it is in the closed-shell ($Zn^{II}TPP$, $Cd^{II}TPP$) or diamagnetic low-energy d orbital ($Pd^{II}TPP$, $ClIn^{III}TPP$) metalloporphyrins, and free-base porphyrins with *meso*-fluorophenyl or chlorophenyl substituents, and their derivatives with reduced macrocycles, that we can expect to find a good balance between stability, long-lived triplet states with high triplet quantum yields and intense red/infrared absorption.

B. Radiationless Transitions

The rates of radiationless transitions between electronic states of porphyrins and their derivatives play a dominant role in their photochemistry because they are the major decay channels of the electronically excited states. Radiative channels, such as fluorescence, rarely exceed 10% of the overall decay rate constant at room temperature. The lifetimes of the lowest electronic states of free-base porphyrins and closed-shell metalloporphyrins vary by more than 10 orders of magnitude with the nature of the substituents. The understanding of such variations is essential to design and control the photochemistry of porphyrins and justifies an incursion on the fundamentals of radiationless transitions.

Internal conversion between electronic states of the same spin multiplicity and intersystems crossing between singlet and triplet states take place because of weak interactions between the initial and final states. The perturbing interaction is usually limited in time and space, and the total Hamiltonian can be considered as the sum of two terms

$$\mathbf{H} = \mathbf{H}_0 + V \tag{1}$$

where the time-independent operator $\mathbf{H_0}$ describes the unperturbed system and V is the perturbation. The probability of electronic transition per unit time is given by the solution of the time-dependent Schrödinger equation

$$(\mathbf{H}_0 + V)\Psi(x,y,z,t) = i\hbar\frac{\mathrm{d}\Psi(x,y,z,t)}{\mathrm{d}t} \tag{2}$$

which has the form (omitting the coordinates)

$$\Psi = \sum_j c_j\psi_j \exp\left(-\frac{i}{\hbar}E_j t\right) \tag{3}$$

where ψ_j represents the full set of eigenfunctions with the associated eigenvalues E_j of the unperturbed system Hamiltonian $\mathbf{H}_0$, when the coefficients c_j are time dependent. The values of c_j obtained in the solution of this set of equations are related to the probability of finding the system in any particular state at any later time. It is not generally possible to find exact solutions, and the time-dependent perturbation theory is usually employed to obtain approximate solutions.

The transition probability per unit time given by the time-dependent perturbation theory, that Fermi named *Golden Rule* in view of its prevalence in radiationless transitions, has the form

$$k_{GR} = \frac{2\pi}{\hbar}|V_{fi}|^2 \rho_f\left(E_i^{(0)}\right) \tag{4}$$

where $\rho_f(E_i^{(0)})$ represents the density of final unperturbed states at the energy of the initial stationary state, and V_{fi} is the matrix element of the perturbation between the initial and final unperturbed states

$$V_{fi} = \int \psi_f^* V \psi_i \mathrm{d}\tau \tag{5}$$

and the integration is over all the space, represented by τ. Equation (4) is valid provided that the final states form a quasi-continuum of states over an energy range δE in the neighborhood of $E_i^{(0)}$ and for values of t that satisfy the relation

$$t \gg \frac{\hbar}{\delta E} \tag{6}$$

These conditions are usually verified for picosecond and nanosecond transitions occurring in large molecules. For example, the density of vibrational states of the ground electronic state of anthracene at the energy of its first excited singlet state ($E_{S1} = 75.5$ kcal/mol) is in the range of 10^{11}–10^{17} states/(cal mol^{-1}) *(48)*.

Using the Born–Oppenheimer approximation and assuming that only the electronic distribution is perturbed, Eq. (5) can be written as

$$V_{fi} = \int \phi_f^* V \phi_i \mathrm{d}\tau_e \int \upsilon_{v'}^* \upsilon_v \mathrm{d}\tau_n \tag{7}$$

where the first factor measures the extension of the electronic redistribution induced by the perturbation from the initial state i to the initial state f

$$V_{\mathrm{fi}}^{\mathrm{e}} = \int \phi_{\mathrm{f}}^{*} V \phi_{\mathrm{i}} \mathrm{d}\tau_{\mathrm{e}} \tag{8}$$

and the second factor is the overlap integral between the vibrational wavefunctions of the initial (v) and final (v') states

$$J_{\mathrm{v}',\mathrm{v}} = \int \upsilon_{\mathrm{v}'}^{*} \upsilon_{\mathrm{v}} \mathrm{d}\tau_{n} \tag{9}$$

which is known as the *Franck–Condon factor* for the f,v′←i,v transition. According to the Golden Rule, Eq. (4), the transition probability is proportional to $|J_{v',v}|^2$.

Jortner and Ulstrup have demonstrated that for isothermic atom transfers and for sufficiently high temperatures, the nonadiabatic transition rate takes the form *(49)*

$$W = \frac{2\pi}{\hbar} |V_{\mathrm{fi}}|^2 \frac{\sqrt{\sinh(\hbar\omega/2k_{\mathrm{B}}T)}}{\omega\sqrt{2\pi S}} \exp\left[-\frac{\sqrt{2\mu}}{\hbar} \sqrt{\Delta E^{\ddagger}}\, d \tanh\left(\frac{\hbar\omega}{4k_{\mathrm{B}}T} \right) \right] \tag{10}$$

where ω is the vibrational frequency of the active vibration with reduced mass μ, the values of the energy barrier $\Delta E^{\ddagger}$ and nuclear displacement d are illustrated in Fig. 6, and S is a reduced displacement defined as

$$S = \frac{d^2}{2} \frac{\mu\omega}{\hbar} \tag{11}$$

This form of the transition rate can be simplified when the argument of the tanh function is larger than 3 because then this function closely approaches unity. For example, a CH stretching vibration, $\omega = 5.65 \times 10^{14}\ \mathrm{s}^{-1}$, gives $\tanh(\hbar\omega/4k_{\mathrm{B}}T) = 0.9986$ at $T = 298$ K. In this limit, the exponential term in Eq. (10) is identical to the transmission coefficient of a barrier formed by two intersecting parabolas in the WKB approximation. In fact, this approximation was employed by Formosinho to calculate the rates of radiationless transitions in large molecules *(50)* and of H-atom abstractions by electronically excited ketones *(51,52)* before the formal demonstration that H-tunneling through intersecting parabolas is isomorphic with the Golden Rule under the limits mentioned above.

Formosinho expressed the radiationless transition probability as the product of a pre-exponential factor containing the electronic coupling between initial and final states and a

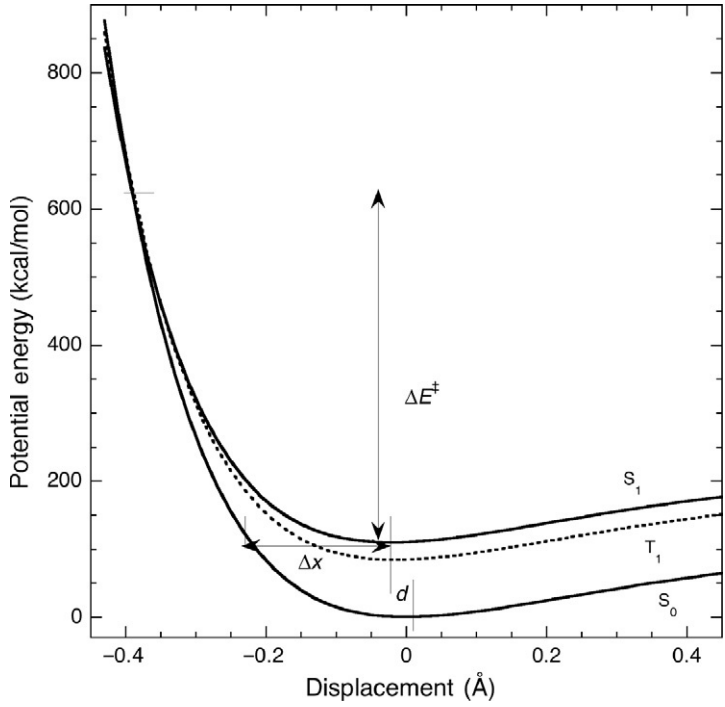

FIG. 6. Generalized bond-length displacement in radiationless transition in large molecules.

Franck–Condon factor with an exponential factor with the form of the WKB approximation for tunneling through intersecting parabolas. This is intrinsically a multidimensional problem, and a generalized bond-length displacement coordinate was introduced to make it tractable. In the process of reducing the coordinates, a measure of the relative number of identical oscillators (same μ and ω) was included in the exponential factor, η, and the tunneling rate was expressed as (*50*)

$$k = \chi \nu \exp\left[-\frac{\sqrt{2\mu}}{\hbar}\sqrt{\Delta E^{\ddagger}}\frac{\Delta x}{2\eta}\right] \tag{12}$$

where $\nu = \omega/(2\pi)$, χ is a nonadiabatic factor ($\chi << 1$ for nonadiabatic transitions such as intersystems crossing), and Δx is the width of the tunneling barrier. The application of Eq. (12) to radiationless transitions provides a simple method to separate electronic and nuclear factors that contribute to the rates of such transitions.

Nonadiabatic factors $\chi << 1$ are expected for intersystems crossings between singlet and triplet states, which are formally spin-forbidden processes. The extent of the prohibition depends significantly on the spin–orbit coupling, and this in turn is related to the atomic spin–orbit coupling constant ζ available from the atomic spectra. The magnitude of the spin–orbit coupling increases rapidly with the atomic number, and its effect on the intersystems crossing rate is usually called *heavy-atom effect*.

The heavy-atom effect of substituents introduced in a porphyrin will depend on the substitution pattern and may be different for $S_1 \rightarrow T_1$ and $T_1 \rightarrow S_0$ transitions. Thus, it should be possible to control the electronic factor to increase the triplet quantum yield without compromising its lifetime. This hypothesis was investigated in detail using various *meso*- and *beta*-substituted free-base and Mg, Zn, or Cd metalloporphyrins (*53*). It was considered that the spin–orbit coupling of atoms in identical substitution patterns gives additive contributions to the nonadiabatic factor

$$\chi = \chi_0 \sum_{i=1}^{n} \left(1 + c_i \zeta_i^2\right) \tag{13}$$

Appropriate consideration of the Franck–Condon factors using Eq. (12) allowed for the fitting the intersystems crossing rates of many diverse systems just by changing the coefficient affecting the heavy-atom effect. It was possible to characterize each substitution patterns by a single value of c, as shown in Table II.

Analysis of Table II shows that only closed-shell metalloporphyrins or *meso*-TPPs with halogens in the *ortho*-positions of the phenyl rings have stronger heavy-atom effects in the rate of the $S_1 \rightarrow T_1$ transition than in the rate of the $T_1 \rightarrow S_0$ transition. Thus, these porphyrins can have long-lived triplet states formed with nearly unit quantum yields. This is a much desired property of PDT sensitizers because only triplet states with tens of microseconds lifetimes in solution can quantitatively react with molecular oxygen and produce ROS. These reactions will be discussed in detail below, but the relevance of long-lived excited states is obvious using simple kinetic arguments. Bimolecular reaction rates of electronically excited porphyrins are limited by diffusion and have to compete with their decay. Diffusion-controlled rate constants of porphyrins approach $3 \times 10^{10}\ M^{-1}\ s^{-1}$ in water (*54*). The most ubiquitous quencher of electronically excited states is molecular oxygen ($^3\Sigma_g^-$ O_2), and its concentration in air-equilibrated water is 2.9×10^{-4} M at 20 °C (*55*). Thus, the reactivity of porphyrins in their singlet states toward molecular oxygen can be characterized by a first-order rate of $8.7 \times 10^6\ s^{-1}$.

TABLE II

EMPIRICAL COEFFICIENTS FITTED TO THE INTERSYSTEMS CROSSING RATES OF FREE-BASE AND METALLOPORPHYRINS[a]

		$S_1 \rightarrow T_1$		$T_1 \rightarrow S_0$	
		c_1	c_2	c_1	c_2
Octaalkylporphyrins	X in alkyl	5×10^{-7}		10^{-5}	
	X in *beta*	2×10^{-5}		5×10^{-4}	
	X in *meso*	10^{-4}		10^{-3}	
Metalloporphyrins			2×10^{-4}		2×10^{-5}
H_2TPP	X in phenyl *ortho*	2×10^{-6}			
ZnTPP	X in phenyl *ortho*	2×10^{-6}	2×10^{-4}	5×10^{-7}	2×10^{-5}

[a]The coefficient c_1 refers to the halogen X, and c_2 refers to the metal (53).

As mentioned before, the singlet state lifetimes of porphyrins rarely exceed 10 ns, and this implies that the efficiency of porphyrin singlet state reactions with molecular oxygen is lower than 8%. A spin-allowed reaction of singlet states with molecular oxygen that was observed in MgTPP and ZnTPP is assisted intersystems crossing to form the triplet state of the photosensitizer while molecular oxygen remains in the ground state (56). More efficient photoreactions can only be obtained with long-lived triplet states formed with high triplet quantum yields.

C. TRIPLET STATE

The phosphorescence of free-base porphyrins is extremely weak. The triplet energy of H_2TPP was reported as 33.5 kcal/mol (57), and Harriman presented a phosphorescence spectrum in methylcyclohexane at 77 K that is consistent with this value (58). Moore and coworkers challenged this triplet energy on the basis of photoacoustic calorimetry (PAC) data and suggested that it could be 3–9 kcal/mol lower in energy (59). However, the photoacoustic measurements of Moore only give the product of the triplet energy by the quantum yield of its formation, $\Phi_T E_T = 21.4$ kcal/mol, and Φ_T is not known with sufficient accuracy to provide a more reliable estimate of E_T. Brauer and coworkers revisited the phosphorescence of H_2TPP with a sensitive near infrared detector and reported $E_T = 33.3$ kcal/mol in

2-methyltetrahydrofuran (MTHF) at 77 K (60). Although this value is consistent with the earlier spectroscopic value reported by Harriman, the phosphorescence spectra of the two studies are appreciably different. It should be noted that Brauer employed H_2TPP available from Aldrich without further purification and that the signal-to-noise ratio of H_2TPP phosphorescence is poor. We used time-resolved PAC to study the triplet state energy of H_2TPP and obtained $\Phi_T E_T = 24 \pm 1$ kcal/mol (32), which indicates that the value reported by Moore is probably too low. More recently, Röder et al. reported the spectral positions of the phosphorescence spectrum of TPP in MTHF at 80 K (61) that are consistent with the spectrum presented by Brauer. At present, the best estimate for the triplet energy of H_2TPP is $E_T = 33 \pm 1$ kcal/mol, which leads to $\Phi_T = 0.73 \pm 0.05$.

The phosphorescence of porphin and its deuterated derivatives was studied in Xe matrices at 10 K (62). This significantly enhances intersystem crossing rates and increases the phosphorescence yield. It was possible to identify the 0–0 band of the phosphorescence at 790–794 nm (36 kcal/mol = 1.57 eV) in Xe matrix and the corresponding band of the fluorescence at 613 nm (46.6 kcal/mol = 2.02 eV) in Ne matrix. The same S_1–T_1 energy splitting for porphin and H_2TPP would imply that the latter would have a triplet state energy of 33.5 kcal/mol.

The extremely weak phosphorescence of the free bases is due to the presence of radiationless decay pathways from the triplet to the ground state competing favorably with phosphorescence. The deactivation of the triplet state was proposed to be mediated by a *cis* NH triplet intermediate, populated in a rate-determining step by proton tunneling, followed by fast intersystem crossing to the ground state of the *cis* form, and finally by return to the ground state *trans* species (62). The *cis* triplet has not been observed, but it is now established that the mechanism of porphin tautomerization involves stepwise migration of two hydrogen atoms, with the formation of a metastable *cis* NH intermediate. The energy of this *cis* singlet intermediate is ca. 5.5 kcal/mol above the ground state (63), and the energy of the *cis* triplet is expected to lie between this intermediate and the *trans* triplet, which is the emissive $^3(\pi,\pi^*)$ state.

The phosphorescence of diamagnetic metalloporphyrins can be easily observed at 77 K. This is consistent with slower radiationless rates, and hence with the absence of metastable *cis* NH intermediates, but the heavy-atom effect exerted by the central metal ion can also contribute to enhance the phosphorescence rate. For example, the phosphorescence lifetimes in the series MgTPP, ZnTPP, and PdTPP decrease in the order 45, 26, and

2.8 ms in methylcyclohexane at 77 K (*64*). The phosphorescence quantum yields tend to increase in the opposite order, and for PdTPP, the phosphorescence becomes so intense that it can be observed in deaerated solutions at room temperature with a lifetime of a few hundred microseconds. The nature of the emissive state for all these metalloporphyrins is the macrocycle (π,π^*) state. With the spectroscopic triplet energy of ZnTPP, it is straightforward to use time-resolved PAC to determine the triplet quantum yield. The values of Φ_T presented in Table III were obtained using the triplet energies given by phosphorescence. It is very clear that introducing heavy atoms in the *ortho*-positions of the phenyl rings further increases the intersystems crossing rate from S_1 to T_1 and the triplet quantum yields approach unity.

Time-resolved PAC was also employed to measure the triplet quantum yields of halogenated H_2TPP, namely, *meso*-tetraphenyl (2,6-dichlorophenyl)porphyrin (H_2TCl_2PP), *meso*-tetraphenyl (2-chlorophenyl)porphyrin (H_2TClPP), *meso*-tetraphenyl(2,6-difluorophenyl)porphyrin (H_2TF_2PP), and their chlorin (H_2TCl_2PC, H_2TClPC, H_2TF_2PC), and bacteriochlorin analogues (H_2TCl_2PB, H_2TClPB, H_2TF_2PB) (*32,66,67*). The emphasis in such halogenated derivatives is justified on the basis of the discussion of the stability of porphyrins. Cl and F substituents raise the oxidation potential of porphyrins and can protect them from oxidative degradation. Table III summarizes the most relevant data on the triplet and

TABLE III

TRIPLET AND SINGLET QUANTUM YIELDS OF HALOGENATED PORPHYRIN OR BACTERIOCHLORIN SENSITIZERS

Sensitizer	Φ_T	Φ_Δ (PAC)	Φ_Δ (phosph.)
H_2TPP[a]	0.73 ± 0.10[b]	0.67 ± 0.14	0.71[c]
ZnTPP[a]	0.86 ± 0.17	0.68 ± 0.19	
$ZnTF_2PP$[a]	0.99 ± 0.04	0.99 ± 0.05	
$ZnTCl_2PP$[a]	1.02 ± 0.01	0.90 ± 0.07	
H_2TF_2PB[d]		0.78 ± 0.04	0.48
H_2TClPB[d]		0.95 ± 0.06	0.59
H_2TCl_2PB[d]		1.06 ± 0.04	0.60
H_2TCl_2PPOH[c]			1.00
H_2TCl_2PBOH[c]			0.85

[a] From Ref. (*32*).

[b] This value of Φ_T was calculated E_{T1} reported by Harriman for H_2TPP, $E_{T1} = 33$ kcal/mol (*58*), which is open to discussion; using the value of porphin, $E_{T1} = 36$ kcal/mol (*62*), we obtain $\Phi_T = 0.67 \pm 0.10$.

[c] From Ref. (*65*).

[d] From Ref. (*66*).

singlet oxygen quantum yields measured by PAC. The heavy-atom effect expected for the halogen substituents is nicely confirmed by PAC, and the effect of four Cl atoms is more important than that of eight F atoms. The values of Φ_T and Φ_Δ approach unity when eight Cl atoms are included in the phenyl rings of TPP. This shows that the triplet states of halogenated free-base porphyrins such as H_2TCl_2PP are also sufficiently long-lived ($\tau_T > 15\ \mu s$ in N_2-saturated toluene (*67*)) to transfer energy quantitatively to singlet oxygen.

It should be emphasized that the measurement of the singlet oxygen phosphorescence intensity at 1270 nm confirmed the values Φ_Δ for the porphyrins but gave systematically lower values for the bacteriochlorins. PAC measures the amount of heat released in the formation of transient species, whereas phosphorescence at 1270 nm measures the amount of singlet oxygen species. The apparent discrepancy between the two techniques may be related to the nature of the species that are formed from the triplet state of bacteriochlorins in the presence of oxygen and will be discussed in the next section.

Closed-shell metal ions (Mg^{2+}, Zn^{2+}) or diamagnetic metal ions with low-lying d orbitals (Pd^{2+}, In^{3+}) accelerate the $S_1 \rightarrow T_1$ intersystems crossing and increase triplet quantum yields. The $T_1 \rightarrow S_0$ intersystems crossing rate is also increased, but in the case of $Pd^{II}TPP$, the triplet state lifetime is still sufficiently long ($\tau_T = 380\ \mu s$ in outgassed methylcyclohexane (*64*)) to transfer its energy quantitatively to singlet oxygen. However, the triplet state lifetime of $ClIn^{III}TPP$ in N_2-saturated DMSO is only 1.6 μs, and this may be at the origin of the modest $\Phi_\Delta = 0.72$ in O_2-saturated DMSO (*68*). The spin–orbit coupling constant ζ of Pd is larger than that of In, and the decrease of the triplet lifetime in $ClIn^{III}TPP$ is probably associated with the concomitant presence of Cl^- as axial ligand.

The macrocycles of conformationally strained porphyrins, and, in particular, 2,3,7,8,12,13,17,18-octaalkyl-5,10,15,20-tetraarylporphrins, tend to adopt nonplanar conformations. This has dramatic consequences in singlet and triplet lifetimes. Increasing the macrocycle distortion with the introduction of four or more ethyl groups in adjacent β positions decreases triplet lifetimes to submicrosecond values and compromises Φ_Δ. This factor adds to the decrease of Φ_T due to decrease of the singlet state lifetime, and $\Phi_\Delta = 0.07$ was reported for 2,3,7,8,12,13-hexaethyl-5,10,15,20-TPP (*61*). Porphyrins with substituents in both β- and *meso*-positions tend to have fast $T_1 \rightarrow S_0$ intersystems crossing and relatively short-lived triplet states (*69*), which are inappropriate for PDT.

We have seen that the strong electronic absorption in the phototherapeutic window observed with bacteriochlorins can be reconciled with photostability increasing the oxidation potential (or the planarity) of the bacteriochlorins with electron-withdrawing substituents. In particular, F or Cl atoms in the *ortho*-positions of the phenyl rings of TPPs have electron-withdrawing effects that stabilize the HOMO and increase Φ_T to values close to unity. Thus, reduced porphyrins with halogen atoms in these positions may combine the desired electronic absorption with stability and long-lived triplet states. A word of caution must be said about the use of electron-withdrawing substituents to stabilize reduced porphyrins. Substituents that are particularly effective for this task, such as the nitro group, may lead to low-lying CT states that effectively deactivate the triplet state (*69*). Coordination with Pd or In also increases Φ_T and, with proper care in the choice of the axial ligand of In complexes, may not compromise Φ_Δ. However, the oxidation potential of $Pd^{II}TPP$ is only 0.07 V higher than that of H_2TPP and can only make a small contribution to the stability of hydroporphyrins. The oxidation potential of $ClIn^{III}TPP$ is 0.21 V higher than that of TPP, and indium hydroporphyrins should be more stable than their palladium analogues. However, care must be exercised in the choice of the axial ligand to allow for long-lived triplet states.

IV. Photoinduced Reactions with Molecular Oxygen

The long-lived triplet states of free-base porphyrins have energies between 33 and 36 kcal/mol (1.43–1.56 eV), and their bacteriochlorin analogues have energies between 25 and 30 kcal/mol (1.08–1.30 eV) (*65*). This is lower than the energy of the second excited state of molecular oxygen ($^1\sum_g O_2$, $E_\sum = 37.5$ kcal/mol) but higher than the energy of singlet oxygen ($^1\Delta_g O_2$, $E_\Delta = 22.5$ kcal/mol). Thus, we can expect that direct energy transfer from triplet porphyrin or bacteriochlorin to molecular oxygen leading to ground state sensitizer and singlet oxygen will be an important decay mechanism in porphyrin-based photosensitizers. In PDT, this is known as type II mechanism.

The mechanism of interaction between the triplet state of a porphyrin and molecular oxygen involves the formation of an encounter pair that may have singlet, triplet, or quintet spin multiplicities. Spin statistics determine the probability of forming each one of these pairs. When two triplets interact, they give nine encounter pair spin states with equal probability, five of which are sublevels of the encounter pair with quintet

multiplicity, three are sublevels of the encounter pair with triplet multiplicity, and the ninth one is the singlet encounter pair. In the absence of perturbations, only the singlet encounter pair eventually leads to singlet oxygen. According to Fig. 7, the singlet path leads to singlet oxygen with a unit quantum yield and the triplet quenching rate constant is (70–72)

$$k_{\Delta} = \frac{1}{9} k_{\text{diff}} \tag{14}$$

In the presence of CT and for small energetic differences between singlet and triplet states of CT intermediates, the singlet quantum yield should drop to 0.25 and the quenching rate constant should increase to (73)

$$k_{\text{CT}} = \frac{4}{9} k_{\text{diff}} \tag{15}$$

The quintet path does not correlate to any products, and the quintet encounter pairs are purely dissociative.

Molecular oxygen is a good electron acceptor, with a reduction potential $E_{\text{A}}^{\text{red}} = -0.78\,\text{V}$ versus SCE in dimethylsulfoxide (74), but not a good electron donor. Thus, CT to molecular oxygen increases as the oxidation potential of the donor decreases. The donor is an electronically excited state, and its oxidation potential is given by

$$E_{\text{D}*}^{\text{ox}} = E_{\text{D}}^{\text{ox}} - E^{*} \tag{16}$$

where we have $E_{\text{D}*}^{\text{ox}} = 0.95 - 1.43 = -0.48\,\text{V}$ for H_2TPP. However, for H_2TPB, the corresponding value is $E_{\text{D}*}^{\text{ox}} = 0.40 - 1.30 = -0.90\,\text{V}$.

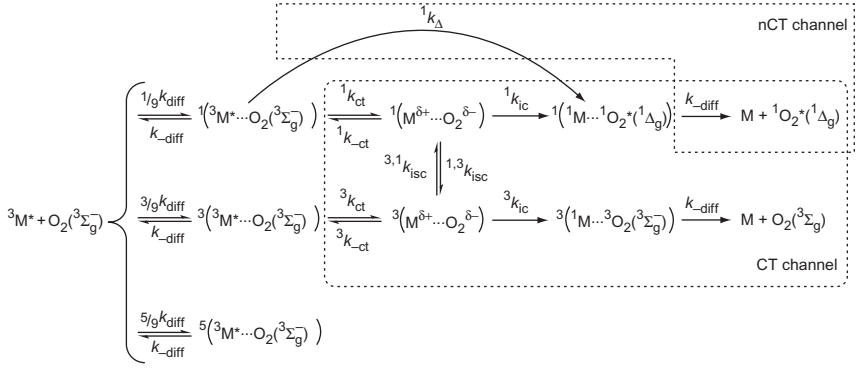

FIG. 7. Wilkinson mechanism for triplet quenching by molecular oxygen.

The free energy of full, outer-sphere, photoinduced electron transfer is given by

$$\Delta G_{ET}^{\varepsilon} = \left(E_{D*}^{ox} - E_{A}^{red}\right)^{\varepsilon} - \frac{e_0^2}{\varepsilon r_{DA}} \tag{17a}$$

where the last term in negligible in polar solvents, and emphasis is given to the measurement of redox potentials in solvents of similar dielectric constant ε. This shows that outer-sphere electron transfer from H_2TPP to O_2 is endothermic, but for H_2TPB, it may become exothermic in polar solvents and lead to the superoxide anion, $O_2^{\bullet -}$.

The generation of superoxide ion is facilitated by photosensitizers with low $E_{D*}{}^{ox}$. This outer-sphere electron transfer should become controlled by diffusion when $\Delta G_{ET} < -0.27$ eV (–6.2 kcal/mol) (*75*), that is, when $E_{D*}{}^{ox} < -1.05$ V (e.g., $E_T = 1.30$ eV and $E_D{}^{ox} < 0.25$ V) versus SCE in polar solvents. Interestingly, for such exothermic electron transfers, the electron transfer rate becomes larger than the statistically limited energy transfer rate, and superoxide ion becomes the predominant product at the expense of singlet oxygen. This does not necessarily mean that large amounts of superoxide ion will be formed at $\Delta G_{ET} = -0.27$ eV because back-electron transfer from $O_2^{\bullet -}$ to the radical cation of the photosensitizer is exothermic by

$$\Delta G_{-ET}^{\varepsilon} = -\left[\left(E_{D}^{ox} - E_{A}^{red}\right)^{\varepsilon} - \frac{e_0^2}{\varepsilon r_{DA}}\right] \tag{17b}$$

and $\Delta G_{-ET} = -1.03$ eV is very close to the driving force of the fastest charge recombinations, at the beginning of Marcus inverted region (*76–78*). Additionally, photosensitizers with low oxidation potentials are more susceptible toward oxidative degradation and may react with $O_2^{\bullet -}$. The free radical route to cellular damage in PDT is called type I mechanism.

The most direct way to assess the competition between type I and type II mechanisms in PDT is to measure the quantum yields of singlet oxygen (Φ_Δ) and of superoxide ion (Φ_O) independently of each other. The value of Φ_Δ is conveniently obtained from the laser energy dependence of the singlet oxygen phosphorescence at 1270 nm because singlet oxygen has microsecond lifetimes in many solvents. This dependence may become nonlinear when a wide range of laser energies are employed and inform on the presence of CT mechanisms (*65*). However, only the value of Φ_Δ can be quantitatively obtained by this method.

In principle, EPR of the spin adduct formed under laser irradiation by a specific spin trap of $O_2^{\bullet -}$ should give a good estimate of Φ_O. In practice, this measurement gives the amount of spin adduct formed and stable in the time window of the experiment, which is only indirectly related to Φ_O. Charge recombination with the photosensitizer radical cation, competitive reactions of $O_2^{\bullet -}$, and decomposition of the spin adduct contribute to diminish the amount of $O_2^{\bullet -}$ measured with this procedure. Lower limits for Φ_O were determined by this method for two photosensitizers in clinical trials, Tookad and Stakel, shown in Fig. 8. The values obtained were $\Phi_O = 0.001$ and 0.003 for Tookad (*79*) and Stakel (*80*), respectively, but are likely to largely underestimate of the actual amount of $O_2^{\bullet -}$ produced. Interestingly, these palladium complexes of bacteriopheophorbide derivatives make use of the heavy-atom effect of Pd to enhance intersystems crossing to the

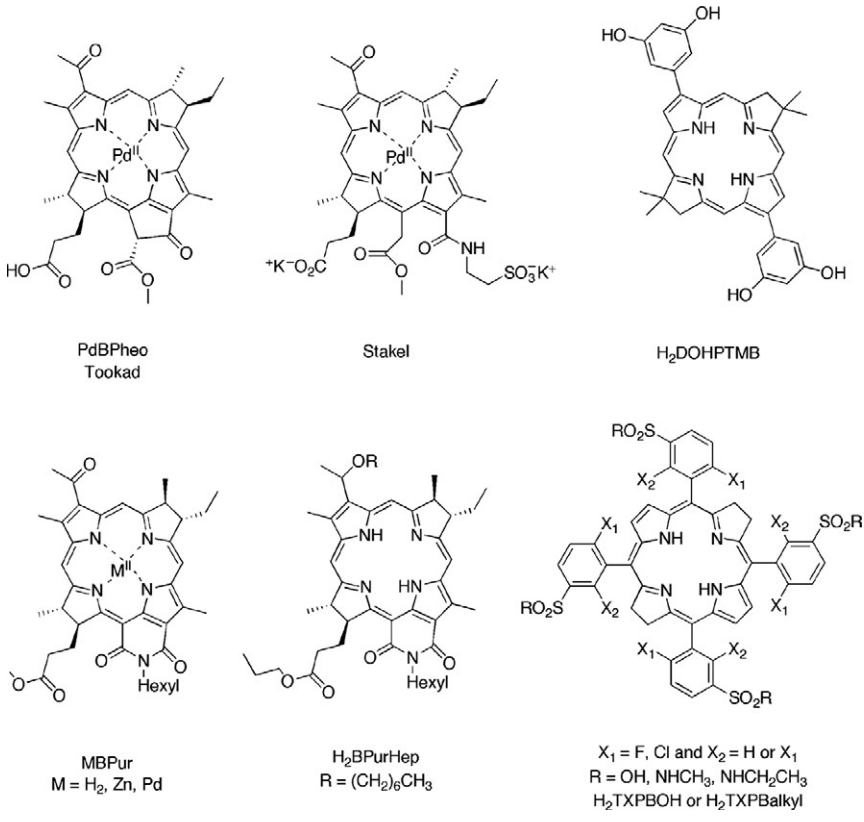

FIG. 8. Molecular structures of photosensitizers employed in photodynamic therapy.

triplet, which is formed with nearly unity quantum yield, but the radiative lifetime of triplet of triplet PdBPheo is still sufficiently long, ca. 3 μs, for Tookad to produce singlet oxygen with $\Phi_\Delta \approx 1$ in organic solvents and $\Phi_\Delta \approx 0.5$ in 3%TX-100/D_2O (*79*). However, Stakel does not produce detectable amounts of singlet oxygen. The predominance of electron transfer in Stakel at the expense of energy transfer, as opposed to Tookad, is in line with their oxidation potentials. The oxidation potential of Tookad is 0.34 V higher than that of MgBChl (*24*) but that of Stakel is only 0.24 V higher which facilitates electron transfer (*80*).

Another spectroscopic technique that should be able to quantify Φ_O is transient absorption of the photosensitizer radical cation. This was attempted in combination with a peculiar approach to lower the value of the oxidation potential of the photosensitizer, and hence to increase the energy of the HOMO and make HOMO–LUMO gap smaller than the triplet state energy. As shown in Table I, this can be achieved with Zn rather than Pd metalloporphyrins derivatives. In fact, the zinc complex of the bacteriopurpurinimide derivative identified in Fig. 8, ZnBPur, has $E_T = 1.4$ eV, $E_{1/2}{}^{ox} = 0.45$ V, and $E_{1/2}{}^{red} = -0.81$ V versus SCE (*81*), and the following sequence of reactions becomes exothermic in polar solvents

$$^3\text{ZnBPur} + \text{ZnBPur} \rightarrow \text{ZnBPur}^{\bullet+} + \text{ZnBPur}^{\bullet-}$$

$$\text{ZnBPur}^{\bullet-} + O_2 \rightarrow \text{ZnBPur} + O_2^{\bullet-}$$

The radical anion and the radical cation of ZnBPur were identified by transient absorption and EPR. The EPR spectra were also consistent with $O_2^{\bullet-}$ forming a complex with the photosensitizer in glassy benzonitrile. ZnBPur yielded $\Phi_\Delta = 0.58$, much smaller than $\Phi_\Delta = 0.94$ of PdBPur but higher than $\Phi_\Delta = 0.33$ of H_2BPur (*81,82*). This is consistent with the expected heavy-atom effect and unrelated to a compensation between Φ_Δ and Φ_O, as expected from the fact that $O_2^{\bullet-}$ is not generated in a competitive reaction mechanism.

Chemical methods can also be employed to assess the competition between the formation of $^1O_2$ and $O_2^{\bullet-}$. A specific chemical probe may react either with $^1O_2$ or $O_2^{\bullet-}$ and yield a fluorescent product. For example, nonfluorescent 3′-(*p*-aminophenyl)fluorescein reacts with hydroxyl radicals, formed subsequently to the formation of $O_2^{\bullet-}$, to give fluorescein as oxidation product (*83*), whereas Singlet Oxygen Sensor Green® (Molecular Probes) specifically reacts with $^1O_2$ to give another fluorescent product (*84*). Admittedly, this again is not a direct comparison between $^1O_2$ and $O_2^{\bullet-}$, and the conversion

from fluorescence intensities to quantum yields is not usually done. Nevertheless, the use of specific fluorescence markers has been used to correlate the relative amounts of $^1O_2$ and $O_2^{\bullet -}$ generated by photosensitizers under the same experimental conditions with their phototoxicities (*85*). It was found that in a series of three bacteriochlorins with a geminal dimethyl group in each pyrroline ring, the best performing bacteriochlorin in PDT of melanoma cell lines, 1,13-bis(3,5-dihydroxyphenyl)-8,8,18,18-tetramethylbacteriochlorin (H_2DOHPTMB), shown in Fig. 8, was also the one that had the highest fluorescein emission (*85*).

Finally, PAC was recently employed to obtain the quantum yields of long-lived species, such as $^1O_2$ and $O_2^{\bullet -}$, formed after laser pulse excitation of halogenated bacteriochlorins in aerated solutions. As mentioned before, the values of Φ_Δ initially reported with PAC seemed to be systematically higher than the values obtained by singlet oxygen phosphorescence (*66*). This discrepancy is removed when it is considered that triplet bacteriochlorins generates both $^1O_2$ and $O_2^{\bullet -}$ in aerated solutions. It should be remembered that PAC measures the amount of heat released in the formation of a transient and that fractions of heat released in the sequential formation of transients with different time scales can be separated (*86,87*). In the time window of a PAC experiment, the triplet state of the bacteriochlorin is formed "instantaneously" and the first heat decay corresponds to the difference between the energy of the light absorbed and the triplet state energy, with appropriate consideration of the triplet quantum yield and of the energy lost by fluorescence. The energy balance of the various fast processes gives

$$\phi_1 E_{h\nu} = E_{h\nu} - \Phi_T E_T - \Phi_F E_S \tag{18}$$

The second heat decay corresponds to the reactions of the triplet. When the triplet reacts by energy and electron transfer with molecular oxygen, the energy balance is (*65*)

$$\phi_2 E_{h\nu} = \Phi_\Delta (E_T - E_\Delta) + \Phi_{CT}(E_T - E_{CT}) + (\Phi_T - \Phi_\Delta - \Phi_{CT})E_T \tag{19}$$

The last term represents nonproductive channels such as the fraction of triplet states that decays by process other than quenching by molecular oxygen or the fraction of bacteriochlorin$^{\bullet +}$/$O_2^{\bullet -}$ ion pairs that undergo charge recombination before they are fully solvated. Additionally, in some cases, there is evidence for a long-lived CT complex with $O_2^{\bullet -}$ (*81*), which may not decay in the time window of the PAC experiment. The halogenated and sulfonated bacteriochlorins shown in Fig. 8 have long-lived triplet states and fast quenching rates with

molecular oxygen. Thus, virtually all triplets will interact with molecular oxygen. The values of Φ_Δ can be reliably measured by singlet oxygen phosphorescence. The energy of the CT state can be estimated from Eqs. (17a and 17b). The major uncertainty in deriving the value of $\Phi_\circ$ from Eq. (19) and an independent measurement of Φ_Δ is the estimate of the fraction of CT states that separate into free ions and of the CT states that recombine. A thorough investigation of the rates and energies of all the processes involved in the interaction between halogenated and sulfonated bacteriochlorins and molecular oxygen leads to the scheme presented in Fig. 9. Typically, these photosensitizers have $\Phi_\Delta = 0.7 \pm 0.1$ and $\Phi_\square = 0.3 \pm 0.1$ (*65*), and lower values of Φ_Δ are closely associated with higher values of $\Phi_\square$.

The generation of $O_2^{\bullet -}$ by chlorinated and sulfonated bacteriochlorins was also investigated by EPR. It was shown that $O_2^{\bullet -}$ is the primary photoproduct of electron transfer in aqueous solution, but it protonates and/or disproportionates to yield molecular oxygen and hydrogen peroxide (*65*). The formation of the hydroxyl radical subsequent to the formation of $O_2^{\bullet -}$ and H_2O_2 was demonstrated by the EPR spectra of spin adducts formed with specific spin traps, and by the inhibition of their formation in the presence of superoxide dismutase or catalase. The hydroxyl radical cannot be formed neither *via* the Haber–Weiss reaction because it is known to be inefficient in water nor *via* the Fenton reaction because a chelating resin was employed to remove metal ions from the solution. Alternatively, the

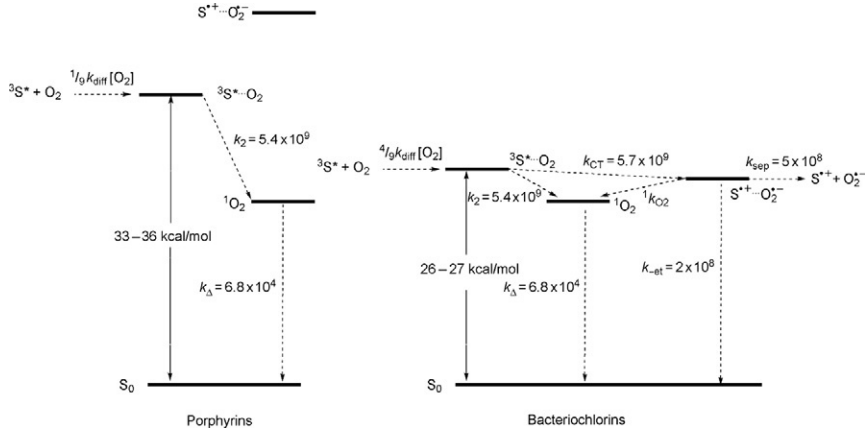

FIG. 9. Rates (in s^{-1}) and energies in the interaction between molecular oxygen and halogenated and sulfonated bacteriochlorins (*65*).

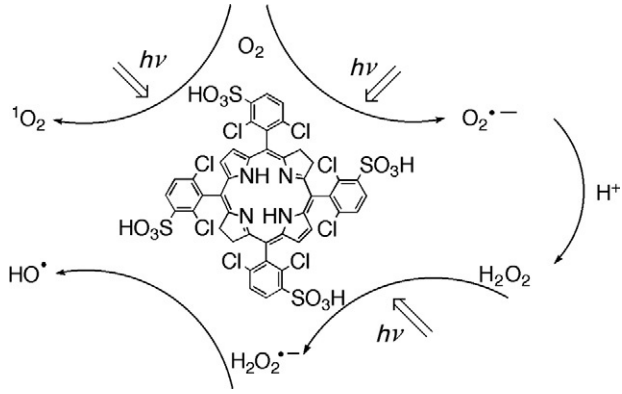

FIG. 10. Mechanism proposed for the interaction between molecular oxygen and halogenated and sulfonated bacteriochlorins (*65*).

photocatalytic mechanism shown in Fig. 10 was proposed to account for the formation of $^1O_2$, $O_2^{\bullet -}$, H_2O_2, and $OH^{\bullet}$ observed in aqueous solutions.

To the best of our knowledge, the first "stable" bacteriochlorins were published in 2002 (*66*), but the concept of "stable" that needs qualification. We classify 5,10,15,20-(2,6-difluorophenyl) bacteriochlorin, H_2TF_2PB, as "stable" because its half-live for degradation in aerated toluene solution under ambient light and at 120 °C exceeds 2 weeks. The preparation of these halogenated bacteriochlorins was criticized for being limited to the synthesis of bacteriochlorins containing inert functionalities (*88*). This criticism was proved unsound (*89*), and more recently, an environmentally friendly method was developed to synthesize $>99\%$ pure halogenated and sulfonated bacteriochlorins in gram batches (*90*).

The remarkable stability of fluorinated and chlorinated TPBs is assigned to the stabilization of their HOMO and was inspired by the increase in oxidation potentials remarked for $Mg^{II}(TF_2PP)$ or $Zn^{II}(TF_2PP)$ (*20*). The other bacteriochlorins presented in Fig. 8 were also developed with the concern of producing more stable photosensitizers than bacteriochlorophyll *a*. Their synthesis was guided by three observations: (i) appropriate metals in the tetrapyrrolic ring increase its oxidation potential and stabilize the bacteriochlorins against oxidation (Tookad), as in metallo-bacteriochlorophylls (*24,91*); (ii) geminal dialkyl groups in each reduced pyrroline ring lock-in the reduction level of the bacteriochlorins (H_2DOH_2PTMB), as in Tolyporphin A (*92*); and (iii) exocyclic rings impart stability toward oxidation

(H_2BPurhep), as in chlorins (*81,93,94*). The success of these strategies can be best evaluated in terms of the photodecomposition quantum yields of the sensitizers.

The photodecomposition quantum yield is defined as

$$\Phi_{pd} = \frac{\text{initial rate of disappearance of photosensitizer molecules}}{\text{initial rate of absorption of photons}} \quad (19)$$

Table IV presents Φ_{pd} values taken from the literature or calculated from data in the literature for various photosensitizers with the structures presented in Fig. 8. Assuming that the oxidation potentials along the series of tetrahydroxyphenyl porphyrin (H_2TOHPP), chlorin (H_2TOHPC, commercialized as Foscan),

TABLE IV

PHOTODEGRADATION AND SINGLET OXYGEN QUANTUM YIELDS OF PHOTOSENSITIZERS, AND TRIPLET QUENCHING RATE CONSTANTS IN AERATED SOLUTIONS

	$\Phi_{pd} \times 10^6$			Φ_Δ	k_q/k_{diff}[a]
	PBS	PBS:methanol	Methanol		
Photofrin[b]	55			0.36	0.12
H_2TOHPP[c]		3.8		0.46	0.17
H_2TOHPC (Foscan)[c]		33		0.43	0.16
H_2TOHPB[c]		1500		0.43	0.23
PdBPheo (Tookad)[d]			1800	≈1	
Stakel (PdBPheo derivative)[e]	2800			≈0	
H_2TClPBOH[f,g]	284	296	35	0.43	0.43
H_2TFPBMet[f]		81		0.63	
H_2TCl$_2$PBEt[f,h]		6		0.66	0.33
H_2BPurHep[i]				0.46	0.33

[a] In methanol, ethanol, benzonitrile, and, in the case of H_2TClPBOH, aqueous solutions, $k_q/k_{diff} = 0.11$ is expected in the absence of charge transfer and should increase to 0.44 with charge transfer.

[b] From Refs. (*95*) and (*96*); the value of Φ_Δ was measured for a 10 μM PBS solution of hematoporphyrin derivative (*97*).

[c] From Refs. (*98,99*) and *99*, with Φ_Δ in methanol.

[d] In acetone using data from Ref. (*79*).

[e] Using data from Ref. (*80*), but the broadening of the absorption bands shows that the photosensitizer is aggregated and this typically diminishes the photodegradation.

[f] From Ref. (*90*).

[g] From Ref. (*100*).

[h] From Ref. (*65*).

[i] From Ref. (*101*), but the rate constants refer to H_2BPur in benzonitrile according to Ref. (*82*).

and bacteriochlorin (H_2TOHPB) follow the same trend as H_2TPP, H_2TPC, and H_2TPB in Table I, the photodecomposition quantum yield in PBS:methanol seems to increase by a factor of 10 as the oxidation potential is reduced in 0.1 V. The presence of two Cl atoms in the *ortho*-positions of the phenyl rings of H_2TCl_2PBEt increase the photostability of this bacteriochlorin to that of a porphyrin. The nature of the substituents and metal ions also influences Φ_{pd}. For example, Tookad has a higher oxidation potential than bacteriochlorophyll *a*, which is similar to that of H_2TPB, but the photodegradation quantum yields of H_2TOHPP and Tookad are similar. Stakel has an oxidation potential 0.1 V less positive than that of Tookad *(80)* and was reported to be less photostable than Tookad. Stakel does not form detectable amounts of $^1O_2$. Its facile photooxidation in PBS leads $O_2^{\bullet -}$ and $OH^{\bullet}$ radicals, and the generation of these species is accompanied by the consumption and degradation of a similar number of Stakel molecules *(80)*.

Table IV also shows that the quenching rate constants of triplet bacteriochlorins by molecular oxygen approach the value of $4/9k_{diff}$, indicative of the formation of CT complexes. The quenching of triplet porphyrins and chlorins is close to $1/9k_{diff}$, which is consistent with the high energy of excited state CT complexes in these systems *(65)*.

The data published over the past 8 years shows the relevance of the CT channel in the quenching of triplet bacteriochlorins by molecular oxygen. These sensitizers contrast with triplet porphyrins that have higher oxidation potentials, lower quenching rates but an upper limit of unity for the singlet oxygen quantum yield. Whereas PDT with triplet porphyrins will be dominated by type II mechanism, triplet bacteriochlorins may also make use of type I mechanism. The comparison between the *in vitro* PDT efficacy of porphyrin and bacteriochlorins may inform on the relevance of type I and type II mechanisms. Additionally, it is of general interest to assess the progress achieved by the photosensitizers presented in Fig. 8 over the most popular photosensitizers in clinical use: Photofrin and Foscan.

V. Photodynamic Therapy

Photofrin (a mixture of hematoporphyrin derivatives including various dimers) and Foscan (H_2TOHPC) are the most widely used sensitizers in oncologic PDT and are indicated for a variety of cancers *(102,103)*. *In vitro* and *in vivo* studies reported for these sensitizers and for the new generation of bacteriochlorin

sensitizers presented in Fig. 8 typically use different experimental conditions, namely, a variety of drug doses and formulations, broad-band and laser light sources, drug-to-light intervals and light doses, and cell lines and animal-models. The rich diversity of studies is dictated by the specific properties of each sensitizer and by the requirements of the clinical cases. This diversity is welcome because each type of cancer (or clinical case) will certainly require a specific therapy and the multiparametric approach offered by PDT may have the flexibility to offer relevant clinical options to various types of cancers. However, the scatter of the experimental details makes the comparison between the performances of the sensitizers very problematic. The aim of this part of our work is only to present some selected examples of PDT with new bacteriochlorin sensitizers and is not intended to be representative of all the therapeutic opportunities they may offer. Thus, the examples presented below are organized in terms of comparable experimental conditions to illustrate how the design of the photochemical properties of sensitizers is reflected in their performance.

Table V presents the limits for cytotoxicity in the dark of porphyrin, chlorin, and bacteriochlorin sensitizers and their phototoxicity under irradiation, in the same lab, by a filtered 500-W halogen lamp with a nearly uniform spectral density from 610 to 800 nm (*54,96,100*). The only exception in that table is Tookad, which was irradiated with a 250-W halogen lamp, with similar filters but in another lab (*106*). Direct comparison between structurally related porphyrins and bacteriochlorins shows that they have similar cytotoxicities in the dark but that the bacteriochlorins are much more phototoxic. In fact, their phototoxicity exceeds what could be expected from the amount of light absorbed, given by ε[PS], and the singlet oxygen quantum yield. Note that H_2TClPPOH has $\varepsilon[PS]\Phi_\Delta = 7.5 \times 10^3\ cm^{-1}$, whereas H_2TClPBOH has $\varepsilon[PS]\Phi_\Delta = 5 \times 10^4\ cm^{-1}$. Thus, considering only the amount of singlet oxygen generated by these sensitizers, for the same incident light dose, the bacteriochlorin should be 6.7 times more potent than the porphyrin. In reality, taking into consideration the drug concentrations and light doses required to kill 90% of melanoma cells, H_2TClPBOH is ca. 65 times more potent than H_2TClPPOH. This difference cannot be assigned to different intracellular localizations because the two sensitizers have similar structures and *n*-octanol:water partition coefficients (P_{OW}). In view of the reactions of bacteriochlorins with molecular oxygen, it is likely that their increased phototoxicity with respect to porphyrins is related to the generation of the hydroxyl radical in water. A word of caution must be said about the limited

TABLE V

PHOTOSENSITIZER PARAMETERS AND LIGHT DOSE ($h\nu_{90}$) UNDER BROAD-BAND IRRADIATION REQUIRED TO KILL 90% OF MELANOMA (S91 OF SKMEL-188) OR COLON CARCINOMA (HT29) CELLS *IN VITRO*

Sensitizer/cell line	λ (nm)	Φ_Δ	ε ($M^{-1}\,cm^{-1}$)	LD_{50Dark} (μM)[a]	LD_{90PDT} (μM)	$h\nu_{90}$ (J/cm^2)	LD_{90} $h\nu_{90}$ (μM J/cm^2)
Photofrin/S91[b]	630	0.36[c]	1170	>25	17	0.175	3.0
H_2TClPPOH/S91[d]	633[e]	0.74[e]	504[e]	>200	20	4.0	80.0
H_2TClPBOH/S91[f]	748[e]	0.43[e]	23,900[e]	>200	5	0.26	1.3
H_2TClPPOH/SKMEL[d]	633[e]	0.74[e]	504[e]	>200	20	5.4	108
H_2TClPCOH/SKMEL[g]	650[e]	0.86[e]	6955[e]	>200	20	0.46	9.2
H_2TClPBOH/SKMEL[g]	742[h]	0.42[h]	61,000[h]		5	0.32	1.6
Tookad/HT29[i]	763	≈1	≈100,000	>5	0.5	12	6.0

[a] The concentrations employed in these studies were not sufficiently high to induce 50% cell death in the dark, but the lower limits presented are higher than the onset of dark toxicity (10–20% cell death).

[b] From Refs. (*96*) and (*102*), the concentrations employed in PDT, 10 μg/ml, were converted to molar units using the nominal molar weight of the mixture (600 g/mol) (*104*) given that the molar weight of Photofrin is ill-defined.

[c] For a 10-μM PBS solution of hematoporphyrin derivative (*97*).

[d] From Ref. (*54*).

[e] In aqueous solutions.

[f] From Ref. (*105*).

[g] From Ref. (*100*).

[h] In ethanol from Ref. (*90*).

[i] From Refs. (*106*) and (*79*), photophysical data in acetone.

generality of these observations. Scherz and coworkers found that phototoxicity of Tookad toward cell cultures is higher than that of Stakel, although Stakel generates mainly hydroxyl radical, as opposed to Tookad (*107*). The contrast with the case of H_2TClPPOH versus H_2TClPBOH is probably related to the fact that Tookad is a hydrophobic sensitizer, whereas Stakel is hydrophilic and their intracellular localizations must be different.

A superficial appraisal of Table V suggests that Photofrin is nearly as good a sensitizer as H_2TClPBOH for PDT of melanoma. A more careful examination reveals that the onset of Photofrin cytotoxicity in the dark occurs at concentrations one order of magnitude lower than those of halogenated and sulfonated TPPs chlorins or bacteriochlorins. In an attempt to compare the *in vitro* efficacy of different sensitizers, Plaetzer defined the IC_{50} of a sensitizer as the ratio between its lethal dose 50% in the dark and induced by light, $IC_{50} = LD_{50dark}/LD_{50PDT}$ (*104*). This is a very convenient index to characterize the effectiveness of a series of sensitizers under the same light dose. However, to compare experiments employing different light doses, it is necessary to incorporate the light dose in the evaluation of sensitizers. We can obtain a figure of merit to characterize the *in vitro* efficacy of a sensitizer using the dark cytotoxicity measured by LD_{50dark}, together with the concentration required to kill 90% of the cells for a given light dose ($h\nu_{90}$)

$$\phi_{PDT} = \frac{LD_{50dark}}{LD_{90PDT} h\nu_{90}} \tag{20}$$

The equation above defines a phototherapeutic index and was applied to *in vitro* studies for which all the parameters are available. Table VI presents a few relevant examples. The comparison between Photofrin and Foscan is straightforward because the same cell line was employed and reveals that the Foscan is a more efficient sensitizer. The comparison between the other sensitizers involves different cell lines and must be made with caution. However, sulfophenylbacteriochlorins with chlorine atoms in the *ortho*-positions of the four phenyl rings have shown similar dark cytotoxicities and phototoxicities toward various cell lines (*89,100,105*) and seem to be promising sensitizers for oncologic PDT.

Sensitizers that are successful *in vitro* may fail *in vivo* because of poor biodistribution/bioavailability, unfavorable pharmacokinetics, or unwanted side effects. As mentioned in Section I, the choice of porphyrin derivatives for the PDT of cancer is driven, in part, by their affinity toward tumors. Hence, biodistribution/bioavailability is not generally a problem with these sensitizers,

TABLE VI

PHOTOSENSITIZER CONCENTRATION AND LASER LIGHT DOSE REQUIRED TO KILL 90% OF THE CELLS *IN VITRO*

Sensitizer*	log P_{OW}	Cell lines	LD_{50Dark} (μM)	LD_{90PDT} (μM)	$h\nu_{90}$ (J/cm^2)	Φ_{PDT} (cm^2/J)
Photofrin[a]	≈0[b]	Epidermoid ca. (A431)	5	60	1.5	0.06
Foscan[a]	5.3	Epidermoid ca. (A431)	8	0.1	1.5	53
H_2BPurhep[c]	11.2	RIF	10	1.5	10	1
H_2DOHPTMB[d]	6.8	HeLa	4	0.2	10	2
H_2TCl_2PBOH[e]	−1.7[f]	Prostate (PC-3)	623	35	6	3

[a]From Refs. (*104*) and (*108*).
[b]For hematoporphyrin IX in Ref. (*108*).
[c]From Ref. (*101*); concentrations between 1.5 and 2.5 μM were tested in the dark, and it was reported that 1.5 μM solutions had no dark toxicity; although IC_{50Dark} was not reported, given the onset of dark toxicity, 10 μM is an educated guess for IC_{50Dark}.
[d]From Ref. (*109*).
[e]From Ref. (*89*).
[f]From Ref. (*90*).

although the most common side effect of clinically approved PDT sensitizers is persistent skin photosensitivity and this is related to a poor distribution between the tumor and skin. For example, Photofrin and Foscan lead to skin photosensitivity that may last from 4 to 6 weeks after treatment (*102*). Improved biodistribution may reduce skin photosensitivity and when associated with a high tumor-to-muscle tissue ratio it may also avoid unwanted side effects in the tissues surrounding the tumor. Favorable pharmacokinetics, namely, a circulation time in the organism that is sufficiently long to take advantage of the good biodistribution of porphyrin derivatives but sufficiently short for satisfactory clearance, is also critical for the success of a PDT sensitizer. Finally, most sensitizers are hydrophobic and require drug formulations with organic solvents that are an additional burden to the organism. Preference for biocompatible sensitizers with low or negative log P_{OW} must be balanced with the evidence for higher *in vitro* PDT efficacy of more lipophilic sensitizers, presumably due to better intracellular localizations (*107,109,110*).

Many examples of tumor regressions in mice with implanted tumors are available in the literature. Table VII results from an effort to select studies with efficient sensitizers that also reported tumor-to-skin and tumor-to-muscle tissue ratios. These ratios are not relevant for Stakel and H_2DOHPTMB because irradiation of the tumors was made starting immediately or 15 min after the intravenous injection of the sensitizers, respectively (*85,113*). The use of these sensitizers and of Tookad is not based on their selectivity toward tumor versus normal tissues. Rather, PDT with these sensitizers targets vascular effects. In fact, it was shown that there is no significant penetration of Tookad in the tissues, and its mechanism is based on the differential response of tumor and normal vasculature to Tookad-PDT (*114*). The photosensitizer in Table VII with the largest tumor-to-skin ratio is H_2TClPBOH, and this is expected to minimize skin photosensitivity. Additionally, more than 90% of this sensitizer is cleared from the blood in 24 h, which are very favorable pharmacokinetics. The stability of this bacteriochlorin due to the presence of electron-withdrawing substituents and the solubility in biocompatible vehicles introduced by the sulfophenyl groups are key factors for the success of this sensitizer *in vivo*. These factors complement the spectroscopic and photochemical properties discussed earlier, namely, the strong absorption of the bacteriochlorin core in the phototherapeutic window, the fast intersystems crossing to the triplet due to the internal heavy-atom effect, the long-lived triplet state, and the efficient formation of both singlet oxygen and superoxide ion. The tumor growth

TABLE VII

ANIMAL-MODEL, TUMOR-TO-NORMAL TISSUE RATIOS, LASER LIGHT DOSE, BLOOD CLEARANCE KINETICS, AND TUMOR GROWTH DELAYS TO PREDETERMINED SIZES IN PDT

Sensitizer	Animal, tumor	Tumor/skin	Tumor/muscle	Light dose (J/cm^2)	Clearance half-life (h)	Tumor growth delay (days)
Photofrin[a]	Nude, HT29	1.05	4.7	100	23[b]	8
Foscan[c]	BDIX, LSBD	3.09	7.57	50	80[b]	7
Stakel[d]	Nude, M2R	≈ 1		30	0.028	20
H_2BPurhep[e]	C3H, RIF-1	2.8		135		18
H_2DOHPTMB[f]	C57BL/6, B16F10			120		6
H_2TClPBOH[g]	DBA, S91	5.3	3	108	5[h]	27

[a]From Ref. (*111*), tumor-to-normal tissue ratios measured 24-h post 30-mg/kg i.p. injection, endpoint of tumor growth 3 cm^3.
[b]Noncompartimental analysis of biological half-life in BDIX rats, from Ref. (*112*).
[c]From Ref. (*112*), tumor-to-normal tissue ratios measured 24-h post 0.3-mg/kg i.v. injection, endpoint of tumor growth 1.8 cm^3.
[d]From Ref. (*113*), tumor-to-normal tissue ratios measured a few minutes post 6-mg/kg i.v. injection, endpoint of tumor growth 1.8 cm^3; a drug dose of 9 mg/kg i.v. further delays tumor growth.
[e]From Ref. (*101*), PDT performed 15-min post 0.4-μmol/kg i.p. injection, endpoint of tumor growth 0.4 cm^3.
[f]From Ref. (*85*), tumor-to-normal tissue ratios measured 24-h post 5 mg/kg i.v. injection, endpoint of tumor growth 1 cm^3.
[g]From Ref. (*105*), tumor-to-normal tissue ratios measured 24-h post 10-mg/kg i.p. injection, endpoint of tumor growth 0.7 cm^3.
[h]There is an initial increase in the concentration of the sensitizer in the blood, followed by a decrease with a half-life of ca. 5 h.

delay observed with H_2TClPBOH illustrates the success of the design of a sensitizer for PDT from spectroscopic, photochemical, and biological principles.

VI. Conclusions

Porphyrin derivatives present a variety of photochemical properties that have been much explored to obtain better sensitizers for the PDT of cancer. Table VIII summarizes some of the more relevant factors that should be considered in the design better photosensitizers for PDT and relates them to structural modifications. Some of these factors are contradictory, and improved photosensitizers are likely to emerge from the best balance between these factors. Free-base and palladium complexes of hydroporphyrins rank among the best sensitizers presently available. Bacteriochlorins are particularly interesting for their intense absorption in the near infrared and were recently shown to be sufficiently stable for PDT when electron-withdrawing groups and/or steric protection are introduced in their molecular structure. In addition to photogenerating singlet oxygen, bacteriochlorins have sufficiently low oxidation potentials to generate

TABLE VIII

GUIDELINES TO DESIGN BETTER PORPHYRIN-BASED PHOTOSENSITIZERS FOR PDT

Objective	Guideline	Limitation
λ_{max} at 720–900 nm	Reduced porphyrins (e.g., bacteriochlorin)	Oxidation potential decreases and oxidative degradation becomes facile
Large ε	Distorted porphyrins (e.g., large groups at β-positions)	
Stability	Increase oxidation potential (e.g., electron-withdrawing substituents, Pd^{2+} or In^{3+} complexes)	Low-energy charge transfer states promote radiationless transitions
Increase Φ_T	Introduce heavy atoms in phenyls at *meso*-positions or diamagnetic heavy metal ions	Excessive heavy-atom effect will reduce τ_T
$\tau_T > 10$ μs	Avoid distortion of the macrocycle, charge transfer states, paramagnetic ions, and excessive heavy-atom effect	
Generate $O_2^{\bullet -}$	Lower the oxidation potential	Compromise with stability
Tumor retention	Moderate lipophilicity	Toxicity of i.v. formulation

also significant amounts of superoxide ion and, in aqueous solutions, hydroxyl radicals. These ROS are very useful in the PDT of cancer and bacteriochlorins rank among the most phototoxic sensitizers presently available. The structure of these macrocycles also allows for the tuning of their intracellular localization and improvement of their biocompatibility and pharmacokinetics.

The rich photochemistry of porphyrin derivatives can serve many other useful applications. A much less explored avenue in photomedicine is the use of porphyrin derivatives for tumor imaging (*115*). Their intrinsic affinity for tumors and their remarkable photochemical properties suggest various roles in the imaging of neoplastic diseases. Recent work described fluorescence imaging with porphyrin derivatives (*116,117*), but their low fluorescence quantum yields and the diffusional nature of light propagation in tissues strongly limit deep tissue imaging with these sensitizers. Alternatively, it was proposed to use porphyrin derivatives as contrast agents in photoacoustic tomography (PAT) (*118*). The design of better contrast agents for PAT should incorporate paramagnetic metal ions that rapidly quench the excited states and rapidly convert all the absorbed energy into heat and, consequently, generate intense acoustic waves.

In view of the ability to predict the effect of substituents in the macrocycle and of the flexibility of the synthetic methods available, it is likely that much improved sensitizers and probes will be made available for photomedicine in the coming years.

Acknowledgments

This work was supported by ERA Chemistry (FCT—Fundação para a Ciência e a Tecnologia—project no. 0002/2008) and FEDER (COMPETE program).

References

1. Dolphin, D. *The Porphyrins*. Academic Press: New York, **1978**.
2. Kadish, K. M.; Smith, K. M.; Guilard, R. *The Phorphyrin Handbook*. Academic Press: San Diego, **2000**.
3. Mirsa, R.; Chandrashekar, T. K. *Acc. Chem. Res.* **2008,** *41*, 265–279.
4. Altman, K. I.; Salomon, K. *Nat. Biotechnol.* **1960,** *187*, 1124.
5. Winkelman, J. *Cancer Res.* **1962,** *22*, 589–596.
6. Castano, A. P.; Demidova, T. N.; Hamblin, M. R. *Photodiagn. Photodyn. Ther.* **2005,** *2*, 91–106.
7. Gouterman, M. *J. Mol. Spectrosc.* **1961,** *6*, 138–163.
8. Schaffer, A. M.; Gouterman, M. *Theoret. Chim. Acta* **1972,** *25*, 62–82.
9. Palummo, M.; Hogan, C.; Sottile, F.; Bagalá, P.; Rubio, A. *J. Chem. Phys.* **2009,** *131*, 084102.

10. Chang, C. K.; Hanson, L. K.; Richardson, P. F.; Young, R.; Fajer, J. *Proc. Natl. Acad. Sci. USA* **1981,** *78*, 2652–2656.
11. Fajer, J.; Borg, D. C.; Forman, A.; Felton, R. H.; Dolphin, D.; Vegh, L. *Proc. Natl. Acad. Sci. USA* **1974,** *71*, 994–998.
12. Terazono, Y.; Dolphin, D. *J. Org. Chem.* **2003,** *68*, 1892–1900.
13. Leroy, J.; Bondon, A. *Eur. J. Org. Chem.* **2008,** *2008*, 417–433.
14. Woller, E. K.; DiMagno, S. G. *J. Org. Chem.* **1997,** *62*, 1588–1593.
15. Wolberg, A.; Manassen, J. *J. Am. Chem. Soc.* **1970,** *92*, 2982–2991.
16. Hansen, C. B.; Drenth, W. *Catal. Lett.* **1993,** *20*, 359–364.
17. Gueutin, C.; Lexa, D.; Momenteau, M.; Savéant, J. -M.; Xu, F. *Inorg. Chem.* **1986,** *25*, 4294–4307.
18. Darwent, J. R.; Douglas, P.; Harriman, A.; Porter, G.; Richoux, M. -C. *Coord. Chem. Rev.* **1982,** *44*, 83–126.
19. Kee, H. L.; Bhaumik, J.; Diers, J. R.; Mroz, P.; Hamblin, M. R.; Bocian, D. F.; Lindsey, J. S.; Holten, D. *J. Photochem. Photobiol. A Chem.* **2008,** *200*, 346–355.
20. Yang, S. I.; Seth, J.; Strachan, J. -P.; Gentemann, S.; Kim, D.; Holten, D.; Lindsey, J. S.; Bocian, D. F. *J. Porphyrins Phthalocyanines* **1999,** *3*, 117–147.
21. Hashimoto, T.; Choe, Y.-K.; Nakano, H.; Hirao, K. *J. Phys. Chem. A* **1999,** *103*, 1894–1904.
22. Liao, M. -S.; Scheiner, S. *J. Chem. Phys.* **2002,** *117*, 205–219.
23. Chen, H. L.; Ellis, P. E.; Jr., Wijesekera, T.; Hagan, T. E.; Groh, S. E.; Lyons, J. E.; Ridge, D. P. *J. Am. Chem. Soc.* **1994,** *116*, 1086–1089.
24. Noy, D.; Fiedor, L.; Hartwich, G.; Scheer, H.; Scherz, A. *J. Am. Chem. Soc.* **1998,** *120*, 3684–3693.
25. Sanders, J. K. M.; Bampos, N.; Clyde-Watson, Z.; Darling, S. L.; Hawley, J. C.; Kim, H.-J.; Mak, C. C.; Webb, S. J. In: "*The Porphyrin Handbook, Vol. 3*"; Eds. Kadish, K. M., Smith, K. M.; Guilard, R.; Academic Press: San Diego, **2000**, p. 1.
26. Kelly, S. L.; Kadish, K. M. *Inorg. Chem.* **1982,** *21*, 3631–3639.
27. Rubio, N.; Prat, F.; Bou, N.; Borrell, J. I.; Teixidó, J.; Villanueva, A.; Juarranz, A.; Cañete, M.; Stockert, J. C.; Nonell, S. *New J. Chem.* **2005,** *29*, 378–384.
28. Kadish, K. M.; Cornillon, J. L.; Cocolios, P.; Taberd, A.; Guilard, R. *Inorg. Chem.* **1985,** *24*, 3645–3649.
29. Parson, W. W.; Nagarajan, V. In: "*Light-Harvesting Antennas in Photosynthesis, Vol. 13*"; Eds. Green, B. R.; Parson, W. W.; Kluwer Academic Press: Dordrecht, **2003**, pp. 83–127.
30. Sternberg, E. D.; Dolphin, D.; Brucker, C. *Tetrahedron* **1998,** *54*, 4151–4202.
31. Takeuchi, T.; Gray, H. B.; Goddard, W. A.III, *J. Am. Chem. Soc.* **1994,** *116*, 9730–9732.
32. Pineiro, M.; Carvalho, A. L.; Pereira, M. M.; Gonsalves, A. M. d. A. R.; Arnaut, L. G.; Formosinho, S. J. *Chem. Eur. J.* **1998,** *4*, 2299–2307.
33. Gentemann, S.; Nelson, N. Y.; Jaquinod, L.; Nurco, J.; Leung, S. H.; Medforth, C. J.; Smith, K. M.; Fajer, J.; Holten, D. *J. Phys. Chem. B* **1997,** *101*, 1247–1254.
34. Goll, J. G.; Moore, K. T.; Ghosh, A.; Therien, M. J. *J. Am. Chem. Soc.* **1996,** *118*, 8344–8354.
35. Spellane, P. J.; Gouterman, M.; Antipas, A.; Kim, S.; Liu, Y. C. *Inorg. Chem.* **1980,** *19*, 386–391.
36. Milgrom, L. R. *The Colours of Life.* Oxford University Press: Oxford, **1997**.

37. Antipas, A.; Dolphin, D.; Gouterman, M.; Johnson, E. C. *J. Am. Chem. Soc.* **1978,** *100*, 7705–7709.
38. Harriman, A. *J. Chem. Soc. Faraday Trans. I* **1981,** *77*, 369–377.
39. Asano, M.; Kaizu, Y.; Kobayashi, H. *J. Chem. Phys.* **1988,** *89*, 6567–6576.
40. Tait, C. D.; Holten, D.; Gouterman, M. *Chem. Phys. Lett.* **1983,** *100*, 268–272.
41. Yu, H. Z.; Baskin, J. S.; Steiger, B.; Wan, C. Z.; Anson, F. C.; Zewail, A. H. *Chem. Phys. Lett.* **1998,** *293*, 1–8.
42. Patchkovskii, S.; Kozlowski, P. M.; Zgierski, M. Z. *J. Chem. Phys.* **2004,** *121*, 1317–1324.
43. Hoshino, M.; Baba, T. *J. Am. Chem. Soc.* **1998,** *120*, 6820–6821.
44. Ohya, T.; Sato, M. *Bull. Chem. Soc. Jpn.* **1996,** *69*, 3201–3205.
45. Boucher, L. J. *Coord. Chem. Rev.* **1972,** *7*, 289–329.
46. Yan, X.; Kirmaier, C.; Holten, D. *Inorg. Chem.* **1986,** *25*, 4774–4777.
47. Jeoung, S. C.; Kim, D.; Cho, D. W. *J. Raman Spectrosc.* **2000,** *31*, 319–330.
48. Arnaut, L. G.; Formosinho, S. J.; Burrows, H. D. *Chemical Kinetics*. Elsevier: Amsterdam, **2007**.
49. Jortner, J.; Ulstrup, J. *Chem. Phys. Lett.* **1979,** *63*, 236–239.
50. Formosinho, S. J. *J. Chem. Soc. Faraday Trans. 2* **1974,** *70*, 605–620.
51. Formosinho, S. J. *J. Chem. Soc. Faraday Trans. 2* **1976,** *72*, 1313–1331.
52. Formosinho, S. J.; Arnaut, L. G. *Adv. Photochem.* **1991,** *16*, 67–117.
53. Azenha, E. G.; Serra, A. C.; Pineiro, M.; Pereira, M. M.; Seixas de Melo, J.; Arnaut, L. G.; Formosinho, S. J.; Gonsalves, A. M. d. A. R. *Chem. Phys.* **2002,** *280*, 177–190.
54. Dabrowski, J. M.; Pereira, M. M.; Arnaut, L. G.; Monteiro, C. J. P.; Peixoto, A. F.; Karocki, A.; Urbanska, K.; Stochel, G. *Photochem. Photobiol.* **2007,** *83*, 897.
55. Murov, S. L.; Carmichael, I.; Hug, G. L. *Handbook of Photochemistry*. Marcel Dekker: New York, **1993**.
56. Kowalska, D.; Steer, R. P. *J. Photochem. Photobiol. Chem.* **2008,** *195*, 223–227.
57. Harriman, A.; Porter, G.; Searle, N. *J. Chem. Soc. Faraday Trans. 2* **1979,** *75*, 1515–1521.
58. Harriman, A. *J. Chem. Soc. Faraday Trans. 1* **1980,** *76*, 1978–1985.
59. Moore, T. A.; Benin, D.; Tom, R. *J. Am. Chem. Soc.* **1982,** *104*, 7356–7357.
60. Völcker, A.; Adick, H.-J.; Schmidt, R.; Brauer, H. -D. *Chem. Phys. Lett.* **1989,** *159*, 103–108.
61. Röder, B.; Büchner, M.; Rückmann, I.; Senge, M. O. *Photochem. Photobiol. Sci.* **2010,** *9*, 1152–1158.
62. Radziszewski, J. G.; Waluk, J.; Nepras, M.; Michl, J. *J. Phys. Chem.* **1991,** *95*, 1963–1969.
63. Arnaut, L. G.; Formosinho, S. J.; Barroso, M. *J. Mol. Struct.* **2006,** *786*, 207–214.
64. Harriman, A. *J. Chem. Soc. Faraday Trans. 2* **1981,** *77*, 1281–1291.
65. Silva, E. F. F.; Serpa, C.; Dabrowski, J. M.; Monteiro, C. J. P.; Arnaut, L. G.; Formosinho, S. J.; Stochel, G.; Urbanska, K.; Simoes, S.; Pereira, M. M. *Chem. Eur. J.* **2010,** *16*, 9273–9286.
66. Pineiro, M.; Rocha Gonsalves, A. M. d. A.; Pereira, M. M.; Formosinho, S. J.; Arnaut, L. G. *J. Phys. Chem. A* **2002,** *106*, 3787–3795.
67. Pineiro, M.; Pereira, M. M.; Gonsalves, A. M.d.A. R.; Arnaut, L. G.; Formosinho, S. J. *J. Photochem. Photobiol. A Chem.* **2001,** *138*, 147–157.
68. da Silva, A. R.; Pelegrino, A. C.; Tedesco, A. C.; Jorge, R. A. *J. Braz. Chem. Soc.* **2008,** *19*, 491–501.

69. Knyukshto, V. N.; Zenkevich, E. I.; Sagun, E. I.; Shulga, A. M.; Bachilo, S. M. *J. Fluoresc.* **2000,** *10*, 55–68.
70. Algar, B. E.; Stevens, B. *J. Phys. Chem.* **1970,** *74*, 3029–3034.
71. Patterson, L. K.; Porter, G.; Topp, M. R. *Chem. Phys. Lett.* **1970,** *7*, 612–614.
72. Gijzemann, O. L. J.; Kaufman, F.; Porter, G. *J. Chem. Soc. Faraday Trans. II* **1973,** *69*, 708–720.
73. Garner, A.; Wilkinson, F. *Chem. Phys. Lett.* **1977,** *45*, 432–435.
74. Huang, C.; Tian, M.; Yang, Y.; Guo, F.; Wang, M. *J. Electroanal. Chem.* **1989,** *272*, 179–184.
75. Formosinho, S. J.; Arnaut, L. G.; Fausto, R. *Prog. React. Kinet.* **1997,** *23*, 1–90.
76. Marcus, R. A.; Sutin, N. *Biochim. Biophys. Acta* **1985,** *811*, 265.
77. Serpa, C.; Gomes, P. J. S.; Arnaut, L. G.; Formosinho, S. J.; Pina, J.; Seixas de Melo, J. *Chem. Eur. J.* **2006,** *12*, 5014-5023.
78. Gomes, P. J. S.; Serpa, C.; Nunes, R. M. D.; Arnaut, L. G.; Formosinho, S. J. *J. Phys. Chem. A* **2010,** *114*, 2778–2787, 10759–10760.
79. Vakrat-Haglili, Y.; Weiner, L.; Brumfeld, V.; Brandis, A.; Salomon, Y.; McIlroy, B.; Wilson, B. C.; Pawlak, A.; Rozanowska, M.; Sarna, T.; Scherz, A. *J. Am. Chem. Soc.* **2005,** *127*, 6487–6497.
80. Ashur, I.; Goldschmidt, R.; Pinkas, I.; Salomon, Y.; Szewczyk, G.; Sarna, T.; Scherz, A. *J. Phys. Chem. A* **2009,** *113*, 8027–8037.
81. Fukuzumi, S.; Ohkubo, K.; Zheng, X.; Chen, Y.; Pandey, R. K.; Zhan, R.; Kadish, K. M. *J. Phys. Chem. B* **2008,** *112*, 2738–2746.
82. Fukuzumi, S.; Ohkubo, K.; Chen, Y.; Pandey, R. K.; Zhan, R.; Shao, J.; Kadish, K. M. *J. Phys. Chem. A* **2002,** *106*, 5105–5113.
83. Price, M.; Reiners, J. J.; Santiago, A. M.; Kessel, D. *Photochem. Photobiol.* **2009,** *85*, 1177–1181.
84. Flors, C.; Fryer, M. J.; Waring, J.; Reeder, B.; Bechtold, U.; Mullineaux, P. M.; Nonell, S.; Wilson, M. T.; Baker, N. R. *J. Exp. Bot.* **2006,** *57*, 1725–1734.
85. Mroz, P.; Huang, Y.-Y.; Szokalska, A.; Zhiyentayev, T.; Janjua, S.; Nifli, A.-P.; Sherwood, M. E.; Ruzié, C.; Borbas, K. E.; Fan, D.; Krayer, M.; Balasubramanian, T.; Yang, E.; Kee, H. L.; Kirmaier, C.; Diers, J. R.; Bocian, D. F.; Holten, D.; Lindsey, J. S.; Hamblin, M. R. *FASEB J.* **2010,** *24*, 3160–3170.
86. Arnaut, L. G.; Caldwell, R. A.; Elbert, J. E.; Melton, L. A. *Rev. Sci. Instrum.* **1992,** *63*, 5381–5389.
87. Schaberle, F. A.; Nunes, R. M. D.; Barroso, M.; Serpa, C.; Arnaut, L. G. *Photochem. Photobiol. Sci.* **2010,** *9*, 812–822.
88. Chen, Y.; Li, G.; Pandey, R. K. *Curr. Org. Chem.* **2004,** *8*, 1105–1134.
89. Pereira, M. M.; Monteiro, C. J. P.; Simões, A. V. C.; Pinto, S. M. A.; Arnaut, L. G.; Sá, G. F. F.; Silva, E. F. F.; Rocha, L. B.; Simões, S.; Formosinho, S. J. *J. Porphyrins Phthalocyanines* **2009,** *13*, 567–573.
90. Pereira, M. M.; Monteiro, C. J. P.; Simões, A. V. C.; Pinto, A. M. A.; Abreu, A. R.; Sá, G. F. F.; Silva, E. F. F.; Rocha, L. B.; Dabrowski, J. M.; Formosinho, S. J.; Simões, S.; Arnaut, L. G. *Tetrahedron* **2010,** *66*, 9545–9551.
91. Fiedor, J.; Fiedor, L.; Kammhuber, N.; Scherz, A.; Scheer, H. *Photochem. Photobiol.* **2002,** *76*, 145–152.
92. Kim, H.-J.; Lindsey, J. S. *J. Org. Chem.* **2005,** *70*, 5475–5486.
93. Kozyrev, A. N.; Zheng, G.; Zhu, C.; Dougherty, T. J.; Smith, K. M.; Pandey, R. K. *Tetrahedron Lett.* **1996,** *37*, 6431–6434.

94. Kozyrev, A. N.; Chen, Y.; Goswami, L. N.; Tabaczynski, W. A.; Pandey, R. K. *J. Org. Chem.* **2006,** *71*, 1949–1960.
95. Bonnett, R.; Martínez, G. *Tetrahedron* **2001,** *57*, 9513–9547.
96. Nowak-Sliwinska, P.; Karocki, A.; Elas, M.; Pawlak, A.; Stochel, G.; Urbanska, K. *Biochem. Biophys. Res. Commun.* **2006,** *349*, 549–555.
97. Tanielian, C.; Wolff, C.; Esch, M. *J. Phys. Chem.* **1996,** *100*, 6555–6560.
98. Bonnett, R.; Djelal, B. D.; Hamilton, P. A.; Martinez, G.; Wierrani, F. *J. Photochem. Photobiol. B Biol.* **1999,** *53*, 136–143.
99. Bonnett, R.; Charlesworth, P.; Djelal, B. D.; McGarvey, D. J.; Truscott, T. G. *J. Chem. Soc. Perkin Trans. 2* **1999,** 325–328.
100. Dabrowski, J. M.; Arnaut, L. G.; Pereira, M. M.; Monteiro, C. J. P.; Urbanska, K.; Simões, S.; Stochel, G. *ChemMedChem* **2010,** *5*, 1770–1780.
101. Chen, Y.; Potter, W. R.; Missert, J. R.; Morgan, J.; Pandey, R. K. *Bioconjug. Chem.* **2007,** *18*, 1460–1473.
102. Detty, M. R.; Gibson, S. L.; Wagner, S. J. *J. Med. Chem.* **2004,** *47*, 3897–3915.
103. Allison, R. R.; Sibata, C. H. *Photodiagn. Photodyn. Ther.* **2010,** *7*, 61–75.
104. Berlanda, J.; Kiesslich, T.; Engelhardt, V.; Krammer, B.; Plaetzer, K. *J. Photochem. Photobiol. B Biol.* **2010,** *100*, 173–180.
105. Dabrowski, J. M.; Urbanska, K.; Arnaut, L. G.; Pereira, M. M.; Abreu, A. R.; Simões, S.; Stochel, G. *ChemMedChem* **2011,** *6*, 465–475.
106. Preise, D.; Mazor, O.; Koudinova, N.; Liscovitch, M.; Scherz, A.; Salomon, Y. *Neoplasia* **2003,** *5*, 475–480.
107. Vakrat, Y.; Weiner, L.; Brandis, A.; Mazor, O.; Hami, R.; Gross, S.; Schreiber, S.; Salomon, Y.; Scherz, A. *Free Radic. Biol. Med.* **1999,** *27*, S129.
108. Cunderlíková, B.; Kaalhus, O.; Cunderlík, R.; Mateásik, A.; Moan, J.; Kongshaug, M. *Photochem. Photobiol.* **2004,** *79*, 242–247.
109. Huang, Y.-Y.; Mroz, P.; Zhiyentayev, T.; Sharma, S. K.; Balasubramanian, T.; Ruzié, C.; Krayer, M.; Fan, D.; Borbas, K. E.; Yang, E.; Kee, H. L.; Kirmaier, C.; Diers, J. R.; Bocian, D. F.; Holten, D.; Lindsey, J. S.; Hamblin, M. R. *J. Med. Chem.* **2010,** *53*, 4018–4027.
110. Henderson, B. W.; Bellnier, D. A.; Greco, W. R.; Amarnath, S.; Pandey, R. K.; Vaughan, L. A.; Weishaupt, K. R.; Dougherty, T. J. *Cancer Res.* **1997,** *57*, 4000–4007.
111. Hajri, A.; Wack, S.; Meyer, C.; Smith, M. K.; Leberquier, C.; Kedinger, M.; Aprahamian, M. *Photochem. Photobiol.* **2002,** *75*, 140–148.
112. Jones, H. J.; Vernon, D. I.; Brown, S. B. *Br. J. Cancer* **2003,** *89*, 398–404.
113. Mazor, O.; Brandis, A.; Plaks, V.; Neumark, E.; Rosenbach-Belkin, V.; Salomon, Y.; Scherz, A. *Photochem. Photobiol.* **2005,** *81*, 342–351.
114. Tremblay, A.; Leroy, S.; Freitag, L.; Copin, M.-C.; Brun, P.-H.; Marquette, C.-H. *Photochem. Photobiol.* **2003,** *78*, 124–130.
115. Pandey, R. K.; Goswami, L. N.; Chen, Y.; Gryshuk, A.; Missert, J. R.; Oseroff, A.; Dougherty, T. J. *Laser Surg. Med.* **2006,** *38*, 445–467.
116. Lassalle, H.-P.; Wagner, M.; Bezdetnaya, L.; Guillemin, F.; Schneckenburger, H. *J. Photochem. Photobiol. B Biol.* **2008,** *92*, 47–53.
117. Goldshaid, L.; Rubinstein, E.; Brandis, A.; Segal, D.; Leshem, N.; Brenner, O.; Kalchenko, V.; Eren, D.; Yecheskel, T.; Salitra, Y.; Salomon, Y.; Scherz, A. *Breast Cancer Res.* **2010,** *12*, R29.
118. Schaberle, F. A.; Arnaut, L. G.; Serpa, C.; Silva, E. F. F.; Pereira, M. M.; Abreu, A. R.; Simões, S. *Proc. SPIE* **2010,** *7376*, 73760X1-7.

PHOTOSENSITIZATION AND PHOTOCATALYSIS IN BIOINORGANIC, BIO-ORGANOMETALLIC AND BIOMIMETIC SYSTEMS

GÜNTHER KNÖR[1] and UWE MONKOWIUS

Institute of Inorganic Chemistry, Johannes Kepler University (JKU), Linz, Austria

ABSTRACT

Inorganic photochemistry has experienced an enormous progress within the past decades. Many branches of current frontier science including sustainable chemistry, solar fuel production, or modern therapeutic strategies critically depend on light-responsive metal complexes. More recently, the various aspects of bioinorganic and bioorganometallic photochemistry have been systematically explored. In the present review, an attempt is made to provide some unifying concepts and rational design guidelines for the development of novel biomimetic and bioinspired systems controlled and driven by photons. Spectral

[1]Corresponding author.

INORGANIC PHOTOCHEMISTRY
VOLUME 63 ISSN 0898-8838 / DOI: 10.1016/B978-0-12-385904-4.00005-6

sensitization of such photoprocesses remains a central challenge for utilizing sunlight as the energy source for enzyme mimetics, artificial photosynthesis, and chemical photocatalysis. Several applications of metal-based drugs in molecular photomedicine also require light sensitivity in clearly defined spectral regions. Therefore, a brief overview on bioinorganic chromophores and their synthetic counterparts is provided. We also focus on the integration of abundant natural resources and the search for novel photocatalysts based on nonprecious metals and environmentally benign materials.

Keywords: Bioinorganic chromophores; Solar photochemistry; Biomimetic catalysis; Artificial photosynthesis; Photoactivated drugs.

I. Introduction

The science of inorganic photochemistry has matured over the past 40 years (*1*). It covers in depth all kinds of chemical effects of photons on inorganic matter. Therefore, it is not surprising that the progress achieved in studying the properties of excited state materials and the photophysics and photochemistry of coordination compounds has significantly driven the frontiers of many other branches of research. Major topics now well established in the field include the detailed characterization of photoexcited metal complexes, photoinduced electron and energy transfer processes, solar energy conversion, homogeneous and heterogeneous photocatalysis, supramolecular photochemistry, semiconductor sensitization, photochromism, luminescent probes, sensors, and the development of light-emitting devices such as OLEDs (*2*).

More recently, the various aspects of light-responsive and photoreactive inorganic compounds in biological and bioinspired systems have been addressed (*3–6*). In the present contribution, some fundamental principles and first advances of the rapidly evolving fields of *bioinorganic photochemistry* and *biomimetic photocatalysis* will be discussed.[1] No attempt will be made to provide a comprehensive coverage of the relevant literature, which is widespread across a bunch of different disciplines

[1]The term *photocatalyst* is used to characterize a substance able to induce catalytic chemical transformations of reaction partners upon the absorption of light (*7*).

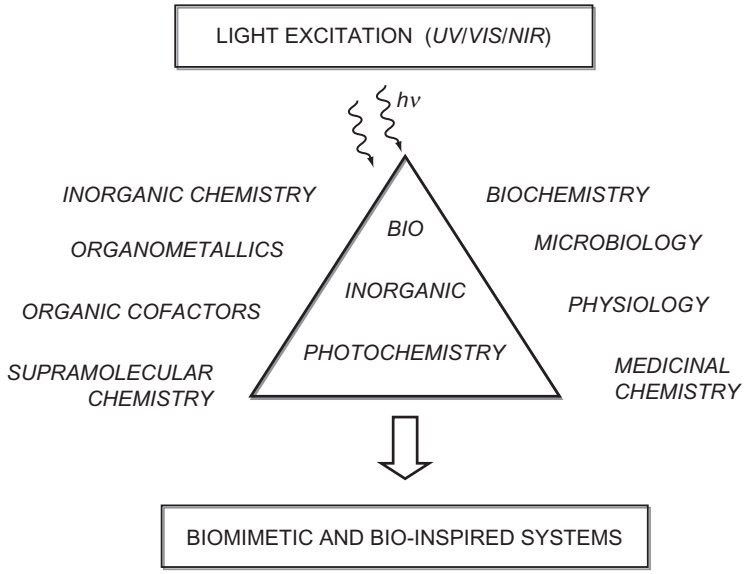

FIG. 1. Origins and impacts of bioinorganic photochemistry.

(Fig. 1). Our intention is rather to visualize current research horizons and to stimulate further endeavors into this exciting new branch of inorganic photochemistry and photocatalysis, which started about a decade ago (*3,8*).

II. Inorganic Photochemistry Inspired by Nature

Studying the inorganic chemistry of life already has a long history (*9*). What we now call biological inorganic (bioinorganic and bio-organometallic) chemistry (*10,11*) is a cross-disciplinary research topic primarily concerned with the role of metals in biology and life sciences. It turned out that approximately one quarter of the known chemical elements has a crucial function for living organisms and that metal ions are of fundamental importance for all biological systems. A large share of the structurally characterized biological macromolecules contains inorganic cofactors. For instance, the majority of all known enzymes are metalloproteins with one or more transition metal ions such as V, (Cr), Mn, Fe, Co, Ni, Cu, Zn, Mo, or W in their respective active site. Coordination chemistry undoubtedly plays a critical part in stabilizing protein structures (*12*). The various other functions of metalloproteins in biological systems are illustrated in Table I.

TABLE I

CLASSIFICATION OF METAL SITES IN BIOLOGY.[a]

Basic role	Typical functions and metal ions involved
Structural	Stabilization of protein configuration (Ca, Mg, Fe, Zn)
Redox	Transfer of electrons or atoms (V, Mn, Fe, Co, Ni, Cu, Mo, W)
Catalytic	Turnover of substrates (V, Cr, Mn, Fe, Co, Ni, Cu, Zn, Mo, W)
Photochemical	Light-harvesting and solar energy conversion (Ca, Mg, Mn, Zn)
Binding	Small molecule coordination, transport, and release (Fe, Ni, Cu)
Storage	Uptake and storage of metal ions, storage of dioxygen (Fe)
Regulation	Switch of protein function (Fe)

[a]Adapted from Refs. *(13) and (14)*.

Metalloenzyme catalysts participate as key compounds in some of the most important biochemical processes of life on earth including nitrogen fixation, respiration, and oxygenic photosynthesis *(15)*. To imitate such natural chemical processes and to develop new compounds which are able to mimic biological materials in their structures or functions are the primary goals of biomimetic chemistry *(16)*. Especially, the construction of robust chemical systems acting as artificial enzyme models (*synzymes, chemzymes*) has always been attracting considerable interest in the field *(17,18)*, as these synthetic counterparts could replace the role of natural enzymes in various applications such as catalytic substrate conversion, bioanalytics, or medicinal chemistry. A representative example is the development of N_5-macrocyclic transition metal complexes, which are able to act as functional mimics of superoxide dismutase (SOD) enzymes *(19)*. The complex **1** shown in Fig. 2 efficiently catalyzes the conversion of $O_2^{\bullet -}$ into peroxide and dioxygen with a rate nearly approaching that of the native manganese redox enzyme MnSOD *(20)*.

It is important to note, however, that synthetic bioinorganic model compounds, which can compete with the reactivity of their natural counterparts, are still extremely rare. This is probably due to the fact that despite huge efforts devoted to this topic, a real breakthrough in simulating the crucial role of the protein matrix which surrounds the native reaction centers has not yet been accomplished.

To mimic the extremely efficient and selective chemistry of biocatalysts in the absence of their dynamic protein environment, novel routes have to be explored *(5,6)*. In this context, we have started to impose light-induced electronic, energetic, and

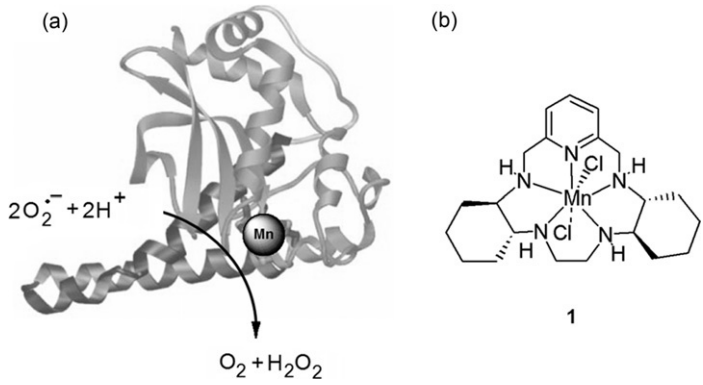

FIG. 2. (a) Structure and function of *H. sapiens* manganese superoxide dismutase (PDP-code: 1ABM) and (b) synthetic low molecular weight substitute of MnSOD optimized for therapeutical purposes (*20*).

structural changes on the substrate binding sites of biomimetic and bioinspired coordination compounds (*artificial photoenzymes*, *photochemical model enzymes*). Already, the first attempts in this direction have proven to be very promising (*3*). As will be shown later in more detail, most of the other functions of metal sites in biological systems summarized in Table I can also be reproduced with bioinspired photochemical model systems.

Efficient light absorption and the population of photoreactive excited states are the minimum requirements for this novel approach. The quantum nature of photons furthermore offers a straightforward strategy to incorporate other interesting properties such as selectivity, switching, and regulation of light-responsive processes. Some basic characteristics of the functional components present in the corresponding bioinorganic and biomimetic systems will be discussed in the following sections.

A. LIGHT ABSORPTION AND SENSITIZATION

The most fundamental principle of photochemistry, which actually was discovered by exposing inorganic compounds to sunlight (*21*), states that light must be absorbed by a chemical substance for a photochemical reaction to occur. We will therefore start our discussion with a brief overview on some of the natural chromophores which are known to be involved in photosensory processes or could be useful for the construction of artificial photoreactive systems.

A.1. Photoresponsive biomolecules

Intensely colored visible-light absorbing molecules are an essential part of our living environment. A quite small number of chromophore types and photoactive pigments seems to be sufficient to deal with the basic photobiological responses and light-dependent functions that have evolved in natural systems. Prominent representatives of organic chromophore molecules in this context (Fig. 3) are the flavins, pterin derivatives such as MTHF **2**, porphyrins and related tetrapyrrole pigments **3**, carotenoids **4**, or conjugated oxidation products of amino acids such as the chromophores of the green fluorescent proteins **5** *(22–24)*.

There are also many building blocks and redox cofactors present in biological systems including purines, quinones, coenzymes such as NADH, and other organic chromophores displaying

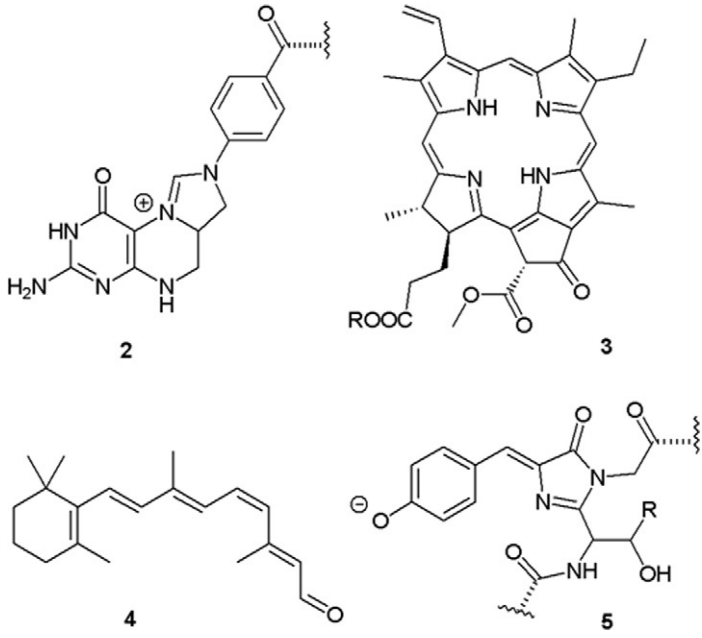

FIG. 3. Examples of natural photoantenna chromophores: (**2**) 5,10-methenyltetrahydrofolate (MTHF), a blue light photoreceptor pigment present in photolyase and some cryptochromes; (**3**) Pheophytin *a*, the primary electron acceptor in cyanobacterial oxygenic photosynthesis. (**4**) 11-*cis*-retinal, which is involved as sensory photoreceptor component in the opsin-based visual process of animals; and (**5**) the *p*-hydroxy-benzylidene-imidazolinone chromophore (HBDI) of the green fluorescent protein from bioluminescent marine species.

characteristic absorption bands (*25*). Most of these compounds are able to interact with metal ions or may serve as ligands in biocoordination chemistry (*10*). Under natural conditions, these chromophores are usually thought not to be directly exposed to electromagnetic radiation. They are therefore considered as irrelevant for photobiological primary processes. Nevertheless, the corresponding compounds frequently turn out to be light sensitive under both *in vitro* and *in vivo* conditions. This feature can be directly exploited to influence biological functions or to construct artificial photoresponsive systems.

Illustrative examples for such a possibility are found with the cytochromes. The name of these proteins comes from the Greek words meaning "colored substances in the cell." Cytochromes are intensely red-colored redox enzymes containing a heme prosthetic group as their dominant chromophore. Hemes are iron complexes of protoporphyrin IX derivatives (*10,26*). One of the most frequently studied metalloproteins of this family is cytochrome *c* (*27*). The ribbon structure of a cytochrome *c* enzyme together with the protein-bound heme *c* cofactor **6** is shown in Fig. 4.

Cytochrome *c* has a number of vital functions inside the cell. As part of the mitochondrial electron transport chain in respiration, it shuttles redox equivalents to cytochrome *c* oxidase (*28*), which can be considered as a kind of natural fuel cell for energy conversion. Mitochondrial dysfunction accompanied with changes in cytochrome *c* oxidase activity, however, seems to be intimately related to aging, neurodegeneration, and disease (*29*). Effects that can manipulate the functions of such redox enzymes are therefore of great importance for many research fields.

Photons are able to cause such effects. Light sensitivity of cytochrome containing systems has been known for a long time. For example, when bacteria of the type *Rhodomicrobium* (red microbe) were exposed to near infrared (NIR) radiation, their cytochrome system was oxidized from the ferrous to the ferric state (*30*). It is important to note that an archaic type of anoxygenic photosynthesis based on the oxidation of Fe(II) species has in the mean time been discovered (*31*), and that *Rhodomicrobium* strains are now known to belong to such types of photoferrotrophic microorganisms (*32*).

More recently, a novel mitochondrial signaling pathway activated by red light in the visible-to-NIR spectral region has been discovered (*33*), which is thought to depend on a direct light absorption by the metal-binding sites of the cytochrome *c* oxidase machinery. These findings may help to understand the beneficial effects of red light therapy for accelerated wound healing and

other medical applications (*34*). Although the detailed mechanisms causing such effects are not fully clear, it seems that the cells directly involved in wound repair are affected upon irradiation. An overall acceleration of the electron transfer processes in the respiratory chain could provide more ATP, which is necessary for the wound-healing process. However, also some other types of bioinorganic photoreactions may be of crucial relevance in this context and have to be discussed (*6*). For example, the nitric oxide generated in injured tissue is well known to inhibit the catalytic center of cytochrome *c* oxidase (*35*), and photoinduced NO release can recover its function (*36*).

Another very interesting example of a photochemical reaction directly involving the two chromophores **5** and **6** (Figs. 3 and 4) has recently been described (*37,38*). The spectral changes of the corresponding photoredox process are shown in Fig. 5.

Oxidative quenching of the photoexcited EGFP protein is not only possible with cytochrome *c* but also achieved with a variety of other electron acceptors, including biologically relevant ones such as NAD^+ or flavins (*37*). Further, the photoinduced electron transfer (PET) seems to favor a net two-electron process. It has been observed both in solution and inside living organisms without any special treatment. These findings give rise to speculations that a possible biological function of green fluorescent proteins might be that of a light-activated electron donor similar to the role of chlorophyll donating electrons to an acceptor in photosynthesis.

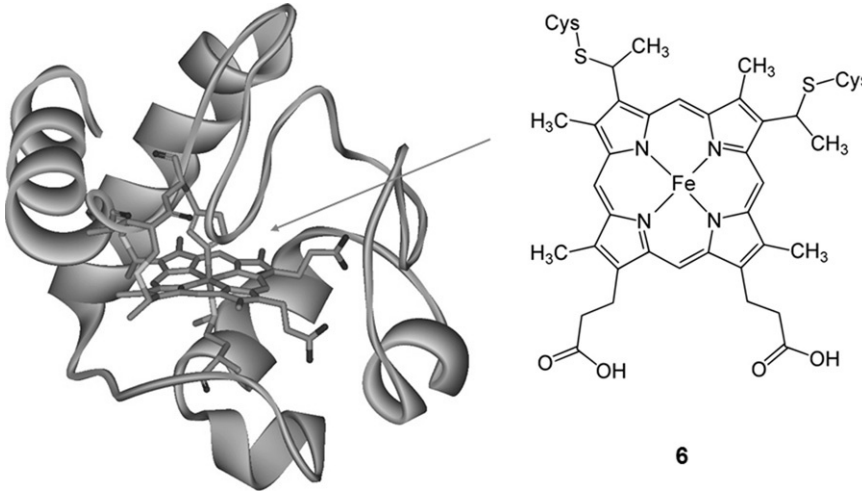

FIG. 4. Structures of cyt *c* (PDB-code: 3CYT) and *c*-type heme (**6**).

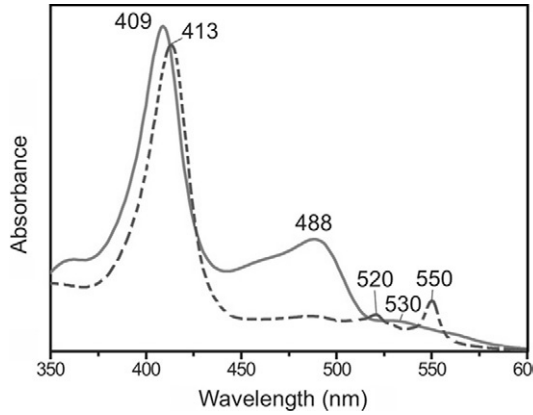

FIG. 5. Electronic spectra of a mixture of ferric cytochrome *c* and enhanced green fluorescent protein EGFP before (—) and after (----) 490 nm photolysis indicating the formation of the ferrous form of heme *c* (**6**) with maxima at 413, 520, and 550 nm. Adapted from Ref. (*37*).

In this context, it is interesting to note that it has been pointed out that enzyme catalysis driven by light represents photosynthesis in its simplest biological form, and that photoenzymes probably played an important role in the early biotic environment on earth (*39*). Today, the only metalloenzyme directly involved in photochemical processes under natural conditions is the visible light-driven water–plastoquinone oxidoreductase, better known as photosystem II (PS II) of oxygenic photosynthetic organisms (*40*). However, the functional properties of many other metal sites in bioinorganic systems are also known to be modified by irradiation. Some of these examples are given below (Table II).

The reasons for light sensitivity in these enzymes are not always well understood, and several other examples will probably be discovered when the nature of the light-absorbing species is clarified. It therefore seems appropriate to provide a brief overview on the basic types of inorganic chromophores occurring in biological metal sites.

A.2. Bioinorganic chromophores

Excitation of proteins, nucleic acids, or organic cofactors acting as ligands in biological systems frequently involves individual functional groups or isolated conjugated π-systems. When a metal is coordinated to such moieties, the resulting molecular orbitals are usually classified as predominately located at the

TABLE II

EXAMPLES OF METALLOPROTEINS INFLUENCED BY LIGHT ABSORPTION

Protein	Metals involved	Effects observed	Reference
Catalase	Fe	Inactivation	(*41*)
Horseradish peroxidase	Fe	Inactivation	(*42*)
[Fe]-Hydrogenase	Fe (?)	Inactivation	(*43*)
Methionine synthase	Co	Inactivation	(*44*)
Ferredoxin nitrate reductase	Mo	Inactivation	(*45*)
Cytochrome P450	Fe	Activation	(*46*)
Cytochrome *c* oxidase	Fe,Cu (?)	Activation	(*47*)
Nitrile hydratase	Fe	Activation	(*48*)
Ethanolamine ammonia-lyase	Co	Activation (?)	(*49*)
CH_3SCoM reductase	Ni (?)	Activation	(*50*)
Tyrosinase	Cu (?)	Activation	(*51*)
Fd-thioredoxin reductase	Fe	Regulation	(*52*)
Ascorbate oxidase	Cu	Regulation	(*53*)
Xanthine oxidase	Mo, Fe (?)	Regulation	(*54*)
Methylamine dehydrogenase	Cu (?)	Switch of function	(*55*)

metal (M) or at the ligands (L). In such a case, three fundamental types of electronic transitions can be distinguished. Transitions localized at the metals (metal-centered, MC), ligands (ligand-centered, LC or intraligand, IL), or charge transfer (CT) transitions with a spatial redistribution of electron density occurring between reducing (donor) and oxidizing (acceptor) subunits of the system (*56,57*).

A schematic representation of the typical classes of electronic transitions (MC, LC, CT) observed in metal complexes is shown in Fig. 6. In bioinorganic chromophores, the MC transitions usually involve metal ions with a partially filled d-electron shell, which are then characterized by the presence of low-energy ligand field ($d \rightarrow d$) electronic transitions or excitations involving metal–metal σ-bonds. The corresponding absorptions are sometimes covered by other bands and therefore hard to detect. It has been pointed out that whenever metallobiomolecules are described as being highly colored and having unique spectral features, this may indicate the presence of intense low-energy CT transitions (*57*). The typical absorption characteristics and the conspicuous colors related to the presence of such inorganic chromophores in biological samples have frequently been used to classify complete enzyme families, to coin names for certain

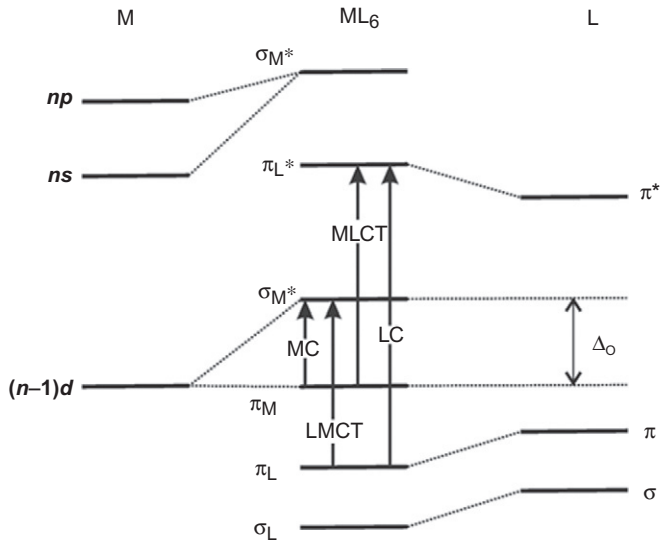

FIG. 6. Molecular orbital diagram for an octahedral transition metal complex ML_6 illustrating different types of electronic transitions based on localized orbital configurations (MC, metal-centered; LC, ligand-centered; MLCT, metal-to-ligand charge transfer; LMCT, ligand-to-metal charge transfer). Adapted from Ref. *(1)*.

compounds, or to identify the involvement of characteristic intermediates or cofactors in biochemical processes. Illustrative examples in this context are metalloproteins with blue copper sites, purple acid phosphatases, or the red iron–sulfur proteins of the rubredoxin type (Fig. 7).

Many of the biological ligands present in metalloproteins (oxide, sulfide, phenolate, thiolate, and peroxide) exhibit low-energy ligand-to-metal charge transfer (LMCT) transitions. Due to the strong donor character of the coordinated groups involved in such systems, this may also reflect the presence of highly covalent ligand–metal bonds, which considerably contribute to the observed reactivity of these active sites in biology. Low-energy metal-to-ligand charge transfer (MLCT) transitions are less frequently assigned in bioinorganic systems. They require the presence of a reducing metal donor site and ligands with sufficiently low-lying acceptor orbitals. This situation is frequently observed in bio-organometallic systems and in the presence of tetrapyrrole macrocycles or redox cofactors.

Besides the CT transitions shown in Fig. 6, several other combinations of donor and acceptor moieties in metalloproteins can

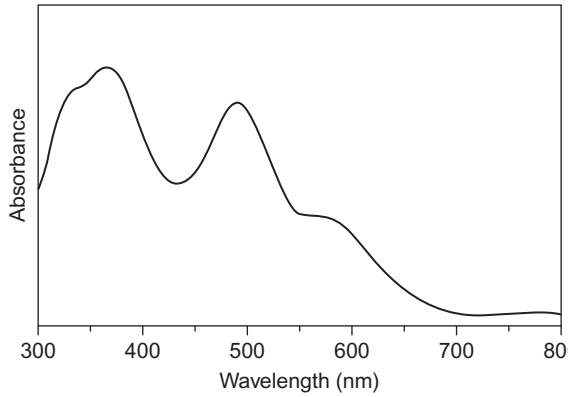

FIG. 7. Electronic absorption spectrum of the oxidized rubredoxin protein from the dinitrogen fixing bacterium *Clostridium pasteurianum*. Adapted from Ref. (*58*).

lead to low-energy CT interactions. This includes the observation of mixed-valent compounds with ligand-to-ligand charge transfer (LLCT) transitions between reducing and oxidizing ligands simultaneously present at a metal-binding site, or the possibility of metal-to-metal charge transfer (MMCT) or intervalence charge transfer transitions in polynuclear metal-binding sites and cluster structures with ligand bridged reducing and oxidizing metal centers (*56*).

In all these cases, the degree of coupling between the donor and acceptor sites crucially determines the electronic structures and optical properties. Whenever strong covalent bonding occurs, as is the case for bioorganometallic systems, the degree of molecular orbital delocalization may become dominant and the description of electronic transitions with localized orbitals and discrete oxidation states is then no longer appropriate. Nevertheless, this simplified classification has proven to be very useful to discuss different types of excited states in both inorganic photochemistry and bioinorganic spectroscopy (*56,57*). A representative overview on the diversity of bioinorganic chromophores following this terminology is given in Table III.

As can be clearly seen from the data provided in Table III, the excitation energies of different bioinorganic chromophores are completely covering the photochemically relevant spectral region from ultraviolet to NIR light. Moreover, the observed intensities of the absorption features directly involving metal-binding sites strongly vary and span many orders of magnitude. To populate a desired excited state manifold more efficiently, it may therefore

TABLE III

SOME BIOINORGANIC CHROMOPHORES

Metalloprotein	Metal	Absorption[a]	Assignment	Reference
Horseradish peroxidase	Fe	400 (100,000)	LC	(42)
Cytochrome P450	Fe	363 (50,000)	LC/LLCT	(59)
Methylmalonyl CoA mutase	Co	376 (12,800)	LC/LLCT	(60)
Methyl CoM reductase	Ni	420 (22,000)	LC	(61)
Bovine serum amine oxidase	Cu	480 (3500)	LC	(62)
Ribonucleotide reductase	Fe/Mn	408 (3400)	LC	(63,64)
Galactose oxidase	Cu	900 (1000)	LLCT	(65)
Deoxyhemerythrin	Fe	1110 (4)	MC	(66)
Nitrile hydratase	Co	575 (30)	MC	(67)
CuZn superoxide dismutase	Cu	610 (155)	MC	(68)
Cytochrome *c* oxidase	Cu–Cu	769 (1500)	MMCT/MC	(69)
Photosystem II	Mn, Mn	820 (?)	MMCT/MC	(70)
Clavaminate synthase	Fe	500 (375)	MLCT	(71)
Taurine α-KG dioxygenase	Fe	530 (140)	MLCT	(72)
Methyl CoM reductase	Ni	754 (2500)	MLCT	(61,73)
Vanadium chloroperoxidase	V	315 (3000)	LMCT (?)	(74)
Mn superoxide dismutase	Mn	480 (800)	LMCT	(75)
Acid phosphatase	Mn	515 (2460)	LMCT	(76)
Formate dehydrogenase	Fe	400(16,000)	LMCT	(77)
Rubredoxin	Fe	490 (8700)	LMCT	(78)
Phenylalanine hydroxylase	Fe	700 (1140)	LMCT	(79)
Thiocyanate hydrolase	Co	340 (?)	LMCT (?)	(80)
Azurin	Cu	630 (5000)	LMCT	(81)
Ascorbate oxidase	Cu	610 (9600)	LMCT	(82)
DMSO reductase	Mo	720 (2000)	LMCT	(83)
DMSO reductase	W	560 (1800)	LMCT	(84)

[a]Wavelength (nm) (ε M^{-1} cm^{-1}); approximate values extracted from the published data.

become necessary to sensitize the systems by introducing additional excited state levels.

A.3. Spectral sensitization

The process of photosensitization occurs, whenever the absorption of radiation by one molecular entity causes photophysical or photochemical alterations in another molecular entity or

material. This may involve either energy transfer or electron transfer (*1*). In a strict mechanistic sense, however, the sensitizer must not be consumed in the process. Scientific work on this topic dates back to the pioneering days of photography, when the sensitivity of silver halides was for the first time extended to longer wavelengths by using various organic dyes and pigments (*85*). Later, the dye sensitization of solids and semiconductors was systematically explored (*86*), which finally led to the development of modern solar cell materials (*87*).

Biological effects of sunlight and synthetic organic dyes on enzymes, microbes, and higher organisms have been discovered in the end of the nineteenth century and soon were exploited for medical applications (*88*). Today, the optimization of sensitizers for photodynamic therapy is still a very active branch of research in bioinorganic photochemistry and molecular photomedicine (*6,89*).

The majority of organic compounds and biological metabolites is colorless but may be severely damaged under UV-light exposure. Therefore, spectral sensitization is a crucial prerequisite for the efficient accumulation of permanent photoproducts in all kinds of synthetic processes driven by light. The big advantage of photosensitized processes avoiding undesired side reactions caused by secondary photolysis now gradually becomes recognized as extremely useful for photocatalytic organic synthesis driven by visible light (*90*).

Here, we will mainly focus on two other important aspects of photosensitization: the fundamental role of deeply colored compounds as light-harvesting antenna chromophores for solar energy conversion and the possibility of reaching spectroscopically hidden, but photochemically active excited state levels by means of spectral sensitization.

Porphyrins and related tetrapyrrole pigments represent the most important class of sensitizers in both natural and artificial photosynthesis (*8,87,91*). These compounds are ideally suited for collecting light in the far-red and NIR spectral region, which represents a natural limit for directly driving energetically uphill bond-formation processes suitable for the photochemical storage of solar energy. To reproduce the spectroscopic and light-harvesting features of the chlorophylls is therefore an important goal of biomimetic and bioinspired chemistry (*5,92,93*). A comparison of natural and synthetic photosensitizers with quite similar absorption characteristics is given in Fig. 8.

Besides metallophthalocyanines **7** as photosensitizers (*91,93*), some intensely colored perylene diimine derivatives such as **8** have also been proposed as functional chlorophyll analogues

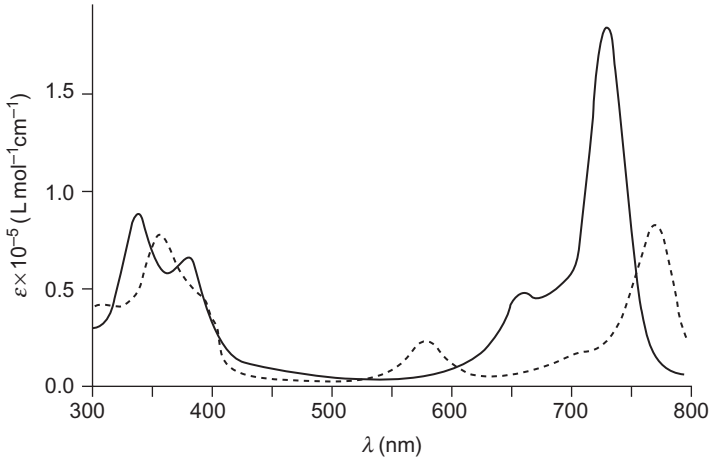

FIG. 8. Electronic spectrum of bacteriochlorophyll *a* (----) extracted from antenna complexes of purple bacteria compared to the spectrum of a synthetic phthalocyanine metal complex (—). Reproduced with permission from Ref. (*5*). Copyright Wiley-VCH.

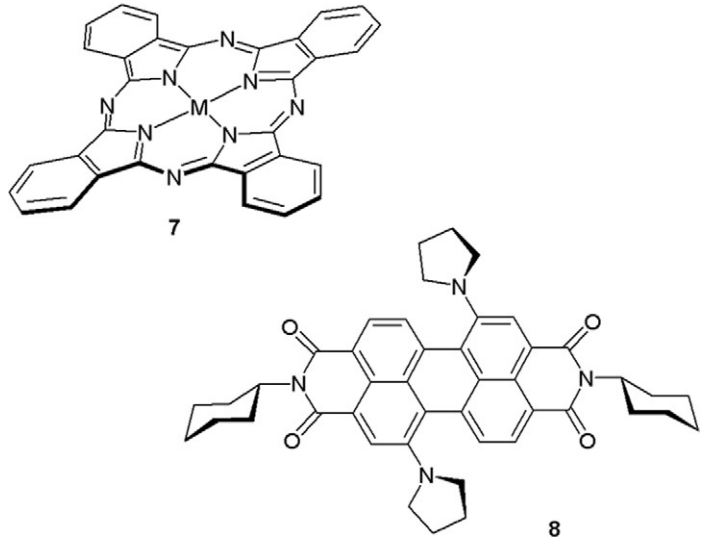

FIG. 9. Structures of robust biomimetic photosensitizers with chlorophyll-like excited state properties (*93,94*).

(*94*). Chlorophyll *a* with a Q_y-band at $\lambda_{max} = 665$ nm (*95*) is the magnesium complex of the dihydroporphyrin derivative **3** already shown in Fig. 3. The chemically quite different structures of compounds **7** and **8** are given in Fig. 9.

In the context of artificial photosynthesis and solar fuel production, the long-wavelength spectral sensitization of photoreactions into the far-red and NIR-region is of prime interest. Without suitable chromophores, a reasonably high efficiency of an abiotic solar energy storage process, which is always characterized by a specific optimum threshold wavelength (*5,96,97*), will not be reached.

As already mentioned above, spectral sensitization may also become indispensable when the light absorption properties of a potentially photoreactive compound do not permit direct excitation in the desired wavelength region. By application of sensitizers with adjusted excited state properties, it is, for example, possible to induce photochemical reactions of otherwise colorless compounds with visible light. Another important application in photochemistry is the sensitized population of excited state levels, which are not easily reached by direct absorption of light due to the limitations of quantum chemical selection rules. This phenomenon has been extensively exploited in mechanistic and synthetic organic photochemistry, where enhanced yields of triplet state population could be achieved in various dye-photosensitized processes (*98*).

In the pioneering years of inorganic photochemistry, the basic inter- and intramolecular sensitization processes were introduced by Vogler and Adamson (*99*), which soon was followed by organometallic examples (*100*). In this decade, also the blue-light absorbing tris(2,2′-bipyridyl)ruthenium(II) cation $[Ru(bpy)_3]^{2+}$, **9** was promoted as an interesting new sensitizer for energy and electron transfer processes (*101,102*). In a plethora of slightly modified forms, $[Ru(bpy)_3]^{2+}$ became an extremely popular prototype of an inorganic photosensitizer (*103*). This also opened fascinating new routes in bioinorganic photochemistry such as probing and modulating the active site properties of metalloenzymes with blue light (*104*). Derivatives of $[Ru(bpy)_3]^{2+}$ continue to be extensively studied in the context of photocatalysis, biomimetics, solar energy conversion, and artificial photosynthesis (*105–109*). The structure of the parent ruthenium polypyridine complex **9** together with a representative application of this structural motif in bioinorganic photocatalysis is depicted below (Fig. 10).

While the MLCT excited state properties of sensitizers such as **9** are easily studied and spectroscopically characterized, these compounds are not yet the best choice for certain applications. This includes all kinds of photosystems requiring to collect a much larger share of the solar spectrum such as artificial photosynthetic architectures or solar cells. Even more severely, in PET

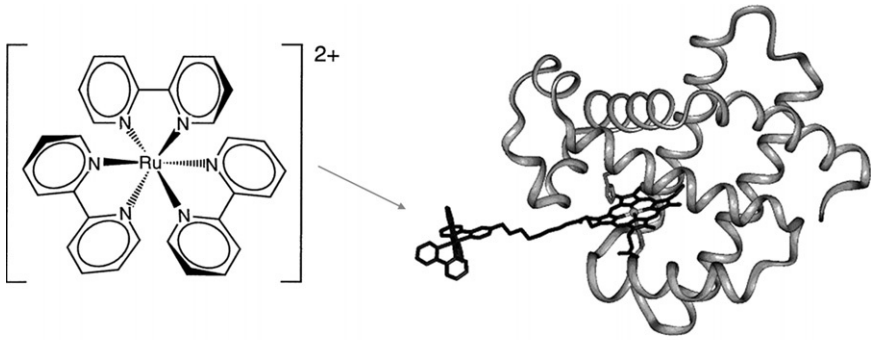

FIG. 10. The photosensititzer $[Ru(bpy)_3^{2+}]$ (**9**, left side) covalently wired to the heme prosthetic group of horse heart apomyoglobin. This hybrid system allows to create and characterize radical intermediates in the enzyme active site triggered by light (*110*).

processes, sensitizers such as $[Ru(bpy)_3]^{2+}$ are acting as a one-electron reagents, while many photocatalytically attractive processes for the synthesis of permanent reaction products require the exchange of more than one electron to avoid destructive side reactions and thermodynamically unfavorable free radical chemistry (*5,8*). Serious efforts are therefore necessary to efficiently couple the photoinduced primary processes to other catalytically competent moieties. As an alternative, a new generation of light-harvesting photocatalysts termed *multielectron transfer (MET) photosensitizers* has been introduced (*8,111*). These compounds are able to directly promote net two-electron processes following the absorption of only one photon.

Besides color, sensitization, and light-harvesting efficiency, the actual reactivity of the excited states populated is therefore a crucial property. Some aspects of relevance for bioinorganic and biomimetic systems will be discussed in the following chapters.

B. PHOTOCHEMICAL REACTIVITY

Absorption of light always leads to an activation of the irradiated compound, as excited state energy levels are situated considerably higher than those of the corresponding ground state species. Thus, it is not surprising that many reactions, which are thermodynamically or kinetically inaccessible in the ground state, can occur with high efficiency from electronically excited states. This general feature makes photochemical activation

under ambient conditions an ideal strategy for the functional modeling of difficult or energetically demanding chemical transformations that are otherwise restricted to biocatalysis and natural photosynthesis. In Table IV, some complementary functions of biological systems and basic types of photochemical reactions are compared.

The design principles for the rational construction of light-driven counterparts of bioinorganic, bio-organometallic, and biocatalytic systems have recently been reviewed in more detail (*5*). Here, we will limit our discussion on the most important aspects and advantages of photoreactive components in bioinspired energy conversion and catalysis.

B.1. Electrons

Light absorption modifies the driving force for electron transfer processes in all kinds of materials. As photoactivated species are always better oxidants *and* reductants than their ground state equivalents, an enhanced redox reactivity is usually observed in the excited state. Photoreactions are therefore ideally suited to trigger, study, and mimic bioinorganic electron transfer.

The typical one-electron redox reactions resulting from PET processes can be applied to control the generation of reactive intermediates similar to the way radical enzymes are performing (*112*). To achieve an accumulation of permanent reaction products, as is the case with most oxidoreductase enzymes and photosynthetic systems, it is very important to provide suitable (photo)-catalytic multielectron transfer (MET) pathways.

TABLE IV

EXCITED STATE PROCESSES AND THEIR FUNCTIONAL COUNTERPARTS

Light-dependent reaction types	Biosystems with related functions
Bond distortion, spin crossover	Enzyme-substrate complexes
Sensitization, energy transfer	Light-harvesting antenna systems
Photoinduced electron transfer	Photosynthetic reaction centers
Hydrogen atom abstraction	Radical enzymes
Photooxidation, photoreduction	Oxidoreductase enzymes
Photoaddition, photosubstitution	Transferases, kinases
Photodissociation, photo-cleavage	Hydrolases, lyases, nucleases
Photoisomerizations	Isomerases, mutases
Photodimerization, photo-polymerization	Ligases, polymerases
Phototriggered release of compounds	Hormones, neurotransmitters
Photodeposition of materials	Biomineralization and storage proteins

The crucial advantage of collecting and coupling redox equivalents is to avoid free-radical side reactions, as these processes tend to decrease both the long-term stability and the overall efficiency of the system. Especially, the light-induced substrate transformations in natural and artificial photosynthesis strongly depend on the feasibility of MET catalysis. For example, the fixation of CO_2 to form carbohydrates in a photocatalyzed four-electron process allows a long-wavelength spectral sensitization down to a photon energy of 1.3 eV, corresponding to an NIR threshold absorption wavelength of about 950 nm. In contrast, a minimum energy of 3.6 eV (340 nm, UV-light) is necessary to drive the reaction in highly unfavorable one-electron steps, and two-thirds of the solar energy suitable for carbon dioxide reduction are wasted (*8*). Also many energetically downhill reactions in bioinorganic and bioinspired catalysis require optimized MET reagents to be sufficiently accelerated and to guarantee a large total number of possible redox cycles.

The qualitative reaction profile given in Fig. 11 shows how a light-induced single-electron transfer process can be coupled to suitable follow-up steps to facilitate the formation of permanent two-electron photoredox products. Larger bond and shape reorganizations of excited state molecules, which typically involve the population of CT states or the formation of Jahn–Teller distorted species, are very helpful to achieve such

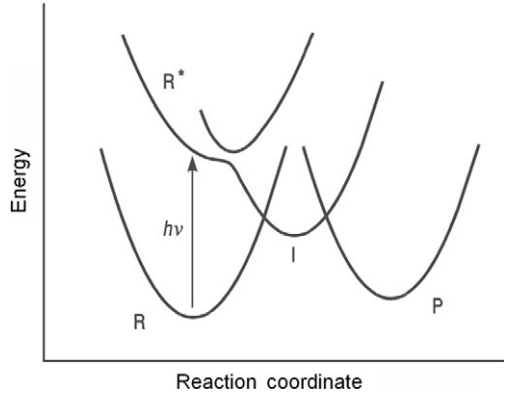

FIG. 11. *Schematic illustration of a net two-electron transfer photoredox process*. Excitation of reactants (R) forms a metastable one-electron intermediate (I), which finally can yield an energy-rich permanent product (P) after a second electron transfer step. Adapted from Ref. (*8*).

a favorable situation of the potential energy surfaces (*5,8*). Ideally, the thermal back reaction of the products formed should have a sufficiently high activation barrier to enable a continuous accumulation of the desired product molecules during many photocatalytic cycles. According to the Hammond postulate (*113,114*), which claims that exothermic reactions have an early barrier, the structural features of the one-electron transfer intermediates formed photochemically should already be as close as possible to the transition state of the follow-up electron transfer step. This requirement gives an important guideline for choosing the type of excited state to be built into such systems.

B.2. Protons

The most common type of biocatalytic reactions is proton transfer (*115*). Nearly, every enzymatic reaction involves one or more proton-coupled steps. Transition-state proton bridging and intramolecular proton transfer (general acid–base catalysis) are important strategies to accelerate substrate conversion processes. Moreover, proton transfer also plays a fundamental role in bioenergetics (*116*).

There are also many well-documented cases of excited state proton transfer reactions. It has been known for a long time that the acid–base properties of organic molecules such as phenols are drastically modified upon light absorption. About 60 years ago, Förster suggested a simple method for estimating the excited state pK^* values of photoactivated species from thermodynamic and spectroscopic data (*117*), which became very popular (Fig. 12).

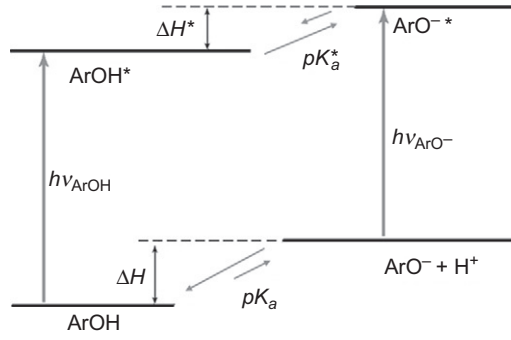

FIG. 12. Förster-cycle for the acid–base equilibria between a phenol derivative (ArOH) and the corresponding phenolate anion (ArO^-) in the ground state S_0 and the first excited singlet state S_1.

The first example of such a reversible proton translocation cycle occurring within a protein core (*118*) was described for the GFP chromophore **5** already mentioned in the previous sections (Fig. 3). In the presence of light, excited state proton transfer should also be relevant for many other biological systems carrying phenols such as tyrosine residues or other deprotonable moieties in their active sites. In inorganic photochemistry, the acid–base properties of the coordinated ligands can also be drastically modified upon excitation. Although some attempts to generalize the Förster concept for coordination compounds have been made (*119*), the possible benefit of utilizing such effects is still underestimated. Nevertheless, it is already quite clear that metal complexes with potential proton translocation sites on the ligand periphery also exhibit immense changes in their nucleophilic character and their acid–base properties upon light absorption (*120*). The chemical bonds most frequently involved in the context of excited state proton transfer reactions include OH, NH, and CH. Typical photoinduced changes in acidity or basicity are characterized by p*K*-value variations of 4–6 units, which is in the range of the transition-state effects observed in hydrolytic enzyme catalysis (*5*). These effects could therefore become a very useful functional tool for many applications in biomimetic and bioinspired photocatalysis.

B.3. Spin

When chemical bonds are formed or broken, the valence electrons of the participating species are redistributed. In some cases, the necessary changes in electron angular momentum (spin) in the course of a chemical reaction may represent the decisive rate-limiting factor (Fig. 13). For example, the majority of stable organic substances are diamagnetic with a singlet ground state. Spontaneous reaction with dioxygen, which has a triplet ground state, is therefore constrained due to spin-barrier effects. These limitations are immediately circumvented, when O_2 is converted into singlet oxygen by photosensitization or by other means.

Rate acceleration is the most fundamental aspect of catalysis. To elucidate the electronic mechanisms of spin–acceleration phenomena therefore represents an important topic in both bioinorganic and biomimetic dioxygen activation (*5,122*). Many other types of substrate transformations catalyzed by metal complexes or redox enzymes also involve key steps with a change in spin along their reaction coordinates. The abundance of such phenomena seems to be much wider than initially thought. This

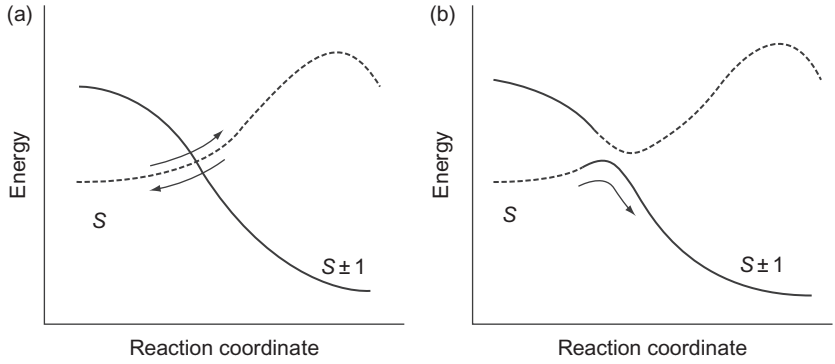

FIG. 13. Energy curves along the reaction coordinate of a spin-forbidden two-state process (a). In such a situation, spin crossover can accelerate product formation by opening up a novel low-energy reaction pathway (b). Adapted from Ref. (*121*).

includes all kinds of radical reactions and electron transfer processes, which can be catalyzed by metal ions (*123*). Some spin-forbidden proton transfer reactions have also been characterized (*124*).

Paramagnetic metal complexes or radical species present in the coordination sphere of active sites can open up initially closed reaction channels when their own spin is combined with those of the reactants. In photosynthetic reaction centers, the fate of the radical-ion pairs generated by photoinduced charge separation is, for example, defined by the exchange interactions with a close-by iron site. Also, the course of bond cleavage processes, hydrogenations, and isomerizations can be influenced by the presence of paramagnetic compounds. All the basic aspects of this ubiquitous phenomenon termed *spin-catalysis* (*125–127*) can also be exploited for bioinspired photocatalytic systems, where spin crossover and intersystem crossing (ISC) processes can be triggered by light, and the degree of spin–orbit coupling can be employed to partially control such effects (*5*).

C. SELECTIVITY AND REGULATION

The interaction between light and matter, unlike thermal activation of compounds in the form of heat, is always a very selective process. Photochemical activation may induce the twisting, stretching, or destabilization of certain bonds located in a specific region of an individual molecule, while other subunits remain

almost unaffected. This resembles the strategies evolved in biocatalytic systems, where activation, regioselectivity, and branching between alternative substrate transformation pathways are carefully controlled by the formation of enzyme–substrate complexes.

The convenient triggering of selective reactions by light and the regulatory effects of light intensity variations are crucial benefits of the photochemical approach toward biomimetic model compounds. These two important aspects of biological systems, which are otherwise hardly achieved in synthetic molecular devices, will be briefly discussed in the following sections.

C.1. Controlling reaction pathways

In photochemical reactions, the population of excited states of different orbital origins can result in quite different reactivity patterns. Therefore, reaction products may occur, which are not accessible at all in thermochemical pathways. Especially in organometallic and coordination compounds, the primary photoproducts obtained are not always resulting from the lowest-lying excited state levels. Wavelength-selective excitation may then be exploited to channel the product formation process and to control a possible branching between different reactivity patterns.

As already mentioned in the previous section, also the fundamental laws of spin conservation may completely close or at least slow down certain reaction channels. ISC and spin inversion thus can strongly influence the balance between competing processes with a different regio- and stereoselectivity (*5*). While such effects are very common in metalloenzyme redox catalysis, their rational exploitation in bioinorganic photochemistry and photocatalysis is still in its infancy (*3,6*).

Successful fine-tuning of the branching reactivity patterns observed in metal complexes and organometallics requires a profound set of experimental and spectroscopic data. Especially in complicated systems with various close-lying electronic excited states of different orbital parentage, an in-depth interpretation of the experimental results can only be supported and further refined by highly sophisticated quantum chemical calculations (*128,129*). A well-documented example of such a situation with a competitive spin-multiplicity- and wavelength-dependent photoreactivity is the selective bond cleavage of $[HMn(CO)_5]$ and related organometallic manganese hydride complexes (Fig. 14).

The carbonyl-hydrido complex $[Mn(H)(CO)_3(DAB)]$ displays nine low-lying singlet and triplet excited states, which all are

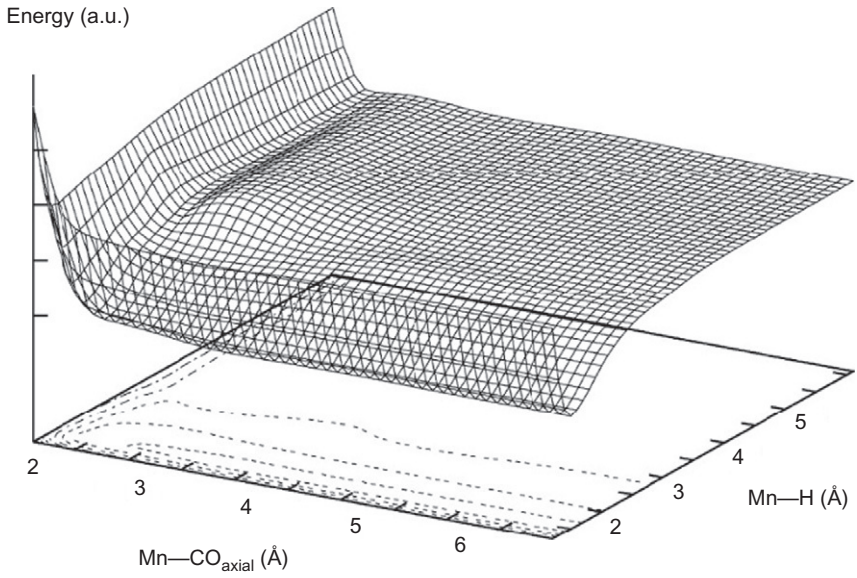

FIG. 14. Calculated potential energy surface of the ^{1}MLCT state of Mn(H)(CO)$_3$(DAB) as a function of the MnH and MnCO bond lengths (DAB, 1,4-diaza-1,3-butadiene). Adapted from Ref. (*128*).

potentially photoreactive. It could be shown (*128*) that only two of those, the singlet metal-to-ligand ^{1}MLCT ($d_{Mn} \rightarrow \pi^*_{DAB}$) state and the triplet sigma-bond-to-ligand ^{3}SBLCT ($\sigma_{MnH} \rightarrow \pi^*_{DAB}$) state, define the photochemistry of the compound. While the lower-lying triplet SBLCT (or mixed MLCT/LLCT) state should induce a homolytic cleavage of the metal-hydride bond, visible light excitation and population of the singlet MLCT state allow an ultrafast direct dissociative process of the axial CO ligand (Fig. 14), which is completed within 400–500 fs.

C.2. Controlling catalytic activity

The metabolic functions of living organisms are maintained by a complex interplay of regulatory networks. Enzymatic activity and gene expression are permanently adapted for an optimum performance and may be completely switched on and off in a reversible manner. Typical mechanisms involved in biological systems include the stimulation and inhibition by control proteins or metabolite molecules, allosteric interactions, proteolytic activation, redox transformations, and reversible covalent bond modifications such as phosphorylation and dephosphorylation (*5*).

In a similar way, photochemical remote control of chemical and biological processes can serve to mimic or influence important aspects of these natural regulatory systems. The most simple version of deactivation and activation of any photochemical process can be achieved by switching between dark- and light-adapted conditions, which is comparable to the presence or absence of an inhibitor. Photosubstitution reactions of metal complexes and light-induced fragmentation processes can be employed to trigger the signal transduction function of small gaseous molecules and other neurotransmitter substances. Another common strategy is the photochemical cleavage of a light-sensitive protection group to trigger the release of otherwise hidden (so-called caged) bioactive or biomimetic compounds (*130,131*). The big disadvantage of most of these simple strategies is that the desired function is only available for one time in an irreversible light-responsive process.

In many types of photocatalytic reactions, however, the variation of incident light intensity is directly related to the actual photostationary concentration of the active species involved (*5*). This feature can then be easily applied for a certain degree of continuous up- and down-regulation of an already running biomimetic process under ambient conditions. An even higher level of control can be reached, whenever a wavelength-selective response of the system is built in. Some photochromic compounds, for instance, (*132*) enable a reversible switching of catalytic activity and other types of light-dependent processes. This is a very powerful tool for the construction of biomimetic and bioinspired enzyme models.

In the field of artificial photosynthetic devices, regulatory strategies could also be advantageous. An interesting recent example for such an approach is given in Fig. 15. The multichromophoric system consists of a covalently linked porphyrin–fullerene donor–acceptor core designed for photoinduced charge separation (*133*). In the periphery, additional aromatic antenna subunits and a photochromic switch are situated. Under intense white-light conditions, the spiro-dihydroindolizine-based regulator subunit **10** opens up to form a larger photostationary concentration of its deeply colored betaine form, which in competition to the donor–acceptor moiety also absorbs in the visible spectral region and efficiently quenches the donor excited state. In a certain sense, this self-regulating molecule mimics the way green plant photosynthesis responds to potentially damaging light levels by controlling the fraction of excitation energy that can drive PET processes.

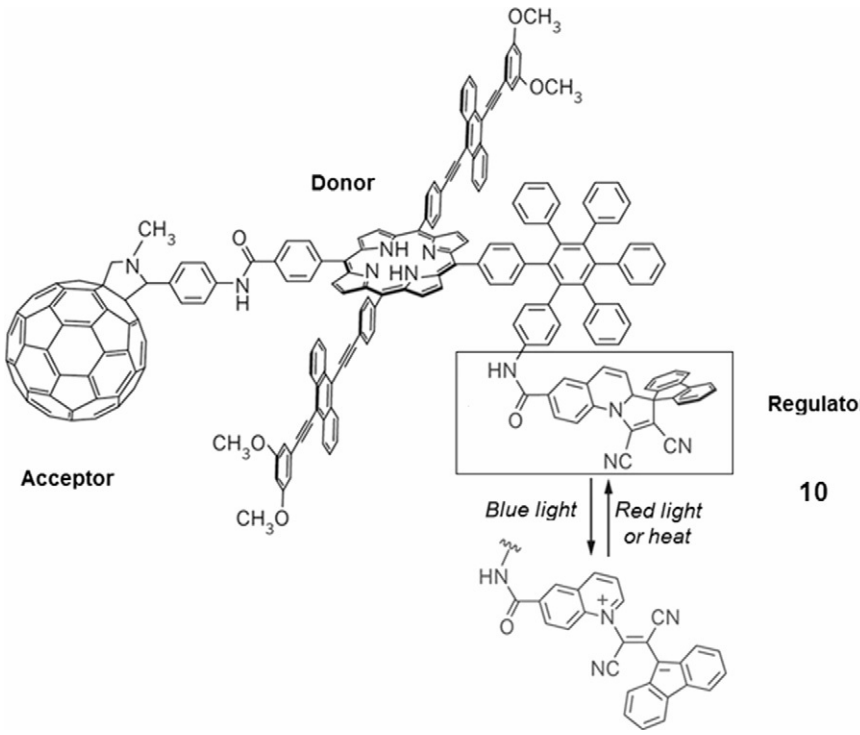

FIG. 15. Example of a covalently linked donor–acceptor system featuring a photochromic control moiety (*11*) for the downregulation of photoinduced electron transfer under intense light conditions. Adapted from Ref. (*133*).

III. Design Strategies and Building Blocks

In the second part of this contribution, we will demonstrate how the basic principles discussed above can be utilized as a starting point for creating artificial biomimetic and bioinspired catalytic and photosynthetic devices. At present, only very few examples of synthetic molecular systems, which are able to replace all important functional aspects of their native counterparts under mild and ambient conditions, have been described in the literature (*6*), including some important results of our own work. In the last sections of this review, several selected case studies from the author's research efforts in this direction will therefore be presented.

Here, we will also try to promote our own personal view on the possible roadmap to be followed for a rational development of such light-controlled photocatalytic systems (*3,5,8*). The first

important step is to analyze the structural and mechanistic details of the natural process to be copied as far as possible. Then, instead of trying to create a synthetic blueprint of all the molecular components involved, the next step should be to define the most fundamental functional requirements for a certain process and to find out, which photoreactive components could possibly fulfill the same kind of function in a more easily accessible way. It is important to note that such a bioinspired design strategy is not at all limited to the bioavailability of certain chemical elements or to the arsenal of biological ligands, which had defined the evolution of the natural systems.

Once a working model for a functional analogue has been identified and tested, available theoretical concepts can serve as a helpful guideline for optimizing the performance of the biomimetic compounds. This may include more detailed insights in multielectron reactivity, proton-coupled steps, conical intersections, stereoselectivity, and selection rule constraints including spin catalysis effects. At this stage of the development, the efficiency and selectivity of important mechanistic key steps of biological systems can already be directly compared with the photochemical reactions chosen to copy the same function. Long-term stability criteria, undesired side reactions, and the possibility of light-dependent regulation should be included in the considerations to optimize the synthetic compounds.

Finally, the best building blocks identified can be coupled in a modular way to complete photocatalytic reaction cycles, which then should be able to mimic a certain biological process. If these bioinspired photocatalytic systems are performing under identical conditions as their native counterparts, a direct comparison of quantitative criteria such as turnover frequencies and the total number of catalytic cycles is possible and should always be the final goal to demonstrate the potential usefulness of the biomimetic process.

A. Identifying Functional Analogies

Nature sometimes solves identical problems with apparently quite different solutions. Important examples of such a convergent evolution at the molecular level are the functional parallels between iron and copper centers in bioinorganic chemistry. The dioxygen-carrier proteins of different organisms may, for instance, be based on mononuclear iron tetrapyrrole complexes or in contrast may involve dinuclear copper sites *(10)*. Synthetic chemistry can even go a step further and try to mimic basic

biological functions with abiotic building blocks. It is therefore very important to identify and compare different types of molecular entities with an intrinsic functional relationship. Some instructive examples of such a possibility, which may become very useful for biomimetic photochemistry, are given below.

A.1. Two-electron redox relays

In many biocatalytic systems, the conversion of substrate molecules is accompanied by the transfer of two electrons and two protons. Several different types of organic ligands are able to assist such a catalytic exchange of multiple redox equivalents. They are either directly acting as electron and proton transfer cofactors or may be coordinated to a redox-active metal site. Typical examples in biological systems are quinone and hydrochinone couples which shuttle redox equivalents between different proteins or porphyrin and hydroporphyrin ligands acting as catalytic subunits in oxidoreductases.

Frequently, such systems undergo reversible structural distortions to better control the redox equilibria and to slow down undesired back reactions. Sometimes, even an irreversible reaction involving cofactor fragmentation is applied to completely shift the redox equilibrium into the desired direction. An important example in this context is the biocatalytic reactivity of α-keto acid-dependent iron enzymes (*134*), where the two-electron oxidation of ferrous active sites to form iron(IV) oxo species is assisted by a decarboxylation process of the coordinated carbonic acid in the presence of dioxygen. Interestingly, quite similar strategies to utilize the efficiency of irreversible processes and thus to better couple two consecutive one-electron radical reactions are well established in the field of inorganic photochemistry. The classical ferrioxalate system for chemical actinometry based on the irreversible LMCT-induced decomposition of iron-coordinated oxalato ligands (*135*) and the more recent development of sacrificial two-electron sensitizers for improving the sensitivity of silver halide photography should be mentioned in this context (*136*).

The employment of robust aromatic ligand architectures able to introduce the same kind of reactivity in a reversible manner is of course much more desirable. For this purpose, biological redox cofactors such as quinones, porphyrins, flavins, and their functional analogues in biomimetic chemistry contain a built-in butadiene-type moiety as part of their π-electron system, which can be considered as a minimum functional motif for assisting the reversible uptake of two electrons and two protons. This

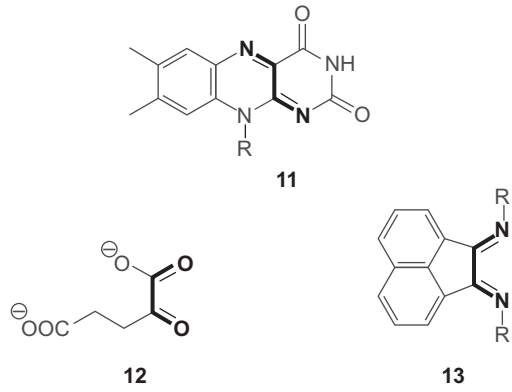

FIG. 16. Structures of different types of ligands acting as two-electron redox relays in natural and artificial systems: Flavins such as (**11**) are the essential constituents of flavodoxines and flavoproteins (*137*). The α-ketoglutarate anion (α-KG, **12**) is a typical example of a sacrificial redox mediator which decomposes during catalysis (*72*). Synthetic chelates such as bis-arylimino-acenaphthene (BIAN, **13**) have been proposed for the development of bio-inspired multielectron transfer photosensitizers (*138*).

property can also be exploited in photochemical model systems involving such types of ligands either directly or in the first or second coordination sphere of redox active metal centers. Some examples of natural and synthetic ligands that can undergo reversible or irreversible two-electron transformations are presented above (Fig. 16).

A.2. Hydride transfer shuttles

Several enzymes such as reductases and dehydrogenases utilize nicotinamide derivatives as reversible carriers of redox equivalents. The reduced dihydronicotinamide moiety NAD(P)H acts by donating a hydride equivalent to other molecules. In the corresponding two-electron oxidized $NAD(P)^+$ form, the cofactor formally accepts a hydride ion from the substrate. Functional models of such reversible hydride transfer processes are of considerable interest for biomimetic chemistry, and the strategies to regenerate nicotinamide-type cofactors are crucial for the performance of many organic transformations involving biocatalytic key steps (*139,140*).

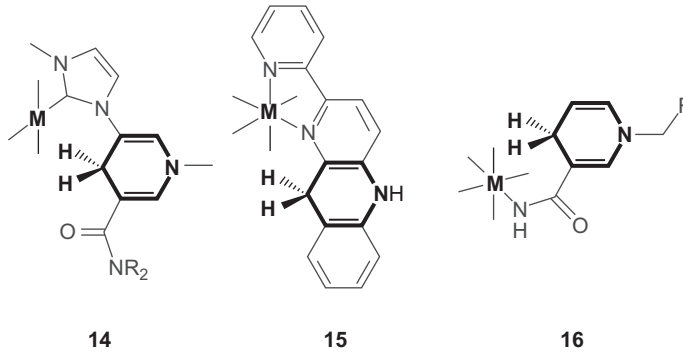

FIG. 17. Some examples of organic ligands acting as nicotinamide cofactor mimetics (*141–143*) with redox-active metals **M** bound to *N*-heterocyclic carbene (**14**), 1,2-diimine (**15**), and amide groups (**16**).

Efficient photochemical systems based on small molecular synthetic compounds with a ligand-based hydride transfer functionality in close proximity to a metal coordination site are still quite rare. In Fig. 17, some possible ligand architectures described in the recent literature are shown.

A.3. Carbon dioxide docking sites

Small carbon-containing molecules such as atmospheric CO_2 are considered to be important renewable feedstocks (*144,145*). In the context of mankind's increasing demand for carbon-based materials, food, and liquid fuels, the photocatalytic reduction of carbon dioxide under solar light irradiation is an attractive option. Such types of artificial photosynthetic processes could greatly enlarge the possibilities of abiotic CO_2 recycling.

To activate carbon dioxide for chemical reactions, it is advantageous to fix and destabilize this rather inert molecule. An important strategy to control and influence the reactivity of CO_2 is its coordination to amines, metal-bound imido moieties, or metal centers (*144*), which leads to a decrease of the CO bond order, while the molecule in most cases becomes considerably bent. In biochemical pathways, the CO_2 adduct of the coenzyme biotin (**17**) is involved in various carboxylation and transcarboxylation reactions (*146*). Similar structural motifs could become important functional building blocks for bioinspired photoreactions involving carbon dioxide activation steps (Fig. 18).

Bocarsly recently described the detailed mechanism of a very interesting photoelectrochemical process with a pyridinium-

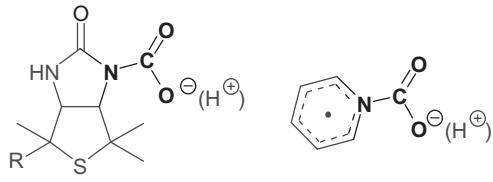

FIG. 18. Ligand architectures for coordinative carbon dioxide activation: structure of the biotin-CO_2 coenzyme (**17**) involved in many biological carboxylations (*146*). Proposed pyridinium-CO_2 adduct (**18**) accelerating electrocatalytic carbon dioxide reduction processes (*147*).

catalyzed multielectron reduction of carbon dioxide in aqueous solution (*147*). An inner-sphere electron transfer mechanism proceeding through coordinative interactions between pyridinium radicals and CO_2-derived species bound to the nitrogen atom of the aromatic heterocycle (**18**) is suggested. A systematic ligand design aiming at an inclusion of this kind of catalytically competent building block might become very advantageous for biomimetic photocatalysis and artificial photosynthetic carbon dioxide conversion.

A.4. Oxyl radical functionality

A widespread structural motif in many biocatalytic oxidations is the presence of electrophilic oxygen species and reactive oxyl radical species in close proximity to pre-organized substrate molecules. The most prominent example is the attachment of a Lewis acid-activated water molecule in the second coordination sphere of a high-valent manganese oxygen center, which is supposed to be involved in catalyzing the crucial first O-O bond formation step in natural oxygenic photosynthesis (*5,148,149*). Some monooxygenase enzymes including the versatile hemoprotein catalysts of the cytochrome P450 family (*3,150*) and the iron- or copper-based enzymes involved in the partial oxidation of methane to methanol are probably operating in a quite similar way (*151,152*). Also many other kinds of oxidoreductases rely on the intermediate generation of oxyl radicals to accelerate substrate conversion and to overcome rate limiting steps such as hydrogen abstraction in a controlled and efficient manner.

In earlier work (*3*), we have already pointed out the striking similarities of such electrophilic oxygen sites and biocatalytic oxyl radical reagents with the electronic structures and

reactivity patterns of certain excited state species. These analogies can be readily exploited for triggering the corresponding substrate transformations in biomimetic photocatalysis. A selection of different building blocks, which, however, can display a very similar chemical reactivity, is given in Fig. 19.

The functional equivalence between the CT excited states of certain metalloporphyrin photosensitizers carrying a high-valent metal-oxo moiety and the porphyrin radical intermediate supposed to be critically involved in cytochrome P450 oxidations has already been recognized several years ago (*155*). Indeed, the biological system and the biomimetic photocatalysts display very similar reactivity patterns. In their electronic ground state, the light-driven enzyme models could be readily characterized and studied (*3,155*). In contrast, despite decades of continuous efforts, a detailed spectroscopic characterization of the Fe(IV)-oxo-porphyrin cation radical thought to be the key intermediate in P450 catalysis has been absent for a long time (*153,156*).

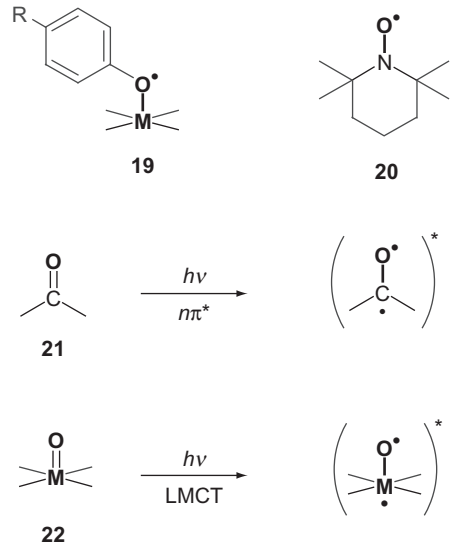

FIG. 19. Different ways to introduce oxyl radical reactivity: nature employs metal bound tyrosyl radicals (**19**) or high-valent metal oxo fragments in many active sites (*65,153*). Nitroxyl radicals such as 2,2,6,6,-tetramethylpiperidin-1-oxyl (TEMPO, **20**) are reactive species used in organocatalysis (*154*). The excited states of carbonyl functional groups (**21**) and metal oxo-fragments (**22**) display a radical pair character, which may become very attractive for biomimetic photoredox processes upon spectral sensitization (*3,5*).

From a mechanistic point of view, the cytochrome P450 enzymes are monooxygenases (*150*) and therefore they release one molecule of water in every catalytic turnover. As the oxygen atom of the formed H_2O molecule is originating from O_2 reduction, it has been tempting to exploit the fundamental principles of microscopic reversibility and detailed balancing (*157,158*), and to photochemically drive the catalytic reaction pathways in a reverse direction, thus resulting in a novel type of bioinspired water oxidation process. In fact, it could be shown that the biomimetic multielectron transfer photocatalysts described above are able to induce an OO bond formation at the metal-oxo site with water as the donor substrate (*111*). In this context, it is important to keep in mind that a quite similar mechanism at a single metal-oxo site has been proposed for the first step in photosynthetic water oxidation (*5,148*), which among other possible pathways becomes more and more plausible with the advent of the crystal structure of oxygen-evolving photosystem II at an atomic resolution (*149*).

B. Emerging Theoretical Frameworks

Once the required functional features for a certain substrate transformation have been defined, individual building blocks such as the structural motifs presented in the previous section have to be combined in a synergistic manner to create an operating photocatalytic system. The choice of suitable metal centers according to their relative atomic energy levels (*159*), and the fine-adjustment of the different components organized in the coordination sphere of the active site is a very crucial stage of development in biomimetic photochemistry. As already discussed before, a rough guideline for potentially useful combinations of the desired fragments can be derived from electrochemical and spectroscopic data, which may serve to predict the predominant orbital parentage and to estimate the relative energetic ordering of the lowest excited states (Fig. 6). When the first experiments at this stage of development have led to promising results, further optimization of such systems can be guided by an arsenal of emerging theoretical models and unifying concepts.

Interestingly, there is a current renaissance of classical bond-theoretical models which are able to illustrate the crucial molecular features of complex systems qualitatively by an interpretation of more or less localized fragment orbitals. Straightforward arguments based, for example, on fundamental aspects of ligand

field theory or on the interpretation of valence-bond state correlation diagrams turn out to be extremely useful for the discussion and prediction of reactivity patterns such as radical coupling mechanisms or bond-formation processes between nucleophilic and electrophilic species (*160,161*). Such types of easily generalized models are very important for the rational design of biomimetic photocatalytic systems, as they are able to directly connect the elementary reactions occurring between reactants, products, and CT excited states in an intuitive and pictorial way (*161*), which can help to adjust the critical reaction barriers as described already before (Fig. 11).

With the continuous development of theoretical and computational photochemistry (*162,163*), also the available quantitative tools for predicting light-induced reactivity are improving rapidly. It is impossible here to cover the immense progress made in this field comprehensively, and therefore, the reader is encouraged to consult and follow the relevant literature. As a starting point, we can only mention a few topics considered to be of prime interest for bioinorganic photosensitization and photocatalysis.

A lot of valuable information can now be derived from a detailed computational analysis of excited state potential energy hypersurfaces. This includes the location of areas where either an extended touching of two surfaces occurs or surface crossing regions such as funnels or conical intersections exist (*164,165*). Studying not only the minima of these crossing points but also a broader energetic region along the so-called extended conical intersection seam (*166*) allows to shape product distributions resulting from branching photochemical pathways, and it is quite clear now that nature makes extensive use of this possibility by exploiting control and selectivity effects induced by the protein environment.

The construction of valence-bond state correlation diagrams (*167*) is also a powerful tool for predicting and shaping critical barriers or describing reactivity patterns in homogeneous catalysis. This conceptual approach can be readily adopted for the field of bioinorganic photocatalysis, as low-lying CT excited states are frequently found to strongly mix with the critical transition states of bioinorganic reactions (*161,167*).

Another important trend already mentioned in previous sections is the increasing attention to angular momentum conservation and spin catalysis (Fig. 13). Attempts are now also made to find analogies between established semiempirical scales such as the spectrochemical and nephelauxetic series and local spin-philicity parameters included in calculations using spin-polarized conceptual DFT descriptors (*168*).

The requirement of spin conservation also seems to be controlling the rates of energy transfer processes, which is directly relevant for the field of bioinorganic and biomimetic photosensitization. Recently, it could be shown, for example, that spin effects can result in significant changes in the rate of Dexter transfer by up to two orders of magnitude at room temperature (*169*). Orbital-specific energy transfer in coordination compounds, occurring preferentially from excited states with a favorable dipole orientation, has also been documented (*170*). These findings especially should be considered for the optimization of all kinds of biomimetic and artificial photosynthetic systems based on polynuclear metal complexes.

Many other important theoretical concepts of paramount importance for biomimetic photochemistry are still in their infancy. This includes the strategies to mediate and accelerate proton-coupled single and multiple electron transfer catalysis (*171–173*), and the fundamental aspects of catalytic hydride transfer and hydrogen tunneling processes (*174–176*) among several others.

C. Photochemical Modeling of Key Steps

Various basic reaction sequences occurring in biological systems can actually be simulated and completely replaced by biomimetic model systems containing light-responsive metal complexes as their active components. Only a few illustrative examples of this strategy will be given below, which have been selected according to our own research interests.

C.1. Charge separation

The primary processes in natural photosynthesis involve the conversion of solar into electrochemical energy (*6,8*). Light absorption by antenna chromophores is followed by energy transfer to a reaction center, where the initial charge separation takes place. Enormous efforts have therefore been made by many research groups to create artificial photosynthetic reaction center models, which are able to integrate light-harvesting and PET properties in large and complex molecular assemblies (*177–179*). A main goal in this field had always been the formation and spectroscopic characterization of long-lived charge-separated states. Coupling of such systems to catalytic sites where multielectron redox processes can occur, however, was largely neglected. Nature has solved this crucial problem by

employing quinone cofactors as the primary electron acceptors in photosynthetic reaction centers, which helps to avoid unproductive charge-recombination processes (*180*).

From a functional point of view, this important property can be readily built into low molecular weight chromophore assemblies acting as artificial reaction centers (*8*). In simple coordination compounds, the population of CT states is directly related to the concept of light-induced charge separation in photosynthesis. Whenever such CT states are photoreactive and lead to the formation of the same kind of permanent redox products as observed in photosynthesis, the most essential features of the primary light reactions have been successfully duplicated. In a more strict sense, this is of course only true, if actinic red or NIR-light of comparable wavelength is absorbed by both the natural and artificial photosynthetic systems.

Biologically relevant electron acceptors such as quinones are able to act as redox-active chelate ligands (*181,182*). Frequently, a coordination of these cofactors leads to intensely colored metal complexes with low-lying CT excited states. With such types of inorganic chromophores, very simple functional model compounds for mimicking the charge separation cascade in photosynthetic reaction centers can be constructed. As an illustrative example (*181*), the organometallic rhenium complex **23** carrying a loosely coordinated 9,10-phenanthrene-quinone (PQ) moiety is presented here (Fig. 20). The deeply colored compound $[Re^{I}(PQ)(CO)_3Cl]$ contains a low-valent diamagnetic metal site which can replace the PET functionality of the primary donor of photosynthetic reaction centers, which usually consists of a special pair of chlorophyll pigments (*6*). At the same time, this compound carries a preorganized quinone cofactor, which can mimic the functional role of the rigidly orientated primary quinone acceptor Q_A present in the PS II-type reaction centers (*180*). The very simple biomimetic system **23** displays a broad and intense CT band in the visible and NIR-spectral region, which has been assigned as a MLCT transition (*181*). Interestingly, the maximum of this band at around 711 nm is almost coinciding with the NIR absorption features of the recently discovered cyanobacterial light-harvesting pigment chlorophyll *f*, which is now believed to represent nature's best choice to match the intrinsic threshold wavelength limits required for oxygenic photosynthesis (*95*).

C.2. Oxygen activation

Modeling the active site features and the mechanistic key steps occurring in biological dioxygen activation is one of the most

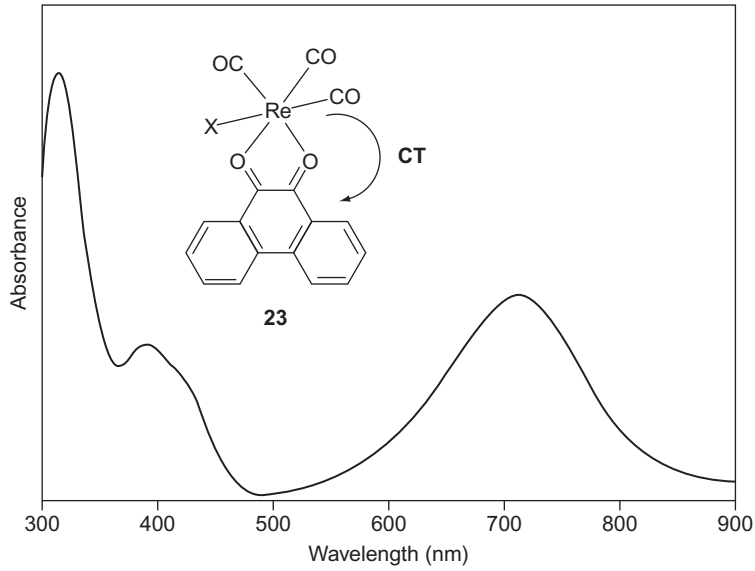

FIG. 20. Electronic spectrum of a rhenium(I) carbonyl complex (**23**) featuring an optical charge transfer transition at $\lambda_{max} = 711$ nm involving a coordinated quinone acceptor ligand *(181)*.

important topics in biomimetic chemistry *(183)*. Detailed knowledge about O_2 activation at metal sites opens the scene for highly selective bioinspired substrate conversions with novel types of redox catalysts. These properties are highly relevant for many environmentally benign technological processes using dioxygen molecules from ambient air as their only oxidant. The investigation of functional chemical models for critical reaction intermediates involved in bioinorganic redox processes of reactive oxygen species is therefore of prime interest for bioinorganic photochemistry.

Nature uses many different types of metalloproteins for the binding, transportation, and controlled activation of oxygen *(10,13)*. An extremely versatile catalyst system is present in the biochemistry of iron-containing heme enzymes (Fig. 21).

The reaction sequence at the heme active site starts with the binding of unactivated triplet dioxygen forming the so-called oxy–heme complexes. The iron center in O_2-activating heme enzymes is then thought to be converted into a peroxo anion species. It can be protonated to form a ferric hydroperoxo intermediate usually termed compound 0 *(183)*, which is a crucial reactive species in catalase and peroxidase enzyme catalysis (Fig. 21). These hydroperoxo intermediates of hemoproteins are important

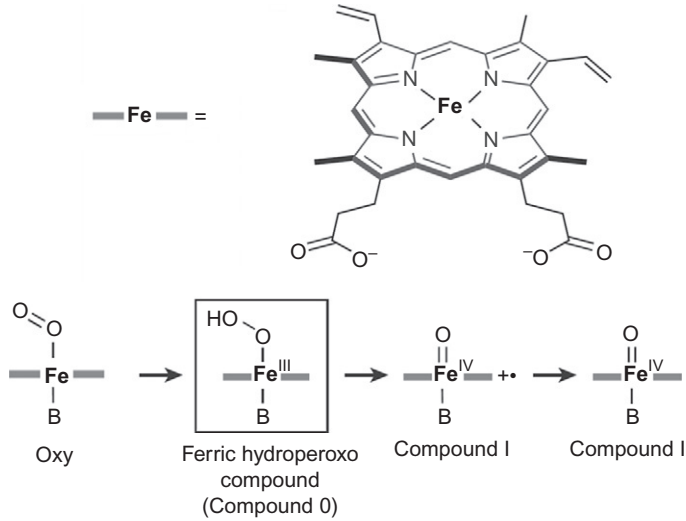

FIG. 21. Typical intermediates in hemoprotein enzyme active sites. The iron protoporphyrin IX cofactor (heme) forms dioxygen adducts termed oxy-species. In the course of oxygen activation and catalytic redox transformations, the oxy form can be consecutively converted into hydroperoxo- and oxo-type intermediates, which are usually referred to as compound 0, compound I, and compound II. Reproduced with permission from Ref. (*183*). Copyright Nature Publishing Group.

precursors for more highly oxidized iron–oxygen species which are formed in the course of an O-O bond cleavage process starting from compound 0. Among those powerful oxidizing catalyst species are the Fe(IV)-oxo-porphyrin cation radicals referred to as compound I (*156*), and the closely related compound II species (*183*), which are also acting as very versatile and strong oxidants (Fig. 21).

Although the knowledge about metal-mediated dioxygen binding and activation has grown immensely within the past decades, there are not many examples of functional biomimetic systems which are able to transfer O-atoms directly from dioxygen to substrate molecules (*184*). With only a few exceptions including some copper peroxo complexes (*185*), most of the reported model compounds and active species are only observable and functional at low temperature, which makes them quite impractical for synthetic oxidative transformations. Several years ago, we have therefore started to search for more robust photochemical model compounds that can be applied in biomimetic dioxygen activation and light-controlled substrate oxidations under ambient conditions (*155*).

For certain reasons described elsewhere in more detail (*8,93*), our first choice fell on the combination of tetrapyrrole photosensitizers including porphyrins or phthalocyanines with redox-active group 14 and group 15 elements such as tin, lead, antimony, or bismuth. Close relationships between the electronic structures of low-valent group 15 metalloporphyrins and the reduced heme groups of cytochrome P450 and chloroperoxidase enzymes had already been recognized before by a comparison of their absorption and magnetic circular dichroism spectra (*186*). Functional similarities with the hemoproteins were also reflected by the facts that the tin complex of protoporphyrin IX is able to act as an efficient competitive inhibitor of heme oxygenase (*187*), and that lead compounds are blocking the natural metallation process of protoporphyrin IX catalyzed by heme synthetase (*188*).

By studying the catalytic properties of a series of antimony(III) porphyrin complexes in the presence of dioxygen, it could be demonstrated that the reactivity of these compounds toward O_2 activation can be triggered and controlled by light activation (*155*). A metal centered sp-excited triplet state of the low-valent main group metal center has been identified to be responsible for this photoreactivity. The population of the dioxygen activating state can be spectrally sensitized by the coordinated porphyrin antenna chromophores, which allows the controlled generation of oxy- and hydroperoxo-metalloporphyrin species with long-wavelength visible light. It could also be shown that catalytic two-electron photoredox processes involving reactive metalloporphyrin species with a direct functional analogy to the hemoprotein compound 0 and compound I intermediates shown in Fig. 21 are involved in the substrate transformations catalyzed by these visible light-driven metalloenzyme models. These compounds, for example, display cytochrome P450 and chloroperoxidase-type reactivity under visible-light and solar irradiation (*3,155,189,190*).

More recently, we have continued to study this interesting kind of bioinspired photocatalysis and expanded our studies toward metallocorrole compounds (Fig. 22), as it is well established that these ring-contracted macrocycles tend to stabilize the formation of high-valent metal complexes (*192*). This strategy for the first time in tetrapyrrole chemistry opened the possibility to create high-valent lead(IV)- and bismuth(V)-oxo species as potential redox catalysts, which are currently investigated in our group (*191,193*). The molecular structures of the heme compound 0 and compound 1 analogous species **24** and **25** obtained in the course of biomimetic oxygen activation

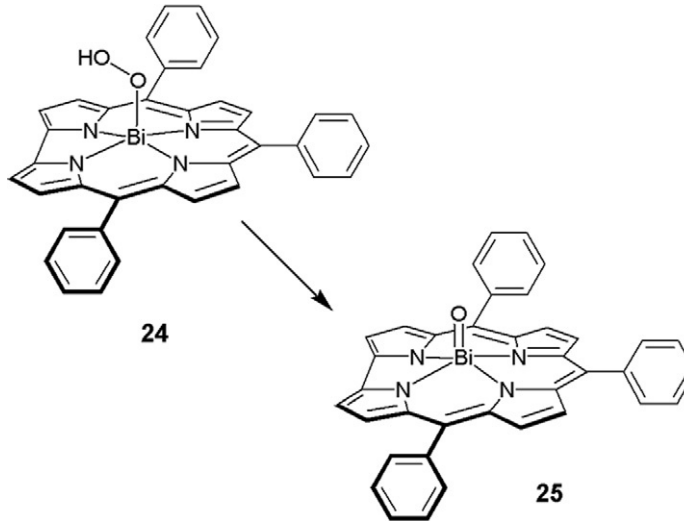

FIG. 22. Structures of hydroperoxo- and oxo-derivatives of bismuth triphenylcorrole photosensitizers (*191*).

photoreactions of the corresponding bismuth corrole catalysts are shown in Fig. 22 (*191*). In this context, it is very interesting to recall the CT properties of high-valent metal-oxo moieties (Fig. 19), which could proof to become very versatile tools for catalyzing the O-O bond formation step in bioinspired artificial photosynthetic water oxidation schemes (*111,193,194*).

C.3. Hydrogen atom transfer

Controlled radical reactivity and H-atom abstraction from substrates are common features of many metalloenzymes (*112,195*). Photochemical strategies can be successfully applied for modeling the biocatalytic transformations involving protein radicals (*3,196*). For example, one of the possibilities to achieve CH bond activation of inert compounds under mild and controlled reaction conditions is to create unpaired spin density at an oxygen atom accessible to the substrate, which should also be preorganized in the microenvironment of this active site. In bioinorganic photochemistry, this can be achieved by introducing oxyl-radical type photoreactivity in low-lying excited states as discussed in the previous sections (Fig. 19). The fundamental design criteria for such types of biomimetic systems based on multielectron transfer (MET) photosensitizers carrying terminal oxo-functionalities and radical-stabilizing cofactors have already been described in more detail elsewhere (*3,5*).

C.4. Release of bioactive molecules

The selective activation of compounds with potential therapeutic effects and the controlled delivery of bioactive molecules triggered by light are topics of intensely growing interest (*6,197–200*). Besides the search for light-sensitive prodrugs activated by photochemical cleavage, isomerization or photoredox processes (*201–203*), especially the release of small molecules such as NO, CO, CS_2, and H_2S, have attracted a lot of interest in the past years (*204–208*).

Inorganic photochemistry offers all the necessary tools required for the design and optimization of such systems. The typical reactivity patterns observed for photoexcited transition metal complexes can be readily exploited for the controlled delivery of therapeutically relevant compounds from physiologically inert precursor species. Such a process was for the first time described in the nineteenth century, when Haldane discovered by serendipity that the dioxygen binding activity of inactivated carboxy-hemoglobin (COHb) was regenerated by the rapid dissociation of CO upon exposure to sunlight (*209*). Today, the basic features of inducing this kind of reactivity are very well settled (*210,211*), and current research efforts can focus on the optimization of the required molecular properties such as bioavailability, solubility, drug-targeting strategies, and photoreactivity in the therapeutically reasonable spectral regions including the improvement of two-photon absorption cross sections or NIR-photosensitivity. The structures of two recent examples of a photoactivated NO-delivering transition metal complex sensitive to NIR light (**26**) and a water soluble organometallic compound (**27**) which was tested for the controlled photorelease of CO are shown in Fig. 23. Efforts in our own group currently focus on

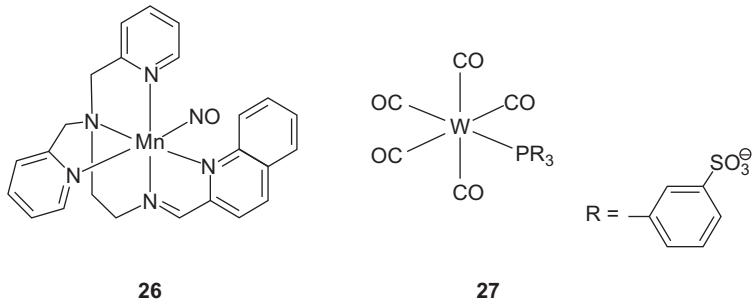

26 **27**

FIG. 23. Examples of photolabile nitrosyl (**26**) and carbonyl complexes (**27**) that have been suggested for the light-triggered release of nitric oxide (*212*) and carbon monoxide (*210*).

the sensitization of related CO-releasing molecules (CORMs) into the red and NIR spectral region to be able to better match the phototherapeutic window of mammalian tissue (*213*).

IV. Selected Applications

Despite the obvious versatility of light-activated key steps and their numerous advantages for the biomimetic modeling of natural systems, up to now, only very few examples are known, where such types of photosensitized processes have been successfully combined to complete reaction cycles with reasonable catalytic turnovers (*6*). In the last section, we are therefore briefly presenting two case studies which describe some recent work performed in our own group focusing on bioinspired catalytic systems that can be controlled and driven by visible light.

A. Toward Artificial Endonuclease Activity

Synthetic compounds able to induce selective damage or scission of DNA strands in a controlled fashion are of prime interest for molecular biology and genetic engineering and for the design of specific diagnostic or chemotherapeutic agents. Therefore, chemical nuclease mimics have actually been among the first examples of bioactive model compounds triggered by light (*214*). The interactions with DNA or nucleobases observed with most of these systems, however, are not operating in a catalytic way, and a reversible regulation of DNA strand cleavage activity with chemically modified restriction enzymes has only recently been reported (*215*). Natural endonucleases are acting as a kind of molecular scissors which can recognize short DNA sequences and cut the phosphodiester bonds of the double helix close to their target sites, which leads to a complete double-strand cleavage.

Several years ago, we have started to explore the possibilities of selective catalytic nucleic acid damage and light-triggered DNA cleavage with bioinspired metalloporphyrin photocatalyts (*216*). In this context, the cationic porphyrinato gold complex **28** shown in Fig. 24 was synthesized as a novel type of potentially tumor localizing electron transfer sensitizer. The choice of the high-valent central metal and the additional aromatic substituents was guided by several reasons. First of all, gold(III) porphyrins were already established as excellent electron acceptors, which should make their low-lying excited states

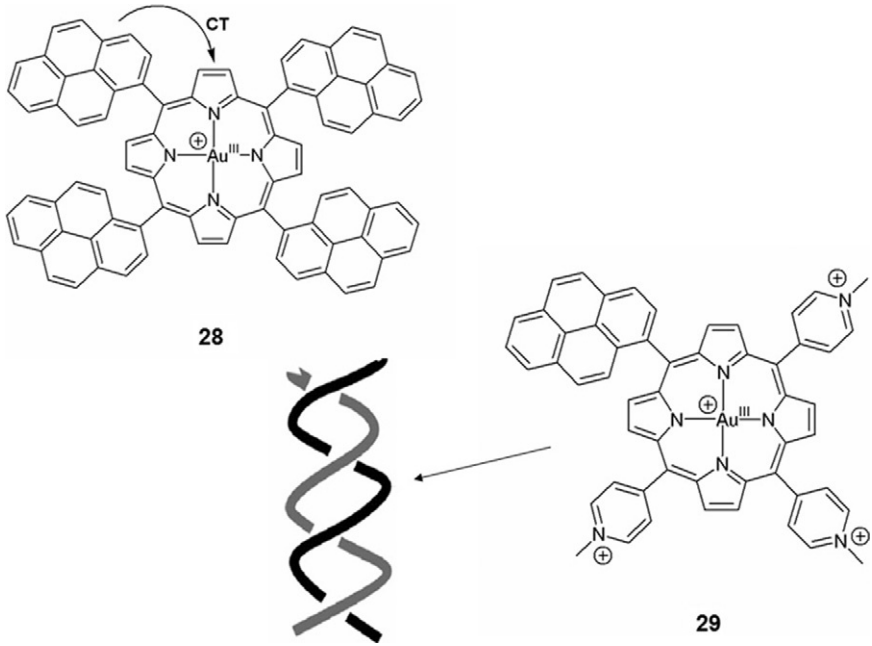

FIG. 24. Structures of cationic gold porphyrins which can bind to DNA and display photocatalytic nucleobase damage and double-strand cleavage controlled by visible light absorption (*216*,*217*).

well-suitable for an oxidative nucleobase damage involving PET steps. Further, we speculated about possible synergistic effects, as the biological activity of gold-based drug compounds had already been studied for more than one century (*218*). Indeed, it turned out in the mean time that gold porphyrin complexes depending on their detailed ligand structures display several promising *in vitro* properties, which seem to indicate a bright future as drug candidates for variety of therapeutic applications (*219*).

The attachment of the pyrenyl substituents in the ligand periphery of **28** was chosen to supply a functional domain that could act as an anchor group with a pronounced affinity for DNA binding and intercalation. This kind of functionalization of the gold(III) porphyrin core structure also introduced novel excited state levels, which led to the occurrence of additional intramolecular CT interactions (*216*). Thus, excitation of the complex **28** with visible light resulted in a direct optical electron transfer process generating a charge-separated state with a pyrenyl radical cation functionality in the molecule periphery and a reduced gold porphyrin center. The redox properties of this

excited state opened the possibility of a selective photodamage of the purine nucleobase guanine (G) under long-wavelength irradiation which should also operate well under hypoxic conditions. When **28** was irradiated in the presence of nucleobase substrates, a photocatalytic oxidative degradation of guanine could be demonstrated. A quantum yield of $\phi = 0.03$ measured for 436-nm photolysis and an initial turnover frequency of $\mathrm{TOF} = 66\ \mathrm{h}^{-1}$ was estimated for guanine degradation. At the same time, a maximum number of approximately 700 turnovers for each photosensitizer molecule was observed (*216*).

Despite these very interesting photocatalytic properties of the gold complex **28**, this compound still had several disadvantages such as moderate water solubility and the existence of atropisomeric mixtures under physiological conditions due to a hindered rotation of the pyrenyl substituents. Therefore, we decided to improve some crucial properties of the system and synthesized the novel gold(III)porphyrin complex **29** (*217*). This compound no longer can form isomeric mixtures and exhibits an excellent water solubility, while keeping one functional pyrenyl group attached. The presence of four positive charges leads to a modification of the possible electrostatic interactions with nucleic acids. Spectroscopic studies revealed that **29** interacts with A-DNA and B-DNA and displays outside binding with self-stacking to DNA duplexes. The modified gold(III) porphyrin sensitizer shows light-induced guanosine and 5′-dGMP oxidation under aerobic and anaerobic conditions. Light-triggered plasmid DNA nicking and photocatalytic double-strand cleavage of oligonucleotide duplex DNA are possible with this artificial photonuclease (*217*). Tumor cell line tests and related studies on other gold(III) tetrapyrrole photosensitizers including substituted corrole complexes are currently underway.

B. Light-Driven Model Enzymes in Catalysis

One of the most challenging areas in inorganic photochemistry is to catalyze the synthesis of valuable and energy-rich compounds from abundant raw materials and sunlight. In this context, the development of homogeneous photocatalysts which are able to completely replace the function of natural enzymes for synthetic applications is a highly desirable goal (*5,18*). As one of the rare examples of such a synthetic model photoenzyme system controlled and driven by visible light, we have chosen an artificial oxidoreductase catalyst investigated in our own group which has already been described in detail elsewhere (*3,6*).

The conception of this functional enzyme mimetic is based on a combination of several individual key steps already discussed in the previous sections. A closed photocatalytic reaction cycle in homogeneous solution could be successfully constructed by coupling a series of complementary functions including bioinspired dioxygen activation with photoexcited main group metals (Fig. 22), hydrogen atom abstraction, controlled formation of substrate radicals with photoactivated metal-oxo species (Fig. 19), and an efficient long-wavelength spectral sensitization of the catalytic system with tetrapyrrole macrocycles acting as robust antenna chromophores (Fig. 8).

The selective transformation of alcohols into carbonyl compounds with this kind of artificial oxidoreductases has been directly compared to a series of native enzymes performing under identical reaction conditions (*3*). In the dark-adapted form of the photocatalyst, which is a high-valent antimony porphyrin complex, the alcohol substrates are already preorganized by hydrogen bonds in the second coordination sphere of the active site. The system displays a certain extent of pH-controlled substrate selectivity, which makes competitive secondary reactions involving the reaction products less favorable. Substrate conversion can be completely switched off in the dark and is readily regulated by variations of light intensity. The system performs under very mild reaction conditions at room temperature and ambient pressure in aqueous solution utilizing dioxygen from air as a two-electron acceptor. Sunlight or even diffuse daylight with a threshold wavelength of approximately 600 nm is activating the catalyst for substrate conversion, which occurs at a rate of $k_{cat} = 0.05\ s^{-1}$ corresponding to a turnover frequency of $TOF = 180\ h^{-1}$ under AM = 2.0 solar irradiation conditions (*3*). A product formation quantum yield of $\Phi = 0.02$ has been determined for monochromatic visible light irradiation at 546 nm. Gradual degradation of the quite robust photocatalyst occurs with a quantum yield of $\Phi \leq 3 \times 10^{-5}$, which is in a typical stability range of natural tetrapyrrole pigments such as chlorophylls and corresponds to an average turnover number of at least 4000 productive photoredox cycles for each catalyst molecule.

The most significant and surprising result of this proof of principle study was the fact that even with such a simple MET photosensitizer system powered by sunlight, a very promising biomimetic performance with reaction rates up to three times higher than that of the natural metalloenzymes catalyzing exactly the same process in the absence of light could be achieved (*3,5*). Further systematic activities heading in this direction are therefore certainly worthwhile.

V. Concluding Remarks

Photoreactivity is a common feature of many components of biological systems and their synthetic functional counterparts. The important role of inorganic photochemistry and photocatalysis as a versatile tool for triggering, driving, and controlling molecular processes by light will therefore certainly be further increasing in the near future.

In this chapter, a unifying description of the most important bioinorganic chromophores and their light-induced properties has been provided. An attempt has been made to collect some general guidelines for the rational design of biomimetic and bioinspired systems based on photoreactive inorganic compounds, which are key constituents of artificial photosynthetic devices, functional enzyme mimetics, and light-sensitive reagents for the controlled release of physiologically active species. Processes based on this kind of photoresponsive molecules inspired by nature are of crucial relevance for many cross-disciplinary research fields and provide a solid foundation for numerous applications at the borderlines of chemistry, biology, and medicine (*5,6*). At present, however, there are only a few pioneering studies demonstrating the power of this novel approach, which have already supplied a convincing proof of principle for the fascinating new research fields of *bioinorganic photochemistry* and *biomimetic photocatalysis* founded about a decade ago (*3,8*). We hope that our current review will be able to stimulate further research efforts in this direction.

Besides novel frontiers in photosensitization and photocatalyis in the context of bioinorganic systems, the photophysics and photochemistry of inorganic materials also continues to be the central discipline in the field of solar energy conversion and renewable fuel production (*87,220*). One of the main future challenges in this direction will be the search for much more versatile types of photosensitizers with improved properties such as intrinsic multielectron reactivity and light-absorption characteristics optimized for solar chemistry. Finally, in the long run, the construction of more efficient systems for powering photocatalysis and artificial photosynthetic energy storage has to be achieved with sustainable, environmentally benign and earth-abundant building blocks (*220,221*). An example illustrating the suggested way to follow (*138*) is given below (Fig. 25).

The widely applied class of photosensitizers derived from the tris(2,2′-bipyridyl)ruthenium(II) cation $[Ru(bpy)_3]^{2+}$ (*101*) is based on one of the rarest metals on earth. Many high-valent compounds of the platinum group metal ruthenium are further

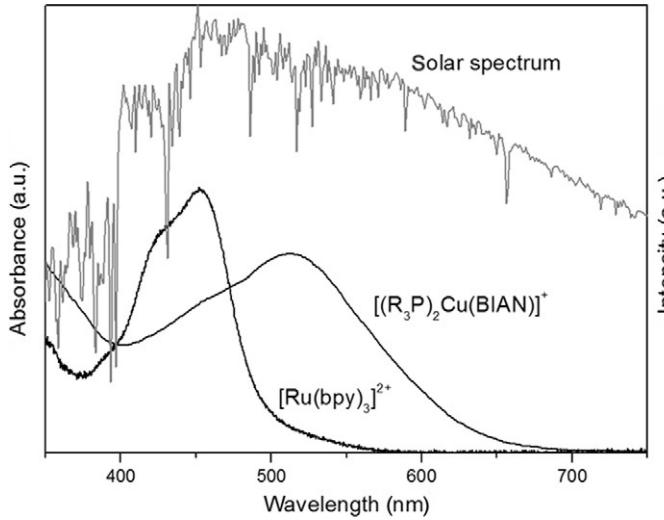

FIG. 25. Comparison of the sunlight harvesting features of tris(2,2′-bipyridyl)ruthenium (**9**) and a copper-based multielectron transfer photosensitizer *(138)* carrying a π-acceptor ligand of the BIAN-type (**13**) already described in Fig. 16.

regarded as toxic or carcinogenic, and reactions involving ruthenium complexes should therefore be considered at least as environmentally problematical. Moreover, $[Ru(bpy)_3]^{2+}$ derivatives absorb only a limited share of the photochemically relevant region of the solar spectrum, and the photoinduced primary processes of such compounds are typically limited to one electron chemistry, which requires further coupling to other redox-active components acting as mediators for multielectron transformations *(173)*.

In contrast, bioinspired compounds such as the copper diimine complex shown in Fig. 25 have been suggested as a versatile and readily tunable alternative to conventional sensitizers used today for various photocatalytic applications, artificial photosynthetic devices, and dye-sensitized solar cells *(138)*. It combines some of the highly desirable features such as long-wavelength absorption well adapted to the solar spectrum and intramolecular coupling of the low-lying excited states to an acceptor ligand providing a preponderance for multielectron reactivity. Further, the compound exclusively consists of abundant and environmentally benign building blocks including a biocompatible redox-active transition metal.

The current state of the art in inorganic photochemistry already offers a large number of possibilities for the development of such alternative approaches. Additional inspiration from natural systems collected in the novel field of bioinorganic photochemistry will certainly lead to further valuable input in this direction. Many other important aspects of biological systems such as the development of self-repair mechanisms to assure a prolonged catalyst lifetime or the control of the microenvironment of active sites by second coordination sphere interactions should also be considered to create robust, selective, and environmentally benign photosensitizers and photocatalysts (*3,5*).

One of the most fascinating aspects of the photochemical approaches in biomimetic chemistry presented in this review is that abiotic reagents are able to accelerate the same overall reactions as biocatalysts in a very promising way. This type of chemistry might even allow to develop systems "realizing processes that enzymes do not perform while displaying comparable high efficiencies and selectivities" (*222*). In the context of artificial photosynthesis and solar fuel production, scientists are now collaborating to find out if they can "beat nature at her own game" (*223*). Bioinorganic photochemistry has already set the stage for this demanding goal, and we are looking forward to the photochemistry of the future (*224*).

Acknowledgments

The Austrian Science Fund (FWF project P21045: "Bioinspired Multielectron Transfer Photosensitizers" and ERA Chemistry project I316: "Selective Photocatalytic Hydroxylation of Inert Hydrocarbons") is gratefully acknowledged. G. K. also thanks the German Research Foundation (DFG Graduate College 640 "Sensory Photoreceptors in Natural and Artificial Systems" and GRK1626 "Chemical Photocatalysis") for partial support of this work.

References

1. Balzani, V.; Bergamini, G.; Campagna, S.; Puntoriero, F. *Top. Curr. Chem.* **2007,** *280*, 1, and refs therein.
2. Haga, M.-a.; Ishitani, O.; Kitamura, N. *Coord. Chem. Rev.* **2010,** *254*, 2477.
3. Knör, G. *ChemBioChem* **2001,** *2*, 593.
4. Szaciłowski, K.; Macyk, W.; Drzewiecka-Matuszek, A.; Brindell, M.; Stochel, G. *Chem. Rev.* **2005,** *105*, 2647.

5. Knör, G. *Chem. Eur. J.* **2009,** *15*, 568.
6. Stochel, G.; Brindell, M.; Macyk, W.; Stasicka, Z.; Szaciłowski, K. *Bioinorganic Photochemistry*. Wiley: Chichester, **2009**.
7. Braslavsky, S. E. *Pure Appl. Chem.* **2007,** *79*, 293.
8. Knör, G. *Coord. Chem. Rev.* **1998,** *171*, 61, p. 68.
9. Beinert, H. *J. Biol. Chem.* **2002,** *277*, 37967.
10. Bertini, I., Gray, H. B., Stiefel, E. I., Valentine, J. S., Eds.; Biological Inorganic Chemistry: Structure and Reactivity. University Science Books: Sausalito, **2007**.
11. Jaouen, G. In: "*Bioorganometallics: Biomolecules, Labeling, Medicine*"; Wiley-VCH: Weinheim, **2006**.
12. Jernigan, R.; Raghunathan, G.; Bahar, I. *Curr. Opin. Struct. Biol.* **1994,** *7*, 256.
13. Reedijk, J.; Bouwman, E. *Bioinorganic Catalysis.* Marcel Dekker: New York, **1999**.
14. Holm, R. H.; Kennepohl, P.; Solomon, E. I. *Chem. Rev.* **1996,** *96*, 2239.
15. Degtyarenko, K. *Bioinformatics Rev.* **2000,** *16*, 851.
16. Breslow, R. *J. Biol. Chem.* **2009,** *284*, 1337, and refs therein.
17. Klotz, I. M.; Royer, G. P.; Scarpa, I. S. *Proc. Natl. Acad. Sci. USA* **1971,** *68*, 263.
18. Kirby, A. J.; Hollfelder, F. *From Enzyme Models to Model Enzymes*. RSC Publishing: Cambridge, **2009**.
19. Riley, D. P. *Chem. Rev.* **1999,** *99*, 2573.
20. Salvemini, D.; Wang, Z. Q.; Zweier, J. L.; Samouilov, A.; Macarthur, H.; Misko, T. P.; Currie, M. G.; Cuzzocrea, S.; Sikorski, J. A.; Riley, D. P. *Science* **1999,** *286*, 304.
21. von Grotthuss, T. *Ann. Phys.* **1819,** *61*, 50.
22. Sancar, A. *Annu. Rev. Biochem.* **2000,** *69*, 31.
23. van der Horst, M. A.; Hellingwerf, K. *Acc. Chem. Res.* **2004,** *37*, 13.
24. Meech, S. R. *Chem. Soc. Rev.* **2009,** *38*, 2922.
25. Kirschenbaum, D. M., Ed.; Bibliographic Atlas of Protein Spectra in the Ultraviolet and Visible Regions. Plenum: New York, **1983**.
26. Lever, A. B. P., Gray, H.B., Eds.; Iron Porphyrins. Addison Wesley: Reading, **1982**.
27. Bertini, I.; Cavallaro, G.; Rosato, A. *Chem. Rev.* **2006,** *106*, 90.
28. Belevich, I.; Verkhovsky, M. I.; Wilkström, M. *Nature* **2006,** *440*, 829, and refs therein.
29. Bishop, N. A.; Lu, T.; Yankner, B. A. *Nature* **2010,** *464*, 529, and refs therein.
30. Morita, S.; Olson, J. M.; Conto, S. F. *Arch. Biochem. Biophys.* **1964,** *104*, 346.
31. Widdel, F.; Schnell, S.; Heising, S.; Ehrenreich, A.; Assmus, B.; Schink, B. *Nature* **1993,** *362*, 834.
32. Heising, S.; Schink, B. *Microbiology* **1998,** *144*, 2263.
33. Karu, T. I.; Pyatibrat, L. V.; Afanasyeva, L. I. *Photochem. Photobiol.* **2004,** *80*, 366.
34. Erdle, B. J.; Brouxhon, S.; Kaplan, M.; van Buskirk, J.; Pentland, A. P. *Dermatol. Surg.* **2008,** *34*, 320.
35. Brown, G. C. *Biochem. Biophys. Acta* **1999,** *1411*, 351.
36. Sarti, P.; Giuffré, A.; Forte, E.; Mastronicola, D.; Barone, M. C.; Brunori, M. *Biochem. Biophys. Res. Commun.* **2000,** *34*, 320.
37. Bogdanov, A. M.; Mishin, A. S.; Yampolsky, I. V.; Belousov, V. V.; Chudakov, D. M.; Subach, F. V.; Verkhusha, V. V.; Lukyanov, S.; Lukyanov, K. A. *Nat. Chem. Biol.* **2009,** *5*, 459.

38. Lukyanov, K. A.; Serebrovskaya, E. O.; Lukyanov, S.; Chudakov, D. M. *Photochem. Photobiol. Sci.* **2010,** *9*, 1301.
39. Begley, T. P. *Acc. Chem. Res.* **1994,** *27*, 394.
40. Guskov, A.; Gabdulkhakov, A.; Broser, M.; Glöckner, C.; Hellmich, J.; Kern, J.; Frank, J.; Müh, F.; Saenger, W.; Zouni, A. *Chem. Phys. Chem.* **2010,** *11*, 1160.
41. Aubailly, M.; Haigle, J.; Giordani, A.; Morlière, P.; Santus, R. *J. Photochem. Photobiol. B* **2000,** *56*, 61.
42. Neves-Petersen, M. T.; Klitgaard, S.; Leitão Carvalho, A. S.; Petersen, S. B.; AiresdeBarro, M. R.; PinhoeMelo, E. *Biophys. J.* **2007,** *92*, 2016.
43. Lyon, E. J.; Shima, S.; Buurman, G.; Chowdhuri, S.; Batschauer, A.; Steinbach, K.; Thauer, R. K. *Eur. J. Biochem.* **2004,** *271*, 195.
44. Jarrett, J. T.; Drennan, C. L.; Amaratunga, M.; Scholten, J. D.; Ludwig, M. L.; Matthews, R. G. *Bioorg. Med. Chem.* **1996,** *4*, 1237.
45. Herrero, A.; Flores, E.; Guerrero, M. G. *Arch. Biochem. Biophys.* **1984,** *234*, 454.
46. Estabrook, R. W.; Cooper, D. Y.; Rosenthal, O. *Biochem. Z.* **1963,** *388*, 741.
47. Karu, T. I.; Afanasyeva, N. I. *Dokl. Akad. Nauk. (Moscow)* **1995,** *342*, 693.
48. Endo, I.; Okada, M.; Yohda, M. *Trends Biotechnol.* **1999,** *17*, 244.
49. Robertson, W. D.; Warnecke, K. *Biochemistry* **2009,** *48*, 140.
50. Olson, K. D.; McMahon, C. W.; Wolfe, R. S. *Proc. Natl. Acad. Sci. USA* **1991,** *88*, 4099.
51. Mikkelsen, R. B.; Tang, D. H.; Triplett, E. L. *Biochem. Biophys. Res. Commun.* **1975,** *63*, 980.
52. Schürmann, P.; Buchanan, B. B. *Antioxid. Redox Signal.* **2008,** *10*, 1235.
53. DeTullio, M. C.; Ciarci, S.; Liso, R.; Arrigoni, O. *J. Plant. Physiol.* **2007,** *164*, 39.
54. Tai, L. A.; Hwang, K. C. *Photochem. Photobiol.* **2001,** *73*, 439.
55. Zhu, Z.; Davidson, V. L. *Biochim. Biophys. Acta* **1998,** *1364*, 297.
56. Vogler, A.; Kunkely, H. *Top. Curr. Chem.* **2001,** *213*, 143.
57. Solomon, E. I.; Hanson, M. A. In: "*Inorganic Electronic Structure and Spectroscopy, Vol. II*"; Eds. Lever, A. B. P.; Solomon, E. I.; Wiley: New York, **1999**.
58. Xiao, Z.; Lavery, M. J.; Ayhan, M.; Scrofani, S. D. B.; Wilce, M. C. J.; Guss, J. M.; Tregloan, P. A.; George, G. N.; Wedd, A. G. *J. Am. Chem. Soc.* **1998,** *120*, 4135.
59. Hanson, L. K.; Eaton, W. A.; Sligar, S. G.; Gunsalus, I. C.; Gouterman, M.; Connell, C. R. *J. Am. Chem. Soc.* **1976,** *98*, 2672.
60. Thomä, N. H.; Meier, T. W.; Evans, P. R.; Leadlay, P. F. *Biochemistry* **1998,** *37*, 4135.
61. Friedmann, H. C.; Klein, A.; Thauer, R. K. *FEMS Microbiol. Rev.* **1990,** *87*, 339.
62. Bossa, M.; Morpurgo, G. O.; Morpurgo, L. *Biochemistry* **1994,** *33*, 4425.
63. Huque, Y.; Fieschi, F.; Torrents, E.; Gibert, I.; Eliasson, R.; Reichard, P.; Sahlin, M.; Sjöberg, B.-M. *J. Biol. Chem.* **2000,** *275*, 25365.
64. Cotruvo, J. A.; Stubbe, J. *Biochemistry* **2010,** *49*, 1297.
65. Whittaker, J. W.; Whittaker, M. M. *Pure Appl. Chem.* **1998,** *70*, 903.
66. Loehr, J. S.; Loehr, T. M.; Mauk, A. G.; Gray, H. B. *J. Am. Chem. Soc.* **1980,** *102*, 6992.
67. Payne, M. S.; Wu, S.; Fallon, R. D.; Tudor, G.; Stieglitz, B.; Turner, I. M.; Jr., Nelson, M. J. *Biochemistry* **1997,** *36*, 5447.

68. Pantoliano, M. W.; Valentine, J. S.; Nafie, L. A. *J. Am. Chem. Soc.* **1982,** *104*, 6310.
69. Gamelin, D. R.; Randall, D. W.; Hay, M. T.; Houser, R. P.; Mulder, T. C.; Canters, G. W.; de Vries, S.; Tolman, W. B.; Lu, Y.; Solomon, E. I. *J. Am. Chem. Soc.* **1998,** *120*, 5246.
70. Boussac, A.; Sugiura, M.; Kirilovsky, D.; Rutherford, W. A. *Plant Cell Physiol.* **2005,** *46*, 837 and refs therein.
71. Pavel, E. G.; Zhou, J.; Busby, R. W.; Gunsior, M.; Townsend, C. A.; Solomon, E. I. *J. Am. Chem. Soc.* **1998,** *120*, 743.
72. Ryle, M. J.; Padmakumar, R.; Hausinger, R. P. *Biochemistry* **1999,** *38*, 15278.
73. Piskorski, R.; Jaun, B. *J. Am. Chem. Soc.* **2003,** *125*, 13120.
74. Renirie, R.; Hemrika, W.; Piersma, S. R.; Wever, R. *Biochemistry* **2000,** *39*, 1133.
75. Barnese, K.; Sheng, Y.; Stich, T. A.; Gralla, E. B.; Britt, R. D.; Cabelli, D. E.; Valentine, J. S. *J. Am. Chem. Soc.* **2010,** *132*, 12525.
76. Sugiura, Y.; Kawabe, H.; Tanaka, H. *J. Am. Chem. Soc.* **1980,** *102*, 6581.
77. Almendra, M. J.; Brondino, C. D.; Gavel, O.; Pereira, A. S.; Tavares, P.; Bursakov, S.; Duarte, R.; Caldeira, J.; Moura, J. J. G.; Moura, I. *Biochemistry* **1999,** *38*, 16366.
78. Coulter, E. D.; Kurtz, D. M. *Arch. Biochem. Biophys.* **2001,** *394*, 76.
79. Cox, D. D.; Benkovic, S. J.; Bloom, L. M.; Bradley, F. C.; Nelson, M. J.; Que, L.; Jr., Wallick, D. E. *J. Am. Chem. Soc.* **1988,** *110*, 2026.
80. Katayama, Y.; Hashimoto, K.; Nakayama, H.; Mino, H.; Nojiri, M.; Ono, T.-a.; Nyunoya, H.; Yohda, M.; Takio, K.; Odaka, M. *J. Am. Chem. Soc.* **2006,** *128*, 728.
81. Lancaster, K. M.; DeBeer George, S.; Yokoyama, K.; Richards, J. H.; Gray, H. B. *Nat. Chem.* **2009,** *1*, 711 and refs therein.
82. Dooley, D. M.; Dawson, J. H.; Gray, H. B. *Biochemistry* **1981,** *20*, 2024.
83. Benson, N.; Farrar, J. A.; McEwan, A. G.; Thomson, A. J. *FEBS Lett.* **1992,** *307*, 169.
84. Stewart, L. J.; Bailey, S.; Bennett, B.; Charnock, J. M.; Garner, C. D.; McAlpine, A. S. *J. Mol. Biol.* **2000,** *299*, 593.
85. Vogel, H. *Ber. Chem. Ges.* **1873,** 1305.
86. Gerischer, H. *Photochem. Photobiol.* **1972,** *16*, 243.
87. Kalyanasundaram, K.; Graetzel, M. *Curr. Opin. Biotechnol.* **2010,** *21*, 298.
88. von Tappeiner, H.; Raab, O. *Münch. Med. Wochenschr.* **1900,** *47*, 5.
89. Nagy, E. M.; Via, L. D.; Ronconi, L.; Fregona, D. *Curr. Pharmaceut. Des.* **2010,** *16*, 1832, and refs therein.
90. Narayanam, J. M. R.; Stephenson, C. R. J. *Chem. Soc. Rev.* **2011,** *40*, 102.
91. Darwent, J.; Douglas, P.; Harriman, A.; Porter, G.; Richoux, M.-C. *Coord. Chem. Rev.* **1982,** *44*, 83.
92. Miyatake, T.; Tamiaki, H. *Coord. Chem. Rev.* **2010,** *254*, 2593.
93. Knör, G. *Inorg. Chem.* **1996,** *35*, 7916.
94. Lukas, A. S.; Zhao, Y.; Miller, S. E.; Wasielewski, M. R. *J. Phys. Chem. B* **2002,** *106*, 1299.
95. Chen, M.; Schliep, M.; Willows, R. D.; Cai, Z.-L.; Neilan, B. A.; Scheer, H. *Science* **2010,** *329*, 1318.
96. Scharf, H.-D.; Fleischauer, J.; Leismann, H.; Ressler, I.; Schleker, W.; Weitz, W. *Angew. Chem. Int. Ed. Eng.* **1979,** *18*, 652.
97. McDaniel, N. D.; Bernhard, S. *Dalton Trans.* **2010,** *39*, 10021.

98. Schönberg, A.; Schenck, G. O.; Neumüller, O.-A. *Preparative Organic Photochemistry*. Springer: New York, **1968**, p. 559.
99. Vogler, A.; Adamson, A. W. *J. Am. Chem. Soc.* **1968,** *90*, 5943.
100. Vogler, A. *Z. Naturforsch.* **1970,** *25*, 1069.
101. Adamson, A. W.; Demas, J. N. *J. Am. Chem. Soc.* **1971,** *93*, 1800.
102. Gafney, H. D.; Adamson, A. W. *J. Am. Chem. Soc* **1972,** *94*, 8238.
103. Juris, A.; Balzani, V.; Barigelletti, F.; Campagna, S.; Belser, P.; von Zelewsky, A. *Coord. Chem. Rev.* **1988,** *84*, 85.
104. Ivan, J.; Dmochowski, I. J.; Crane, B. R.; Wilker, J. J.; Winkler, J. R.; Gray, H. B. *Proc. Natl. Acad. Sci. USA* **1999,** *96*, 12987.
105. Kuo, C.-H.; Fruk, L.; Niemeyer, C. M. *Chem. Asian J.* **2009,** *4*, 1064.
106. Duan, L.; Xu, Y.; Zhang, P.; Wang, M.; Sun, L. *Inorg. Chem.* **2009,** *49*, 209.
107. Streich, D.; Astuti, Y.; Orlandi, M.; Schwartz, L.; Lomoth, R.; Hammarström, L.; Ott, S. *Chem. Eur. J.* **2010,** *16*, 60.
108. Tucker, J. W.; Nguyen, J. D.; Narayanam, J. M. R.; Krabbe, S. W.; Stephenson, C. R. J. *Chem. Commun.* **2010,** *46*, 4985.
109. Jakubikova, E.; Martin, R. L.; Batista, E. R. *Inorg. Chem.* **2010,** *49*, 2975.
110. Immoos, C. E.; Di Bilio, A. J.; Cohen, M. S.; Van der Veer, W.; Gray, H. B.; Farmer, P. J. *Inorg. Chem.* **2004,** *43*, 3593.
111. Knör, G.; Vogler, A.; Roffia, S.; Paolucci, F.; Balzani, V. *Chem. Commun.* **1996,** 1643.
112. Stubbe, J.; van der Donk, W. A. *Chem. Rev.* **1998,** *98*, 705.
113. Hammond, G. S. *J. Am. Chem. Soc.* **1955,** *77*, 334.
114. Caldin, E. F. *The Mechanisms of Fast Reactions in Solution*. IOS Press: Amsterdam, **2001**, p. 278.
115. Kirby, A. J. *Acc. Chem. Res.* **1997,** *30*, 290.
116. Brzezinski, P. *Biochim. Biophys. Acta Bioenerg.* **2000,** *1458*, 1.
117. Förster, T. *Naturwissenschaften* **1949,** *36*, 186.
118. Youvan, D. C.; Michel-Beyerle, M. E. *Nat. Biotechnol.* **1996,** *14*, 1219.
119. Grabowski, Z. R.; Rubaszewska, W. *J. Chem. Soc. Faraday Trans. 1* **1977,** *73*, 11.
120. Zambrana, J. L.; Jr., Ferloni, E. X.; Gafney, H. D. *J. Phys. Chem. A* **2009,** *113*, 13457.
121. Poli, R. *J. Organomet. Chem.* **2004,** *689*, 4291.
122. Minaev, B. F. *Russ. Chem. Rev.* **2007,** *76*, 988.
123. Fukuzumi, S.; Itoh, S. *Adv. Photochem.* **1999,** *25*, 107.
124. Janaway, G. A.; Braumann, J. I. *J. Phys. Chem. A* **2000,** *104*, 1795, and refs therein.
125. Buchachenko, A. L.; Berdinsky, V. L. *Chem. Rev.* **2002,** *102*, 603.
126. Poli, R.; Harvey, J. N. *Chem. Soc. Rev.* **2003,** *32*, 1.
127. Buchachenko, V. L.; Berdinsky, V. L. *Russ. Chem. Rev.* **2004,** *73*, 1033.
128. Daniel, C. *Top. Curr. Chem.* **2004,** *241*, 119.
129. Vlček, A. Jr., *Top. Organomet. Chem.* **2010,** *29*, 73.
130. Goeldner, M.; Givens, R. *Dynamic Studies in Biology: Phototriggers, Photoswitches and Caged Biomolecules*. Wiley-VCH: Weinheim, **2005**.
131. Bochet, C. G.; Blanc, A. In: "*Handbook of Synthetic Photochemistry*"; Eds. Albini, A.; Fagnoni, M.; Wiley-VCH: Weinheim, **2010**.
132. Irie, M. *Chem. Rev.* **2000,** *100*, 1683.
133. Straight, S. D.; Kodis, G.; Terazono, Y.; Hambourger, M.; Moore, T. A.; Moore, A. L.; Gust, D. *Nat. Nanotechnol.* **2008,** *3*, 280.
134. Solomon, E. I.; Decker, A.; Lehnert, N. *Proc. Natl. Acad. Sci. USA* **2003,** *100*, 3589.

135. Hatchard, C. G.; Parker, C. A. *Proc. R. Soc. Lond. Ser. A* **1956,** *235A*, 518.
136. Gould, I. R.; Lenhard, J. R.; Muenter, A. A.; Godleski, S. A.; Farid, S. *J. Am. Chem. Soc.* **2000,** *122*, 11934.
137. Kaim, W.; Schwederski, B.; Heilmann, O.; Hornung, F. M. *Coord. Chem. Rev.* **1999,** *182*, 323.
138. Kern, T.; Monkowius, U.; Zabel, M.; Knör, G. *Eur. J. Inorg. Chem.* **2010,** 4148.
139. Hollmann, F.; Arends, I. W. C. E.; Buehler, K. *ChemCatChem* **2010,** *2*, 762.
140. Berenguer-Mucia, A.; Fernandez-Lafuente, R. *Curr. Org. Chem.* **2010,** *14*, 1000.
141. McSkimming, A.; Bhadbhade, M.; Colbran, S. B. *Dalton Trans.* **2010,** *39*, 10581.
142. Fukushima, T.; Fujita, E.; Muckerman, J. T.; Polyansky, D. E.; Wada, T.; Tanaka, K. *Inorg. Chem.* **2009,** *48*, 11510.
143. Matsubara, Y.; Koga, K.; Kobayashi, A.; Konno, H.; Sakamoto, K.; Morimoto, T.; Ishitani, O. *J. Am. Chem. Soc.* **2010,** *132*, 10547.
144. Aresta, M. In: "*Activation of Small Molecules: Organometallic and Bioinorganic Perspectives*"; Ed. Tolman, W. B.; Wiley-VCH: Weinheim, **2006**.
145. Aresta, M. In: "*Carbon Dioxide as Chemical Feedstock*"; Wiley-VCH: Weinheim, **2010**.
146. Knappe, J. *Annu. Rev. Biochem.* **1970,** *39*, 757.
147. Cole, E. B.; Lakkaraju, P. S.; Rampulla, D. M.; Morris, A. J.; Abelev, E.; Bocarsly, A. B. *J. Am. Chem. Soc.* **2010,** *132*, 11539.
148. Brudvig, G. *Coord. Chem. Rev.* **2008,** *252*, 231, and refs therein.
149. Umena, Y.; Kawakami, K.; Shen, J.-R.; Kamiya, N. *Nature* **2011,** *473*, 55.
150. de Montellano, P. R. O. Ed.; Cytochrome P450: Structure, Mechanism and Biochemistry. Kluwer: New York, **2005**.
151. Xue, G.; De Hont, R.; Münck, E.; Que, L.Jr., *Nat. Chem.* **2010,** *2*, 400.
152. Balasubramanian, R.; Smith, S. M.; Rawat, S.; Yatsunyk, L. A.; Stemmler, T. L.; Rosenzweig, A. *Nature* **2010,** *465*, 115.
153. Rittle, J.; Green, M. T. *Science* **2010,** *330*, 933.
154. Tromp, S. A.; Matijošyte, I.; Sheldon, R. A.; Arends, I. W. C. E.; Mul, G.; Kreutzer, M. T.; Moulijn, J. A.; de Vries, S. *ChemCatChem* **2010,** *2*, 827.
155. Knör, G.; Vogler, A. *Inorg. Chem.* **1994,** *33*, 314.
156. Sligar, S. G. *Science* **2010,** *330*, 924.
157. Tolman, R. C. *Proc. Natl. Acad. Sci. USA* **1925,** *11*, 436.
158. Gold, V.; Loening, K. L.; McNaught, A. D.; Shemi, P. *IUPAC Compendium of Chemical Terminology.* (2nd edn.). Blackwell Science: Oxford, **1997** (1994, 66, 1105).
159. http://physics.nist.gov/PhysRefData/ASD/levels_form.htm.
160. Betley, T. A.; Surendranath, Y.; Childress, M. V.; Alliger, G. E.; Fu, R.; Cummins, C. C.; Nocera, D. G. *Philos. Trans. R. Soc. Lond. B Biol. Sci.* **2008,** *363*, 1293.
161. Shaik, S.; Lai, W.; Chen, H.; Wang, Y. *Acc. Chem. Res.* **2010,** *43*, 1154.
162. Olivucci, M. Ed.; Computational Photochemistry. Elsevier: Amsterdam, **2005**.
163. Kutateladze, A. Ed.; Computational Methods in Photochemistry. CRC Press: Boca Raton, **2005**.
164. Turro, N. J.; Ramamurthy, V.; Scaiano, J. C. *Principles of Molecular Photochemistry.* University Science Books: Sausalito, **2009**.
165. Bernardi, F.; Olivucci, M. *Chem. Soc. Rev.* **1996,** 321.

166. Boggio-Pasqua, M.; Bearpark, M. J.; Robb, M. A. *The Spectrum* **2008,** *21*, 28.
167. Shaik, S. *Phys. Chem. Chem. Phys.* **2010,** *12*, 8706.
168. Moens, J.; Jaque, P.; De Proft, F.; Geerlings, P. *ChemPhysChem* **2009,** *10*, 847.
169. McCusker, J. K. *Book of Abstracts, 237th ACS National Meeting, Salt Lake City, UT,* p. INOR-062.
170. Knight, T. E.; McCusker, J. K. *J. Am. Chem. Res.* **2010,** *132*, 2208.
171. Stubbe, J.; Nocera, D. G.; Yee, C. S.; Chang, M. C. Y. *Chem. Rev.* **2003,** *103*, 2167.
172. Dempsey, J. L.; Winkler, J. R.; Gray, H. B. *Chem. Rev.* **2010,** *110*, 7024.
173. Jurss, J. W.; Concepcion, J. C.; Norris, M. R.; Templeton, J. L.; Meyer, T. J. *Inorg. Chem.* **2010,** *49*, 3980.
174. Hammes-Schiffer, S. *Acc. Chem. Res.* **2009,** *42*, 1881.
175. Ess, D. H.; Schauer, C. K.; Meyer, T. J. *J. Am. Chem. Soc.* **2010,** *132*, 16318.
176. Roston, D.; Kohen, A. *Proc. Natl. Acad. Sci. USA* **2010,** *107*, 9572.
177. Gust, D.; Moore, T. A.; Moore, A. In: "*Artificial Photosynthesis*"; Eds. Collings, A. F.; Critchley, C.; Wiley-VCH: Weinheim, **2005**.
178. Hammarström, L.; Hammes-Schiffer, S. *Acc. Chem. Res.* **2009,** *42*, 1859, and refs therein.
179. Yamada, H.; Ohkubo, K.; Kuzuhara, D.; Takahashi, T.; Sandanayaka, A. S. D.; Kujima, T.; Ohara, K.; Ito, O.; Uno, H.; Ono, N.; Fukuzumi, S. *J. Phys. Chem. B* **2010,** *114*, 14717.
180. Flores, M.; Savitsky, A.; Paddock, M. L.; Abresch, E. C.; Dubinski, A. A.; Okamura, M. Y.; Lubitz, W.; Möbius, K. *J. Phys. Chem. B* **2010,** *114*, 16894.
181. Leirer, M.; Knör, G.; Vogler, A. *Z. Naturforsch.* **1999,** *54b*, 1039.
182. Pierpont, C. G. *Coord. Chem. Rev.* **2001,** *219*, 415.
183. Karlin, K. D. *Nature* **2010,** *463*, 168.
184. Borovik, A. S.; Zinn, P. J.; Zart, M. K. In: "*Activation of Small Molecules: Organometallic and Bioinorganic Perspectives*"; Ed. Tolman, W. B.; Wiley-VCH: Weinheim, **2006**.
185. Würtele, C.; Sander, O.; Lutz, V.; Waitz, T.; Tuczek, F.; Schindler, S. *J. Am. Chem. Soc.* **2009,** *131*, 7544.
186. Dawson, J. H.; Trudell, J. R.; Barth, G.; Linder, R. E.; Bunnenberg, E.; Djerassi, C.; Gouterman, M.; Connell, C. R.; Sayer, P. *J. Am. Chem. Soc.* **1977,** *99*, 641.
187. Stevenson, D. K.; Wong, R. J. *Semin. Fetal Neonat. Med.* **2010,** *15*, 164, and refs therein.
188. Taketani, S.; Ishigaki, M.; Mizutani, A.; Uebayashi, M.; Numata, M.; Ohgari, Y.; Kitajima, S. *Biochemistry* **2007,** *46*, 15054.
189. Inoue, H.; Sumitani, M.; Sekita, A.; Hida, M. *J. Chem. Soc. Chem. Commun.* **1987,** *22*, 1681.
190. Knör, G. *Chem. Phys. Lett.* **2000,** *330*, 383.
191. Reith, L. M.; Himmelsbach, M.; Schöfberger, W.; Knör, G. *J. Photochem. Photobiol. A Chem.* **2011,** *218*, 247.
192. Gross, Z.; Gray, H. B. *Comments Inorg. Chem.* **2006,** *27*, 61.
193. Schöfberger, W.; Lengwin, F.; Reith, L. M.; List, M.; Knör, G. *Inorg. Chem. Commun.* **2010,** *13*, 1187.
194. Gao, Y.; Åckermark, T.; Liu, J.; Sun, L.; Åckermark, B. *J. Am. Chem. Soc.* **2009,** *131*, 8726.
195. Toraya, T. *Chem. Rev.* **2003,** *103*, 2095.

196. Hisaeda, Y.; Shimakoshi, H. In: "*Handbook of Porphyrin Science, Vol. 10*"; Eds. Kadish, K. M., Smith, K.; Guilard, R.; World Scientific: New Jersey, **2010**.
197. Stochel, G.; Wanat, A.; Kuliś, E.; Stasika, Z. *Coord. Chem. Rev.* **1998,** *171*, 203.
198. Mann, B.; Motterlini, R. *Chem. Commun.* **2007,** 4197.
199. Ford, P. C. *Acc. Chem. Res.* **2008,** *41*, 190.
200. Schatzschneider, U. *Eur. J. Inorg. Chem.* **2010,** 1451.
201. Zhang, Z.; Hatta, H.; Ito, T.; Nishimoto, S.-i. *Org. Biomol. Chem.* **2005,** *3*, 592.
202. Rose, M. J.; Mascharak, P. K. *Coord. Chem. Rev.* **2008,** *252*, 2093.
203. Farrer, N. J.; Woods, J. A.; Salassa, L.; Zhao, Y.; Robinson, K. S.; Clarkson, G.; Mackay, F. S.; Sadler, P. J. *Angew. Chem.* **2010,** *122*, 9089.
204. Ignarro, L. J.; Buga, G. M.; Wood, K. S.; Byrns, R. E.; Chaudhuri, G. *Proc. Natl. Acad. Sci. USA* **1987,** *84*, 9265.
205. Motterlini, R.; Clark, J. E.; Foresti, R.; Sarathchandra, P.; Mann, B. E.; Green, C. J. *Circ. Res.* **2002,** *90*, e17.
206. Pryor, W. A.; Houk, K. N.; Foote, C. S.; Fukuto, J. M.; Ignarro, L. J.; Squadrito, G. L.; Davies, K. J. A. *Am. J. Physiol. Regul. Integr. Comp. Physiol.* **2006,** *291*, R491.
207. Li, L.; Moore, P. K. *Pharmacol. Sci.* **2008,** *29*, 84.
208. Tang, G.; Wu, L.; Wang, R. *Clin. Exp. Pharmacol. Physiol.* **2010,** *37*, 753.
209. Haldane, J.; Smith, J. *J. Physiol.* **1896,** *20*, 497.
210. Rimmer, R. D.; Richter, H.; Ford, P. C. *Inorg. Chem.* **2009,** *49*, 1180, and refs therein.
211. Kratochwil, N. A.; Bednarski, P. J.; Mrozek, H.; Vogler, A.; Nagle, J. K. *Anti-Cancer Drug Des.* **1996,** *11*, 155 and refs therein.
212. Hoffman-Luca, C. G.; Eroy-Reveles, A. A.; Alvarenga, J.; Mascharak, P. K. *Inorg. Chem.* **2009,** *48*, 9104.
213. Knör, G.; Preiss, U., unpublished results.
214. Armitage, B. *Chem. Rev.* **1998,** *98*, 1171.
215. Schierling, B.; Noël, A.-J.; Wende, W.; Hien, L. T.; Volkov, E.; Kubareva, E.; Oretskaya, T.; Kokkinidis, M.; Römpp, A.; Spengler, B.; Pingoud, A. *Proc. Natl. Acad. Sci. USA* **2010,** *107*, 1361.
216. Knör, G. *Inorg. Chem. Commun.* **2001,** *4*, 160.
217. Häubl, M.; Reith, L. M.; Gruber, B.; Karner, U.; Müller, N.; Knör, G.; Schöfberger, W. *J. Biol. Inorg. Chem.* **2009,** *14*, 1037.
218. Koch, R. *Wien. Med. Bl.* **1890,** *13*, 531.
219. Sun, R. W.-Y.; Li, C. K.-L.; Ma, D.-L.; Yan, J. J.; Lok, C.-N.; Leung, C.-H.; Zhu, N.; Che, C.-M. *Chem. Eur. J.* **2010,** *16*, 3097, and refs therein.
220. Cook, T. R.; Dogutan, D. K.; Reece, S. Y.; Surendranath, Y.; Teets, T. S.; Nocera, D. G. *Chem. Rev.* **2010,** *110*, 6474.
221. Bullock, M. R. Ed.; Catalysis Without Precious Metals. Wiley-VCH: Weinheim, **2010**.
222. Lehn, J.-M. *Supramolecular Chemistry: Concepts and Perspectives*. VCH: Weinheim, **1995** p. 67.
223. Listorti, A.; Durrant, J.; Barber, J. *Nat. Mater.* **2009,** *8*, 929.
224. Ciamician, G. A. *Science* **1912,** *36*, 385.

TRANSITION METAL COMPLEXES AS SOLAR PHOTOCATALYSTS IN THE ENVIRONMENT: A SHORT REVIEW OF RECENT DEVELOPMENT

ZOFIA STASICKA

Faculty of Chemistry, Jagiellonian University, Ingardena 3, Kraków, Poland

ABSTRACT

The role of photocatalysis by transition metal complexes in the environment is reviewed, and its influence on composition of the environmental compartments, transport between them, and activation of the environmental self-cleaning behavior is characterized. In description of atmospheric processes, the attention is paid to coordination compounds as photocatalysts of the transfer and redox reactions of nitrogen oxides. In the case of hydrosphere and soils, various mechanisms of organic pollutant photodegradations are presented in which the iron, copper, and chromium complexes play

INORGANIC PHOTOCHEMISTRY
VOLUME 63 ISSN 0898-8838 / DOI:10.1016/B978-0-12-385904-4.00004-4

crucial roles. Mono- or mixed-metal photocatalytic cycles are stimulated, in which the complex photoreduction is accompanied by oxidation of ligands and/or external molecules (sacrificial electron donors), whereas the sacrificial acceptor, closing of the photocatalytic cycle, is predominantly molecular oxygen. The self-cleaning mechanisms by photocatalysis and photosensitization apply also to organic matter included in microorganisms, thus they can lead as well to the environmental self-disinfection. The review shows fast progress in our understanding of the natural processes driven by the solar energy and catalyzed by transition metal complexes; treating the cycles as anti-photosynthesis is also discussed.

Keywords: Environmental homogeneous photocatalysis; Photoreduction of transition metal complexes; NO-carriers; Photodegradation of organic pollutants; Photocatalytic cycles stimulated by iron, copper and chromium complexes.

I. Introduction

The metal reservoirs are lithosphere and deeper Earth shells. The presence of metal species in the atmosphere and hydrosphere, and their migration between the environmental compartments, depend predominantly on the nearest surroundings and especially on ligands present in their direct neighborhood. Metal oxidation state and ligand nature belong thus to the most important factors controlling metal transport in the environment. The best illustration of this relation can be seen in mercury transport from the solid phase (e.g., in the form of HgS or Hg_2Cl_2) to the hydrosphere (e.g., as $HgCl_2$) and atmosphere (e.g., as $Hg(CH_3)_2$ or Hg). Other examples can be chromium compounds, which are composed of mobile and water-soluble CrO_4^{2-} anions, or sparingly soluble hydroxo and macrocyclic complexes of Cr(III). A similar difference in solubility is observed between Fe(III) and Fe(II) compounds.

The role of photochemistry in nature is difficult to overestimate especially when we consider conversion of solar energy into the chemical energy in natural photosynthesis or ozone production, which protects the Earth from hazardous UV radiation. Much less is known about the role of sunlight in environmental self-cleaning processes.

The latter processes are stimulated by transition metal compounds and mostly by iron, copper, and chromium complexes,

which solar photoreduction is of crucial environmental relevance because it is accompanied by organic pollutant oxidative degradations. The compounds existing or formed in the environment are able to remove or at least abate a lot of natural and anthropogenic pollutants, even those which are nonbiodegradable and persistent.

II. Environmental Matter Under Sunlight Impact

The composition of environmental compartments undergoes continuous changes, the main driving force of which is solar radiation. The most spectacular changes are brought about by photosynthesis, which is beyond the subject of this chapter. However, beside photosynthesis a variety of photochemical processes are observed in nature that results in the removal of many diverse substances, in particular superfluous, degraded or even harmful organic compounds.

The reactivity is influenced both by radiation and chemical factors. In the former case, all parameters controlling sunlight intensity and spectral range are important, such as intensity of solar emission, altitude, latitude, season, day-time, etc. The chemical factors originate from the characteristics of the substrate and its surroundings. The relevant substrate features consist of spectral fitting to the solar light, chemical reactivity at low energetic excited states and high enough quantum yields. More complex is the influence of the surroundings; for instance, dispersed matter in the atmosphere favors photodissociation processes, whereas the clay layers provide reaction fields which stabilize charge-separated species generated in the photoredox processes (*1*). In many cases, however, the effect is much more drastic: chromate(VI), for example, in neat aqueous solution can be stored in glass or quartz bottles without any decomposition induced by sunlight; when, however, in aqueous milieu, where electron donors, such as aliphatic alcohol, phenol, and its halogen derivates or oxalate, appear (*2*) – photoreduction of chromate(VI) is observed, leading to formation of the corresponding Cr(III) complex.

The photochemical reactions induced by sunlight are of essential relevance to pollution abatement only when they lead to oxidative degradation of waste organic material. This can be done either through direct or indirect photoredox reactions. The direct photodecomposition of organic pollutants under sunlight is not very common and applies mostly to aromatic compounds. Much more common is indirect photoreactivity in which solar light is

absorbed by a photosensitizer or photocatalyst and transferred to the substrate molecule.

Due to sunlight energy that is limited at the ground level to $\varepsilon \leq 415$ kJ/mol ($\lambda \geq 290$ nm), only unique organic substrates (S) are able under these conditions to undergo photoconversion into products (P):

$$\mathrm{S} \xrightarrow{h\nu(\text{sunlight})} {}^{*}\mathrm{S} \rightarrow \mathrm{P} \tag{1}$$

The Cr(VI) example quoted above illustrates, however, that besides the monomolecular also bimolecular photoprocesses are effective:

$$\mathrm{S} \xrightarrow{h\nu(\text{sunlight})} {}^{*}\mathrm{S} \xrightarrow{\mathrm{Q}} \mathrm{P} \tag{2}$$

where Q represents a molecular entity that deactivates (quenches) an excited state of the substrate molecule, either by energy transfer or electron transfer or by a chemical mechanism.

Moreover, photosensitization processes are observed in which a reaction of a nonabsorbing substrate is induced by energy transfer or electron transfer from an excited light-absorbing photosensitizer (Sens):

$$\mathrm{Sens} \xrightarrow{h\nu(\text{sunlight})} {}^{*}\mathrm{Sens} \xrightarrow{\mathrm{S}} \mathrm{P} \tag{3}$$

The electron transfer sensitization is called reductive or oxidative, depending on the action of the excited sensitizer as electron donor or acceptor, respectively. Photosensitization may be treated as one branch of the more general family of catalytic reactions called photocatalysis, which involves light absorption by a catalyst precursor (pC) or by a substrate:

$$\mathrm{pC} \xrightarrow{h\nu(\text{sunlight})} \mathrm{C} \xrightarrow{\mathrm{S}} \mathrm{P} \tag{4}$$

$$\mathrm{S} \xrightarrow{h\nu(\text{sunlight})} {}^{*}\mathrm{S} \xrightarrow{\mathrm{C}} \mathrm{P} \tag{5}$$

Photocatalysis includes various reactivity types which may be divided into two categories depending on the role of light on: (i) photogenerated catalysis consisting of reactions catalytic in photons and (ii) catalyzed photolysis, in which processes are noncatalytic in photons (Fig. 1).

The photoinduced catalytic reactions in which both light and catalyst are not consumed, are of importance in organic syntheses, but are of minor significance in environmental chemistry. Much more important are those in which the solar energy is consumed

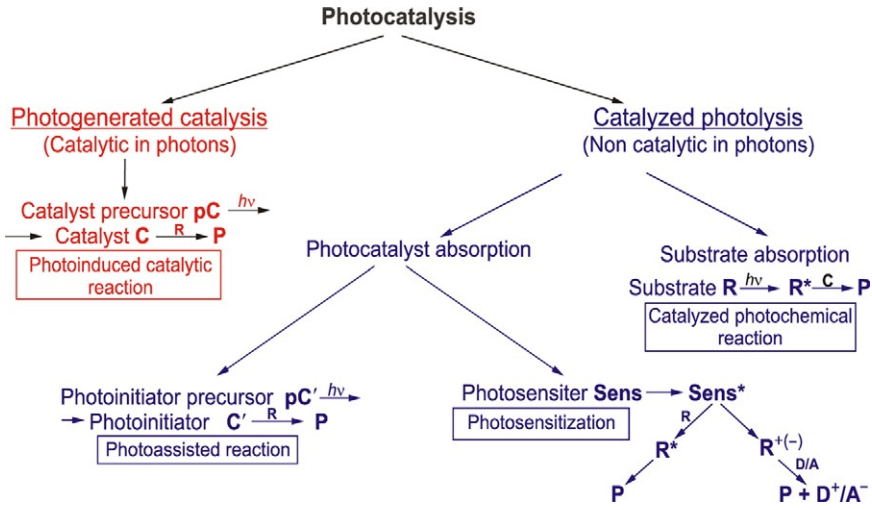

FIG. 1. Classification of photocatalysis.

and is the main driving power of environmental reactivity. Among catalyzed photolysis those reactions that follow substrate absorption are limited mainly to those cases when solar radiation induces photodegradation of a pollutant that is enabled or accelerated by some natural or anthropogenic catalyst.

The most essential pathways of pollutant photodegradation start from photocatalyst absorption followed by photosensitization or photoassisted reactions. The former consists in the energy or charge transfer from an excited photosensitizer to the substrate (quencher) molecule, whereas the latter results in generation of a "catalyst for one cycle," called photoinitiator. To guarantee the continuity of the charge transfer reactions both photosensitizers and photoinitiators should be recycled; the common practice is their regeneration by means of adequate electron donors and/or acceptors. These are not restored in a subsequent redox process but destroyed by irreversible chemical conversion; thus they are called sacrificial donors and acceptors, respectively.

The most common sacrificial electron acceptor in the environment is molecular oxygen, whereas the main sacrificial donors are organic compounds. In consequence, the self-cleaning processes consist in oxidation of organic pollutants by molecular oxygen in its triplet ground state; the reactions are driven by energy from solar radiation. In nature, many different photoinitiators or photosensitizers are reactive, but the most common environmental photosensitizers include humic substances (HS), whereas the best photoinitiators are transition metal complexes.

Coordination compounds are known for their photochemical properties, which may result in photodissociation, photosubstitution, photoisomerization, photoreduction, or photooxidation, for example (*3*). In addition to inner-sphere rearrangements, the complexes in excited states are susceptible to transfer their energy or charges into other species, such as solvent molecules, ion-pair partners, and other nonbonded quenchers.

Photoreactions can change forms and the physicochemical behavior of coordination compounds and thereby are responsible for transition metal transport between the environmental compartments. Some of these photoreactions are also of significance in natural cleaning: to ensure continuity of the processes, catalyst reproducibility should be guaranteed, that is, the relevant photoreactions should belong to the photocatalytic family.

III. Effect of Complexation and Photochemistry on Composition of Individual Compartments and Transport Between Them

A. Role of Natural Chelating Ligands

One of the most important agents controlling metal transport and their function in nature are chelating and macrocyclic ligands. The former are ubiquitous in the environment coming from both natural and anthropogenic sources. Their main natural reservoirs are HS or natural organic matter, widespread existing in water or soil environmental systems. These are heterogeneous mixtures of a variety of organic compounds, consisting of aromatic, aliphatic, phenolic, and quinolic functional groups with varying molecular sizes and properties. HS arise from decomposition of plant and animal tissues in soils, waters, and sediments, which cannot be classified as any other chemical class of compounds. Humic materials consist of a skeleton of alkyl or aromatic units cross-linked mainly by oxygen and nitrogen groups with the major functional groups being carboxylic acid, phenolic and alcoholic hydroxyls, ketone, and quinone groups. Their size, molecular weight, elemental composition, structure, number, and positions of functional groups vary depending on the origin and age of the material. According to their solubility, HS are divided into fulvic acids, humic acids, and humins. The structures of fulvic acids are somewhat more aliphatic and less aromatic than humic acids, and fulvic acids are richer in carboxylic, phenolic, and ketonic groups. This composition is

responsible for their higher solubility in water at all pH values. Humic acids, being more aromatic, become insoluble when the carboxylate groups are protonated at low pH values. This structure allows the humic materials to function as chelating ligands with the ability to bind various metal centers (*4*). The effective distribution of metal ion affinities for binding to a HS measured under typical freshwater conditions showed that the three groups of cations could be distinguished: (a) Al, H, Pb, Hg, and Cr, which are preferentially bound to the phenolic sites of the fulvic ligand; (b) Ca, Mg, Cd, Fe(II), and Mn, which display a greater effective affinity for carboxylic sites; and (c) Fe(III), Cu, Zn, and Ni, for which phenolic and carboxylic distributions overlap (*5*).

Complexation in combination with detergent and colloidal properties, make humic and fulvic materials, effective agents to transport both inorganic and organic contaminants in the environment. Organic contaminants that are associated with HS are essentially unavailable for uptake by biota, but these natural organic acids can enhance or retard the photochemical decomposition of waste or toxic organics. Consequently, dissolved organic matter (DOM) can either enhance or inhibit the rate of photodegradation of organic contaminants in water basins and thus the effect of HS on photodegradation of organic contaminants on soil surfaces is broadly investigated (*4*).

The HS found in most natural waters absorb solar light in the range 300–500 nm, and upon laser (355 nm) excitation three primary transient species were detected: triplet state (^{3}HS), hydrated electron (e^-_{hydr}), and radical cation ($HS^{\bullet +}$):

$$^1\text{HS} \xrightarrow{h\nu} {}^*\text{HS} \begin{cases} \rightarrow {}^3\text{HS} \\ \rightarrow \text{HS}^{\bullet +} + e^-_{hydr} \end{cases} \qquad (6)$$

The results of steady-state irradiation suggested, however, that hydrated electrons are mostly trapped by molecular oxygen and their role in sunlight-irradiated natural surface waters is likely to be minor. Thus, the main species responsible for the photoinduced degradation of aquatic pollutants are triplet excited states of HS. The triplet state lifetime was estimated as longer than 2 μs with an energy of 170 kJ mol^{-1} (*6*). These parameters are adequate to generate the excited singlet O_2 state ($^1\Delta_g$ or $^1\Sigma_g$), first of which is relatively low lying (94 kJ mol^{-1}) and thus can be easily populated by the energy transfer from the triplet states

of most dyes; the second O_2 singlet state ($^1\Sigma_g$) is more difficult to reach (157 kJ mol^{-1}), but is much more reactive.

The ^{3}HS may react with triplet O_2 or with an oxidizable reactant by energy, hydrogen or electron transfer reactions (Fig. 2). Direct reactions between ^{3}HS and organic substrates seem less favored since the triplet state reaction with oxygen is very efficient (7). The quantum yield of singlet oxygen production determined at 365 nm as 1–3%, depends strongly on the irradiation wavelength and the HS nature (6).

Moreover, due to the extremely short $^1O_2$ lifetime in water (4 μs), the competing reaction rate constants should be at least 2 orders of magnitude higher than that of solvent quenching (2.3×10^5 s^{-1}) (8). Furthermore, singlet oxygen ($^1\Delta$) was found to be quenched not only by water molecules but also by HS. These characteristics make the steady-state concentration of singlet oxygen in natural waters of the order of 10^{-13}–10^{-14} and thus can oxidize only the most reactive acceptor molecules, such as tryptophan (3-indolylalanine, $C_6H_4NHCHCCH_2CH(NH_2)COOH$), histidine ($C_6H_9O_3N_3$), phenolates ($C_6H_5OM$) (9).

Photosensitized oxidations by molecular oxygen are however important because of their impact on living organisms. It is known that, microorganisms and other living cells can be killed in the presence of light, molecular oxygen, and sensitizing dye. Moreover, some of the anthropogenic hazardous organic pollutants can undergo degradation photosensitized by HS. To this group belong both pesticides and herbicides, such as DDT (dichloro-diphenyl-dichloroethane) (10), atrazine (2-chloro-4-(ethylamino)-6-(isopropylamino)-*s*-triazine) (11), different

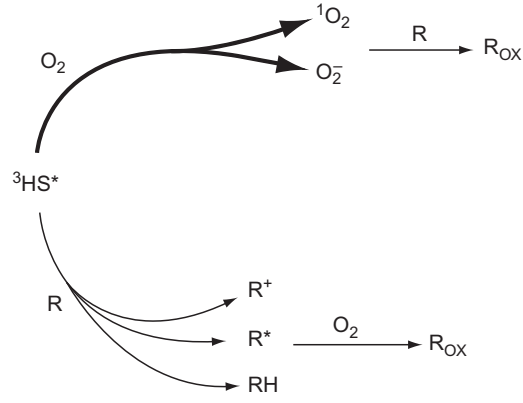

FIG. 2. Reactions of humic substances in the excited triplet state with molecular oxygen and with organic reactants.

organophosphorus pesticides (*12*), and irgarol 1051 (2-methylthio-4-terbutylamino-6-cyclopropylamino-*s*-triazine) (*13*).

HS form thermally stable complexes with transition metals, among others with iron and chromium. On irradiation the Fe (III) complexes undergo photoreduction producing Fe(II) and organic radicals (*6,14*).

B. Involvement of Anthropogenic Agents

Among anthropogenic chelating agents the most ubiquitous in the environment are aminopolycarboxylates and phosphonates, which, unfortunately, are not or only slowly biodegradable and are therefore rather persistent in the environment. Strong chelating agents occur in natural waters predominantly in the form of metal complexes; they have thus the potential to upset the natural speciation of metals and to influence metal bioavailability. High concentrations of chelating agents may lead to the remobilization of metals from sediments and aquifers, consequently posing a risk to ground and drinking water (*15*).

Coordination to a metal affects not only the compound solubility but also changes most of the metal and ligand features. Among others, coordination affects essentially the photochemical behavior. Ethylenediaminetetraacetic acid (edta) for example, which concentration in European surface water is higher than any other identified anthropogenic organic compound, is resistant to chemical, photochemical, and bio-degradation in the environment. However, when $edta^{4-}$ is coordinated to Fe(III) or Cr(III) it undergoes efficient solar photodegradation (*16–18*). This case illustrates the role of complex formation in the photochemical self-cleaning processes.

IV. Transition Metal Photochemistry in Conversion of Some Atmospheric Gases

The atmosphere is a complex medium in which several phases coexist: gas, aerosol particles, condensed water, liquid, and ice particles. All of the interactions that may occur between these various phases are included in the term “multiphase or heterogeneous chemistry.” Clouds favor the development of atmospheric multiphase chemistry, as they are composed of all three atmospheric phases (i.e., gas, liquid, and solid phases that stimulate a full set of reactions). Moreover, clouds modify radiative properties by diffusion of short-wavelength radiation coming from

the sun, absorption or diffusion infrared radiation emitted by the terrestrial surface, as well as by increase in the albedo of the Earth/atmosphere system (*19*).

In an effort to understand atmospheric chemical and photochemical behaviors, chemists have traditionally examined homogeneous gas-phase radical (mainly $OH^{\bullet}$) reactions of natural and anthropogenic pollutants. In subsequent studies the role of multiphase chemistry within the atmosphere was taken into account. Thus, although in general the homogeneous gas-phase model has been successful, some observations suggest that other pathways exist that may contribute significantly to the overall mechanism. These observations include processes occurring within cloud droplets or raindrops or layers at the surface of ice crystals, inside which the photochemical reactions are much stronger than in interstitial air. Among others, in atmospheric waters beside the $OH^{\bullet}$ radicals, also superoxide radical ions, $O_2^{\bullet -}$, are active in redox reactions: they can be the dominant source of transition metal compounds at low oxidation states (e.g., Cu(I)), whereas hydroperoxyl radicals, $HOO^{\bullet}$, or organic peroxyl radicals, $ROO^{\bullet}$, can be involved in oxidation of reduced forms of metals such as Cu(I) or Fe(II) (*20*).

The role of multiphase photochemistry in the atmosphere needs to be evaluated, especially as surface of metal oxide particles and other solid aerosols exceeds by far the total surface of the globe. Atmospheric photochemistry, which alters dust properties, may influence atmospheric metal cycling. Mixing of mineral dust with acid aerosol in result of coalescence processes within clouds may be an important mechanism of increasing the solubility of atmospheric iron in cloud water and photochemical reduction of iron (III) to iron(II) during the long-range transport of particles. Thus, the mobilization of metals might be strongly dependent on the history of the aerosol particles in the atmosphere. Consequently, we can assume that iron probably undergoes repeated cycles of very rapid Fe(III) photoreduction and slower Fe(II) oxidation on a time scale of a few minutes (*19*). Photolysis plays a similar role in atmospheric pathways of copper compounds.

A. Volatile Organic Compounds

The described processes result in changes in the atmospheric composition, which can be observed in the case of trace gases, such as volatile organic compounds (VOCs), sulfur oxides, nitric oxides, etc.

Aromatic, olefinic, and acetylenic hydrocarbons, but especially saturated hydrocarbons belong to persistent pollutants difficult to eliminate from the troposphere. The only exceptions are some aromatic compounds that undergo direct photodegradation in result of solar irradiation. Alkanes are undoubtedly much less reactive than other organic compounds including unsaturated hydrocarbons, surely because they are more completely saturated and their activation involves cleavage of the relatively strong C—H bond ($\varepsilon = 415$ kJ).

The C—H bond can be activated by a metal complex, particularly when the complex plays the role of catalyst or photocatalyst. The reactions of hydrocarbons with metal complexes occur at low temperatures and can be selective. There are different pathways for C—H bond activation: (i) by low-valence metal complexes, (ii) by high-valent metal-oxo compounds, (iii) by molecular oxygen and oxygen atom donors, (iv) by biological oxidation, or (v) by photocatalytic enhancement (*21*).

The cleavage of the C—H bond by direct participation of a transition metal ion proceeds via an oxidative addition mechanism or an electrophilic substitution mechanism. Metals in low oxidation states undergo oxidative addition while high oxidation state metals take part in electrophilic substitutions. Another function of the metal complex in these reactions consists of abstracting an electron or a hydrogen atom from the hydrocarbon, RH. The $RH^{\bullet+}$ radical ions or $R^{\bullet}$ radicals which are formed then interact with other species, such as molecular oxygen which is present in the solution or in one of the ligands of the metal complex (*21*).

To the main metal-containing systems which are capable to react with hydrocarbons and other C—H compounds belong also those producing the $OH^{\bullet}$ radicals, as Fenton and photo-Fenton reagents (see Section V.A.1). Other strong enough oxidizers may be generated as result of sunlight excitation of some transition metal complexes. For example, cyclohexene (C_6H_{10}) was reported to undergo photochemical oxygenation by Ru (II)–porphyrin complexes chemically activated upon visible light irradiation (*22*).

Some diverse VOCs (halocarbons, isoprene ($CH_2C(CH_3)CH_2CH_2$), monoterpenes, ethanol, and methyl *tert*-butyl ether, ($(CH_3)_3COCH_3$)) were found to be photooxidized efficiently on solid aerosols. Solid photocatalyst particles, such as TiO_2, ZnO, and Fe_2O_3, were here of special importance, but the VOC oxidation was photoassisted also by dessert sand, volcanic ash, or even by chalk particles (*23–25*). Similarly, sulfur dioxide was found to

be photooxidized to S(VI) species on an aqueous suspension of Fe_2O_3 (*20,26*) as well as by means of oxidants produced in nature by transition metal compounds (*27*).

B. Nitrogen Oxides

VOCs react readily with nitrogen oxides especially under favorable atmospheric conditions (intensive sunlight, high humidity, oxygenation, presence of transition metal species, etc.). To date, only few of the reactions are recognized, but the results of extensive studies focusing on the reactivity between NO_x and the VOC parent compounds in various biochemical systems are accessible and may be useful in solving environmental problems; thus, the most relevant of these experiences are presented in this chapter.

Nitrogen oxides (NO, NO_2) belong to the most important species active in tropospheric photochemistry, whereas N_2O is not degradable in the troposphere and undergoes photodegradation only in higher atmospheric parts, where more energetic ($\lambda < 250$ nm) UV radiation is available. Nitrogen monoxide plays an important role in the formation of ground-level ozone in highly populated areas, and in acid depositions. NO is emitted by various anthropogenic and natural sources, such as fossil fuel combustion, biomass burning, lightning, microorganism activity in the soil. Nitric oxide (NO) is also naturally generated from the amino acid arginine ($C_6H_{14}O_2N_4$) in the reaction catalyzed by an enzyme called NO synthase. In the atmosphere, NO is converted fast to NO_2 by O_3 and peroxy radicals ($HO_2^\bullet$, $RO_2^\bullet$, where $RO_2^\bullet$ represents peroxy radicals derived from VOCs). NO_2 dissociates to NO and $O(^3P)$ by exposure to solar radiation ($\lambda \leq 420$ nm):

$$NO_2 \xrightarrow{h\nu} NO + O(^3P) \tag{7}$$

$O(^3P)$ combines rapidly with an oxygen molecule to form ozone and in this way NO_x is the most important precursor of O_3 in the troposphere. NO and NO_2 interconvert in a few minutes. In daytime, the lifetime of NO_x in the lower part of troposphere is typically 1–2 days and is determined by the oxidation of NO_2 by the $OH^\bullet$ radical to produce nitric acid:

$$NO_2 + OH^\bullet + M \rightarrow HNO_3 + M \tag{8}$$

and by the reaction between NO_2 and O_3 in which the $NO_3^{\bullet}$ radical is formed that is a key compound in nighttime atmospheric chemistry. $NO_3^{\bullet}$ reacts with various VOCs and oxidizes them rapidly (*28*).

NO forms complexes with almost all transition metal ions and these compounds have unique physical and chemical properties imparted by the presence of the strongly electron-withdrawing NO ligands (*29*). The reactions of NO play an important role in environmental and biological processes, since they are implicated in a number of diseases coupled to its over- or underproduction. Transition metal complexes can be both efficient NO-scavengers and NO-donors, and thus belong to the important agents capable of regulating the NO-level in nature. The most characteristic feature of the interaction between NO and metal complexes is the redox character of nitrosyl complex formation accompanied by reduction or oxidation of the metal center and coordination of the NO^+ or NO^- ligand, respectively. This is related to the unique dual nature of the NO molecule that can act as a ligand and/or as a redox partner due to its radical character in the ground state. As a consequence, NO is formally oxidized to NO^+ by the metal ion that is reduced by one electron (reductive nitrosylation) as in met-myoglobin, where the Fe^{III} center binds NO in the form of $Fe^{II}—NO^+$. The reaction of reduced vitamin B_{12} with gaseous NO to give Co^{II} bound to NO in the form of $Co^{III}—NO^-$ represents an example of oxidative nitrosylation (*30*).

Redox-active metal ions may assist in the nitrosylation of organic substrates such as alcohols, amines, and thiols:

$$NO + M^{n+} + E - H \rightarrow E - NO + M^{(n-1)+} + H^+ \qquad (9)$$

where E = RO, R_2N, RS. In such reductive nitrosylation reactions, NO is formally oxidized to NO^+ by the metal ion that is reduced by one electron (*31*).

NO is a fascinating diatomic radical in the context of coordination chemistry due to its notorious non-innocent behavior in transition metal complexes. For example, NO adducts of ferrous iron complexes could have electronic structures that vary all the way from a $Fe(I)—NO^+$ to a $Fe(III)—NO^-$ extreme with the Fe(II)—NO (radical) case being intermediate. This distinction is significant, as it can be expected that NO^+, NO (radical), and NO^- will show very different reactivities. However, characterizing the exact electronic structures of transition metal nitrosyls is difficult, which led to the establishment of the famous Enemark–Feltham $[Fe—NO]^x$ notation (the superscript x

corresponds to the total number of ($d+\pi^*NO$) electrons) that allows for a general classification of transition metal nitrosyls without the need to define an exact electronic structure. Another complication of the coordination chemistry of NO is that many transition metal complexes catalyze the oxidative or reductive transformation of NO into other NO_x species, most prominently nitrite (NO_2^-), nitrate (NO_3^-), hyponitrite, nitrous oxide (N_2O), or HNO (*32*).

NO release takes place in the redox reaction backward to the synthetic procedure induced thermally by UV/visible or even by near infrared (NIR) radiation. There is also a possibility of the gaseous NO release by a homolytic cleavage of the N—O bond in some nitrito complexes.

$$[L_nMONO] \xrightarrow{h\nu} [L_nMO] + NO \qquad (10)$$

Such a behavior was observed in the case of the [M(TTP)(ONO)] complexes of Mn(III), Cr(III), and the Mo(TPP)(O)(ONO) complex of Mo(V) (TPP = tetraphenylporphyrin) (*33*).

The special role of transition metal NO complexes, or metal nitrosyls, in the environment consists in the photoreversibility of NO binding, as consequence of which the compounds are significant photocatalysts enabling NO cycling (*34,35*). Moreover, NO is one of the most important signaling and regulatory molecule in all animal and plant organisms. In contact with biofluids, a main sink for NO occurs through the very fast reactions with oxymyoglobin, oxyMb, and oxyhaemoglobin, oxyHb, giving NO_3^-. Also bio-relevant is the use of the so-called NO-donor drugs: *N*-hydroxyurea ($(OH)NHCONH_2$), hydroxylamine (NH_2OH), sodium nitroprusside ($Na_2[Fe(CN)_5NO]$), organic nitrates and nitrites (first of all glyceryl trinitrate, $C_3H_5(ONO)_3$), etc., which must be metabolized in the body through oxidative or reductive processes up to NO generation in order to be rendered physiologically active (*32,36–40*).

B.1. Iron NO complexes

Most of the target receptors of NO contain iron centers (*34*). This behavior illustrates the important role of iron complexes in the binding, storage, transport, and release of NO_x species in biological and environmental processes, controlling the local atmospheric nitrosity.

It is known since long that aqua complexes of Fe(II) are able to bind gaseous NO producing reversibly nitrosyl complexes:

$$[FeL_5(H_2O)]^{2+} + NO \rightleftarrows [FeL_5(NO)]^{2+} + H_2O \qquad (11)$$

The overall binding constant K_{NO} representing the ratio of the rate constants for the "on" and "off" reactions, that is, $K_{NO} = k_{on}/k_{off}$, was found to depend on the nature of L. It varied between 1×10^2 (for $L = H_2O$) and 1×10^6 M^{-1} (for $L_5 = edta^{4-}$) (*30,41*). The tendency of the Fe^{II} compounds to reversibly bind NO was reported to correlate with the oxygen sensitivity of the Fe^{II} complexes, suggesting that $[FeL_5(NO)]$ is stabilized in the form of $[Fe^{III}L_5(NO^-)]$ similar to that found for the binding of dioxygen, viz., $[Fe^{III}L_5(O_2^-)]$.

Iron complexes are involved in various steps of NO metabolism; most of these complexes also contain various sulfur ligands. Iron nitrosyls and nitrosothiols are the most relevant agents responsible for storage and transport of NO and related compounds; nitrosothiols and metal nitrosyl complexes belong to the most important external sources of NO (NO-donors) (*42*).

The most complex interactions are observed in ternary iron–sulfur–nitrosyl systems. Depending on the bond nature, the ternary iron–sulfur–nitrosyl species may be classified into two groups: (i) iron complexes with the *S*-nitrosothiol ligand containing the [Fe—N(SR)O] moiety and (ii) RS—Fe—NO compounds, where both NO and sulfur are coordinated to the Fe-center. Irrespective of the structural details, the mutual interactions of all components are very strong due to considerable bond delocalization within both ternary systems.

The iron–sulfur clusters constitute an integral part of several natural structures occurring in a large family of biologically relevant metalloproteins. These [Fe—S] units form active sites of enzymes, which play a crucial role in living organism processes such as: electron transfer chain, photosynthesis (photosystem I), isomerization, respiratory chain, nitrogen fixation, and many various catalytic reactions; they can also operate as biosensors for oxidants and iron. The [Fe—S] clusters are even supposed to be the interface between the biological and inorganic worlds, because they catalyze redox transformations of such likely components of the Earth's primordial atmosphere, as N_2, CO, and H_2. The iron–sulfur units form mono-, di-, tri-, tetra-, and hexanuclear species in which iron atoms are connected through S bridges, with thiolates and/or NO as terminal ligands.

The family encompasses species like $[Fe_2(\mu_2\text{-}S)_2(NO)_4]^{2-}$ (known as Roussin's red salt), $[Fe_2(\mu_2\text{-}SR)_2(NO)_4]$ (Roussin's red salt ester), $[Fe_4(\mu_3\text{-}S)_3(NO)_7]^-$ (Roussin's black salt), $[Fe_4(\mu_3\text{-}S)_4(NO)_4]$, and $[Fe_6(\mu_3\text{-}S)_6(NO)_6]$. Two of these complexes, $[Fe_4(\mu_3\text{-}S)_3(NO)_7]^-$ and $[Fe_4(\mu_3\text{-}S)_4(NO)_4]$, have been studied as

possible thermal- and photoinitiated precursors of nitrovasodilators and anticancer agents. Experiments in various biological systems showed that light strongly enhances their vasodilatory and cytotoxic properties, and the biological activity of the clusters strongly correlates with the generation of NO (*41,42*).

Special attention was also paid to understanding the basic properties and reactivity patterns of the dinitrosyl iron complexes and Roussin's red salt esters, and to resolve the mechanism of their biological functions and NO emission (*43–47*). The quantum yield of NO release from $[Fe_2(\mu_2\text{-}SR)_2(NO)_4]$ under visible light irradiation can be considerably enhanced by incorporating into the ester a proper chromophore; then single- or two-photon processes were observed (*46,48,49*).

Experimental work in model systems supplemented with theoretical investigations proved that the main photoreaction mode of Roussin's black salt is a photoredox reaction leading to generation of NO and a Fe(II) compound. The π*NO–d transitions were assumed to be responsible for the photochemical reactivity of these compounds, which result in photodissociation of the NO group (*33,36,50–52*). It has been found, however, that irradiation of $[Fe_4(\mu_3\text{-}S)_3(NO)_7]^-$ in the presence of S^{2-}, thiolate anions or other *S*-nucleophiles produces Fe(III) species and N_2O, instead of NO (*53*).

From biological and medical aspects, the primary targets for NO in bioregulatory functions are metal centers, chiefly heme- and nonheme iron proteins (*33,41,54–57*). A fast reaction with its biological targets would be necessary for NO to serve as an effective regulatory agent at the submicromolar concentrations found *in vivo*. This is indeed the case for the reaction of NO with the ferroheme enzyme soluble guanylyl cyclase for which $k_{on} = 1.4 \times 10^8\ M^{-1}\ s^{-1}$ (277 K) (*41*). The rates tend to be very fast when the NO ligand enters a previously unoccupied coordination site or substitutes a very labile leaving group like the H_2O ligand.

Detailed kinetic and mechanistic studies on the reaction between NO and metmyglobin (Mb(III)) using laser flash photolysis and stopped-flow techniques, demonstrated the reversible binding of NO:

$$[\text{metMb}(H_2O)] + NO \rightleftharpoons [\text{metMb}(NO)] + H_2O \qquad (12)$$

From a mechanistic perspective, the nitrosyl complex of metmyoglobin is of particular interest because both association and dissociation of NO are conveniently observable under

physiological temperatures and pH (*54,58*). In the reaction of NO with oxymyoglobin, an iron(III)–nitrato complex was identified as the millisecond intermediate (*59*).

NO reacts with both ferric and ferrous centers in hemoproteins to form the respective iron(II) and iron(III) nitrosyl adducts, whose structural features are similar to those observed for iron (II) and iron(III) porphyrin nitrosyls. These analogies are also reflected in similar chemical reactivity observed for nitrosylated ferri- and ferroproteins and their respective porphyrin models. For example, NO-adducts of Fe(III) undergo reductive nitrosylation in the presence of an excess of NO, and a similar process is commonly observed for synthetic Fe(III) porphyrins. The first step of this reaction involves nucleophilic attack of OH^- on the nitrosyl ligand coordinated to the iron center, as presented in reaction (13) (*33,60*):

$$[(\text{porph})\text{Fe} - \text{N} = \text{O}] + \text{OH}^- \rightleftarrows [(\text{porph})\text{Fe} - \text{N} = \text{O}_2\text{H}] \rightarrow [(\text{porph})\text{Fe}] + \text{HONO} \quad (13)$$

The reversible reaction of NO with water-soluble iron(III) porphyrins proceeds via a dissociative mechanism (*41,61*). Kinetic and mechanistic studies on the reductive nitrosylation as a function of pH, revealed a significant decrease in the rate of NO binding to $[(\text{porph})\text{Fe}^{\text{III}}(\text{OH})]$ as compared to that of $[(\text{porph})\text{Fe}^{\text{III}}(\text{H}_2\text{O})_2]$ (*62,63*). On the other hand, trace impurities can also interact with a catalytically active species and therefore accelerate or decelerate the reaction, or even change its mechanism (*64*). Electron-donating substituents on the porphyrin slow down the reductive nitrosylation process, whereas electron-withdrawing substituents accelerate the reaction, suggesting that they induce the formation of $[(\text{porph})\text{Fe}^{\text{II}}(\text{H}_2\text{O})(\text{NO}^+)]$ and increase the electrophilicity of coordinated NO^+ (*65*). The nature and charge of substituents in the porphyrin periphery affect the dynamics of both the binding and release of NO (*66*). Ferric porphyrins are able to form nitrosyl complexes by rapid trapping of nitroxyl anions (NO^-) (*67*).

The ferriheme protein metmyoglobin (metMb) at the physiological pH 7.4 was reported to bind the NO molecule reversibly yielding the nitrosyl adduct [metMb(NO)]; the kinetics of the association and dissociation processes were investigated and a limiting dissociation mechanism was proposed (*58,68*). 2-His-1-Glu nonheme iron center engineered into myoglobin was reported capable to bind Fe(II) and reduce NO to N_2O (*69*).

The reaction of NO with the ferric(met) nitrite derivative of human adult hemoglobin Hb was investigated using thin films

of sol-gel encapsulated Hb, and the patterns observed were consistent with a mechanism whereby NO reacts with the ferric nitrite derivative to generate N_2O_3 (*70*).

Flavodi-iron proteins containing a distinctive nonheme diiron/flavin mononucleotide active site, catalyze reductive scavenging of dioxygen and NO in air sensitive microorganisms. Anaerobic addition of NO up to one NO per diferrous unit results in formation of a diiron mononitrosyl complex, whereas further addition of NO results in two reaction pathways, one of which produces N_2O and the diferric site and the other which produces a stable diiron–dinitrosyl complex. The production of N_2O upon addition of NO to the mononitrosyl deflavo-protein was interpreted in terms of the hyponitrite mechanism (*71*).

The DFT method was used to study the adsorption of NO on various metal phthalocyanines, MPc, (M = Mn, Fe, Co). The NO adsorption induces significant changes in the geometry and the electronic structures of the MPc. The geometry of the M—N—O grouping was found linear in the case of the Mn center, whereas bent for Fe and Co phthalocyanines. The observed difference in the geometry and the electronic structures was interpreted in terms of the hybridization of NO π^* orbitals and d orbitals of the metal atoms, as well as charge transfer between the NO molecule and MPc. The calculation and parallel experimental results have shown that metal phthalocyanines are potential sensor devices for detecting NO gas (*72*).

Transition metal complexes binding efficiently enough to eliminate NO from some compartments have attracted much interest because of their potential use as NO acceptors, donors, and/or carriers important not only in therapy but also in pollution abatement. Among these complexes the iron(II) aminocarboxylates are characterized by their high solubility in aqueous solution and ability of rapid and reversible NO-binding. These features are useful in reducing both the NO content in exhaust gases and the NO level in human body during NO mediated pathological events (*73–77*).

The photolabile $[Fe—NO]^6$ iron nitrosyl complexes with a pentadentate ligand *N*,*N*-bis(2-pyridylmethyl)amine-*N*-ethyl-2-pyridine-2-carboxamide, $PaPy_3H$, and its derivative $[(PaPy_3)Fe(NO)](ClO_4)$ have been synthesized in which the binding of NO is reversible and the bound NO is released rapidly under irradiation with visible light (*78–80*).

Among the studied aminocarboxylates, the ethylenediaminetetraacetate complex of Fe(II) proved to be the most promising NO-scavenger and the reaction:

$$\left[Fe^{II}(edta)(H_2O)\right]^{2-} + NO \rightleftarrows [Fe(edta)(NO)]^{2-} + H_2O \qquad (14)$$

is characterized by the extremely fast NO-uptake (rate constant of $2.4 \times 10^8\ M^{-1}\ s^{-1}$ and high stability constant of $2.1 \times 10^6\ M^{-1}$ at 25 °C (*60,81–87*)). The Fe^{II}(edta) complex also reacts fast with dioxygen:

$$2\left[Fe^{II}(edta)(H_2O)\right]^{2-} + O_2 + H_2O \rightarrow 2\left[Fe^{III}(edta)(H_2O)\right]^{-} + H_2O_2 \qquad (15)$$

but the reaction is slower than that with NO ($k = 320\ M^{-1}\ s^{-1}$ at 25 °C and pH 6 (*88,89*)). Moreover, its oxidized form, the $[Fe^{III}(edta)(H_2O)]^-$ complex, is inactive toward NO. This means that to ensure effective NO-uptake under atmospheric conditions, the Fe(III) product should be rapidly reduced:

$$\left[Fe^{III}(edta)(H_2O)\right]^{-} + e^- \rightarrow \left[Fe^{II}(edta)(H_2O)\right]^{2-} \qquad (16)$$

and different chemical and biological methods for the reduction of Fe(III) were proposed (*90–92*).

To avoid any additional pollution by the oxidation products and to ensure the low cost of the process, the BiodeNOx procedure was proposed, which is a novel technique for NO_x removal from industrial flue gases. In principle, BioDeNOx is based on NO absorption into an aqueous $[Fe^{II}(edta)(H_2O)]^{2-}$ solution (Eq. 14) followed by NO reduction and $[Fe^{II}(edta)]^{2-}$ regeneration by the denitrifying bacteria:

$$6\left[Fe^{II}(edta)(NO)\right]^{2-} + C_2H_5OH \rightarrow 6\left[Fe^{II}(edta)\right]^{2-} + 3N_2 + 2CO_2 + 3H_2O \qquad (17)$$

The technical and economical feasibility of the BioDeNOx concept is strongly determined by high rate biological regeneration of the scrubber liquid and by edta degradation. Detailed studies showed, however, a contradiction between the optimal redox state of the aqueous $[Fe^{II}(edta)]^{2-}$ solution for NO absorption and the biological regeneration. $[Fe^{III}(edta)(H_2O)]^-$ reduction was found to be too slow to keep all [Fe(edta)] in the reduced state. Moreover, since flue gases generally contain oxygen, part of the $[Fe^{II}(edta)]^{2-}$ is oxidized to $[Fe^{III}(edta)]^-$ (Eq. 15). Therefore, not NO reduction but $[Fe^{III}(edta)]^-$ reduction was found to be the rate limiting factor of BioDeNOx reactors treating flue gas that contains more than 1% oxygen (*77,92*).

Recently (*93*), a photochemical method for NO-separation from an gaseous mixture was proposed, in which the Fe^{II} substrate is generated and regenerated by photoreduction:

$$\left[Fe^{III}(edta)(H_2O)\right]^- + edta^{4-} \xrightarrow{h\nu} \left[Fe^{II}(edta)(H_2O)\right]^{2-} + edta^{\bullet 3-} \quad (18)$$

The free edta plays here the role of sacrificial electron donor and undergoes degradation, similarly as in the BioDeNOx technique (*77*). The photoreduction course was found to be almost independent of pH. This finding is of practical meaning because $[Fe^{II}(edta)(H_2O)]^{2-}$ oxidation by molecular oxygen (Eq. 15) is slower at higher pH values (*89*) and in an excess of edta (*94*). Thus, the photochemical generation of the $[Fe(edta)(NO)]^{2-}$ complex should be more effective under these conditions (*93*). The process seems to be especially economic and environmentally friendly as it can be driven by sunlight (*16,17,95*).

B.2. Ruthenium NO complexes

Complexes of other transition metals, such as Ru, Mn, Cr, Cu, Co, are also capable of regulating the level of NO in biological and environmental systems by the binding and chemical or photochemical release of gaseous NO. In recent years, various transition metal complexes have been synthesized to modulate NO concentrations in cellular environments and control physiological processes that are regulated by NO (*33,46,54,75,96*).

The high affinity of ruthenium for NO is well documented. Since ruthenium complexes are in general stable, various ruthenium nitrosyls have been isolated and studied in detail in terms of their NO donating capacities. Ruthenium compounds with readily available coordination sites can be used as NO scavengers, whereas ruthenium nitrosyl complexes are investigated as agents controlling the NO-release for medicinal applications, in particular for the control of high blood pressure, and as anti-tumor agents that might release cytotoxic NO within tumor cells, thus leading to cell death.

Modulation of NO release can be induced by one-electron reduction, which occurs at NO^+ to yield coordinated $NO^\bullet$, or by photolysis (*41,46*). Thus, the ruthenium complexes were studied in search for an ideal system for the site-directed NO delivery from thermally stable precursors which can release NO when triggered by light. A large number of $[Ru—NO]^6$ nitrosyls release NO upon exposure to UV light and their potential as NO donors under the control of light has been surveyed. In general, the

nitrosyls with nonporphyrin ligands (such as amines, Schiff bases, thiolates, and ligands with carboxamide groups) readily release NO upon illumination and generate Ru(III) photoproducts. In contrast, photolysis of ruthenium nitrosyls derived from porphyrins is followed by a rapid recombination that reduces the release of NO. To date, notable progress has been made in the area of $[Ru—NO]^6$ species derived from polydentate ligands with strong absorption bands in the visible/NIR region that could be used for site-specific light induced NO delivery (*75,97–101*).

Dinuclear hydrotris(pyrazolyl)borate complexes of ruthenium were reported to be N—N coupled by two nitrosyl ligands. These complexes undergo transformation of the N—N bridged into the oxo-bridged dinuclear complexes with the release of N_2O. The N—N bond is easily cleaved by oxidation and regenerated again by reduction. This observation would provide significant information regarding the mechanism of NO reduction to N_2O by nitrosyl complexes (*102*).

Similarly to the iron complexes, the nitrite ruthenium compounds might serve as photochemical NO delivery agents (*103*).

Also the triruthenium cluster, $[Ru_3(\mu_3\text{-}O)(\mu\text{-}CH_3COO)_6(CO)(L_1)(L_2)]$ (where $L_1 = [(NC_5H_4)CH_2NHC(O)(CH_2)_{10}S^-]_2$, $L_2 = 4$-methylpyridine), which forms a self-assembled monolayer is able to coordinate NO. The NO ligand can be selectively introduced into the cluster to replace the originally bound CO ligand when the Ru_3 cluster is oxidized by one electron, and part of the coordinated NO can also be desorbed from the resultant NO-bound monolayer when the cluster is reduced by one-electron from its original oxidation state (*104*). These findings demonstrate also new prospects for the NO reactivity pathways in the interfacial environmental space.

B.3. Copper NO complexes

NO is scavenged by Cu(II) complexes and diverse reaction pathways were reported (*34*):

i. Gaseous NO forms stable adducts with copper complexes as in the case of dithiocarbamates, that changes their toxic properties (*35,105*).
ii. Cu(II) compounds are reduced, whereas NO is oxidized to NO_2^-; such a pathway was suggested for copper complexes with 1,10-phenantroline and its derivatives, for example:

$$\left[\mathrm{Cu(dmp)_2}\right]^{2+} + \mathrm{NO} \overset{\leftarrow}{\rightarrow} \left[\mathrm{Cu(dmp)_2}\right]^{+} + \mathrm{NO}^{+} \quad (19)$$

$$\mathrm{NO}^{+} + \mathrm{H_2O} \rightarrow \mathrm{HNO_2} + \mathrm{H}^{+} \quad (20)$$

where dmp = 2,9-dimethyl-1,10-phenanthroline (*106*).

iii. The redox reaction between NO and a Cu(II) complex leads to the production of Cu(I) species and nitrosation of the ligand, as in the case of a tripodal tetraamine ligand and its derivatives, which undergo concomitant nitrosation at all three secondary amine sites (*107*). A similar effect has been observed for the fluorescein-derived ligands (Fl):

$$\left[\mathrm{Cu^{II}{}_2(Fl)_2}\right] \xrightarrow{2\mathrm{NO}} 2\mathrm{Cu^{I}} + \mathrm{(Fl)_2(NO)_2} \quad (21)$$

The reaction (Eq. 21) is accompanied by fluorescence enhancement and for this reason the copper fluorescein complexes can be used as NO-sensors (*108*).

The reactions of NO with copper proteins as possible NO targets *in vivo* are not as well characterized as those with iron proteins. Recent studies indicate, however, that redox reactions can be very fast even at low NO concentrations and in the presence of oxygen, and therefore the reactions may be of physiological relevance. In general, it is assumed that different spectroscopic types of copper centers react differently with NO (*54*).

The 2-His-1-Glu metal center commonly found in natural non-heme iron enzymes was engineered into myoglobin, and this new protein appears capable of binding not only Fe(II) but also Cu(I), and the sites are active in reducing NO to N_2O via different intermediates (*69*).

Reaction of the monovalent complex [Me_2NN]Cu(η^2-ONAr) with NO(g) to give divalent [Me_2NN]Cu(κ^2-O_2N_2Ar) represents an example of oxidative nitrosylation (where Ar = 3,5-$Me_2C_6H_3$ or Ph). The *C*-nitroso adducts reported herein are capable of incorporating one equivalent of NO into the coordinated ONAr ligand to form diazeniumdiolates [Cu](κ^2-O_2N_2Ar), which represents oxidative nitrosylation of the formally monovalent [Me_2NN]Cu(η^2-ONAr). This serves as a well-defined example that illustrates the possibility of oxidizing a metal center via functionalization of a bound ligand with NO (*31*). The liberation of NO from the copper nitrosyl complexes was not characterized in detail, but the nitritophenylophosphino complex of Cu(I) was recently reported to release NO upon protonation (*109*).

Copper and its compounds are also known to catalyze and photocatalyze NO transformations (*110*).

B.4. Cobalt NO complexes

Cobalt is present in human organisms in the form of vitamin B_{12} derivatives, and the physiological actions of NO on vitamin B_{12} derivatives were intensively studied (*54*). It was reported that the reduced form of vitamin B_{12}, [Cbl(II)], reacts with gaseous NO to form a stable nitrosyl complex.

$$[\mathrm{Cbl(II)}] + \mathrm{NO} \rightleftarrows [\mathrm{Cbl(NO)}] \rightarrow [\mathrm{Cbl(III)NO^-}] \qquad (22)$$

The large value of the formation constant for this complex indicates that the binding of NO by cob(II)alamin is very efficient, and thus may account for the observed physiological effects. In analogy to porphyrin Co(II) nitrosyl complexes, the cob(II)alamin nitrosyl adduct was formally described as [Cbl (III)NO^-].

Irradiation of the [Cbl(III)NO^-] complex by visible light in aqueous solution leads to the formation of Cbl(II) and free NO, after which re-formation of [Cbl(III)NO^-] could be observed (*54,60,111*).

$$[\mathrm{Cbl(III)NO^-}] \xrightarrow{h\nu(532\,\mathrm{nm})} [\mathrm{Cbl(II)}] + \mathrm{NO} \rightarrow [\mathrm{Cbl(III)NO^-}] \qquad (23)$$

The reaction between aquacobalamin, [Cbl(H_2O)], and NO at low pH was studied repeatedly and it is now accepted that under such conditions nitrous acid impurities are responsible for the reaction observed between vitamin B_{12} and NO (*112–118*).

The reaction of NO with [Co^{II}(TPPS)] (where TPPS = tetrameso-(4-sulfonatophenyl)porphinate) was found to approach diffusion limited rates, similarly to the reaction with the [Fe^{II}(TPPS)] and [Fe^{II}(TMPS)] (TMPS=tetrameso (sulfonatomesityl)porphinate) (*68*).

An untypical behavior of gaseous NO in the presence of [Co^{II}(salen)] nanoparticles was reported. Under these conditions NO underwent disproportionation generating different N_xO_y products (*119*).

B.5. NO complexes of other transition metals

Thermally stable chromium(III) dinitrito complexes undergo photocleavage of the Cr–O—O bond in coordinated nitrite leading to the generation of NO and a Cr^{IV}=O intermediate.

$$\left[L_n Cr^{III}(ONO)\right]^+ \xrightarrow{h\nu} \left[L_n Cr^{IV}{=}{=}O\right)]^+ + NO \qquad (24)$$

For example, *trans*-$[Cr(cyclam)(ONO)_2]^+$ (cyclam = 1,4,8,11-tetraazacyclotetradecane) was suggested as photochemical precursor for NO delivery to physiological targets (*33*). This water-soluble and thermally stable system, which demonstrates a large Φ_{NO} for NO release with UV light, seems very promising. However, its absorption cross section in the visible is very small, since these transitions are ascribed to the Laporte forbidden ligand field (d–d) bands. To improve the photosensitivity range, several new macrocyclic ligands L with pendant aromatic chromophores were prepared. Photoexcitation of aqueous solutions containing these complexes at wavelengths corresponding to the chromophore absorption bands led to the generation of NO (*46,48*). Nanocrystal quantum dots were found to offer important advantages as photosensitizing chromophores, including high optical cross-sections for both single and two photon excitations and the ability to tune the optical properties by varying the QD diameter (*120,121*). Also visible light excitation of *trans*-$[Cr(cyclam)(ONO)_2]^+$ in solutions containing thiol reducers such as the biological antioxidant glutathione leads to a permanent reaction even under anaerobic conditions, resulting in a high quantum yield for the release of NO (*122*).

Density functional theory (DFT) studies of the series of complexes $[Cr(L)(H_2O)_5]^{n+}$ (where $L = N_3^-$, NO, NS, or NSe) show that the unpaired electron resides in a metal-based d_{xy} orbital and that the electronic structure in the equatorial plane is similar in all four complexes and resembles Cr^{3+}. The σ donating ability was found to follow the order $N_3^- \gg NO < NS \approx NSe$, whereas the π accepting ability followed the order $NO > NS \approx NSe$. Time dependent DFT calculations gave in all four complexes a $d_x2_{-y}2 \leftarrow d_{xy}$ transition energy around 17,500 cm^{-1} (*123*).

The Mn(III) complexes with pyridine derivatives, $[Mn(PaPy_3)(NO)]ClO_4$ and $[Mn(PaPy_2Q)(OH)]ClO_4$ (where $PaPy_3H$ = *N*, *N*-bis(2-pyridylmethyl)amine-*N*-ethyl-2-pyridine-2-carboxamide and $PaPy_2QH$ = *N*,*N*-bis(2-pyridylmethyl)-amine-*N*-ethyl-2-quinoline-2-carboxamide), though insensitive to dioxygen, react with NO to afford the nitrosyl complexes $[Mn(PaPy_3)(NO)]ClO_4$ and $[Mn(PaPy_2Q)(NO)]ClO_4$ via reductive nitrosylation. These diamagnetic nitrosyl $[Mn{-}NO]^6$ complexes are soluble in water, and release NO after exposure to visible radiation with high quantum yields (0.385 and 0.694 at $\lambda_{irr} = 550$ nm, respectively). The quantum yield of the quinoline derivative at $\lambda_{irr} = 500$ nm

is even higher ($\Phi = 0.742$) and the compound is also sensitive to NIR light (800–900 nm), which results in bleaching of its maroon solution and release of NO. These results show that properly designed manganese nitrosyls can also effectively deliver NO under light, and their photoactivity can be modulated by alterations in the ligand frame (*124*).

In the reaction of a dinuclear Ni(I) complex with NO, one $[Me_2NN]Ni$ fragment is trapped as the nickel nitrosyl compound $[Me_2NN]Ni(NO)$ (*31*).

S-Nitrosothiols undergo a reversible transnitrosation reaction at zinc tris(pyrazolyl)boratozinc thiolates, ^{iPr2}TpZn-SR. These zinc thiolates are unreactive toward anaerobic NO but rapidly react with NO in the presence of O_2 or anaerobically with NO_2 to release the *S*-nitrosothiol RSNO with formation of the corresponding zinc nitrate (*125*).

The reactivity of Zn_7- and Cd_7-metallothionein (MT) with *S*-nitrosopenicillamine (SNAP), *S*-nitrosoglutathione (GSNO), and 2-(*N*,*N*-diethylamino)-diazenolate-2-oxide (DEA/NO) demonstrated that MT is a significant site for cellular reaction of NO or its compounds. Zn_7-MT reacts with SNAP or GSNO under aerobic conditions and in the presence of light, which stimulates the decomposition of *S*-nitrosothiolates to NO and Zn^{2+}, whereas protein thiols are modified (*126*).

NO_x can also undergo photoredox reactions on solid photocatalysts modified by coordination compounds, for example, on TiO_2 modified by H_2PtCl_6 (*127*) or on bismuth tungstate photocatalysts (*128*).

To date, research on light-activated NO donors has almost exclusively focused on the chemical reactivity of NO in biochemical systems, but detecting and understanding the role of NO in the environmental processes is an exciting new field of endeavor (*129*). The prerequisites of these operations were presented in this review, but still new details appear that prove the environmental importance of cooperation between transition metal ions, natural ligands, NO, and solar light. A significant example may be found in the recent report on the role of copper(II) and other divalent metal ions (zinc, cobalt, and iron) in N_2O reduction to N_2 in the presence of sulfides, which is an essential stage of denitrification processes proceeding both in natural environments (marine sediments) and industry (activated sludge, methanogenic sludge, BioDeNOx process) (*130*). The photocatalytic release of NO is accessible also in multiphase systems, as was demonstrated in case of the encapsulated iron and ruthenium nitrosyl complexes (*101*).

V. Photooxidation of Organic Pollutants by Transition Metal Complexes in Hydrosphere and Soils

One of the most significant stimulus of photocatalytic processes in water basins and soils are transition metal ions. Although abundance of naturally occurring transition metals is in general less than 100 ppm and concentrations of their water soluble forms are even several orders lower, their presence has relevant effects on the environmental processes and compositions. The important prerequisites are readiness to decrease their oxidation numbers in photoredox reactions and the possibility to generate higher oxidation numbers in contact with molecular oxygen. As a consequence, transition metal ions present in the aquatic compartments are involved in photochemical cycles that play an important role in the degradation of various pollutants.

A. Iron Complexes

Especially important for the cleaning of aquatic systems are water-soluble iron(III) complexes, although in colloidal systems Fe(III) species can also be light-activated (*76*). One of the controlling parameters is the nature of the ligand (*131*). A special role is played by hydroxo complexes, but ligands forming chelate complexes are also of relevance, among them HS. The OH^- ligand undergoes photooxidation at the expense of the Fe(III) center:

$$\left[Fe^{III}(OH)L_5\right] + H_2O \xrightarrow{h\upsilon(\mathrm{LMCT})} \left[Fe^{II}(H_2O)L_5\right] + OH^{\bullet} \qquad (25)$$

and $OH^{\bullet}$ radicals that belong to the strongest environmental oxidants are responsible for most of the degradative oxidations of organic pollutants. Alternatively, organic ligands coordinated to Fe(III) are oxidized directly by the excited center:

$$\left[Fe^{III}(LL)_3\right] \xrightarrow{h\upsilon(\mathrm{LMCT})} \left[Fe^{II}(LL)_2(H_2O)_2\right] + LL^{\bullet} \qquad (26)$$

Typically sunlight absorption can excite Fe(III) complexes to ligand-to-metal charge transfer (LMCT) excited states, which decay via photoinduced electron transfer (PET) to the Fe-center from the inner (ligand) or external electron donor. The photochemically generated Fe(II) species is then reoxidized to the initial Fe(III) compound or its derivative (e.g., aqua complex) closing the photocatalytic cycle. As result many environmental pollutants are oxidized by molecular oxygen in reactions driven

by solar energy, that is in photoassisted processes catalyzed by Fe complexes (cf. Fig. 1).

Among Fe(III) chelate complexes those with HS are of special relevance due to abundant occurrence of these ligands in the nature. They are thermally very stable compounds, whereas under sunlight undergo photoredox reactions yielding ferrous species and free $HS^{\bullet+}$ radicals (see Section III.A) *(6,132)*.

A.1. Fenton and photo-Fenton reactions

The most common oxidation reaction induced by iron complexes is generation of $OH^{\bullet}$ radicals from H_2O_2 by Fe(II) salts in the so-called Fenton reaction *(133)*:

$$Fe^{2+} + H_2O_2 \rightarrow Fe^{3+} + OH^{\bullet} + OH^{-} \qquad (27)$$

The reaction can be converted into a photocatalytic process by photoreduction of Fe(III) complexes; when at least one of the ligands is hydroxide, then the second $OH^{\bullet}$ radical is produced (Eq. 25); such a reaction sequence is known as the photo-Fenton reaction. It belongs to photoassisted processes because oxidation of organic compounds requires the consumption of radiation energy, whereas the iron photocatalyst is regenerated. However, during this operation instead of molecular oxygen another sacrificial acceptor (H_2O_2) is required. Although hydrogen peroxide does exist in the environment, its concentration is too low to play any significant role in the natural photo-Fenton processes. Moreover, any continuous course of the reaction needs continuous delivery of hydrogen peroxide, and thereby the photo-Fenton role in natural processes is limited *(134)*.

Instead, the photo-Fenton reaction is strongly recommended as one of the most efficient and convenient among the advanced oxidation methods resulting in effective oxidative degradation of organic pollutants in waste and sewage treatments *(135)*. Kinetics and mechanism of the photo-Fenton processes *(136–141)*, process parameters and control *(142)*, pH influence *(143)*, effect of iron source *(144,145)*, and anchored oxygen-donor coordination to iron *(146)*, were all studied extensively. The rate of Fe(II) reoxidation necessary to close the photocatalytic cycle was investigated as function of naturally occurring ligands, molecular oxygen and radical scavenger availability, solution pH, and temperature *(147)*.

The conventional homogeneous photochemical system was proposed to be enhanced by using electro-(photo)-Fenton *(148,149)*

or heterogeneous Fenton techniques especially with the use of semiconductors or resins (*146,150–168*).

Both conventional and improved photo-Fenton methods play a significant role in the degradation of various organic compounds, differing in their structure (aliphatic or aromatic), such as hydrocarbons (*169*), alcohols and their derivatives (*170*), organic acids: salicylic (OHC_6H_4COOH) (*171*), oxalic $(COOH)_2$ (*157*), citric $(OH)C_3H_4(COOH)_3$ (*172*), maleic $(CHCOOH)_2$ (*158*), formic (HCOOH) (*173–175*), phenol (C_6H_5OH) and its derivatives (*159,163,176,177*), poly(ethylene glycol) ($H(OCH_2CH_2)_nOH$) (*178*), and many others organic pollutants (*2,179*).

The photo-Fenton processes are explored as photochemical pretreatment of nonbiodegradable and ubiquitous environmental pollutants and/or extremely toxic compounds in wastewaters, such as persistent organic dyes under visible light irradiation (*151,154,180,181*) and under UV irradiation (*139,182*), azo dye factory wastewaters (*140,162,183–185*), herbicides (*186–188*), pesticides (*152,153,189,190*), insecticides (*191*), pharmaceuticals and wastewaters from medical laboratories (*192–197*), surfactants (*198*), industrial effluents with persistent toxic pollutants (*199*), industrial solvents and wastewaters (*167,200*), chlorinated solvents (*201*), and municipal wastewater (*202*). The photo-Fenton process was proposed to improve the biodegradability of especially biorecalcitrant wastewater, coming from textile industry, and the method was also suggested for water disinfection (*203–205*).

A.2. Photoreduction in other iron systems

A similar oxidative photodegradation of organic substances in the presence of iron(III) complexes without any added H_2O_2 was explored over a long time (*2,16,17,95,206,207*). The studies proved that generation of $LL^{\bullet}$ (Eq. 26) or $OH^{\bullet}$ radicals (Eq. 25) in the photoreduction of $[Fe^{III}(LL)_3]$ or $[Fe^{III}(OH)L_5]$, respectively, leads simultaneously to direct or indirect oxidation of organic ligands (LL) or other substances (via $OH^{\bullet}$ radicals). The Fe(II) re-oxidation by atmospheric molecular oxygen is strongly pH dependent and in general too slow (*147*) to be used for sewage treatment, although it works perfectly under natural environmental conditions.

The Fe(II)/Fe(III) cycling and consequent radical generation was studied repeatedly and effects of various parameters were considered. DOM, oxygenation, and solar irradiance were found to be the most important factors controlling the nature and concentrations of Fe(II) and Fe(III) complexes in water basins. There is a large number of possible thermal and photochemical

reactions involving DOM and both ferrous and ferric iron, along with various reactive oxygen species (superoxides, peroxy radicals, hydrogen peroxide, hydroxo radicals); a net photooxidation process may indicate the importance of the reactive oxygen species in the overall observations (*208–211*). Some inorganic ingredients, such as phosphate or nitrate ions, are also of significance in the photodegradation processes (*212,213*).

The solution pH is of special significance. Most of the processes are favored by alkaline medium that is connected to the formation of hydroxo complexes and generation of the hydroxo radicals (Eq. 25), which are the main oxidizers in photoinduced degradation of pollutants such as: phenol (C_6H_5OH), 2-aminophenol ($NH_2C_6H_4OH$), 3-chlorophenol (ClC_6H_4OH), cyclohexanol ($C_6H_{11}OH$), and nitrobenzene ($C_6H_5NO_2$) (*132,214–219*). A similar mechanism was also suggested in the case of benzoic acid (C_6H_5COOH) removal by homogeneous Fe(III) photocatalysis (*220*), although a maximum rate was noted for pH $\sim$3.5, and at pH values higher than 5.5 the system showed no reactivity at all. The results are thus inconsistent with the effect of pH on the concentration of the $[Fe^{III}(OH)(H_2O)_5]^{2+}$ form ($pK_a = 3.05$).

Quite another mechanism was suggested in case of ligands which form strong complexes with Fe(III), such as mono- and polycarboxylates: acetate (CH_3COO^-), citrate ($(OH)C_3H_4(COO)_3^{3-}$), malonate $(CHCOO)_2^{2-}$, oxalate ($C_2O_4^{2-}$), and ethylenediaminetetraacetate $(OOCCH_2)_2NCH_2CH_2N(CH_2COO)_2^{4-}$, being common constituents of environmental compartments. Moreover, these polycarboxylate complexes undergo rapid photochemical reactions under sunlight irradiation leading to the formation of oxidative species. It was reported that light irradiation of Fe(III)-polycarboxylate complexes initiates the series of redox reactions by LMCT excitation followed by producing both Fe(II) and ligand free radicals.

Thus for Fe(III) acetate the pathway of homogeneous photocatalytic mineralization of the acetate ligand was proposed to start from $R^\bullet = CH_3^\bullet$ radical generation and CO_2 release (*221*):

$$\left[Fe^{III}(RCO_2)\right]^{2+} \xrightarrow{h\upsilon(\mathrm{LMCT})} Fe^{II} + R^\bullet + CO_2 \qquad (28)$$

A somewhat other mechanism was concluded from laser flash photolysis experiments carried out for chelate Fe(III) complexes, such as $[Fe(edta)(H_2O)]^-$ and $[Fe(edta)(OH)]^{2-}$ (*16,17,87,95,222*). The edta complexes were suggested to undergo inner-sphere photoreduction induced by LMCT excitation:

$$\left[Fe^{III}(edta)(H_2O)\right]^- \xrightarrow{h\nu(LMCT)} {}^*\left[Fe^{II}(edta^{\bullet})(H_2O)\right]^- \quad (29)$$

with the $edta^{\bullet 3-}$ radical coordinated to the Fe^{II} center by means of five COO^- groups with a radical $CH_2COO^{\bullet}$ grouping pending free in the transient species. The simultaneous presence of a vacant coordination site and radical ligand in a complex anion is responsible for quenching the transient by both electron donors and acceptors, or even for self-quenching (*16,17*):

$$\begin{aligned} {}^*\left[Fe^{II}(edta^{\bullet})(H_2O)\right]^- + \left[Fe^{III}(edta)(H_2O)\right]^- \rightarrow \\ \left[(H_2O)(edta^{\bullet})Fe^{II}(\mu - OH_x)Fe^{III}(edta)\right]^{x-4} \end{aligned} \quad (30)$$

Within milliseconds the Fe(II)/Fe(III) intermediate undergoes inner-sphere electron transfer:

$$\begin{aligned} \left[(H_2O)(edta^{\bullet})Fe^{II}(\mu - OH_x)Fe^{III}(edta)\right]^{x-4} + xH_2O \rightarrow \\ \left[(edta)Fe^{III}(\mu - O)Fe^{III}(edta)\right]^{4-} + xH_3O^+ \end{aligned} \quad (31)$$

and regenerates the original Fe(III) complex:

$$[(edta)Fe(\mu-O)Fe(edta)]^{4-} + 2H_3O^+ \overset{\leftarrow}{\rightarrow} 2\left[Fe^{III}(edta)(H_2O)\right]^- + H_2O \quad (32)$$

Quenching ${}^*[Fe^{II}(edta^{\bullet})(H_2O)]^-$ by electron donors leads in a deoxygenated medium to the regeneration of the $edta^{4-}$ ligand from the $edta^{\bullet 3-}$ radical and formation of the reduced Fe(II) complex and oxidized donor molecule (D = aliphatic alcohol, sulfate (IV), nitrate(III) or even extraneous $edta^{4-}$ ligand):

$${}^*\left[Fe^{II}(edta^{\bullet})(H_2O)\right]^- + D \rightarrow \left[Fe^{II}(edta)(H_2O)\right]^{2-} + D^+ \quad (33)$$

whereas in the presence of O_2 or another external electron acceptor (e.g., $A = CrO_4^{2-}$), the excited state undergoes oxidative quenching:

$${}^*\left[Fe^{II}(edta^{\bullet})(H_2O)\right]^- + A \rightarrow \left[Fe^{III}(ed3a)(H_2O)\right] + A^- + edta_{ox} \quad (34)$$

producing a stable Fe(III) complex with pentadentate ethylenediaminetriacetate ligand ($(OOCCH_2)_2NCH_2CH_2NH(CH_2COO)^{3-}$, ed3a), and oxidation products of one part of the $edta^{4-}$ ligand ($CH_2COO^{\bullet}$ radical) (*6*).

Laser flash photolysis experiments carried out for a wide range of initial parameters, provided new evidence that intramolecular electron transfer from a ligand to the Fe(III) center is the main photochemical process in the photochemistry of $[Fe^{III}(C_2O_4)_3]^{3-}$ (222). As primary transient species, the radical complex $[(C_2O_4)_2Fe^{II}(C_2O_4^{\bullet})]^{3-}$ was detected; the yield of organic radicals in the primary photoprocess was found to be negligible. A kinetic scheme for the photolysis of $[Fe^{III}(C_2O_4)_3]^{3-}$ was proposed, including formation of $[(C_2O_4)_2Fe^{II}(C_2O_4^{\bullet})]^{3-}$, its reversible dissociation to the oxalate ion and secondary radical complex $[(C_2O_4)Fe^{II}(C_2O_4^{\bullet})]^{-}$, and the decay of both radical complexes. Quite a similar behavior was reported for the heteroleptic Fe(II) oxalate complexes with *N*,*N*-ethylenebis(benzoylacetoneiminato) Schiff base derivatives (223).

Recently, the photochemical redox cycling of iron coupled to the oxidation of the malonate ligand $(CHCOO)_2^{2-}$ has been investigated under conditions that are representative of atmospheric waters (224). Malonate exhibited significantly different characteristics from oxalate and other dicarboxylates. Spin-trapping electron spin resonance experiments proved the formation of both the $CH_2COOH^{\bullet}$ and $OH^{\bullet}$ radicals at lower total malonate concentration, but only $CH_2COOH^{\bullet}$ at higher concentrations of malonate, providing strong evidence for competition between malonate and OH^{-} ligands, and subsequent different photoreaction pathways. The study is of relevance to advance our understanding of iron cycling in acidified carbon-rich atmospheric waters.

Moreover, recent studies on Fe(III) complexes with ethylenediamine-*N*,*N*-disuccinate ($(CH_2NHCHCH_2(COO)_2)_2^{4-}$, edds), which is a structural isomer of edta, proved that the photolysis of Fe-polycarboxylates can be diverse (2,95,225). Irradiated solutions of $[Fe(edds)]^{-}$ showed generation of $OH^{\bullet}$ radicals with a quantum yield dependent on pH and independent of the complex concentration. Thus, the proposed reaction scheme was as follows:

$$\left[Fe^{III}(edds)\right]^{-} \xrightarrow{h\nu(LMCT)} Fe^{II} + edds^{\bullet} \tag{35}$$

$$Fe^{II} \xrightarrow{edds,O_2} \left[Fe^{III}(edds)\right]^{-} \tag{36}$$

$$edds^{\bullet 3-} + OH^{-} \rightarrow edds^{4-} + OH^{\bullet} \tag{37}$$

This study gave evidence for the potential role of $[Fe^{III}(edds)]^{-}$ as a photoactive species in natural waters.

The ligand radicals generated by mono- and polycarboxylate iron(III) complexes can also be the driving force for photocatalytic oxidative degradation of external pollutants directly or upon their

conversion into $OH^{\bullet}$ radicals (e.g., Eqs. 34 and 37). The yield and convenience of the solar photocatalytic degradation can be enhanced by Fe(III) species coupled with TiO_2 (*145,158,159,226–229*).

B. Copper Complexes

Other potential transition metal photocatalysts occur in water basins in much lower concentrations and thus the effect of their photoreactivity is decidedly smaller. Among them only the copper contribution was more extensively studied. In soils most of the metal is in an insoluble form or bound to various inorganic and organic ligands. Only in storm water and subsequently urban rivers, the copper concentration frequently exceeds the freshwater quality criteria. Generally, the main inorganic cupric species present in freshwater systems are Cu^{2+}, $Cu(OH)^{+}$, $Cu(OH)_2$, and $[Cu(CO_3)_2]^{2-}$, and these make up 98% of the dissolved inorganic copper; the rest 2% of dissolved inorganic copper is coordinated mostly by chlorides and phosphates. In seawater, however, copper complexes with naturally occurring organic ligands are predominant. Dissolved organic copper complexes include those with amino acids, carboxylic acids and humic acids. Substantial organic-copper complexation may occur even in water with relatively low organic content, and increases with decreasing pH and increasing salinity. Chloride can strongly bind to Cu(I) and this explains the presence of Cu(I) in seawater (*2*).

The photoredox behavior of Cu(II) complexes, similarly to those of Fe(III), is derived mostly from the reactive decay of their LMCT states. Excitation to LMCT excited states can be attainable by direct sunlight, when the ligands coordinated to Cu(II) are good enough electron donors. As a consequence of the reactive decay of the LMCT excited state by inner-sphere electron transfer, the Cu(II) central atom is reduced to Cu(I), whereas the ligand or another available electron donor is oxidized to its radical, for example:

$$\left[Cu^{II}(LL)_2\right] \xrightarrow{h\nu(\mathrm{LMCT})} Cu^{I} + LL^{\cdot+} \tag{38}$$

or

$$\left[Cu^{II}Cl_x\right]^{2-x} \xrightarrow{h\nu(\mathrm{LMCT})} \left[Cu^{I}Cl_{x-1}\right]^{2-x} + Cl^{\bullet} \tag{39}$$

$$Cl^{\bullet} + Cl^{-} \rightarrow Cl_2^{\bullet -} \quad (40)$$

The $Cl_2^{\bullet -}$ radicals are strong oxidation and chlorination agents. For instance, they are able to oxidize phenol and its derivatives to *para*-benzochinone and/or CO_2 (*230*).

The secondary reactions depend on many factors such as solution pH, oxygenation, DOM, but the Cu(II) photoreduction (Eq. 38) may lead to photodegradation of the chelate ligands or external electron donors.

Cu(II) complexes with carboxylate ligands (acetate, malonate, oxalate) undergo photodecarboxylation during irradiation within their LMCT bands, for example (*231*):

$$[CuOOCCH_3]^{+}{}_{solv} \xrightarrow{LMCT} {}^{*}[CuOOCCH_3]^{+}{}_{solv} \rightarrow Cu^{+}{}_{solv} + CH_3^{\bullet} + CO_2 \quad (41)$$

The electron donor ability of several carboxylic acids to Cu(II) reduction photoassisted by TiO_2 has been compared and formate was found to be a better electron donor than oxalate.

Aminocarboxylate ligands, such as glycine (NH_2CH_2COOH), glutamine ($NH_2CO(CH_2)_2(NH_2)COOH$), alanine (CH_3CHNH_2COOH), nta ($N(CH_3COOH)_3$), ida ($NH(CH_3COOH)_2$), and edta ($C_2H_4N_2(CH_2COOH)_4$), are able to undergo photooxidation under these conditions. Complete photooxidation of these ligands yields among other products carbon dioxide and ammonia. For example, Cu(II) nitrilotriacetate irradiated at 350 nm demonstrated a significant photodecomposition of the ligand to CH_2O, iminodiacetic acid (ida), and CO_2 (*206,230*), whereas Cu(II) iminodiacetate underwent photodegradation to Cu(I) species, NH_4^{+}, HCHO, and CO_2 (*207*).

Ethylenediamine and others polyamine Cu(II) complexes can also be oxidatively photodegraded producing NH_3 and CO_2. Phenanthroline ($C_{12}H_8N_2$) and related compounds in mixed ligand Cu(II) complexes were reported to undergo copper photoreduction and generation of the different radicals that originated from the co-ligands, such as $OH^{\bullet}$, $CH_3O^{\bullet}$, and $CH_3OH^{\bullet +}$. The radicals are able to oxidize many organic compounds, such as primary and secondary aliphatic alcohols or aromatic hydrocarbons (benzene, toluene) and phenol (*230*).

UV-irradiation of Cu(II) diketonate complexes generate Cu(0), which can originate from a disproportionation of Cu(I) produced in photodegradation of β-diketonate of Cu(II). The quantum yields of these reactions are relatively high for UV-irradiation, and solar light is also active (*2*).

Cu(I) produced by photoreduction of Cu(II) undergoes relatively fast reoxidation mostly in the reaction with molecular oxygen:

$$Cu^{+} + O_2 \rightarrow Cu^{2+} + O_2^{\bullet -} \quad (42)$$

which makes the Cu(I) disappearance in oxic environments very fast (in ms). In suboxic rivers, however, the Cu(I) concentration varies with solar UV-irradiance and can reach even 50% of the dissolved copper (2). Chloride ions retard the Cu(I) oxidation through its stabilization in the CuCl form. Conversely, oxygen dissolved in water reduces the Cu(I) concentration, and $O_2^{\bullet -}$ and H_2O_2 are produced instead:

$$O_2^{\cdot -} + H^{+} \rightarrow HO_2^{\bullet} \rightarrow H_2O_2 + O_2 \quad (43)$$

These species play an important role in the copper cycle as they can behave either as oxidants or as reducing agents. The Cu(I) oxidation proceeds in two steps: slow (Eq. 44) and fast (Eq. 45).

$$Cu^{+} + H_2O_2 \rightarrow Cu^{2+} + OH^{\bullet} + OH^{-} \quad (44)$$

$$Cu^{+} + OH^{\bullet} \rightarrow Cu^{2+} + OH^{-} \quad (45)$$

Similarly, Cu(II) reduction goes through the slow (Eq. 46) and the fast steps (Eq. 47)

$$Cu^{2+} + HO_2^{-} \rightarrow Cu^{+} + O_2^{\bullet -} + H^{+} \quad (46)$$

$$Cu^{2+} + O_2^{\bullet -} \rightarrow Cu^{+} + O_2 \quad (47)$$

Dissolved Cu(II) compounds show exceptional susceptibility to scavenge hydroperoxide ($HO_2^{\bullet}$) and superoxide ($O_2^{\bullet -}$) radicals (*230*). Peroxide and superoxide species are thus not only formed in the copper cycle but they have also an influence on the Cu(I)/Cu(II) interconversion, which is of importance in natural waters.

The reaction of Cu(I) with H_2O_2 generating $OH^{\bullet}$ radicals (Eq. 44) resembles that of the iron(II) complexes (Eq. (27), Fenton reaction) and although it is followed by a fast opposite reaction (Eq. 45) that consumes the radicals, copper can contribute to the oxidative degradation in the Fenton-type processes (*205,232–235*). On the other hand, the photophysical properties of copper(I) bis(phenanthroline) complexes induced by a MLCT excitation were interpreted as formation of the Cu(I)→Cu(II) excited state (*236*).

Photooxidation of pollutants with participation of Cu(II) complexes may also occur in heterogeneous systems, viz. on semiconductor surfaces. Since this system requires the presence

of other substances such as TiO_2 or WO_3, it seems to be more useful rather for wastewater cleaning from hazardous species than for environmental self-cleaning (237–242).

C. Chromium Compounds

Chromium environmental abundance is much lower than that of iron. Moreover, the chemistry and photochemistry of chromium(III) complexes are significantly distinct from those of iron(III). The main symptoms are lower stability of Cr(II) species and lower solubility of Cr(III) complexes. Moreover, chromium forms compounds in several higher oxidation states, among which only Cr(VI) species are stable. As a consequence, in the environment chromium occurs in two oxidation states, that is, Cr(III) and Cr(VI), which are drastically different in charge, physicochemical properties, as well as chemical and biochemical reactivity. The immobile Cr(III) form is one of the trace elements essential for the proper functioning of living organisms, whereas mobile Cr(VI) exerts strong toxic effects on biological systems. Their conversion into each other is possible but needs specific reaction conditions, such as solution pH, oxygen concentration, presence of appropriate electron donors, acceptors, and mediators acting as reagents, ligands, or catalysts (243,244).

These prerequisites do not favor anticipation of any observable chromium contribution to pollutant photodegradation in the environment. But yet, cyclic fluctuations of the Cr(VI)/Cr(III) concentration ratio in seawater, dependent on solar irradiance, were detected, which is indicative for the detectable photoconversion that had to entail an oxidative photodegradation of DOM (243). Moreover, the photochemical conversion between Cr(VI) and Cr(III) was investigated with respect to the possible existence in the nature of complete photocatalytic cycles functioning in day-and-night intervals. Under conditions mimicking the natural ones, the model system consisted of $[Cr(C_2O_4)_3]^{3-}$, CrO_4^{2-}, and $C_2O_4^{2-}$, the concentration ratio was oscillating according to light and dark sequences, suggesting the cyclic conversions of Cr(III) to Cr(VI) and Cr(VI) to Cr(III) (95,245).

C.1. Cr(III) complexes

Current knowledge of chromium(III) photochemistry relates mostly to the decay of the metal-centered (MC) excited states (246). Photosubstitution and photoisomerization are, however, of minor

environmental relevance, because only the photoredox behavior is able to induce oxidative photodegradation of the pollutants.

To undergo a photoredox reaction, the central atom should coordinate an electron donor good enough for electron transfer toward the Cr(III) center in the LMCT excited state. Photoredox reactivity was reported for Cr(III) complexes with ligands such as N_3^- (*247*), CN^- (*248*), NCS^- (*249*), edta (*18,244*), and $C_2O_4^{2-}$ (*245*). The LMCT excitation within the UV range was shown to induce Cr(III) photoreduction to Cr(II) in $[Cr(CN)_{6-x}(OH)_x]^{3-}$ (*248*), $[CrA_2(NCS)_4]^-$ (A = NH_3, aniline ($C_6H_5NH_2$), *n*-propylamine ($C_3H_7NH_2$), morpholine ($NHCH_2CH_2OCH_2CH_2$)), and $[Cr(A—A)(NCS)_4]^-$ (A–A = 1,2-diaminethane or 1,2-diaminopropane) complexes (*250*). The Cr(III) complexes with edta are able to undergo photoreduction upon excitation by solar light (*18,244*), whereas the photoreactivity of oxalate and citrate complexes needs some more energetic radiation (*245,251,252*).

The LMCT excitation of the Cr(III) complex with edta:

$$\left[Cr^{III}(edta)OH\right]^{2-} \xrightarrow{h\nu(LMCT)} {}^*\left[Cr^{II}(edta^{\bullet})OH\right]^{2-} \qquad (48)$$

is followed by back electron transfer

$${}^*\left[Cr^{II}(edta^{\bullet})OH\right]^{2-} \rightarrow \left[Cr^{III}(edta)OH\right]^{2-} \qquad (49)$$

and/or PET accompanied by dissociation of the oxidized part of the ligand. In the presence of molecular oxygen, $*[Cr^{II}(edta^{\bullet})OH]^{2-}$ is quenched reproducing Cr(III) or even yielding Cr(VI) species. The latter Cr(II) oxidation (Eq. 50) is possible under specific conditions, that is, in alkaline medium and at a relatively large excess of O_2 over the Cr(II) concentration (*18,244,248–250*).

$$Cr(II)_{aq} + O_2 \xrightarrow{OH^-} CrO_4^{2-} \qquad (50)$$

Another hypothesis concerning the mechanism of the Cr(II) → Cr(VI) oxidation is based on the assumption that in alkaline medium the $edta^{\bullet 3-}$ radical ligand, similar to the free $edds^{\bullet 3-}$ radical (Eq. 37), produces $OH^{\bullet}$ radicals (*225,252*).

The crucial role of $OH^{\bullet}$ radicals in Cr(II) → Cr(VI) oxidation was suggested also in the case of UV irradiated citrate complexes $[Cr^{III}(cit)]$ and $[Cr^{III}(cit)OH]^-$ (*252*). The reaction series is initiated by photoreduction:

$$\left[Cr^{III}(cit)\right] \xrightarrow{h\nu(LMCT)} {}^*\left[Cr^{II}(cit^{\bullet})\right] \rightarrow Cr^{II}{}_{aq} + cit^{\bullet} \qquad (51)$$

and followed by oxidation of both products by O_2:

$$\text{cit}^{\bullet 2-} + O_2 \rightarrow 3\text{-oxoglutarate} + CO_2 + O_2^- \quad (52)$$

$$Cr^{II}{}_{aq} + O_2 \rightarrow Cr^{III}{}_{aq} + O_2^- \quad (53)$$

$$2O_2^{\bullet -} + 2H^+ \rightarrow 2HO_2^{\bullet} \rightarrow H_2O_2 + O_2 \quad (54)$$

$$H_2O_2 \xrightarrow{h\nu<300\,\text{nm}} 2OH^{\bullet} \quad (55)$$

$$Cr^{II}{}_{aq} + 4OH^{\bullet} + 4OH^- \rightarrow CrO_4^{2-} + 4H_2O \quad (56)$$

Consistent with the proposed reaction scheme, the quantum yield of chromate(VI) production increased significantly with pH, that is, for $[Cr^{III}(cit)OH]^-$ it was higher than for $[Cr^{III}(cit)]$.

In the case of trisoxalatochromate(III), $[Cr(C_2O_4)_3]^{3-}$, a similar pathway of LMCT photochemistry was suggested, although distinct from $edta^{\bullet 3-}$, the $C_2O_4^{\bullet -}$ radical ligand is more susceptible to release (*95,245*). The LMCT excitation:

$$\left[Cr^{III}(C_2O_4)_3\right]^{3-} \xrightarrow{h\nu(\text{LMCT})} {}^*\left[Cr^{II}(C_2O_4)_2(C_2O_4^{\bullet -})\right]^{3-} \quad (57)$$

is followed by back electron transfer

$${}^*\left[Cr^{II}(C_2O_4)_2(C_2O_4^{\bullet -})\right]^{3-} \rightarrow \left[Cr^{III}(C_2O_4)_3\right]^{3-} \quad (58)$$

and/or by PET accompanied by dissociation of the oxidized ligand:

$${}^*\left[Cr^{II}(C_2O_4)_2(C_2O_4^{\bullet -})\right]^{3-} \rightarrow \left[Cr^{II}(C_2O_4)_2\right]^{2-} + C_2O_4^{\bullet -} \quad (59)$$

Quenching of the Cr(II) species by molecular oxygen yields $[Cr^{III}(C_2O_4)_2(H_2O)_2]^-$ and/or CrO_4^{2-}, whereas the $C_2O_4^{\bullet -}$ radicals readily generate $OH^{\bullet}$ radicals and finally are oxidized to CO_2 (*222,225*).

Recent flash photolysis results showed, however, that beside the photoredox mechanism illustrated by Eqs. (51)–(53), also solvated electron generation could be recorded within nanoseconds ($\tau_{1/2} = 0.16\ \mu s$) (*251*).

$$\left[Cr^{II}(C_2O_4)_2(C_2O_4^{\bullet -})\right]^{3-} \rightarrow \left[Cr^{III}(C_2O_4)_2(C_2O_4^{\bullet -})\right]^{2-} + e^-{}_{aq} \quad (60)$$

The $e^-{}_{aq}$ lifetime increased significantly when one oxalate ligand in $[Cr^{III}(C_2O_4)_3]^{3-}$ was substituted by a more electrophilic

ligand like pyridinedicarboxylate (pda). This behavior was interpreted by the reaction series:

$$\left[Cr^{III}(C_2O_4)_2(pda)\right]^{3-} \xrightarrow{h\nu(LMCT)} \left[Cr^{II}(C_2O_4^{\bullet-})(C_2O_4)(pda)\right]^{3-} \tag{61}$$

$$\left[Cr^{II}(C_2O_4^{\bullet-})(C_2O_4)(pda)\right]^{3-} \rightarrow \left[Cr^{III}(C_2O_4^{\bullet-})(C_2O_4)\left(pda^{\bullet 3-}\right)\right]^{3-} \tag{62}$$

$$\left[Cr^{III}(C_2O_4^{\bullet-})(C_2O_4)\left(pda^{\bullet 3-}\right)\right]^{3-} \rightarrow \left[Cr^{III}(C_2O_4^{\bullet-})(C_2O_4)(pda)\right]^{2-} + e^-_{aq} \tag{63}$$

$$\left[Cr^{III}(C_2O_4^{\bullet-})(C_2O_4)(pda)\right]^{2-} + 2H_2O \rightarrow \left[Cr^{III}(C_2O_4)(pda)(H_2O)_2\right]^{-} + C_2O_4^{\bullet-} \tag{64}$$

demonstrating that photoinduced innersphere charge transfer from the oxalate ligand to the Cr(III) center (Eq. 61) was followed by secondary inner-sphere CT from the Cr(II) center to the pyridinedicarboxylate ligand (Eq. 62) and by outer-sphere electron transfer to the solvent (Eq. 63).

Molecular oxygen competes effectively with inner- or outersphere electron transfer, and production of chromate(VI) was recorded both in the case of oxygenated homo- and heteroleptic complexes with the quantum yield decreasing within the series 2,3-pda > 2,4-pda > 2,5-pda ≈ $(ox)_3$. However, Cr(VI) production was never recorded in the photoreaction of homoleptic complexes containing only pyridinedicarboxylate ligands *(251)*.

The photoredox reaction of chromium(III) complexes with ligands such as oxalate, citrate, or edta can proceed under environmental conditions. In consequence, these pollutants undergo oxidative degradation, but simultaneously the harmful and toxic chromate(VI) is generated. To close the photocatalytic cycle, Cr(VI) had to undergo successive photoredox processes.

C.2. Chromate(VI) compounds

In the environment, chromate(VI) occurs in two forms, depending on the solution pH (pK = 6.5):

$$HCrO_4^- \rightleftarrows CrO_4^{2-} + H^+ \tag{65}$$

and its concentrations are too low for the existence of the dimeric $Cr_2O_7^{2-}$ form. Both monomeric anions absorb the near-UV part of the solar spectrum ($\lambda_{max} = 374$ nm, $\varepsilon = 4880$ for CrO_4^{2-} and $\lambda_{max} = 352$ nm, $\varepsilon = 1350$ for $HCrO_4^-$ (*253*)) and the absorbed radiation generates the LMCT excited state, which undergoes a photoreaction only when a proper electron donor is accessible to activate the PET between two sites localized in the same molecular entity (innersphere PET, Eq. 66) or from one molecular entity to another (outersphere PET, Eq. 67).

Oxidation of alcohols at the expense of photoreduction of Cr (VI) was initially interpreted in terms of the photochemical reactivity of chromate(VI) esters, but time-resolved spectroscopic studies (*253*) proved that the photoreaction mode depends on the bond strength between chromate and secondary alcohol. In the case of the strong bond, innersphere transfer of two electrons was recorded (Fig. 3):

$$^*R_1R_2CHOCrO_3^- + 5H^+ + 3H_2O \rightarrow R_1R_2CO + \left[Cr(H_2O)_6\right]^{4+} \quad (66)$$

whereas in the case of weak interaction between chromate(VI) and an electron donor, outersphere quenching yields one electron transfer:

$$^*HCrO_4^- + R_1R_2CHOH \rightarrow H_2Cr^{V}O_4^- + R_1R_2CHO^{\bullet} \quad (67)$$

In the environment, there are many external electron donors, which are susceptible to contribute to the Cr(VI) photoreduction, among others alcohols, oxalate, cysteine ($HSCH_2CH(NH_2)COOH$), phenol, and its derivatives (*2,95,244,245,253–255*).

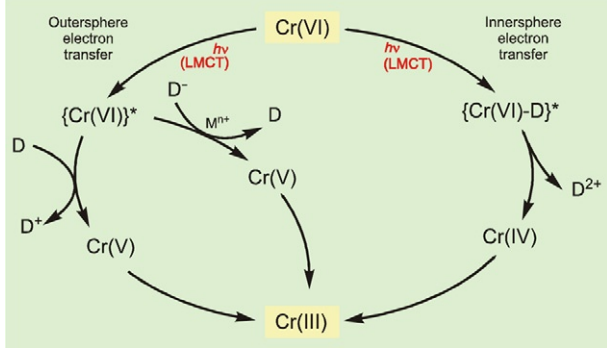

FIG. 3. Scheme for photoinduced charge transfer between excited chromate(VI) anions and electron donors via inner- or outer-sphere pathway.

Their oxidative degradation starts from PET analogous to that shown for alcohols (Eq. 67). In the case of anionic electron donors, electron transfer is assisted by external cations yielding ion pairs (*245*) (Fig. 3).

Chromium(V) species, the main photoreduction products, are stable only in exceptional cases (as in the polyvinylalcohol matrix (*256*)). The reduction of chromium(V) to chromium(III) is a far slower process when chromium is in the presence of strong chelating agents such as polycarboxylate derivatives (*257*), but in general, Cr(V) undergoes a series of redox reactions and, in absence of other redox and coordinating partners, is transformed in part into a Cr(III) species and in part to Cr(VI), for example:

$$3\mathrm{Cr(V)} \rightarrow \mathrm{Cr(III)} + 2\mathrm{Cr(VI)} \qquad (68)$$

D. Photocatalytic Cycles

Photochemical and photocatalytic processes are responsible for self-cleaning of the atmosphere, soils, and water basins. Transition metal complexes contribute mainly to cleaning of the hydrosphere, although their cooperation with atmospheric gases is as yet underestimated and the progress needs more detailed investigations.

The photoassisted activity is especially useful for degradation of strongly hazardous substances or recalcitrant pollutants, which are resistant to removal in chemical and/or biochemical processes. Transition metal photocatalysts are able to stimulate the indirect photodegradation of molecules that resist direct photolysis. Thus, they can activate species not absorbing sunlight, or those whose excited states populated by sunlight absorption are chemically inefficient.

Photocatalysis processes are environmental friendly, heading for sustainable development because their driving force is sunlight, their oxidizing agent is atmospheric molecular oxygen and most photodegradations result in complete mineralization of the DOM without any pollution by risky side-products.

Among the coordination compounds involved in environmental photocatalysis, iron, copper, and chromium species belong to the most effective. The photoassisted cycles driven by most transition metals need one photon excitation; the exception is the chromium cycle, which needs twofold excitations of the chromium species to close the cycle (Fig. 4).

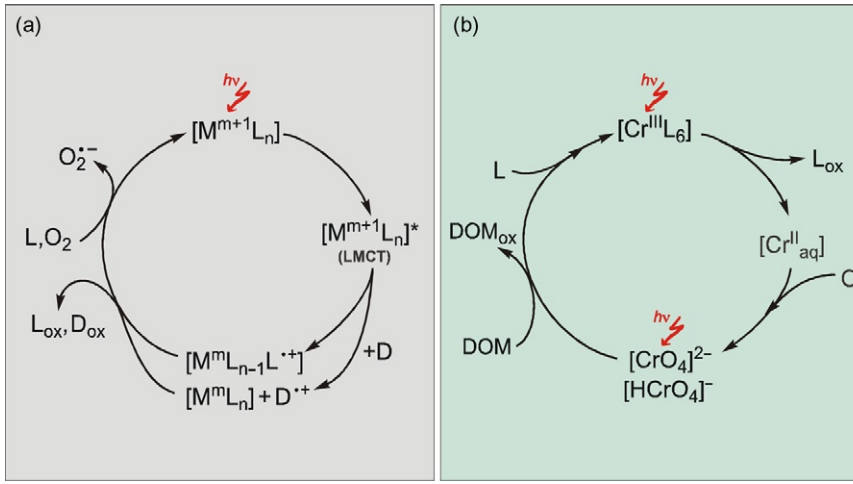

FIG. 4. Two alternative pathways for the redox cycles photocatalyzed by Fe(III) or Cu(II) complexes (a) and by chromium compounds (b); L, ligand; D, external electron donor; DOM, dissolved organic matter.

The former case is illustrated in Fig. 4a, showing two alternative pathways for the redox cycles photocatalyzed by Fe(III) or Cu(II) chelate complexes: (i) innersphere PET with ligand (L) as electron donor and (ii) outersphere PET with an external electron donor (D). The latter way of degradation by Fe(III) photocatalysts is of special meaning in the case of anthropogenic pollutants, such as herbicides and pesticides (*164,186,189,258,259*).

The iron photocatalytic cycles have relevant activity in nature not only due to their cleaning and disinfection functions (*203*) but also for inducing key biological processes, including amino acid synthesis, oxygen transport, respiration, nitrogen fixation, methanogenesis, the citric acid cycle, photosynthesis, and DNA biosynthesis. Moreover, the vast majority of bacteria require for growth iron in a definite oxidation state (*260*).

It is now realized that copper as metal next to iron and chromium participates in photoredox cycles and its role cannot be ignored. The most important part of the cycle is photoreduction of Cu(II) to Cu(I) induced by solar light and oxidation of ligands to their environmentally benign forms. Then Cu(I) is easily re-oxidized to Cu(II), which can coordinate the next ligand molecule, and thereby the Cu photocatalytic cycles contribute to continuous environmental cleaning. Besides oxidation/reduction, other critical processes relevant to the copper cycles are adsorption/desorption and precipitation/dissolution

that control the Cu environmental speciation and thus its bioavailability and toxicity.

The role of chromium compounds (Fig. 4b) is quite special. Although two photons are needed to excite two different Cr forms in one cycle, each photoreduction entails an organic pollutant oxidation, which possibly means higher efficiency and larger diversification of degraded pollutants. Moreover, the processes result not only in the degradation of organic compounds but also assist in decreasing the concentration of chromate(VI), one of the most dangerous and toxic pollutants.

Beside monometallic cycles, mixed metal systems are also active in nature. The cooperation between the photocatalytic cycles of two transition metals can lead to diversification of the degraded pollutants, but their efficiency can be either higher or lower compared to that of the single metal cycle.

Photocatalysis of the mixed Cu(II)/Fe(III)/TiO_2/edta system was investigated and edta photooxidation was found accompanied by simultaneous metal cation reduction, the rate of which was directly correlated with the initial Cu(II) concentration *(229)*.

In aspect of its toxicity, any pathway leading to abatement of chromate(VI) pollution arouse a vivid interest. One of such pathways seems to be created by cooperations between the iron and chromium photocatalytic cycles, which were reported as effectively converting chromate(VI) into Cr(III) species. Photochemical coupling reactions between polycarboxylate Fe(III) complexes and chromate(VI) were studied and strong collaboration between both photocatalysts was demonstrated, which was significantly affected by the oxygen concentration *(16,17,95,261)*. On the other hand, chromium(VI) reduction photoinduced by iron(III) nitrilotriacetate accompanied by nta degradation was found to be independent of the O_2 concentration, whereas the oxidation state of the chromium product depended on the pH *(257)*.

In the Fe(III)/Cr(VI)/BPA ternary system (BPA = bisphenol A, $(CH_3)_2C(C_6H_4OH)_2$), simultaneous photocatalytic reduction of Cr(VI) and oxidation of bisphenol A was observed in the presence of Fe(III)—OH complexes, and the reaction rate was affected by Fe(III) and H^+ concentrations *(262)*.

The study of Cr(VI) photoreduction in the presence of ferric ion and inorganic anions showed that direct irradiation of acidic wastewaters containing Cl^-, NO_3^-, and Fe(III) is a feasible strategy for eliminating Cr(VI) *(263)*.

A synergistic photoreduction of Cr(VI) and Cu(II) mediated by TiO_2, or photocatalytic reduction of Cr(VI) and oxidation of

organic matter by environmental polyoxometallates as photocatalysts may constitute alternative possibilities (*264*).

VI. Concluding Remarks

The mutual stimulation of scientists coming from different disciplines, viz. photochemistry, electrochemistry, coordination chemistry, analytical chemistry, biology, medicine, material chemistry, surface science, electronics, and catalysis, resulted in the extremely rapid development of photocatalysis (*265*). This review shows the fast progress made in our understanding of the processes occurring in nature that are catalyzed by metal complexes and driven by solar energy, and demonstrates their general trends and fine details.

In the environment there are two general opposing trends, viz. to build organic substances from carbon dioxide and water in photosynthesis, and to decompose them by O_2 oxidation, photocatalyzed by transition metal compounds. The photocatalytic cycles may be treated as "anti-photosynthesis" as they consume atmospheric oxygen and organic compounds and thus disperse energy accumulated by photosynthesis. These processes are of vital importance, because theoretically, most atmospheric oxygen could be consumed, which would be a threat to life on Earth. Fortunately, photosynthesis is dominating in nature and photocatalysis by transition metals plays a minor, although a very useful, role in cleaning the environment from the excess of useless and harmful organic matter. The natural processes may as well be used in environmental protection procedures of the pollution abatement and in solar purification of water in arid countries.

The relevance of photocatalysis in solving the environmental problems manifests itself in effective degradation of many pollutants, which are not sensitive to biodegradation, like the majority of synthetic polymers, among others poly(*N*-vinylpyrrolidone) (PVP) (*266*).

Moreover, the environmental systems demonstrate unique diversity and versatility of the processes depending on the actual conditions, viz. the reaction directions and rates are sensitive to many diverse parameters, sometimes even difficult to be perceived. The example may be the dependence of the photocatalytic activity of Sr—Al—Nb—O double perovskite on the cation ordering in the oxides (*267*), or the effect of the in-plane twist of the quinoline-based co-ligand on the thermal stability and yield of NO photorelease from the $[Ru(NO)]^6$ nitrosyl complexes (*96*).

Environmental photosensitization processes may be stimulated not only by natural but also by anthropogenic pollutants, such as phenols and dihydroxybenzenes, which are efficient photosensitizers. Among others, phenol was found to sensitize the dehalogenation of halogenophenols (*268*). This behavior shows that the simultaneous presence of the adequate sensitizer and quencher in polluted environment can lead to the photosensitized decomposition of the latter and thereby to pollution abatement.

One of the most relevant activators is traces of solid semiconductors present in atmospheric or hydrospheric compartments. This role may be played not only by typical semiconductors but also by many different substances even dessert sand and volcanic ash (*23–25,269–271*).

The self-cleaning mechanisms by photocatalysis and photosensitization apply also to organic matter included in microorganisms, thus it can also lead to environmental self-disinfection. This is especially expected in the vicinity of a semiconductor (especially TiO_2) and/or iron deposits, which are responsible for solar photogeneration of reactive oxygen substances capable of water disinfection (*272–275*).

Acknowledgments

The technical assistance of Mr. Zygmunt Wołek in preparation of the chapter is greatly appreciated.

References

1. Shichi, T.; Takagi, K. *J. Photochem. Photobiol. C. Photochem. Revs.* **2000,** *1*, 113.
2. Ciesla, P.; Kocot, P.; Mytych, P.; Stasicka, Z. *J. Mol. Catal. A. Chem* **2004,** *224*, 17.
3. Balzani, V.; Bergamini, G.; Campagna, S.; Puntoriero, F. In "*Photochemistry and Photophysics of Coordination Compounds I*" Vol. I;. In: Eds. Balzani, V.; Campagna, S. Verlag: Berlin, **2007**, p. 1.
4. Gaffney, J. S.; Marley, N. A.; Clark, S. B. In "*Humic and Fulvic Acids*"; *ACS Symposium Series*,, **1996,** Vol. 651, p. 2.
5. Rey-Castro, C.; Mongin, S.; Huidobro, C.; David, C.; Salvador, J.; Garces, J. L.; Galceran, J.; Mas, F.; Puy, J. *Environ. Sci. Technol.* **2009,** *43*, 7184.
6. Boule, P.; Bolte, M.; Richard, C. In: "*Environmental Photochemistry*"; Ed. Boule, P.; Springer: Berlin, **1999**, p. 181.
7. Rontani, J. F. In: "*Environmental Photochemistry*"; Ed. Boule, P.; Springer-Verlag: Berlin, **1999**, p. 263.
8. Larson, R. A.; Marley, K. A. In: "*Environmental Photochemistry*"; Ed. Boule, P.; Springer: Berlin, **1999**, p. 123.

9. Hessler, D. P.; Frimmel, S. H.; Oliveros, E.; Braun, A. M. *J. Photochem. Photobiol. B. Biol.* **1996,** *36*, 56.
10. Zhao, X.; Quan, X.; Zhao, H.; Chen, S.; Zhao, Y.; Chen, J. *J. Photochem. Photobiol. A Chem* **2004,** *167*, 177.
11. Chan, K. H.; Chu, W. *Water Res.* **2005,** *39*, 2154.
12. Kamiya, M.; Kameyama, K. *Chemosphere* **1998,** *36*, 2337.
13. Sakkas, V. A.; Lambropoulou, D. A.; Albanis, T. A. *J. Photochem. Photobiol. A Chem* **2002,** *147*, 135.
14. Kyziol, J.; Twardowska, I.; Schmitt-Kopplin, P. *Chemosphere* **2006,** *63*, 1974.
15. Nowack, B.; VanBriesen, J. M. In "*Biogeochemistry of Chelating Agents*"; *ACS Symposium Series,* **2005,** Vol. 910, p. 1.
16. Kocot, P.; Karocki, A.; Stasicka, Z. *J. Photochem. Photobiol. A Chem* **2006,** *179*, 176.
17. Kocot, P.; Szaciłowski, K.; Stasicka, Z. *J. Photochem. Photobiol. A Chem* **2007,** *188*, 128.
18. Ciesla, P.; Karocki, A.; Stasicka, Z. *J. Photochem. Photobiol. A Chem.* **2004,** *162*, 537.
19. Deguillaume, L.; Leriche, M. D. K.; Mailhot, G.; George, C.; Chaumerliac, N. *Chem. Rev.* **2005,** *105*, 3388.
20. Faust, B. C. In: "*Environmental Photochemistry*"; Ed. Boule, P.; Springer: Berlin, **1999**, p. 101.
21. Shilov, A. E.; Shul'pin, G. B. *Chem. Rev.* **1997,** *97*, 2879.
22. Funyu, S.; Kinai, M.; Masui, D.; Takagi, S.; Shimada, T.; Tachibana, H.; Inoue, H. *Photochem. Photobiol. Sci.* **2010,** *9*, 931.
23. Isidorov, V.; Klokova, E.; Povarov, V.; Kalkova, S. *Catal. Today* **1997,** *39*, 233.
24. Idriss, H.; Miller, A.; Seebauer, E. G. *Catal. Today* **1997,** *33*, 215.
25. Idriss, H.; Seebauer, E. G. *Langmuir* **1998,** *14*, 6146.
26. Faust, B. C.; Hoffmann, M. R.; Bahnemann, D. W. *J. Phys. Chem.* **1989,** *93*, 6371.
27. Brandt, C.; van Eldik, R. *Chem. Rev.* **1995,** *95*, 119.
28. Sadanaga, Y.; Matsumoto, J.; Kajii, Y. *J. Photochem. Photobiol. C. Photochem. Revs.* **2003,** *4*, 85–104.
29. Hayton, T. W.; Legzdins, P.; Sharp, W. B. *Chem. Rev.* **2002,** *102*, 935.
30. Wanat, A.; Schneppensieper, T.; Stochel, G.; van Eldik, R.; Bill, E.; Wieghardt, K. *Inorg. Chem.* **2002,** *41*, 4.
31. Wiese, S.; Kapoor, P.; Williams, K. D.; Warren, T. H. *J. Am. Chem. Soc.* **2009,** *131*, 18105.
32. Lehnert, N.; Scheidt, W. R. *Inorg. Chem.* **2010,** *49*, 6223.
33. Ford, P. C.; Wecksler, S. *Coord. Chem. Rev.* **2005,** *249*, 1382.
34. Macyk, W.; Franke, A.; Stochel, G. *Coord. Chem. Rev.* **2005,** *249*, 2437.
35. Roy, S.; Hegde, M. S.; Madras, G. *Appl. Energy* **2009,** *86*, 2283.
36. Roncaroli, F.; Videla, M.; Slep, L. D.; Olabe, J. A. *Coord. Chem. Rev.* **2007,** *251*, 1903.
37. Lim, M. H.; Lippard, S. J. *Acc. Chem. Res.* **2007,** *40*, 41.
38. Ostrowski, A. D.; Ford, P. C. *Dalton Trans.* **2009,** *48*, 10660.
39. Rose, M. J.; Mascharak, P. K. *Curr. Opin. Chem. Biol.* **2008,** *12*, 238.
40. Hubbard, C. D.; van Eldik, R. *Inorg. Chim. Acta* **2010,** *363*, 2357.
41. Ford, P. C.; Laverman, L. E. *Coord. Chem. Rev.* **2005,** *249*, 391.
42. Szaciłowski, K.; Chmura, A.; Stasicka, Z. *Coord. Chem. Rev.* **2005,** *249*, 2408.

43. Harrop, T. C.; Tonzetich, Z. J.; Reisner, E.; Lippard, S. J. *J. Am. Chem. Soc.* **2008,** *130*, 15602.
44. Chen, Y. J.; Ku, W. C.; Feng, L. T.; Tsai, M. L.; Hsieh, C. H.; Hsu, W. H.; Liaw, W. F.; Hung, C. H.; Chen, Y. J. *J. Am. Chem. Soc.* **2008,** *130*, 10929.
45. Tsou, C. C.; Lin, Z. S.; Lu, T. T.; Liaw, W. F. *J. Am. Chem. Soc.* **2008,** *130*, 17154.
46. Ford, P. C. *Acc. Chem. Res.* **2008,** *41*, 190.
47. Grapperhaus, C. A.; Patra, A. K.; Mashuta, M. S. *Inorg. Chem.* **2002,** *41*, 1039.
48. DeRosa, F.; Bu, X.; Ford, P. C. *Inorg. Chem.* **2005,** *44*, 4157.
49. Wecksler, S. R.; Mikhailovsky, A.; Korystov, D.; Buller, F.; Kannan, R.; Tan, L. S.; Ford, P. C. *Inorg. Chem.* **2007,** *46*, 395.
50. Chmura, A.; Szaciłowski, K.; Stasicka, Z. *Nitric Oxide* **2006,** *15*, 370.
51. Jaworska, M.; Stasicka, Z. *New J. Chem.* **2005,** *29*, 604.
52. Jaworska, M.; Stasicka, Z. *J. Mol. Struct.* **2006,** *785*, 68.
53. Chmura, A.; Szaciłowski, K.; Waksmundzka-Gora, A.; Stasicka, Z. *Nitric Oxide* **2006,** *14*, 247.
54. Wanat, A.; Wolak, M.; Orzel, L.; Brindell, M.; van Eldik, R.; Stochel, G. *Coord. Chem. Rev.* **2002,** *229*, 37.
55. Fernandez, B. O.; Lorkovic, I. M.; Ford, P. C. *Inorg. Chem.* **2003,** *42*, 2.
56. Goodrich, L. E.; Paulat, F.; Praneeth, V. K. K.; Lehnert, N. *Inorg. Chem.* **2010,** *49*, 6293.
57. Rose, M. J.; Betterley, N. M.; Oliver, A. G.; Mascharak, P. K. *Inorg. Chem.* **2010,** *49*, 1854.
58. Laverman, L. E.; Wanat, A.; Oszajca, J.; Stochel, G.; Ford, P. C.; van Eldik, R. *J. Am. Chem. Soc.* **2001,** *123*, 285.
59. Yukl, E. T.; de Vries, S.; Moenne-Loccoz, M. *J. Am. Chem. Soc.* **2009,** *131*, 7234.
60. Wolak, M.; van Eldik, R. *Coord. Chem. Rev.* **2002,** *230*, 263.
61. Laverman, L. E.; Hoshino, M.; Ford, P. C. *J. Am. Chem. Soc.* **1997,** *119*, 12663.
62. Wolak, M.; van Eldik, R. *J. Am. Chem. Soc.* **2005,** *127*, 13312.
63. Jee, J. E.; Eigler, S.; Hampel, F.; Jux, N.; Wolak, M.; Zahl, A.; Stochel, G.; van Eldik, R. *Inorg. Chem.* **2005,** *44*, 7717.
64. Schmeisser, M.; van Eldik, R. *Inorg. Chem.* **2009,** *48*, 7466.
65. Jee, J. E.; van Eldik, R. *Inorg. Chem.* **2006,** *45*, 6523.
66. Jee, J. E.; Wolak, M.; Balbinot, D.; Jux, N.; Zahl, A.; van Eldik, R. *Inorg. Chem.* **2006,** *45*, 1326.
67. Bari, S. E.; Martı, M. A.; Amorebieta, V. T.; Estrin, D. A.; Doctorovich, F. *J. Am. Chem. Soc.* **2003,** *125*, 15272.
68. Laverman, L. E.; Ford, P. C. *J. Am. Chem. Soc.* **2001,** *123*, 11614.
69. Lin, Y. W.; Yeung, N.; Gao, Y. G.; Miner, K. D.; Lei, L.; Robinson, H.; Lu, Y. *J. Am. Chem. Soc.* **2010,** *132*, 9970.
70. Roche, C. J.; Friedman, J. M. *Nitric Oxide* **2010,** *22*, 180.
71. Hayashi, T.; Caranto, J. D.; Wampler, D. A.; Kurtz, J. D. M.; Moenne-Loccoz, P. *Biochemistry* **2010,** *49*, 7040.
72. Nguyen, T. Q.; Escano, M. C. S.; Kasai, H. *J. Phys. Chem. B* **2010,** *114*, 10017.
73. Fricker, S. P. *Platinum Met. Rev.* **1995,** *39*, 150.
74. Serli, B.; Zangrando, E.; Gianferrara, T.; Yellowlees, L.; Alessio, E. *Coord. Chem. Rev.* **2003,** *245*, 73.
75. Rose, M. J.; Mascharak, P. K. *Curr. Opin. Chem. Biol.* **2008,** *12*, 238.

76. Stochel, G.; Brindell, M.; Macyk, W.; Stasicka, Z.; Szaciłowski, K. *Bioinorganic photochemistry* (1st edn.). Wiley: Chichester, **2009** p. 382.
77. van der Maas, P.; van den Brink, P.; Utomo, S.; Klapwijk, B.; Lens, P. *Biotechnol. Bioeng.* **2006,** *94*, 574.
78. Patra, A. K.; Rowland, J. M.; Marlin, D. S.; Bill, E.; Olmstead, M. M.; Mascharak, P. K. *Inorg. Chem.* **2003,** *42*, 6812.
79. Afshar, R. K.; Patra, A. K.; Olmstead, M. M.; Mascharak, P. K. *Inorg. Chem.* **2004,** *43*, 5736.
80. Eroy-Reveles, A. A.; Hoffman-Luca, C. G.; Mascharak, P. K. *Dalton Trans.* **2007,** *45*, 5268.
81. Littlejohn, D.; Chang, S. G. *J. Phys. Chem.* **1982,** *86*, 537.
82. Rudziński, K. J.; Sada, E.; Kumazawa, H. *Ind. Eng. Chem. Res.* **1987,** *26*, 2012.
83. Zang, V.; Kotowski, M.; van Eldik, R. *Inorg. Chem.* **1988,** *27*, 3279.
84. Zang, V.; van Eldik, R. *Inorg. Chem.* **1990,** *29*, 4462.
85. Schneppensieper, T.; Finkler, S.; Czap, A.; van Eldik, R.; Heus, M.; Nieuwenhuizen, P.; Wreesmann, C.; Abma, W. *Eur. J. Inorg. Chem.* **2001,** *2*, 491.
86. Schneppensieper, T.; Wanat, A.; Stochel, G.; van Eldik, R. *Inorg. Chem.* **2002,** *41*, 2565.
87. Maigut, J.; Meier, R.; Zahl, A.; van Eldik, R. *Inorg. Chem.* **2007,** *46*, 5361.
88. Zang, V.; van Eldik, R. *Inorg. Chem.* **1990,** *29*, 1705.
89. Seibig, S.; van Eldik, R. *Inorg. Chem.* **1997,** *36*, 4115.
90. Huasheng, L.; Wechi, F. *Ind. Eng. Chem. Res.* **1988,** *27*, 770.
91. Jin, Y.; Veiga, M. C.; Kennes, C. *J. Chem. Technol. Biotechnol.* **2005,** *80*, 483.
92. Gambardella, F.; Galán Sánchez, L. M.; Ganzeveld, K. J.; Winkelman, J. G. M.; Heeres, H. J. *Chem. Eng. J.* **2006,** *116*, 67.
93. Jaworska, M.; Stopa, G.; Stasicka, Z. *Nitric Oxide* **2010,** *23*(3), 227.
94. Sada, E.; Kumazawa, H.; Machida, H. *Ind. Eng. Chem. Res.* **1987,** *26*, 1468.
95. Ciesla, P.; Mytych, P.; Kocot, P.; Stasicka, Z. *Sep. Sci. Technol.* **2007,** *42*, 1651.
96. Fry, N. L.; Heilman, B. J.; Mascharak, P. K. *Inorg. Chem.* **2011,** *50*, 317.
97. Rose, M. J.; Mascharak, P. K. *Coord. Chem. Rev.* **2008,** *252*, 2093.
98. Patra, A. K.; Rose, M. J.; Murphy, K. A.; Olmstead, M. M.; Mascharak, P. K. *Inorg. Chem.* **2004,** *43*, 4487.
99. Rose, M. J.; Patra, A. K.; Alcid, E. A.; Olmstead, M. M.; Mascharak, P. K. *Inorg. Chem.* **2007,** *46*, 2328.
100. Maji, S.; Sarkar, B.; Patra, M.; Das, A. K.; Mobin, S. M.; Kaim, W.; Lahiri, G. K. *Inorg. Chem.* **2008,** *47*, 3218.
101. Bordini, J.; Ford, P. C.; Tfouni, E. *Chem. Commun.* **2005,** *33*, 4169.
102. Arikawa, Y.; Asayama, T.; Moriguchi, Y.; Agari, S.; Onishi, M. *J. Am. Chem. Soc.* **2007,** *129*, 14160.
103. da Rocha, Z. N.; Marchesi, M. S. P.; Molin, J. C.; Lunardi, C. N.; Miranda, K. M.; Bendhack, L. M.; Ford, P. C.; da Silva, R. S. *Dalton Trans.* **2008,** *32*, 4282.
104. Zhou, W.; Zhang, Y.; Abe, M.; Uosaki, K.; Osawa, M.; Sasaki, Y.; Ye, S. *Langmuir* **2008,** *24*, 8027.
105. Rhenals, M. V.; Strasberg-Rieber, M.; Rieber, M. *J. Med. Chem.* **2010,** *53*, 1627.
106. Tran, D.; Skelton, B. W.; White, A. H.; Laverman, L. E.; Ford, P. C. *Inorg. Chem.* **1998,** *37*, 2505.

107. Sarma, M.; Kalita, A.; Kumar, P.; Singh, A.; Mondal, B. *J. Am. Chem. Soc.* **2010,** *132*, 7846.
108. McQuade, L. E.; Lippard, S. J. *Inorg. Chem.* **2010,** *49*, 7464.
109. Chuang, W. -J.; Lin, I. -J.; Chen, H. -Y.; Chang, Y. -L.; Hsu, S. C. N. *Inorg. Chem.* **2010,** *49*, 5377.
110. Centi, G.; Perathoner, S. *Appl. Catal. A: General* **1995,** *132*, 179.
111. Wolak, M.; Zahl, A.; Schneppensieper, T.; Stochel, G.; van Eldik, R. *J. Am. Chem. Soc.* **2001,** *123*, 9780.
112. Zheng, D.; Birke, R. L. *J. Am. Chem. Soc.* **2001,** *123*, 4637.
113. Zheng, D.; Birke, R. L. *J. Am. Chem. Soc.* **2002,** *124*, 9066.
114. Wolak, M.; Stochel, G.; van Eldik, R. *J. Am. Chem. Soc.* **2003,** *125*, 1334.
115. Sharma, V. S.; Pilz, R. B.; Boss, G. R.; Magde, D. *Biochemistry* **2003,** *42*, 8900.
116. Selcüki, C.; van Eldik, R.; Clark, T. *Inorg. Chem.* **2004,** *43*, 2828.
117. Wolak, M.; Stochel, G.; van Eldik, R. *Inorg. Chem.* **2006,** *45*, 1367.
118. Roncaroli, F.; Shubina, T. E.; Clark, T.; van Eldik, R. *Inorg. Chem.* **2006,** *45*, 7869.
119. Nguyen, J. G.; Johnson, C. A.; Subramaniam, B.; Borovik, A. S. *Chem. Mater.* **2008,** *20*, 5939.
120. Neuman, D.; Ostrowski, A. D.; Absalonson, R. O.; Strouse, G. F.; Ford, P. C. *J. Am. Chem. Soc.* **2007,** *129*, 4146.
121. Neuman, D.; Ostrowski, A. D.; Mikhailovsky, A. A.; Absalonson, R. O.; Strouse, G. F.; Ford, P. C. *J. Am. Chem. Soc.* **2008,** *130*, 168.
122. Ostrowski, A. D.; Deakin, S. J.; Azhar, B.; Miller, T. W.; Franco, N.; Cherney, M. M.; Lee, A. J.; Burstyn, J. N.; Fukuto, J. M.; Megson, I. L.; Ford, P. C. *J. Med. Chem.* **2010,** *53*, 715.
123. Dethlefsen, J. R.; Døssing, A.; Hedegard, E. D. *Inorg. Chem.* **2010,** *49*, 8769.
124. Eroy-Reveles, A. A.; Leung, Y.; Beavers, C. M.; Olmstead, M. M.; Mascharak, P. K. *J. Am. Chem. Soc.* **2008,** *130*, 4447.
125. Varonka, M. S.; Warren, T. H. *Inorg. Chem.* **2009,** *48*, 5605.
126. Zhu, J.; Meeusen, J.; Krezoski, S.; Petering, D. H. *Chem. Res. Toxicol.* **2010,** *23*, 422.
127. Ishibai, Y.; Sato, J.; Akita, S.; Nishikawa, T.; Miyagishi, S. *J. Photochem. Photobiol. A Chem.* **2007,** *188*, 106.
128. Li, G.; Zhang, D.; Yu, J. C.; Leung, M. K. H. *Environ. Sci. Technol.* **2010,** *44*, 4276.
129. Tonzetich, Z. J.; McQuade, L. E.; Lippard, S. J. *Inorg. Chem.* **2010,** *49*, 6338.
130. Bartacek, J.; Manconi, I.; Sansone, G.; Murgia, R.; Lens, P. N. L. *Nitric Oxide* **2010,** *23*, 101.
131. Szaciłowski, K.; Macyk, W.; Stochel, G.; Stasicka, Z.; Sostero, S.; Traverso, O. *Coord. Chem. Rev.* **2000,** *208*, 277.
132. Smejkalova, D.; Piccolo, A. *Environ. Sci. Technol.* **2006,** *40*, 1644.
133. Dunford, H. B. *Coord. Chem. Rev.* **2002,** *233/234*, 311.
134. Miller, W. L.; King, D. W.; Lin, J.; Kester, D. R. *Marine Chem.* **1995,** *50*, 63.
135. Andreozzi, R.; Caprio, V.; Insola, A.; Marotta, R. *Catal. Today* **1999,** *53*, 51.
136. Pignatello, J. J.; Liu, D.; Huston, P. *Environ. Sci. Technol.* **1999,** *33*, 1832.
137. Rodrıguez, M.; Malato, S.; Pulgarin, C.; Contreras, S.; Curco, D.; Gimenez, J.; Esplugas, S. *Sol. Energy* **2005,** *79*, 360.

138. Kusic, H.; Koprivanac, N.; Lon, A.; Bozic, L.; Selanec, I. *J. Hazard. Mater. B* **2006,** *136*, 632.
139. Kusic, H.; Koprivanac, N.; Horvat, S.; Bakija, S.; Bozic, A. L. *Chem. Eng. J.* **2009,** *155*, 144.
140. Devi, L. G.; Rajashekhar, K. E.; Raju, K. S. A.; Kumar, S. G. *J. Mol. Catal. A. Chem* **2009,** *314*, 88.
141. Duesterberg, C. K.; Waite, T. D. *Environ. Sci. Technol.* **2006,** *40*, 4189.
142. Gernjak, W.; Fuerhacker, M.; Fernandez-Ibanez, P.; Blanco, J.; Malato, S. *Appl. Catal. B: Environ.* **2006,** *64*, 121.
143. Vermilyea, A.; Voelker, B. *Environ. Sci. Technol.* **2009,** *43*, 6927.
144. Nogueira, R. F. P.; Silva, M. R. A.; Trovo, A. G. *Sol. Energy* **2005,** *79*, 384.
145. Meštánková, H.; Krýsa, J.; Jirkovský, J.; Mailhot, G.; Bolte, M. *Appl. Catal. B* **2005,** *58*, 185.
146. Ji, H.; Song, W.; Chen, C.; Yuan, H.; Ma, W.; Zhao, J. *Environ. Sci. Technol.* **2007,** *41*, 5103.
147. Craig, P. S.; Shaw, T. J.; Miller, P. L.; Pellechia, P. J.; Ferry, J. L. *Environ. Sci. Technol.* **2009,** *43*, 337.
148. Brillas, E.; Sires, I.; Oturan, M. A. *Chem. Rev.* **2009,** *109*, 6570.
149. Oturan, N.; Zhou, M.; Oturan, M. A. *J. Phys. Chem. A* **2010,** *114*, 10605.
150. Cermenati, L.; Pichat, P.; Guillard, C.; Albini, A. *J. Phys. Chem. B* **1997,** *101*, 2650.
151. Feng, J.; Hu, X.; Yue, P. L.; Zhu, H. Y.; Lu, G. Q. *Ind. Eng. Chem. Res.* **2003,** *42*, 2058.
152. Malato, S.; Caceres, J.; Aguera, A.; Mezcua, M.; Hernando, D.; Vial, J.; Fernandez-Alba, A. R. *Environ. Sci. Technol.* **2001,** *35*, 4359.
153. Malato, S.; Blanco, J.; Cáceres, J.; Fernández-Alba, A. R.; Agüera, A.; Rodrıguez, A. *Catal. Today* **2002,** *76*, 209.
154. Parra, S.; Guasaquillo, I.; Enea, O.; Mielczarski, E.; Mielczarki, J.; Albers, P.; Kiwi-Minsker, L.; Kiwi, J. *J. Phys. Chem. B* **2003,** *107*, 7026.
155. Parra, S.; Henao, L.; Mielczarski, E.; Mielczarski, J.; Albers, P.; Suvorova, E.; Guindet, J.; Kiwi, J. *Langmuir* **2004,** *20*, 5621.
156. Cheng, M.; Ma, W.; Li, J.; Huang, Y.; Zhao, J. *Environ. Sci. Technol.* **2004,** *38*, 1569.
157. Quici, N.; Morgada, M. E.; Piperata, G.; Babay, P.; Gettar, R. T.; Litter, M. I. *Catal. Today* **2005,** *101*, 253.
158. Franch, M. I.; Ayllon, J. A.; Peral, J.; Domenech, X. *Catal. Today* **2005,** *101*, 245.
159. Lam, S. W.; Chiang, K.; Lim, T. M.; Amal, R.; Low, G. K. -C. *J. Catal.* **2005,** *234*, 292.
160. Gumy, D.; Fernandez-Ibanez, P.; Malato, S.; Pulgarin, C.; Enea, O.; Kiwi, J. *Catal. Today* **2005,** *101*, 375.
161. Mestankova, H.; Mailhot, G.; Jirkovsky, J.; Krysab, J.; Bolte, M. *Appl. Catal. B* **2005,** *57*, 257.
162. Dantas, T. L. P.; Mendonca, V. P.; Jose, H. J.; Rodrigues, A. E.; Moreira, R F P M *Chem. Eng. J.* **2006,** *118*, 77.
163. Tryba, B.; Morawski, A. W.; Inagaki, M.; Toyoda, M. *J. Photochem. Photobiol. A Chem* **2006,** *179*, 224.
164. Kwan, C. Y.; Chu, W.; Lam, W. S. *J. Mol. Catal. A: Chem.* **2007,** *274*, 50.
165. Lee, J.; Kim, J.; Choi, W. *Environ. Sci. Technol.* **2007,** *41*, 3335.
166. Rincon, A. -G.; Pulgarin, C. *Appl. Catal. B* **2006,** *63*, 222.
167. Bozzi, A.; Yuranova, T.; Mielczarski, E.; Mielczarski, J.; Buffat, P. A.; Lais, P.; Kiwi, J. *Appl. Catal. B* **2003,** *42*, 289.

168. Yu, H.; Irie, H.; Shimodaira, Y.; Hosogi, Y.; Kuroda, Y.; Miyauchi, M.; Hashimoto, K. *J. Phys. Chem. C* **2010,** *114*, 16481.
169. Moraes, J. E. F.; Quina, F. H.; Nascimento, C. A. O.; Silva, D. N.; Chiavone-Filho, O. *Environ. Sci. Technol.* **2004,** *38*, 1183.
170. Masarwa, A.; Rachmilovich-Calis, S.; Meyerstein, N.; Meyerstein, D. *Coord. Chem. Rev.* **2005,** *249*, 1937.
171. Goi, A.; Veressinina, Y.; Trapido, M. *Chem. Eng. J.* **2008,** *143*, 1.
172. Quici, N.; Morgada, M. E.; Gettar, R. T.; Bolte, M.; Litter, M. I. *Appl. Catal. B* **2007,** *71*, 117.
173. Rossetti, G. H.; Albizzati, E. D.; Alfano, O. M. *Ind. Eng. Chem. Res.* **2002,** *41*, 1436.
174. Rossetti, G. H.; Albizzati, E. D.; Alfano, O. M. *Sol. Energy* **2004,** *77*, 461.
175. Farias, J.; Rossetti, G. H.; Albizzati, E. D.; Alfano, O. M. *Ind. Eng. Chem. Res.* **2007,** *46*, 7580.
176. Benitez, F. J.; Beltran-Heredia, J.; Acero, J. L.; Rubio, F. J. *Ind. Eng. Chem. Res.* **1999,** *38*, 1341.
177. Gernjak, W.; Krutzler, T.; Glaser, A.; Malato, S.; Caceres, J.; Bauer, R.; Fernandez-Alba, A. R. *Chemosphere* **2003,** *50*, 71.
178. Giroto, J. A.; Teixeira, A C S C; Nascimento, C. A. O.; Guardani, R. *Ind. Eng. Chem. Res.* **2010,** *49*, 3200.
179. Hermosilla, D.; Cortijo, M.; Huang, C. P. *Chem. Eng. J.* **2009,** *155*, 637.
180. Chacon, J. M.; Leal, M. T.; Sanchez, M.; Bandala, E. R. *Dyes Pigm.* **2006,** *69*, 144.
181. Gazi, S.; Ananthakrishnan, R.; Singh, N. D. P. *J. Hazard. Mater.* **2010,** *183*, 894.
182. Tryba, B.; Piszcz, M.; Grzmil, B.; Pattek-Janczyk, A.; Morawski, A. W. *J. Hazard. Mater.* **2009,** *162*, 111.
183. Herrera, F.; Kiwi, J.; Lopez, A.; Nadtochenko, V. *Environ. Sci. Technol.* **1999,** *33*, 3145.
184. Fotiadis, C.; Xekoukoulotakis, N.; Mantzavinos, D. *Catal. Today* **2007,** *124*, 247.
185. Arslan-Alaton, I.; Tureli, G.; Olmez-Hanci, T. *J. Photochem. Photobiol. A Chem.* **2009,** *202*, 142.
186. Poulain, L.; Mailhot, G.; Wong-Wah-Chung, P.; Bolte, M. *J. Photochem. Photobiol. A Chem.* **2003,** *159*, 81.
187. Katsumata, H.; Kaneco, S.; Suzuki, T.; Ohta, K.; Yobiko, Y. *Chemosphere* **2006,** *63*, 592.
188. Katsumata, H.; Kaneco, S.; Suzuki, T.; Ohta, K.; Yobiko, Y. *J. Photochem. Photobiol. A Chem.* **2006,** *180*, 38.
189. Catastini, C.; Sarakha, M.; Mailhot, G.; Bolte, M. *Sci. Total Environ.* **2002,** *298*, 219.
190. Zapata, A.; Oller, I.; Rizzo, L.; Hilgert, S.; Maldonado, M. I.; Sánchez-Pérez, J. A.; Malato, S. *Appl. Catal. B: Environ.* **2010,** *97*, 292.
191. Evgenidou, E.; Konstantinou, I.; Fytianos, K.; Poulios, I. *Water Res.* **2007,** *41*, 2015.
192. Perez-Estrada, L. A.; Malato, S.; Gernjak, W.; Agüera, A.; Thurman, E. M.; Ferrer, I.; Fernandez-Alba, A. R. *Environ. Sci. Technol.* **2005,** *39*, 8300.
193. Sioi, M.; Bolosis, A.; Kostopoulou, E.; Poulios, I. *J. Photochem. Photobiol. A Chem.* **2006,** *184*, 18.
194. Bautitz, I. R.; Nogueira, R. F. P. *J. Photochem. Photobiol. A Chem.* **2007,** *187*, 33.

195. Trovo, A. G.; Melo, S. A. S.; Nogueira, R. F. P. *J. Photochem. Photobiol. A Chem.* **2008,** *198*, 215.
196. Bautitz, I. R.; Nogueira, R. F. P. *Catal. Today* **2010,** *151*, 94.
197. Yaping, Z.; Jiangyong, H. *Appl. Catal. B: Environ.* **2008,** *78*, 250.
198. Amat, A. M.; Arques, A.; Miranda, M. A.; Seguir, S. *Sol. Energy* **2004,** *77*, 559.
199. Malato, S.; Blanco, J.; Maldonado, M. I.; Oller, I.; Gernjak, W.; Perez-Estrada, L. *J. Hazard. Mater.* **2007,** *146*, 440.
200. Son, H. S.; Im, J. K.; Zoh, K. D. *Water Res.* **2009,** *43*, 1457.
201. Rodrıguez, S. M.; Galvez, J. B.; Rubio, M. I. M.; Ibanez, P. F.; Gernjak, W.; Alberola, I. O. *Chemosphere* **2005,** *58*, 391.
202. Antoniadis, A.; Takavakoglou, V.; Zalidis, G.; Poulios, I. *Catal. Today* **2007,** *124*, 260.
203. Rincon, A. -G.; Pulgarin, C. *Catal. Today* **2007,** *122*, 128.
204. Spuhler, D.; Rengifo-Herrera, J. A.; Pulgarin, C. *Appl. Catal. B* **2010,** *96*, 126.
205. Nieto-Juarez, J. I.; Napierzchła, K.; Sienkiewicz, A.; Kohn, T. *Environ. Sci. Technol.* **2010,** *44*, 3351.
206. Andrianirinaharivelo, S.; Mailhot, G.; Bolte, M. *Solar Energy Mater. Solar Cells* **1995,** *38*, 459.
207. Mailhot, G.; Bordes, A. L.; Bolte, M. *Chemosphere* **1995,** *30*, 1729.
208. Borman, C. J.; Sullivan, B. P.; Eggleston, C. M.; Colberg, P. J. S. *Chem. Geol.* **2010,** *269*, 33.
209. Burns, J. M.; Craig, P. S.; Shaw, T. J.; Ferry, J. L. *Environ. Sci. Technol.* **2010,** *44*, 7226.
210. Baker, A. R.; Croot, P. L. *Mar. Chem.* **2010,** *120*, 4.
211. Crisponi, G.; Remelli, M. *Coord. Chem. Rev.* **2008,** *252*, 1225.
212. Fisher, J. M.; Reese, J. G.; Pellechia, P. J.; Moeller, P. L.; Ferry, J. L. *Environ. Sci. Technol.* **2006,** *40*(7), 2200.
213. Rijkenberg, M. J. A.; Gerringa, L. J. A.; Carolus, V. E.; Velzeboer, I.; de Baar, H. J. W. *Geochim. Cosmochim. Acta* **2006,** *70*, 2790.
214. Feng, W.; Nansheng, D. *Chemosphere* **2000,** *41*, 1137.
215. Andreozzi, R.; Caprio, V.; Marotta, R. *Water Res.* **2003,** *37*, 3682.
216. Mazellier, P.; Bolte, M. *Chemosphere* **2001,** *42*, 361.
217. Garrel, L.; Bonetti, M.; Tonucci, L.; d'Alessandro, N.; Bressan, M. *J. Photochem. Photobiol. A Chem.* **2006,** *179*, 193.
218. Rodrıguez, M.; Abderrazik, N. B.; Contreras, S.; Chamarro, E.; Gimenez, J.; Esplugas, S. *Appl. Catal. B: Environ.* **2002,** *37*, 131.
219. Andreozzi, R.; Canterino, M.; Marotta, R. *Water Res.* **2006,** *40*, 3785.
220. Andreozzi, R.; Marotta, R. *Water Res.* **2004,** *38*, 1225.
221. Imanishi, M.; Hashimoto, K.; Kominami, H. *Appl. Catal. B: Environ.* **2010,** *97*, 213.
222. Pozdnyakov, I. P.; Kel, O. V.; Plyusnin, V. F.; Grivin, V. P.; Bazhin, N. M. *J. Phys. Chem. A* **2008,** *112*, 8316.
223. Izakovic, M.; Šima, J.; Brezová, V. *J. Photochem. Photobiol. A Chem* **2004,** *167*, 81.
224. Wang, Z.; Chen, X.; Ji, H.; Ma, W.; Chen, C.; Zhao, J. *Environ. Sci. Technol.* **2010,** *44*, 263.
225. Li, J.; Mailhot, G.; Wu, F.; Deng, N. *J. Photochem. Photobiol. A Chem.* **2010,** *212*, 1.
226. Fàbrega, C.; Andreu, T.; Cabot, A.; Morante, J. R. *J. Photochem. Photobiol. A Chem.* **2010,** *211*, 170.

227. Adan, C.; Martınez-Arias, A.; Malato, S.; Bahamonde, A. *Appl. Catal. B: Environ.* **2009,** *93*, 96.
228. Mansilla, H. D.; Bravo, C.; Ferreyra, R.; Litter, M. I.; Jardim, W. F.; Lizama, C.; Freer, J.; Fernandez, J. *J. Photochem. Photobiol. A Chem.* **2006,** *181*, 188.
229. Park, E. H.; Jung, J.; Chung, H. H. *Chemosphere* **2006,** *64*, 432.
230. Sýkora, J. *Coord. Chem. Rev.* **1997,** *159*, 95.
231. Sykora, J.; Sima, J. *Coord. Chem. Rev.* **1990,** *107*, 1.
232. Hu, X.; Lam, F. L. Y.; Cheung, L. M.; Chan, K. F.; Zhao, X. S.; Lu, G. Q. *Catal. Today* **2001,** *68*, 129.
233. Yip, A. C. K.; Lam, F. L. Y.; Hu, X. *Ind. Eng. Chem. Res.* **2005,** *44*, 7983.
234. Lam, F. L. Y.; Yip, A. C. K.; Hu, X. *Ind. Eng. Chem. Res.* **2007,** *46*, 3328.
235. Zou, S. W.; How, C. W.; Chen, J. P. *Ind. Eng. Chem. Res.* **2007,** *46*, 6566.
236. Lavie-Cambot, A.; Cantuel, M.; Leydet, Y.; Jonusauskas, G.; Bassani, D. M.; McClenaghan, N. D. *Coord. Chem. Rev.* **2008,** *252*, 2572.
237. Yang, J. K.; Davis, A. P. *Environ. Sci. Technol.* **2000,** *34*, 3796.
238. Yang, J. K.; Davis, A. P. *Environ. Sci. Technol.* **2001,** *35*, 3566.
239. Chen, F.; Deng, Z.; Li, X.; Zhang, J.; Zhao, J. *Chem. Phys. Lett.* **2005,** *415*, 85.
240. Yeber, M. C.; Onate, K. P.; Vidal, G. *Environ. Sci. Technol.* **2007,** *41*, 2510.
241. Shimizu, K.; Maruyama, R.; Hatamachi, T.; Kodama, T. *J. Phys. Chem. C* **2007,** *111*, 6440.
242. Yamazaki, S.; Iwai, S. *J. Phys. Chem. A* **2001,** *105*, 11285.
243. Kotaś, J.; Stasicka, Z. *Environ. Pollution* **2000,** *107*, 263.
244. Mytych, P.; Ciesla, P.; Stasicka, Z. *Intern. J. Photoenergy* **2001,** *3*, 181.
245. Mytych, P.; Ciesla, P.; Stasicka, Z. *Appl. Catal. B: Environ.* **2005,** *59*, 161.
246. Kane-Maguire, N. A. P. In: "*Photochemistry and Photophysics of Coordination Compounds*"; Eds. Balzani, V.; Campagna, S.; Vol. I; Springer: Berlin, **2007**, p. 37.
247. Kirk, A. D. *Chem. Rev.* **1999,** *99*, 1607.
248. Marchaj, A.; Stasicka, Z.; Rehorek, D. *Polyhedron* **1983,** *2*, 1281.
249. Mainusch, B.; Wasgestian, F.; Stasicka, Z.; Karocki, A. *J. Inf. Rec. Mats.* **1994,** *21*, 687.
250. Mainusch, B.; Karocki, A.; Guldi, D. M.; Stasicka, Z.; Wasgestian, F. *Inorg. Chim. Acta* **1997,** *255*, 87.
251. Wi□niewska, J.; Marai, H.; Karocki, A.; Szaciłowski, K.; Kita, E.; Stasicka, Z. *J. Photochem. Photobiol. A Chem.* **2010,** *209*, 121.
252. Dai, R.; Yu, C.; Liu, J.; Lan, Y.; Deng, B. *Environ. Sci. Technol.* **2010,** *44*, 6959.
253. Mytych, P.; Karocki, A.; Stasicka, Z. *J. Photochem. Photobiol. A Chem.* **2003,** *160*, 163.
254. Mytych, P.; Stasicka, Z. *Appl. Catal. B: Environ.* **2004,** *52*, 167.
255. Cakir, S.; Bicer, E. *Bioelectrochem.* **2005,** *67*, 75.
256. Pizzocaro, C.; Lafond, C.; Bolte, M. *J. Photochem. Photobiol. A Chem.* **2002,** *151*, 221.
257. Abida, O.; Mailhot, G.; Mestankova, H.; Litter, M.; Bolte, M. *Photochem. Photobiol. Sci.* **2010,** *9*, 823.
258. Chen, Y.; Wu, F.; Lin, Y.; Deng, N.; Bazhin, N.; Glebov, E. *J. Hazard. Mater.* **2007,** *148*, 360.
259. Burrows, H. D.; Canle, M.; Santaballa, J. A.; Steenken, S. *J. Photochem. Photobiol. B: Biol.* **2002,** *67*, 71.
260. Sandy, M.; Butler, A. *Chem. Rev.* **2009,** *109*, 4580.

261. Wang, Z.; Ma, W.; Chen, C.; Zhao, J. *Environ. Sci. Technol.* **2008,** *42*, 7260.
262. Liu, Y.; Deng, L.; Chen, Y.; Wu, F.; Denga, N. *J. Hazard. Mater. B* **2007,** *139*, 399.
263. Tzou, Y. M.; Hsu, C. L.; Chen, C. C.; Chen, J. H.; Wu, J. J.; Tseng, K. J. *J. Hazard. Mater.* **2008,** *156*, 374.
264. Goeringer, S.; Chenthamarakshan, C. R.; Rajeshwar, K. *Electrochem. Commun.* **2001,** *3*, 290.
265. Herrmann, J. M. *J. Photochem. Photobiol. A: Chem.* **2010,** *216*, 85.
266. Hassouna, F.; Mailhot, G.; Morlat-Thérias, S.; Gardette, J. -L. *J. Photochem. Photobiol. A Chem.* **2011,** *218*, 239.
267. Iwakura, H.; Einaga, H.; Teraoka, Y. *Inorg. Chem.* **2010,** *49*, 11362.
268. Richard, C.; Grabner, G. In: "*Environmental Photochemistry*"; Ed. Boule, P.; Springer Verlag: Berlin, **1999**, p. 217.
269. Castillo, N. C.; Ding, L.; Heel, A.; Graule, T.; Pulgarin, C. *J. Photochem. Photobiol. A Chem.* **2010,** *216*, 221.
270. González-Bahamón, L. F.; Mazille, F.; Benítez, L. N.; Pulgarín, C. *J. Photochem. Photobiol. A Chem.* **2011,** *217*, 201.
271. Genuino, H. C.; Njagi, E. C.; Benbow, E. M.; Hoag, G. E.; Collins, J. B.; Suib, S. L. *J. Photochem. Photobiol. A Chem.* **2011,** *217*, 284.
272. Li, Q.; Xie, R.; Li, Y. W.; Mintz, E. A.; Shang, J. K. *Environ. Sci. Technol.* **2007,** *41*, 5050.
273. Rincon, A. -G.; Pulgarin, C. *Appl. Catal. B* **2006,** *63*, 222.
274. Rincon, A. -G.; Pulgarin, C. *Catal. Today* **2007,** *122*, 128.
275. Sichel, C.; Blanco, J.; Malato, S.; Fernandez-Ibanez, P. *J. Photochem. Photobiol. A Chem.* **2007,** *189*, 239.

PHOTOCHEMICAL ACTIVATION AND SPLITTING OF H_2O, CO_2, AND N_2 INDUCED BY CT EXCITATION OF REDOXACTIVE METAL COMPLEXES

ARND VOGLER[1] and HORST KUNKELY

Institut für Anorganische Chemie, Universität Regensburg, 93040 Regensburg, Germany

ABSTRACT

The cleavage of the ubiquitous and abundant molecules H_2O, CO_2 (or CO_3^{2-}, respectively) and N2 is of is of considerable interest. Owing to their stability this splitting should be facilitated by light and may thus be applied for solar energy utilization. Under ambient conditions the direct photocleavage can certainly not be accomplished but assistance by suitable redox-active metal complexes is conceivable. Light absorption should induce charge redistribution between metal and molecules to be split. CT excitation is expected to initiate the generation of redox products in the first photochemical step. Indeed, the redox couples $Os^{II}Cp_2$/$Os^{IV}Cp_2$ with Cp = cyclopentadienyl anion, Cu(I)/Cu(II) and $Os^{II}N_2Os^{III}$/Os^{VI}(N) have been successfully applied to photo cleave H_2O, CO_3^{2-} and N_2, respectively. Future attempts are directed to improve the efficiency of these photoreactions. In particular, the inclusion of such reactions in photocatalytic cycles is a challenging task.

[1]Corresponding author.

INORGANIC PHOTOCHEMISTRY
VOLUME 63 ISSN 0898-8838 / DOI: 10.1016/B978-0-12-385904-4.00003-2

Keywords: Photocatalysis; Photo splitting; Solar energy utilization; H_2O, CO_2, CO_3^{2-}, N_2; Last Glacial Maximum.

I. Introduction

The reactivity of the ubiquitous and abundant chemicals H_2O, CO_2, and N_2 is of fundamental importance in its own right but also with regard to applications related to climate change and utilization of solar energy. A rather significant aspect of this chemistry deals with the splitting of these molecules, for example

$$2H_2O \rightarrow 2H_2 + O_2 \tag{1}$$

$$CO_2 \rightarrow CO + \frac{1}{2}O_2 \tag{2}$$

$$N_2 + 3H_2 \rightarrow 2NH_3 \tag{3}$$

Owing to the simple composition and structure of H_2O, CO_2, and N_2, this chemistry might be expected to be simple, too. However, due to the extreme stability of these species their splitting is rather difficult to achieve, at least under ambient conditions and requires a sophisticated mechanism and much energy. It is an attractive idea to supply this energy by light (solar energy). Nevertheless, the direct activation and cleavage need light of extremely short wavelength (<200 nm), which is usually not available at ambient conditions. Accordingly, some type of long-wavelength sensitization is required to photochemically split the very strong bonds in these molecules. Guidelines may be derived from natural photosynthesis:

$$CO_2 + H_2O \rightarrow \frac{1}{n}(CH_2O)_n + O_2 \tag{4}$$

The electrons that are provided by photosystem I are finally used to reduce CO_2 to carbohydrates, while in photosystem II, water is oxidized to oxygen. Intense research over many decades has partially revealed the extremely complicated mechanism of natural photosynthesis. It follows that it is obviously rather difficult to imitate this in an artificial photosynthesis that is intended to convert and store solar energy in simple but energy-rich chemicals. Different approaches have been developed to solve this problem (*1*). It has been suggested to facilitate artificial photosynthesis by the assistance of redoxactive metal complexes in homogeneous systems. Generally, photoredox reactions of metal

complexes are initiated by CT excitation, which in simple cases leads to a one-electron transfer between metal and ligand or another substrate (2,3). Accordingly, radicals are generated that are very reactive. They undergo various secondary reactions including recombinations. In principle, such one-electron photoredox reactions can be combined to produce relatively stable products that are formally the result of a multielectron transfer. However, to put this in reality is extremely difficult. Fortunately, such interferences may be avoided by the introduction of suitable metal complexes that undergo multielectron transfer (4).

There are essentially two possibilities to accomplish two-electron or multielectron transfer at metal complexes without formation of one-electron transfer intermediates (e.g., radicals). Appropriate metal centers should have available stable oxidation states that differ by at least two units. Typical examples that represent such photoredox reactions are reductive eliminations such as (X^- = halide, pseudohalide) (5):

$$\left[Pt^{IV}(CN)_4X_2\right]^{2-} \xrightarrow{h\nu} \left[Pt^{II}(CN)_4\right]^{2-} + X_2 \qquad (5)$$

LMCT (X^- to Pt^{IV}) excitation is associated with a shift of electron density from X^- to Pt^{IV} but finally yields Pt(II) because Pt(III) is not easily accessible. In cases that are restricted to one-electron transfer at single metal centers a simultaneous multielectron transfer can be achieved by assembling two or more metal centers in binuclear or polynuclear complexes (4). This applies, for example, to the redox couple Fe(II) and Fe(III) ($PctsH_2$ = phthalocyaninetetrasulfonate) (6):

$$(Pcts)Fe^{III}\left(O_2{}^{2-}\right)Fe^{III}(Pcts) \xrightarrow{h\nu} 2Fe^{II}(Pcts) + O_2 \qquad (6)$$

LMCT ($O_2{}^{2-}$ to Fe^{III}) excitation finally leads to the formation of Fe(II) and molecular oxygen.

In conclusion, photochemical multielectron transfer of metal complexes has been frequently studied with the intension to realize artificial photosynthesis. In the following sections, this is emphasized when appropriate. However, such reactions are also very interesting in their own right and are described below irrespective of particular applications.

II. Water Splitting

Photochemical water splitting (1,7) can be viewed as the simplest version of artificial photosynthesis:

$$2H_2O \rightarrow 2H_2 + O_2, \quad \Delta H = +289\,kJ \qquad (7)$$

Numerous molecular metal complexes have been examined as photocatalysts in homogenous solution. The reduction of water to hydrogen and the oxidation to oxygen can be studied as independent processes. The photoreduction of water or protons to hydrogen is a two-electron transfer that may be mediated by various mononuclear and binuclear (or polynuclear) metal complexes. They can undergo an oxidation to a stable oxidation state that is higher by two units. A prominent type of a metal complex that generates H_2 is a hydride complex which undergoes reductive elimination upon irradiation, for example (7,8),

$$Ir^{III}Cl(H^-)_2(PPh_3)_3 \xrightarrow{h\nu} Ir^{I}Cl(PPh_3)_3 + H_2 \qquad (8)$$

Generally, hydride is an electron donor or reductant. Accordingly, (H^- to Ir^{III}) LMCT excitation could initiate the observed photolysis. However, how can this photoredox reaction be related to water or proton reduction? While various hydride complexes undergo such a reductive elimination of H_2 their synthesis is generally based on complicated procedures and cannot be formed by a simple reaction with water or protons in aqueous solution (8).

Even more difficult, the photooxidation of water to oxygen is associated with the transfer of four electrons. In natural photosynthesis, this is accomplished by photosystem II, which contains a tetranuclear manganese cluster as active oxidation center. In artificial systems, various complexes have been shown to generate oxygen upon irradiation (9). This applies also to permanganate but the mechanism of oxygen release seems to be a sequence of quite complicated steps (10). An interesting example is a binuclear complex containing the $Fe^{III}OFe^{III}$ moiety, for example (edta = ethylendiaminetetraacetate) (11):

$$2\left[(edta)Fe^{III} - O - Fe^{III}(edta)\right]^{4-} \xrightarrow{h\nu} 4\left[(edta)Fe^{II}\right]^{2-} + O_2 \qquad (9)$$

It is suggested that ($O^{2-} \rightarrow Fe^{III}$) LMCT and/or ($Fe^{III} \rightarrow Fe^{III}$) MMCT excitation initially leads to the disproportionation of Fe(III).

$$\left[(edta)Fe^{III} - O - Fe^{III}(edta)\right]^{4-} \rightarrow \left[(edta)Fe^{IV}{=}O\right]^{2-} + \left[(edta)Fe^{II}\right]^{2-} \qquad (10)$$

The oxoferryl fragment $Fe^{IV}O$ is not stable. The subsequent reaction of two such complexes yields Fe^{II} and oxygen:

$$2\left[(edta)Fe^{IV}{=}O\right]^{2-} \rightarrow 2\left[(edta)Fe^{II}\right]^{2-} + O_2 \qquad (11)$$

This reaction is facilitated by the high oxidizing power of Fe(IV).

When suitable independent reactions for the reduction and oxidation of water are available, it still would not be simple to combine them to a cyclic process with Eq. (1) as net reaction. Accordingly, it is desired to perform reduction and oxidation by an interconvertible redox pair based on the same metal complex. This background motivated our recent study with osmocene ($OsCp_2$, $Cp^- = C_5H_5^-$) as photoredox catalyst (*12*).

A. Water Splitting by Light with Osmocene as Photocatalyst

Osmocene dissolves in water only in the presence of acids. The protonation of osmocene leads to the formation of a well-known hydride complex Eq. (12) (*13*):

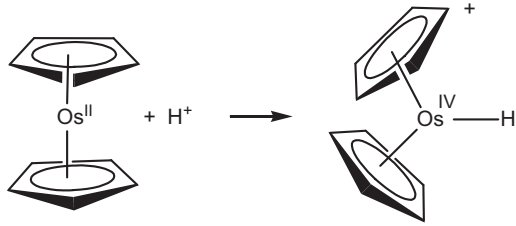

(12)

Generally, osmocene is not light sensitive, but undergoes a photolysis in acidic (e.g., H_2SO_4 or HBF_4) aqueous solutions. The irradiation with UV–light ($\lambda_{irr} = 254$ nm) is accompanied by characteristic spectral changes (Fig. 1) that unambiguously indicate the formation of $[Cp_2Os^{III}Os^{III}Cp_2]^{2+}$ (*14*). Simultaneously, hydrogen is released. Both photolysis products are formed approximately in a 1:1 ratio. This photoreaction can thus be described by a simple stoichiometric equation:

$$2\left[Cp_2Os^{IV}(H^-)\right]^+ \xrightarrow{h\nu} \left[Cp_2Os^{III} - Os^{III}Cp_2\right]^{2+} + H_2 \qquad (13)$$

Product formation could take place via the intermediate formation of a radical pair:

$$\left[Cp_2Os^{IV}(H^-)\right]^+ \rightarrow \left[Cp_2Os^{III}\right]^+ + H - \text{atom} \xrightarrow{2\times} \left[Cp_2Os^{III} - Os^{III}Cp_2\right]^{2+} + H_2 \qquad (14)$$

However, this reaction path can be excluded since $[Cp_2Os^{III}]^+$ radicals disproportionate immediately under these conditions (see below) Eq. (15):

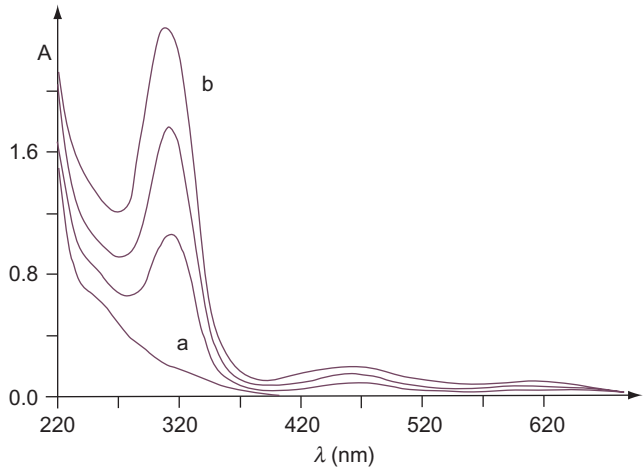

FIG. 1. Spectral changes during the photolysis of 2.37×10^{-4} M osmocene in 5 M H_2SO_4 under argon at room temperature after 0 min (a), 20, 40, and 80 min (b) irradiation times with $\lambda_{irr} = 254$ nm 1-cm cell.

$$2\left[Cp_2Os^{III}\right]^{+} \rightarrow \left[Cp_2Os^{IV}\right]^{2+} + Cp_2Os^{II} \qquad (15)$$

Accordingly, we suggest that the photolysis is preceded by a reversible dimerization of the hydride complex that subsequently undergoes a reductive elimination without the formation of radicals:

$$2\left[Cp_2Os^{IV}(H^{-})\right]^{+} \rightleftarrows \left[Cp_2Os^{IV}H\cdots HOs^{IV}Cp_2\right]^{2+} \xrightarrow{h\nu} \left[Cp_2Os^{III} - Os^{III}Cp_2\right]^{2+} + H_2 \qquad (16)$$

This special type of a hydrogen bonding has also been considered to occur in other cases (*15*). Since this bonding is certainly rather weak, the monomer is expected to prevail in the equilibrium. The apparent quantum yield for the formation of $[Cp_2Os^{III}Os^{III}Cp_2]^{2+}$ amounts to $\phi = 10^{-3}$ ($\lambda_{irr} = 254$ nm). However, it must be taken into account that the photoactive dimeric hydride complex is probably present only in small concentrations while the monomer absorbs most of the light. A comparable photolysis has been described earlier but without discussion of the mechanism: $2HIr^{I}(PF_3)_4 \rightarrow H_2 + (PF_3)_4Ir^0 - Ir^0(PF_3)_4$ (*16*).

In coordinating solvents (L) such as CH_3CN the Os(III) dimer is well known to undergo a slow disproportionation Eq. (17) (*14*):

$$\left[Cp_2Os^{III} - Os^{III}Cp_2\right]^{2+} + L \rightarrow Cp_2Os^{II} + \left[Cp_2Os^{IV}L\right]^{2+} \qquad (17)$$

This reaction proceeds also photochemically as indicated by the concomitant spectral changes that are identical in both cases. When the irradiation is carried out in acidic solution ($L = H_2O$) comparable spectral variations are observed. Since the photolysis products are apparently stable under these conditions and interfering inner-filter effects are absent the photolysis can be performed to completion. The Os(III) dimer disappears with $\phi = 8 \times 10^{-3}$ at $\lambda_{irr} = 436$ nm. Disproportionations of this kind that take place as a consequence of the photochemical splitting of a metal–metal bond are an important reaction type in organometallic chemistry *(17,18)*.

The stoichiometry of Eq. (17) has been confirmed experimentally. Osmocene was extracted from the acidic solution with hexane and spectroscopically identified *(19)* as well as quantitatively determined. The comparison of the spectra of the extracted solutions of the photolyzed samples and those kept in the dark yielded a molar ratio of nearly 1:1.

When the photolysis of $[Cp_2Os^{IV}H]^+$ is performed with white light instead of UV light the spectral variations do not follow a simple pattern because the primary photolysis of the hydride complex and the secondary photolysis of the Os(III) dimer are superimposed. The combined photolysis with white light proceed then according to the equation

$$Cp_2Os^{II} + 2H^+ + H_2O \rightarrow H_2 + \left[Cp_2Os^{IV}(H_2O)\right]^{2+} \qquad (18)$$

The aqua complex ($L = H_2O$) is apparently light stable and does not undergo any further photolysis. Various salts with the cation $[Cp_2Os^{IV}L]^{n+}$ (L = halide or coordinating solvent) have been prepared and characterized by Taube and coworkers *(14)*. The reddish brown hydroxo complex $[Cp_2Os^{IV}(OH)]PF_6$ described by Fischer and Gruber *(20)* is also a compound of this type. Aqueous solutions of this salt are acidic and light sensitive. They are bleached upon irradiation with visible light. As photoproducts only osmocene and oxygen could be detected. From the spectral changes it can be deduced that the hydroxo complex is converted to osmocene nearly quantitatively. In addition, osmocene and oxygen are formed in the molar ratio 1:0.5. These observations are consistent with the equation:

$$\left[Cp_2Os^{IV}(OH)\right]^+ \xrightarrow{h\nu} Cp_2Os^{II} + \frac{1}{2}O_2 + H^+ \qquad (19)$$

The quantum yield for the disappearance of $[Cp_2Os^{IV}(OH)]^+$ amounts to $\phi = 2 \times 10^{-3}$ ($\lambda_{irr} = 405$ nm). In the solid state, this complex apparently undergoes this decomposition also thermally, but only at 185 °C *(20)*. In the photolysis, oxygen is

generated in the singlet state, at least partially. When the photolysis is carried out in acetonitrile in the presence of diphenylacetylene, benzil was formed and identified by its characteristic luminescence at $\lambda_{max} = 507$ nm. The addition of $^1O_2$ to diphenylacetylene has been previously used for the detection of singlet oxygen (*21*).

We suggest that the photolysis of the hydroxo complex consists of the following consecutive steps:

$$\left[Cp_2Os^{IV}(OH)\right]^+ \rightleftarrows Cp_2Os^{IV}{=}{=}O + H^+ \tag{20}$$

$$2Cp_2Os^{IV}{=}{=}O \underset{\rightarrow}{\leftarrow} Cp_2OsO_2OsCp_2 \tag{21}$$

$$Cp_2OsO_2OsCp_2 \overset{h\nu}{\rightarrow} 2Cp_2Os^{II} + O_2 \tag{22}$$

The electronic structure of the fragment $[OsO_2Os]^{4+}$ is not clear. However, we assume that this binuclear cation exists as peroxo complex, $Cp_2Os^{III}(O_2^{2-})Os^{III}Cp_2$. Binuclear peroxo complexes of this type frequently photolyze under elimination of oxygen in general and $^1O_2$ in particular (*22*).

Recently, we have studied such a photoredox reaction (*6*) that proceeds in analogy to the photolysis of the binuclear osmium complex Eq. (23):

$$(\text{porphyrin})Fe^{III}(O_2^{2-})Fe^{III}(\text{porphyrin}) \overset{h\nu/\text{LMCT}}{\rightarrow} 2(\text{porphyrin})Fe^{II} + O_2(^1O_2) \tag{23}$$

In this context, it is of interest that the complex $[Cp_2Os^{III}(S_2^{2-})Os^{III}Cp_2]^{2+}$ is apparently not stable but thermally decomposes to osmocene and sulfur (*23*). In any case, the product formation is certainly facilitated by the high stability of osmocene.

In summary, the photochemical water splitting can be described in a simplified version by the cyclic process shown in Scheme 1.

The protonation of osmocene (Eq. 12) can be viewed as an oxidative addition leading to the formation of Os(IV). Since Os(IV) is an oxidant, the complex $Cp_2Os^{IV}H^+$ should be characterized by a $(H^- \rightarrow Os^{IV})$ LMCT transition at relatively low energies. Although a corresponding absorption band was not identified the photolysis of the hydridic complex (Eq. 12) seems to originate from such a LMCT state. Moreover, $[Cp_2Os^{IV}(OH)]^+$ should have available a low-energy $(OH^- \rightarrow Os^{IV})$ LMCT state. The corresponding LMCT absorption of the hydroxo complex or its deprotonated form $Cp_2Os^{IV}O$ appears at $\lambda_{max} = 390$ nm.

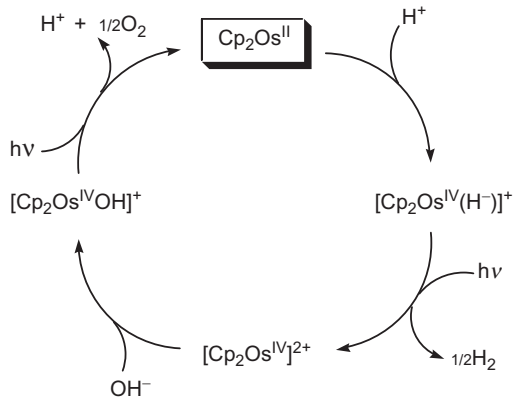

SCHEME 1. Photochemical water splitting.

Finally, LMCT excitation leads to the reduction to Os(II) and oxidation of hydroxide, oxide, or peroxide to oxygen.

It is apparent from Scheme 1 that the reductive and oxidative part of the water splitting by osmocene shows interesting analogies to photosystems I and II of natural photosynthesis which also take place as separate processes.

III. Carbon Dioxide Splitting

For artificial photosynthesis most efforts have been devoted to photochemical water splitting (Eq. 7) while other possibilities have also been considered. Natural photosynthesis

$$CO_2 + H_2O \rightarrow \frac{1}{n}(CH_2O)_n + O_2, \quad \Delta H = +470\,\text{kJ} \qquad (24)$$

yields carbohydrates as energy-storing products (Eq. 24). Surprisingly, very little is known about photosplitting of CO_2 Eqs. (2) and (4) as another simple version of artificial photosynthesis.

$$CO_2 \rightarrow CO + \frac{1}{2}O_2, \quad \Delta H = +238\,\text{kJ} \qquad (25)$$

$$CO_2 + H_2O \rightarrow CO + H_2O_2, \quad \Delta H = +281\,\text{kJ} \qquad (26)$$

Equation (26) can be easily transformed to Eq. (25) by disproportionation of hydrogen peroxide. It is quite interesting that the products of reaction (25) have been labeled as carbon monoxide detonating gas more than 70 years ago (*24*). This emphasizes also the analogy of splitting water (Eq. 7) and carbon dioxide (Eq. 25).

A. Photoreduction of Carbonate in a Copper(I) Phosphine Complex

The photoreduction of CO_2 to CO by metal complexes has been studied in some detail (*25–27*). Frequently, complexes that contain CO_2 as ligand have been examined. In general, such complexes are not available by simple procedures. In this context, it is quite surprising that the photoreactivity of carbonate complexes has been investigated only to a rather limited extent although the photoreduction of carbonate ligands has been anticipated (*28*).

Carbonate complexes are known since the beginning of coordination chemistry. Generally, they are rather stable and easily accessible. The reduction of CO_3^{2-} to CO should be facilitated in mononuclear or binuclear carbonate complexes with metal centers that provide two excess electrons. The requested photoexcitation corresponds to an MLCT transition that terminates at the carbonate ligand as acceptor. However, MLCT absorptions of this type are unknown. They are expected to occur at very short wavelength since the π^* acceptor orbital of CO_3^{2-} is certainly located at rather high energies (*29*).

As a suitable candidate, we selected the complex (prophos) $Cu^I(CO_3)Cu^I$(prophos) (**I**) (Scheme 2) with prophos = 1,3-bis(diphenylphosphino)propane for a recent study (*30*).

Copper(I) is a MLCT donor and as a d^{10} metal it has not available interfering LF states (*31*). The oxidation of both metal centers to Cu(II) leads to the release of two electrons that are required for the reduction of carbonate to CO. Our expectation that complex ***I*** should photochemically split off CO was based on various observations. The thermal release of CO from CO_2 catalyzed by Cu (I) at higher temperatures was already reported in 1976 (*32,33*). Quite recently, a related reaction has been discovered (*34*). Moreover, complex ***I*** shows certain analogies to $(P\phi_3)_2Cu^I(NO_3)$ (*35*). As CT acceptor, it contains NO_3^-, which is isoelectronic to CO_3^{2-}. In this case, the irradiation leads to the population of a reactive MLCT state that initiates the oxidation of Cu(I) and the reduction of nitrate. The triphenylphosphine ligand does not only serve to

(prophos)$Cu^I(CO_3)Cu^I$(prophos)

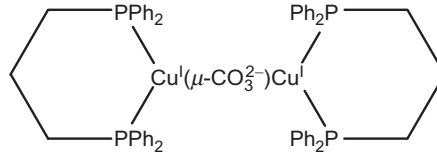

Scheme 2.

stabilize Cu(I) but provides also an IL state for light absorption. For our purpose, the complex $(P\phi_3)_2Cu^I(\mu\text{-}CO_3^{2-})Cu^I(P\phi_3)_2$ should be a suitable candidate. It was synthesized and characterized already in 1995 (*36*). For further stabilization we replaced $P\phi_3$ by the bidentate ligand prophos.

Complex ***I*** is colorless, well soluble in organic solvents and does not decompose in humid air. The absorption spectrum of ***I*** ($\lambda_{max} = 279$ nm; $\varepsilon = 15{,}400\ M^{-1}\ cm^{-1}$ and $\lambda_{max} = 268$ nm; $\varepsilon = 16{,}800\ M^{-1}\ cm^{-1}$) in CH_3CN (Fig. 1) remains unchanged for days. However, ***I*** is light sensitive. The irradiation is accompanied by spectral variations including an isosbestic point at 231 nm (Fig. 1). During the photolysis a continuous decrease of the absorption at $\lambda > 231$ nm takes place. The photoproduct shows a characteristic spectrum (Fig. 1) with a maximum at 263 nm and further features at $\lambda_{max} = 256$, 271, 284, and 296 nm. Complex ***I*** displays a weak luminescence at $\lambda_{max} = 440$ nm (Fig. 2), which disappears during the photolysis and is replaced by a much more intense luminescence at $\lambda_{max} = 304$ nm (Fig. 2). Further, maxima appear at 282 (sh), 290, and 318 nm (sh).

The absorption and emission spectrum of the photolyzed solution can be unambiguously attributed to 1,3-bis(diphenylphosphino)propane monoxide (prophos oxide, ***II***) as shown by comparison with the spectra of an authentic sample of ***II***. The phosphine oxide ***II*** is formed with a quantum yield of

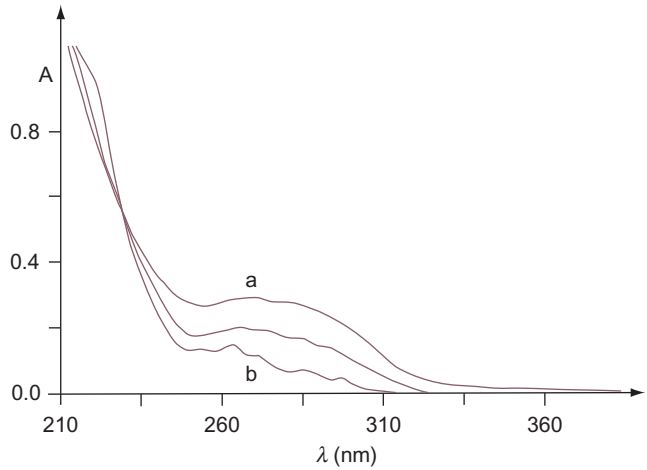

FIG. 2. Spectral changes during the photolysis of 2.68×10^{-5} M (prophos)$Cu^I(CO_3)Cu^I$(prophos) in acetonitrile at room temperature under argon at 0 (a), 15 and 40 min (b) irradiation times with $\lambda_{irr} = 313$ nm (Osram HBO 200 W/2 lamp), 1-cm cell.

$\phi = 0.01$ at $\lambda_{irr} = 313$ nm. Even at higher concentrations of ***I*** characteristic LF bands of Cu(II) cannot be detected in the spectrum of the photolyzed solution.

The photolysis of ***I*** is accompanied by the formation of a gas that already in the beginning becomes visible as small bubbles. This gas is not CO_2 but CO. The photolysis can be described by the simple stoichiometric equation:

$$CO_2 + \text{prophos} \rightarrow CO + \text{prophos monoxide} \qquad (27)$$

On the basis of our observations and further considerations we suggest that the photolysis proceeds by the following molecular mechanism. In analogy to other Cu(I) phenylphosphine complexes (*37*) including $(P\phi_3)_2Cu^I(NO_3)$ (*35*) the long-wavelength absorption of ***I*** is attributed to an IL (phosphine) transition. Accordingly, the irradiation of ***I*** is associated with an IL excitation. Partially, the deactivation leads to an IL luminescence ($\lambda_{max} = 440$ nm). The IL emissions of comparable complexes (*37*) such as $(P\phi_3)_2Cu^I(NO_3)$ at $\lambda_{max} = 450$ nm (*35*) or $[Cu^I(\text{prophos})_2]^+$ at $\lambda_{max} = 430$ nm appear in the same spectral region. Another deactivation path terminates at a reactive $(Cu^I \rightarrow CO_3^{2-})$ MLCT state which with participation of a suitable vibration leads to the dissociation of CO from the carbonate bridge (Fig. 3).

According to this description, the release of CO should be accompanied by the generation of a CuO_2Cu moiety in the primary photochemical step. This fragment may contain $Cu^I(O_2^{2-})Cu^I$ or its redox isomer $Cu^{II}(O^{2-})_2Cu^{II}$. Calculations have shown

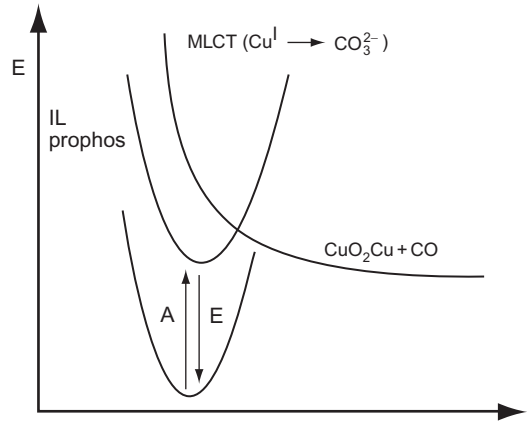

FIG. 3. Potential energy diagram for the ground state and the lowest energy excited states of $(\text{prophos})Cu^I(CO_3)Cu^I(\text{prophos})$.

that they are close in energy, although such complexes are unknown (*38,39*). Since the CuO_2Cu fragment should be quite oxidizing it is not unexpected that it undergoes an oxygen transfer to a phosphine in agreement with our observation. It is well known that a variety of oxygen transfer agents are able to convert phosphines to phosphine oxides.

B. Splitting of Alkyl Carbonates Photocatalyzed by Copper Hydrotris Pyrazolylborate Complexes

While indeed a clean photoreduction of CO_3^{2-} to CO in the complex (prophos)$Cu^I(CO_3)Cu^I$(prophos) was observed the concomitant oxidation did not yield oxygen or hydrogen peroxide but phosphine oxide (*30*). In order to prevent this dead end, phosphines have to be replaced by ligands that do not act as oxygen atom acceptors. For this purpose we selected the tridentate ligand hydrotris (3,5-dimethyl-1-pyrazolyl)borate (Tp*) as a suitable ligand (*40*). Various Cu(I) and Cu(II) complexes of Tp* or other Tp derivatives have been prepared and characterized (*41–45*). Unfortunately, we were not able to obtain simple carbonate complexes of the Cu^ITp^* moiety (Structure 1). In the presence of CO_3^{2-}, Cu^ITp^* underwent a decomposition.

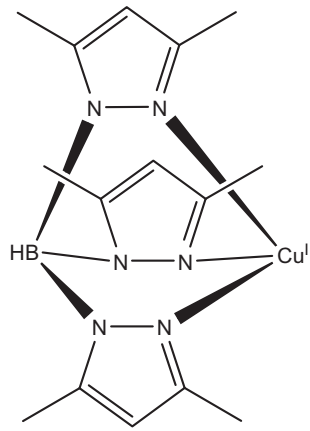

However, Cu^ITp^* (*41–45*) can be dissolved in an aqueous solution of carbonic acid esters $CO(OR)_2$ with $R = CH_3$, C_2H_5, and $½CH_2CH_2$ without decomposition. The photolysis of these solutions smoothly proceeds according to Eq. (5).

$$2Cu^{I}Tp^{*} + CO(OR)_2 + 2H_2O \rightarrow Tp^{*}Cu^{II}(\mu\text{–}OH)_2 \quad Cu^{II}Tp^{*} + CO + 2ROH \tag{28}$$

The photoreduction to CO was also observed when $CO(OR)_2$ was replaced by urea. A detailed analysis was carried out for the photolysis in the presence of dimethyl carbonate. The irradiation of $Cu^{I}Tp^{*}$ ($\lambda_{max} = 279$ nm; $\varepsilon = 16{,}180\,M^{-1}\,cm^{-1}$ and $\lambda_{max} = 227$ nm (sh); $\varepsilon = 8600\,M^{-1}\,cm^{-1}$) in a water/dimethylcarbonate mixture was accompanied by spectral changes (Fig. 4) that indicated a clean conversion to $Tp^{*}Cu^{II}(OH)_2Cu^{II}Tp^{*}$. The spectrum of an authentical sample of this complex (*42*) shows absorptions at $\lambda_{max} = 260$ nm, $\varepsilon = 6800$ and $\lambda_{max} = 653$ nm, $\varepsilon = 120\,M^{-1}\,cm^{-1}$. Moreover, a gas was formed that already in the beginning becomes visible as bubbles. This gas is not CO_2 but apparently CO. The quantitative determination of the gas was carried out by measuring the volume with a gas burette. The stoichiometric ratio of $Tp^{*}Cu^{II}(OH)_2Cu^{II}Tp^{*}$ to CO was found to be roughly 1:1 confirming the product ratio in Eq. (5). The quantum yield for the disappearance of $Cu^{I}Tp^{*}$ was $\phi = 1.5 \times 10^{-3} \pm 5\%$ ($\lambda_{irr} = 313$ nm). At later stages of the photolysis, secondary reactions took place as indicated by the irregular pattern of the spectral changes and the loss of the isosbestic points at 230 and 440 nm.

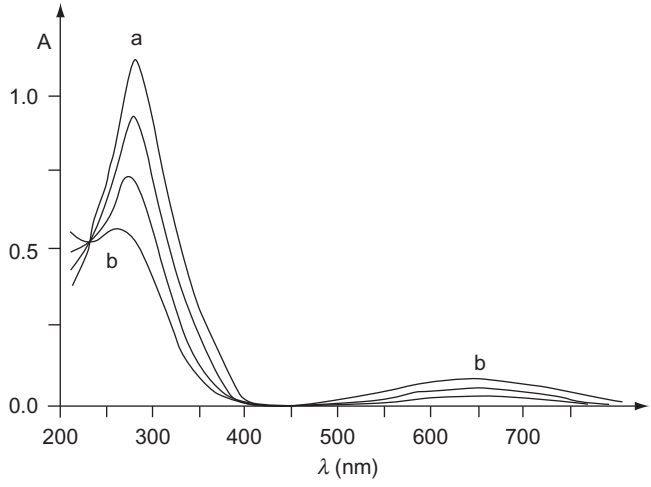

FIG. 4. Spectral changes during the photolysis of 6.89×10^{-5} M $Cu^{I}Tp^{*}$ in a water/dimethylcarbonate mixture under argon at room temperature after 0 min (a), 40, 80, and 160 min (b) irradiation times with $\lambda_{irr} > 290$ nm, 1-cm cell, spectral region 450–800 nm with 10-fold extension of absorbance.

The primary photoproduct $Tp^*Cu^{II}(OH)_2Cu^{II}Tp^*$ is itself also photoactive. The photolysis of $Tp^*Cu^{II}(OH)_2Cu^{II}Tp^*$ in CH_3CN at rather low concentrations ($<10^{-4}$ M) was accompanied by spectral changes that are roughly the reversal of those in Fig. 4. At higher concentrations of $Tp^*Cu^{II}(OH)_2Cu^{II}Tp^*$, this photolysis led to the precipitation of $Cu^{I}Tp^*$, which is rather insoluble in most solvents. It was identified by its absorption and emission spectrum with $\lambda_{max}=594$ nm. As further products O_2 and H_2O_2 were detected and determined. The ratio of H_2O_2 to O_2 decreased with increasing irradiation times. After extensive photolysis essentially only oxygen was detected while in the beginning only H_2O_2 was apparently formed. A quantitative analysis roughly established Eq. (29) for this photolysis after short irradiation times.

$$Tp * Cu^{II}(\mu\text{-}OH)_2Cu^{II}Tp^* \rightarrow 2Tp^*Cu^{I} + H_2O_2 \qquad (29)$$

The quantum yield for the disappearance of $Tp^*Cu^{II}(OH)_2Cu^{II}Tp^*$ was $\phi=3\times10^{-3}$ at $\lambda_{irr}=313$ nm. The complex was not light sensitive upon long wavelength irradiation ($\lambda>450$ nm) in the region of the Cu(II) LF bands.

It follows from Eqs. (28) and (29) that the photosplitting of dialkyl carbonates should be catalytic. This is expressed by Eq. (30) or (31), which includes the disproportionation of H_2O_2.

$$CO(OR)_2 + 2H_2O \rightarrow CO + H_2O_2 + 2ROH \qquad (30)$$

$$CO(OR)_2 + H_2O \rightarrow CO + \frac{1}{2}O_2 + 2ROH \qquad (31)$$

Indeed, extended irradiation ($\lambda>290$ nm) of $Cu^{I}Tp^*$ in $CO(OR)_2$/H_2O mixtures was associated with formation of CO exceeding the amount calculated for Eq. (28) with TON>5. The limitation of photocatalysis in our system is apparently caused by an accompanying irreversible photodecomposition of Cu(I) and/or Cu(II) Tp* complexes as indicated by the precipitation of a slightly colored material after continued irradiation.

At this point a few comments about the mechanism of the photochemical splitting of carbonate are appropriate. We suggest that in agreement with the excited state properties of Tp complexes in general *(46,47)* the photoexcitation of $Cu^{I}Tp^*$ leads to the population of an IL excited state followed by electron transfer to the carbonate. A radical anion is thus formed as an intermediate which is subsequently reduced by a second $Cu^{I}Tp^*$ complex forming CO. Simultaneously, two $Cu^{II}Tp^*$ fragments are generated as oxidation products. Under these conditions

(Eq. 28) they combine to the well-known binuclear hydroxy-bridged complex $Tp^*Cu^{II}(OH)_2Cu^{II}Tp^*$ (*42*). Generally, Cu(II) complexes have available low-energy LF and LMCT states. While Cu(II) LF states are not reactive, LMCT states initiate the reduction of Cu(II) to Cu(I) and oxidation of ligands (*48,49*). As a reductive elimination of H_2O_2, Eq. (6) finds a logic explanation in this way. Reductive elimination of two hydroxide ligands yielding H_2O_2 has been reported previously (*50,51*). Another observation related to our work is also quite important. The photolysis of $Tp^*Cu^{II}OCu^{II}Tp^*$ in the presence of dimethyl sulfide or cyclohexene is accompanied by oxygen transfer to these organic substrates (*52*).

In summary, the photocatalysis Eq. (30) or (31) can be considered as proof of principle for photocatalytic splitting of CO_3^{2-} or CO_2 itself (Eq. 3 or 4). However, in order to improve this photocatalysis, a few shortcomings of the present system should be mentioned. Of course, alkyl carbonates or amides (urea) must be replaced by CO_3^{2-}. Since carbonate complexes of Cu(I) are known (*36*), the instability of $CuTp^*/CO_3^{2-}$ mixtures is probably associated with the Tp* ligand. Accordingly, Tp* should be replaced by another ligand that forms also stable Cu(I) and Cu(II) complexes but does not facilitate a decomposition in the presence of carbonate and the photooxidation of the spectator ligand as it takes place in the case of copper phosphines (see above). Finally, the present system needs UV light, but this is certainly not an inherent energy requirement. An intermolecular or intramolecular long-wavelength sensitization might circumvent this problem.

IV. Dinitrogen Splitting

The lack of reactivity of dinitrogen which complicates its chemical conversion has been a challenge to chemists for many decades (*53,54*). This difficulty is based on the extreme stability of the nitrogen–nitrogen triple bond. The huge energy difference between HOMO and LUMO (23 eV) makes N_2 rather redox inert. Moreover, the conversion of N_2 to simple species, such as ammonia or nitride, requires the transfer of six electrons. Such multielectron transfer processes are generally associated with large activation barriers. Nevertheless, the reduction of N_2 to NH_3 occurs in nature through the utilization of the enzyme nitrogenase as catalyst. This conversion also takes place in the Haber–Bosch process; however, extreme conditions are required. However, this catalysis occurs only under extreme conditions.

Accordingly, it is of considerable interest to accomplish this reaction at ambient conditions. In principle, catalysis can be replaced by a photochemical procedure. The activation energy is then supplied by light. In favorable cases, the photoactivation is selective and avoids interfering processes. Moreover, light may not only provide the activation energy but also the energy for an endothermic reaction that does not occur in catalysis at lower temperatures.

In this context, it has been reported that $(Mes)_3Mo{=}N{=}N{=}Mo(Mes)_3$ with Mes = 2,4,6-$Me_3C_6H_2$ is light sensitive and the photoproducts imply the intermediate formation of $(Mes)_3Mo{\equiv}N$ (*55*). This photolysis was carried out under conditions that are usually applied for synthetic purposes. It may be thus difficult to elucidate the photochemical mechanism. For example, the photolysis mentioned above was performed for 18 h. In such cases, the photoproducts could be the result of subsequent reactions that may not be easily related to the primary photochemical steps.

Quite recently, a detailed study of the thermal and photochemical reactivity of $(\mu\text{-}N_2)[Mo(N[tert\text{-}Bu]Ar)_3]_2$ has been reported by Cummins *et al.* (*56*). It is rather interesting that the N_2 bridge is thermally cleaved to generate the nitride complex $NMo(N[tert\text{-}Bu]Ar)_3$ while the photolysis leads to the same result, but in a second reaction path also liberates N_2 yielding $Mo(N[tert\text{-}Bu]Ar)_3$. The ground state of the $\mu\text{-}N_2$ complex has been suggested to contain the MoNNMo fragment implying that dinitrogen is present in a reduced form. The nature of the reactive excited state is not immediately obvious and could be identified only by density functional theory (*56*). In contrast, the reductive splitting of the NN triple bond in a molecular complex is certainly much more difficult to achieve and has previously not yet been accomplished, neither thermally nor photochemically.

Accordingly, we decided to examine a binuclear complex with a bridging N_2 ligand that largely preserves its integrity as dinitrogen molecule. For this purpose, we selected the cation $[(NH_3)_5Os^{II}(\mu\text{-}N_2)Os^{III}(NH_3)_5]^{5+}$ (*57,58*) (***I***) for a recent study (*59*).

A. Photoreduction of N_2 in a Binuclear Osmium Complex

The cation $[(NH_3)_5Os^{II}(\mu\text{-}N_2)Os^{III}(NH_3)_5]^{5+}$ (*59*) (scheme 3) offers several attractive features.

This complex offers several attractive features. It is easily accessible and rather stable in aqueous solution in the absence of light. Owing to the intense color of ***I*** its disappearance can be precisely monitored. Although it is a mixed-valence system

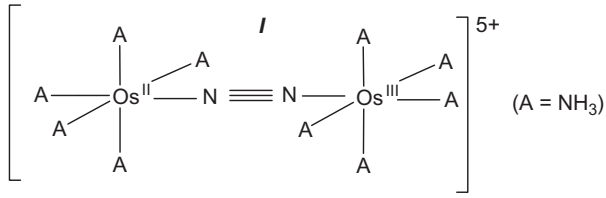

SCHEME 3.

with considerable electronic delocalization between both metal centers, the triple bond of free N_2 is also present in the coordinated state as indicated by vibrational spectroscopy. Finally, the splitting of N_2 in the complex can be anticipated to proceed by a simple intramolecular redox reaction that produces only one excess electron that can lead to complications (Eq. 32):

$$\left[(NH_3)_5Os^{II}(\mu\text{-}N_2)Os^{III}(NH_3)_5\right]^{5+} \rightarrow 2\left[Os^{VI}(NH_3)_4N\right]^{3+} + 2NH_3 + 1e^- \quad (32)$$

The expected photoproduct $[Os(NH_3)_4N]^{3+}$ is also quite stable and well characterized *(60–62)*. In this context, it should be stressed that the reverse reaction has been observed as photochemical *(60,61)* and thermal *(63,64)* process. It is obviously much easier to couple two nitride complexes containing the $Os^{VI}N|$ moiety to a binuclear N_2 complex owing to the extreme stability of the NN triple bond.

The irradiation of ***I*** (absorption spectrum *(5)*: $\lambda_{max} = 700$ nm, $\varepsilon = 4000$ M^{-1} cm^{-1}; $\lambda_{max} = 260$ (sh), $\varepsilon = 21{,}000$; and $\lambda_{max} = 238$ nm; $\varepsilon = 41{,}000$) is associated with a bleaching of the green color owing to the disappearance of the 700 nm absorption (Fig. 1). While ***I*** is not luminescent, the photoproduct shows an orange emission at $\lambda_{max} = 570$ nm (Fig. 2) which grows with increasing irradiation time. The emission is attributed to the formation of $[Os^{VI}(NH_3)_4N]^{3+}$ *(60–62)* ***II***. This assignment is confirmed by the excitation spectrum of the photolyzed solution (Fig. 2), which closely resembles the absorption spectrum *(60–62,65)* ($\lambda_{max} = 410$ nm, $\varepsilon = 25$; $\lambda_{max} = 325$ (sh), $\varepsilon = 75$; $\lambda_{max} = 270$ nm, $\varepsilon = 1350$; and $\lambda_{max} = 236$ nm, $\varepsilon = 3100$), and the excitation spectrum of an authentic sample of ***II*** (Figs. 5 and 6).

The photolysis of ***I*** does not take place upon irradiation of the 700 nm band but only upon shorter-wavelength irradiation ($\lambda_{irr} < 450$ nm). The quantum yield amounts to $\phi = 0.002$ at $\lambda_{irr} = 254$ nm and $\phi = 0.003$ at $\lambda_{irr} = 365$ nm. Complex ***I*** is not completely converted to ***II***. The molar ratio of ***I*** to ***II*** was found

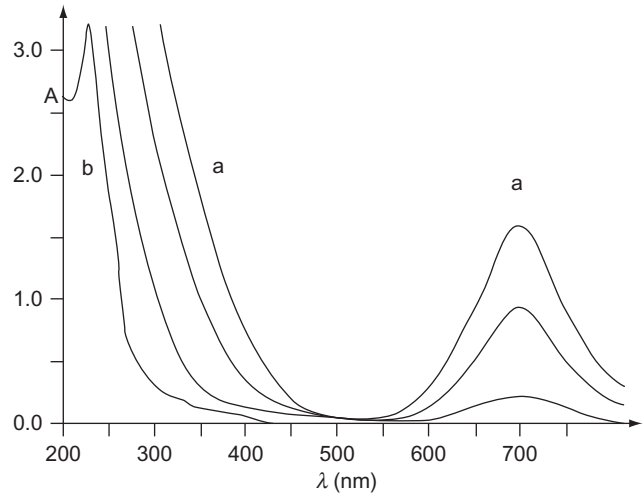

FIG. 5. Spectral changes during the photolysis of 4.1×10^{-4} M $[(NH_3)_5Os^{II}(\mu\text{-}N_2)Os^{III}(NH_3)_5](CF_3SO_3)_5$ in 10^{-3} M CF_3SO_3H under argon at room temperature after 0 min (a), 30, 60, and 120 min (b) irradiation times with $\lambda_{irr} = 250$–390 nm (UV filter Schott UG 11/2) 1-cm cell.

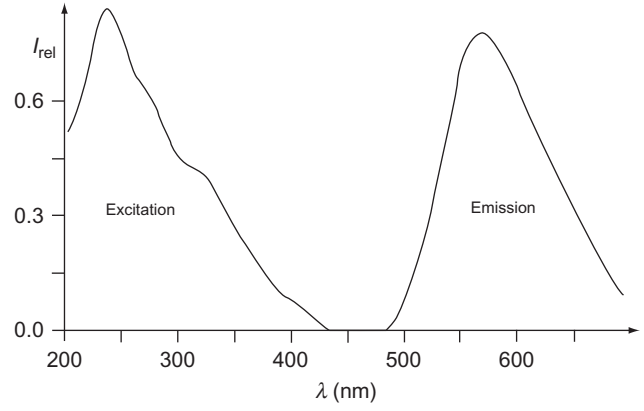

FIG. 6. Electronic excitation ($\lambda_{em} = 570$ nm) and emission ($\lambda_{exc} = 380$ nm) spectrum of 4.1×10^{-4} M $[(NH_3)_5Os^{II}(\mu\text{-}N_2)Os^{III}(NH_3)_5](CF_3SO_3)_5$ in 10^{-3} M CF_3SO_3H under argon at room temperature after 120 min irradiation time with $\lambda_{irr} = 250$–390 nm (UV filter Schott UG 11/2), 1-cm cell, intensity in arbitrary units.

to be roughly 1:2. Accordingly, a further Os complex should have been formed. It was assumed to be $[Os^{III}(NH_3)_5(H_2O)]^{3+}$ (see below) which cannot be identified in the photolyzed solution by its absorption spectrum. This spectrum consists only of a short-wavelength shoulder at $\lambda_{max} = 220$ nm of moderate intensity ($\varepsilon = 1100$). However, upon addition of iodide the aquo complex undergoes a facile substitution yielding $[Os^{III}(NH_3)_5I]^{2+}$ (*66*). This complex shows a long-wavelength LMCT band ($\lambda_{max} = 407$ nm, $\varepsilon = 1970$). Indeed, this absorption appears in the spectrum of the photolyzed solution when iodide is added. The molar ratio of ***I*** to $[Os^{III}(NH_3)_5I]^{2+}$ was found to be nearly 3. Neither ***I*** nor ***II*** was observed to react with iodide. Ammonia was detected as a further photoproduct of ***I***. Any interference by ***I*** or the constituents of the photolyzed solution could be excluded. The molar ratio of ***I*** to NH_3 was found to be approximately 2. Finally, the photolysis of ***I*** is not accompanied by the evolution of a gas. In contrast, the irradiation of $[Os^{II}(NH_3)_5(N_2)]^{2+}$ leads to the release of N_2 (*67*). In this case at higher complex concentrations N_2 appears as gas bubbles even at the beginning of the photolysis.

The long-wavelength absorption of ***I*** at 700 nm has been assigned to an intervalence transition within the delocalized Os^{II}/Os^{III} system while the UV bands have been attributed to MLCT transitions terminating at the bridging N_2 ligand (*57*). These assignments are also reflected by the photoreactivity of ***I***. Light absorption by the 700 nm band is not associated with any photoactivity. In contrast, MLCT excitation leads to the oxidation of the metal and reduction of N_2 as anticipated in Eq. (1). Of course, MLCT excitation and product formation do not imply the transfer of six electrons to N_2, but only the shift of electron density owing to the covalent nature of the complexes. However, the occurrence of this photoredox reaction is certainly facilitated by the simple stoichiometry of the intramolecular photoredox process for the conversion of ***I*** to ***II***. In distinction to ***I***, MLCT excitation of $[Os^{II}(NH_3)_5(N_2)]^{2+}$ does not result in the reduction of N_2 but leads only to the release of N_2 (*67*) probably because a simple photochemical mechanism yielding stable reduction products of N_2 is apparently not available in this case.

The distribution of the photoproducts of ***I*** as obtained by analytical measurements suggests that the presence of an excess electron in Eq. (1) causes complications. It is reasonable to assume that the primary photochemical step takes place according to Eq. (33) since the reversal of this reaction type as

$$\left[(NH_3)_5Os^{II}(N_2)Os^{III}(NH_3)_5\right]^{5+} \rightarrow \left[Os^{VI}(NH_3)_4N\right]^{3+} + \left[Os^{V}(NH_3)_4N\right]^{2+} + 2NH_3 \quad (33)$$

thermal (*63,64*) and photochemical (*61,62*) process has been previously observed. The release of ammonia (Eq. 33) occurs due to the strong trans-effect of nitride.

In distinction to $[Os^{VI}(NH_3)_4N]^{3+}$, the complex $[Os^{V}(NH_3)_4N]^{2+}$ (*68*) is not stable and subsequent disproportionations may lead to product formation, as, for example,

$$2\left[Os^{V}(NH_3)_4N\right]^{2+} \rightarrow \left[Os^{VI}(NH_3)_4N\right]^{3+} + \left[Os^{IV}(NH_3)_4N\right]^{+} \quad (34)$$

$$2\left[Os^{IV}(NH_3)_4N\right]^{+} + 3H^{+} + H_2O \rightarrow \left[Os^{V}(NH_3)_4N\right]^{2+} + \left[Os^{III}(NH_3)_5(H_2O)\right]^{3+} \quad (35)$$

These reactions or their modifications would result in the following overall stoichiometry:

$$3\left[(NH_3)_5Os^{II}(N_2)Os^{III}(NH_3)_5\right]^{5+} + 3H^{+} + H_2O \rightarrow 5\left[Os^{VI}(NH_3)_4N\right]^{3+} + \left[Os^{III}(NH_3)_5(H_2O)\right]^{3+} + 6NH_3 \quad (36)$$

The analytical results roughly agree with this equation.

In general, $Os^{V}N$ complexes are not stable (*60–62,68*) owing to the fact that Os(V) is strongly oxidizing and reducing (*69*). In the absence of a suitable redox partner, Os(V) undergoes disproportionation to Os(VI) and Os(IV) (see above). Accordingly, it should also be possible to intercept Os(V) by other redox agents such as oxygen. Indeed, O_2 is apparently able to oxidize $[Os^{V}(NH_3)_4N]^{2+}$ to $[Os^{VI}(NH_3)_4N]^{3+}$. With regard to Eq. (32), oxygen takes up the excess electron. In agreement with this assumption, the photolysis of $[(NH_3)_5Os^{II}(\mu\text{-}N_2)Os^{III}(NH_3)_5]^{5+}$ yields more $[Os^{VI}(NH_3)_4N]^{3+}$ and less $[Os^{III}(NH_3)_5(H_2O)]^{3+}$ in the presence of oxygen compared to that which was performed under argon. The amount of $[Os^{VI}(NH_3)_4N]^{3+}$ increased by 13% when the 5+ ion (4×10^{-4} M) was photolyzed in the presence of oxygen. This comes close to a complete conversion (17%).

In the context of these observations, the question arises what happens when $[(NH_3)_5Os^{III}(\mu\text{-}N_2)Os^{III}(NH_3)_5]^{6+}$ (*70*) is

irradiated. Does the photolysis take place according to the simple Eq. (37)?

$$\left[(NH_3)_5Os^{III}(\mu\text{-}N_2)Os^{III}(NH_3)_5\right]^{6+} \rightarrow 2\left[Os^{VI}(NH_3)_4N\right]^{3+} + 2NH_3 \quad (37)$$

Unfortunately, $[(NH_3)_5Os^{III}(\mu\text{-}N_2)Os^{III}(NH_3)_5]^{6+}$ is rather labile and undergoes a facile decomposition in aqueous solution even at 5 °C (*57,70*). Accordingly, a detailed study is very difficult to perform, but a qualitative experiment is quite revealing. In distinction to the photolysis of $[(NH_3)_5Os^{II}(\mu\text{-}N_2)Os^{III}(NH_3)_5]^{5+}$, the irradiation of $[(NH_3)_5Os^{III}(\mu\text{-}N_2)Os^{III}(NH_3)_5]^{6+}$ is accompanied by the vigorous evolution of nitrogen which takes place also thermally but with a much smaller rate. The photochemical behavior of the 6+ ion can be explained by its excited state properties. It is well known that MLCT transitions of Os(III) complexes occur at much higher energies than those of Os(II) (*71*). A reactive ($Os \rightarrow N_2$) MLCT state of the 6+ ion is apparently not anymore accessible by conventional light sources. As an alternative or additional effect, LF states of the 6+ ion are now populated. These LF states initiate the release of N_2 in agreement with the general behavior of LF states.

While the photoactivation of dinitrogen in $[(NH_3)_5Os^{II}(\mu\text{-}N_2)Os^{III}(NH_3)_5]^{5+}$ in an aqueous solution leading to the reductive cleavage of N_2 has been achieved it is of considerable importance if the nitride ligand of the photoproduct can be utilized for the formation of useful nitrogen compounds (*56*). Although the study of further reactions of $[Os^{VI}(NH_3)_4N]^{3+}$ was not within the scope of the present investigation, it is well known that $Os^{VI}N$ complexes are able to undergo nitrogen atom transfer reaction or reduction to Os^{II} or Os^{III} (*69,72,73*). In the latter case, protonation of the nitride ligand yields NH_3. In this sense, our observations can be directly related to the Haber–Bosch process, which takes place at a solid interphase. In this context, it is of interest that Schrauzer (*74*) and Kisch (*75*) observed the photoreduction of N_2 at TiO_2.

In summary, the photolysis of aqueous $[(NH_3)_5Os^{II}(N_2)Os^{III}(NH_3)_5]^{5+}$ induced by MLCT excitation leads to the reductive splitting of the bridging N_2 ligand yielding $[Os^{VI}(NH_3)_4N]^{3+}$ as main photoredox product. It should be emphasized that the electronic CT excitation does not only provide a suitable intramolecular redox reaction but may supply also the necessary energy for activation and cleavage of the very stable N_2 molecule.

V. Conclusion

Even the most stable and least reactive molecules such as H_2O, CO_2, and N_2 can be photocleaved by intramolecular electron transfer between suitable redoxactive metal centers and these molecules or simple derivatives such as carbonate instead of carbon dioxide. The photoactivation is achieved by CT excitation which corresponds to a shift of electron density. The formation of stable products is determined by the availability of appropriate oxidation states at the metal centers. While these photoreactions are very interesting in their own right, applications are conceivable in particular for solar energy utilization. Especially, organometallic approaches to water splitting have been anticipated to be rather promising in the future (*76*).

VI. Abbreviations

CT transitions are classified according to the redox sites at the metals and ligands (*2,77*). Their energy depends roughly on the reducing and oxidizing strength of the donor and acceptor, respectively. Accordingly, the labels M_{ox}, M_{red}, L_{ox}, and L_{red} are used to stress the possibility of a low-energy transition:

M_{ox}–L_{red}	Ligand-to-metal	LMCT
M_{red}–L_{ox}	Metal-to-ligand	MLCT
M_{red}–L–M_{ox}	Metal-to-metal	MMCT
M_{red}–M_{ox}	Metal-to-metal	MMCT
L_{red}–M–L_{ox}	Ligand-to-ligand	LLCT
M–L (L = A_{ox}–D_{red})	Intraligand	ILCT

Acknowledgment

We are grateful for financial support from the DFG (Grant VO 211/18-1).

References

1. Lewis, N. S.; Nocera, D. G. *Proc. Natl. Acad. Sci. USA* **2006,** *103*, 15729–15735.

2. Vogler, A.; Kunkely, H. In: "*Photosensitization and Photocatalysis*"; Eds. Kalyanasundaram, K.; Grätzel, M.; Kluwer Academic Publishers: **1993** pp. 71–111.
3. Horvath, O.; Stevenson, K. L. *Charge Transfer Photochemistry of Coordination Compounds.* VCH: Weinheim, **1993**.
4. Nocera, D. G. *Acc. Chem. Res.* **1995,** *28*, 209–217.
5. Vogler, A.; Kern, A.; Fußeder, B.; Hüttermann, J. *Z. Naturforsch.* **1978,** *33b*, 1352–1356.
6. Kunkely, H.; Vogler, A. *Inorg. Chim. Acta* **2005,** *358*, 4086–4088.
7. Geoffroy, G. L.; Pierantozzi, R. J. *Am. Chem. Soc.* **1976,** *98*, 8054.
8. Geoffroy, G. L.; Wrighton, M. S. In "*Organometallic Photochemistry*"; Academic Press: New York, **1979** pp. 277–299 chapter 7.
9. Muckerman, J. T.; Polyansky, D. E.; Wada, T.; Tanaka, K.; Fujita, E. An invited paper for forum on "Making Oxygen" *Inorg. Chem.* **2008,** *47*, 1697.
10. Lee, D. G.; Moylan, C. R.; Hayashi, T.; Brauman, J. I. J. *Am. Chem. Soc.* **1987,** *109*, 3003.
11. Kunkely, H.; Vogler, A. *J. Chem. Soc., Chem. Commun.* **1994,** 2671–2672.
12. Kunkely, H.; Vogler, A. *Angew. Chem. Int. Ed.* **2009,** 1685–1687.
13. Shubina, E. S.; Krylov, A. N.; Kreindlin, A. Z.; Rybinskaya, M. I.; Epstein, L. M. J. *Organomet. Chem.* **1994,** *465*, 259–262.
14. Droege, M. W.; Harman, W. D.; Taube, H. *Inorg. Chem.* **1987,** *26*, 1309–1315.
15. Crabtree, R. H.; Eisenstein, O.; Sini, G.; Peris, E. J. *Organomet. Chem.* **1998,** *567*, 7–11.
16. Kruck, T.; Sylvester, G.; Kunau, I. -P. *Angew. Chem.* **1971,** *17–18*, 725.
17. Stiegmann, A. E.; Tyler, D. R. *Acc. Chem. Res.* **1984,** *17*, 61–66.
18. Stiegmann, A. E.; Tyler, D. R. *Coord. Chem. Rev.* **1985,** *63*, 217–240.
19. Kunkely, H.; Vogler, A. *Trans. Met. Chem.* **2000,** *25*, 234–236.
20. Fischer, E. O.; Grubert, H. *Chem. Ber.* **1959,** *92*, 2302–2309.
21. Sugimoto, H.; Sawyer, D. T. J. *Am. Chem. Soc.* **1984,** *106*, 4283–4285.
22. Vogler, A.; Kunkely, H. *Coord. Chem. Rev.* **2006,** *250*, 1622–1626.
23. Droege, M. W.; Taube, H. *Inorg. Chem.* **1987,** *26*, 3316–3318.
24. Leschewski, K.; Möller, H.; Steinmann, B. *Z. Anorg. Allg. Chem.* **1938,** *239*, 180–188.
25. Fujita, E. *Coord. Chem. Rev.* **1999,** *185–186*, 373–384.
26. Hayashi, Y.; Kita, S.; Brunschwig, B. S.; Fujita, E. *J. Am. Chem. Soc.* **2003,** *125*, 11976–11987.
27. Lin, W.; Frei, H. J. *Am. Chem. Soc.* **2005,** *127*, 1610–1611.
28. Henary, M.; Kaska, W. C.; Zink, J. I. *Inorg. Chem.* **1989,** *28*, 2995–2997.
29. Leirer, M.; Knör, G.; Vogler, A. *Inorg. Chem. Commun.* **1998,** *1*, 49–50.
30. Kunkely, H.; Vogler, A. *Inorg. Chem. Commun.* **2010,** *13*, 137–138.
31. Kunkely, H.; Vogler, A. *Chem. Phys. Lett.* **2003,** *368*, 49–52.
32. Tsuda, T.; Sanada, S. -I.; Saegusa, T. J. *Organomet. Chem.* **1976,** *116*, C10–C12.
33. Tsuda, T.; Chujo, Y.; Saegusa, T. J. *Am. Chem. Soc.* **1980,** *102*, 431–433.
34. Laitar, D. S.; Müller, P.; Sadighi, J. P. J. *Am. Chem. Soc.* **2005,** *127*, 17196–17197.
35. Kunkely, H.; Vogler, A. J. *Am. Chem. Soc.* **1995,** *117*, 540–541.
36. Darensbourg, D. J.; Holtcamp, M. W.; Khandelwal, B. J.; Reibenspies, H. *Inorg. Chem.* **1995,** *34*, 5390–5394.
37. Kutal, C. *Coord. Chem. Rev.* **1990,** *99*, 213–252.
38. Ruiz, E.; de Graaf, C.; Alemany, P.; Alvarez, S. *J. Phys. Chem.* **2002,** *A 106*, 4938–4941.

39. Blanchet-Boiteux, C.; Mouesca, J. -M. *J. Phys. Chem.* **2000,** *A 104*, 2091–2097.
40. Kunkely, H.; Vogler, A. *Inorg. Chem. Commun.* **2001,** *14*, 96–98.
41. Mealli, C.; Arcus, C. S. J. *Am. Chem. Soc.* **1976,** *98*, 711–718.
42. Kitajima, N.; Koda, T.; Hashimoto, S.; Kitagawa, T.; Moro-oka, Y.; Kitajima, N.; Koda, T.; Hashimoto, S.; Kitagawa, T.; Moro-oka, Y. *J. Am. Chem. Soc.* **1991,** *113*, 5664–5671.
43. Kitajima, N.; Fujisawa, K.; Fujimoto, C.; Moro−oka, Y.; Hashimoto, S.; Kitagawa, T.; Toriumi, K.; Tatsumi, K.; Nakamura, A. *J. Am. Chem. Soc.* **1992,** *114*, 1277–1291.
44. Lobbia, G. G.; Pettinari, C.; Marchetti, F.; Bovio, B.; Cecchi, P. *Polyhedron* **1996,** *15*, 881–890.
45. Díaz-Requejo, M. M.; Mairena, M. A.; Belderrain, T. R.; Nicasio, M. C.; Trofimenko, S.; Pérez, P. *J. Chem. Commun.* **2001,** 1804–1805.
46. Kunkely, H.; Pawlowski, V.; Strasser, A.; Vogler, A. *Inorg. Chem. Commun.* **2008,** *11*, 415–417.
47. Kunkely, H.; Vogler, A. J. *Photochem. Photobiol. A Chem.* **1998,** *119*, 187–190.
48. Kunkely, H.; Vogler, A. *Inorg. Chim. Acta* **2004,** *357*, 888–890.
49. Horváth, O.; Stevenson, K. L. *Charge Transfer Photochemistry of Coordination Compounds.* VCH Publishers: New York, **1993** 49.
50. Knör, G.; Vogler, A.; Roffia, S.; Paolucci, F.; Balzani, V. *Chem. Commun.* **1996,** 1643–1644.
51. Becht, A.; Vogler, A. *Inorg. Chem.* **1993,** *32*, 2835–2837.
52. Kitajima, N.; Koda, T.; Moro-oka, Y. *Chem. Soc. Jpn. Chem. Lett.* **1988,** 347–350.
53. Gambarotta, S.; Scott, J. *Angew. Chem. Int. Ed Engl.* **2004,** *43*, 5298–5308.
54. Fryzuk, M. D.; Johnson, S. A. *Coord. Chem. Rev.* **2000,** *200–202*, 379–409.
55. Solari, E.; Da Silva, C.; Iacono, B.; Hesschenbrouck, J.; Rizzoli, C.; Scopelliti, R.; Floriani, C. *Angew. Chem.* **2001,** *113*, 4025–4027.
56. Curley, J. J.; Cook, T. R.; Reece, S. Y.; Müller, P.; Cummins, C. C. J. *Am. Chem. Soc.* **2008,** *130*, 9394–9405.
57. Richardson, D. E.; Sen, J. P.; Buhr, J. D.; Taube, H. *Inorg. Chem.* **1982,** *21*, 3136–3140.
58. Lay, P. A.; Magnuson, R. H.; Sen, J.; Taube, H. J. *Am. Chem. Soc.* **1982,** *104*, 7658–7659.
59. Kunkely, H.; Vogler, A. *Angew. Chem. Int. Ed.* **2010,** *49*, 1591–1593.
60. Che, C. -M.; Lau, T. -C.; Lam, H. -W.; Poon, C. -K. *J. Chem. Soc., Chem. Commun.* **1989,** 114–116.
61. Che, C. -M.; Lam, H. -W.; Tong, W. -F.; Lai, T. -F.; Lau, T. -C. *J. Chem. Soc., Chem. Commun.* **1989,** 1883–1884.
62. Lam, H. -W.; Che, C. -M.; Wong, K. -Y. *J. Chem. Soc. Dalton Trans.* **1992,** 1411–1416.
63. Buhr, J. T.; Taube, H. *Inorg. Chem.* **1979,** *18*, 2208–2212.
64. Ware, D. C.; Taube, H. *Inorg. Chem.* **1991,** *30*, 4605–4610.
65. Buhr, J. T.; Winkler, J. R.; Taube, H. *Inorg. Chem.* **1980,** *19*, 2416–2425.
66. Lay, P. A.; Magnuson, R. H.; Taube, H. *Inorg. Chem.* **1989,** *28*, 3001–3007.
67. Matsubara, T.; Bergkamp, M.; Ford, P. C. *Inorg. Chem.* **1978,** *17*, 1604–1607.
68. Che, C. -M.; Yam, V. W. -W. *Adv. Inorg. Chem.* **1992,** *39*, 233–325.
69. Pipes, D. W.; Bakir, M.; Vitols, S. E.; Hodgson, D. J.; Meyer, T. J. J. *Am. Chem. Soc.* **1998,** *112*, 5507–5514.

70. Lay, P. A.; Magnuson, R. H.; Taube, H. J. *Am. Chem. Soc.* **1985,** *107*, 2551–2552.
71. Lay, P. A.; Magnuson, R. H.; Taube, H. *Inorg. Chem.* **1988,** *27*, 2848–2853.
72. Bakir, M.; White, P. S.; Dovletoglou, A.; Meyer, T. J. *Inorg. Chem.* **1991,** *30*, 2835–2836.
73. Ware, D. C.; Taube, H. *Inorg. Chem.* **1991,** *30*, 4598–4605.
74. Schrauzer, G. N.; Guth, T. D. J. *Am. Chem. Soc.* **1977,** *99*, 7189–7193.
75. Kisch, H.; Linnik, O. *Mendeleev Commun.* **2008,** *18*, 10–11.
76. Piers, W. E. *Organometallics* **2011,** *30*, 13–16.
77. Vogler, A.; Kunkely, H. *Comments Inorg. Chem.* **1997,** *19*, 283–306.

VISIBLE LIGHT PHOTOCATALYSIS BY METAL HALIDE COMPLEXES CONTAINING TITANIA AS A SEMICONDUCTOR LIGAND

HORST KISCH

Department of Chemistry and Pharmacy, Institute of Inorganic Chemistry, Friedrich-Alexander-Universität Erlangen-Nürnbegrg, Egerlandstraße 1, Erlangen, Germany

ABSTRACT

Reaction of an aqueous suspension of titania with $H_2[PtCl_6]$ or RhX_3 (X = Cl, Br) affords halogenometalate complexes of composition $\{[TiO_2]OMX_nL\}^{z-}$; $z = 1, 2$, L = H_2O, OH^-, M = Pt: $n = 4$, M = Rh, $n = 3$. In these hybrid materials, titania can be viewed as a semiconducting "inorganic ligand" bound via oxygen to a platinum(IV) or rhodium(III) center. The quasi-Fermi level of electrons in the titania ligand is shifted anodically by 0.2–0.3 V as compared to the free "ligand." In the case of the platinum complex, visible light irradiation results in a platinum centered excitation followed by homolytic Pt–Cl bond cleavage and electron injection of Pt(III) into the titania conduction band. Thus, the reducing and oxidizing surface sites can be described as a trapped electron, that is, a Ti(III) center, and a loosely bound

INORGANIC PHOTOCHEMISTRY
VOLUME 63 ISSN 0898-8838 / DOI: 10.1016/B978-0-12-385904-4.00002-0

chlorine atom. In the case of the rhodium surface complex, the excitation is of rhodium-to-titanium charge-transfer type resulting in a Ti(III) center and a Rh(IV) species. These heterosupramolecular metal complexes in the presence of air photocatalyze the exhaustive visible light oxidation of pollutants like halocarbons and atrazine. They are active even in diffuse indoor daylight.

Keywords: Chloroplatinate(IV); Flatband potential; Halogenorhodate(III); Photocatalysis; Solar detoxification; Titanium dioxide; Visible light.

I. Introduction

In connection with the chemical utilization of solar energy the photochemistry of inorganic compounds has received increasing attention. It started in the 1970s, declined in the 1990s, and came up again in the present decade. For the desired conversion of light to chemical energy, three key steps can be considered as schematically summarized by Eqs. (1)–(7) for the sensitization of the redox reaction $A+D=A_{red}$ and D_{ox} by a transition metal complex. They consist of photo-induced charge separation (Eq. 1), electron exchange with substrates affording primary redox products (Eqs. 3 and 4), and conversion of the latter to stable final products (Eqs. 5 and 6). In the case of *solar energy storage*, the over-all reaction has to be endergonic, whereas for *solar energy utilization* it can also be exergonic. It is noted that although many systems undergo the first reaction step, only a few enable also the crucial electron exchange steps due to the highly favored charge recombination (Eq. 2). Even if these two steps proceed (Eqs. 3 and 4), efficient back electron transfer (BET) between the primary redox products (Eq. 7) in many cases prevents efficient formation of the final redox products (Eqs. 5 and 6). Thus, the basic problem of the conversion of light to chemical energy is how to inhibit the primary and secondary charge recombination processes according to Eqs. (2) and (7), respectively. In homogeneous systems, the problem is partially solved by making one of the redox steps, for example, Eq. (4), so fast that it successfully competes with recombination. A typical example is the evolution of hydrogen upon irradiating an aqueous solution of a tris(bipyridyl)ruthenium(II) complex in the presence of methylviologen (corresponds to A) and a reducing agent like triethylamine (corresponds to D). In this system, the

radical cation generated in the reaction step according to Eq. (4) undergoes a fast and irreversible decomposition (Eq. 6) rendering the BET (Eq. 7) too slow to successfully compete with formation of A_{red} (Eq. 5), which corresponds to the reduction of water by the reduced methylviologen (*1*). In summary, the function of the transition metal complex is to photosensitize two *consecutive homogeneous* electron exchange reactions with a donor and acceptor.

$$[M] - L \xrightarrow{h\nu} [M]^{+\cdot} \rightarrow L^{-\cdot} \tag{1}$$

$$[M]^{+\cdot} - L^{-\cdot} \rightarrow [M] - L + h\nu/\text{heat} \tag{2}$$

$$[M]^{+\cdot} - L^{-\cdot} + A \rightarrow [M]^{+\cdot} - L + A^{-\cdot} \tag{3}$$

$$[M]^{+\cdot} - L + D \rightarrow [M] - L + D^{+\cdot} \tag{4}$$

$$A^{-\cdot} \rightarrow A_{red} \tag{5}$$

$$D^{+\cdot} \rightarrow D_{ox} \tag{6}$$

$$A^{-\cdot} + D^{+\cdot} \rightarrow A + D \tag{7}$$

The reaction sequence discussed above differs significantly from photosensitization by a semiconductor, in general just named *photocatalysis*, a reaction system wherein a solid photocatalyst *simultaneously* sensitizes two *heterogeneous* redox reactions (*2*). By analogy with Eqs. (1)–(7), the basic reaction steps may be summarized in a simplified way according to Eqs. (8)–(10). Light absorption generates, *inter alia*, reactive electron–hole pairs trapped at the surface. It is expected that the distance between these redox centers should be larger than in a molecular sensitizer and therefore charge recombination may become slow enough to allow the desired interfacial electron transfer (IFET) between the solid and adsorbed or dissolved substrates. The subsequent reaction steps are described by Eqs. (5)–(7).

$$SC \xrightarrow{h\nu} SC\left(e_r^-, h_r^+\right) \tag{8}$$

$$SC\left(e_r^-, h_r^+\right) \rightarrow SC + h\nu/\text{heat} \tag{9}$$

$$SC\left(e_r^-, h_r^+\right) + A + D \rightarrow SC + A^{-\cdot} + D^{+\cdot} \tag{10}$$

Scheme 1 summarizes the primary processes occurring after light absorption by a titania crystal. Due to the band gap of about 3.2 eV, ultraviolet light of wavelength shorter than 391 nm is

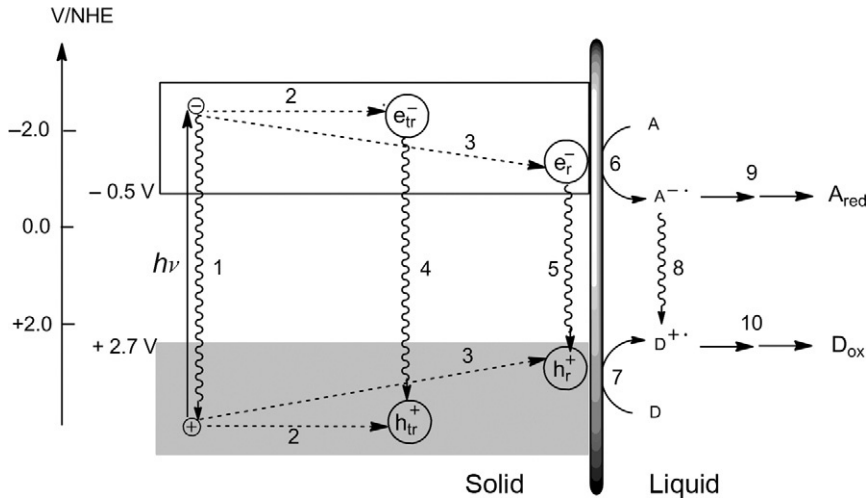

SCHEME 1. Schematic description of primary processes occurring during a semiconductor photocatalyzed redox reaction. The thick vertical bar symbolizes the solid/liquid interface. For the sake of simplicity emissive and photocorrosive processes are omitted. (1) Light absorption and primary charge recombination; (2) charge trapping at unreactive or (3) reactive surface sites; (4, 5) secondary charge recombination; (6, 7) IFET processes; (8) back electron transfer; (9, 10) secondary reactions.

necessary for excitation. The positions of the upper valence band and lower conduction band edge are given as electrochemical potentials and apply for the anatase modification in contact with water of pH 7. Surface defects and an inhomogeneous electric field of a thin surface layer induce trapping of the light-generated charges at the surface forming redox centers of different chemical reactivity.

Centers which undergo primarily recombination are termed in the scheme as *trapped* electron–hole pairs (e_{tr}^-, h_{tr}^+) whereas those involved in the IFET are named *reactive* electron–hole pairs (e_r^-, h_r^+). Only in a very few cases the existence of both types of redox centers is experimentally proven (*3*). In general, only one type of electron–hole pairs is considered. In competition with the primary processes depicted in Scheme 1, the photogenerated charges may exchange electrons also with the semiconductor itself resulting in a deactivation of the photocatalyst. Depending on the detailed reaction conditions like presence or absence of oxygen, this photocorrosion termed process affords, for example, in the case of the n-semiconductor zinc sulfide elemental zinc and sulfur and zinc sulfate.

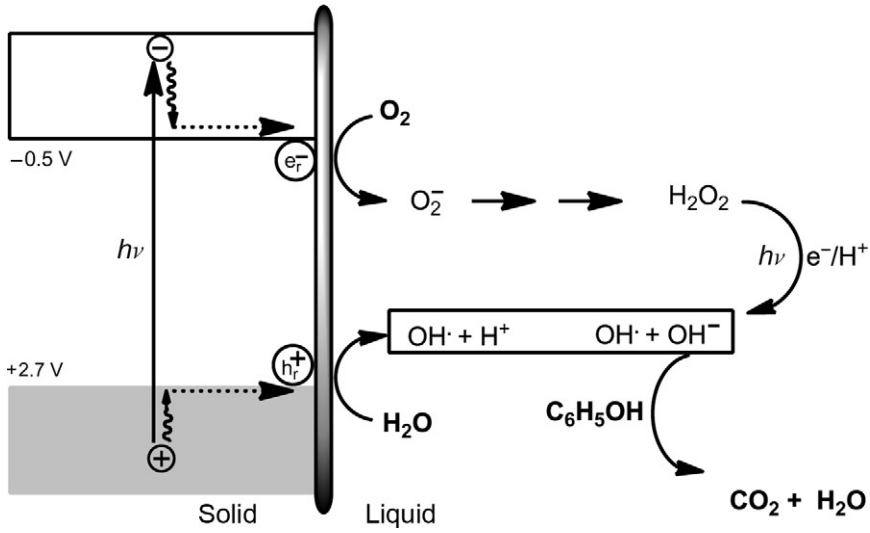

SCHEME 2. Simplified mechanistic scheme of the titania photocatalyzed mineralization of phenol.

Once formed, the primary redox products are converted in subsequent thermal reactions steps to the final compounds A_{red} and D_{ox}. When oxygen is the electron acceptor and a pollutant like phenol is the electron donor, carbon dioxide and water are the final redox products (Scheme 2). The primary reductive redox product is superoxide which can be converted to the strongly oxidizing OH radical via protonation, disproportionation of HO_2 and reductive photocleavage of the produced H_2O_2. Instead of water oxidation, the oxidative primary step may consist of the oxidation of the pollutant producing a phenoxy radical and a proton. Such complete photooxidation reactions are often termed as *mineralization* and in general titania is employed as the photocatalyst (*4–7*).

Thermodynamics requires that the redox potentials of acceptors and donors (D and A) are located within the potential range given by the reactive electron–hole pair. Since the latter in general is not known, the positions of the band edges may be taken as approximate values. It is noted that this is reliable only in the absence of any crystal defects prone of charge trapping, a rather rare case in experimental photocatalysis. Thus, the reduction and oxidation potentials of these surface centers in general may be a few hundred of millivolts smaller than estimated by this approach. A more detailed discussion is given by Gerischer for an n-type semiconductor (Scheme 3) (*8*). Absorption of light

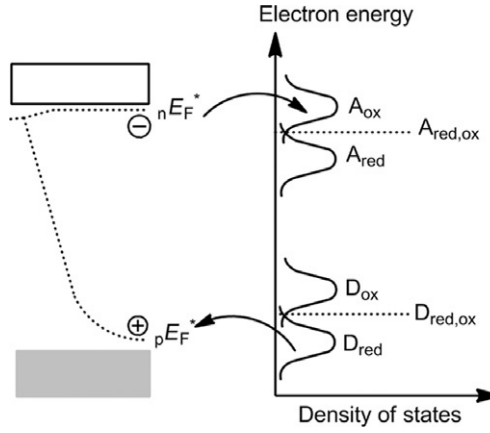

SCHEME 3. Thermodynamics of interfacial electron transfer (IFET) between a photoexcited n-type semiconductor solid and dissolved donor and acceptor molecules. The depicted density of states maxima apply for equal concentrations of reduced and oxidized forms.

induces a splitting of the Fermi level into quasi-Fermi levels of electrons and holes indicated as $_nE_F^*$ and $_pE_F^*$, respectively. Since redox reactions are connected with reorganization energies (χ), the density of states has a maximum not at the standard potential ($D_{red,ox}$ and $A_{red,ox}$) but at an energy higher (D_{ox} and A_{ox}) and lower (D_{red} and A_{red}) by the amount of χ. As a consequence, both reductive and oxidative IFET reactions are thermodynamically feasible only when the energies of A_{ox} and D_{red} are equal or below and above the quasi-Fermi level of electrons and holes, respectively. Whereas standard potentials are usually easy obtainable, this is not true for reorganization energies which may reach values of up to 0.5 eV. Thus, a large uncertainty is connected with a precise calculation of the free energy change of such type of interfacial electron exchange reactions. These basic aspects are often overlooked when discussing the energetic requirements for water splitting. Instead of taking the ideal value of 1.23 eV, a value of about 2 eV seems more realistic.

To estimate the thermodynamic feasibility of interfacial redox reactions at a hitherto unknown semiconductor surface, it is therefore of basic importance to know the position of the quasi-Fermi level. The quasi-Fermi level of electrons of powders or thin films of modified titania photocatalysts can be easily obtained by the "suspension method" developed by Bard *et al.* (*9,10*) and modified by Roy *et al.* (*11*) for titania and cadmium sulfide. It is based on the pH-dependence of the flat-band potential of TiO_2.

Since the procedure requires irradiation, different to the classical Mott–Schottky method, it is more correct to replace E_{fb} by the quasi-Fermi energy of electrons ($_nE_f$*). Bard *et al.* (*9*) measured the photocurrent generated in the presence of methylviologen (MV^{2+}) and a reducing agent as function of the pH value, whereas Roy recorded the photovoltage in the absence of a reducing agent. In the latter method, the shape of the sigmoidal voltage/pH curve depends on the potential of the reference electrode, the $[MV^{2+}]/[MV^{+\bullet}]$ ratio, the pH value, k, and on $_nE_f$*. At the pH value of the inflection point (pH_o), the quasi-Fermi level is equal to the one electron reduction potential of the methylviologen cation. From this the quasi-Fermi potential of electrons at any pH can be calculated according to Eq. (11) (*11*) if the factor k is known. For titania, k is usually equal to 59 mV (*12*). Roy *et al.* obtained it from

$$_nE_f^*(\mathrm{pH}) = E^\circ_{MV^{2+/+\bullet}} + k(\mathrm{pH}_o - \mathrm{pH}) \qquad (11)$$

the slope of the voltage/current plot above the inflection point whereas Bard *et al.* calculated it from the slope of the onset of photocurrent versus pH (*10*). However, in our hands, both methods afforded only poorly reproducible results due to considerable voltage fluctuations and too low photocurrents. We have determined the k value by an alternative method through measuring the pH_0 value not only for one but also for a serious of redox couples (*13*).

With the knowledge of the quasi-Fermi level of electrons, the level of holes can be estimated by adding the band-gap energy as obtained from diffuse reflectance spectra. This rough but helpful procedure is based on the assumption that both Fermi levels are located very close to the corresponding band edges. Since most of the employed powders represent highly doped semiconductors, this seems a reliable approximation.

Unfortunately, titania can utilize only the very small UV part (about 3%) of solar light and therefore practical applications like cleaning of air require the use of UV lamps. However, also the much larger visible part ($\lambda > 400$ nm) may induce photocatalysis when titania is surface modified by dyes and transition or main group elements. Whereas dye sensitization can be an efficient method in photoelectrochemical devices operating in the absence of oxygen, it is not suited for photocatalytic aerial oxidation reactions since the photogenerated reactive oxygen compounds in general attack not only the substrate but also the dye. Accordingly, we thought that modification by oxidation-stable high-valent transition metal complexes may be a promising method.

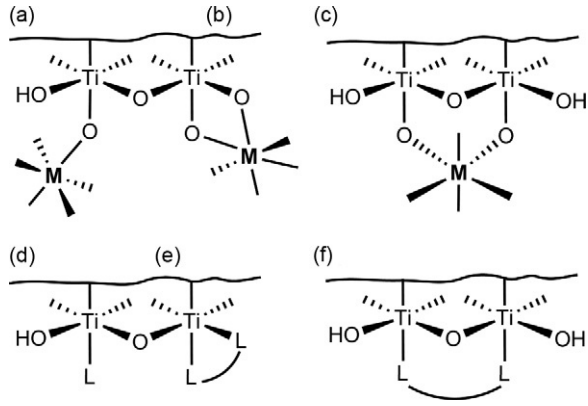

FIG. 1. The dual role of the titania surface in coordination chemistry.

In the following, we discuss our results on the characterization and photocatalytic properties of titania–halogenometal complexes of Pt(IV) and Rh(III). Considering that the surface of titania contains about 3–6 OH groups per nm^2 *and* under-coordinated titanium atoms it may act both as a mono- and bidentate ligand (Fig. **1**a–c) and as a coordination centre (Fig. **1**d–f). Research on the latter topic was recently summarized (*14*).

II. Titania–Chloroplatinum(IV) Complexes

In the very first investigations, we have found that simple metal chloride complexes like $Na_2[PtCl_6]$, $AuCl_3$, and $RhCl_3$ introduced into the bulk of amorphous microporous titania (*15–17*) by sol-gel methods induce a photomineralization of the water pollutant 4-chlorophenol (4-CP) by visible light. Surprisingly, in the platinum doped material isolated $PtCl_4$ units are present in an amorphous titania matrix exhibiting no bonding interactions with the lattice components. Thus, the visible light absorption is located at the $PtCl_4$ units. It is noted that a physical mixture of $PtCl_4$ and silica does not afford a visible light active photocatalyst. Recalling that photocatalysis is a surface phenomenon we replaced the sol-gel method by a simple surface modification procedure in order to introduce chemical bonding between titania and the metal halide complex. The aim of this work was to investigate how the photoredox properties of titania are changed by the covalent attachment to chloroplatinate or chlororhodate and how the primary photoprocesses of charge

separation and IFET can be described. Detailed information is available from recent original publications (*13,18–20*).

A. Preparation and Characterization of Photocatalysts

Upon stirring a suspension of titania powders in an aqueous solution of $H_2[PtCl_6]$ in the dark, different maximum amounts were adsorbed. For the anatase hydrate and anatase/rutile samples *TH* (*Kronos*) and *P25* (*Degussa*), there were taken up 4.0% and 1.1%, respectively, whereas only traces were adsorbed onto the rutile material *Ald*. The almost four times larger amount adsorbed by *TH* corresponds with the about four times larger surface area as compared to *P25* (vide infra). Subsequent heat treatment at 200 °C afforded the desired photocatalyst (*21*). Surface modification may be performed also by simple grinding with $PtCl_4$, but the resulting powders are of lower photocatalytic activity and less stability (*18,20*).

Analysis by transmission electron microscopy (TEM) and X-ray powder diffraction (XRD) of 4.0%$H_2[PtCl_6]$/TH revealed the presence of about 200 nm large aggregates composed of 2–4 nm sized anatase crystallites (*22*). Specific surface areas of unmodified *P25* (50 m^2/g) and *Ald* (3 m^2/g) were not changed upon modification whereas a significant decrease from 334 to 260 m^2/g was found for *TH*.

To find out if the chlorplatinate is physically or chemically adsorbed onto the tiania surface, 4.0%$H_2[PtCl_6]$/TH was stirred in 0.01 M potassium fluoride at ambient conditions. It is known that fluoride irreversibly chemisorbs through replacement of titania bound OH groups (*23–27*). Surprisingly, no desorption of a chloroplatinate complex was observable under these experimental conditions. However, desorption became feasible upon decreasing the pH value. These observations strongly suggest that chloroplatinate is chemically bound to titania as summarized in Eq. 14) ($L = Cl^-$, OH^-) and that desorption is an acid catalyzed process. From

$$[TiO_2] - OH + PtCl_5L^{n-} \rightarrow [TiO_2] - O - PtCl_4L^{n-} + HCl \quad (12)$$

the amount of chloride released after stirring an NaOH suspension of 4.0%$H_2[PtCl_6]$/TH in the dark, the composition $[Ti]OPtCl_4L^{n-}$, $L = H_2O$, OH^-, $n = 1, 2$, was proposed for the titania surface complex. In corresponding photochemical desorption experiments ($\lambda \geq 455$ nm) with 4.0%$H_2[PtCl_6]$/TH suspended in

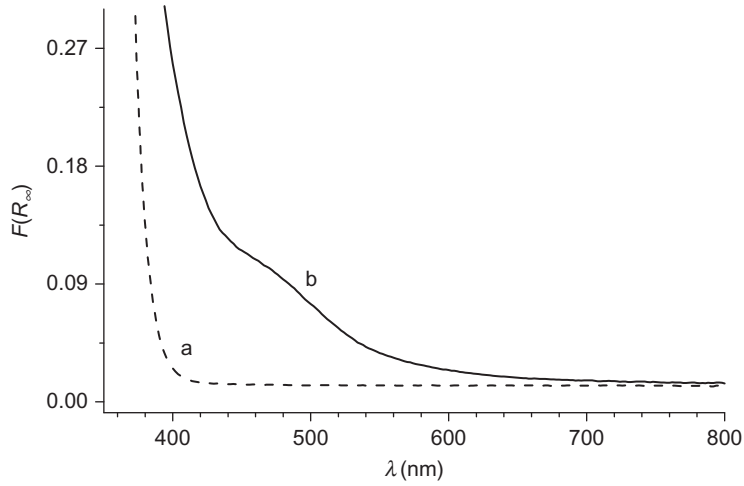

FIG. 2. Diffuse reflectance spectra of *TH* (a) and 4.0%$H_2[PtCl_6]$/TH (b). The Kubelka–Munk function, $F(R_\infty)$, is equivalent to absorbance.

water no desorption occurred within 24 h of irradiation time, whereas in the presence of 0.1 M HCl desorption of $[PtCl_6]^{2-}$ was almost complete.

The diffuse reflectance spectra of *TH* and 4.0%$H_2[PtCl_6]$/TH are compared in Fig. 2. The pronounced absorption of the modified material in the visible region is tentatively assigned to a metal-centered transition of the platinum(IV) chloride component, by analogy with the solution spectrum of $Na_2[PtCl_6]$ (*18,28,29*). Below 400 nm the steep absorption increase of the modified sample originates from the band-gap transition of TiO_2. For an indirect crystalline semiconductor, the band-gap energy is obtained by extrapolation of the linear part of the plot of $(F(R_\infty)h\nu)^{1/2}$ versus $h\nu$ (*30*). In the case of 4.0%$H_2[PtCl_6]$/TH, it amounts to 3.21 eV, what is slightly smaller than the value of unmodified *TH* (3.27 eV). The absorption of these materials extends down to 620–650 nm corresponding to about 2.0 eV.

To locate the approximate redox potentials of the reactive electron–hole pair, the quasi-Fermi levels of the powders were measured as summarized above. The plots of photovoltage versus pH for *TH* and a series of $H_2[PtCl_6]$/TH materials are summarized in Fig. 3. From the inflection point (pH_o), the corresponding quasi-Fermi potentials at pH 7, as obtained via Eq. (11) taking $k = 0.059$ V, are -0.58 V (P25) and -0.54 V (TH). The flat-band potential of a single crystal of anatase was reported to be -0.59 V (pH 7) (*31*). Relative to the value of *TH* the quasi-Fermi level is shifted anodically by 0.05, 0.09, and

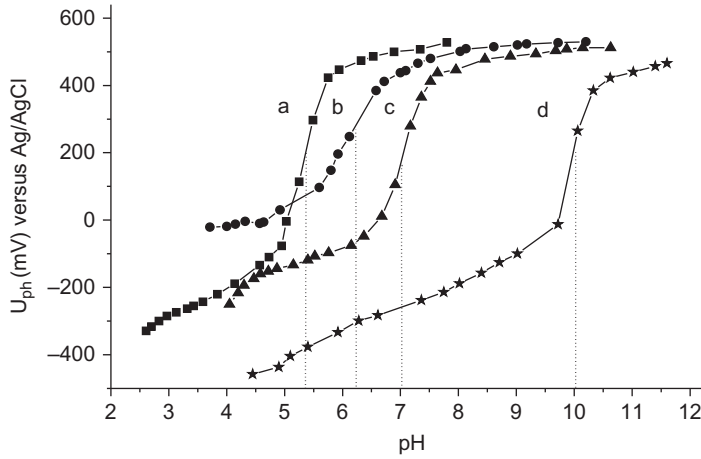

FIG. 3. Photovoltage recorded for *TH* (a), 1.0% (b), 2.0% (c), and 4.0% $H_2[PtCl_6]$/TH (d) suspensions in 0.1 M KNO_3 in the presence of $(MV)Cl_2$ irradiated with the full light of an XBO-lamp. The position of the inflection point pH_0 is marked with a dotted line.

0.26 V in the case of 1%, 2%, and 4.0%$H_2[PtCl_6]$/TH, respectively. The reproducibility of quasi-Fermi potential and photocatalytic activity measurements was in the range of ± 0.02 V and $\pm 10\%$, respectively. Since the onset of the TiO_2 part in the 4.0% $H_2[PtCl_6]$/TH reflectance spectrum remains nearly unchanged, the band gap is not altered and the anodic shift of the conduction band edge is therefore accompanied by an anodic shift of the valence band edge.

B. PHOTOCATALYTIC DEGRADATION WITH ARTIFICIAL VISIBLE LIGHT ($\lambda \geq 455$ nm)

Figure 4 illustrates the photodegradation of 4-CP (*32*) with visible light. Since reaction rates increased with increasing photocatalyst concentration, reaching a constant value at 0.5 g/L, all experiments were conducted at this value (*33*). Whereas the rutile based $H_2[PtCl_6]$/Ald was inactive (Fig. 4, curve a), in accord with the very small surface area and the trace amounts of chemisorbed chloroplatinate, 1.1.%$H_2[PtCl_6]$/P25 and 4.0% $H_2[PtCl_6]$/TH were active, inducing 50% degradation after 95 and 15 min, respectively (Fig. 4, curves b, c). 4.0%$H_2[PtCl_6]$/TH also initiated a fast mineralization as indicated by curve d in Fig. 4.

Since the mineralization process produces CO_2, H_2O, and HCl, the initial pH value of 3.4 decreased to 3.0 at 120 min

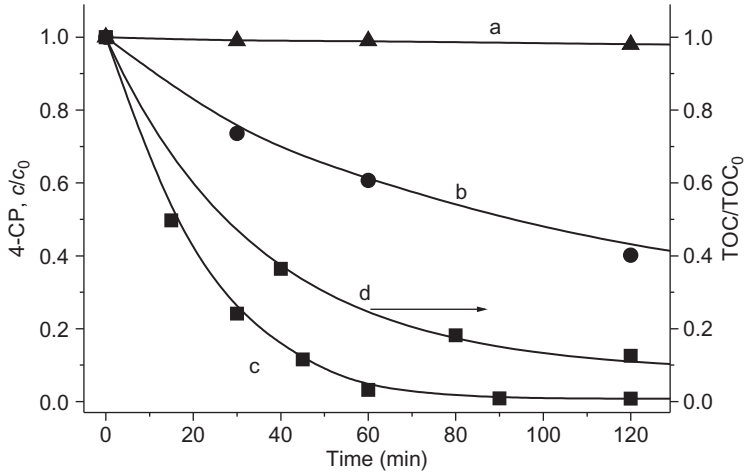

FIG. 4. 4-CP degradation upon visible light irradiation; $H_2[PtCl_6]$/Ald (a), 1.1%$H_2[PtCl_6]$/P25 (b), 4.0%$H_2[PtCl_6]$/TH (c), 4-CP mineralization as catalyzed by 4.0%$H_2[PtCl_6]$/TH (d) (19).

irradiation time. These conditions should favor photodesorption (vide supra) and therefore a long-term irradiation was conducted in the presence of $NaHCO_3$ to neutralize the acid generated. In this experiment, the concentration of 4-CP was readjusted to its original value when the c/c_0 values approached zero. Whereas in the absence of bicarbonate the activity decreased to 50% of its original value already at the third cycle, it changed only little even after 19 cycles when bicarbonate was present. This clearly proofs the catalytic nature of the photodegradation reaction.

Also other pollutants like atrazine, dichloroacetic acid, lindane, and trichloroethylene were almost completely mineralized ($\lambda \geq 455$ nm). The degradation of atrazine in general affords cyanuric acid as the final product when unmodified titania were employed as photocatalysts (*34*). However, when 4.0%$H_2[PtCl_6]$/TH was used, even cyanuric acid was mineralized as indicated by TOC and nitrate determinations.

C. Photodegradation with Natural Indoor and Outdoor Daylight

The excellent photocatalytic activity of 4.0%$H_2[PtCl_6]$/TH became even more evident, when the reaction was conducted in diffuse indoor laboratory daylight (4–10 Wm^{-2} at 400–1200 nm). Under these conditions both unmodified *P25* and *TH* were inactive

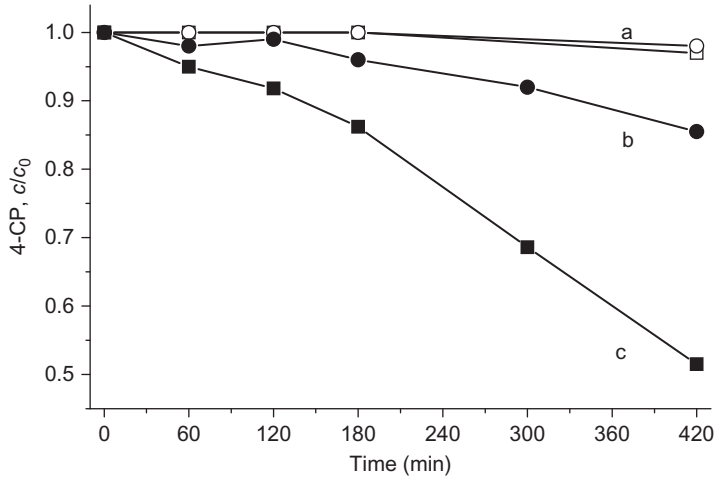

FIG. 5. Diffuse indoor daylight induced degradation of 4-CP in the presence of *TH* and *P25* (a), 1.1%$H_2[PtCl_6]$/P25 (b), 4.0%$H_2[PtCl_6]$/TH (c).

whereas the 1.1% and 4.0% surface modified counterparts after 420 min exhibited 10% and 50% degradation, respectively (Fig. 5).

The superior activity of modified titania was demonstrated also when the degradation of 4-CP was conducted with outdoor sunlight. Surprisingly, 2.0%$H_2[PtCl_6]$/TH was more active than *P25*. This higher reactivity was even more pronounced when the solar irradiation was replaced by artificial UV light. 2.0% $H_2[PtCl_6]$/TH induced 90% degradation already after 12 min, the time by which only 50% were degraded by *P25*. In the case of 4.0%$H_2[PtCl_6]$/TH only traces of unreacted 4-CP could be detected after this irradiation time.

D. MECHANISM

Since the chloroplatinate component is the light absorbing species, we proposed the primary photoprocess to be a homolytic PtCl cleavage affording a Pt^{III} intermediate and an adsorbed chlorine atom, by analogy with the known photochemistry of hexachloroplatinate in solution (*29,35*). Electron injection from the platinum(III) complex into the titania conduction band reforms Pt^{IV}. Thus, the reductive and oxidative centers become spatially separated rendering charge recombination less probable. The trapped conduction band electron reduces oxygen to superoxide and finally hydroxyl radicals as evidenced by

scavenging experiments with benzoic acid and tetranitromethane, an alternative electron acceptor. The adsorbed chlorine atom is assumed to oxidize 4-CP under deprotonation to the corresponding oxyl radical which is eventually converted to CO_2 and HCl, by analogy with the photomineralization catalyzed by unmodified titania upon UV-excitation (*36,37*). It is noted that the alternative mechanism, that is, electron injection from the excited chloroplatinate resulting in a platinum(V) intermediate cannot be completely ruled out.

As summarized above, the primary photoprocess generates two surface redox centers. The oxidative one can be described as a kind of Cl/Cl^- redox pair weakly coordinated to a metal center. It is reasonable to assume that this oxidant is weaker than the free Cl/Cl^- pair ($E^\circ_{Cl/Cl^-} = 2.6$ V, value for aqueous solution (*38*), but stronger than the couple $\frac{1}{2}Cl_2/Cl^-$ ($E^\circ = 1.3$ V (*39*) and the oxidation potential of 4-CP (1.18 V). Further, the potential has to be lower than 2.4 V, the estimated redox potential of the OH/OH^- couple, because no hydroxyl radical formation could be observed in the presence of benzoic acid and tetranitromethane as OH and electron acceptor, respectively (*18*). Thus, the potential of the oxidative center should be in the range of 1.3–2.4 V.

Unfortunately, the redox potential of the $Pt^{4+/3+}$ couple is not known in the literature. Although some stable Pt^{III} compounds have been isolated and characterized (*40*), the oxidation state III is reached usually only in unstable intermediates of photoaquation reactions (*41–43*) and on titania surfaces as detected by time resolved diffuse reflectance spectroscopy (*44*). The redox potential of the surface $Pt^{4+/3+}$ couple should be equal or more negative than -0.28 V, that is, the quasi-Fermi potential of $4.0\%H_2[PtCl_6]/TH$ at pH 7. Assuming a value of -0.40 V and recalling that the potential difference between the reactive charges cannot be higher than the absorbed light energy divided by the elemental charge, which is about 2.00 V upon excitation at the absorption onset (620–650 nm), the potential of $E_{Pt\text{-}(Cl/Cl^-)}$ is obtained as 1.6 V (Scheme 4). These chlorine based surface centers are absent in unmodified titania and very likely enable the degradation of otherwise reluctant cyanuric acid (vide supra).

III. Titania–Halogenorhodium(III) Complexes (X = Cl, Br)

To find out whether or not sensitization of titania as described above is feasible also with halides of other d^6 metals, surface modification was also attempted with RhX_3 (X = Cl, Br) (*45*). The novel hybrid photocatalysts $x\%RhCl_3/TH$ containing 0.5,

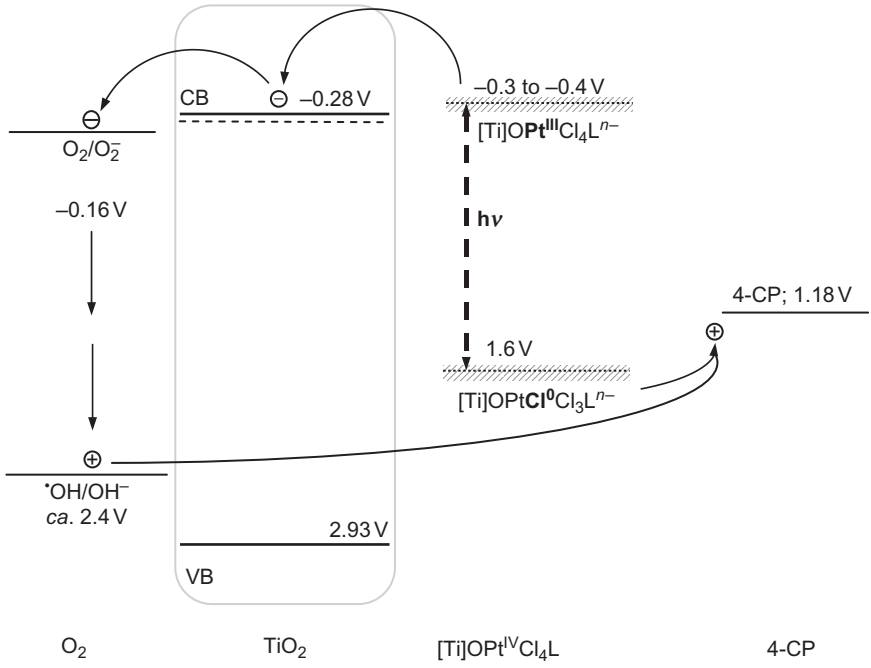

SCHEME 4. Potential diagram for 4.0%$H_2[PtCl_6]$/TH at pH 7. All potentials are given versus NHE.

1.0, 2.0, and 5.0 wt% of rhodium and 2%$RhBr_3$/TH were prepared as described above for the chloroplatinate complexes. Again the titania hydrate *TH* afforded photocatalysts which were very active in the photodegradation of 4-CP, whereas *Hombikat* 100 (Sachtleben) and *P25* based materials were less efficient. Maximum loading was observed at 5.0 wt% of rhodium whereas the use of higher metal halide concentrations afforded powders from which excess rhodium is completely removed during washing.

A. CHARACTERIZATION

$RhCl_3$/TH and $RhBr_3$/TH have a pink and a dark yellow color, respectively, and are surprisingly stable to desorption of the rhodium component as compared to chloroplatinate modified *TH* (*13,19,20*). In aqueous suspension upon stirring either in the dark or under irradiation with visible light, no dissolved rhodium complex was detectable by UV–Vis absorption spectroscopy.

Both 4.0%$RhCl_3$/TH and 4.0%$RhBr_3$/TH did not undergo desorption of the rhodium surface complex even after stirring for five days in the dark in 0.5 M KF. Thus, one can conclude that Rh (III) is covalently bound to titania through a bridging oxygen ligand (*45*). Whereas 4.0%H_2PtCl_6/TH in 0.1 M HCl upon UV irradiation (*19*) for 24 h suffered almost complete desorption to $[PtCl_6]^{2-}$, only 40% of $[RhCl_6]^{3-}$ were detectable in the case of 4.0%$RhCl_3$/TH.

This difference may reflect the fact that the metal–oxygen bond is about 40 kJ mol^{-1} stronger in the case of rhodium (*46*). In strongly alkaline suspension the chloride ligands are completely displaced, as also observed for 4.0%H_2PtCl_6/TH (*19*). Since from the amount of chloride produced in this experiment, one can conclude that three chloride ligands are present in the surface rhodium complex, a composition of $[TiO_2]ORhCl_3(H_2O)_2^-$ is suggested.

Comparison of the diffuse reflectance spectra of TH and 2.0% Rh(III)/TH clearly indicates novel absorptions at 400–500 and 500–700 nm (Fig. 6). The shoulder at about 500 nm compares well with the lowest metal-centered transition of $[RhCl_6]^{3-}$ observed in hydrochloric acid at 518 nm (*47*). At wavelengths shorter than about 550 nm a strong absorption increase suggests that it does not originate exclusively from the second metal-centered transition occurring in $[RhCl_6]^{3-}$ at 410 nm with about the

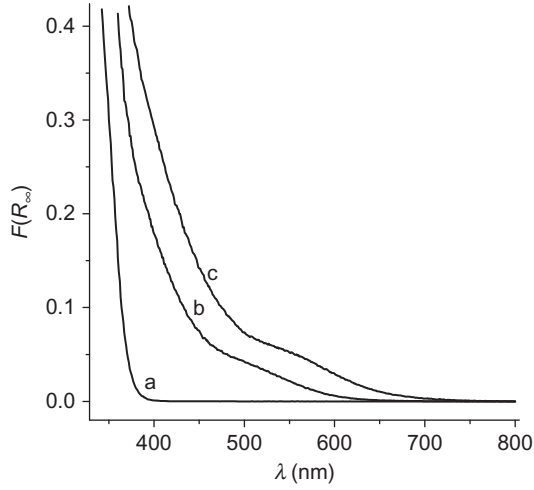

FIG. 6. Diffuse reflectance spectra of *TH* (a), 2.0%$RhCl_3$/TH (b), and 2.0%$RhBr_3$/TH (c). The Kubelka–Munk function, $F(R_\infty)$, is equivalent to absorbance.

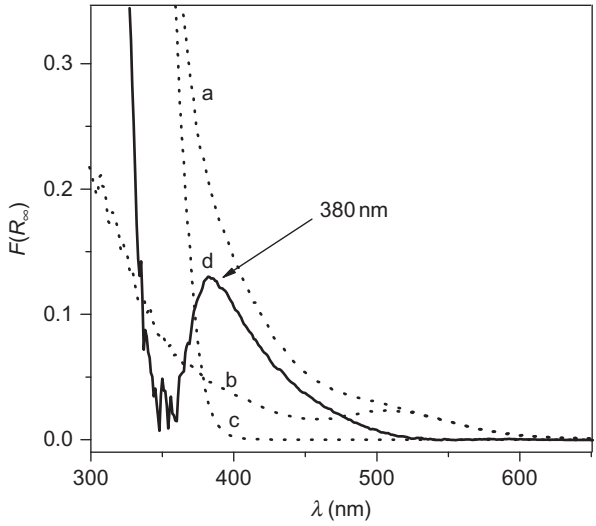

FIG. 7. Diffuse reflectance spectra of 2.0%$RhCl_3$/TH (a), 2.0%$RhCl_3$/SiO_2 (b), TH (c). Spectrum $d = a - (b + c)$.

same intensity as the 510 nm band. It rather may originate from a rhodium-to-titanium charge-transfer transition. This is corroborated by the fact that the silica analogue 2.0%$RhCl_3$/SiO_2 does not exhibit a strong absorption increase at $\lambda \leq 550$ nm, most likely because, different from titania, silica does not have a low lying conduction band (Fig. 7, curve b). In the corresponding difference spectrum an unsymmetrical absorption band is observed at a maximum at about 380 nm. In the case of 2.0% $RhBr_3$/TH a similar comparison with 2.0%$RhBr_3$/SiO_2 afforded the MMCT maximum at about 390 nm *(48)*.

Assuming that all samples are indirect crystalline semiconductors, as is anatase, the band-gap energy can be obtained by extrapolation of the linear part of a plot of $[F(R_\infty)\ h\nu]^{1/2}$ versus the energy of exciting light *(30)*. From this the band gap of TH, 0.5, 1.0, 2.0, and 5.0%$RhCl_3$/TH and of 2.0%$RhBr_3$/TH, can be calculated as 3.29, 3.26, 3.25, 3.22, 3.21, and 3.10 eV, respectively (Table I).

B. PHOTOCATALYTIC ACTIVITY

To investigate the photocatalytic activity, the disappearance and mineralization of 4-CP was performed in the presence of air. Surprisingly, the activity of 5.0%$RhCl_3$/TH was very high

TABLE I

BANDGAP ENERGIES AND QUASI-FERMI POTENTIALS OF ELECTRONS

Photocatalyst	E_{bg} (eV)[a]	${}_nE_F{}^*$(pH 7, NHE) (V)[b]
TH	3.29	−0.54
0.5% $RhCl_3$/TH	3.26	−0.53
1.0% $RhCl_3$/TH	3.25	−0.48
2.0% $RhCl_3$/TH	3.22	−0.46
5.0% $RhCl_3$/TH	3.21	−0.34
2.0% $RhBr_3$/TH	3.10	−0.32

[a,b]Reproducibility was better than ±0.05 and ±0.02 V, respectively.

and after 60 min of visible light irradiation ($\lambda \geq 455$ nm) 95% of 4-CP had disappeared whereas 75% of 4-CP mineralized. 2.0% $RhBr_3$/TH exhibited a photoactivity comparable to that of 2.0% $RhCl_3$/TH. The unmodified powders *TH* and *P25* were inactive under these experimental conditions. The photocatalytic activity increases with increasing rhodium loading, exhibiting the highest value for 5.0%$RhCl_3$/TH (Fig. 8). This resembles the findings on the surface-loading of *TH* with $[PtCl_6]^{2-}$ (*13,19,20*).

Photoelectrochemical measurements of the photovoltage as function of pH value (*11*) indicate that the quasi-Fermi level of electrons is shifted gradually more anodic upon increasing the rhodium loading. Thus, the value of −0.55 V (vs. NHE, at pH 7) as observed for unloaded TH is shifted to −0.53, −0.48, −0.46, and −0.34 V upon loading with 0.5, 1.0, 2.0, and 5.0% $RhCl_3$/TH, respectively (Table I). In the case of 2.0%$RhBr_3$/TH, the quasi-Fermi level was found at −0.32 V.

To obtain experimental evidence for a mutual formation of OH radicals under visible light irradiation ($\lambda \geq 400$ nm), the photodegradation of benzoic acid in the presence of 4.0%$RhCl_3$/TH and oxygen was investigated by monitoring the production of salicylic acid (*18,49,50*). Surprisingly, no salicylic acid was detectable in solution. A likely reason for this could be a fast photodegradation of small amounts of initially produced salicylic acid. To test this hypothesis, photodegradation of salicylic acid was carried out under identical experimental conditions. It turned out that salicylic acid is efficiently adsorbed onto 4.0% $RhCl_3$/TH and that its photodegradation is very fast. About 96% of salicylic acid had disappeared after 10 min of irradiation. These results suggest that salicylic acid formed from benzoic acid largely remains adsorbed and is efficiently decomposed before being desorbed into solution.

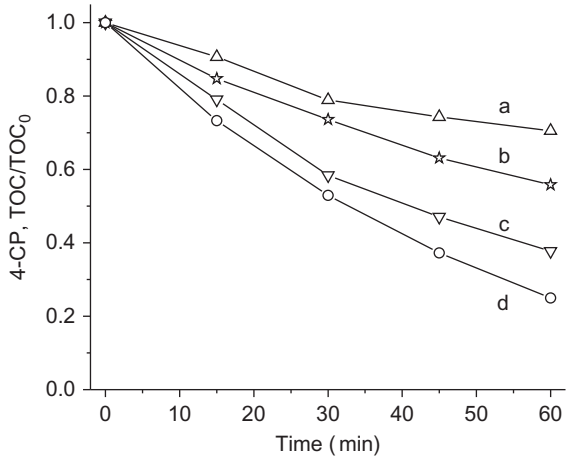

FIG. 8. Mineralization of 4-CP as function of rhodium content; photocatalyst concentration: 0.5 gL^{-1}; (a) 0.5%$RhCl_3$/TH, (b) 1.0% $RhCl_3$/TH, (c) 2.0%$RhCl_3$/TH, (d) 5.0%$RhCl_3$/TH.

C. MECHANISM

To test if the photocatalytic activity of $RhCl_3$/TH is also initiated by a homolytic MCl bond cleavage, as proposed previously for platinum(IV) chloride modified TH, the photodegradation of phenol under visible light irradiation ($\lambda \geq 455$ nm) was carried out. Formation of chlorophenol would evidence the presence of intermediate chlorine atoms. However, no significant amount of chlorophenol was detectable (*51*). This differs from Pt(IV)/TH, in which case chlorophenol formation was observable (*18*). Further, cyanuric acid, a molecule which is mineralized in the presence of platinum (IV) modified TH (*20*) (vide supra), is not decomposed by 4.0% $RhCl_3$/TH. These significant differences indicate that in the case of rhodium(III) modification visible light-induced cleavage of the metal–halogen bond is not a major primary photoprocess. More likely seems a mechanism as proposed for UV light-induced oxidation reactions in the presence of Rh(III) doped titania colloids (*52*).

$$[TiO_2]O - Rh^{3+} + h\nu \rightarrow [TiO_2]O - Rh^{4+} + e^-_{CB} \quad (13)$$

$$[TiO_2]O - Rh^{4+} + 4{-}CP \rightarrow [TiO_2]O - Rh^{3+} + 4{-}CP^{+\bullet} \quad (14)$$

$$O_2 + e^-_{CB} \rightarrow O_2{}^{-\bullet} \quad (15)$$

$$O_2{}^{-\bullet} + H^+ \rightarrow HO_2{}^{\bullet} \quad (16)$$

$$HO_2^{\bullet} + HO_2^{\bullet} \rightarrow H_2O_2 + O_2 \quad (17)$$

$$H_2O_2 + O_2^{-\bullet} \rightarrow OH^{\bullet} + OH^{-} + O_2 \quad (18)$$

$$H_2O_2 + e_{CB}^{-} \rightarrow OH^{\bullet} + OH^{-} \quad (19)$$

Visible light excitation within the rhodium-to-titanium charge-transfer band of $RhCl_3$/TH affords as primary products an electron in the titania conduction band and a Rh(IV) center (Eq. 13). The energetic position of the latter can be estimated by adding the energy of the Vis absorption onset (2.25 eV) to the quasi-Fermi level as depicted in Scheme 5. Approximate the same position has been assigned to the Rh(III/IV) level in Rh(III) doped $BaTiO_3$ (*53*). The resulting potential of 1.91 V is positive enough to oxidize water or more likely 4-chlorophenol to the radical cation (Eq. 14), which finally breaks down to CO_2, HCl, and H_2O, as well known from the UV photodegradation in the presence of unmodified TiO_2 (*54–56*). The electron generated in the conduction band reduces oxygen to superoxide (Eq. 15) which through the reaction sequence according to Eqs. (16)–(19)

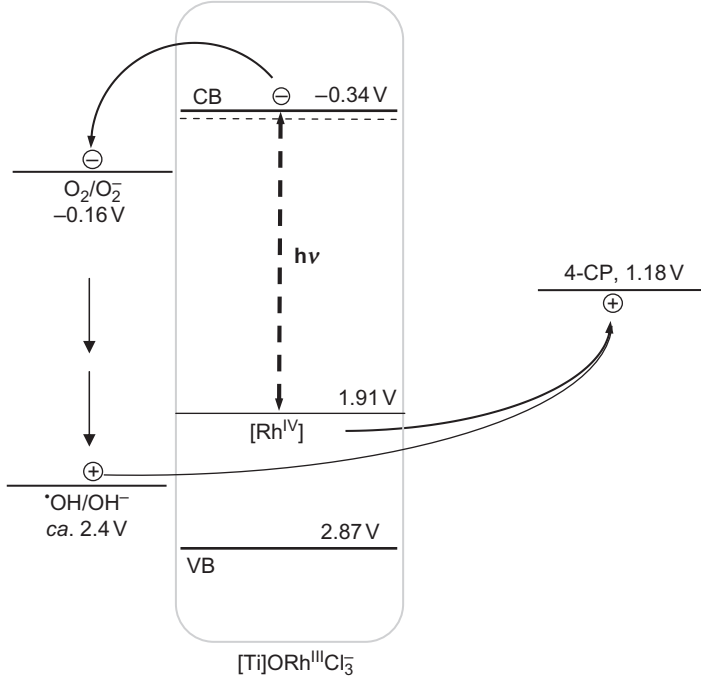

SCHEME 5. Mechanistic scheme of titania sensitization by rhodium (III) complexes. Depicted values apply for 5.0%$RhCl_3$/TH at pH 7.

(*57–59*) is converted to an OH radical. The latter subsequently induces oxidation of 4-CP.

Recently, it was reported that also the halogenides of Ru(III), Ir(IV), and Au(III) are able to form visible light active titania photocatalysts (*60*).

IV. Summary and Outlook

Modification of titania powders by halogenometal compounds affords surface transition metal complexes that are efficient semiconductor photocatalysts for the visible light mineralization of organic pollutants. In these hybrid materials, titania can be considered as a semiconducting "inorganic ligand" bound via oxygen to a platinum(IV) or rhodium(III) center. Different to a conventional ligand titania has a peculiar electronic structure and provides also a solid surface for the adsorption of substrates. The quasi-Fermi level of electrons in the titania ligand is shifted anodically by 0.2–0.3 V as compared to the free "ligand." In the case of the platinum complex visible light irradiation results in a platinum centered excitation followed by homolytic PtCl bond cleavage and electron injection of Pt(III) into the titania conduction band. Thus, the reducing and oxidizing surface sites can be described as a trapped electron, that is, a Ti(III) center, and a loosely bound chlorine atom. In the case of the rhodium surface complex, the excitation is of the rhodium-to-titanium charge-transfer type resulting in a Ti(III) center and a Rh(IV) species.

The few investigations hitherto performed on the photochemical properties of transition metal complexes having titania as a ligand clearly proof the general importance of the field. Until now this applies only for the high photocatalytic activity in exhaustive photooxidation reactions. Since this is based on an efficient light-induced charge separation such type of supramolecular coordination complexes are promising systems also for other relevant processes like nitrogen fixation and artificial photosynthesis.

Acknowledgments

This work was supported by the Bavarian State Program BayFORREST and by Deutsche Forschungsgemeinschaft.

References

1. Lehn, J. M.; Sauvage, J. P. *Nouv. J. Chim.* **1977,** *1*, 449.
2. Serpone, N.; Pelizzetti, E. E. *"Photocatalysis. Fundamentals and Applications"* Wiley: New York, Chichester, Brisbane, Toronto, Singapore, **1989**.
3. Zeug, N.; Buecheler, J.; Kisch, H. *J. Am. Chem. Soc.* **1985,** *107*, 1459.
4. Fujishima, A.; Rao, T. N.; Tryk, D. A. *J. Photochem. Photobiol. C Photochem. Rev.* **2000,** *1*, 1.
5. Hoffmann, M. R.; Martin, S. T.; Choi, W.; Bahnemann, D. W. *Chem. Rev.* **1995,** *95*, 69.
6. Carp, O.; Huisman, C. L.; Reller, A. *Prog. Solid State Chem.* **2004,** *32*, 33.
7. Thompson, T. L.; Yates, J. T.Jr., *Top. Catal.* **2005,** *35*, 197.
8. Gerischer, H. *Electrochim. Acta* **1990,** *35*, 1677.
9. Ward, M. D.; White, J. R.; Bard, A. J. *J. Am. Chem. Soc.* **1983,** *105*, 27.
10. White, J. R.; Bard, A. J. *J. Phys. Chem.* **1947,** *1985*, 89.
11. Roy, A. M.; De, G. C.; Sasmal, N.; Bhattacharyya, S. S. *Int. J. Hydrogen Energy* **1995,** *20*, 627.
12. Bolts, J. M.; Wrighton, M. S. *J. Phys. Chem.* **1976,** *80*, 2641.
13. Kisch, H.; Burgeth, G.; Macyk, W. *Adv. Inorg. Chem.* **2004,** *56*, 241.
14. Macyk, W.; Szacilowski, K.; Stochel, G.; Buchalska, M.; Kuncewicz, J.; Labuz, P. *Coord. Chem. Rev.* **2010,** *254*, 2687.
15. Kisch, H.; Zang, L.; Lange, C.; Maier, W. F.; Antonius, C.; Meissner, D. *Angew. Chem. Int. Ed.* **1998,** *37*, 3034.
16. Zang, L.; Lange, C.; Abraham, I.; Storck, S.; Maier, W. F.; Kisch, H. *J. Phys. Chem. B* **1998,** *102*, 10765.
17. Zang, L.; Macyk, W.; Lange, C.; Maier, W. F.; Antonius, C.; Meissner, D.; Kisch, H. *Chem. Eur. J.* **2000,** *6*, 379.
18. Macyk, W.; Kisch, H. *Chem. Eur. J.* **1862,** *2001*, 7.
19. Burgeth, G.; Kisch, H. *Coord. Chem. Rev.* **2002,** *230*, 41.
20. Macyk, W.; Burgeth, G.; Kisch, H. *Photochem. Photobiol. Sci.* **2003,** *2*, 322.
21. For the case of simplicity, the modified TH powders are abbreviated as x% H_2PtCl_6 wherein x% describes the mass% of platinum employed in the preparation.
22. Burgeth, G.; Fernandez, A.; Kisch, H. unpublished results.
23. Boehm, H. P.; Herrmann, M. *Z. Anorg. Allg. Chem.* **1967,** *352*, 156.
24. Herrmann, M.; Boehm, H. P. *Z. Anorg. Allg. Chem.* **1969,** *368*, 73.
25. Flaig-Baumann, R.; Herrmann, M.; Boehm, H. P. *Z. Anorg. Allg. Chem.* **1970,** *372*, 296.
26. Herrmann, M.; Kaluza, U.; Boehm, H. P. *Z. Anorg. Allg. Chem.* **1970,** *372*, 296.
27. van Veen, J. A. R. *Z. Phys. Chem. Neue Folge* **1989,** *162*, 215.
28. Cox, L. E.; Peters, D. G. *Inorg. Chem.* **1927,** *1970*, 9.
29. Cox, L. E.; Peters, D. G.; Wehry, E. L. *J. Inorg. Nucl. Chem.* **1972,** *34*, 297.
30. Tauc, J.; Grigorovici, R.; Vanuc, A. *Phys. Stat. Sol.* **1966,** *15*, 627.
31. Kavan, L.; Graetzel, M.; Gilbert, S. E.; Klemenz, C.; Scheel, H. J. *J. Am. Chem. Soc.* **1996,** *118*, 6716.
32. All photodegradations discussed in this review were performed on a 2.5×10^{-4} M 4-CP solution. If not otherwise mentioned a cut-off filter of ($\lambda \geq$ 455 nm) was employed.
33. Rates are comparable only if this optimum catalyst concentration is selected and if the amount of light absorbed is the same for each

experiment. Thus, comparisons are justified only of results within one figure but not between different figures, except mentioned otherwise.
34. Tetzlaff, T. A.; Jenks, W. S. *Org. Lett.* **1999,** *1*, 463.
35. Davidson, C. M.; Jameson, R. F. *Trans. Faraday Soc.* **1965,** *61*, 2462.
36. Mills, A.; Davies, R. H.; Worsley, D. *Chem. Soc. Rev.* **1993,** *22*, 417.
37. Linsebigler, A. L.; Lu, G.; Yates, J. T.Jr., *Chem. Rev.* **1995,** *95*, 735.
38. Malone, S. D.; Endicott, J. F. *J. Phys. Chem.* **1972,** *76*, 2223.
39. Lide, D. R. In "*CRC Handbook of Chemistry and Physics*"; (76 edn.). CRC Handbook of chemistry and Physics. CRC Press: Boca Raton, New York, London, Tokyo, **1995**.
40. Usón, R.; Forniés, J.; Tomás, M.; Menjón, B.; Sünkel, K.; Bau, R. *J. Chem. Soc., Chem. Commun.* **1984,** 751.
41. Wright, R. C.; Laurence, G. S. *J. Chem. Soc. Chem. Commun.* **1972,** 132.
42. Rehorek, D.; Dubose, C. M.; Janzen, E. G. *Inorg. Chim. Acta* **1984,** *83*, L7.
43. Waltz, W. L.; Lilie, J.; Goursot, A.; Chermette, H. *Inorg. Chem.* **1989,** *28*, 2247.
44. Draper, R. B.; Fox, M. A. *Langmuir* **1990,** *6*, 1396.
45. Dai, Z. -M.; Burgeth, G.; Parrino, F.; Kisch, H. *J. Organomet. Chem.* **2009,** *694*, 1049.
46. Cundari, T. R.; Moody, E. W. *THEOCHEM* **1998,** *425*, 43.
47. Alimarin, I. P.; Shlenshaya, V. I.; Efremenko, O. A. *Russ. J. Inorg. Chem.* **1970,** *15*, 530.
48. We thank a referee for pointing out that instead of measuring a simple difference spectrum, a detailed factor analysis should have been performed. Although this may give more accurate values for the wavelength of the new absorption maximum, it would not alter the main conclusion that a novel absorption band is present in the hybrid photocatalysts.
49. Sakthivel, S.; Kisch, H. *Angew. Chem. Int. Ed.* **2003,** *42*, 4908.
50. Sakthivel, S.; Kisch, H. *Chemphyschem* **2003,** *4*, 487.
51. The sensitivity of HPLC instrument is about 1.0 μmol dm^{-3}.
52. Choi, W.; Termin, A.; Hoffmann, M. R. *J. Phys. Chem.* **1994,** *98*, 13669.
53. Schirmer, O. F.; Veber, C.; Meyer, M. *Phys. Solid State* **2002,** *44*, 1426.
54. For the mechanism of the further reactions steps see, e.g.
55. Cunningham, J.; Al-Sayyed, G. *J. Chem. Soc. Faraday Trans.* **1990,** *86*, 3935.
56. Theurich, J.; Lindner, M.; Bahnemann, D. W. *Langmuir* **1996,** *12*, 6368.
57. Carraway, E. R.; Hoffman, A. J.; Hoffmann, M. R. *Environ. Sci. Technol.* **1994,** *28*, 786.
58. Carraway, E. R.; Hoffman, A. J.; Hoffmann, M. R. *Environ. Sci. Technol.* **1994,** *28*, 776.
59. Kormann, C.; Bahnemann, D. W.; Hoffmann, M. R. *Environ. Sci. Technol.* **1988,** *22*, 798.
60. (a) Kominami, H.; Sumida, K.; Yamamoto, K.; Kondo, N.; Hashimoto, K.; Kera, Y. *Res. Chem. Intermed.* **2008,** *34*, 587. (b) Ishibai, Y.; Sato, J.; Akita, S.; Nishikawa, T.; Miyagishi, S. J. *J. Photochem. Photobiol. A: Chem.* **2007,** *188*, 106.

PHOTOCATALYSIS BY INORGANIC SOLID MATERIALS: REVISITING ITS DEFINITION, CONCEPTS, AND EXPERIMENTAL PROCEDURES

B. OHTANI

Catalysis Research Center, Hokkaido University, Sapporo, Japan

INORGANIC PHOTOCHEMISTRY
VOLUME 63 ISSN 0898-8838 / DOI: 10.1016/B978-0-12-385904-4.00001-9

Abstract

This review has been written in order to clarify fundamental aspects of photocatalysis, an important subject in inorganic and material chemistry, not to present a list of studies on photocatalysis reported so far, since it seems rather difficult to make a complete review by introducing all or a large part of the reported studies on photocatalysis of relatively long history. This review is based on the author's experience in studies on photocatalysis and topics are limited to so-called semiconductor photocatalysis; definition and examples of photocatalysis, its principle and kinetics, visible light-induced photocatalysis, and design of active photocatalysts are discussed in detail.

Keywords: Photocatalysis and catalysis; Photocatalytic activity; Band structure and excitation; Energy conversion; Langmuir-Hinshelwood mechanism; Electron–hole recombination; Quantum efficiency; Physical property–activity correlation; Synergetic effect.

I. Introduction

After the relatively long history of studies on photocatalysis, it seems unnecessary to explain the importance of photocatalysis in both fundamental and application aspects; for example, coatings of window glass and exterior walls with photocatalysts have already been commercialized worldwide due to its highly beneficial effect of "self-cleaning" which enables the surface to be kept clean under conditions of sunlight exposure and rain (*1*). Since results of many scientific studies on photocatalysis have been reported, it seems rather difficult, at least for the author, to make a complete review by introducing all or a large part of the reported studies on photocatalysis, while, of course, successful reviews (2,3) have been published by talented researchers in this field. This review has been written in order to clarify fundamental aspects of photocatalysis, not to present a list of studies on photocatalysis reported so far. Some of the aspects have not been discussed so far as "common sense" in papers relating to photocatalysis. This review is based on the author's experience in studies on photocatalysis for more than 25 years and topics are therefore limited to so-called semiconductor photocatalysis (Sections II.A and III.A), and consequently the author's results and interpretations are highlighted. It is the author's pleasure

to suggest reading also his recent review (*4*) on photocatalysis, which may be helpful for understanding the outline of studies on photocatalysis.

II. Photocatalysis

A. Definition

Although various definitions and interpretations of the term "photocatalysis" have been proposed, "photocatalysis" or "photocatalytic reaction" is defined, in this chapter, as a chemical reaction induced by photoabsorption of a solid material, or "photocatalyst," which remains chemically unchanged during and after the reaction. In other words, the solid acts catalytically, without any changes in its composition or structure, under photoirradiation, and this explanation may be consistent with most other definitions. "Photocatalysis" is the conceptual name for photocatalytic reactions. In this context, data can be obtained by measuring consumption of the starting materials and/or formation of reaction products initiated by photoirradiation and then examining whether the photocatalyst or its properties have been modified during the reaction. This seems to be a relatively easy procedure. However, various problems are, in fact, encountered when trying to prove a given phenomenon as being photocatalytic (Section V.C).

B. Photocatalysis and Catalysis

The most significant difference between photocatalysis and catalysis lies in their thermodynamics. In a general definition, a catalyst reduces activation energy of a given chemical reaction by changing the intermediate states and thereby accelerates the reaction which proceeds spontaneously with negative Gibbs-energy change, that is, catalysis is limited to thermodynamically possible reactions. On the other hand, it is well known that photocatalysis can drive energy-storing reactions, for example, splitting water into hydrogen and oxygen. In this sense, "photocatalysis" must be recognized as a concept completely different from that of "catalysis." Actually, apparent activation energy of photocatalysis estimated by an Arrhenius plot has been reported to be very small compared with that of catalytic reactions (*5*).

C. Photocatalytic Activity

The term "activity" is often used in papers on photocatalysis as "photocatalytic activity." Although the author does not know who first started using this term in the field of photocatalysis, people involved in the field of catalysis were using this term before the 1980s, when photocatalysis studies had begun to be accelerated by the famous study of the so-called Honda–Fujishima effect on photoelectrochemical water splitting using a single-crystal titania electrode (*6*). Most authors, including the present author, use the term "photocatalytic activity," but in almost all cases the meaning is the same as that of absolute or relative reaction rate. One reason why we like to use the term "photocatalytic activity" may be that it can make readers think of "photocatalytic reaction rate" as one of the properties or abilities of a photocatalyst, that is, photocatalysts have individual activity, while "reaction rate" is controlled by the activity under given reaction conditions. In the field of catalysis, "catalytic activity" has been used to show a property or performance of a catalyst, since an "active site" (Fig. 1) on a catalyst accounts for the catalytic reaction. The reaction rate per active site can be estimated and should be "catalytic activity." In a similar sense, "turnover frequency," that is, number of turnover per unit time of reaction to show how many times one active site produces a reaction product(s) within unit time, is also used. On the other hand, there are no active sites on a photocatalyst (*7*), and the reaction rate strongly depends on various factors such as the intensity of irradiated light which initiates a photocatalytic reaction. Considering at least that the dark side of a photocatalyst or suspension

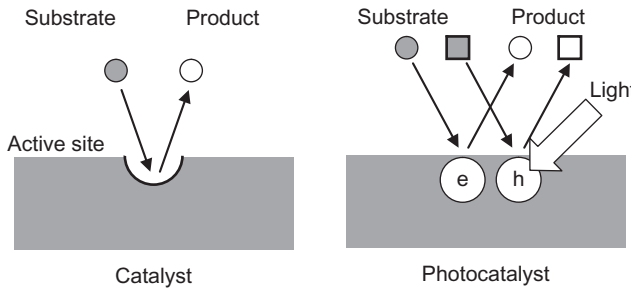

Fig. 1. Difference in concepts of catalytic and photocatalytic reactions: A catalyst contains active sites at which a substrate is converted into a product, while no active sites are present on a photocatalyst.

is not directly involved in the photocatalytic reaction, the use of the term "active site" is inappropriate, and a relationship of photocatalytic activities with active sites therefore cannot be expected.

III. Principle of Photocatalysis

A. Generally Accepted Explanation

The principle of photocatalysis is often explained with an illustration like Fig. 2, a schematic representation of the electronic structures of semiconducting materials, a band model. An electron in an electron-filled valence band (VB) is excited by photoirradiation to a vacant conduction band (CB), which is separated by a forbidden band, a band gap, from the VB, leaving a positive hole in the VB (Section III.B). These electrons and positive holes drive reduction and oxidation, respectively, of compounds adsorbed on the surface of a photocatalyst. Such an interpretation accounts for the photocatalytic reactions of semiconducting and insulating materials absorbing photons by the bulk of materials. In the definition of "photocatalysis" given above, however, no such limitation based on the electronic structure of a photocatalyst is included. For example, isolated

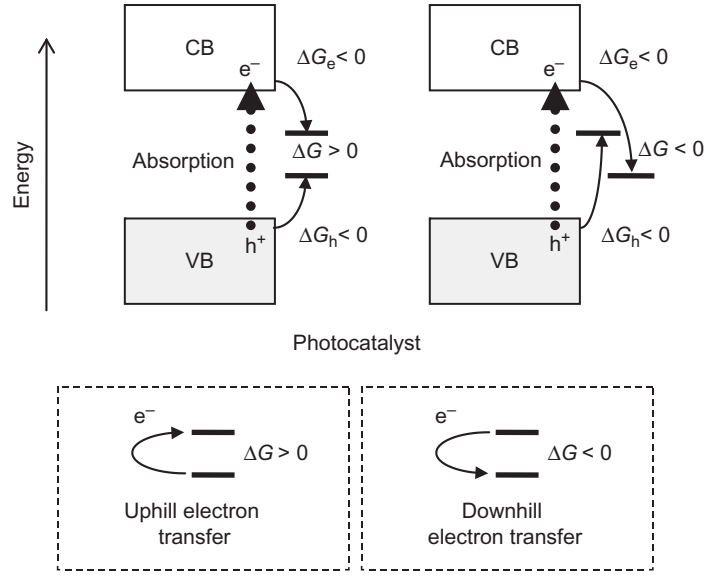

Fig. 2. Gibbs-energy change in photocatalytic reactions.

chemical species, not having the above mentioned band structure, on or in a solid can be a photocatalyst, and even when a bulk material is used, the photoabsorption and resultant photocatalytic reaction may proceed at a localized site when, for example, photocatalysts are photoirradiated at a wavelength near the band gap. An example is a gold-modified titania photocatalyst which induces "photocatalytic" decomposition of organic compounds under aerated conditions by photoabsorption of surface-plasmon resonance of gold particles (*8*). Therefore, the interpretation using a band model is not always adequate for understanding photocatalysis. In this sense, the term "heterogeneous photocatalytic reaction (photocatalysis)" seems better than "semiconductor photocatalytic reaction" based on the electronic band structure.

B. Band Structure and Excitation

An important point in general understanding of the mechanism of photocatalysis is that photoabsorption and (e^-–h^+) generation (Fig. 3) are inextricably linked; a VB electron is not excited after photoabsorption. This interband (band-to-band) excitation is often illustrated by three bands, CB, forbidden band (band gap) and VB, in which an electron moves vertically from the VB to CB, that is, no spatial change in the position of electron, though the author sometimes encounters misunderstanding that

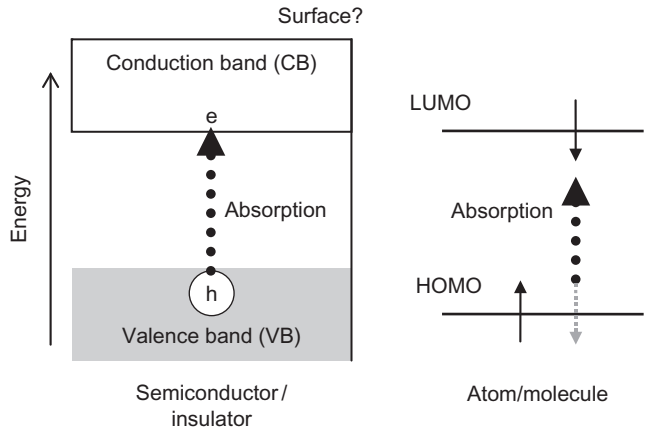

Fig. 3. Photoabsorption by transition of electrons in the VB or HOMO to the CB or LUMO in a semiconductor/insulator or atom/molecule, respectively.

an electron migrates from VB to CB spatially. Anyway, the above mentioned interpretation seems a little strange considering the meaning of band structure and band-to-band transition, in which electrons are not localized and therefore electrons and positive holes can migrate within a crystal; an unlocalized excitation state may be described as "photoexcited crystal," for example, an excited state of titania, without showing localized e^-–h^+. Do e^- and h^+ migrate in the CB and VB, respectively, after photoabsorption, that is, photoexcitation? When we illustrate the electronic structure of a molecule, lines are drawn to show the electronic state (Fig. 3); the length of these lines does not mean spatial distribution of electrons in those states. This should also be the case for semiconducting (or insulating) materials, and band-to-band transition just means that an electron in the VB is excited to the CB without clarifying the location of e^- and h^+. Sometimes we, at least the present author, misunderstand that e^- and h^+ migrate to the surface. (Right or left end of the CB and VB in Fig. 3 is often assigned to "surface.")

A possible interpretation for better understanding for e^-–h^+ location is that there are sites trapping e^- or h^+ in the crystal lattice and that e^- and h^+ are trapped by these sites "immediately" after the band-to-band transition, that is, photoabsorption (*9*). Location of e^- and h^+ in the initial stage of photocatalysis as well as the rate should be controlled by the density and spatial distribution of these traps in a photocatalyst. However, there is little information on the density and spatial distribution of traps, since the structure of traps has not been fully clarified (*10*).

C. Positive Hole

A significant problem in studies on photocatalysis is the definition of "positive hole." Positive hole is defined as a defect of an electron (i.e., a positive hole must be included in a substance, while an electron is a real substance). Therefore, not only h^+ produced by photoinduced band-to-band transition in solid materials but also a hydroxyl radical, which is a one-electron deficient hydroxyl anion, can be a positive hole. If this definition is accepted, there should be no difference in the photocatalytic oxidation mechanisms between "direct hole transfer" and "surface-adsorbed hydroxyl radical reaction," since it is well known that the surface of a metal oxide is covered with chemically or physically adsorbed water and a positive hole passing through this water layer into a solution may be a hydroxyl radical or its protonated or deprotonated species (Fig. 4). Actually, hydroxyl

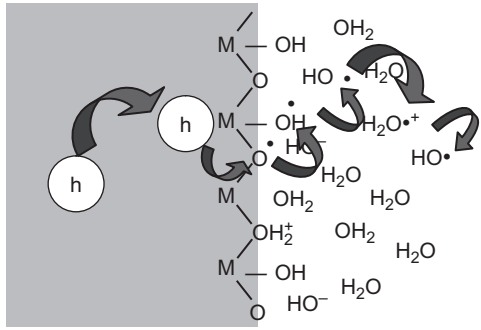

FIG. 4. Transfer of positive holes from bulk of a photocatalyst through the interface to aqueous solution phase. Surface-adsorbed and free (hydrated) hydroxyl radicals and its derivatives can be a possible form of positive holes.

radicals were detected in a suspension of titania particles under ultraviolet irradiation (11,12). Although the author does not know from when people in this field believed that photocatalysis, especially by titania, includes oxidation of organic substrates by hydroxyl radicals that are liberated by the reaction of positive holes and surface-bound water or hydroxyl groups, the detection of hydroxyl radicals might be the reason for this misunderstanding. A problem is the difficulty in obtaining proof for a certain reaction intermediate; one acceptable way to show intermediacy of a species is to show the disappearance of an intermediate, when a reaction substrate is added, with the rate being the same (but in the opposite direction) as that of liberation of a product. However, as far as the author knows, there have been no reports showing this for hydroxyl radical.

D. FERMI LEVEL

Fermi level is a kind of measure of equilibrium electronic energy of a solid material. It is thought that Fermi level is located just below the CB bottom and above the VB top for n-type and p-type semiconducting materials (*13*), respectively. Most metal oxides are categorized as n-type semiconductors with Fermi levels more cathodic (higher) than the standard electrode potential of electrolyte in contact with the metal oxide and thereby electrons in donor levels a little below the CB are injected into the electrolyte to form a space charge (depletion) layer with an electric field, that is, Schottky barrier. In the

1980s, it was thought that this inner electric field separates e^-–h^+ effectively; that is, e^- and h^+ migrate to the bulk and surfaces of semiconductor electrodes and particles, but it seems that this is not the case for untreated photocatalyst particles because of the expected large thickness of this layer due to very low density of donor levels in ordinary photocatalyst particles.

E. Overall Thermodynamics

Change in Gibbs energy (ΔG) of a given reaction is often discussed in chemistry. If ΔG is negative ($\Delta G < 0$) and positive ($\Delta G > 0$), the reaction releases and absorbs energy, respectively, and both situations are possible for photocatalytic reactions. Why can photocatalysts drive a reaction of positive ΔG which does not proceed spontaneously? A possible answer is that a redox reaction can be achieved, even if the overall ΔG is positive, in a system in which reduction and oxidation steps are spatially or chemically separated, otherwise reaction between reduction and oxidation products proceeds to give no net products. Under these conditions, both of Gibbs-energy change for reactions of e^- with oxidant (ΔG_e) and h^+ with reductant (ΔG_h) are required to be negative, that is, reactions by e^- and h^+ proceed spontaneously after photoexcitation (Fig. 2). As discussed in Section III.A, it is often emphasized that a thermodynamic requirement for photocatalytic reaction is more cathodic and anodic levels of the CB bottom and VB top compared with the standard electrode potential of an oxidant and a reductant, respectively, to make Gibbs-energy change of both reactions negative. However, this is only one of necessary conditions and another important necessary condition, though negligibly discussed, is separation of reduction and oxidation by e^- and h^+, respectively, for both types of reaction with positive and negative ΔG (*14*). Actually, many studies have revealed "potential photocatalysts" for photoinduced water splitting using two kinds of model reaction for hydrogen and oxygen production from aqueous methanol and an aqueous solution of silver salt; production of hydrogen and oxygen in each reaction proved that positions of the CB bottom and VB top are more cathodic and anodic compared with the standard electrode potentials for H^+/H_2 and O_2/H_2O systems, respectively, though only a few photocatalysts could produce hydrogen and oxygen at the same time in the absence of sacrificial electron donors and acceptors.

F. Energy Conversion

Photocatalytic and photoelectrochemical cleavage of water produces hydrogen (H_2), as an ideal fuel emitting only water, and oxygen (O_2) and many researchers are trying to establish a highly efficient system for water splitting under solar radiation. Since this reaction requires input of energy due to its positive Gibbs energy, energy of light is used. The efficiency of conversion of light energy to chemical energy thus becomes important (*15*). It should be noted that there are at least two kinds of methods for calculation of the efficiency: number (molar amount)-based and energy-based methods. The former is the same as "quantum efficiency," which is calculated as a number ratio of product(s) and photons absorbed by (quantum efficiency) or incident on the reaction system (apparent quantum efficiency; ϕ in Fig. 5) per time unit. For discussion on energy conversion, the latter energy-based calculation should be used. Since the energy of H_2 (and O_2) shown in the difference in electrochemical potential, that is, electromotive force (emf), is 1.23 eV, energy-conversion efficiency is 100% when light of 1.23-eV energy (ca. 1000-nm wavelength) is absorbed completely by a photocatalyst and all liberated e^- and h^+ are used for water cleavage. The most significant point of photocatalysis and photoelectrochemical reaction is that even if light of energy much greater than the band gap of semiconducting materials as a photocatalyst or photoelectrode is used, potential of e^- and h^+ is fixed at the position of the CB bottom and VB top, respectively. Therefore, the energy-conversion efficiency is halved when 2.46-eV light (504 nm) is used with constant apparent quantum efficiency (Fig. 5a). Although it is often claimed that extension of the limiting wavelength of absorption by photocatalysts and photoelectrodes is necessary in order to utilize solar energy more efficiently, relatively low energy-conversion efficiency at a shorter wavelength has still not been improved. It should also be pointed out that there is a limitation of the longer-wavelength side depending on the reaction to drive, for example, ca. 1000 nm at longest for water splitting as described above (*16*).

There is still a problem in calculation of energy-conversion efficiency when electrochemical or chemical bias is also applied in photoelectrochemical or photocatalytic reaction of positive Gibbs energy. For example, as shown in Fig. 5c, energy-conversion efficiency for a photoelectrochemical system consisting of an n-type semiconductor and metal counter electrodes with bias voltage Δb is possibly expressed as follows:

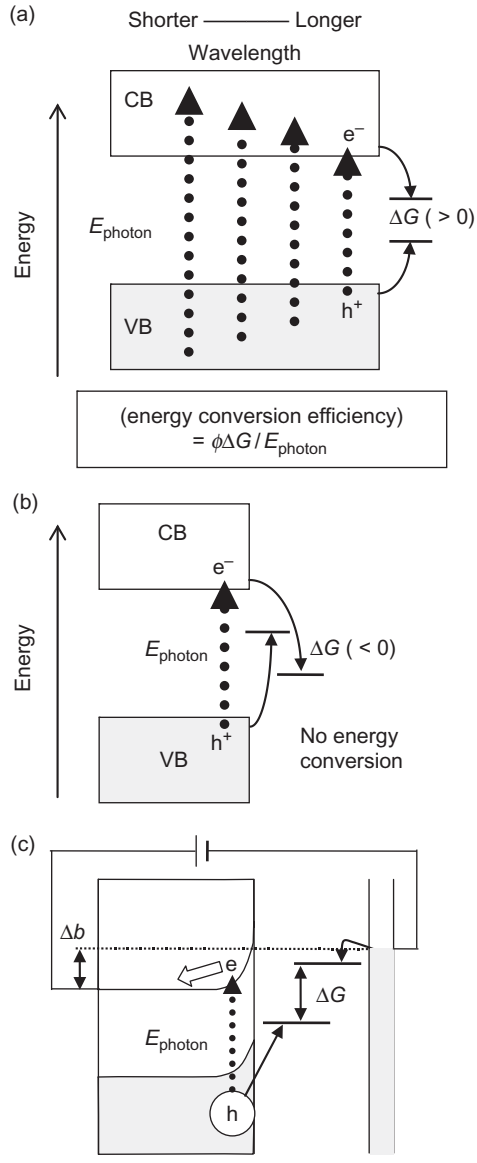

FIG. 5. (a) Photo-to-chemical energy-conversion efficiency of photocatalytic reaction calculated as an integral of the product of apparent quantum efficiency (ϕ) and Gibbs-energy change (storage) divided by photon energy (E_{photon}) as a function of wavelength. (b) In the case where Gibbs-energy change is negative, energy-conversion efficiency cannot be defined, or is defined to be zero. (c) Electrochemically biased (Δb) photoelectrochemical cell consisting of an n-type semiconductor and metal counter electrodes.

$$(\text{energy conversion efficiency}) = \varphi \frac{\Delta G - \Delta b}{E_{\text{photon}}}. \quad (1)$$

However, the reasonability of this calculation has been scarcely discussed so far.

IV. Kinetics

A. First-Order Kinetics

It is well known that first-order kinetics is commonly observed for reactions occurring in homogeneous phases, that is, reactions in homogeneous solutions or in gas phase. Ideally, rate of a monomolecular reaction obeys first-order rate expression which is explained by that the proportion (number) of molecules that have kinetic energy larger than the activation energy is determined only by the temperature of reaction and actual number of molecules with energy for activation is proportional to the concentration (or pressure) of molecules. For these reactions, kinetic data are analyzed by plotting the logarithm of concentration of a substrate or a product against time of the reaction (*17*) to obtain a linear line, and absolute value of the slope of the line is a rate constant, k (Fig. 6). The rate (r) of consumption of a substrate (A) is shown by the following equation.

$$r = -\frac{\mathrm{d[A]}}{\mathrm{d}t} = k[\mathrm{A}]. \quad (2)$$

On the other hand, kinetics of reactions occurring on a solid surface, that is, catalysis or photocatalysis, must be significantly different. There may be two representative extreme cases. One is so-called a diffusion controlled process, in which surface reactions and the following detachment process occur very rapidly to give a negligible surface concentration of adsorbed molecules, and the overall rate coincides with the rate of adsorption of substrate molecules. In this case, the overall rate is proportional to concentration of the substrate in a solution or gas phase (bulk), that is, first-order kinetics is observed (*18*). The other extreme case is so-called surface-reaction limited, in which surface adsorption is kept in equilibrium during the reaction and the overall rate coincides with the rate of reaction occurring on the surface, that is, reaction of e^- and h^+ with surface-adsorbed substrate (*19*). Under these conditions, the overall rate is not proportional to concentration of the substrate in the bulk unless the adsorption isotherm obeys a Henry-type equation, in which the amount of adsorption is proportional to concentration in the bulk (*20*). In the former case, the rate

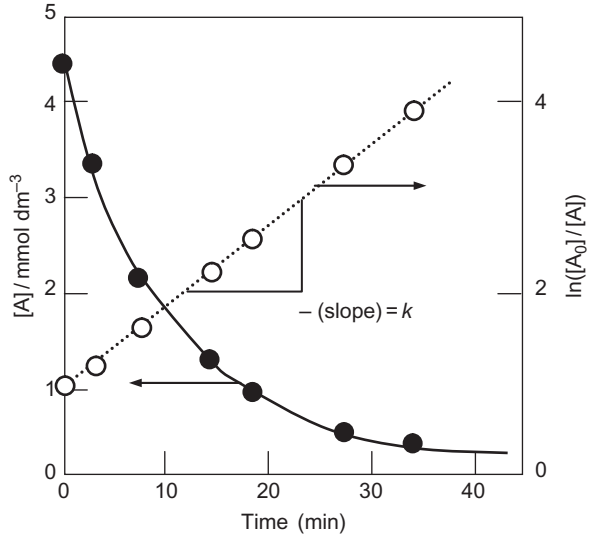

FIG. 6. First-order kinetic analysis for a reaction consuming a substrate A. Plot of logarithm of relative consumption (in the present plot, ratio of initial concentration of substrate A and concentration of A at a given time).

of photocatalytic reaction obeys the first-order rate law, but this is only formal and does not mean the mechanism of monomolecular reaction with activation energy.

One of the most significant points that we must consider in scientific studies, not limited to studies on photocatalysis, is distinction between "evidence" and "consistency," as least as far as the author thinks. In other words, it is necessary to recognize every fact to be a "necessary condition" but not a "sufficient condition" in a strict scientific sense. For example, the fact that a reaction rate obeys the first-order rate law giving a linear relation in a plot of data as in Fig. 6 is only a necessary condition for a monomolecular reaction in homogeneous phase and also a necessary condition for heterogeneous photocatalytic reaction in diffusion-limited conditions or that in surface-reaction limited conditions with a Henry-type adsorption or a Langmuir-type adsorption in the lower-concentration region.

B. LANGMUIR–HINSHELWOOD MECHANISM

The term "Langmuir–Hinshelwood mechanism" has often been used in discussion of the mechanism of photocatalytic reaction in suspension systems, but, as far as the author knows, there has

been no definition given for the Langmuir–Hinshelwood (L–H) mechanism in photocatalytic reactions. In most cases, authors have claimed that a photocatalytic reaction proceeds via the L–H mechanism when a linear reciprocal relation is observed between the reaction rate and the concentration of reaction substrate in a solution. These experimental results seem to be consistent with the following equation:

$$r = \frac{ksKC}{KC + 1}, \tag{3}$$

where r, k, K, s, and C are rate of the reaction, rate constant of the reaction of the surface-adsorbed substrate with e^- (h^+), adsorption equilibrium constant, limiting amount of surface adsorption, and concentration of substrate in the bulk at equilibrium, respectively *(21)*, when the substrate is adsorbed by a photocatalyst obeying a Langmuir isotherm and the adsorption equilibrium is maintained during the photocatalytic reaction, that is, the rate of adsorption is faster than that of the reaction with electrons or holes (Section IV.A). Such a situation is often called "light-intensity limited," that is, photoabsorption is the rate-determining step *(22)*. Several methods for linearization of Eq. (3) have been reported, but two kinds of plots are often employed for analysis. As shown in Fig. 7, the most popular one is a plot of reciprocal rate against reciprocal concentration, and another one is a plot of ratio of concentration to rate against concentration. Both plots give ideally the same values of parameters, ks and K, while the former plot reflects mainly lower-concentration data with probable relatively large experimental error.

The original meaning of the term "Langmuir–Hinshelwood mechanism" in the field of catalysis is, to the author's knowledge, a reaction of two kinds of molecules proceeding on a surface in which both molecules are adsorbed at the same surface adsorption sites with the surface reaction being the rate-determining step (in the original meaning of "rate-determining step"). Of course, the general rate equation for the L–H mechanism (not shown here) includes two sets of parameters for two kinds of molecules, and when one set of parameters is neglected, the equation is for a monomolecular reaction, similar to the photocatalytic reaction of a substrate adsorbed in Langmuirian fashion. However, at least in the field of catalysis, the term L–H mechanism is rarely used for such monomolecular surface reactions, since the L–H mechanism has been discussed for a bimolecular surface reaction by comparing with the Rideal-Eley

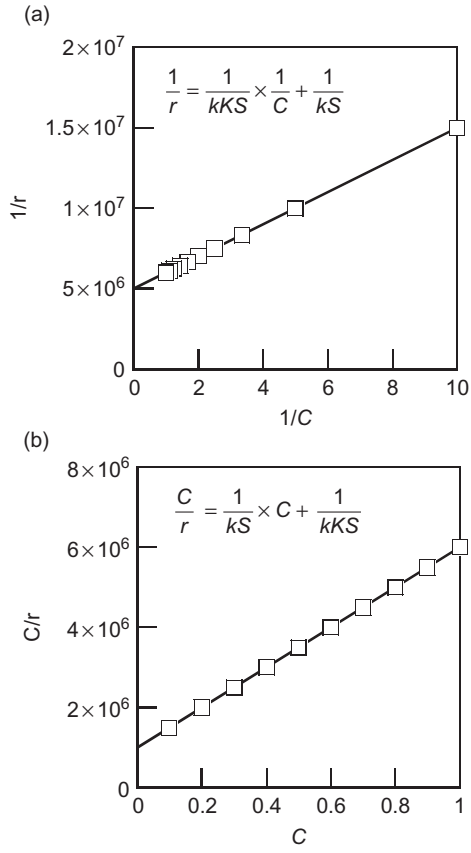

FIG. 7. Simulation of linearized plots for kinetics governed by surface concentration of substrates adsorbed on the photocatalyst surface in a Langmuirian fashion, where r, C, k, K, and S are rate of reaction (mol s^{-1}), concentration of a substrate (mol L^{-1}), rate constant (10^{-4} s^{-1}), adsorption equilibrium constant (5 L mol^{-1}), and saturated amount of adsorption (2×10^{-3} mol).

mechanism, in which a surface-adsorbed molecule reacts with a molecule coming from the bulk.

Even if the L–H mechanism is defined as the reaction of a surface-adsorbed substrate obeying a Langmuir isotherm governing the overall rate, the frequently reported experimental evidence, a reciprocal linear relation between concentration of the substrate in solution and rate of photocatalytic reaction is not always proof of this mechanism. From the linear plot, two parameters are calculated (*23*). One (often shown as "k," not as "ks") is a limiting rate of the reaction at the infinite concentration

giving maximum adsorption, that is, ks, and the other is the adsorption equilibrium constant, K. The former parameter is a product of rate constant and adsorption capacity of a photocatalyst and this may be a photocatalytic activity. The latter parameter shows the strength of adsorption and must be the same as that estimated from an adsorption isotherm measured in the dark. If kinetically obtained K is different from that obtained in dark adsorption measurement, the L–H mechanism cannot be adopted. Therefore, dark adsorption measurement is always required. Finally, it should be noted also in this case that a linear relation fitting to a Langmuir-type adsorption isotherm and similarity of adsorption equilibrium constant evaluated using photocatalytic reaction rate and by dark adsorption experiments are only necessary conditions; the observed reaction rate is "consistent" with kinetics of a substrate undergoing Langmuir-type adsorption and does not exclude the possibility of other reaction kinetics (*24*).

C. Electron–Hole Recombination

Recombination of e^- and h^+ occurs in photocatalysts in some degree and it has been believed that this reduces quantum efficiency, that is, efficiency of e^-–h^+ used in the chemical reaction (s), and overall photocatalytic reaction rate. Since recombination does not produce any chemicals, it is not easy to estimate the rate of recombination directly. One possible way for estimation of recombination rate is to subtract the overall rate of chemical reaction by e^-–h^+ from the rate of photoabsorption, but the obtained data cannot give any other information.

Kinetics of e^-–h^+ recombination may depend on its mode; if one electron is excited and this is recombined with h^+, the recombination rate obeys the first-order rate law, while if multiple e^-–h^+ appears at the same time within a photocatalyst particle, the rate obeys the second-order rate law. Actually, in a femtosecond pump–probe diffuse reflection spectroscopic analysis of titania samples, photoabsorption at 620 nm by trapped electrons showed second-order decay with a component of baseline as follows:

$$(\text{absorption}) = \alpha\left\{\frac{[e_0]}{1 + k_r[e_0] \times t} + \text{BL}\right\}, \tag{4}$$

where α, $[e_0]$, k_r, t, and BL are a constant, initial concentration of trapped electrons at time zero, second-order rate constant, time

after pump pulse (310 nm), and baseline component, respectively (*25*). A baseline component might correspond to electrons trapped in deep traps. Different from kinetic analysis based on the first-order rate law (Section IV.A), analysis based on the second-order rate law requires absolute values of concentration ($[e_0]$ in Eq. (4)) and photoabsorption coefficient (α in Eq. (4)) of a target compound, but these cannot be determined experimentally, at least when the analyses are performed and calculation is performed assuming α to be unity. An example of these kinetic analyses is shown in Fig. 8 for Degussa (Evonic) P25 (*26*). Although the thus-obtained second-order rate was relative, it was observed that k_r's of different titania samples in the form of powder are proportional to those in suspension systems, suggesting that k_r can be a measure of rate of recombination. However, it must be noted that such a second-order recombination process cannot be reproduced in an ordinary photoirradiation process in which lower light intensity induces single-electron photoexcitation and mutual recombination occurs obeying the first-order rate law (*27*).

D. Quantum Efficiency

The term "quantum efficiency" or "quantum yield" was originally defined as a ratio of number of products (or consumed starting material) to that of absorbed photons in photoreaction in homogeneous phase, that is, in solutions or gas phase,

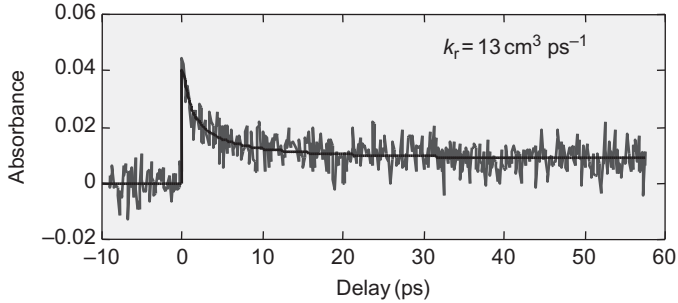

Fig. 8. An example of picosecond-time-region decay of photoabsorption (620 nm) of trapped electrons in Degussa (Evonic) P25 particles after excitation by a ca. 100-fs pump pulse (310 nm). The curve was analyzed by a second-order rate law (Eq. (4)) with a baseline component (BL), and a second-order rate constant (k_r) was obtained to be $13\ cm^{-1}\ ps^{-1}$.

assuming that one photon induces reaction or change in one molecule since a multiple-photon process and subsequent multiple-electron transfer can be neglected in ordinary photoirradiation conditions with relatively low photon flux. Confusion might arise when this concept is applied to photocatalysis, in which a multiple-photon process and at the same time radical chain reaction may be included, especially in reaction in the presence of oxygen.

In a heterogeneous photocatalytic reaction, in which multiple photons are absorbed due to the relatively large size of particles compared with the size of molecules, multiple-electron (positive hole) transfer may occur. For example, photocatalytic silver metal deposition accompanied by molecular oxygen (O_2) liberation proceeds with the following stoichiometry (*28*):

$$4Ag^+ + 2H_2O \rightarrow 4Ag + O_2 + 4H^+ \tag{5}$$

For the determination of quantum efficiency, it is necessary to make an assumption on how many photons are required for the reaction. One of the possible and the most frequently employed assumptions is that four photons are required for liberation of one oxygen molecule, four silver metal atoms, or four protons, and when the O_2 yield is used, the quantum efficiency is calculated to be

$$\frac{4n(O_2)}{n(\text{photon})}, \tag{6}$$

where n is the number of molecules or photons. Thus, for the calculation of quantum efficiency of heterogeneous photocatalytic reactions, it is reasonable to consider the efficiency of utilization of electrons–positive holes assuming that an electron and positive-hole pair is produced by absorption of a photon. However, since neither a photoexcited electron nor a positive hole appears in stoichiometry, the above-mentioned consideration may not always be straightforward. For example, acetic acid dissolved in air-saturated water is decomposed into carbon dioxide by an appropriate suspended photocatalyst with the following proposed stoichiometry:

$$CH_3COOH + 2O_2 \rightarrow 2CO_2 + 2H_2O. \tag{7}$$

How many photons are required for this reaction? Assuming that only O_2 is reduced by photoexcited electrons in this reaction and that reduction of an O_2 molecule requires four electrons, this reaction is an eight-electron process. However, since the photocatalytic reaction of acetic acid may include a radical chain mechanism or at least addition of O_2 to intermediate radicals, an

acetic acid molecule could be decomposed by less than eight electrons. It is impossible to calculate intrinsic quantum efficiency, that is, efficiency of utilization of electron–positive-hole pairs, only from the product yield. Therefore, quantum efficiency is reported with the description that a given reaction is assumed to proceed through a proposed multiple-electron process (e.g., eight for the acetic acid decomposition in Eq. (7)).

Another problem for the determination of quantum efficiency is the difficulty in determining the number of absorbed photons. Unlike measurement for homogeneous solutions, solid materials scatter incident photons to reduce the light intensity arriving at a detector in a spectrophotometer. In the wavelength region in which only some of the photons are absorbed, that is, around the band-edge wavelength, it is difficult to measure the photoabsorption efficiency. Therefore, apparent quantum efficiency (photonic efficiency) has often been used instead of quantum efficiency, and apparent quantum efficiency is calculated by the number of incident photons rather than the number of photons used for quantum efficiency calculation. Since quantum efficiency is defined as efficiency of electron–positive-hole utilization, apparent quantum efficiency is a product of efficiencies of photoabsorption and electron–positive-hole utilization. Of course, both quantum efficiency and apparent quantum efficiency depend on the irradiation wavelength and sometimes on the irradiation intensity, and thereby the data should be shown with wavelength and preferably with intensity. In this sense, such measurement must be performed by monochromatic irradiation; irradiation with sharp-cut optical filters is inappropriate.

E. Rate-Determining Step

Assuming that a certain reaction proceeds through a series of steps without any branching reactions, the rate must be the same as the rate of the slowest step, the rate-determining step, that is, the overall activation energy is that of the rate-determining step (Fig. 9). This original definition cannot be directly applied to photocatalysis. A possible reason is that reactions by photoexcited electrons and positive holes occur in parallel, not in series (Fig. 9). Considering the requirement of photocatalysis for the same numbers of electrons and positive holes to be used (consumed), it seems possible to compare the rates of electron and positive-hole reactions. However, it seems that the overall reaction rate is also influenced by recombination of e^-–h^+. In ordinary photochemistry in homogeneous phase, steady

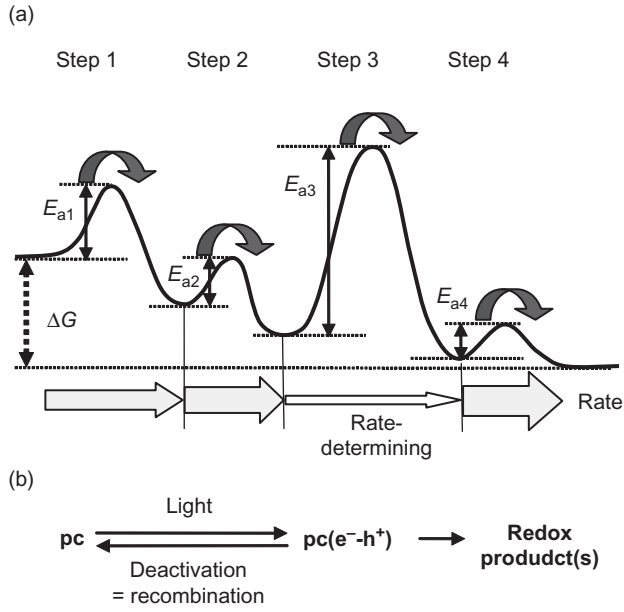

FIG. 9. (a) Model interpreting a rate-determining step in a four-step series reaction. Step 3 with largest activation energy determines the overall rate. (b) Simplified scheme of photocatalytic reaction with a photocatalyst "pc." It is clear that this process is not a series reaction since a "deactivation step" is included.

(stationary)-state approximation is used to analyze the kinetics, assuming forward reaction to give products and backward reaction, that is, de-excitation. In such analyses, there may be no rate-determining step.

V. Visible Light-Induced Photocatalysis

A. Background

It has been claimed since the early stage of studies on photocatalysis that only one possible drawback of titania is its photoabsorption wavelength range shorter than ca. 400 nm; titania can absorb ultraviolet light included a little in solar radiation (*29*). Since solar radiation includes light of wavelengths from 280 to 4000 nm, use of photocatalysts that absorb light in visible and near-infrared regions is highly desired. However, light of longer wavelength has smaller energy, leading to a decrease in

potential for redox reactions, and thereby reactions driven by visible-light irradiation are limited to those satisfying the thermodynamic and kinetic requirements (Sections III.E and III.F). Many studies have been performed to design and develop photocatalysts that work under visible-light irradiation.

First, the boundary wavelength between ultraviolet light and visible light should be defined. The meaning of the term "visible light" is light that can be seen, and the limiting wavelength differs among individuals. Many studies demonstrating that visible light induced, as expected, a photocatalytic reaction used the condition of photoirradiation through an optical cut-off filter, L-42 or its equivalent, and the irradiation wavelength under such conditions used to be described as ">420 nm." However, this is inadequate because this filter transmits light of wavelength >ca. 390 nm (*30*). Actually, in the author's experience, appreciable photocatalytic activity of not only rutile but also anatase titania photocatalysts could be observed by irradiation through the filter. When this optical filter is used for irradiation, at least comparison of the photocatalytic activity with that of a representative titania photocatalyst, such as P25 (Degussa (Evonic)) or ST-01 (Ishihara Sangyo), is necessary. Otherwise, optical cut-off filters of longer transmission limits should be used. One of the possible and smart ways is to define "visible light" as light that gives photocatalytic reaction product less than the detection limit of analyses by titania and to use an appropriate optical filter to realize this, considering the history of studies on photocatalysis.

B. Doping

Strategies that have usually been employed, since the discovery of visible light-induced activity of nitrogen-containing titania particles by Asahi *et al.* (*31*), in studies on visible light-induced photocatalysis are modification (doping) of titania to give visible-light absorption or use of colored mixed metal oxide and nitride. Although it is expected that such doping of crystalline and mixed metal oxide/nitride may induce production of lattice defects, which enhance electron–hole recombination, resulting in lower photocatalytic activity (*32*), discussion of the strategies is not a purpose of this review. Some problems in the studies on visible light-photocatalytic activity are discussed here.

One possible reason for the explosive growth in the number of papers on doped material is an unclear definition of the term "doping." As far as the author knows, the meaning of "doping"

is incorporation of atoms or ions in a crystalline lattice, that is, modification of the bulk structure of crystallites, but not modification of surfaces. However, as far as the author knows, such location of hetero atoms or ions has negligibly been discussed (*33*). If an adequate analytical method(s), if any, is (are) employed, average density of hetero atoms/ions can be determined, and if mapping of elements can be performed with higher sensitivity, spatial distribution may be elucidated. The effect of doping must be discussed on the basis of this structural information, though there have been few reports containing such discussion so far. In relation to this problem, recent papers claimed that in procedure for nitrogen doping using urea, heptazine derivatives are produced on the surface of titania particles and work as a photosensitizer and/or photocatalyst (*34*), that is, nitrogen is not "doped" in the titania lattice but is included as a surface modifier.

C. Proof for Visible Light-Induced Photocatalysis

Even if introduced hetero atoms/ions are not "doped" in the lattice, it is useful to prepare modified photocatalysts with visible-light absorption by introducing hetero atoms/ions. One problem, however, is that only newly appearing visible-light photoabsorption and photoinduced reaction rate under visible-light photoirradiation are often described in papers. As the author's group reported, the use of organic dyes for a photoinduced degradation test is inappropriate because those dyes might be adsorbed and work as visible-light photosensitizers, and it is preferable to show resemblance of absorption (diffuse reflection) and actions spectra, that is, photocatalysis by doped (modified) photocatalysts can be proved through action spectrum analysis. Figure 10 presents representative results proving visible-light response of sulfur-doped titania (*35*), as a rare case among studies on visible light-sensitive photocatalysts, showing the resemblance of a diffuse-reflectance spectrum with an action spectrum for photocatalytic oxidative decomposition of acetic acid in aerated aqueous solution; doping of (or at least modification with) sulfur induced photoabsorption and photocatalytic activity in the visible-light region. In other words, showing that a certain reaction proceeds under the above mentioned visible-light irradiation conditions is not proof of visible light-induced photocatalytic activity unless an appropriate compound is used for the photocatalytic activity test. Dyes have relatively large photoabsorption (extinction) coefficients (This is the reason why

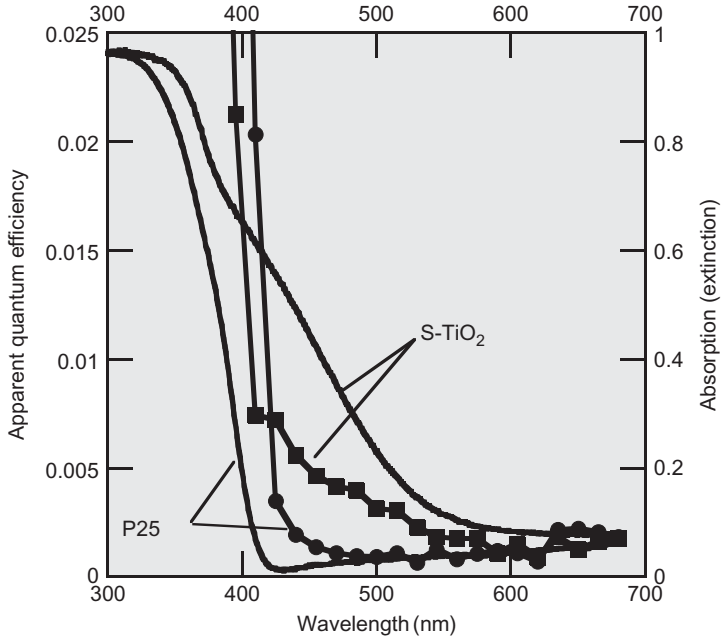

FIG. 10. Diffuse reflectance (photoabsorption) and action spectra for acetic acid, having no absorption in the visible-light wavelength range, decomposition in aerated aqueous solutions of sulfur–doped titania (S–TiO_2) and Degussa (Evonic) P25.

they are used as dyes, i.e., coloring agents.) and therefore measurements of their concentrations in solutions are easy even if the concentrations are very low. However, the fact that dyes absorb visible light indicates that a photoreaction might be induced by visible-light photoabsorption (dye sensitization) as well as by photoabsorption of a photocatalyst. Although this problem had been pointed out earlier, there have been no clear experimental results showing the self-photodecomposition of dyes, presumably due to the difficulty in determining the mechanism of this photoreaction. Actually, determination of the extent to which incident photons are absorbed by a dye and photocatalyst is difficult. A paper has been published to show that methylene blue (MB), the most frequently employed dye, as well as, presumably, other kinds of organic dyes, is inappropriate as a model compound, particularly for testing visible light-induced photocatalytic activity (*36*). There are at least three reasons for its inappropriateness. One is that the dye molecules absorb photons, especially in the visible-light range, and thus photoexcited electrons may be injected into photocatalyst

particles as has been suggested by similarity of the action spectrum similar to the photoabsorption spectrum of the dye (37–39) (Fig. 11). Another reason is that the absolute molar amount of dye contained in the reaction system can be much smaller than that of a solid photocatalyst. The concentration of dye in the solution should be relatively low since the absorption coefficient is large. These two facts are closely related to the problem of how we can prove a given reaction to be "photocatalytic," as discussed in Section II.A. The third reason is that the mechanism of dye degradation is so complicated that efficiency of the photocatalytic reaction, for example, quantum efficiency, cannot be measured. Measuring the consumption (decrease) of a dye during photoirradiation requires only a spectrophotometer, but the use of dyes as model compounds is inappropriate, and if dyes are used, care must be taken in the analysis of experimental results.

An action spectrum is a plot of apparent quantum efficiency, not quantum efficiency, against wavelength of light used for apparent quantum efficiency measurement. Therefore, it is clear that monochromatic light irradiation is required to record an action spectrum. Usually, a grating-type monochromator is used with a light source such as a xenon arc lamp. Interference-type optical filters, transmitting at only a certain wavelength region, are also used for monochromatic irradiation, though wavelengths of possible irradiation are limited. Because of possible dependence of apparent quantum efficiency on light intensity *(40)*, it is preferable to adjust the light intensity at each wavelength *(41)*. Wavelength-selective irradiation can be carried out using optical filters

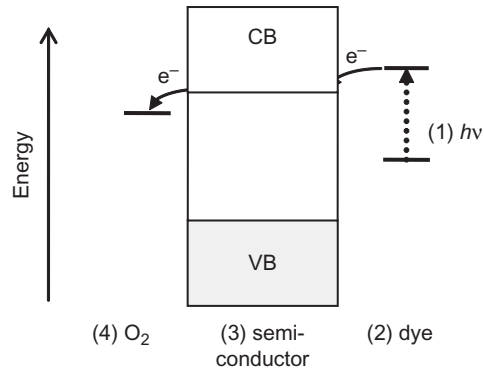

FIG. 11. Possible mechanism of "dye-sensitized" photoinduced oxidative decomposition of dye in the presence of oxygen. Components (1)–(4) are necessary conditions for "dye-sensitized reaction" and they are also necessary conditions for ordinary photocatalytic reaction.

that transmit light of wavelength longer than a certain limit, that is, "cut-off filters." By using a number of filters with different cut-off wavelengths, a plot of apparent quantum efficiency against the cut-off wavelengths can be obtained, and this "pseudo-action spectrum" seems like a "true" action spectrum obtained by the above-described monochromatic irradiation. However, those are completely different; a pseudo-action spectrum is an integrated (from longer to shorter wavelengths) form of a "true" action spectrum based on the assumption that light intensity is constant in the whole range of irradiation, because of the difference in irradiation wavelength region (Fig. 12). Consequently, the corresponding action spectrum should be estimated by differentiation of the pseudo-action spectrum; a horizontal part in a pseudo-action spectrum (Fig. 12), if any, shows that apparent quantum efficiency at the wavelength is negligible even if an appreciable value is seen in the pseudo-action spectrum.

D. Cocatalyst Loading for Multiple Electron Transfer

As has been discussed in Section III.E, a photocatalytic reaction can proceed if the CB bottom and VB top are more cathodic and anodic than the standard electrode potentials of electron acceptors and donors, respectively. Therefore, band-edge position

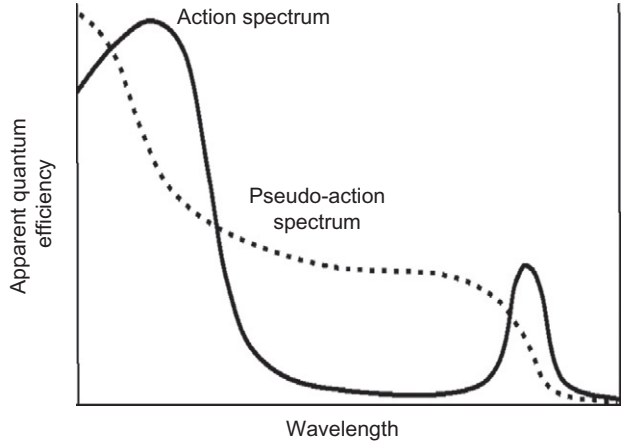

Fig. 12. Examples of action and pseudo-action spectra for photoinduced reaction by an ordinary semiconductor photocatalyst (shorter wavelength) and an organic dye (longer-wavelength peak). A pseudo-action spectrum taken by cut-off filters corresponds to integration of the "true" action spectrum from the longer-wavelength side.

is very important to predict the possibility for driving a photocatalytic reaction. On the other hand, the gap between the CB bottom and VB top, a band gap, determines the photoabsorption spectrum, that is, wavelength range to be absorbed by a photocatalyst. For ordinary simple and mixed metal oxides, it has been reported in the 1980s that change in the metal induces a shift of the CB bottom position, while the VB top position is unchanged because the VB is mainly composed of oxygen 2p atomic orbitals commonly contained in metal oxides (*42*). This means that narrowing the band gap of a metal-oxide photocatalyst shifts the CB bottom position to more anodic, that is, decreasing the ability of reduction by e^-. In most applications of photocatalysis, molecular oxygen is reduced by e^-, and its standard electrode potential of one-electron reduction of oxygen to give superoxide anion radical ($O_2^{\bullet -}$) lies just below the CB bottom of anatase titania, absorbing only ultraviolet light. A shift of the absorption range of titania to visible means a shift of the CB bottom below the potential for one-electron reduction of oxygen. The reason for negligible photocatalytic activity of tungsten(VI) oxide (tungstena), absorbing visible light of wavelength up to ca. 470 nm, for oxidative decomposition of organic and inorganic compounds in air is accounted for by the lower CB bottom position. Thus, ordinary metal oxides cannot be a photocatalyst being active for oxidative decomposition under visible-light irradiation (*43*).

Recently, it was reported that loading small amount of platinum onto tungsten(VI) oxide enhances the visible-light photocatalytic activity significantly and this is caused by the catalytic action of platinum to induce multiple-electron transfer to oxygen (*44*). Reactions of two and four-electron transfer processes are as follows (potential in parentheses is standard electrode potential versus standard hydrogen electrode at pH 0).

$$O_2 + 2H^+ + 2e^- \rightarrow H_2O_2 (0.695\,V), \tag{8}$$

$$O_2 + 4H^+ + 4e^- \rightarrow 2H_2O (1.23\,V). \tag{9}$$

The standard electrode potentials are far more anodic than that of one-electron transfer process, –0.284 V (SHE) and the visible-light photocatalytic activity of platinum-loaded tungsten(VI) oxide could be interpreted by enhanced multiple-electron transfer process by deposited platinum (*45*), since it is well known that platinum and the other noble metals catalyze such multiple-electron transfer processes. Similar phenomena, cocatalyst promoted visible-light photocatalytic activity, have been reported with palladium (*46*) and copper oxide (*47*). Thus, change of reaction process seems beneficial to realize visible-light photocatalytic activity.

VI. Design of Active Photocatalysts

A. Physical Property–Activity Correlation

A.1. Nanostructured photocatalysts

There have been many reports on preparation of photocatalysts with nanometer-sized structures, for example, nanoparticles, nanoplates, nanocubes, nanorods, nanotubes or nanowires, as well as their photocatalytic activities, and the number of such reports is still increasing (*48*). A possible reason for such an explosive increase in studies on nanostructured photocatalysts is popularization of low-priced pressure-tolerant Teflon bottles for hydrothermal reactions. By using this type of apparatus, a variety of inorganic compounds can be prepared and morphology can be changed depending on the reaction conditions. Scanning or transmission electron microscopic images of those nanostructured photocatalysts (even non-photocatalysts) are attractive and interesting. However, considering that we do not know what structural parameters of photocatalysts govern the photocatalytic activity or how they govern the photocatalytic activity, there seems to be no assured reason why nanostructured materials, rather than ordinary nonstructured ones, should be employed.

A.2. Dependence of photocatalytic activities on physical and structural properties

It can be said that not only the above mentioned "nano-structure" but also other ordinary physical or structural properties measured for photocatalysts have not been proved to be decisive factors for the photocatalytic activities. It is true that photocatalytic activities of photocatalysts of certain components prepared or treated in different ways or under different conditions may be different and this is because physical and structural properties of those photocatalysts differ depending on the preparation/treatment conditions, that is, physical and structural properties must control the photocatalytic activity (*49*). A problem is we, at least the author, do not know how properties affect photocatalytic activity. A possible reason is that those properties, though we do not know how many properties are required for analysis, are changed at the same time. For example, when titania photocatalysts are prepared by hydrolysis of a titanium compound such as titanium(IV) sulfate or tetra (2-propoxide) followed by calcination in air, higher-temperature

calcination gives higher crystallinity, smaller specific surface area and rutile crystallites, while lower-temperature calcination gives lower crystallinity, larger specific surface area and anatase crystallites. It has been reported that photocatalytic activity of titania particles prepared in such a way decreased drastically at the temperature at which anatase–rutile transformation occurred. Since both crystalline form and specific surface area were changed drastically at the same time and there have been no reported ways to extract the intrinsic effect of each property, it is difficult to determine which property (or both of them) is significant. Discussions on property–activity correlations reported so far, including those reported by a group of the author, may involve such a problem. It can be said that rutile titania samples with a small surface area that are prepared at a high temperature show low photocatalytic activity, but it is scientifically (logically) impossible to state that the conversion of crystalline form or drastic reduction of specific surface area is the reason for the low photocatalytic activity.

A.3. Extraction of intrinsic effects of physical and structural properties

A plausible method to extract the intrinsic effect of each physical and structural property is statistical analysis of data on physical and structural properties and photocatalytic activities for samples of the same composition, such as titania. In a recent study by the author's research group, photocatalytic activities and physical and structural properties of 35 commercial titania powders were statistically analyzed to find the predominant property (properties) determining the activity of a given reaction system (*50*): standardized photocatalytic activities for five kinds of reactions were fairly well reproduced by a linear combination of six kinds of physical and structural properties of photocatalysts, that is, specific surface area, density of crystalline defects, primary particle size, secondary particle size, and existence of anatase and rutile phases. Recently, decahedral-shaped anatase titania particles (DAPs) have been prepared by controlled gas-phase reaction of titanium(IV) chloride and oxygen at 1473 K (Fig. 13) (*51*). The photocatalytic activity of DAPs was reported to be much higher than the photocatalytic activities of commercial titania particles, for example, Degussa (Evonic) P25, presumably due to relatively large specific surface area to adsorb a large amount of the substrate(s) and high crystallinity, that is, less crystalline defects to reduce e^-–h^+ recombination. Then, how does the decahedral shape itself affect the photocatalytic activity? It was suggested that high levels of

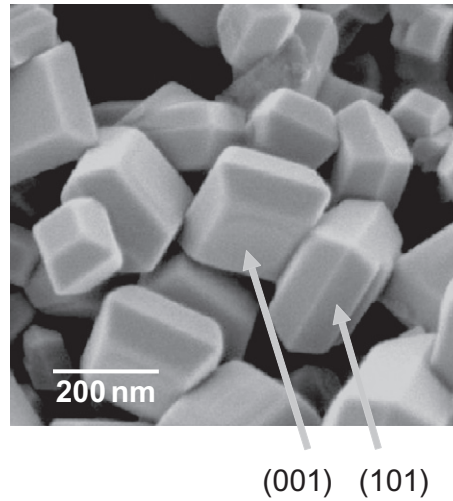

FIG. 13. A representative SEM image of decahedral anatase titania particles prepared by controlled gas-phase reaction of titanium(IV) chloride and oxygen at 1473 K. Most particles expose two square (001) facets and eight trapezoidal (101) facets.

photocatalytic activity of DAPs could not be reproduced by correlation equations derived in the above mentioned multivariable analysis *(52)*.

B. SYNERGETIC EFFECT

A hypothesis not proved scientifically regarding titania photocatalysts, especially P25, is that the copresence of anatase and rutile crystallites induces a high level of photocatalytic activity; transfer of photoexcited electrons and positive holes between interconnecting anatase and rutile particles may enhance charge separation and hence improve the efficiency of utilization of electron–hole pairs. However, as far as the author knows, there have been no reports showing direct evidence of such interparticle charge migrations and the expected lower level of activity of pure anatase or rutile particles alone. In a scientific sense, isolation of anatase and rutile crystallites from P25 is necessary to determine the crystalline composition and to check the synergetic effect of anatase and rutile.

The term "synergetic effect" in photocatalysis could be defined as follows: when more than two kinds of photocatalysts are used as a mixture, the overall photocatalytic activity exceeds the sum

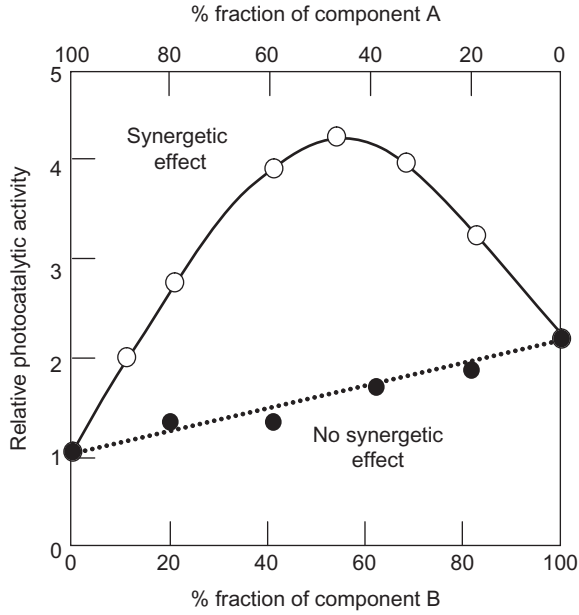

FIG. 14. Hypothetical representation of relative photocatalytic activities of mixtures of components A and B. A synergetic effect can be suggested at least when a mixture shows better photocatalytic activity compared with those of pure components A and B.

of activities of each photocatalyst (Fig. 14). When a certain component alone is not a photocatalyst and a mixture with another photocatalyst shows improved activity, that component should be called "cocatalyst" or "enhancer," and the improvement cannot be attributed to a synergetic effect. One of the representative discussions on the synergetic effect is for anatase–rutile mixed crystalline photocatalysts, such as Degussa P25 (*53*). The author thinks that a synergetic effect has not yet been proved for P25, and the effect seems to be speculation. This is natural considering that each component, anatase and rutile, in P25 had not been isolated before the isolation of anatase by the author's group. Even if all of the components are isolated from the mixture, how can we show a synergetic effect? Taking into consideration the fact that a photocatalytic reaction proceeds by photoabsorption of the photocatalyst and the fact that total number of absorbed photons is not directly proportional to the mass (volume) of the photocatalyst, a control experiment using each component should be carried out with adjustment to make the flux of absorbed photons the same as that for the mixture. However,

discussion is still needed to establish a method to clarify the synergetic effect in photocatalysis.

VII. Concluding Remarks

When the author started the study on photocatalysis in 1981, there appeared to be no laboratories doing research work only on photocatalysis, that is, photocatalysis studies were preformed in laboratories in the field of catalysis, electrochemistry, photochemistry, materials chemistry, etc. This means that results of those studies have been discussed, presumably, on the basis of different concepts, analytical methods or understanding depending on the fields, and this might give rise to misunderstandings, misconceptions, or speculations, some of which are described in this review. It is time now to fix the field of "photocatalysis" having common unified understandings. It would be the author's great pleasure if this review builds a momentum for unified understandings of photocatalysis.

Acknowledgments

This work was partly supported by Project to Create Photocatalyst Industry for Recycling-oriented Society supported by NEDO, New Energy and Industrial Technology Development Organization and Grant-in-Aid for "Scientific Research (A) (General)" from the Ministry of Education, Culture, Sports, Science and Technology (MEXT) of Japan.

References

1. Fujishima, A.; Hashimoto, K.; Watanabe, T. In "*TiO_2 Photocatalysis Fundamentals and Applications*"; Bkc, Inc.: Tokyo, **1999**.
2. Hoffmann, M. R.; Martin, S. T.; Choi, W. Y. *Chem. Rev.* **1995,** *95*, 69.
3. (a) Fujishima, A.; Zhang, X. T.; Tryk, D. A. *Surf. Sci. Rep.* **2008,** *63*, 515. (b) Fujishima, A.; Zhang, X.; Tryk, D. A. *Int. J. Hydrogen Energy* **2007,** *32*, 2664.
4. Ohtani, B. *Chem. Lett.* **2008,** *37*, 216.
5. Papers reporting activation energy of photocatalytic reactions in the period 2000–2004. Figures and compounds in square brackets and parentheses, respectively, show activation energy in the unit of kJ mol-1 and substrate. (a)Vorontsov, A. V.; Stoyanova, I. V.; Kozlov, D. V.; Simagina, V. I.; Savinov, E. N. *J. Catal.* **2000,** *189*, 360 [10.9 (acetone)]. (b) Xu, Y. M. *Chem. J. Chin. Univ. Chin.* **2000,** *21*, 1539 [4.2-4.6 (acetophenone)]. (c) Su, W. Y.; Fu, X. Z.; Wei, K. M. *Chem. J. Chin. Univ.*

Chin. **2001,** *22*, 272 [13.7 (bromomethane)]. (d) Lea, J.; Adesina, A. A. *J. Chem. Tech. Biotech.* **2001,** *76*, 803 [7.83 (nitrophenol)]. (e) Kartal, O. E.; Erol, M.; Oguz, H. *Chem. Eng. Tech.* **2001,** *24*, 645 [16.2 (phenol)]. (f) Okte, A. N.; Resat, M. S.; Inel, Y. *J. Catal.* **2001,** *198*, 172 [17.1 (1,3-dihydroxy-5-methoxybenzene)]. (g) Tada, H.; Suzuki, F.; Yoneda, S.; Ito, S.; Kobayashi, H. *Phys. Chem. Chem. Phys.* **2001,** *3*, 1376 [19.7/29.4 (bis(2-dipyridil)disulfide)]. (h) Lee, N. C.; Choi, W. Y. *J. Phys. Chem. B* **2002,** *106*, 11818 [18.7 (soot)]. (i) Cui, W. Q.; Feng, L. R.; Xu, C. H.; Lu, S. J.; Qiu, F. *Chin. J. Catal.* **2003,** *24*, 937 [8.46 (methanol)]. (j) Kozlov, D. V.; Panchenko, A. A.; Bavykin, D. V.; Savinov, E. N.; Smirniotis, P. G. *Russ. Chem. Bull.* **2003,** *52*, 1100 [6.3 + 0.4 (benzene)]. (k) Mills, A.; Hill, G.; Bhopal, S.; Parkin, I. P.; O'Neill, S. A. *J. Photochem. Photobiol. A Chem.* **2003,** *160*, 185 [19 (stearic acid)]. (l) Al-Rasheed, R.; Cardin, D. *J. Chemosphere* **2003,** *51*, 925 [17 + 0.6 (fumic acid)]. (m) Garcia, J. C.; Takashima, K. *J. Photochem. Photobiol. A Chem.* **2003,** *155*, 215 [24.8 (imazaquin)]. (n) Machado, A. E. H.; de Miranda, J. A.; de Freitas, R. F.; Duarte, E T F M; Ferreira, L. F.; Albuquerque, Y. D. T.; Ruggiero, R.; Sattler, C.; de Oliveira, L. *J. Photochem. Photobiol. A Chem.* **2003,** *155*, 231 [7.9–10.5 (organic matter)]. (o) Parra, S.; Stanca, S. E.; Guasaquillo, I.; Thampi, K. R. *Appl. Catal. B: Environ.* **2004,** *51*, 107 [10.9 (atrazine)].

6. Fujishima, A.; Honda, K. *Nature* **1972,** *238*, 37 "Honda-Fujishima effect" is a well-known chemical phenomenon closely related to photocatalysis and the paper published in Nature in 1972 had undoubtedly promoted research activity of photocatalysis but not an origin of heterogeneous photocatalysis in the bibliographic sense (Ref. 3(a)).
7. Sometimes the term "active site" is used for a photocatalytic reaction system with dispersed chemical species, e.g., metal complexes or atomically adsorbed species, on support materials. Even in this case, a photocatalytic reaction occurs only when the species absorb light, and species not irradiated therefore cannot be active sites.
8. (a) Kowalska, E.; Abe, R.; Ohtani, B. *Chem. Commun.* **2009,** *45*, 241. (b) Kowalska, E.; Prieto-Mahaney, O. O.; Abe, R.; Ohtani, B. *Phys. Chem. Chem. Phys.* **2010,** *12*, 2344. (c) Zielinska, A.; Kowalska, E.; Sobczak, J. W.; Izabela, L.; Gazda, M.; Ohtani, B.; Hupka, J.; Zaleska, A. *Separ. Purif. Tech.* **2010,** *72*, 309.
9. In femto-second pump-prove transition photoabsorption measurements, titania photocatalysts gave visible-light photoabsorption of trapped e^- within ca. 100 fs pump pulse without showing photoabsorption of e^- in the CB. See Section IV.C.
10. (a) Ikeda, S.; Sugiyama, N.; Murakami, S.-y.; Kominami, H.; Kera, Y.; Noguchi, H.; Uosaki, K.; Torimoto, T.; Ohtani, B. *Phys. Chem. Chem. Phys.* **2003,** *5*, 778–783. (b) Murakami, N.; Prieto-Mahaney, O. O.; Abe, R.; Torimoto, T.; Ohtani, B. *J. Phys. Chem. C* **2007,** *111*, 11927–11935.
11. A probable first report on photocatalytic liberation of hydroxyl radical Jaeger, C. D.; Bard, A. J. *J. Phys. Chem.* **1979,** *83*, 3146.
12. Recent papers on photocatalytic production of hydroxyl radical: (a) Hirakawa, T.; Nosaka, Y. *Langmuir* **2002,** *18*, 3247. (b) Nosaka, Y.; Komori, S.; Yawata, K.; Hirakawa, T.; Nosaka, A. Y. *Phys. Chem. Chem. Phys.* **2002,** *5*, 4731. (c) Tryba, B.; Toyoda, M.; Morawski, A. W.; Nonaka, R.; Inagaki, M. *Appl. Catal. B Environ.* **2007,** *71*, 163. (d) Murakami, Y.; Endo, K.; Ohta, I.; Nosaka, Y. *J. Phys. Chem.* **2007,** *111*, 11339. (e) Hirakawa, T.; Yawata, K.; Nosaka, Y. *Appl. Catal. A Gen.*

2007, *325*, 105. (f) Sroiraya, S.; Triampo, W.; Morales, N. P.; Triampo, D. *J. Ceram. Proc. Res.* **2008,** *9*, 146. (g) Chang, C. Y.; Hsieh, Y. H.; Hsieh, L. L.; Yao, K. S.; Cheng, T. C. *J. Hazard. Mater.* **2009,** *166*, 897 and references therein.

13. Since the band structure of semiconductors, as well as insulators, consists of a filled valence band (VB) and vacant conduction band (CB), their Fermi level must be located between the VB and CB.
14. Backward electron (hole) transfer can be avoided thermodynamically only when the CB bottom and VB top are more positive and negative than standard electrode potentials of a reductant and an oxidant, respectively.
15. In other words, it is impossible to discuss "energy conversion efficiency" for reaction of negative Gibbs energy change as shown in Fig. 5(b).
16. It is thought that there should be at least ca. 200-mV "overpotential" in both reduction by e^- and oxidation by h^+, and this shifts the limiting wavelength for water splitting by ca. 250 nm.
17. In this analysis of first-order kinetics, any value can be plotted against time of reaction, unless the value is proportional to the molar amount of a substrate or product; for example, absorbance of a compound at a given wavelength can be used even if the molar absorption (extinction) coefficient is unknown and thereby absolute concentration can not be determined. Moreover, taking the logarithm means a reciprocal value can also be used, e.g., $[A_0]/[A]$, where $[A_0]$ is initial concentration of a substrate A (See Fig. 6).
18. Under these conditions, rate constant k obtained by the first-order kinetic analysis does not reflect the reactivity of a photocatalyst; k contains diffusion constant of a substrate and surface area of a substrate (strictly speaking, area of the diffusion layer on the "photoirradiated active" surface).
19. It should be noted that the overall rate obeys the first-order rate law in regard to surface concentration of a substrate but not concentration in the bulk.
20. In the lower concentration region of a Langmuir adsorption isotherm, similar linear dependence is also observed. However, if a given reaction condition is considered to be in this region, a Henry-type adsorption isotherm, not a Langmuir-type one, should be used, since the most significant characteristic of a Langmuir isotherm is saturation at a high concentration.
21. Another point to check is adequate use of substrate concentration in analysis. Since a Langmuir isotherm is derived on the basis of the adsorption equilibrium between species adsorbed and desorbed in solution, the isotherm is a function of concentration of the adsorbate (molecules to be adsorbed on surfaces) in solution, not concentration of the adsorbate in feed. Therefore, the actual concentration, which must be reduced from that in feed due to appreciable adsorption, must be measured at least before photoirradiation.
22. The author thinks that the use of "rate-determining step" for photoreactions is misleading, since a photoreaction in principle proceeds via species in their excited state and they undergo both chemical reaction and deactivation (deexcitation). The assumption for rate-determining step is that the reaction proceeds sequentially, not in parallel, such as photoreactions. See Section IV.E.
23. In some reports on photocatalytic reaction, it has been stated that the time-course curve obeys the first-order rate law and that the rate of reaction changes following Langmuir-type adsorption behavior (so-called

"Langmuir-Hinshelwood mechanism") when the substrate concentration is changed, though these two facts are incompatible. A possible situation is that a double reciprocal plot of rate and substrate concentration (Fig. 7 (a)) is linear but that the line passes through the origin, suggesting that the rate is proportional to the substrate concentration.

24. An example of papers showing the coincidence of equilibrium adsorption constants obtained from the photocatalytic reaction rate and adsorption in the dark, see: Amano, F.; Nogami, K.; Ohtani, B. *Langmuir* **2010,** *26*, 7174. Examples of papers reporting adsorption in the dark are as follows: (a) Cunningham, J.; Sedlak, P. *J. Photochem. Photobiol. A: Chem.* **1994,** *77*, 255. (b) Minero, C. *Catal. Today* **1999,** *54*, 205. (c) Xu, Y.; Langford, C. H. *J. Photochem. Photobiol. A: Chem.* **2000,** *133*, 67.
25. (a) Colombo, D. P.; Jr., Bowman, R. M. *J. Phys. Chem.* **1995,** *99*, 11752. (b) Colombo, D. P.; Jr., Bowman, R. M. *J. Phys. Chem.* **1996,** *100*, 18445. (c) Colombo, D. P.; Jr., Roussel, K. A.; Saeh, J.; Skinner, D. E.; Cavaleri, J. J.; Bowman, R. M. *Chem. Phys. Lett.* **1995,** *232*, 207.
26. Ohtani, B.; Kominami, H.; Bowman, R. M.; Colombo, D. P.; Jr., Noguchi, H.; Uosaki, K. *Chem. Lett.* **1998,** *27*, 579.
27. Tamaki, Y.; Hara, K.; Katoh, R.; Tachiya, M.; Furube, A. *J. Phys. Chem. C* **2009,** *113*, 11741.
28. This stoichiometry was clarified for the first time by the author's group and reported as: Nishimoto, S.-i.; Ohtani, B.; Kajiwara, H.; Kagiya, T. *J. Chem. Soc., Faraday Trans. 1* **1983,** *79*, 2685 Before submission to this journal, we submitted a part of the experimental results to Chemistry Letters as the first paper in the author's career in the field of photocatalysis, but the paper was rejected presumably due to a reviewer's comment that the content had been reported in a Russian journal without showing bibliographic data (We could not find this.). To submit the results as a full paper, additional experiments were carried out to support the stoichiometry. For example, an oxygen-isotope experiment was performed and showed the origin of molecular oxygen to be water. As a result, we were able to have the paper published, and it has been cited more than 100 times, including recent citations. This is an example of rejection of a submitted paper not always being disadvantageous for the authors.
29. This small content of ultraviolet light in solar radiation has been often described in papers, but an explanation of how this content was determined is rare. See Ref. 4, but the calculation in this review included some mistakes.
30. In the Japanese Industrial Standards (JIS B7113, discontinued), limiting transmission wavelength is defined as the center of wavelengths giving 72% and 5% transmission. For example, the limiting transmission wavelength for an Asahi Technoglass L-42 cut-off filter is 420 nm based on the standard, and this filter transmits ca. 60% at 420 nm. The number "42" indicates only that 420 nm is the limiting transmission wavelength defined in JIS, and a sample is practically irradiated at >390 nm through this filter. Statements such as "visible-light irradiation at >420 nm was performed using an optical sharp cut filter" seem misleading when L-42 has been used.
31. Asahi, R.; Morikawa, T.; Ohwaki, T.; Aoki, K.; Taga, Y. *Science* **2001,** *293*, 269 Fifteen years before the publication of this paper, Sato had reported the nitrogen incorporation in titania lattice, but he reported this to be "NO_x doping". Sato, S. *Chem. Phys. Lett.* **1986,** *123*, 126.
32. Amano, F.; Abe, R.; Ohtani, B. *Trans. Mater. Res. Soc. Jpn* **2008,** *33*, 173.

33. Highfield, J. G.; Pichat, P. *New J. Chem.* **1989,** *13*, 61.
34. (a) Mitoraj, D.; Beranek, R.; Kisch, H. *Photochem. Photobiol. Sci.* **2010,** *9*, 31. (b) Mitoraj, D.; Kisch, H. *Chem. Euro. J.* **2010,** *16*, 261.
35. Yan, X.; Ohno, T.; Nishijima, K.; Abe, R.; Ohtani, B. *Chem. Phys. Lett.* **2006,** *429*, 606 This paper claimed inappropriate use of organic dyes as test compounds for visible light-sensitive photocatalysts. Citation of this paper was not expected at all, since the authors using methylene blue (MB) as a model compound for photocatalytic reaction never want to refer to this and, on the other hand, those who do not use MB need not to refer to this. However, there has been an appreciable number of citations and, to the author's surprise, approximately half of the citations of this paper were for reasonable use of MB, indicating that authors of those papers did not read the paper.
36. Watanabe *et al.* have reported similar action spectrum analysis of photoinduced degradation of Rhodamine B with a cadmium sulfide suspension and pointed out a similar dye-sensitization mechanism: Watanabe, T.; Takizawa, T.; Honda, K. *J. Phys. Chem.* **1977,** *81*, 1845. Photocatalytic reaction of MB in aerated titania suspensions was reported in 1937 by a Japanese photochemist: Horio, M. *Nihon Gakujutsu Kyokai Hokoku* **1937,** *12*, 204 (in Japanese). As far as the author knows, this is the first report on titania photocatalysis.
37. Mills, A.; Wang, J. *J. Photochem. Photobiol. A: Chem.* **1999,** *127*, 123.
38. The fact that irradiation of a dye solution in the absence of a photocatalyst decomposes the dye negligibly has often been described in the papers to support negligible photoinduced reaction by photoexcited dye molecules. However, the photoinduced electron injection requires an acceptor, such as titania, and thereby there are no ideal control experiments to exclude the possibility of photoinduced electron injection, as shown in Fig. 11.
39. When organic dyes themselves are a pollutant to be decomposed, visible light-induced, but not photocatalytic, reaction can be a useful technique, e.g., Chen, X.; Zheng, Z.; Ke, X.; Jaatinen, E.; Xie, T.; Wang, D.; Guo, C.; Zhao, J.; Zhu, H. *Green Chem.* **2010,** *12*, 414.
40. Torimoto, T.; Aburakawa, Y.; Kawahara, Y.; Ikeda, S.; Ohtani, B. *Chem. Phys. Lett.* **2004,** *392*, 220 This paper showed that the rate of photocatalytic reaction in the presence of molecular oxygen, i.e., photocatalytic oxidative decomposition, may strongly depend on the intensity of light irradiation, while the rate of reaction in the absence of oxygen seems to be almost independent of light intensity.
41. Strictly speaking, when apparent quantum efficiency is discussed, the light intensity should be adjusted to be the same in number of photons, not in energy.
42. Scaife, D. E. *Sol. Energy* **1980,** *25*, 41.
43. Some exceptions have been reported, e.g., bismuth tungstate (Bi_2WO_6) shows a relatively high level of photocatalytic activity for oxidative decomposition of acetaldehyde in air: (a) Amano, F.; Nogami, K.; Ohtani, B. *J. Phys. Chem. C* **2009,** *113*, 1536. (b) Amano, F.; Nogami, K.; Abe, R.; Ohtani, B. *J. Phys. Chem. C* **2008,** *112*, 9320–9326.
44. Abe, R.; Takami, H.; Murakami, N.; Ohtani, B. *J. Am. Chem. Soc.* **2008,** *130*, 7780.
45. It was proved that tungsten(VI) oxide produces a negligible amount of hydrogen from an aqueous solution containing electron donors such as methanol even when loaded with platinum, and this is consistent with

the assumption of platinum-catalyzed multiple-electron transfer to oxygen.
46. Arai, T.; Horiguchi, M.; Yanagida, M.; Gunji, T.; Sugihara, H.; Sayama, K. *Chem. Commun.* **2008,** 5565.
47. Irie, H.; Kamiya, K.; Shibanuma, T.; Miura, S.; Tryk, D. A.; Yokoyama, T.; Hashimoto, K. *J. Phys. Chem. C* **2009,** *113*, 10761.
48. A recent review on nanostructured titania photocatalysts: Chen, X.; Mao, S. S. *Chem. Rev.* **2007,** *107*, 2891.
49. Examples of papers discussing the property-activity correlation are: (a) Enríquez, R.; Agriosa, A. G.; Pichat, P. *Catal. Today* **2007,** *120*, 196. (b) Ryu, J.; Choi, W. *Environ. Sci. Technol.* **2008,** *42*, 294.
50. (a) Prieto-Mahaney, O. O.; Murakami, N.; Abe, R.; Ohtani, B. *Chem. Lett.* **2009,** *38*, 238. (b) Ohtani, B.; Prieto-Mahaney, O. O.; Amano, F.; Murakami, N.; Abe, R. *J. Adv. Oxidat. Tech.* **2010,** *13*, 247.
51. Amano, F.; Prieto-Mahaney, O. O.; Terada, Y.; Yasumoto, T.; Shibayama, T.; Ohtani, B. *Chem. Mater.* **2009,** *21*, 2601.
52. Ohtani, B.; Amano, F.; Yasumoto, T.; Prieto-Mahaney, O. O.; Uchida, S.; Shibayama, T.; Terada, Y. *Top. Catal.* **2010,** *53*, 455.
53. It was suggested that transfer of photoexcited electrons and positive holes between interconnecting anatase and rutile particles may enhance charge separation and hence improve the efficiency of utilization of electron–hole pairs: Hurum, D. C.; Agrios, A. G.; Gray, K. A.; Rajh, T.; Thurnauer, C. *J. Phys. Chem. B* **2003,** *107*, 4545. Ohtani, B.; Prieto-Mahaney, O. O.; Li, D.; Abe, R. *J. Photochem. Photobiol. A Chem.* **2010,** *216*, 179.

INDEX

CONTENTS OF PREVIOUS VOLUMES

VOLUME 45

VOLUME 46

VOLUME 47

VOLUME 52

VOLUME 53

VOLUME 54

VOLUME 57

VOLUME 58

VOLUME 59

VOLUME 60

VOLUME 61

VOLUME 62